Regional Geology Reviews

Bastien Linol
Maarten J. de Wit
Editors

Origin and Evolution of the Cape Mountains and Karoo Basin

Springer

Regional Geology Reviews

More information about this series at http://www.springer.com/series/8643

Ode to Fieldwork

Arthur Fuller with his field equipment exploring the Cape-Karoo on his motorcycle in 1960. Today young geo-scientists are less attracted by such basic fieldwork (and freedom), yet the Cape Mountains and Karoo hinterland is a unique natural laboratory to observe, discover, learn and preserve

Bastien Linol · Maarten J. de Wit
Editors

Origin and Evolution of the Cape Mountains and Karoo Basin

AEON Earth Stewardship Science Research Institute
Nelson Mandela Metropolitan University for tomorrow
Springer

Editors
Bastien Linol
AEON-ESSRI
Nelson Mandela Metropolitan University
Port Elizabeth
South Africa

Maarten J. de Wit
AEON-ESSRI
Nelson Mandela Metropolitan University
Port Elizabeth
South Africa

ISSN 2364-6438 ISSN 2364-6446 (electronic)
Regional Geology Reviews
ISBN 978-3-319-40858-3 ISBN 978-3-319-40859-0 (eBook)
DOI 10.1007/978-3-319-40859-0

Library of Congress Control Number: 2016943862

Cover illustration: View through a window of columnar joints of a Karoo sill at the top of the Great Escarpment looking south, through Desolation Valley, towards the distant Cape Mountain ranges, all features reported on in this book

Printed on acid-free paper

This Springer imprint is published by Springer Nature
The registered company is Springer International Publishing AG Switzerland

This book is dedicated to three extraordinary lovers of nature and of the geology across Cape-Karoo routes—and advocates of "do your own thing" Arthur O. Fuller, Samuel O. Bowing and David L. Roberts

For years during his early career, Arthur Fuller traversed the Cape and the Karoo on his motorcycle. He seldom documented his observations in writing, but he photographed every nook and cranny, and freely shared his vast knowledge and understanding of the stratigraphy, sedimentology and geomorphology of iconic Cape-Karoo landscapes that he memorized and knows by hard. During one of these 'motorcycle maintenance' trips, Arthur discovered a dilapidated farmhouse near Laingsburg, and persuaded the farmer Colenso van Wyk to long-lease it as a field-work station. Since that day, literally hundreds and possibly thousands of students have tasted their first exposure to and mapping of 'Cape-Karoo' rocks from there; and listened to some legendary Arthur Fuller stories around campfires. Today, Arthur still has vivid geological and motorcycle memories of Cape-Karoo challenges that he loves to share.

On and off, over 20 odd years, Sam Bowring traversed Cape-Karoo routes with numerous South African geologists. He recognized early on that his high-precision chronology tools would prove to be of immense value to record the paleo-history of the Karoo. And so it has. In 1996 Sam was the first person to date zircons collected from the Collingham Formation, establishing 'proof of concept' that the age of Karoo tuff beds could be measured at 100 Kyr levels using the time-consuming mechanical and chemical abrasion systems with the TIMS that he developed at MIT, and which are even now well established by several of his graduate students at leading universities in the USA. Sam continued to work unselfishly with South African paleontologists, under his motto '*no dates, no rates*', to track the evolutionary paths of Karoo fossils. Sam had an unrivalled memory of thousands of outcrops he visited throughout his career. Sadly, Sam recently

suffered brain damage; and whilst his long-term knowledge appears intact, his unique short-term memory is locked away. Thankfully his deep empathy remains as ever.

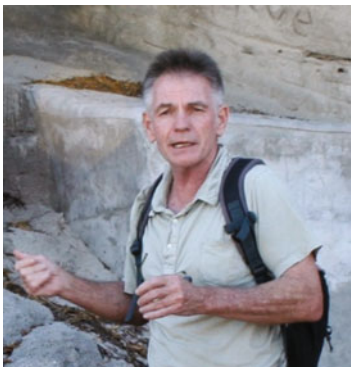

Dave Roberts was the ultimate field geologist. He walked the mountains and the beaches of southern Africa, and made stunning observations that he analysed in detail. He had deep first-hand knowledge of paleo-sea levels and erosion surfaces from scrambling across them, and interpreting their histories based on his interdisciplinary connections with sedimentology, stratigraphy, paleontology and archeology—and contributed widely to appreciation of our relatively recent geological history. Dave found the oldest fossilized Homo *sapiens* footprints ('Eve's Footprints' near Langebaan in the West Coast National Park in 1995 along both the east and south coasts of South Africa, and was protective of these 'global heritages'). Whilst a 'loner'—and what good field geologist is not—he shared his enthusiasm of his new discoveries and interpretations with anyone who showed the slightest interest, and even those who didn't. Sadly whilst still in his geologic prime and with lots of ideas and goals, he passed away late in 2015; his vast geologic memory suddenly disappeared like a 'burnt library'. Those who read his published work will gain deep insights in how to excel as an outstanding field-observer and, following his footsteps, will appreciate his astuteness as a guide towards further unravelling Cape-Karoo geo-bio narratives.

Preface

1 Introduction

What Is in This Book and Why?
This book has 18 chapters that summarize advances made over the last 25 odd years towards better understanding the wealth and value of the geological heritage of southernmost Africa, and in particular its Phanerozoic history across the Cape-Karoo landscapes. This region is a unique natural laboratory from which to reconstruct, predominantly, the terrestrial evolution of our southern hemisphere continents over the last 500 million years or so. We have tried to summarize this history in Fig. 1.1.

This book, a follow-up of an earlier book (de Wit and Ransome 1992), is an outcome of the 2015 Cape-Karoo 'Imbizo' (=South African meeting or dialogue, especially a gathering of the Zulu people called by the king or a traditional leader to exchange ideas) with a focus to stimulate cross-disciplinarity in future research of the Cape-Karoo archives. We asked contributors to be brief in summarizing their recent work within limited space, and to address their findings without jargon, so that both students and professionals could easily understand their aims and analyses, and to stimulate young researchers to identify new challenges and to get involved.

What Is Not in This Book?
Inevitably not all ongoing work is represented in this book, and some classic missing segments are major shortcomings. For example, the history of the Cape Mountains along the west coast of South Africa (e.g. Cedarberg/Piketberg) are barely mentioned, nor is its flanking Karoo stratigraphy, or their (Gariep) basement and Cape Granites. This (Saldanian) region has unique narratives to tell, particularly about the early Cape Supergroup sequences, such as the Ordovician glaciation and related fossil record, especially so because these Cape-Karoo sections are less affected by the Cape Orogeny, since the western part of the Cape Fold Belt is linked to tectonic strike-slip rather than "head-on" convergence (we expand on this a little in this Preface). Similarly, the structural history of 'syntaxis' linking the two Cape tectonic domains, and the related foreland depositional environment in the delta-turbidite sequences of the Tanqua Karoo that best record this tectonic history, are not documented here (the interested reader might consult Fildani et al. 2007 and references therein). Similarly, a detailed examination of the Karoo and related magmatism is wanted. However, Chaps. 6 and 12 explore some outstanding Karoo volcanic problems that have been neglected for some time, and highlight the need for more careful geochemical and geochronological data to separate those sequences that are related to Karoo magmatism and those with affinities to South American sources. The lack of coastal marine and off-shore continental margin work, as well as the details related to geomorphology and landscaping, is also obvious. To highlight these 'black holes' we have added some relevant sections in this Preface. Not because we understand them well, but precisely because there is severe lack of knowledge and cross-disciplinary communication; and thus to highlight where there is a real need for transformation in Cape-Karoo research in the future. Additionally the reference lists of the preface and the chapters provide ample opportunities to explore further.

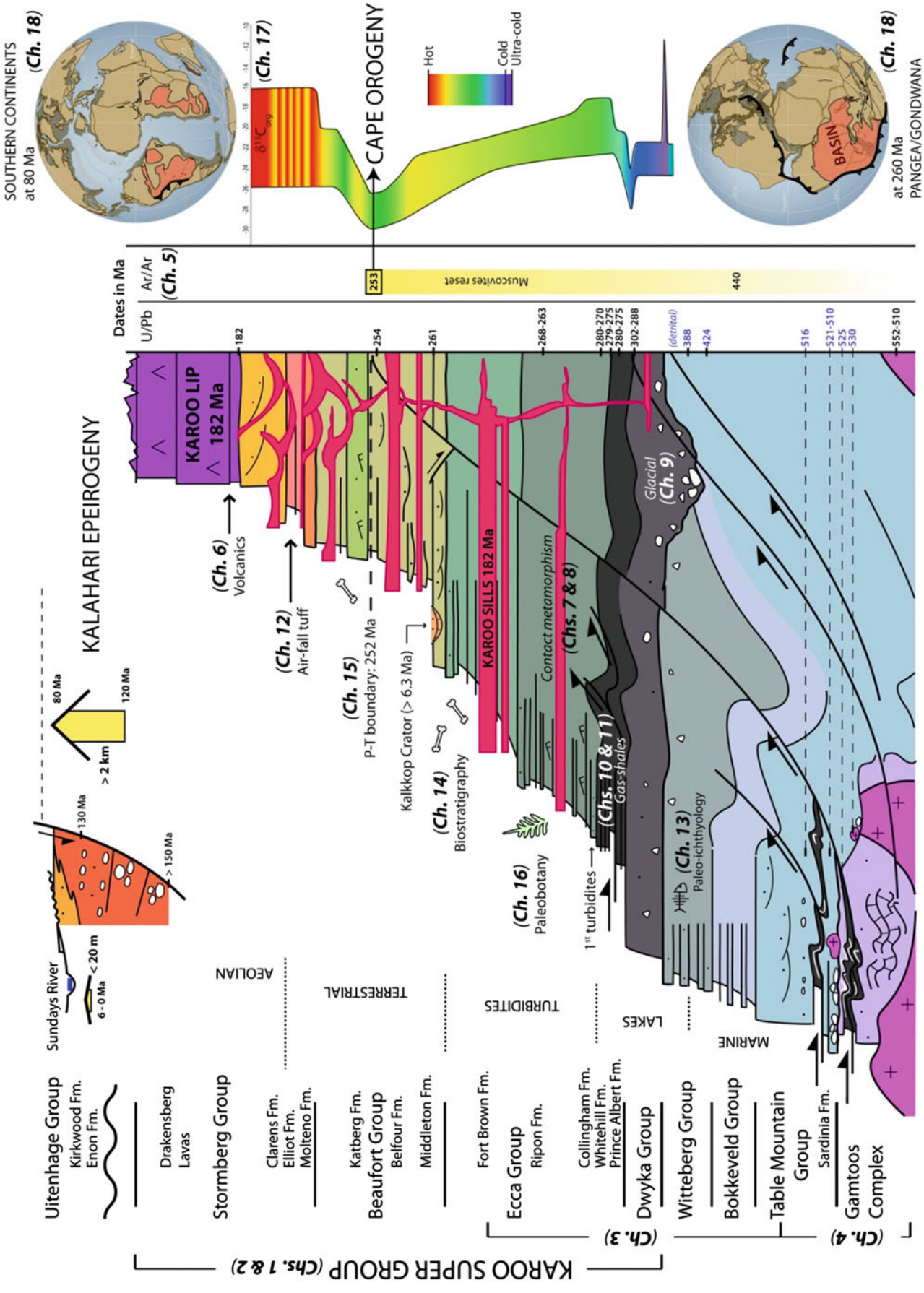
KAROO SUPER GROUP (Chs. 1 & 2)
Uitenhage Group
Kirkwood Fm.
Enon Fm.
Drakensberg Lavas
Stormberg Group
Clarens Fm.
Elliot Fm.
Molteno Fm.
Katberg Fm.
Beaufort Group
Belfour Fm.
Middleton Fm.
Fort Brown Fm.
Ecca Group
Ripon Fm.
Collingham Fm.
Whitehill Fm.
Prince Albert Fm.
Dwyka Group
Witteberg Group
Bokkeveld Group
Table Mountain Group
Sardinia Fm.
Gamtoos Complex
(Ch. 3)
(Ch. 4)
AEOLIAN
TERRESTRIAL
TURBIDITES
LAKES
MARINE
Sundays River
< 20 m
6 - 0 Ma
130 Ma
> 150 Ma
80 Ma
120 Ma
> 2 km
KALAHARI EPEIROGENY
KAROO LIP 182 Ma
(Ch. 6) Volcanics
(Ch. 12) Air-fall tuff
(Ch. 15) P-T boundary: 252 Ma
Kalkkop Crater (> 6.3 Ma)
(Ch. 14) Biostratigraphy
KAROO SILLS 182 Ma
Contact metamorphism
(Chs. 7 & 8)
(Ch. 16) Paleobotany
1st turbidites
(Chs. 10 & 11) Gas-shales
(Ch. 13) Paleo-ichthyology
Glacial (Ch. 9)
Dates in Ma
U/Pb
Ar/Ar (Ch. 5)
182
254
261
268-263
280-270
279-275
280-275
302-288
(detrital)
388
424
516
521-510
525
530
552-510
253
Muscovites reset
440
(Ch. 17)
$\delta^{13}C_{org}$
CAPE OROGENY
Hot
Cold
Ultra-cold
SOUTHERN CONTINENTS
at 80 Ma
(Ch. 18)
BASIN
at 260 Ma
PANGEA/GONDWANA
(Ch. 18)

◄ **Fig. 1.1** Graphic summary of the generalized Cape-Karoo stratigraphy linked to the chapters of this book. The oldest sequences (e.g. the Kango, Kaaimans and Gamtoos complexes—*pale purple*) comprise deformed carbonates, black phyllites with voluminous polyphase quartz veins, and dacite-granitoids (*pink*) that are dated between 550 and 510 Ma. These are overlain by conglomerates (the Sardinia Bay Formation in eastern Cape; the Klipheuvel Formation in western Cape) containing youngest detrital zircons dates of 521–510 Ma, and thick sequences of cross-bedded quartzites with interbedded micaceous mudrocks of the Cape Supergroup (the Table Mountain, Bokkeveld and Witteberg Groups; *blues*). Major décollement zones are rooted in the black phyllites, and from there propagate upward as thrusts, duplicating overlying siliclastic sequences (Chap. 4). In the uppermost part, Devonian shales contain a rich fossil vertebrate fauna, including fish (Chap. 13). The top of the Cape Supergroup is either a continuous transition to glacial sediments or an abrupt erosion surface, with incised paleo-glacial valleys and eskers (Chap. 9) of the Dwyka Group (*grey*) that, near its base record pronounced peaks of δ^{13} C_{org} indicating ultra-cold conditions (Chap. 17), perhaps reflecting a lake below an Antarctic-like ice-cap that prevailed for some 50 million years. Onset of deglaciation, just before 288–291 Ma, is marked by accumulation of organic-rich black shale (the Prince Albert and Whitehill Formations; *dark grey*). The latter is the host of potential unconventional shale-gas reservoirs (Chaps. 10 and 11). These are also locally deformed along décollement surfaces. Thick overlying turbidites and fluvial-deltaic sequences form most of the Ecca and Beaufort Groups of the lower Karoo Supergroup (*greens*) and likely related to variable uplift of the proto Cape Mountain ranges, culminating in the Cape Orogeny that is now best dated using Ar/Ar on metamorphic muscovites at 253.3 ±1.9 Ma (Chap. 5); e.g. within error of the Permo-Triassic extinction. These syn-tectonic basin sequences contain numerous interlayered tuffs dated between 280 and 250 Ma and the terrestrial Permian-Triassic boundary at 252.2 Ma, as best defined by vertebrate paleontology and related ecosystems (Chaps. 14 and 15). The uppermost Karoo Supergroup, comprising the Molteno, Elliot and Clarens Formations (*yellows),* is rich in flora and fauna (Chap. 16) despite becoming increasingly arid with marked δ^{13} C_{org} excursions reflecting episodic droughts before the onset of 50 million years of the southern Gondwana Desert (Chaps. 12 and 17). The Karoo Supergroup is widely intruded by 182 Ma dolerite dykes and sill complexes (*red*), and is covered by the Drakensberg basalts of the Karoo Large Igneous Province (LIP) that erupted at 182–183 Ma (Chap. 6), and whose related sills have affected (metamorphosed) the siliciclastic rocks at their contacts (with growth of andalusite) and reduced the porosity of the gas-shales (Chaps. 7 and 8). Associated with the break-out of Africa from Gondwana (200–130 Ma), Jurassic-Cretaceous rift sequences were deposited during this extensional tectonics along the flanks of the Cape-Karoo (the Uitenhage Group; *oranges*), and offshore along the 'passive' continental margin of southern Africa (not discussed in any of the chapters). Thereafter the Kalahari epeirogeny (120–80 Ma) uplifted the continent interior during relatively hot and humid conditions, inducing extreme high rates of exhumation and sculpturing of the Cape and Karoo Mountains, and farther inland the Kalahari Plateau (as discussed in this Preface). The present-day topography preserves numerous erosion surfaces between the coast and escarpments, one surface of which is impacted by the Kalkkop crater now estimated to be older than 6.3 Ma (Miocene) from nearby Neogene-Quaternary erosion rates that are extremely low (1–20 m/Ma), as determined from cosmogenic isotopes along river terraces and catchment valleys (e.g. Sundays River), Table Mountain and Cape Mountain ridges, dolerite sill and recent alluvial plains (Sect. 7 in this Preface). Much of the Mesozoic and more recent geomorphology, including spectacular coastal canyons along the south and east coasts (e.g. Storms River Mouth), were induced by changing sea levels and possibly minor episodes of tectonic uplift and subsidence. Details of how these coastal processes affected the inland geomorphology (including the Great Escarpment and the complexity of adjacent surfaces and inland canyons) and ecosystems remain to be resolved using modern techniques such as Sr-isotope analyses of marine fossils, and geo-ecodynamics based on interlinked genetic studies of the living Cape-Karoo flora and fauna, integrated with numerical modelling

Content

The 18 chapters in this book address a large variety of topics relevant towards unravelling the origin and evolutionary history of the Cape-Karoo in its larger Gondwana context. The aim is to try and solidify more interdisciplinary thinking about local and global Phanerozoic geo-bio-evolution. Much of the Karoo tells a unique terrestrial story that can be linked to the greater Gondwana interior basins, whilst the Cape Fold Belt, which formed part of the Gondwanides as recognized long ago by Alex du Toit and his South American peer Juan Keidel, is of direct interest to natural scientist on other Gondwana continents where segments of this iconic orogenic system are preserved (Fig. 1.2).

Fig. 1.2 *Left* Dispersal of the fold and thrust belts of the Gondwanides (*yellow*) into its tectonic fragments that are now dispersed on many continents thousands of kilometers away. *Right* Copy of original drawing of Alex du Toit (1937; from the UCT archives) showing the extent of the orogenic zone to the south of the Cape Fold Belt, and flanked to the north by "foreland" and "foredeep" complexes. Du Toit used the term "Samfrau Orogenic Zone" (*Samfrau* an acronym of South AMerica, aFRica and AUstralia) instead of the presently preferred term Gondwanide Orogenic Belt, or Gondwanides

Below, we first summarize the contents of this book, chapter by chapter, and thereafter expand on some peripheral topics and emerging ideas that are not directly addressed in the chapters, but that are an integral part of consolidating a more comprehensive history of the origin and evolution of the Cape-Karoo. The chapters in the book are divided into five technical subdivisions:

I. Subsurface geology and geophysics

In Chap. 1, Bastien Linol et al. describe the litho-stratigraphy and structure of the southern Karoo Basin reconstructed from detailed re-logging of 11 deep boreholes drilled by SOEKOR in the 1960s. The Karoo Supergroup here is between 750 and 5,540 m thick, including 79–569 m thick black shales of the lowermost Ecca Group that were deposited during rapid deglaciation, marking a relatively short-lived, deep-water time-horizon as the most obvious sequence to function as a baseline for stratigraphic correlations. These shales also happen to be rich in organic matter, and are believed to be unconventional gas-reservoirs. Overlying successions become regionally sandier and thicker-bedded upward, and include a transition to fluvial sections of the Beaufort Group that cannot at this stage be delineated with confidence. Along the southern margin, flanking the Cape Fold Belt, the Karoo successions are variably deformed, whilst farther north increasingly abundant dolerite sills intrude progressively to greater depths, all of which complicate unraveling the basin-wide stratigraphy.

The next two chapters describe seismic data with which the deep subsurface make-up of the Cape-Karoo might be interpreted, although it is acknowledged that there is a lack of reliable data. Nevertheless, in Chap. 2, Stephanie Scheiber-Enslin et al. reinterpret old (SOEKOR) seismic data to provide insight into the subsurface structure of dolerite sills that have intruded the Karoo Basin at multiple levels. This is especially the case in the far eastern part of the basin, north of East London, where cumulatively, dolerites are known to reach great thicknesses that occur as far down as the Ecca black shales and Dwyka tillites, some 2,000 m below surface here. Farther southward, the number of sills decreases rapidly (close to East London there are very few at Ecca depths), and no dolerite is found further south, defining a 'dolerite line'. This 3D change in spatial distribution of the sills will likely influence the location of early shale gas exploration. The seismic data confirm the presence at relatively shallow stratigraphic levels of the

Karoo Basin of small to medium saucer-shaped sills, some 5–30 km in diameter and with vertical thicknesses up to 300 m, and dips of between 2° and 8°. Larger 'saucers' up to 150 km widths, with dips of between 3° and 13° occur down to depths of 5 km. The change in geometry of the sills and associated dykes are likely related to variable mantle supply and source locations, but it remains a mystery how these processes distributed sill and dyke complexes over thousands of kilometers across the Karoo Basin and beyond (in Namibia, Botswana and Zimbabwe). There is also no agreement on how far the overlying Karoo lavas, now mostly preserved only across Lesotho, might have extended across the Karoo Basin. Whilst this Karoo Large Igneous Province is dated at 182 Ma and intuitively linked to mantle processes during opening of the proto-Indian Ocean as southern Africa separated from East Antarctica, there is just too little data yet from geophysics (especially off-shore) and geochemistry to unravel the details of this story.

In contrast, in Chap. 3 Lucian Bezuidenhout and coworkers describe new seismic results using ambient seismic signals derived from 17 stations installed along swath in the south-eastern Cape-Karoo. This new technique creates velocity models to depths of at least 5 km. Their early results reveal two different velocity regions broadly flanking the divide between the Cape Fold Belt and the Karoo Basin. The higher group velocity anomalies (3–5 km in thickness) most likely represent the Carboniferous-Permian sequences of the Karoo Basin (Dwyka-Ecca-Beaufort Groups). A lowermost velocity region in the south-eastern study area coincides with the younger Jurassic-Cretaceous sequences of the Algoa Basin that directly overlie the Cape Fold Belt. What is exciting about this work is that it leads the way towards rapid non-invasive seismic mapping of the subsurface of the Karoo Basin.

II. Structure and Tectonics

In context of a regional tectonic model for the origin of the Cape Orogeny, Warren Miller et al. in Chap. 4, interpret new structural field observations and U-Pb zircon geochronology from rock sequences of the Gamtoos Complex along the easternmost sector of the Cape Fold Belt. They describe for the first time thick tectonic wedges of poly-deformed black phyllites that are transected by multiple phases of closely spaced quartz-veins. These accretionary-like wedges contain south-dipping décollement zones that in turn extend up-sequence as splay-thrusts into the overlying quartzites of the Table Mountain Group. Combined with recent seismic profiling, these observations are consistent with south-dipping plate subduction and emplacement of the Cape Fold Belt as Jura-like duplexes during the evolution of the larger Gondwanide Orogen.

However, in part because of the low grades of metamorphism, there is still an unsatisfactory resolution of the age of deformation structures of the Cape Fold Belt, against which a consistent tectonic model must be tested. Whilst recent $^{40}Ar/^{39}Ar$ results from single muscovite grains and aggregate samples imply at least two tectonic events (ca. 270 Ma and ca. 250 Ma) for the Cape Fold Belt, in Chap. 5, Scarlett Blewett and David Phillips present preliminary high-precision $^{40}Ar/^{39}Ar$ step-heating analyses on more than 100 single muscovite grains from the Cape Supergroup of the Eastern Cape region that yield concordant muscovite ages at ca. 253 Ma. This constrains the final stage(s) of the low-grade deformation close to the Permian-Triassic boundary. By contrast to the previous studies, intermediate ages between 255 and 440 Ma appear to represent mixed age populations of detrital and metamorphic micas. Thus a reliable age of an earlier (if any) phase of Cape deformation remains to be recorded. Presently, U/Pb dates of zircons from volcanic ashes interbedded within the first turbidite sequences of the Ecca Group (the Collingham Formation), and linked to a switch in provenance sources for the Karoo sediments, provide only circumstantial evidence for an early tectonic phase to the south of the Fold Belt at about 275 Ma.

III. Magmatism and Metamorphism

The origin and tectonic significance of tholeiitic basalts of the Mimosa Formation, which constitute the uppermost stratigraphic unit of the Jurassic Suurberg Group in the northern part of the Algoa Basin, have long remained contentious: do they belong to the 182 Ma-aged Karoo Large Igneous Province, or are they related to the Jurassic-Cretaceous

rift basins, or both? In Chap. 6, Goonie Marsh describes for the first time the geochemical, age and paleo-magnetic signatures of these basalts from two drill cores. $^{40}Ar/^{39}Ar$ dating of plagioclase suggests an age of 194 ± 12 Ma, which is within error of the age of the relatively short-lived Karoo volcanism in Lesotho. This, and geochemistry, as well as magnetic polarity fingerprints, indicates that the Mimosa basalts are equivalent to flows in the upper part of the Lesotho sequence. The question remains how these Suurberg lavas can help to reconstruct the wider paleo-cover of lavas across the Karoo Basin and beyond that many workers predict have since been eroded away during the Cretaceous-Paleocene.

Host rock alterations related to high heat and fluid flow during the emplacement of the Karoo igneous intrusions, and specifically its sills, are believed to have changed the reservoir characteristics of gas-bearing Ecca shales, through reducing their porosity and permeability. Chapters 7 and 8 describe the petrography and mineralogy of the host rocks along the margins of such intrusions and at various distances away, above and below their igneous contacts. In Chap. 7, Vhuhwavhohau Nengovhela et al. document distinct changes in mineralogy and chemistry of the shale host rocks and their organic matter. Analysis of drill core samples of the Karoo black shales close to upper and lower contacts of several dolerite sills indicate increased quartz content, decrease in hydrous minerals, and formation of metamorphic minerals including chiastolite (andalusite). Most notable is the distinct decrease of porosity in these samples.

In Chap. 8, David Moorcroft and Nicolas Tonnelier describe similar metamorphic changes in these shales at various distances away from dolerite sills. Together with Ti-biotite geo-thermometry, they develop a conductive heat flow model that shows thin sills heat host shales at their contacts up to 650–700 °C, and up to 350 °C at 45 m away from the contacts. Mineral phase equilibrium modelling constrains minimum temperatures of ca. 375 °C up to 13 m above two closely spaced sills, and cooler temperatures farther away and below these sills.

IV. Stratigraphy and Sedimentary Systems

Sinuous north–south orientated gravel ridges on a flat erosional surface flanking the northwest margin of the Karoo Basin have been mined for diamonds in the Lichtenburg-Ventersdorp area for 90 years, yet the origin of these gravel ‘runs’ has remained unresolved. In Chap. 9, Mike de Wit describes these gravels in detail, as well as glacial pavements and isolated remnants of thin Karoo sediments found across the erosional surface. These new field observations, together with age dating of diamonds and zircons separated from the gravels, indicate that the runs are paleo-eskers of up to 30 km long that formed during final deglaciation and ice retreat of the Permo-Carboniferous Dwyka continental ice cap. The paleo-eskers represent the infillings of ice-walled stream channels and record deposition of poorly sorted sediment in subglacial drainage networks. The absence of Mesozoic age diamonds supports the interpretation that the runs are of Karoo age and are not recent river deposits as previously thought.

The overlying Early Permian black shales, especially those of the Whitehill Formation in the southern sections of the Karoo Basin have recently been identified as potential unconventional gas reservoirs. Because successful gas recovery is strongly influenced by host rock properties, characterizing the spatio-temporal variations in these black shales, is necessary. In Chap. 10, Kenneth Chukwuma and Emese Bordy report on these rock property variations and their sedimentological controls by combining field descriptions, petrographic observations and geochemical proxies. They distinguish five sedimentary facies (F1–F5) that suggest changes in the depositional conditions from overall low-energy environments where pelagic snow aggregates covered the basin floor in the deep southern sections of the Karoo Basin, to higher energy farther north where terrestrial detritus was deposited via mud flows that originated from melting of glaciers flanking the northern margin of the Karoo Basin. It is not always clear, however, if some of these variations may also be due to post-depositional diagenesis, fluid-flow and weathering.

Nethertheless, these observations are consistent with a broader regional deglaciation model for the deposition of black shales of the lower Ecca Group (the Prince Albert and Whitehill Formations) preserved in the southern Karoo Basin. Hans-Martin Schultz and coworkers show in Chap. 11 that the chemical and mineral signals of these black shales indicate that organic carbon production and preservation changed in time and space to variations in marine incursions into a deep fresh water lake. This chapter presents for the first time a realistic modern analogue for the Early Permian deposition of Karoo carbon-rich sediments, based on the post-Pleistocene glaciation history of the Baltic Sea of northern Europe.

Dating of the Karoo sequences have for some time now relied on U/Pb dating of interbedded ash-fall layers. Whilst this has been relatively successful in the lower turbidite sequences of the Ecca Group, where the tuffs are thick and well preserved, this technique hampered by sedimentary reworking in fluvial systems higher in the Karoo sequences (the Beaufort and Drakensberg Groups). In Chap. 12, Emese Bordy and Miengah Abrahams address this with the aim to pinpoint with more confidence the Triassic-Jurassic boundary within the red beds of the upper Elliot Formation. Here they focus on the Pronksberg bentonite within the lowermost Jurassic deposits, by analyzing in details its sedimentological, mineralogical, and major and trace element geochemical characteristics, and conclude that the bentonite formed by devitrification of felsic volcanic ash clouds that originated in southwest Gondwana (now South America) where explosive silicic igneous activity has been documented throughout the Permian to Early Jurassic. The ash was subsequently reworked in an ephemeral lake where intense chemical weathering of the ash occurred. With that detailed knowledge, future U/Pb dating on remnant zircons may still yield useful chronostratigraphic information towards identifying the precise location of the Triassic-Jurassic extinction zone in the Karoo.

V. Paleontology and Paleo-Environments

Life thrived throughout Cape-Karoo times and preserves an almost complete evolutionary history from trilobites to dinosaurs and mammals; and from Glossopteris to modern flora that is now under preservation in Cape and Karoo heritage sites. This evolutionary story is unique too because Cape-Karoo ecosystems survived at least five well-known Phanerozoic extinction events, three of which are exceptionally well preserved and two of which are classic, globally important terrestrial archives.

In Chap. 13, Robert Gess describes in detail the bottle-neck during mid-Paleozoic life (the second major Phanerozoic extinction) recorded in the Witteberg Group rocks exposed along the southern margin of the proto-Karoo Basin. Globally, the Devonian/Carboniferous boundary (ca. 359 Ma) is characterized by mass extinction of the entire grade of placoderm (armored) fish, and a radically reduced diversity of sarcopterygian (tetrapods such as coelacanths and lungfish) and acanthodian (early jawed fishes, shark-like with sharp spines along the leading edges of all fins). In the Cape Supergroup a fauna of sharks, acanthodians and an increasing diversity of placoderms dominated from the Silurian Bokkeveld Group through the upper Witteberg Group. Overlying strata contain no placoderms or sarcopterygians, but present are some relict sharks and acanthodians, and an increasing abundance of ray-finned fishes. This rapid change defines the positions the Devonian/Carboniferous boundary within the Witteberg Group and uplifts its status as an important transition zone for further unravelling the causes and effects of the second Phanerozoic mass extinction (the first, at the Ordovician-Silurian transition (ca. 444 Ma) must also be present in the Table Mountain Group, but a 'hunt' for this event in these marine sequences is not covered in this book).

The following non-marine Permian-Jurassic deposits of the Karoo Supergroup have long been a world standard for terrestrial biostratigraphy that contain the next two major global extinction events: across the Permian-Triassic (ca. 252 Ma) and across the Triassic-Jurassic (ca. 201 Ma) boundaries.

The Permian stratigraphy of the Karoo Supergroup of South Africa is best known for its evolutionary record of mammal-like reptiles, conifers, insects and early flowering plants.

In Chap. 14, Bruce Rubidge, together with many specialized coworkers, summarize their recent and new research that is documenting these paleo-archives at an unprecedented level of precision based on U/Pb dating of zircons from interbedded tuff horizons. The bio-chronostratigraphic work confirms that there is a marked diversity drop in tetrapods well before the Permian-Triassic boundary, and is perfecting understanding of the global terrestrial vertebrate evolution. This exciting work is dramatically enhancing our understanding of the link between major punctuated events in terrestrial ecosystems and tectonic processes related, at least in the Karoo, to the Gondwanide orogeny, and subsequent rifting during the Early Jurassic start of Gondwana disintegration.

The Karoo Basin is considered also to contain the type terrestrial record of the third major Phanerozoic mass extinction. A detailed extinction model, based on bio-lithostratigraphy, has proposed rapid ecosystem changes to have been caused by onset of rapid global aridity. However, in Chap. 15, Johann Neveling et al. describe their detailed transdisciplinary data collected over many years across several boundary sections exposed along the Great Escarpment, to demonstrate that ecological change was subtle and protracted, reflecting a more complex way in which the ancient Karoo landscape responded to, for example, tectonic forces; and that feedback links between life's global terrestrial and marine turnover across the Permian-Triassic boundary are far from understood.

Complementing all these faunal narratives are well-preserved silicified 'forest' fossils (woods) that are scattered through the Karoo sequences. In Chap. 16, Marion Bamford, South Africa's leading 'paleo-carpenter', shows how this wood-record can be used to track past climate changes, from Dwyka ice-times, across the Permian extinction into warmer Triassic environments when seed-producing plants (gymnosperms) that include conifers, cycads, ginkgo and gnetales exploded during Molteno times. Preliminary research on the growth rings of these gymnospermous woods is presented here and shows that there appear to be both longitudinal and latitudinal variations in climate, so that these signals likely reflect both local and global climate fluctuations, as indeed is the case across southern Africa during more recent times. Indeed there is a lot to be learned from this Karoo work to ponder the future evolution of its vegetation.

In Chap. 17, Maarten de Wit (and collaborators) picks up the challenge to explore paleo-connectivity and feed-back between ecosystems and climate variability, by providing a chemical-stratigraphic baseline based on carbon isotopes from selective organic materials collected throughout the upper Cape-Karoo formations. Such stable isotope systematics is being used increasingly for high resolution chemo-stratigraphy to reconstruct temperature and/or microbial bio-genic shifts (e.g. Rothman et al. 2014). They present the first Karoo terrestrial organic carbon isotope curve calibrated against U/Pb zircon dates. This preliminary curve can be used for correlation between separate terrestrial Gondwana basins and with marine sequences elsewhere. The data identify a number of distinct shifts in the carbon isotope stratigraphy of the Karoo Supergroup that record punctuated and gradational changes over a span of about 200 million years, from ultra-cold conditions under polar ice caps to desert conditions. The carbon isotope signatures are consistent with a gradual climate change and/or bacterial activity before the Permian-Triassic boundary; and also confirms that the Karoo Basin includes the bio-engineered invention of a new photosynthetic pathway (CAM) during protracted periods of fluctuating droughts across the Triassic-Jurassic transition that herald the onset of a vast sub-Sahara desert that lasted until the initial opening of the South Atlantic.

VI. Geodynamics

Understanding these larger regional affects requires better linking of the Cape-Karoo evolution with other iconic stratigraphic sequences of West Gondwana. In the last chapter of this book, Bastien Linol et al. link the Cape-Karoo of southern Africa with its time-equivalent sequences in the less well-known Congo Basin of central Africa, and the Paraná and Parnaíba Basins of south-east and north-central South America, respectively. They summarize the main stratigraphic data of these four very large basins of Central West Gondwana to discuss possible correlations and paleogeographic reconstructions during

Fig. 1.3 Location map (Google Earth view) of the studied areas in the chapters of this book

and following the period of amalgamation of Gondwana and Pangea (ca. 600–300 Ma), and during the subsequent period of break-up of these two supercontinents (ca. 200–130 Ma). The aim is to provide a geologic framework against which global dynamic models and climatic variability can be tested and verified during supercontinental times.

Next, we now first provide a geologic and geophysical summary of the Cape-Karoo region to contextualize above mentioned chapters (Figs. 1.1 and 1.3) and, in addition, to consolidate some of the areas of research not covered directly in this book.

2 General Geology and Geophysics

Below we present a simplified geological map of South Africa together with an N-S cross section and selected Cape-Karoo geophysical profiles.

The cross-sections highlight the relatively shallow extend of the Karoo Basin and its link to the southern, E-W branch of the Cape Fold Belt (CFB), where maximum tectonic depths of the

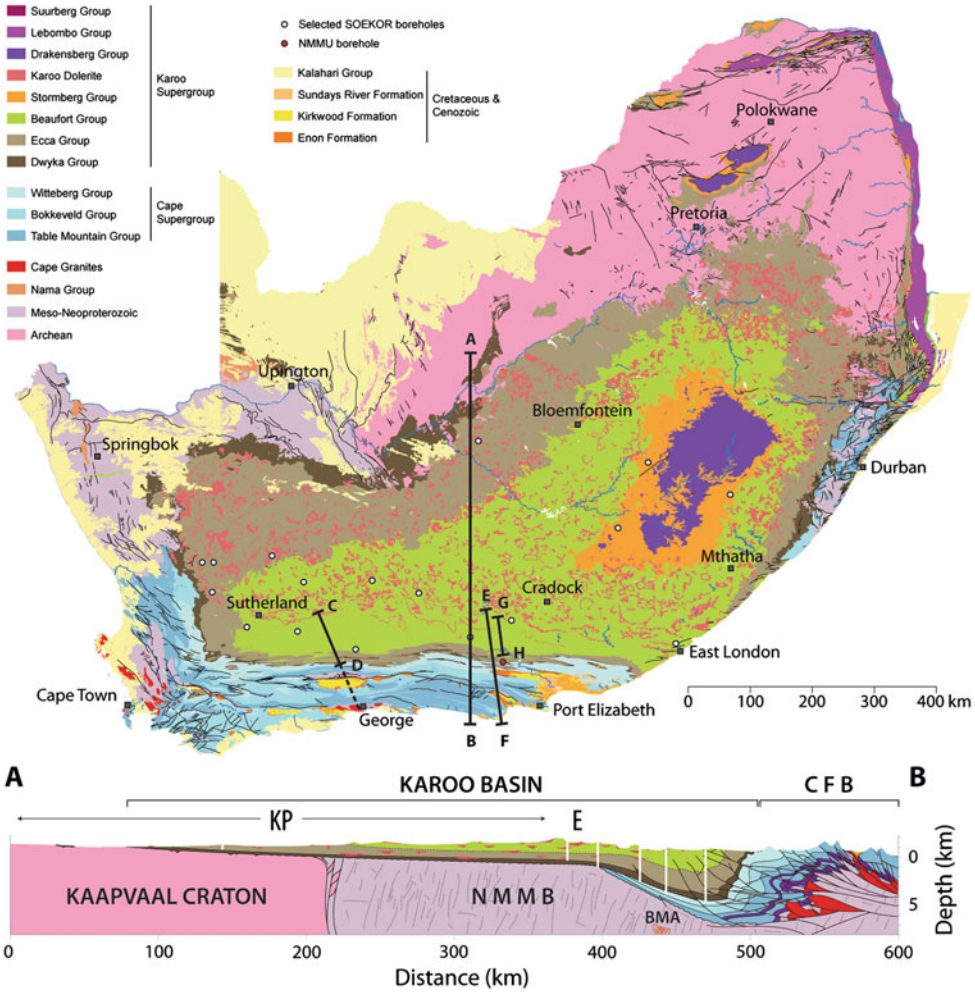

Fig. 2.1a Geology of South Africa (GIS, Council for Geoscience) and N-S cross-section, 700 km long across the Cape Fold Belt (CFB) and southern Karoo Basin, based on deep boreholes (*white vertical lines*) and seismic profiles (*black lines*; see also Chaps. 1 and 2). Note that the topographic heights of the Cape Mountains and the Karoo escarpment reach close to 2 km (the vertical exaggeration of the section is about 10:1). *NMMB* Namaqua Natal Mobile Belt; *BMA* Beattie Magnetic Anomaly; *E* Escarpment; *KP* Kalahari Plateau

Cape and Karoo Supergroups reach down to about 7 and 5 km, respectively. Thrust duplexes, normal and reversed thrust faults related to the Cape Orogeny extend at least 100–170 km to the north of major south-dipping décollements exposed along the south coast, just west of Port Elizabeth (Shone and Booth 2005; Booth and Goedhart 2014; Miller et al. 2016 and Chap. 4). Blind thrust faults propagate well into the Karoo Basin, where they likely influenced sedimentary processes at surface right up to the time of the Permian-Triassic (P-T) boundary, and possibly beyond, as witnessed, for example, by widespread preservation of well-rounded boulders of Cape Supergroup quartzites in the Triassic Molteno Formation, especially across erosional surfaces exposing Molteno coal fields (Sect. 6).

Regional correlations between these Karoo sequences remain uncertain due to complexity of the basin geometry and limited 3-D information (there is only one modern seismic reflection line across the southern Cape-Karoo Basin—Fig. 2.1b). Re-analyses of cores from 11 deep (0.8–5.5 km) boreholes (Chap. 1); and from old seismic data derived in the 1960s–1970s

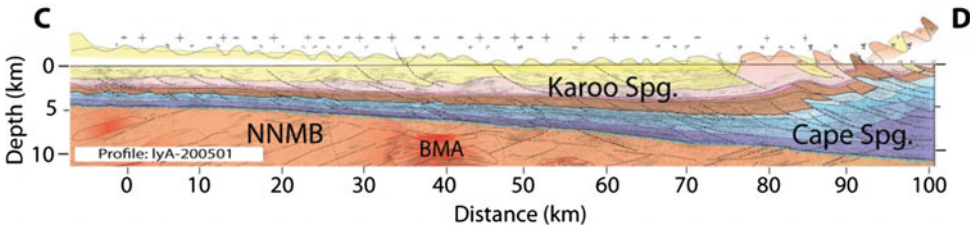

Fig. 2.1b High-resolution seismic reflection profile, about 100 km long across the south-western Karoo (Figs. 2.1a, c for location). Thrust faults duplicate the Cape and Karoo Supergroups (Spg.) to more than 12 km thickness in the southernmost section and propagate northward as blind thrust faults into the Karoo Basin. *NNMB* Namaqua Natal Mobile Belt; *BMA* Beattie Magnetic Anomaly (modified from Lindeque et al. 2007, 2011)

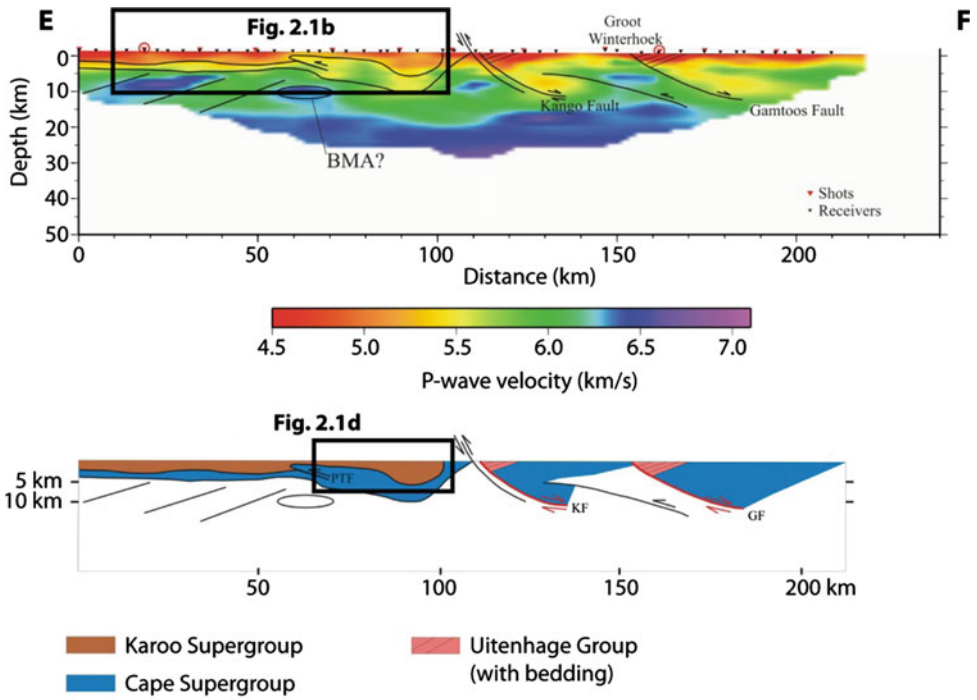

Fig. 2.1c Seismic refraction profile, 220 km long across the eastern Cape-Karoo (Fig. 2.1a for location), together with geologic interpretations (*bottom section*; modified from Stankiewicz et al. 2007, 2008; Parsiegla et al. 2009). *Black rectangles* show the projected position of sections CD and GH

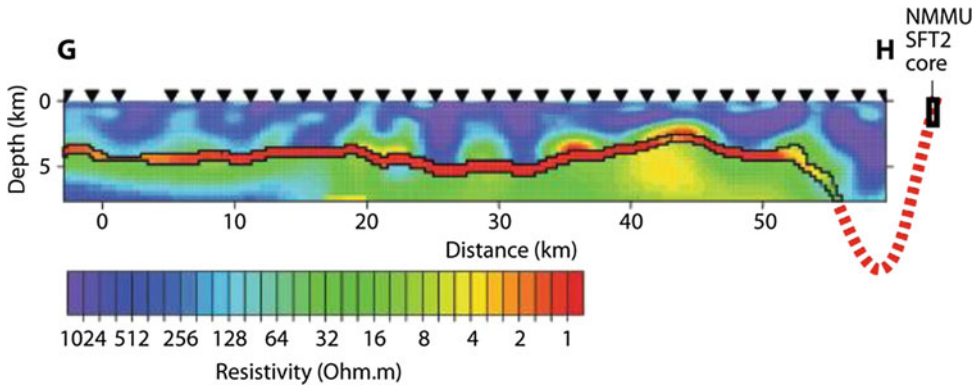

Fig. 2.1d Resistivity section across the southern Karoo Basin (Figs. 2.1a, c for location) highlighting the depth of the black shales of the Ecca Group (*red layer*; modified from Branch et al. 2007 and Weckmann et al. 2007a, b, 2012). SFT2 represents the NMMU borehole core that reached the conductive layer (Whitehill Formation) 200 m below surface, as predicted using structural analyses (*red broken red line*) and is described in detail in Geel et al. (2013, 2015) and Black et al. (2016)

(Chap. 2), sheds new light on the complex thickness variations of both sedimentary and igneous rocks across the Cape-Karoo, as well as depth to basement.

Other geophysical work using magneto-telluric signatures have clearly demarked the location of the shale-gas horizons in the Karoo Basin flanking the CFB (Fig. 2.1d; Branch et al. 2007; Weckmann et al. 2007a, b, 2012). Whilst the resolution of this electrical method is not yet at levels where robust stratigraphic inferences can be made, the highly conductive black shales with high organic materials content and graphite are distinctly marked (*red layer* in Fig. 2.1d). Slightly more resistant 'hotspots' (*yellows* in Fig. 2.1d) closely above and below the distinctly conductive layer may represent deep saline groundwater reservoirs. Clearly more

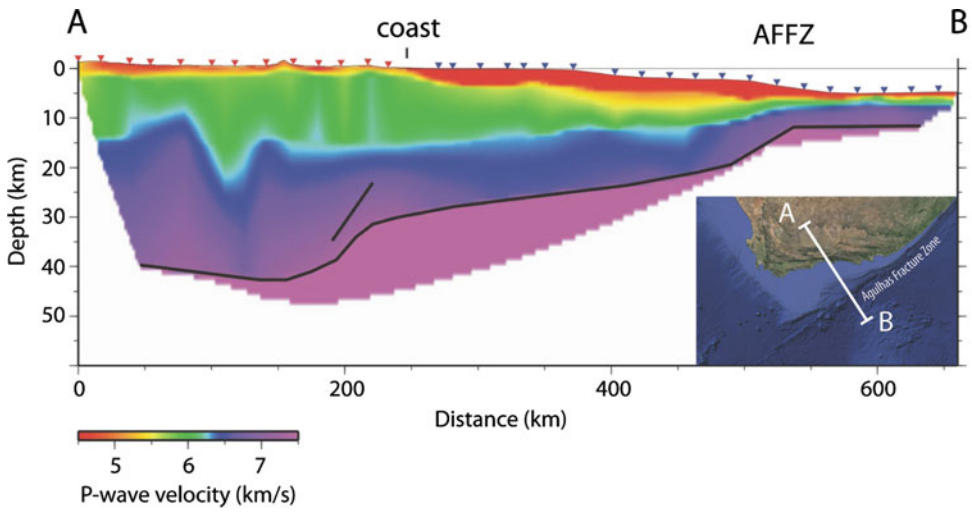

Fig. 2.2 Onshore/offshore seismic refraction line (*red triangles* onshore shots; *black triangles* offshore shots), some 600 km long from the southern Karoo across the Agulhas Fracture Zone towards the Agulhas Plateau (*inset* for location), highlighting the absence of a tectonic root below the Cape Mountains such as is generally recorded beneath orogenic collision zones (modified from Stankiewicz et al. 2007, 2008; Parsiegla et al. 2009). The seismic refraction line clearly outlines the abrupt 10 km crustal thinning (*black line*) from some 40 km below the Cape-Karoo sequence to 30 km at the coastal margin and from there more gently by another 10 km up until the Agulhas-Falklands Fracture Zone (AFFZ) across which the 20 km continental crust abuts oceanic crust of about 10 km. Unfortunately detailed seismic reflection lines across the Cape Mountains are still wanted, particularly to trace the surface faults and folds to greater depth with the aim to test just how much tectonic repetition of the sequences can be identified

detailed geophysics is required to unravel these observations ahead of potential shale gas developments.

In reality, the tectonic and related geodynamics of the Gondwanides remain poorly understood, and there are very strong conflicting tectonic models for the origin of the CFB and its linked Karoo Basin (Chaps. 4 and 5 and Sect. 6). Resolving this will require more concerted efforts of dating of metamorphic minerals and mineralisation in fluid-induced veins, as well as greater association between structural mapping, sedimentology, and volcanism within southern Africa as well as across the greater Gondwanides. There is only one detailed geophysical section (magnetic-telluric) across the CFB (Weckmann et al. 2012). This is a major shortcoming in knowledge of the CFB. However the regional seismic refraction profile (Fig. 2.2) suggests an absence of a tectonic root beneath the Cape Mountains. The section also highlights the crustal thinning across the southern continental shelf, where the major extensional depocentres are filled with Jurassic-Cretaceous sequences that record the complex history of Gondwana fragmentation and Africa mobility since its separation from the adjacent continents and microcontinent fragments of West Antarctica and Patagonia (Sects. 6 and 7). The greatest volumes of sediment fill off-shore was derived predominantly during the time of uplift of southern Africa during the Kalahari Epeirogeny (120–80 Ma; de Wit 2007; Tinker et al. 2008a, b). Linking these onshore-offshore processes remains a major challenge, which this book does not explore in detail (but see Sect. 7).

New seismic techniques, using ambient noise (Chap. 3), are now being employed with encouraging success towards 3-D mapping the Cape-Karoo contacts at significant depths, and future work will likely continue to map the Karoo Basin and individual stratigraphic layers in considerable detail, especially where combined with electromagnetic methods that are presently ongoing.

3 Paleo-environments and Changing Climates During Gondwana Times

The Cape-Karoo sequences record co-evolving paleo-environments and climate changes following the amalgamation of Gondwana supercontinent (750–550 Ma) until its break-up into Africa, South America, India and Antarctica (200–130 Ma). Below we present schematic paleo-geographic reconstructions based on stratigraphic and sedimentological data (see also Chap. 18).

The Gondwana history is recorded within vast marginal silicilastic platforms that encircle the supercontinent during the Early Paleozoic (Fig. 3.1a), through major glaciation during the Late Paleozoic (Fig. 3.1b) and within intracontinental basins during the formation of the Variscan and Cape Fold Belts at around 270–250 Ma (Fig. 3.1c), to progressively terrestrial, hot and arid deposition during the Early Mesozoic, terminating with the eruption of Large Igneous Provinces (LIPs) during successive break-up episodes of Gondwana (Fig. 3.1d). This broad evolution of southern Gondwana is relatively well-known (e.g. du Toit 1937; Cole 1992; Catuneanu et al. 2005; Milani et de Wit 2008; Linol et al. 2015), however more detailed regional sedimentary basin analyses of the Cape-Karoo Basin and its equivalents on the other Gondwana continents are needed before robust correlations and global climate and tectonic models can be established.

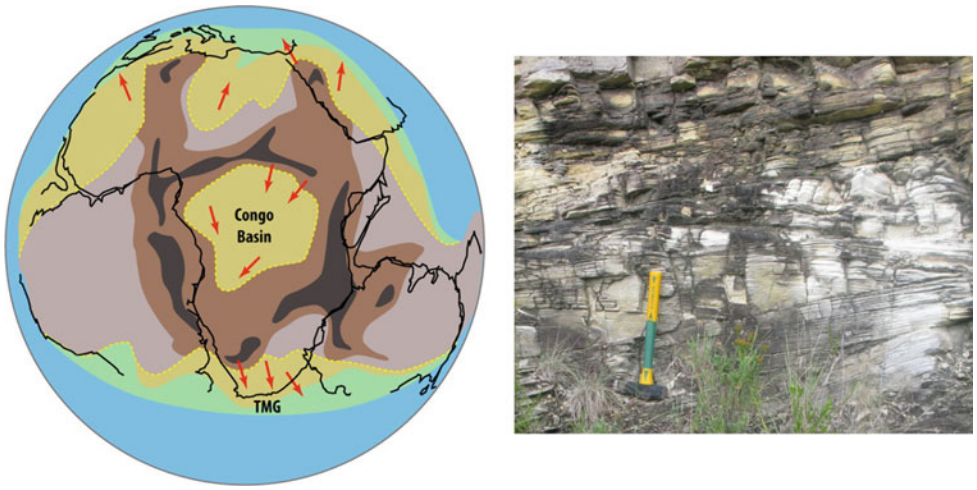

Fig. 3.1a Early Cambrian (~540 Ma) reconstruction of Gondwana, showing extensive Himalaya-Tibetan like mountain systems (*pale and dark brown*) across Central Gondwana, with sediment dispersal directions (*red arrows*), and (*right*) overturned (upside-down) cross-bedded quartzites of the Peninsula Formation from the Eastern Cape. Continental sediments (*yellow*) were regionally deposited southward across southern and central Africa, and northward across northern Africa and south-western Europe, derived predominantly from upper Mesoproterozoic-lower Neoproterozoic sources (0.9–1.1 Ga), as revealed by detrital zircons dating (Avigad et al. 2003; Andersen et al. 2016; Linol et al. 2016; Miller et al. 2016). Contribution of zircons by recycling of older sedimentary sequences and within the Cape-Karoo Province need to be better understood through complementary Lu-Hf isotope analyses to fingerprint the complexity of the original sources and potentially eroded thick cover sequences. *TMG* Table Mountain Group

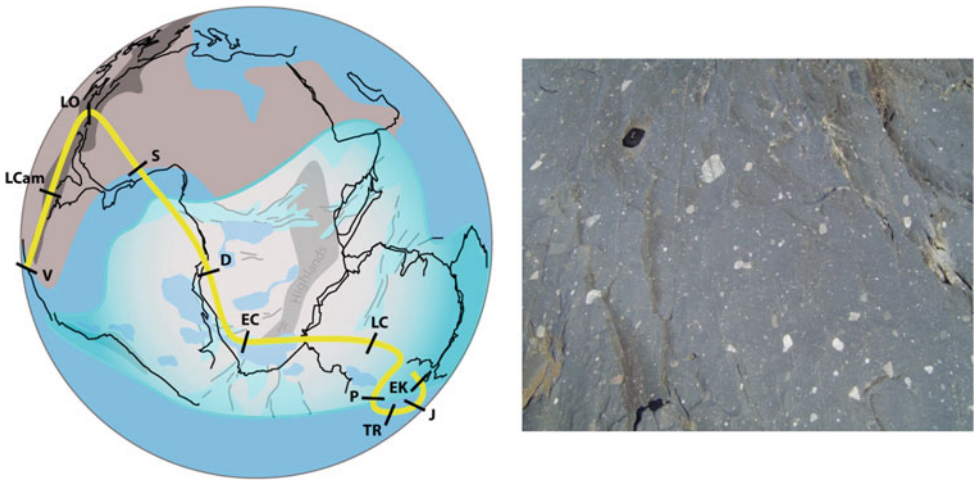

Fig. 3.1b Mid-Carboniferous (~320 Ma) ice-age, when the South Pole traversed across southern Africa (*yellow line* Phanerozoic Polar path: *LCam* Late Cambrian; *LO* Late Ordovician; *S* Silurian; *D* Devonian; *EC* Early Carboniferous; *LC* Late Carboniferous; *P* Permian; *TR* Triassic; *J* Jurassic; *EK* Early Cretaceous), and (*right*) Dwyka tillite from the Karoo Basin—a Gondwana-type glacial deposit. During Late Devonian to Mid-Carboniferous, a major Antarctica-like ice-cap across southern Gondwana carved wide subglacial valleys and lakes systems beneath and marginally to this Gondwana ice-sheet. By about 300 Ma (LC-P), as the South Pole moved across toward Antarctica there was rapid deglaciation across southern Africa, as witnessed by terrestrial eskers along the northern margin of the Karoo Basin and black shale accumulations across the southern basin (see Chaps. 9, 10 and 11). It is not at present possible to accurately construct the expansion and contraction of the regional ice-caps and glaciers across southern Gondwana and sub-Saharan Africa, for lack of accurately dated (and thus correlatable) regional litho-, bio- and magneto-stratigraphy. Indeed, reliable paleomagnetic data is scarce, so that there is still considerable uncertainty about the precise Polar wander path (*yellow line*). The reader is referred to Isbell et al. (2008), López-Gamundí and Buatois (2010) and Milleson et al. (2016) for an early attempt to overcome some of these uncertainties, but clearly a better geologic understanding of this circa 50 million years long cold period, and ecosystem adaptations during and after this time, deserve much greater attention

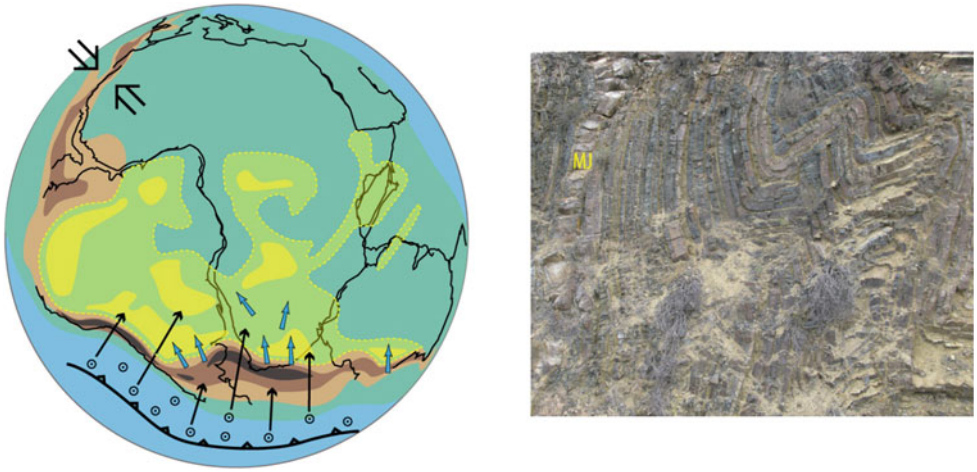

Fig. 3.1c Permian-Triassic reconstruction (~250 Ma) during and following the amalgamation of Gondwana into Pangea, and (*right*) deformed, characteristic turbidites with abundant interbedded volcanic tuffs (*yellow layers*) of the Collingham Formation (*MJ* Matjiesfontein Chert). Collision between north-western Africa, eastern United States and western Europe (*doubled black arrows*) formed a large orogen comprising the Appalachian-Mauritanian-Variscan Belts (330–270 Ma), whilst orogenesis along southern Africa and southern South America resulted in the formation of the Cape-Sierra de la Ventana Fold Belts (270–250 Ma). This period of convergent tectonic regimes resulted in large-scale intracontinental deformation and lithosphere buckling providing space for widespread deposition of thick continental sequences (*yellows*) from paleocurrents (*blue arrows*) regionally directed to the north in the southern basins, and which was associated with ash-fall tuffs (*black arrows*) from intense volcanism (Θ) along the southern magmatic-arc margin of Gondwana (e.g. Linol et al. 2015)

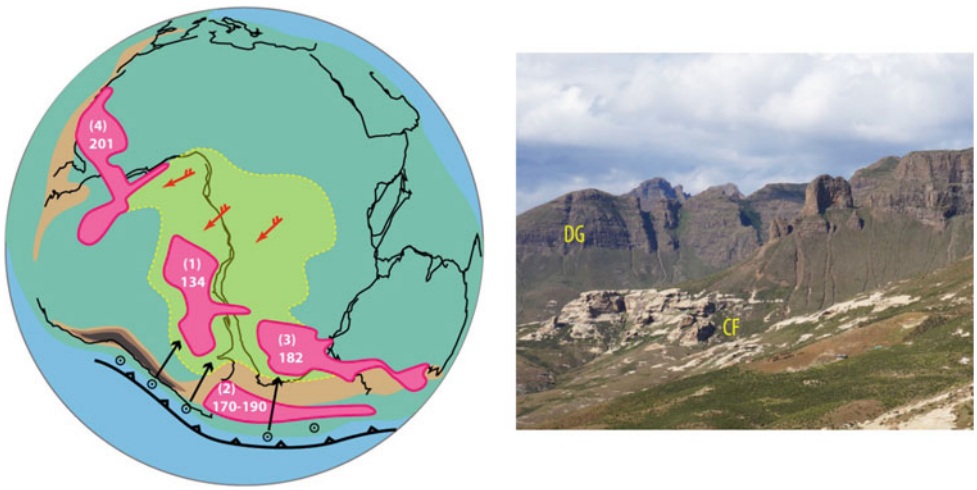

Fig. 3.1d Late Triassic-Early Cretaceous (~200–130 Ma) reconstruction showing the vast extent of aeolian sequences that attest of a Sahara-like desert across Central West Gondwana (*yellow*), and (*right*) the upper Karoo aeolian Clarens Formation (*CF*) covered by thick lavas of the Drakensberg Group (*DG*). Surface winds (*red arrows*) were blowing predominantly to the southwest across central Africa and eastern Brazil. This arid sedimentation was repeatedly interrupted by eruptions of Large Igneous Provinces (*pink*): (*1*) Etendeka, (*2*) Tobifera, (*3*) Karoo, (*4*) CAMP (with *white number* = age of their respective rapid continental volcanism), related to successive phases of supercontinental break-up (LIPs not shown are Deccan = 66 Ma and Kerguelan = 120 Ma)

4 Igneous Processes and Mantle Dynamics

Topping the Karoo Basin are the Drakensberg Group lavas, erosional remnants of a series of basaltic to basaltic-andesite flows (ca. 140,000 km^2) that once covered an estimated region in excess of 2 million km^2 (but in reality of unknown extend), and which reach a thickness of 1.7 km in central Lesotho, but which is also a minimum because subsequent erosion, likely in the order of 1–5 km affected the entire Cape-Karoo region (Sect. 7). The volcanics are underlain by feeder dykes and sills that extend below surface to depths exceeding 4 km, measured in drill cores and seismic sections (Chaps. 1 and 2). These Karoo igneous rocks have similar chemical compositions, and are part of a larger world-class continental flood basalt province that stretches across southern Africa (Erlank 1984; Eales et al. 1984; Cox 1988; Duncan and Marsh 2006), Antarctica and Tasmania/Australia as part of the Karoo-Ferrar Large Igneous Province (LIP; see Fig. 3.1d).

A clearly defined transition tracing the connectivity between the lavas and their underlying intrusive 'feeders' is still wanted. These transitionary sequences require detailed building on the classic mapping of the Karoo sills and dykes by Du Toit (between 1902 and 1915) and his colleagues of the Geological Survey (Department of Mines and Industries—Geological Survey of the Union of South Africa) in the early parts of the last century (du Toit 1954). This, and the thermo-mechanical analyses of the emplacement mechanisms of the sills that has only recently attracted modern techniques (Chevallier and Woodward 1999; Svenson et al. 2007; Polteau et al. 2008; Chere 2010; Schofield et al. 2010; Aarnes et al. 2011; Walker 2016; see also

Fig. 4.1 Drakensberg Group (*DG*) lavas and related intrusions in Lesotho and the Eastern Cape. **a** Spectacular vesicular lavas appear sub-conformable above the underlying sand- and mud-stones of the Clarens Formation (*white*) in turn underlain by the Elliot Formation (*EF*) near Sterkspruit. North of Barkly East (S30° 53′29.7″; E27°33′59.0″) there is good field evidence of erosion and interaction between the lavas and significant surface-water (lakes?) and ground-water bodies, by extensive pillow lavas **b**, **c** that are directly covered (*yellow arrow*) by sandy layers with accretionary lapilli and hyalo-clastic deposits. However, there is no clearly defined regional boundary or an inferred paleo-topographic relief that has been mapped-out since the classic work of Lock et al. (1974). The chemical- and magneto-stratigraphy of the volcanics (Duncan and Marsh 2006), whilst impressive, is incomplete and requires renewed chemical data in conjunction with detailed field analyses

Fig. 4.2 The upper Karoo sequences (*BG* Beaufort Group) provide ample exposures of **a** progressive stepped sills associated with fractures and local trusts that can be observed to have transgressively induced **b** visicular fluid escape textures (likely including oil/gas flow) well-preserved beneath, but not above the sill; and **c** hydrothermal vent (*HV*), e.g. near Telle Bridge (Lundean Nek Pass) cutting through the Elliot Formation (*EF*). Detailed analyses of such structures will be of great interest to testing for hydrocarbon potential throughout the Karoo Basin (e.g. Svenson et al. 2006)

Chaps. 7 and 8), are needed before a better understanding of the crustal plumbing system and links to the mantle can fully determine the origin and evolution of Karoo magmatism.

Because Karoo magmatism was active long before the main uplift of southern Africa during the Kalahari Epeirogeny (ca. 120–80 Ma), it is also of great interest to determine at what height above sea-level the Karoo lavas were extruded, perhaps through careful analyses of amygdales and sedimentary layers (e.g. Fig. 4.1c) with possible micro-organisms and plant-leave fragments.

Almost 40 years ago, Keith Cox suggested a geodynamic mantle link between long term subduction along the paleo-Pacific and the origin of the 182 Ma Karoo flood basalts (Cox 1978). Since Cox's insightful work, the general focus has shifted towards unravelling a direct link between the Karoo-Ferrar LIP (whose age equivalents have recently been unequivocally been established at 182 Ma; Burgess et al. 2015) and a deep mantle upwelling (or plume as preferred by some workers) as part of the southern African mantle superswell (Burke and Torsvik 2004; Torsvik et al. 2010). However, Cox's model has not gone away (e.g. Nicolaysen 1985): a regional overlap in age with the bimodal Tobifera-Chon Aike Province of southern South America (190–170 Ma, Fig. 3.1d; Stern and de Wit 2004), as well as mantle tomography that has traced oceanic slabs beneath South America down to the lower mantle (e.g. French and Romanowicz 2015), point to long term (~300 milion years) subduction processes linked to lower mantle dynamics and mantle upwelling below Gondwana and during its subsequent fragmentation history (see Fig. 6.5 in Sect. 6). The details of these interconnected geodynamic systems remain to be tested and resolved (e.g. Steinberger and Torsvik 2012); and how these igneous processes relate to the formation and leakage of hydrocarbons in the Karoo Basin; and to greenhouse gas emissions during its most prominent punctuated event (within less than 700 kyrs at around 182 Ma) that many believe to be linked to the Early Jurassic mass extinction (Sell et al. 2014; Guex et al. 2016).

The outcomes of this 'mantle-atmosphere debate' may yet come from better quantifying surface processes across the Cape-Karoo, especially the erosion and sculpturing of its landscapes that for long have also been acknowledged as an iconic laboratory for geomorphology, championed most famously by Lester King (1942), and which continue to mesmerize and challenge researchers across the world (e.g. Braun et al. 2014 and references therein), as summarized in Sect. 7.

5 Cape-Karoo Life: Evolution from Fish to Dinosaurs

The Cape-Karoo is not only rich in proven and potential natural resources, but is also internationally acclaimed for its wealth of fossilized remains of ancient life. Below, we present some selected fossil specimens from the upper Cape Supergroup to the uppermost parts of the Karoo Supergroup to highlight the abundance and value of this paleontological laboratory.

Devonian

The recent discovery of a 360 million year old lagoon system in the Witteberg Group (upper Cape Supergroup) in the Eastern Cape region has yielded hundreds of fossilized plants, fish and arthropods (e.g. Fig. 5.1). This menagerie of fossils sheds new light on the Devonian biodiversity of southern Gondwana, and includes some of the oldest and rarest known coelacanths in the world (a fitting tribute to Grahamstown's former JLB Smith Institute; Fig. 5.2).

Permian

The Permian Karoo rocks hosts the longest-ranging and richest diversity of therapsid mammal-like reptile fossils in the world (e.g. Fig. 5.3). Their fossil record chronicles the distant ancestry of mammals in remarkable detail, and they have been used in an internationally applicable biozonation scheme for the Beaufort Group (Rubidge 2005; Chap. 14 and references therein). Large collections of therapsids, collected by generations of paleontologists, are curated by the Albany Museum, Council for Geoscience, Ditsong Museum, Iziko Museum, National Museum, University of the Witwatersrand, and the Rubidge Museum in Wellwood Farm near Graaff-Reinet. Current research has highlighted the importance of these Karoo vertebrates in stratigraphy and basin development studies as well as understanding the cause and effects of the end-Capitanian (260 Ma) and end-Permian (252 Ma) global mass extinctions in the terrestrial realm of the Karoo, as popularized in Rubidge and McCarthy (2005, see also Chap. 15).

Field studies in the lower Beaufort Group strata around Fraserburg (Northern Cape) highlighted the increased abundance of dicynodont burrows in the aftermath of the

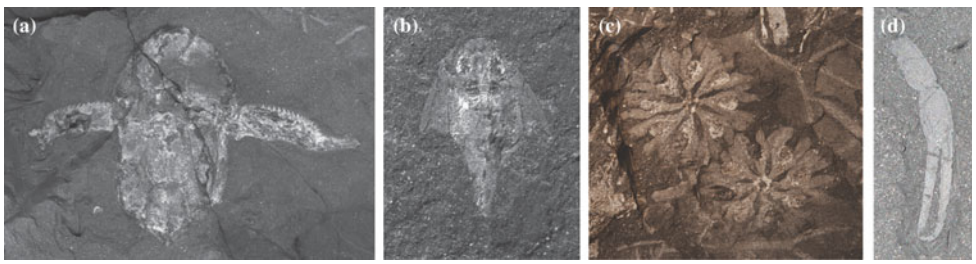

Fig. 5.1 Paleontologist Dr. Rob Gess of the Albany Natural History Museum has found hundreds of fossilized plants, fish, and arthropods from 70-odd tons of fossil-rich shale exposed during recent road works near Grahamstown. His findings have provided new insights into the ecosystems of a southern hemisphere Devonian estuary. Shown above are a selection of Gess' fossils from the Upper Devonian (Famennian) Witpoort Formation, lagerstätten: **a** *Bothriolepis africana*, subadult antiarch placoderm head and trunk armour in dorsal view, 4 cm long; **b** 2.5 cm long hatchling of the arthrodire placoderm, *Groenlandaspis* showing head and trunk armour as well as an impression of the soft tissue tail; **c** 2.4 cm wide oogonia-bearing whorls of the aquatic charophyte alga, *Octochara crassa*; **d** 2.5 cm long pincer of the scorpion *Gondwanascorpio emzantsiensis*, Gondwanas oldest known terrestrial animal (*Photos* by Rob Gess; see also Chap. 13)

Fig. 5.2 Coelacanth juvenile (*top*) *Serenichthys kowiensis* holotype and (*bottom*) reconstruction of Serenichtys juvenile emerging from a bed of charophytes in brackish waters. This is the oldest coelacanth from Africa; and Waterloo Farm (near Grahamstown) is the oldest known coelacanth nursery in the world. The species from that collection most closely resemble the line leading to modern coelacanths ('a living fossil') that thrive in the Indian Ocean off the East coast of Africa and south of Indonesia (*Photos* supplied by Rob Gess)

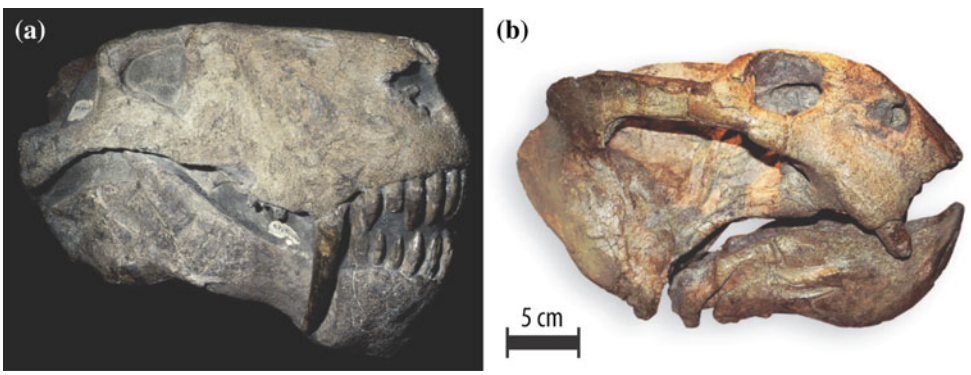

Fig. 5.3 Therapsid skulls representative of two families that went extinct in the Permian: **a** flesh eating gorgonopsian, and **b** the herbivore dicynont *Daptocephalus* (*Photos* supplied by Bruce Rubidge)

Fig. 5.4 2.5 m long fossilized cast of an ancient burrow in the lower Beaufort Group that contains a complete adult skeleton of the small herbivorous therapsid *Diictodon feliceps*. The skull is visible protruding from the infilling of the terminal chamber. Scratch marks left on the roof and walls of the tunnel match the dimensions of the spatulate claws of this tortoise-beaked like, dassie-sized dicynodont. This specimen has been partially prepared to reveal the skeleton and resides in the collections of Iziko South African Museum, Cape Town (*Photo* supplied by Roger Smith)

end-Guadalupian mass extinction (Fig. 5.4; Smith 1987; Smith and Evans 1996; Sullivan et al. 2003). It is proposed that these mega-burrows were opportunistically excavated as a buffer to the rapid climate change that accompanied this extinction event some 260 million years ago. The host rocks were deposited on expansive floodplains flanking large Mississippi-sized meandering river, and the burrows were excavated into the proximal floodplain soils on a constant 35° decline terminating around 1 m below surface in the calcareous B-horizon. Some of these tunnels are helical with two dextral whorls leading into a straight terminal chamber.

Triassic

The Upper Triassic Molteno of the Karoo Basin, dating at around 230 Ma, ranks as one of the richest plant/insect bearing formations anywhere globally. It is certainly the richest and most thoroughly sampled in the Triassic and portrays the heyday of the gymnosperms at the height of the Triassic explosion of renewed diversity after the end-Permian extinction (Fig. 5.5). Statistical projections, from observed to preserved to existed diversity suggest that the Molteno might well represent the peak of plant diversity through geological time. It was along

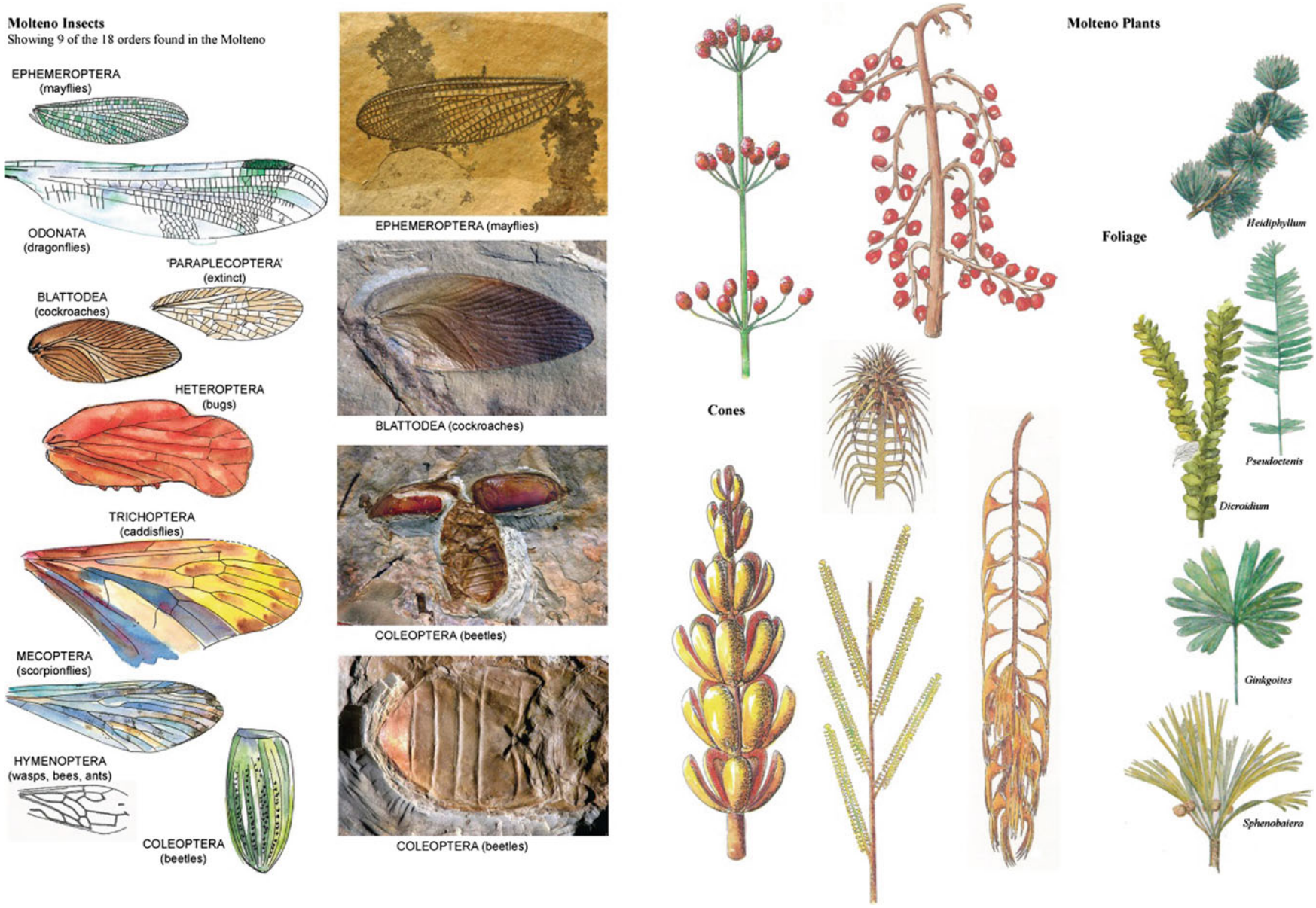

Fig. 5.5 Triassic fossils of co-evolving insects and plants found in the Molteno Formation, suggesting the very first bio-pollination of plants by insects. The gut contents, wing structures, and mouthpart morphologies of fossilized beetles and flies suggest that they acted as pollinators (*photos* and drawings by John Anderson)

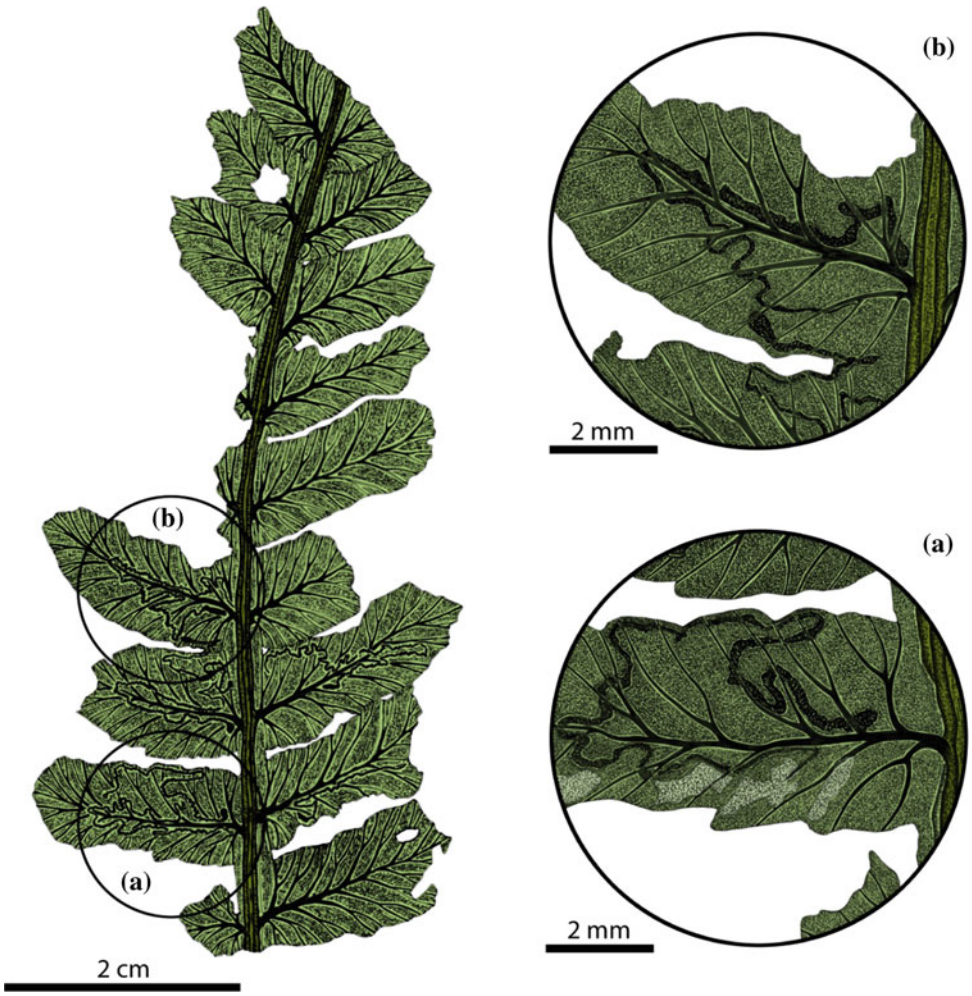

Fig. 5.6 Example of leaf mining preserved in the Molteno fossils. The fern leaf (DT41) is from the Dordrecht 111 site and is on *Cladophlebis janetae* (Osmundales). This damage type is probably attributable to a basal, leaf-mining lepidopteran clade (*photos* and drawings supplied by Conrad Labandeira)

with this rebound of plant diversity that the dinosaurs first appeared and that the mammals evolved from the mammal-like reptiles. And in parallel with this, there occur, amongst the 86 described Molteno Gymnosperm cones, some that begin to show angiosperm (flowering plant) like features. These might be referred to as angiosperm-like gymnosperms.

With over 2,000 insect specimens from 43 of the 100 sampled plant assemblages, close on 350 species (in 18 orders) have been recognized. Around half the total species are beetles: by far the most diverse of the insect orders. This, for the first time, pre-empts the extant world where the beetles are clearly the most diverse group of insects, in fact of any group of multicellular organisms. Just as bees and butterflies co-evolved to diversity as pollinators with the flowering plants in the Cretaceous, so the beetles radiated to great diversity along with the cone-bearing plants in the Triassic.

The full range of ways that insect herbivores are seen to impact on plants today, are commonly found amongst the different groups of Molteno plants. These modes of interaction (as researched by Dr. Conrad Labandeira of the Smithsonian Institute, Washington) spread widely through from external foliage feeding, piercing and sucking, oviposition, mining, galling and seed predation to wood boring (Fig. 5.6).

Distinguishing both the wood and the trees at that time and their circa 150 million years of evolution throughout the Karoo times (from the Carboniferous to the Jurassic), are discussed by Marion Bamford in detail in Chap. 16.

Fig. 5.7 Skeleton of the sauropodomorph dinosaur *Massospondylus* from the Elliot Formation (*Photo* supplied by Bruce Rubidge)

Fig. 5.8 Theropod dinosaur footprints from the Lower Jurassic Elliot Formation. Scale bar = 15 cm (*Photos* supplied by Emese Bordy)

Jurassic

Jurassic fossils from the Karoo tell us about the early diversification of dinosaurs and crocodilians (e.g. McPhee et al. 2016). The Elliot Formation, in particular, is known for its basal sauropodomorph dinosaurs (Fig. 5.7),—animals that paved the way for the evolution of 60-ton behemoths.

The abundance of trace fossils (ichnofossils) from the Karoo is also important in providing insights into the interactions among organisms and their sustaining ecosystems (Fig. 5.8). Ichnofossils can provide clues about the organismal behaviour that cannot be derived from fossil bones alone; for example, clusters of dinosaur footprints can assist in deducing the social habits of the animals (solitary vs. gregarious).

6. Structure and Tectonics

The origin and structural history of the Cape Orogeny, during which the Cape Fold Belt (CFB) emerged, has long been under debate. In the 1970s, Brian Lock, a recently graduated Ph.D. student under guidance of John Dewey during the early emergence of models linking plate tectonics and mountain building, proposed a most innovative geodynamic model for the Cape Orogeny, based on the concept of a north-directed flat paleo-subducting plate beneath the CFB. Such a model was conceived because the assumed related subduction plate boundary along the paleo-Pacific margin flanking Gondwana was more than 1,000 km away from the CFB. At that time, it was proposed that a section of this Paleozoic subduction zone remained fossilized in the mid-lower crust beneath the southernmost Karoo Basin, preserved as a large magnetic anomaly, the Beattie Magnetic Anomaly (BMA; Figs. 2.1b, c) that had been identified there (Lock 1980).

By then, the most detailed structural analysis and interpretations of the CFB, conducted under the leadership of Ingo Hälbich as part of the South African National Geodynamic Program (Söhnge and Hälbich 1983; Hälbich 1992; Hälbich et al. 1993; see also Dingle et al. 1983) was in full swing. This work continued to build on Lock's "flat subduction model". Hälbich's investigations for the first time also identified complex, multi-stage deformation events (often referred to as paroxysms), based on many years of field mapping and K/Ar and Ar/Ar dating of selected rocks and minerals. These studies became the benchmark for many subsequent interpretations for the origin of the Karoo Basin and its stratigraphic hinge-lines during their evolution in a foreland basin model. However, the isotopic dates obtained were of

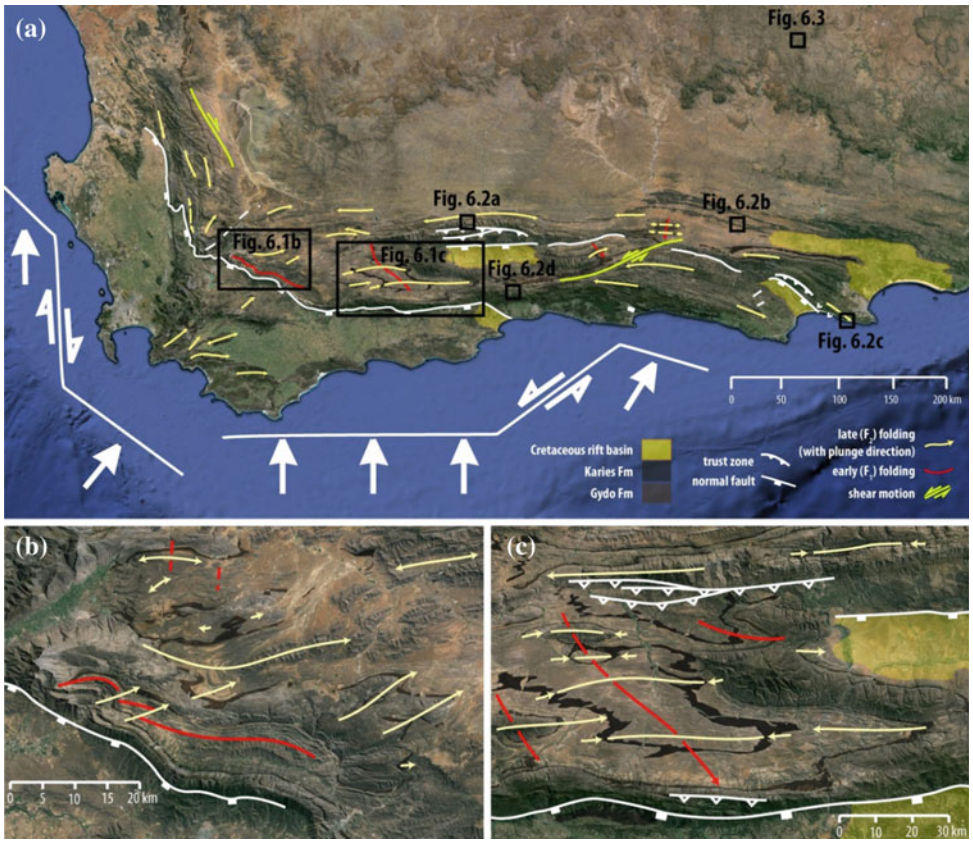

Fig. 6.1 **a** Simplified structural map of the CFB, showing at least two generations of folding (*red and yellow arrows* = fold axes with plunges), linked to inferred shearing and differential collisional block movements (*large white arrows*). **b**, **c** Areas with both early (*red*) and late folding (*yellow*) with related thrust sequences (Fig. 6.2a, b). Large areas with downward facing Table Mountain Group sequences are exposed in Port Elizabeth and surroundings, as well as along the Outeniqua Pass (Figs. 6.2c, d; see also Fig. 3.1a)

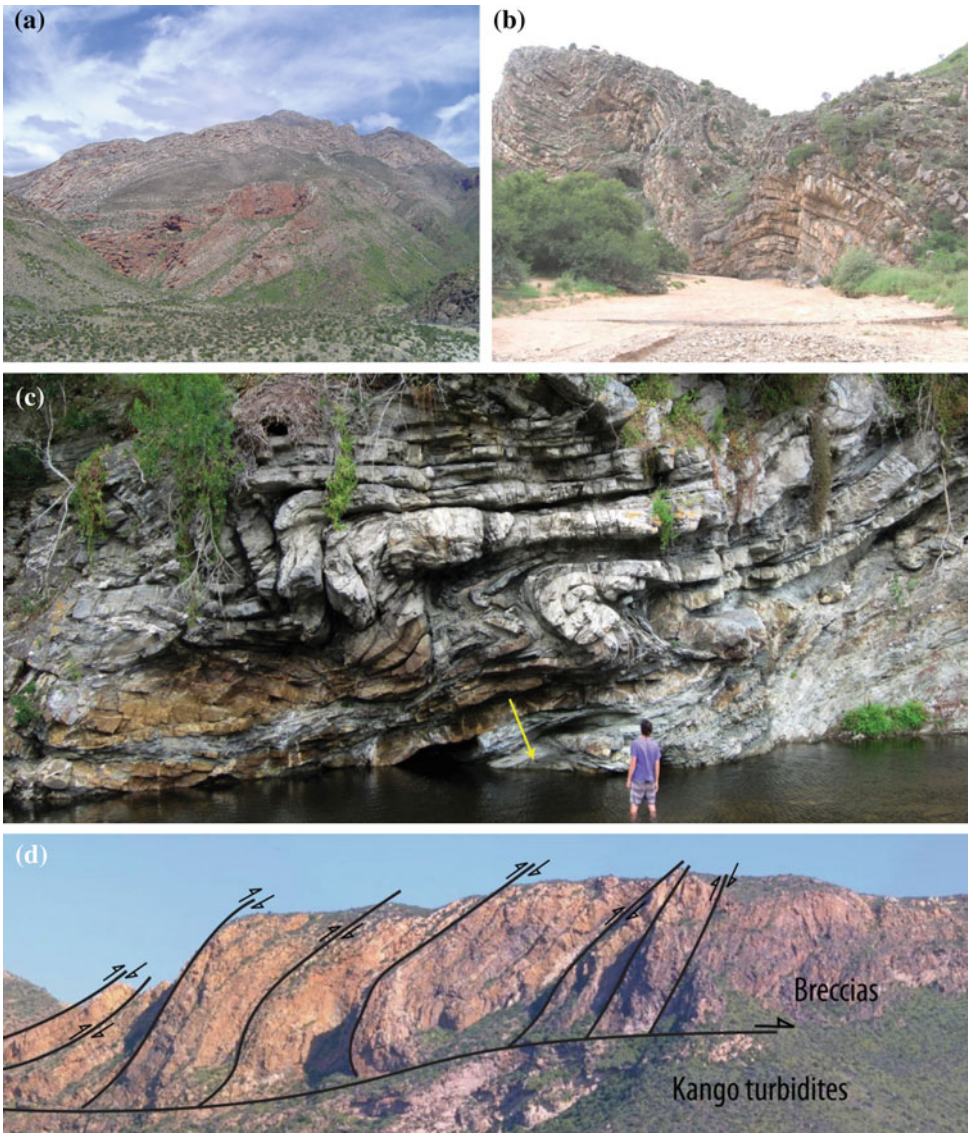

Fig. 6.2 Variable styles of folding and thrusting across the CFB. **a** Large-scale overturned folding of the Table Mountain Quartzites along the Swartberg Ranges (in the Hell); **b** upright folding in the Witteberg Group near Jansenville; **c** subhorizontal folding of shear zones/thrust systems in the Table Mountain Group near Port Elizabeth (*arrow* shows the younging direction); and **d** early large-scale thrust duplexes of Peninsula Formation quartzites over-riding Kango turbidites on the western side of Huisriver (see Fig. 6.1a for locations; *photos* by M. de Wit, W. Miller and S. Moore)

relatively low resolution, with large error bars; and with modern hindsight possibly misleading, especially in light of more advanced geochronology and dating techniques. This is discussed in detail in Chap. 5. Of the three to five paroxysms identified by the early 1980s, today only a robust date of 253 Ma remains; and possibly one around 275 Ma (Hansma et al. 2015). Clearly a lot more work on tectonic minerals is needed to build on this. In addition, the location and shape of the BMA is now more accurately identified with new geophysical data (Lindeque et al. 2011; Weckmann 2007a, b; see also Figs. 2a, b) to be part of the Mesoproterozoic basement beneath the Cape-Karoo sequence, and cannot therefore be related to a Paleozoic flat subduction model.

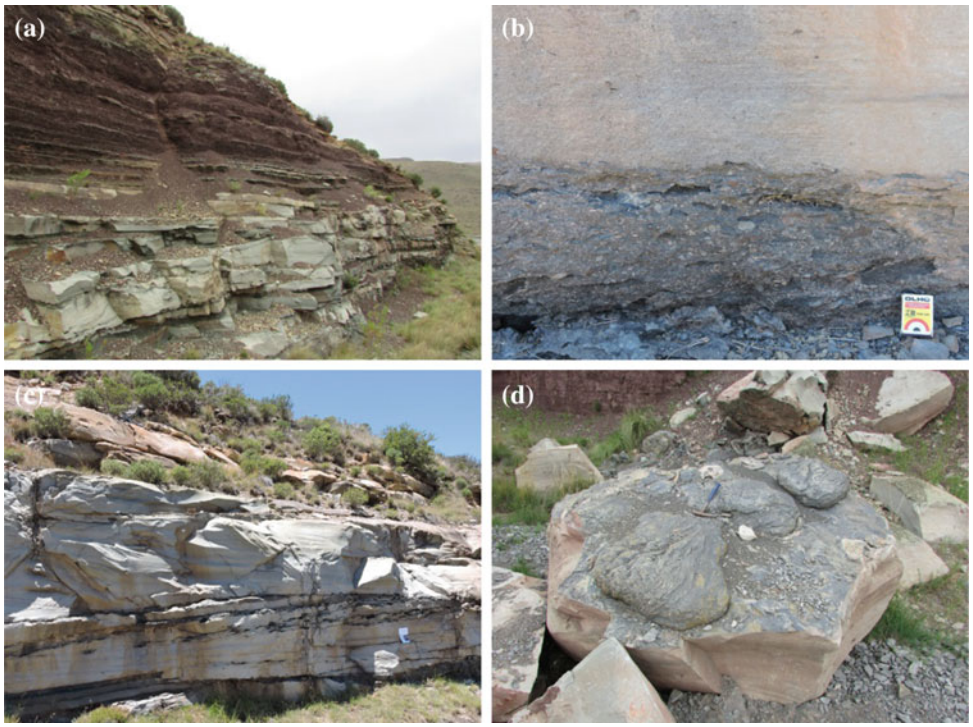

Fig. 6.3 **a** Bedded red purplish mudstone and amalgamated grey-green sandstone channels of the Beaufort Group, exposed along the Lootsberg Pass—a Permian-Triassic type-section of the Karoo Basin, with **b** basal gravel lag composed of bone fragments and small rounded mud and carbonate pebbles (matchbox for scale), **c** low-angle cross stratifications with abundant rip-up clasts (notebook for scale), and **d** giant scour marks at the base of beds (hammer for scale), all of which indicate (rapid) flash flood deposition possibly related to continuous north propagation of Cape folding and thrusting (see Fig. 6.1a for location; *photos* by B. Linol)

More recently, new models have emerged based on either strike-slip deformation parallel to the CFB ridges (e.g. the strike-slip orogeny of Johnson 2000; Tankard et al. 2009), or as a south dipping subduction zone related to a marginal basin located to the south of the present CFB (Lindeque et al. 2011; Miller et al. 2016 and Chap. 4).

The style of deformation along and across the CFB varies considerably and suggests a complex structural history, perhaps driven by accretion of multiple tectonic blocks at different times (Fig. 6.1; e.g. de Wit and Ransome 1992). It has also become apparent that there are at least two major fold-and-thrust events, each at distinctly different angles, based on sustained mapping and detailed outcrop observations. One of the first to identify this on a regional scale was Peter Booth (Booth and Shone 2002; Booth et al. 2004; Booth 2011), as is clearly seen on Fig. 6.1.

Both Ingo Hälbich and Peter Booth also identified large sections in the lower Table Mountain sequence that are downward-facing (upside down), and contain isoclinal folds with near-horizontal axial planes that in turn are re-folded by more upright folds and thrust duplexes (Figs. 6.1 and 6.2). Clearly there is a need for much more detailed structural mapping in the CFB, in conjunction with high-resolution geochronology, before a consistent model for its origin can be constructed. This is important not only to tease-out the geodynamic evolution of the CFB, but also to better interpret stratigraphic observations in the linked Karoo Basin to the north.

Attempts to link CFB deformation events (paroxysms) with changes in the Karoo stratigraphy were first explored by Brian Turner (Turner 1978, 1983, 1990), and more recently by Catuneanu et al. (1998), and are now widely accepted. For example in Chap. 15 of this book, across the Permian-Triassic boundary changes in the biostratigraphic record are linked to

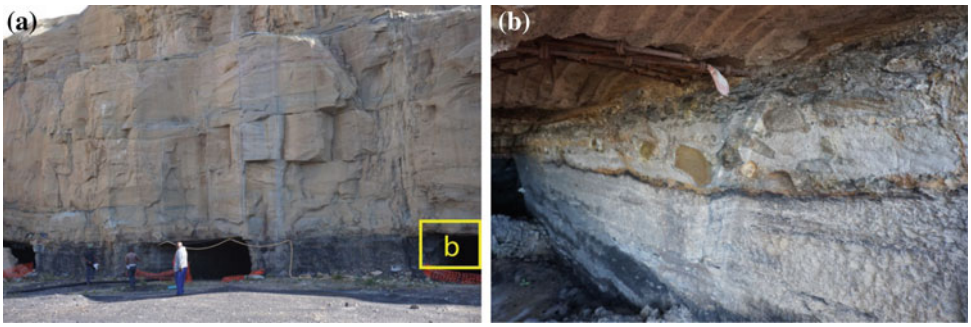

Fig. 6.4 **a** 1.2 m coal deposits (*dark grey*) sharply overlain **b** by pebbles and cobbles mainly of TMG quartzites, which resemble molasse deposits, and cross-bedded coarse sandstones (*white*) of the Molteno Formation, at Elitheni Coal Mine (S31°31′59.5″; E27°16′14.3″)

possible late CFB tectonism. Indeed many subtle sedimentary structures across the boundary (Fig. 6.3) support contemporaneous tectonic activity (and as is explored also in Chap. 5).

Turner has also pointed to tectonic activity in the CFB to explain the prominent and widespread occurrence of rounded boulders and pebbles of Table Mountain quartzites in the Triassic Molteno Formation (Fig. 6.4). It is clear from his and subsequent work that these deposits define a time of non-preservation/erosion for example of the Molteno coal deposits (the CO_2 side effects of which must have contributed to global warming; Faure et al. 1995). These observations implicate, and may thus confirm, CFB activity well into the Triassic. Identifying such stratigraphic signatures require much greater collaboration between sedimentologist, palaeontologist, and structural field geologist if we are to test and unravel subtle details of the linked CFB and Karoo Basin evolution.

At a greater Gondwana-scale, geological evidence now suggests that southern Africa was the lower plate during the Cape Orogeny and that the subducted slab dropped south-westward beneath the Gondwana composite ribbon continent that we here informally refer to as Patagonian microplate(s). This collage of small continental blocks collided with southern Africa around 275 Ma, shortly after the end of the Dwyka glaciation; and the Table Mountain Group was tectonically transported northwards during the Cape-de la Ventana tectonism around 253 Ma, in turn affecting sedimentation in the Karoo Basin up to, and possibly beyond the Permo-Triassic transition (Fig. 6.5).

Northward migration of the early Karoo foredeep during the Cape Orogeny, and subsequent terrestrial sedimentation during the upper Karoo times, was complex and affected cannibalization and re-deposition processes up to 400 km northward, creating a series of non-linear depositional hinge-lines that are poorly constrained at present (Chap. 14).

In this model, the CFB and Gondwanides resemble in size and structure of the Rocky Mountain thrust belt of the North American Cordillera, respectively, and this is similar to the new exciting models for the evolution of the North American Cordillera as recently explored by Hildebrand (2009, 2013, 2015). How all this links farther with orogenesis in Antarctica (e.g. Ross Orogeny; Paulsen et al. 2007) and South America (e.g. Castillo et al. 2015; Ramos 2008) remains unresolved. Mantle tomography has delineated a huge cold slab below present-day South America that extends vertically down to the lower mantle (French and Romanowicz 2015), marking the site of a sustained period of subduction beneath Gondwana-South America for nearly 300 million years as the overriding geodynamic connectivity with the lower mantle upwelling that also shaped the uplift of southern Africa (Kalahari Plateau) described below.

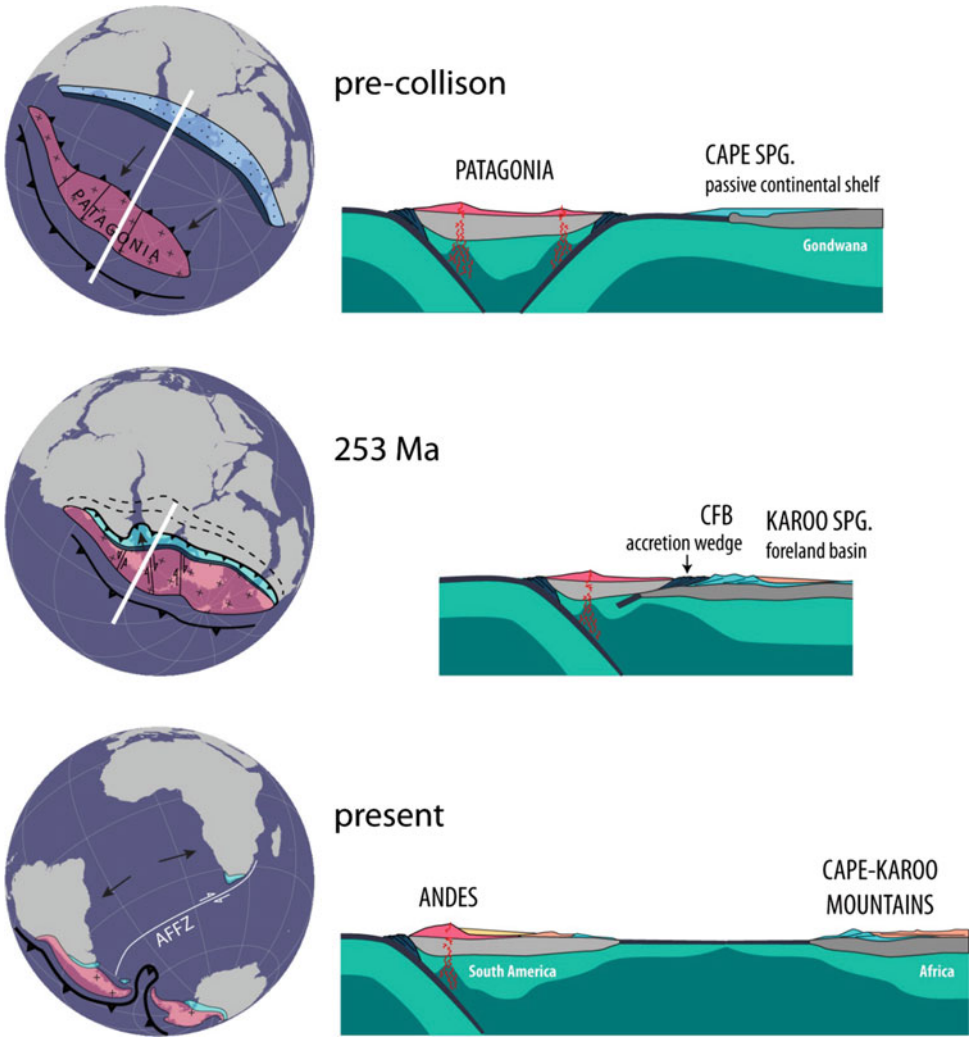

Fig. 6.5 Schematic plate model for the formation and break-up of the Gondwanides, resulting in the Cape Mountains in southernmost Africa, the Sierra de la Ventana in northern Argentina and Chile, mountains of the Falkland Island, and the Ellsword Mountains in Antarctica. *Bold white lines* sections; *stippled black lines* schematic stratigraphic hinge-lines

7. Landscapes, Sculpturing, and Erosion Rates

The iconic landscapes of sub-Saharan Africa have deeply influenced global geomorphology theories. In southern Africa much of this was guided by the work of Lester King (1951, 1967; see Summerfield 1985; Partridge and Maud 1987; Decker et al. 2013 for overviews and references), but this work has remained within the realm of qualitative observations. On the other hand, much has been achieved over the last two decades towards quantifying exhumation and erosion rates of the Cape Mountains and Karoo Basin; and across southern Africa (the Kalahari Plateau) in general. Most of this is because of significant advances in thermochronology, using for example Apatite Fission Track analyses (AFT; Fig. 7.1), and cosmogenic dating.

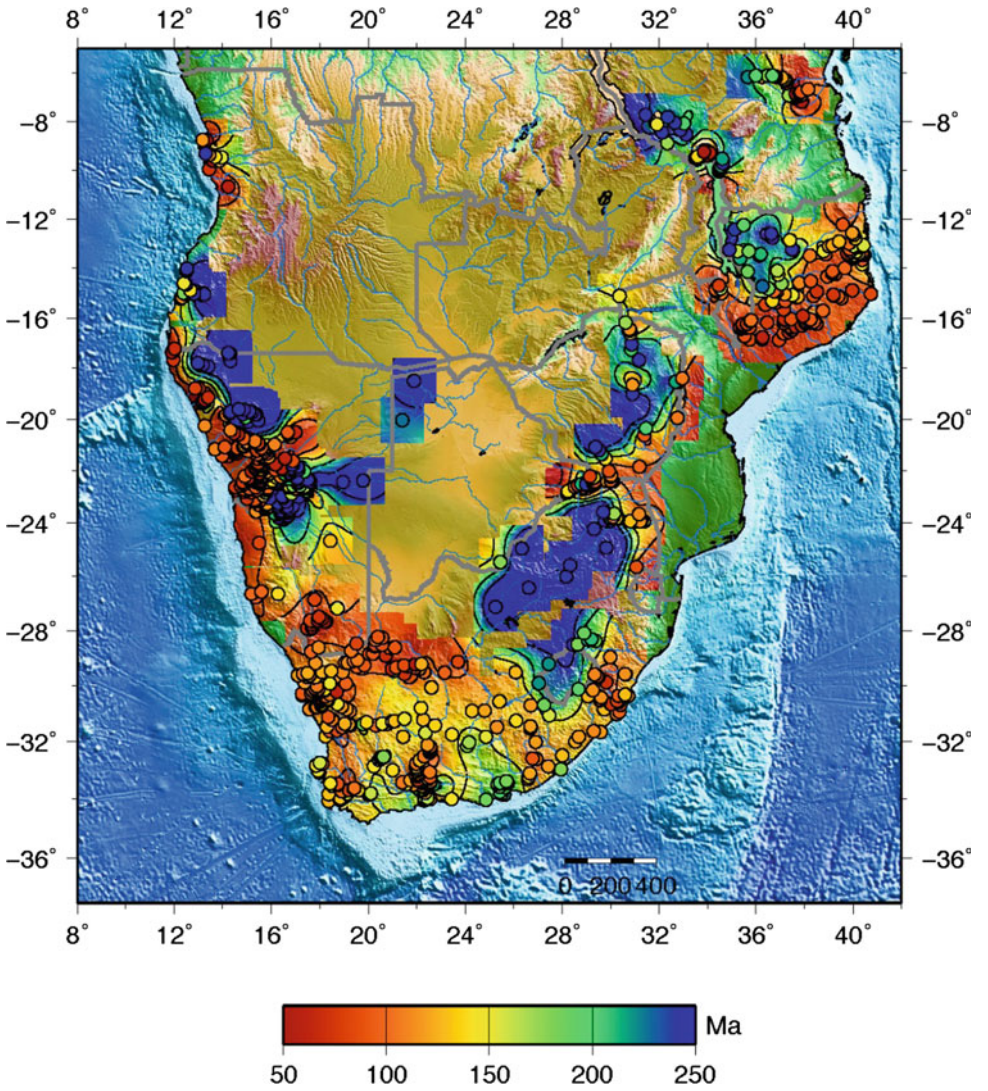

Fig. 7.1 Map showing the pattern of apatite fission track age (*circles*) measured for surface samples across southern Africa overlaying a digital terrain model (SRTM30 Plus 1 km DEM, http://topex.ucsd.edu/WWW_html/srtm30_plus.html). The AFT data comprise a compilation of data from the literature (Van der Beek et al. 1998; Tinker et al. 2008a, b; Brown et al. 1990, 2000, 2002; Cockburn et al. 2000), as well as significant unpublished data from the University of Glasgow thermochronology research group. The AFT age map provides a qualitative proxy for the relative timing and depth of erosion; with young ages (< c. 150 Ma) indicating significant (>3–4 km typically) post Gondwana break-up erosion and the older ages (> c. 200 Ma) indicating much less (c. 1 km or less), and typically protracted, slow erosion (Map provided by Roderick Brown)

The AFT ages of surface samples by themselves do not directly date the timing of any geological or geomorphic event because the detailed thermal history for a particular sample depends on the track length distribution. However, the striking pattern of AFT ages across southern Africa does provide important clues to the post break-up morphotectonic evolution of the sub-continent and several important features are apparent from this broad pattern of AFT age. Firstly, the older ages (older than c. 200 Ma) are clearly restricted to the high elevation areas of the continent that make up the Kalahari Plateau. Moreover they appear to be restricted to the Azanian (Kaapvaal+Zimbabwe) and southern Congo Craton areas of the interior. The second obvious feature of Fig. 7.1 is that AFT ages younger than 100 Ma occur in many places well inland of the coastal plain and extend across bordering parts of the elevated, low relief Kalahari Plateau. This pattern is strikingly different from that expected from models

of passive margin evolution that envisage post break-up erosion being largely governed by retreat of a major coast parallel escarpment zone that divides a deeply eroded coastal plain from an interior, elevated, low relief paleo-plain of some antiquity. This broad pattern indicates that the spatial distribution of post break-up erosion across southern Africa has been strongly influenced by the regional tectonic architecture of the sub-continent, and suggests that significant Cretaceous tectonic reactivation and consequent differential displacement and erosion has occurred across many older basement structures (e.g. Brown et al. 2014; Wildman et al. 2015, 2016; Green et al. 2016).

This rapidly growing database has provided a firm confirmation that present day landscapes across southern Africa are close to equilibrium and in a geomorphic steady state with denudation rates of less than 20 m/Ma—low to insignificant in geological time. A surprising example from studies across the alpine-like relief of the Cape Mountains reveals some of the lowest denudation rates in the world (Figs. 7.2 and 7.3).

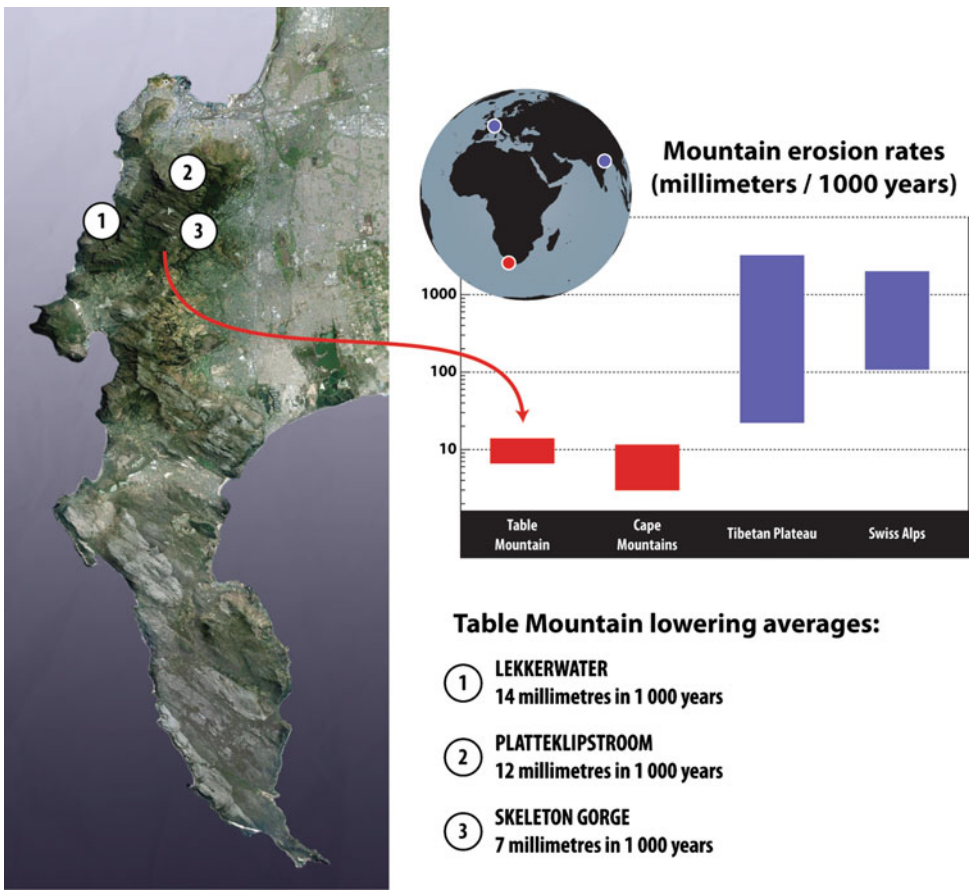

Fig. 7.2 Erosion rates of the Table Mountains. Rivers draining Table Mountain across the Cape Peninsula remove each year around 30 tons of sediment per each square kilometre. The sediment that ultimately ends up in the ocean, results from the continuous action of wind and water. Table Mountain is slowly 'washed into the sea' becoming 10 mm slimmer every 1000 years (from de M.J. Wit and A.T. Codilean 2015 unpublished)

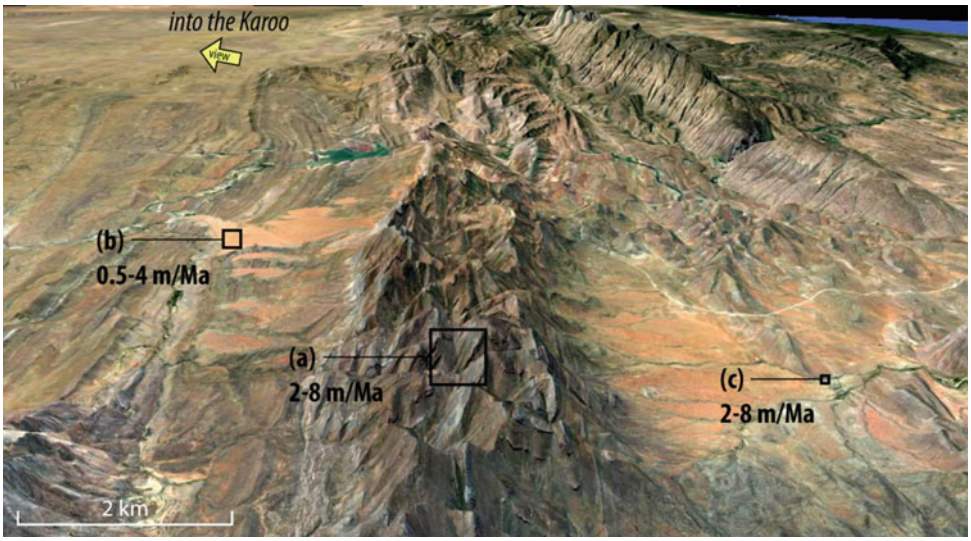

Fig. 7.3 Relief view (Google image) along the Witteberg Ranges, looking toward the Eastern Cape (see Fig. 7.4 for location), showing the transition between the Cape Mountains and the Karoo Basin. Note the exposure of the folded surfaces beneath the alluvial fans along both edges of the Witteberg Mountains. Present erosion rates of the quartzite ridges (**a**), the alluvial plains (**b**), and their catchments (**c**), are in all cases <4 m/Ma on average. By contrast erosion rates across this same landscape were up to 2 orders of magnitude greater in the Cretaceous (100–80 Ma). Thus, the present day Cape-Karoo landscape represents 'frozen-in' sculptures of end Cretaceous-early Cenozoic times

Within the Cape Mountains, where slope angles are often in excess of 30° and relief frequently exceeds 1 km, Be-denudation rates on the interfluves of the mountains range between 2–4 m/Ma, and catchment-averaged denudation rates between 2–8 m/Ma (Scharf et al. 2013). This Cape Mountain maintenance of its rugged topography and suppression of denudation rates can be attributed primarily to the physically strong and chemically inert quartzites of the Table Mountain Group that constitute the backbone of the high mountain ranges (Fig. 7.4a). This includes the iconic Table Mountain, where the range of erosion rates, whilst nearly double that of the inland quartzite ranges, are still low between 7–14 m/Ma (Fig. 7.2), and thus assuring its survival over geological time and into the future, despite the Cape storms that episodically release large boulders from its 'Table cloth'.

Yet strong Cape quartzites cannot be the explanation for the old topographic relief inland across the Karoo, where denudation are similarly low, ca. <4 m/Ma (Fleming et al. 1999; Kounov et al. 2007; Decker et al. 2011; Keen-Zebert et al. 2016). Here, denudation rates are controlled by the relatively strong dolerite sills that sustain large parts of the landscape (Figs. 7.4b and 7.5). However, the same dolerites often retain deeply weathered Cretaceous paleo-surfaces (Figs. 7.6a, b). One explanation is that dolerites weather fast under humid and hot climates, as was the case in the Cretaceous, but not so under the progressively cooler and dry conditions during the late Cenozoic (de Wit 2007; Uenzelmann-Neben et al. 2016), and quartzites may be less so affected by climate variations.

Indeed, the AFT work on surface and borehole samples by Justine Tinker across the Cape Mountains and southern Karoo up onto the escarpment showed that Cretaceous erosion rates along this region range between 200 and 400 m/Ma (Tinker et al. 2008a, b). There has therefore been a drastic reduction of weathering and erosion since the mid-Cretaceous (~80–100 Ma). It is likely that this reduction is related to long term cooling from the hot (and humid) conditions in the Late Cretaceous-Early Paleogene, for which there is ample record in the form of local remnant deep weathering profiles (Fig. 7.6). Across the Karoo interior and along the east coast this is dominated by weathered dolerites, while along the Cape Mountains this has left in places thick sections of kaolin.

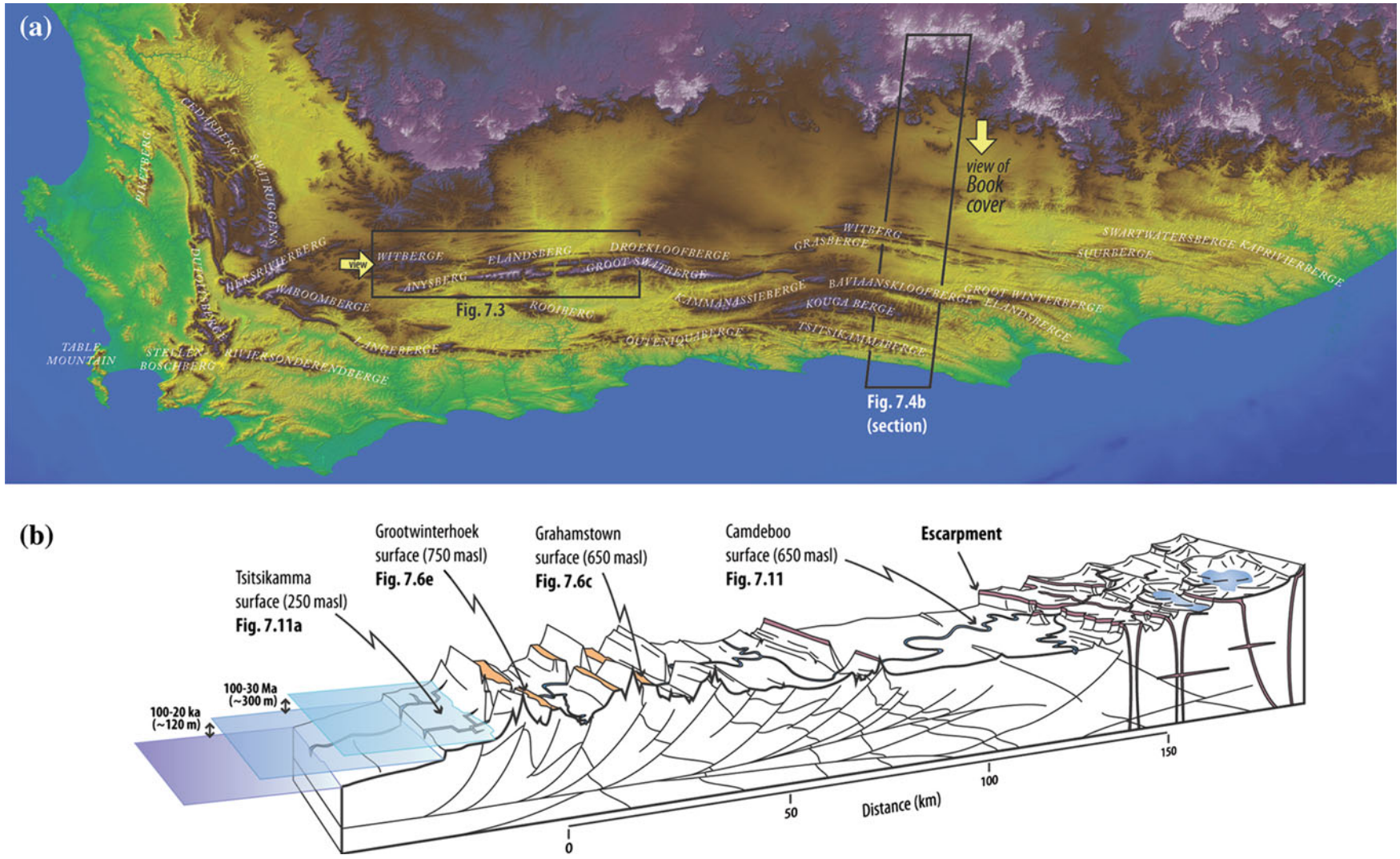

Fig. 7.4 **a** Cape-Karoo relief map showing the names of Cape Mountain ridges and the rugged edge of the Karoo escarpment into the Kalahari Plateau (*purple and white*). **b** N-S schematic section, from the coast to the escarpment showing main geomorphic features referred to in the text. Note sea-level fluctuations of more than 300 m along the south coast

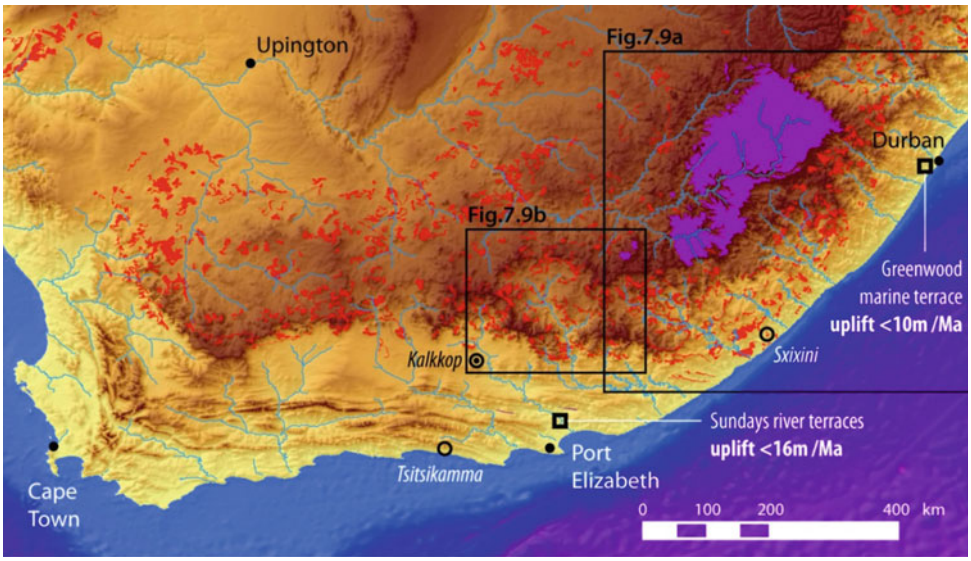

Fig. 7.5 Shaded digital elevation model (SRTM30) of southernmost Africa highlighting the remnants of Karoo LIP lavas (*purple*) and dolerite sills (*red*). These igneous rocks have 'engineered' a regional drainage divide across the central Karoo and define the Great Escarpment across the southern Karoo Basin. Note the striking meandering pattern of many of the south-draining rivers that cut through and traverse parallel to ridges of the Cape Mountains, and similarly along the east coast where the rivers cut across or terminate within dolerite saucer-shaped sills (e.g. Fig. 7.4b). Note also that meandering rivers occur at the highest elevations (Lesotho) incising the lavas, which suggest that meanders are inherited from incision into subhorizontal sequences that must have covered a vast region above the Karoo lavas. Modern AFT analysis, U/Th/He and cosmogenic dating suggest that these overburden thicknesses ranged between 1–2 km above the Kalahari Plateau and 2–7 km south of the escarpment (Stanley et al. 2013 and Tinker et al. 2008a, b, respectively). □ Dated river and marine terraces where uplift rates have been determined at <10–20 m/Ma over at least the last 4 million years (Erlanger et al. 2012)

It has been argued for long that the topography along the coastal regions, which all reveal young AFT ages (Fig. 7.1), and specifically along the east coast flanking the escarpment, relate to recent (Miocene) tectonic uplift of up to 700–900 m (Partridge and Maud 1987; Partridge 1998) on the basis that flat erosional plains, presently occurring at different elevations above sea-level (asl), originally developed at the same elevation (referred in the literature to as the 'African Surface'). But, more recent cosmogenic isotope analyses along the coastal marine platforms, river terraces and faults (Erlanger et al. 2012; Bierman et al. 2014; Kounov et al. 2015; Fig. 7.5) have shown that such tectonic uplift is unlikely to have been greater than at most 100 m over the last 4 million years and at present may even be subsiding.

These now well-established low late Cenozoic erosion rates have, for example, been successfully used to estimate the age of the Kalkkop Crator (Mthembi et al. 2016), impacted on the Camdeboo Plains of the Karoo interior, just below the escarpment (Fig. 7.7). With the assumption that the eroded rim of the crater was originally of 50 m height, and a moderately low erosion rate of 6–7 m/Ma, the age of Kalkkop (and thus its flat plains) may be about 6.5 Ma (Miocene) old, and possibly older if the established lower erosion rates of 1–4 m/Ma of the nearby peneplains (Fig. 7.3; Kounov et al. 2015) are applied.

Understanding the geomorphology of coastal and inland areas along the east coast of South Africa, between the high plateau covered by Drakensberg lavas across Lesotho (circa 2.6–3.4 km asl) and the numerous Karoo dolerite sills exposed from about 2,000 m elevation down to sea-level (Fig. 7.9b), requires a different analysis than the sculptures found along the Cape and Karoo regions south of the escarpment (Fig. 7.4). Across the latter major meandering rivers cut deeply through the quartzites Cape ranges (Fig. 7.6e). Across the former meandering rivers traverse and cut into basalts, dolerites and interbedded softer sandstones and shales (Fig. 7.8). Such an inheritance of incised meandering rivers was first pointed out by King (1953); and

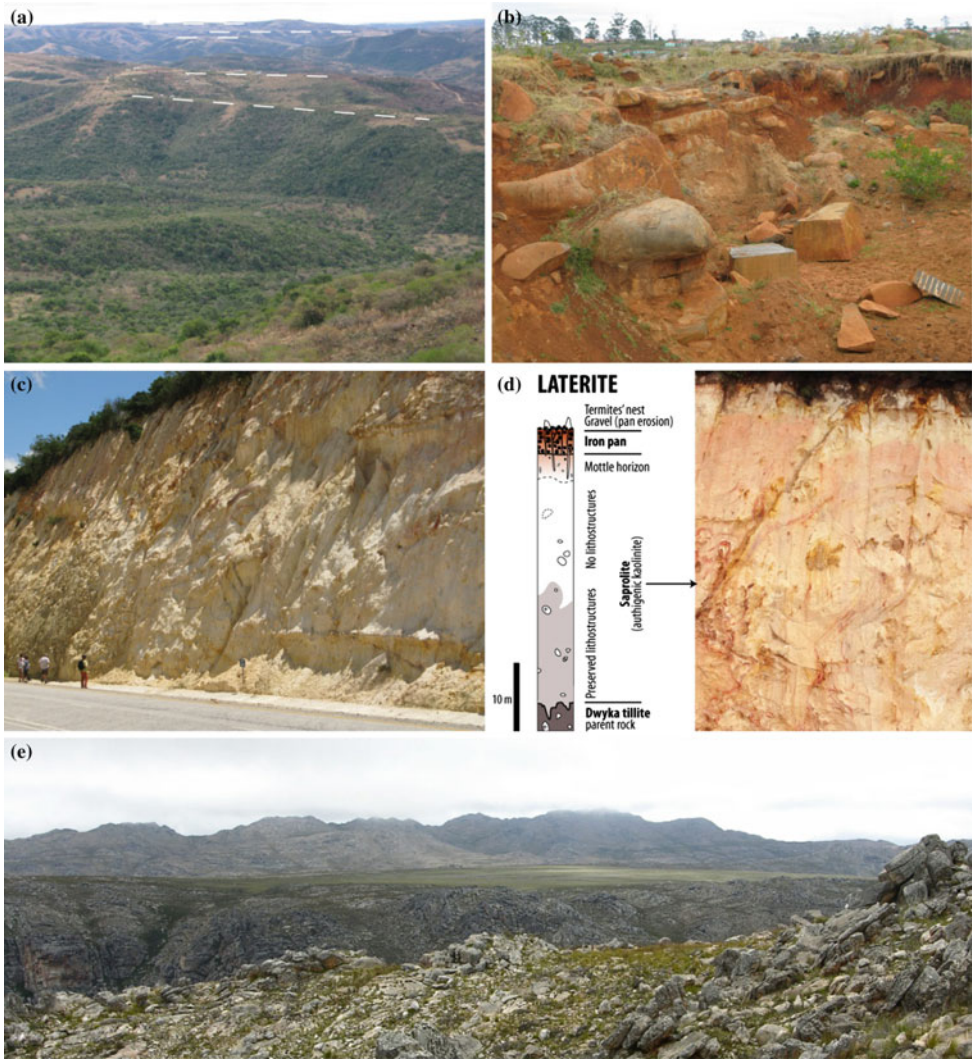

Fig. 7.6 Relics of deep weathering profiles: **a** majority of dolerite sill surfaces (*white stipples*) are covered by **b** iron-rich laterites with large core stones (e.g. Sxixini area; Fig. 7.5 for location); **c** 30–40 m thick section of kaolinite from highly weathered Dwyka rocks (**d**) is preserved below the Grahamstown surface of silcretes and ferricretes; and **e** 200 m deep canyon cut into remnant erosion surface of the Cape Supergroup quartzite flanking the Grootwinterhoek Mountains (far distance; Fig. 7.4b for location; *photos* by B. Linol, M. de Wit and W. Illenberger)

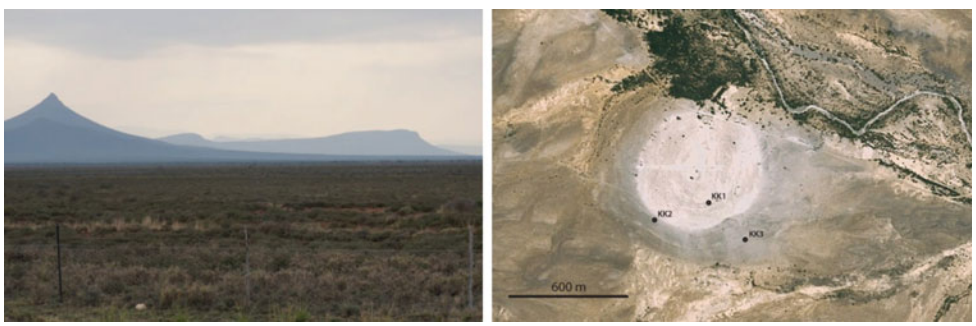

Fig. 7.7 The Camdeboo Plain near Pearston (*left*) impacted by the Kalkkop Crator (*right*). This crator has the shape of a saucer (and underlain by breccias, suggesting a possible meteorite impact origin) with a diameter of 600 m; its rim is raised 9 m above the level of the surrounding flat country of gently folded Beaufort sandstones and mudstones. The depression is covered with lacustrine fossiliferous carbonates and calcretes (*white*) that provide a unique record of Cenozoic climate and ecosystems (Mthembi et al. 2016)

Fig. 7.8 **a** Flat erosional plains at 1,950 masl (S30°45′04.9″; E28°11′58.1″) and **b** incised meandering river (1,700 masl; S30°53′29.7″; E27°33′59.0″) steep into basalts, dolerites, and gently sloped across upper Karoo shales in the Drakensberg Mountains

recent AFT data confirm that this is likely related to an old inherited meandering system from river-incision into thick and subhorizontal softer cover of sediments above the present landscape that has since been eroded (e.g. Tinker at al. 2008a, b; de Wit 2007; Fig. 7.10).

A first order observation is that the sills, which have an overall geometry of regional 'saucers' of various size (see also Chap. 2), can act as barriers and local sources for rivers (Figs. 7.9a, b). This can explain the apparent paradox between the low rock uplift rates and river incision of 10–20 m/Ma over the last 1–5 Ma, the inferred late Cenozoic tectonic uplifts along the east coast of South Africa (700–900 m; Partridge and Maud 1987; Burke and Gunnell 2008), and yet significant decrease in offshore sedimentation during the same period (e.g. Tinker et al. 2008b; Guillocheau et al. 2012; Braun et al. 2014).

There is yet another fundamental challenge in that the present models are unable to account for all the coastal and inland landscape. Clearly new models are needed to explain the topography of the complex transition from the coast to the hinterland plateau, with meandering rivers, deep canyons, multiple steep escarpments and flat erosion surfaces. There are at least two parameters to inculcate. First, it is clear that strong basalts and dolerite sills play a significant role in controlling river incision modes and erosion rates (Fig. 7.9a, b). Second, there needs for a better understanding of the links and lag-times between inland stream retreat (back-erosion), isostatic readjustments and coastal marine terraces (Figs. 7.10 and 7.11): how much river incision and back-wearing of inland canyons is driven by the substantial long and short term sea-level changes? To unravel that there is need for greater integration between the earth and life sciences.

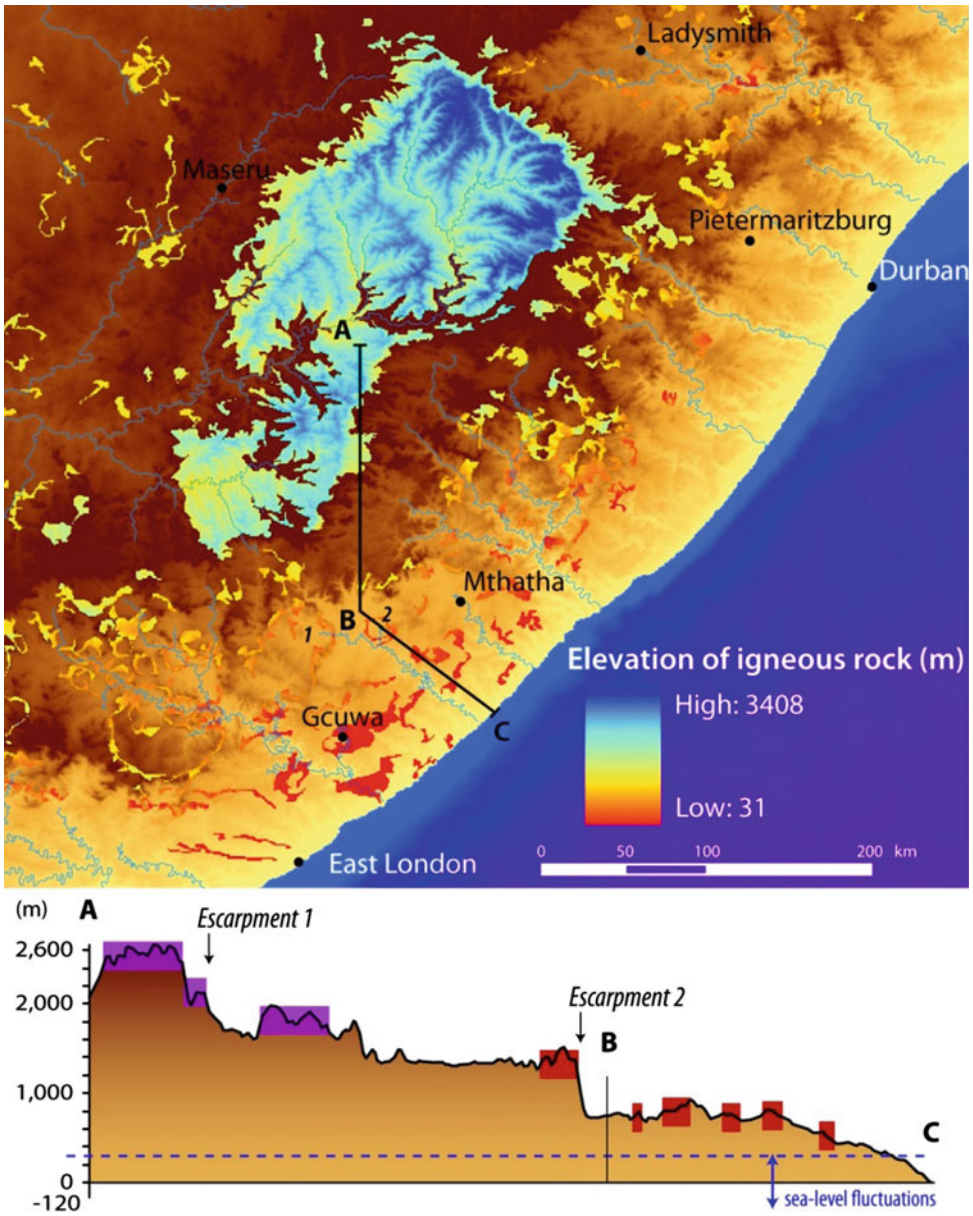

Fig. 7.9a Standard deviation of elevations of Karoo igneous rocks across the Drakensberg and eastern coastal region of South Africa (Fig. 7.5 for regional location). The topographic profile (*bottom*) shows outcropping resistant basalts (*purple*) and dolerites (*red*), rock types that are significantly controlling the landscape evolution. Note the position of at least two major escarpments (>500 m scarps), both of which have very low present-day erosion rates (2–5 m/Ma; Decker et al. 2011). In many places, meandering rivers cut across the resistant sills; in other they originate within saucer-shaped sills (rings, *1* and *2* as examples) from where they drop-down once a break has been forced through the edge of the saucer (Fig. 7.9b)

While the present geologic and thermochronology data does not support the concept that planation surfaces ('African Surface') across the coastal region represent recent differential phases of uplift, the coastal marine terraces over the last 100 million years or so have consistently fluctuated between present day to about 330 m above and 150 m below (Figs. 7.4b and 7.11), as has been inferred from marine fossils, sedimentary sequences, and phylogeography based on microcondrial DNA (mtDNA) sequence variations of fish (e.g. Swartz et al. 2007). It is likely, for example that the deep inland and coastal canyons cutting the planation surfaces (schematically shown on Fig. 7.4b) are related to these sea-level fluctuations and are

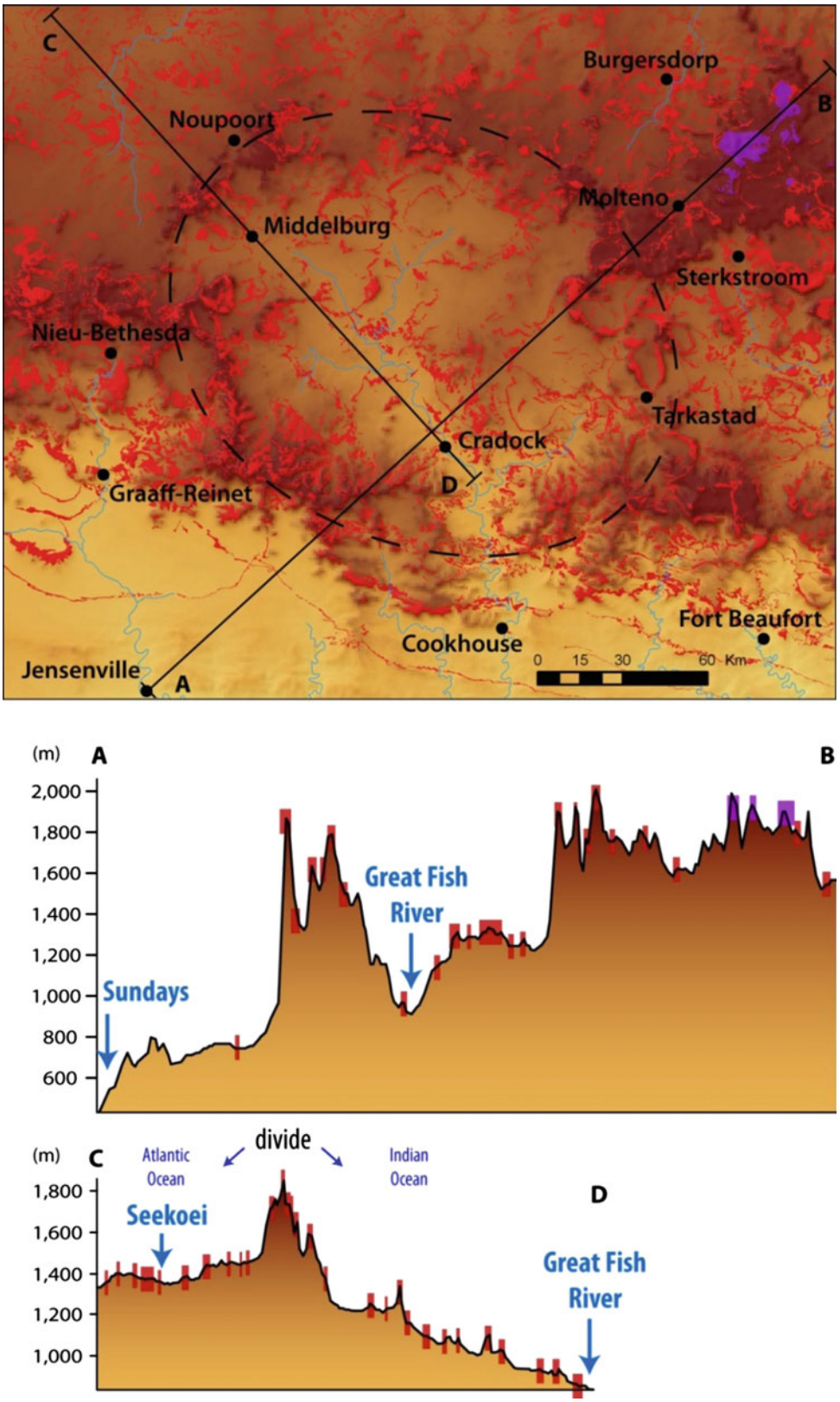

Fig. 7.9b Map and cross-sections across nested sills, ranging in diameter between 150 to less than 10 km within the southern Karoo escarpment (Fig. 7.5 for regional location). Many dolerite sills and dykes form the highest local reliefs (*dotted line* delineates approximately the edges). Note that the main river (Great Fish) meanders across the floor of the large sill complex but has tributaries sourced within smaller internal sills

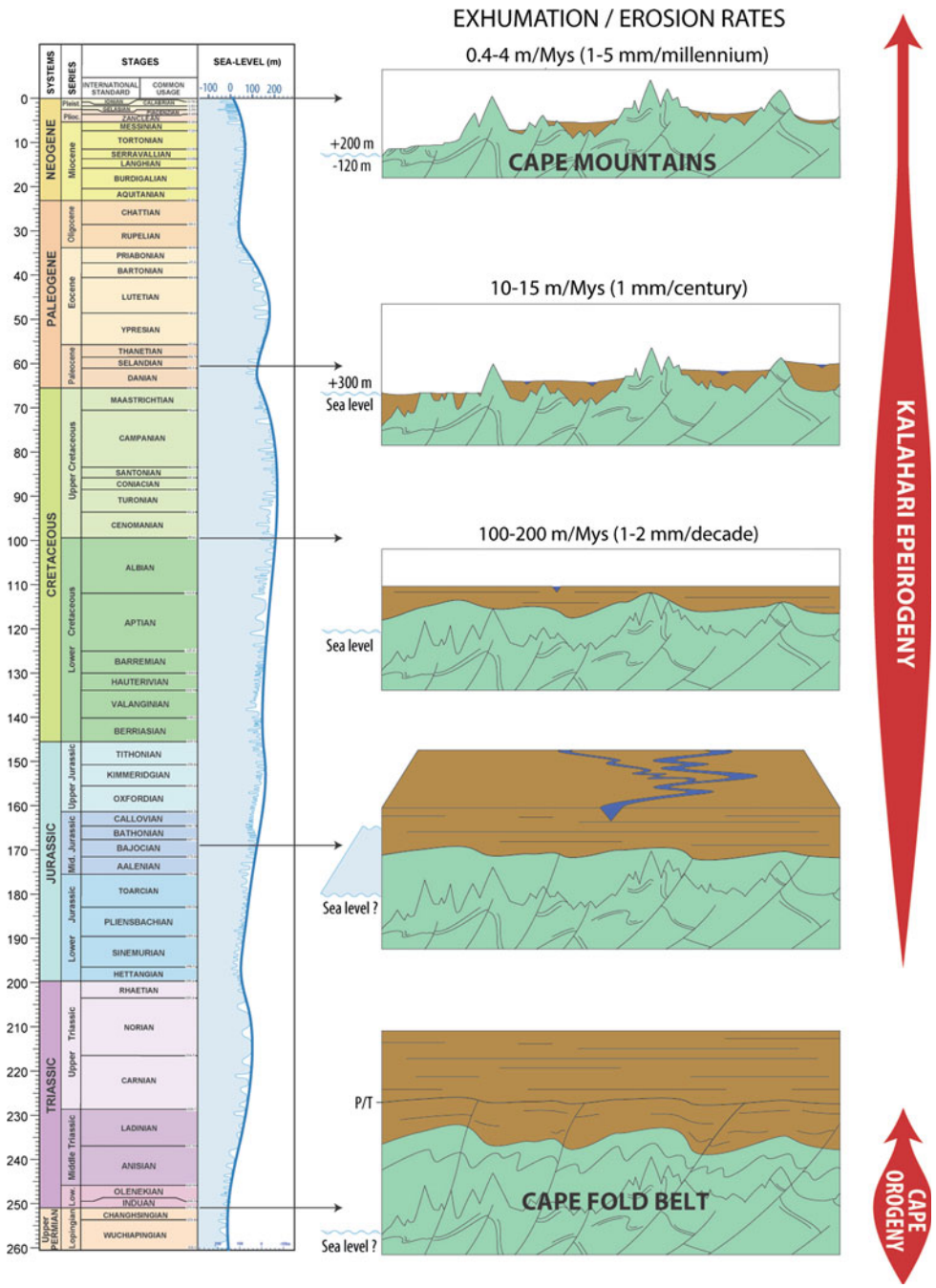

Fig. 7.10 Schematic summary of estimated exhumation and erosion rates related to the Kalahari Epeirogeny (uplift at 120–80 Ma) following the end of the Cape Orogeny (at 253 Ma) with relative erosion rates, calculated using both shallow crustal thermochronology (AFT, U/Th/He) and cosmogenic isotope analysis (^{3}He, ^{21}Ne, ^{10}Be, ^{26}Al, ^{36}Cl). Sea-level stands are rough estimates and require future work. For simplicity, the extensional Jurassic-Cretaceous fault systems are not shown

Fig. 7.11b Cretaceous-Cenozoic sea-level curves (from Haq et al. 1987 and Miller et al. 2011) during ► Gondwana break-up (Scotese 2014). Note there is considerable uncertainty about the paleo-sea levels (e.g. Müller et al. 2008; Rowley 2013). Note also the transition from Cretaceous to Cenozoic climate is largely driven by unique circulation changes in the southern Oceans, driven by opening and closing of ocean gateways to the Pacific (e.g. Uenzelmann-Neben et al. 2016)

Fig. 7.11a Regional wave-cut platform into Table Mountain quartzites 250 masl along the south-eastern Cape coastal region (e.g. Tsitsikamma; Figs. 7.4b and 7.5 for location), extending from George to Van Stadens Bridge, west of Port Elizabeth. This plane can be followed intermittently farther east to beyond East London, where it is preserved above the weathered dolerite sills (330 masl)

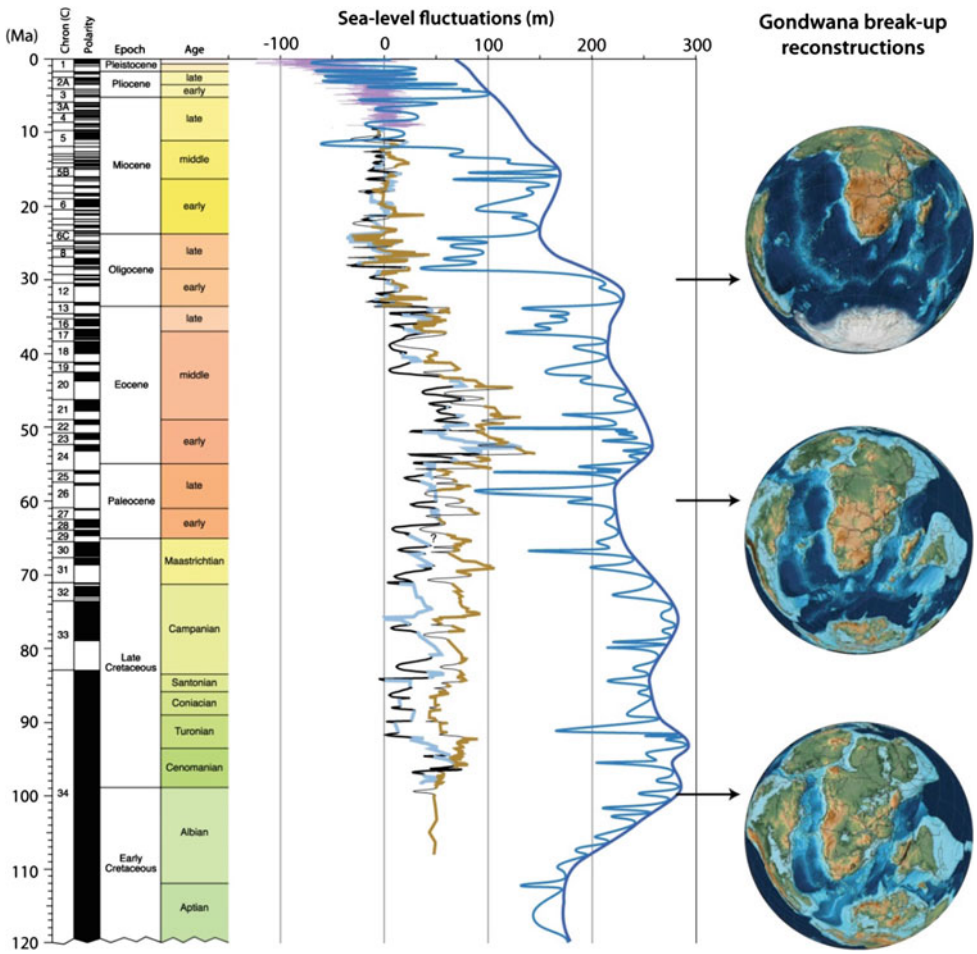

thus climate driven. The latter show a strong association with paleo-river systems, sea-level and landscape changes (Swartz et al. 2007). Similar genetic work incorporating geomorphic evolution of animal and plant diversification across the Cape-Karoo will prove to open up new ways of testing the landscape sculpturing across the Cape-Karoo (Cowling et al. 2009; Verboom et al. 2008; Hoffmann et al. 2015). When such genetic analysis is linked with new thermochronology, cosmogenic isotopes analysis, field work on rock and weathering features, and numerical modelling (Braun et al. 2014), then a better understanding can emerge of how surface processes and mantle dynamic flows can best explain the topographic evolution of southern Africa. With such potential advances in geoecodynamics, the Cape-Karoo region will continue to be a driving force for global geodynamic models and geomorphic theory; and the unique laboratory from which to quantify and differentiate the contributions of surface processes and of mantle dynamics to its regional landscape evolution.

8. Neotectonics, Microseismicity, and Fluid Induced Earthquakes

Within the Cape Mountains, and likely in the basement beneath the Karoo Basin, there are significant active and passive (dormant) faults (Andreoli et al. 1996; Ben-Avraham et al. 1997; Bird et al. 2006; Kounov et al. 2008, 2013; Wildman 2015; Lindeque et al. 2007, 2011; Tankard et al. 2009, 2012; Smit et al. 2015). In addition a number of seismically active sites have been identified ever since the 6.3 ML Ceres-Tulbagh Earthquake in 1969 (Fig. 8.1). The origin of this intraplate seismicity is not known, but is likely associated with the well-known fault systems that stretch along the Cape Mountains, and for some of which there is strong evidence for geologically recent surface ruptures (Bierman et al. 2014). Most models relate this seismic activity to far-field tectonic activity along the South Atlantic mid-oceanic ridge (ridge push), transcurrent forces along the Agulhas-Falkland Fracture Zone (Fig. 6.5), or to southward propagation of the East African Rift (Reeves 1972; Nguuri et al. 2001; Singh et al. 2011; Wildman et al. 2016).

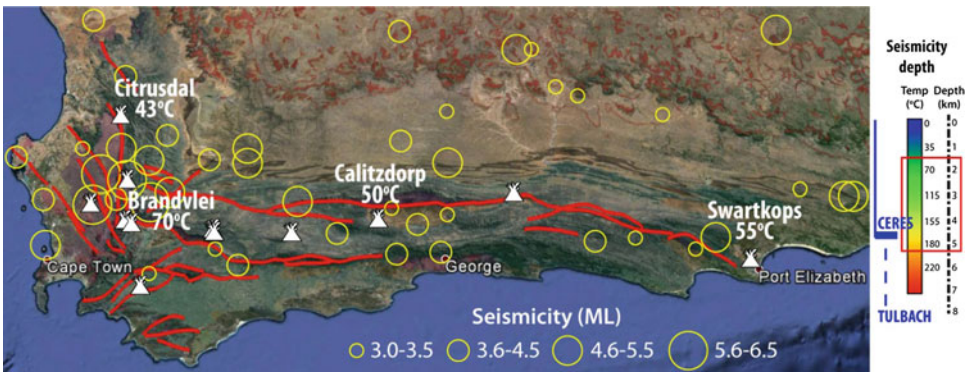

Fig. 8.1 Regional exposed dormant to active faults (*red lines*) across the Cape Mountains and location of major hot springs (*white triangles*) with surface temperatures in degrees Celsius (°C). Also shown is the distribution of micro-seismicity clusters (*yellow circles*) and location of historical earthquakes for the period between 1620 and 2007 (compiled by R. Ebrahim-Trollop). Depths of micro-seismicity and the historic earthquake at Ceres/Tulbach, together with estimated temperatures and potential depth penetration of meteoric water that 'feed' the hot-springs are shown on the right-hand figure (Smit et al. 2015; Diamond and Harris 2000). Local high paleo-heat anomalies and local high potential geotherms (not shown here) have been documented elsewhere in the southern Karoo Basin (Duane and Brown 1992; Brown et al. 1994; Dansay et al. 2014)

It is also possible that the seismicity is induced by deeply penetrating meteoric water that in places returns to the surface in concentrated areas of 'hot-springs' (Fig. 8.1). It is known that fluids play a key role in modifying the chemical and physical properties of fault zones (Guglielmi et al. 2015), which may prime them for repeated ruptures (inducing earthquake) by the generation of high pore fluid pressure and precipitation of weak secondary minerals following deep penetration of meteoric water, as has been shown in New Zealand's Alpine Fault (Cox et al. 2015; Menzies et al. 2016).

Thus, understanding the surface precipitation and deep hydrogeology of the Cape-Karoo fault- and hot spring-systems is a great challenge both for predicting naturally occurring earthquakes and potential induced earthquakes in the future during possible shale gas development and related fluid re-injections (Walsh and Zobach 2015). Whilst hydraulic fracturing operations induce minute earthquakes, minor earthquakes are most often caused not by the hydraulic fracturing itself, but by wastewater re-injection and water extraction in the USA (Ellsworth 2013; van der Elst et al. 2013 and 2016; McGarr 2014; Hornbach et al. 2015). Indeed, with the ubiquitous vertical and horizontal connected joint systems in the rock formations of southern Africa (Muedi 2014), and the presence of likely subsurface fault systems beneath the Karoo Basin that could potentially be activated during artificial fluid injections, new structural and material analyses across the Karoo Basin are sorely needed; and local and regional rock mechanical studies, micro-seismic analyses, as well as deep geo-hydrology must be undertaken before hydraulic fracturing for shale gas extraction in the Karoo can proceed so that monitoring during operations can diminish this risk within a predetermined risk-envelope. Chapter 3 describes a new way to monitor such systems using ambient noise with small portable recording stations.

Presently, the Karoo shale gas is a resource with estimated volumes of 19–23 tcf (trillion cubic feet) of available free gas across an area of approximately 79–92,000 km^2 (Decker and Marot 2012; Geel et al. 2011; Chere 2015). However, the 3-D subsurface geology of the Karoo is poorly known, and remote geophysical sensing and deep-cored drill-holes will need to be implemented during a first exploration phase to determine subsurface distribution of gas-shales and allow for greater accuracy in determining the total potential recoverable amount of shale gas in place.

However before any potential shale-gas development can proceed, the risk of induced seismicity and pollution of natural water systems by injection of waste fluids must be minimized through careful site selection, monitoring and management (Guglielmi et al. 2015; Walsh III and Zobach 2015; Walters et al. 2015). It is clear that it is very difficult to predict the possible impacts of hydraulic fracturing on South Africa's water resources due to the lack of information on shallow to deep groundwater systems (Egle 1996; Chevallier et al. 2004). As emphasized elsewhere (de Wit 2011), comprehensive natural baseline studies must be undertaken on a local as well as regional scale to develop a clear understanding and continuous monitoring of the existing state of the Karoo, including a robust quantitative knowledge about groundwater resources, prior to any decisions leading to possible shale gas development (and uranium mining) across the region.

9. Conclusion

What Still Needs to be Done in the Cape-Karoo?

Despite geologic observations for more than 200 years, the history of the Cape-Karoo remains relatively poorly constrained. But increasingly, with greater geochronology precision and mapping accuracy, aided by new geophysical methods, a 4-D model for the origin and evolution of the crust of southern Africa may become a reality in the near future. Such developments will help unravelling the origin and evolution of the Cape-Karoo region, answer critical questions related to geo-biosciences, and above all, manage the resources and heritage of this unique natural laboratory with care and confidence.

Below, we list some (but by no means a comprehensive list) sets of questions (in geo-chronological order):

- What is the stratigraphic position and sedimentology of the 'pre-Cape' sequences (e.g. the Kango, Kaaimans and Gamtoos Complexes)?
- How can we improve the chronostratigraphy of the Cape-Karoo sequences? For example, can modern micro-magnetic technology reveal more about the magneto-stratigraphy that is difficult to measure from conventional core analyses? And can this help to improve the polar wander path during the Paleozoic and refine Gondwana paleogeographical reconstructions?
- How can we best improve the details of transitions during the 4 recorded major (and several less intense) Phanerozoic mass extinctions? Where are they best and most fully preserved? And can we link them better with their respective terrestrial or marine counterparts? Do any link to Gondwana LIPs and/or global tectonic events?
- How many (marine) transgressions are recorded within the Lower to Mid-Paleozoic sedimentary platform sequences (the Cape Supergroup and Dwyka Group)? Can they be correlated with precision to the other Gondwana passive margin deposits and linked to global sea-level changes?
- What is the cause of the apparent 50 million years long Dwyka glaciation? Can we better resolve if there were major interglacial episodes and the cause and effects of the final deglaciation during the Early Permian?
- Can we retrace the evolution of the gas-shale formations (the Prince Albert and Whitehill Formations), from deposition (to reconstruct the paleo-water depth), through diagenesis and burial to great depth, to exhumation and weathering?
- Where is the contact between the overlying Permian-Triassic Ecca and Beaufort Groups? It represents a transition from subaqueous to subaerial sedimentation, marked by a change from turbidite to deltaic and then river deposits. However robust evidence of emersion (such as terrestrial burrows and paleosoils) is scarce in the lowermost Beaufort and its fluvial sedimentology is often out-dated, based on traditional meandering-stream facies models from the 1990s.
- Can we link the peak(s) of deformation of the CFB (253 Ma) to the sedimentological and biostratigraphic record? Also, because subsurface fluid flow through the Karoo is known to be extensive (but of low temperatures), how have these processes affected the conventional Ar/Ar dates? And what is the linkage between the Gondwanides, CFB, Karoo Basin and subsequent extensional processes during the onset of Karoo magmatism?
- Where are the significant hiati, and how much time is missing in the Karoo sedimentary record, such as for example within the Molteno erosional surfaces?
- The Karoo LIP erupted rapidly between 182 and 183 Ma; but at what elevation? What is the relationship and relative timing of dolerite intrusions at different levels (from −4 to +2 km asl) and widespread extrusions of the Drakensberg lavas? Do they link to rifting and the associated younger Jurassic-Cretaceous alluvial fan sedimentation (Enon conglomerates)? And did these syn-rift conglomerates fossilize the Cretaceous weathering profiles (the 'African surfaces')?
- Erosion rates have been shown to decrease from >200 m to <20 m/Ma between the Cretaceous and the Cenozoic. Is this simply linked to global paleo-climate cooling?
- Along the coastal region, wave-cut platforms and overlying marine deposits are preserved at various elevations, up to 330 masl. Can they be coupled to paleo-sea level changes and/or limited regional subsidence and uplift? How can we distinguish between the two?
- How much of the inland topography, river canyons, valleys and soil erosion have been shaped by sea-level fluctuations? Can modern genetics of coastal flora and fauna help provide a high-resolution age dating of these events?

- How can geo-bio-scientists contribute towards developing a robust natural baseline of the Karoo before and during likely shale gas exploration in the near future, across this iconic landscape? If exploration is successful, development of unconventional gas industries will have a major effect on this receiving laboratory and its communities.

Port Elizabeth, South Africa — Bastien Linol
May 2016 — Maarten J. de Wit

References

Aarnes I, Svensen H, Polteau S and Planke S (2011) Contact metamorphic devolatilization of shales in the Karoo Basin, South Africa, and the effects of multiple sill intrusions. Chem Geol 281: 181–194.

Andreoli MAG, Doucouré M, Van Bever Donker J, Brandt D and Andersen NJB (1996) Neotectonics of southern Africa. Afr Geosci Rev 3: 1–16.

Andersen T, Kristoffersen M and Elburg MA (2016) How far can we trust provenance and crustal evolution information from detrital zircons? A South African case study. Gondwana Res 34: 129–148, doi:10.1016/j.gr.2016.03.003.

Avigad D, Kolodner K, McWilliams M, Persing H and Weissbrod T (2003) Origin of northern Gondwana Cambrian sandstone revealed by detrital zircon SHRIMP dating. Geology 31(3): 227, http://dx.doi.org/10.1130/0091-7613(2003)031<0227:OONGCS>2.0.CO;2.

Ben-Avraham Z, Hartnady CJH and Kitchin KA (1997) Structure and tectonics of the Agulhas–Falkland fracture zone. Tectonophysics 282(1): 83–98.

Bierman PR, Coppersmith R, Hanson K, Neveling J, Portenga EW and Rood DH (2014) A cosmogenic view of erosion, relief generation and the age of faulkting in southern Africa. GSA today 24: 4–11, doi:10.1130/GSATG206A.1.

Bird P, Ben-Avraham Z, Schubert G, Andreoli M and Viola G (2006) Patterns of stress and strain rate in southern Africa. J Geophys Res Solid Earth (1978–2012) 111(B8).

Black D, Booth P and de Wit M (2016) Petrographic, geochemical and petro-physical analysis of the Collingham Formation near Jansenville, Eastern Cape, South Africa—potential cap rocks to shale gas in the Karoo. S Afri J Geol 119(1), doi:10.2113/gssajg.119.1.0.

Booth PWK (2011) Stratigraphic, structural and tectonic enigmas associated with the Cape Fold Belt: challenges for future research. S Af J Geol 114(3-4): 235-248.

Booth PWK and Shone RW (2002) A review of thrust faulting in the Eastern Cape Fold Belt, South Africa, and the implications for current lithostratigraphic interpretation of the Cape Supergroup. J Afr Earth Sci 34: 179–190.

Booth PWK, Brunsdon G and Shone RW (2004) A Duplex Model for the Eastern Cape Fold Belt? Evidence from the Palaeozoic Witteberg and Bokkeveld Groups (Cape Supergroup), Near Steytlerville, South Africa. Gondwana Res 7(1): 211–222.

Booth PWK and Goedhart ML (2014) Thrust faulting in the northernmost foreland zone of the Cape Fold Belt, Fort Beaufort, Eastern Cape, South Africa. S Afri J Geol 117(2): 301–315.

Branch T, Ritter O, Weckmann U, Sachsenhofer RF and Schilling F (2007) The Whitehill Formation—a high conductivity marker horizon in the Karoo Basin. S Afr J Geol 110: 465–476.

Braun J, Guillocheau F, Robin C, Baby G and Jelsma H (2014) Rapid erosion of the Southern African Plateau as it climbs over a mantle superswell. J Geophys Res 119(7): 6093–6112.

Brown RW, Rust DJ, Summerfield MA, Gleadow AJ and de Wit MC (1990) An Early Cretaceous phase of accelerated erosion on the south-western margin of Africa: Evidence from apatite fission track analysis and the offshore sedimentary record. Int J Rad Appl Instrum D. Nuclear Tracks and Radiation Measurements 17(3): 339–350.

Brown RW, Gallagher K and Duane M (1994) A quantitative assessment of the effects of magmatism on the thermal history of the Karoo sedimentary sequence. J Afr Earth Sci 18(3): 227–243.

Brown RW, Gallagher K, Gleadow AJ and Summerfield MA (2000) Morphotectonic evolution of the South Atlantic margins of Africa and South America. In: Summerfield MA (ed) Geomorphology and global tectonics, John Wiley and Sons Ltd, p 255–281.

Brown RW, Summerfield MA, Gleadow AJW (2002) Denudation history along a transect across the Drakensberg Escarpment of southern Africa derived from apatite fission track thermochronology. J Geophys Res 107(B12), 2350, http://dx.doi.org/10.1029/2001JB000745.

Brown R, Summerfield M, Gleadow A, Gallagher, K, Carter A, Beucher R and Wildman M (2014) Intracontinental deformation in southern Africa during the Late Cretaceous. J Afr Earth Sci 100: 20–41.

Burgess SD, Bowring SA, Fleming TH and Elliot DH (2015) High-precision geochronology links the Ferrar large igneous province with early-Jurassic ocean anoxia and biotic crisis. Earth Planet Sci Lett 415: 90–99.
Burke K and Gunnell Y (2008) The African Erosion Surface: A Continental-Scale Synthesis of Geomorphology, Tectonics and Environmental Change over the Past 180 Million Years. Geol Soc Am Mem 201. GSA, Boulder.
Burke K and Torsvik TH (2004) Derivation of large igneous provinces of the past 200 million years from long-term heterogeneities in the deep mantle. Earth Planet Sci Lett 227: 531–538.
Castillo P, Fanning CM, Hervé F and Lacassie JP (2015) Characterisation and tracing of Permian magmatism in the south-western segment of the Gondwanan margin; U–Pb age, Lu–Hf and O isotopic compositions of detrital zircons from metasedimentary complexes of northern Antarctic Peninsula and western Patagonia. Gondwana Res, http://dx.doi.org/10.1016/j.gr.2015.07.014.
Catuneanu O, Hancox P and Rubidge B (1998) Reciprocal flexural behaviour and contrasting stratigraphies: a new basin development model for the Karoo retroarc foreland system South Africa. Basin Res 10(4): 417–439.
Catuneanu O, Wopfner H, Eriksson PG, Cairncross B, Rubidge BS, Smith RMH and Hancox PJ (2005) The Karoo basins of south-central Africa. J Afr Earth Sci 43(1-3): 211–253.
Chere N (2010) Geology and geochemistry of breccia pipes in the Karoo Basin, South Africa. Unpublished Honours thesis, University of Cape Town.
Chere N (2015) Sedmentological and geochemical investigations on borehole cores of the Lower Ecca Group black shales, for their gas potential—Karoo Basin, South Africa. Unpublished Master thesis, Nelson Mandela Metropolitan University.
Chevallier L and Woodward AC (1999) Morpho-tectonics and mechanism of emplacement of the dolerite rings and sills of the western Karoo, South Africa. S Afr J Geol 102: 43–54.
Chevallier L, Gibson LA, Nhleko LO, Woodford AC, Nomquphu W and Kippie I (2004) Hydrogeology of fractured-rock aquifers and related ecosystems within the qoqodala dolerite ring and sill complex, Great Kei catchment, Eastern Cape. WRC Report No.1238/1/04.
Cockburn HAP, Brown RW, Summerfield MA and Seidl MA (2000) Quantifying passive margin denudation and landscape development using a combined fission-track thermochronology and cosmogenic isotope analysis approach. Earth Planet Sci Lett 179(3): 429–435.
Cole DI (1992) Evolution and development of the Karoo Basin. In: De Wit MJ and Ransome ID (eds) Inversion tectonics of the Cape Fold Belt, Karoo and Cretaceous basins of Southern Africa. Balkema, Rotterdam, p. 87–100.
Cowling RM, Procheş S and Partridge TC (2009) Explaining the uniqueness of the Cape Flora: incorporating geomorphic evolution as a factor for explaining its diversification. Molecular Phylogenetics and Evolution 51: 64–74.
Cox KG (1978) Flood basalts, subduction, and the break-up of Gondwanaland. Nature 274: 47–49.
Cox KG (1988) The Karoo Provence. In: Macdougall JD (ed) Continental Flood Basalts. Kluwer Acadenic Publishers, Dordrecht, p. 239–271.
Cox SC, Menzies CD, Sutherland R, Denys PH, Chamberlain C and Teagle DAH (2015) Changes in hot spring temperature and hydrogeology of the Alpine Fault hanging wall, New Zealand, induced by distal South Island earthquakes. Geofluids 15(1-2): 216–239, doi:10.1111/gfl.12093.
Dhansay T, de Wit M and Patt A (2014) An evaluation for harnessing low-enthalpy geothermal energy in the Limpopo Province, South Africa. S Afr J Sci 110 (3/4), Art. #2013-0282, 10 pages, http://dx.doi.org/10.1590/sajs.2014/20130282.
Decker JE, Niedermann S and de Wit MJ (2011) Soil erosion rates in South Africa compared with cosmogenic 3He-based rates of soil production. S Afr J Geol 114: 475–488 (Spec Inkaba yeAfrica).
Decker J and Marot J (2012) Investigation of hydraulic fracturing in the Karoo of South Africa. Annexure A: Resource Assessment. Petroluem Agency SA, http://www.dmr.gov.za/publications/viewdownload/182/854.html.
Decker JE, Niedermann S and de Wit MJ (2013) Climatically influenced denudation rates of the southern African plateau: Clues to solving a geomorphic paradox. Geomorphology 190: 48–60.
De Wit MJ (2007) The Kalahari Epeiorogeny and climate change: differentiating cause and effect from Core to Space. S Afr J Geol 110: 367–392 (Spec Inkaba yeAfrica).
De Wit MJ (2011) The great shale debate in the Karoo. S Afr J Sci 107(7-8) Art. #791, 9 pages, doi:10.4102/sajs.v107i7/8.791.
De Wit MJ and Ransome I (eds) (1992) Inversion Tectonics of the Cape Fold Belt, Karoo and Cretaceous Basins of Southern Africa, Balkema, Rotterdam. ISBN 90 54 10 0478.
Diamond RE and Harris C (2000) Oxygen and hydrogen isotope geochemistry of thermal springs of the Western Cape, South Africa: recharge at high altitude? J Afr Earth Sci 31(3/4): 467–481.
Dingle RV, Siesser WG and Newton AR (1983) Mesozoic and Tertiary Geology of Southern Africa. Balkema, Rotterdam, 375 pp.
Duane M and Brown R (1992) Geochemical open-system behaviour related to fluid flow and metamorphism in the Karoo Basin. In: De Wit MJ and Ransome ID (eds) Inversion tectonics of the Cape Fold Belt, Karoo and Cretaceous basins of Southern Africa. Balkema, Rotterdam, p. 127–140.
Duncan AR and Marsh JS (2006) The Karoo Igneous Province. In: Johnson MR, Anhaeusser CR and Thomas RJ (eds) The Geology of South Africa. Geol Soc S Afr, Johannesburg, p. 501–520.

Du Toit AL (1937) Our wandering continents. Oliver and Boyd, Edinburgh.
Du Toit AL (1954) The Geology of South Africa. Haughton and Boyd, London.
Eales HV, Marsh JS and Cox KG (1984) The Karoo Igneous Province: an Introduction. In: Erlank AJ (ed), Petrogenesis of the volcanic rocks of the Karoo Province. Spec Publ Geol Soc S Afr 13: 1–26.
Egle S (1996) Paleo-hydrology of the Cape Fold Belt and the Karoo Basin, South Africa. Unpublished PhD, University of Vienna, Austria.
Ellsworth WL (2013) Injection-induced earthquakes. Science 341: 1–7, doi:10.1126/SCIENCE.1225942.
Erlanger ED, Granger DE and Gibbon RJ (2012) Rock uplift rates in South Africa from isochron burial dating of fluvial and marine terraces. Geology 40: 1019–1022.
Erlank AJ (ed) (1984) Petrogenesis of the volcanic rocks of the Karoo Province. Spec Publ Geol Soc S Afr 13, 395 pp.
Faure K, de Wit MJ and Willis J (1995) Late Permian global coal hiatus linked to 13C-depleted CO2 flux into the atmosphere during the final consolidation of Pangea. Geology 23: 507–510.
Fildani A, Drinkwater NJ, Weislogel A, McHargue, T, Hodgson, DM and Flint SS (2007) Age Controls on the Tanqua and Laingsburg Deep-Water Systems: New Insights on the Evolution and Sedimentary Fill of the Karoo Basin, South Africa. J Sediment Res 77(11): 901–908.
Fleming A, Summerfield MA, Stone JOH, Fifield LK and Cresswell RG (1999) Denudation rates for the southern Drakensberg escarpment, SE Africa, derived from in-situ-produced cosmogenic 36Cl: initial results. J Geol Soc London 156: 209–212.
French SW and Romanowicz B (2015) Broad plumes rooted at the base of the Earth's mantle beneath major hotspots. Nature 525: 95–99.
Geel C, Schulz H-M, Booth P, de Wit MJ and Horsfield B (2013) Shale gas characteristics of Permian black shales in South Africa: results from recent drilling in the Ecca Group (Eastern Cape). Energy Procedia 40: 256–265.
Geel C, de Wit M, Booth P, Schulz H-M and Horsfield B (2015) Palaeo-environment, diagenesis and characteristics of Permian black shales in the Lower Karoo Supergroup flanking the Cape Fold Belt near Jansenville, eastern Cape, South Africa: Implications for the shale gas potential of the Karoo Basin. S Afr J Geol 118(3): 249–274.
Green PF, Duddy IR, Japsen P, Bonow JM and Malan JA (2016) Post-breakup burial and exhumation of the southern margin of Africa. Basin Res, doi:10.1111/bre.12167.
Guex J, Pilet S, Müntener O, Bartolini A, Spangenberg J, Schoene B, Sell B and Schaltegger U (2016) Thermal erosion of cratonic lithosphere as a potential trigger for mass-extinction. Nature Sci Rep 6: 23168, doi:10.1038/srep23168
Guglielmi Y, Cappa F, Avouac J-P, Henry P and Elsworth D (2015) Seismicity triggered by fluid injection–induced aseismic slip. Science 348: 1224–1226.
Guillocheau F, Rouby D, Robin C, Helm C, Rolland N, Carlier L, de Veslud C and Braun J (2012) Quantification and causes of the terrigeneous sediment budget at the scale of a continental margin: A new method applied to the Namibia-South Africa margin. Basin Res 24: 3–30.
Hälbich IW (1992) The Cape Fold Belt orogeny: state of the art 1970s–1980s. In: de Wit MJ and Ransome ID (eds) Inversion tectonics of the Cape Fold Belt, Karoo and Cretaceous basins of Southern Africa. Balkema, Rotterdam, p. 141–158.
Hälbich IW, de Beer JH, du Plessis A, Dürrheim RJ, Maher MJ, Pitts BE and Smith G (1993) The Cape Fold Belt—Agulhas Bank Transect across the Gondwana Suture in Southern Africa. Global Science Transect 9. American Geophysical Union & Inter-union Commission on Lithosphere, Washington, USA.
Hansma J, Tohver E, Jourdan F, Schrank C and Adams D (2015) The Timing of the Cape Orogeny: New 40Ar/39Ar age constraints on deformation and cooling of the Cape Fold Belt, South Africa. Gondwana Res, doi:10.1016/j.gr.2015.02.005.
Haq BU, Hardenbol J and Vail PR (1987) Chronology of fluctuating sea levels since the Triassic. Science 235(4793): 1156–67.
Hildebrand RS (2009) Did westward subduction cause Cretaceous-Tertiary Orogeny in the North American Cordillera? Geol Soc Am Spec Pap 457, 71p.
Hildebrand RS (2013) Mesozoic Assembly of the North American Cordillera. Geol Soc Am Spec Pap 495, 169p.
Hildebrand RS (2015) Geology, mantle tomography, and inclination corrected paleogeographic trajectories support westward subduction during Cretaceous orogenesis in the North American Cordillera. In: Hibbard JP, Pollock JC, Murphy JB, van Staal CR and Greenough JD (eds) Reeltime Geological Syntheses—Remembering Harold 'Hank' Williams. Geoscience Canada Reprint Series 10, p. 439–456.
Hoffmann V, Verboom GA and Cotterill FPD (2015) Dated Plant Phylogenies Resolve Neogene Climate and Landscape Evolution in the Cape Floristic Region. PLoS ONE 10(9): e0137847, doi:10.1371/journal.pone.0137847.
Hornbach MJ, DeShon HR, Ellsworth WL, Stump BW, Hayward C, Frohlich C, Oldham HR, Olson JE, Magnani MB, Brokaw C and Luetgert JH (2015) Causal factors for seismicity near Azle, Texas. Nature Comm 6, doi:10.1038/ncomms7728.
Isbell JL, Cole DI and Catuneanu O (2008) Carboniferous—Permian glaciation in the main Karoo Basin, South Africa: Stratigraphy, depositional controls, and glacial dynamics. In: Fielding CR, Frank TD and Isbell JL (eds) Resolving the Late Paleozoic Ice age in Time and Space. Geol Soc Am Spec Pap 441: 71–82.

Johnson ST (2000) The Cape fold belt and syntaxis and the rotated Falkland Islands: dextral transpressional tectonics along the southwest margin of Gondwana. J Afr Earth Sci 31: 51–63.
Keen-Zebert A, Tooth S and Stuart FM (2016) Cosmogenic 3He measurements provide insight into lithologic controls on bedrock channel incision: examples from the South African interior. J Geol 124, doi:10.1086/685506.
King LC (1942) South African Scenery—a textbook of geomorphology. Oliver and Boyd Ltd. Edinburg and London.
King LC (1951) South African Scenery, Second ed. Oliver and Boyd, Edinburgh.
King LC (1953) Canons of landscape evolution. Geol Soc Am Bull 64: 721–751.
King LC (1967) Morphology of the Earth, Second ed. Oliver and Boyd, Edinburgh.
Kounov A, Niedermann S, de Wit MJ, Viola G, Andreoli M and Erzinger J (2007) Present denudation rates across selected sections of the South African escarpment based on cosmogenic 3He and 21Ne. S Afr J Geol 110: 235–248.
Kounov A, Viola G, de Wit MJ and Andreoli M (2008) A Mid Cretaceous paleo-Karoo River valley across the Knersvlakte plain (northwestern coast of South Africa): Evidence from apatite fission-track analysis. S Afr J Geol 111(4): 409–420.
Kounov A, Viola G, Dunkl I and Frimmel HE (2013) Southern African perspectives on the long-term morphotectonic evolution of cratonic interiors. Tectonophysics, 601: 177–191.
Kounov A, Niedermann S, de Wit MJ, Viola G, Andreoli M, Codilean AT and Kubik PW (2015) Cosmogenic 21Ne and 10Be Reveal a more than 2 Ma Alluvial Fan flanking the Cape Mountains, South Africa. S Afr J Geol 118: 129–144, doi:10.2113/gssajg.118.2.129.
Lindeque AS, Ryberg T, Stankiewicz J, Weber MH and de Wit MJ (2007) Deep crustal seismic reflection experiment across the southern Karoo Basin, South Africa. S Afr J Geol 110: 419–438.
Lindeque A, de Wit MJ, Ryberg T, Weber M and Chevallier L (2011) Deep Crustal Profile across the Southern Karoo Basin and Beattie Magnetic Anomaly, South Africa: an Integrated Interpretation with Tectonic Implications. S Afr J Geol 114(3–4): 265–292.
Linol B, de Wit MJ, Milani EJ, Guillocheau F, Scherer C (2015) Chapter 13: New regional correlations between the Congo, Paraná and Cape-Karoo Basins of southwest Gondwana. In: de Wit MJ, Guillocheau, F, de Wit MJC (eds) The Geology and Resource Potential of the Congo Basin, Regional Geology Reviews. Springer-Verlag, Berlin Heidelberg, pp. 246–268, http://dx.doi.org/10.1007/978-3-642-29482-2_13.
Linol B, de Wit MJ, Barton E, de Wit MJC and Guillocheau F (2016). U-Pb detrital zircon dates and source provenance analysis of Phanerozoic sequences of the Congo Basin, central Gondwana. Gondwana Res 29(1): 208–219, doi:10.1016/j.gr.2014.11.009.
Lock BE, Paverd AL and Broderick TJ (1974) Stratigraphy of the Karoo volcanic rocks of the Barkly East District. Trans Geol Soc S Afr 77: 117–129.
Lock BE (1980) Flat-plate subduction and the Cape Fold Belt of South Africa. Geology 8: 35–39.
López-Gamundí and Buatois (eds) (2010) Late Paleozoic Glacial Events and Postglacial Transgressions in Gondwana. Geol Soc Am Spec pap 468, 207p.
McGarr A (2014) Maximum magnitude earthquakes induced by fluid injection. J Geophys Res Solid Earth 119: 1008–1019, doi:10.1002/2013JB010597.
McPhee B, Mannion PD, de Klerk WJ and Choiniere JN (2016) High diversity in the sauropod dinosaur fauna of the Lower Cretaceous Kirkwood Formation of South Africa: Implications for the Jurassic-Cretaceous transition. Cretaceous Res 59: 228–248.
Menzies CD, Teagle DAH, Niedermann S, Cox SC, Craw D, Zimmer M, Cooper MJ and Erzinger J (2016) The fluid budget of a continental plate boundary fault: Quantification from the Alpine Fault, New Zealand. Earth Planet Sci Lett, http://dx.doi.org/10.1016/j.epsl.2016.03.046.
Milani EJ and de Wit MJ (2008) Correlations between the classic Paraná and Cape Karoo sequences of South America and southern Africa and their basin infills flanking the Gondwanides: du Toit revisited. In: Pankurst RJ, Trouw RAJ, Brito Neves BB and de Wit MJ (eds) West Gondwana: Pre-Cenozoic Correlations Across the South Atlantic Region. Geol Soc London Spec Publi 294: 319–342.
Miller KG, Mountain GS, Wright JD and Browning JV (2011) A 180-million-year record of sea level and ice volume variations from continental margin and deep-sea isotopic records. Oceanography 24(2): 40–53, doi:10.5670/oceanog.2011.26.
Miller W, Armstrong R and de Wit MJ (2016) Geology and U/Pb geochronology of the Gamtoos Complex and lower Paleozoic Table Mountain Group, Cape Fold Belt, Eastern Cape, South Africa. S Afri J Geol 119(1), doi:10.2113/gssajg.119.1.0.
Milleson M, Myers TS and Tabor NJ (2016) Permo-carboniferous paleoclimate of the Congo Basin: Evidence from lithostratigraphy, clay mineralogy, and stable isotope geochemistry. Palaeogeogr Palaeoclimatol Palaeoecol 441: 26–240, http://dx.doi.org/10.1016/j.palaeo.2015.09.039.
Mthembi P, Roberts DL and Harris C (2016) Chemical stratigraphy of lake deposits from the Kalkkop Impact Crater, South Africa, and its palaeoenvironmental significance. S Afr J Geol 119(1): 215–230.
Muedi TT (2014) Cretaceous dyke swarms and brittle deformation structures in the upper continental crust flanking the Atlantic and Indian margins of Southern Africa, and their relationship to Gondwana break-up. Unpublished Master thesis, Nelson Mandela Metropolitan University.
Müller RD, Sdrolias M, Gaina C, Steinberger B and Heine C (2008) Long-term sea-level fluctuations driven by ocean Basin Dynamics. Science 319: 1357–1362.

Nguuri TK, Gore J, James DE, Webb SJ, Wright C, Zengeni TG, Gwavava O, Snoke JA, Kaapvaal Seismic Group (2001) Crustal structure beneath southern Africa and its implications for the formation and evolution of the Kaapvaal and Zimbabwe cratons. Geophys Res Lett 28(13): 2501–2504, doi:10.1029/2000GL012587.

Nicolaysen LO (1985) On the physical basis for the extended Wilson cycle, in which most continents coalesce and then disperse again. S Afr J Geol 88: 562–580.

Parsiegla N, Stankiewicz J, Gohl K, Ryberg T and Uenzelmann-Neben G (2009) Southern African continental margin: dynamic processes of a transform margin. Geochem Geophy Geosy 10, Q03007, doi:10.1029/2008GC002196.

Partridge TC (1998) Of diamonds, dinosaurs and diastrophism: 150 million years of landscape evolution in southern Africa. S Afr J Geol 101: 167–184.

Partridge TC and Maud RR (1987) Geomorphic evolution of southern Africa since the Mesozoic. S Afr J Geol 90: 179–208.

Paulsen TS, Encarnación J, Grunow AM, Layer PW and Watkeys M (2007) New age constraints for a short pulse in Ross orogeny deformation triggered by East-West Gondwana suturing. Gondwana Res 12: 417–427.

Polteau S, Ferre EC, Planke S, Neumann E-R and Chevallier L (2008) How are saucer-shaped sills emplaced? Constraints from the Golden Valley Sill, South Africa J Geophy Res 113, B12104, doi:10.1029/2008JB005620.

Ramos VA (2008) Patagonia: a Paleozoic continent adrift? J South Amer Earth Sci 26(3): 235–251.

Reeves C (1972) Rifting in the Kalahari? Nature 237(5350): 95–96.

Rothman DH, Fournier GP, French KL, Alm EJ, Boyle EA, Cao C and Summons RE (2014) Methanogenic burst in the end-Permian carbon cycle. PNAS 111(15): 5462–5467. www.pnas.org/cgi/doi/10.1073/pnas.1318106111.

Rowley DB (2013) Sea level: Earth's dominant elevation—Implications for duration and magnitudes of sea level variations. J Geol 121: 445–454, doi:10.1086/671392.

Rubidge BS (2005) Re-uniting lost continents—Fossil reptiles from the ancient Karoo and their wanderlust. S Afr J Geol 108(1): 135–172, doi:10.2113/108.1.135.

Rubidge B and McCarthy T (eds) (2005) The Story of Earth & Life. SBN: 9781770071483.

Scharf TE, Codilean AT, de Wit M, Jansen JD and Kubik PW (2013) Strong rocks sustain ancient postorogenic topography in southern Africa. Geology 41: 331–334.

Schofield N, Stevenson C and Reston T (2010) Magma fingers and the importance of host rock fluidization in sill emplacement. Geology 38: 63–66.

Scotese CR (2014) PaleoAtlas for ArcGIS, PALEOMAP Project, Evanston, IL.

Sell B, Ovtcharova M, Guex J, Bartolini A, Spangenberg JE, Vicente J-C and Schaltegger U (2014) Evaluating the temporal link between the Karoo LIP and climatic-biologic events of the Toarcian Stage with high-precisaion U-Pb geochronology. Earth Planet Sci Lett 408: 48–56.

Shone RW and Booth PWK (2005) The Cape Basin, South Africa: a review. J Af Earth Sci, 43(1-3): 196–210.

Singh M, Kijko A and Durrheim R (2011) Seismotectonic Models for South Africa: Synthesis of Geoscientific Information, Problems, and the Way Forward. Seismol Res Lett 80(1): 71–80, doi:10.1785/gssrl.80.1.71.

Smit L, Fagereng A, Braeuer B and Stankiewicz J (2015) Microseismic Activity and Basement Controls on an Active Intraplate Strike-Slip Fault, Ceres–Tulbagh, South Africa. Bull Seismol Soc Am 105(3), doi:10.1785/0120140262.

Smith RMH (1987) Helical burrow casts of therapsid origin from the Beaufort Group (Permian) of South Africa. Palaeogeog Palaeoclimatol Palaeoecol 60: 155–170.

Smith RMH and Evans SE (1996) New material of Youngina (Reptilia: Diapsida) and evidence for juvenile aggregation in Permian diapsids. Palaeontology 39(2): 289–303.

Söhnge APG and Hälbich IW (1983) Geodynamics of the Cape Fold Belt. Geol Soc S Afr Spec Publ 12, 184p.

Stankewicz J, Ryberg T, Schultze A, Lindeque A, Weber MH and de Wit MJ (2007) Initial results from the wide-angle seismic refraction lines in the southern Cape. Inkaba yeAfrica special volume, S Afr J Geol 110: 407–418, doi:10.2113/gssajg.110.2/3.407.

Stankiewicz J, Parsiegla N, Ryberg T, Gohl K, Weckmann U, Trumbull R and Weber M (2008) Crustal Structure of the Southern Margin of the African Plate: results from geophysical experiments. J Geophys Res 113: B103103.

Stanley JR, Flowers RM and Bell DR (2013) Kimberlite (U-Th)/He dating links surface erosion with lithospheric heating, thinning, and metasomatism in the southern African Plateau. Geology 41: 1243–1246.

Steinberger B and Torsvik TH (2012) A geodynamic model of plumes from the margins of Large Low Shear Veolocity Provinces. Geochem Geophys Geosyst 13(1): Q01W09, doi:10.1029/2011GC003808.

Stern CR and de Wit MJ (2004) Rocas Verdes ophiolite, southernmost South America: remnants of progressive stages of development of oceanic type crust in a continental back arc basin. In: (de Dilek Y and Robinson PT). Geol Soc London Spec Publ 218: 665–683.

Sullivan C, Reisz R and Smith RMH (2003) The Permian mammal-like herbivore Diictodon, the oldest known example of sexually dimorphic armament. Proc R Soc London B 270: 173–178.

Summerfield MA (1985) Plate tectonics and landscape evolution on the African continent. In: Morisawa M amd Hack JT (eds) Tectonic Geomorphology. Allen and Unwin, Concordia.

Svenson H, Jamtveit B, Planke S and Chevallier L (2006) Structure and evolution of hydrothermal vent complexes in the Karoo Basin, South Africa. J Geol Soc London 163 (4): 671–682.

Svenson H, Planke S, Chevallier L, Malthe-Sorenssen A, Corfu F and Jamtviet B (2007) Hydrothermal Venting of Greenhouse Gases Triggering Early Jurassic Global Warming. Earth Planet Sci Lett 256: 554–266.

Svenson H, Corfu F, Ploteau S, Hammer O and Planke S. (2012) Rapid magma emplacement in the Karoo Large igneous Province. Earth Planet Sci Lett 325/326: 1–9.

Swartz ER, Skelto PH and Bloomer P (2007) Sea-level changes, river capture and the evolution of populations of the Eastern Cape and fiery redfins (*Pseudobarbus afer* and *Pseudobarbus phlegethon*, Cyprinidae) across multiple river systems in South Africa. J Biogeogr 34(12): 2086–2099, doi:10.1111/j.1365-2699.2007.01768.x.

Tankard A, Welsink H, Aukes P, Newton R and Stettler E (2009) Tectonic evolution of the Cape and Karoo basins of South Africa. Mar Pet Geol 26(8): 1379–1412.

Tankard A,Welsink H, Aukes, P, Newton R and Stattker E (2012) Chapter 23: geodynamic interpretation of the Cape and Karoo basins, South Africa. In: Roberts DG and Bally AW (eds) Phanerozoic Passive Margins, Cratonic Basins and Global Tectonics Maps. Elsevier, Amsterdam, p. 869–945.

Tinker J, de Wit M and Brown R (2008a) Mesozoic exhumation of the southern Cape, South Africa, quantified using apatite fission track thermochronology. Tectonophysics 455(1): 77–93.

Tinker J, de Wit MJ and Brown R (2008b) Linking source and sink: Evaluating the balance between onshore erosion and offshore sediment accumulation since Gondwana break-up, South Africa. Tectonophysics 455(1): 94–103.

Torsvik TH, Burke K, Steinberger B, Webb SC and Ashwal LD (2010) Diamonds sourced by plumes from the core mantle boundary. Nature 466, doi:10.1038/nature09216352.

Turner BR (1978) Sedimentary patterns of Uranium mineralisation in the Beaufort Group of the Southern Karoo (Gondwana) Basin, South Africa. In: Miall AD (ed) Fluvial Sedimentology, vol. 5. Canadian Soc Pet Geol Memoir, p. 831–848.

Turner BR (1983) Braidplain deposition of the upper Triassic Molteno formation in the main Karoo (Gondwana) basin, South Africa. Sedimentology 30: 77–89.

Turner BR (1990) Continental sediments in South Africa. J Afr Earth Sci 10: 139–149.

Uenzelmann-Neben G, Tobias W, Jens G and Maik T (2016) Transition from the Cretaceous ocean to Cenozoic circulation in the western South Atlantic—A twofold reconstruction. Tectonophysics. http://dx.doi.org/10.1016/j.tecto.2016.05.036.

Van der Beek P, Mbede E, Andriessen P and Delvaux D (1998) Denudation history of the Malawi and Rukwa Rift flanks (East African Rift System) from apatite fission track thermochronology. J Afr Earth Sci 26(3): 363–385.

Van der Elst NJ, Savage HM, Keranen KM and Abers GA (2013) Enhanced Remote Earthquake Triggering at Fuid-Injection Sites in the Midwestern United States. Science 341:164–167.

Van der Elst NJ, Page MT, Weiser DA, Goebel THW and Hosseini SM (2016) Induced earthquake magnitudes are as large as (statistically) expected. J Geophys Res Solid Earth 121(6): 4575–4590, doi:10.1002/2016JB012818.

Verboom GA, Archibald JK, Bakker, FT, Bellstedt DU, Ferozah C, Dreyer LL, Forest F, Galley C, Goldblatt P, Henning JF, Mummenhoff K, Linder HP, Muasya AM, Oberlander KC, Savolainen V, Snijman DA, van der Niet T and Nowell TL (2009) Origin and diversification of the Greater Cape flora: Ancient species repository, hot-bed of recent radiation, or both? Molecular Phylogenetics and Evolution 51: 44–53, doi:10.1016/j.ympev.2008.01.037.

Walker RJ (2016) Controls on transgressive sill growth. Geology 44: 99–102.

Walsh III FR and Zobach MD (2015) Oklahoma's recent earthquakes and saltwater disposal. Science Advances 1(5) e1500195, doi:10.1126/sciadv.1500195.

Walters RJ, Zoback MD, Baker JW and Beroza GC (2015) Characterizing and Responding to Seismic Risk Associated with Earthquakes Potentially Triggered by FluidDisposal and Hydraulic Fracturing. Seismol Res Lett 86(4): 1–9, doi:10.1785/0220150048.

Weckmann U, Ritter O, Jung A, Branch T and de Wit M (2007a) Magnetotelluric measurements across the Beattie magnetic anomaly and the Southern Cape Conductive Belt, South Africa, J Geophys Res 112, B05416, doi:10.1029/2005JB003975.

Weckmann U, Jung A, Branch T and Ritter O (2007b) Comparison of electrical conductivity structures and 2D magnetic modelling along two profiles crossing the Beattie Magnetic Anomaly, South Africa. S Afr J Geol 110: 449–464.

Weckmann U, Ritter O, Chen X, Tietze K and de Wit M (2012) Magnetotelluric image linked to surface geology across the Cape Fold Belt, South Africa. Terra Nova 24(2): 207–212, doi:10.1111/j.1365-3121.2011.01054.

Wildman M, Brown R, Watkins R, Carter A, Gleadow A and Summerfield M (2015) Post break-up tectonic inversion across the southwestern cape of South Africa: New insights from apatite and zircon fission track thermochronometry. Tectonophysics 654: 30–55.

Wildman M, Brown R, Beucher R, Persano C, Stuart F, Gallagher K, Schwanethal J and Carter A (2016) The chronology and tectonic style of landscape evolution along the elevated Atlantic continental margin of South Africa resolved by joint apatite fission track and (U-Th-Sm)/He thermochronology. Tectonics, doi:10.1002/2015TC004042.

Acknowledgements

This Cape-Karoo book emerged from a recent '*Imbizo*' organized by AEON-ESSRI at the Nelson Mandela Metropolitan University (recently renamed NMU-Nelson Mandela University) in Port Elizabeth (NMMU) between 23rd–30th November 2016. The goal was for geoscientists to share knowledge and to collaborate and, together, contribute towards advancing research and development in the Karoo Basin and flanking Cape Mountains.

Ninety-one participants attended the 3-days conference, dominated by students and academics from South African universities (NMMU/NMU, Cape Town, Western Cape, Stellenbosch, Johannesburg, Witwatersrand, Pretoria, Free States), and professionals from natural museums (Rhodes, Iziko) and national agencies (Council for Geoscience, Petroleum Agency, PetroSA), and with participants from Norway, Germany and Brazil, as well as private (some retired) professionals from industry. This event resulted in 55 presentations and 15 posters covering a wide range of disciplines such as, but not limited to: subsurface geology and geophysics, structural geology, magmatism and metamorphism, sedimentology, paleontology, geochronology, petroleum systems, geomorphology and geodynamics. The conference was preceded by a 2-days workshop on oil and gas, focused on unconventional resources (shale-gas), and followed by 3-days field trip across the Eastern Cape region, from the Algoa coast near Port Elizabeth, through the Cape Mountains and vast areas of the Karoo hinterland, including the Kalkkop crator site, and the South African Great Escarpment in the vicinity of Graaff-Reinet. We would like to warmly thank all participants for their interactions and stimulated discussions. We hope that this book highlights some of their ongoing research and interdisciplinary discourse, as well as encourage and inspire new ideas to others.

We are grateful to the following for contributing to the Preface: John Anderson (SA), Emese Bordy (SA), Rod Brown (UK), Jonah Choiniere (SA), Rob Gess (SA), Conrad Labandeira (USA), Warren Miller (SA), Bruce Rubidge (SA) and Roger Smith (SA).

In addition, we would like to sincerely thank the following referees for their peer reviews of the chapters in this book:

John Anderson, AEON, Nelson Mandela Metropolitan University, South Africa
David Bell, AEON, Nelson Mandela Metropolitan University, South Africa
Antoine Bercovici, Smithsonian Institution, Washington, USA
Peter Booth, Nelson Mandela Metropolitan University, South Africa
Emese Bordy, University of Cape Town, South Africa
Steffen Buettner, Rhodes University, South Africa
Mike Coates, University of Chicago, USA
Doug Cole, Council for Geoscience, South Africa
Mike Daly, Oxford University, UK
David Elliot, Ohio State University, USA
Chris Fielding, University of Nebraska-Lincoln, USA
Robert Gastaldo, Colby College, USA
Jan Kramers, University of Johannesburg, South Africa
Spencer Lucas, New Mexico Museum of Natural History and Science, USA
Mike Lynn, Newfield Resources, Perth, Australia

Gerrit Olivier, Institute of Mine Seismology, Tasmania, Australia
Bruce Rubidge, University of the Witwatersrand, South Africa
Hans-Martin Schulz, Helmholtz Research Centre for Geosciences—GFZ, Germany
Jacek Stankiewicz, European Centre for Geophysics and Seismology, Luxemburg
Jurie Viljoen, Council for Geoscience, South Africa

Financial support was provided by the NRF—National Research Foundation and the DST—Department of Science and Technology through the '*Iphakade'* programme, and UNESCO—United Nations Educational Scientific and Cultural Organization via the IGCP-628 Gondwana Project.

Port Elizabeth, South Africa — Bastien Linol
May, 2016 — Maarten J. de Wit

Contents

Part I
Subsurface Geology and Geophysics

1 Deep Borehole Lithostratigraphy and Basin Structure of the Southern Karoo Basin Re-Visited

Bastien Linol, Naledi Chere, Thomas Muedi, Vhuhwavhohau Nengovhela, and Maarten J. de Wit

Abstract

The lithostratigraphy and structure of the southern Karoo Basin is analyzed based on detailed re-logging of 11 deep boreholes drilled by SOEKOR in the 1960s. The Karoo Supergroup here is between 750 and 5540 m thick. The sequence starts with an extensive cover of glaciomarine and/or glaciolacustrine bedded diamictites with black shales of the mid-Carboniferous to Lower Permian Dwyka Group (353–744 m thick), capped by 79–569 m black shales of the lowermost Ecca Group deposited during rapid deglaciation that mark a relatively short-lived time horizon. The black shales are overlain by middle- to outer-fan turbidites in the southernmost deeper part of the basin that grade over a distance of 50 km northward into alternating dark gray silty shales with fine sandstones and carbonated mudstones characteristic of shallower shelf-slope deposits. The successions become regionally sandier and thicker bedded upward, implying a first-order regression that is marked by at least two second-order regressive surfaces, but the transition to the fluvial, Middle Permian to Triassic Beaufort Group cannot at this stage be mapped with confidence. In addition, along the southern margin, flanking the Cape Fold Belt, the Karoo successions are variably deformed, whilst farther north increasingly abundant dolerite sills intrude progressively to greater depths, all of which complicate unraveling the basin-wide stratigraphy.

Keywords

Karoo Supergroup • Borehole stratigraphy • Basin structure • Dolerite intrusions

1.1 Introduction

The Karoo Basin developed within the continental interior of Southwest Gondwana (Milani and de Wit 2008; Linol et al. 2015). It covers half of South Africa (ca. 600,000 km^2; Fig. 1.1) and preserves 3–6 km thick, mid-Paleozoic to Lower Jurassic sedimentary rock sequences that are in places duplicated along thrusts and folds along the southern margin of the basin, where it flanks the Cape Mountains; and to the north these sequences are widely intruded by dolerite sills and capped by basalts related to the eruption of the Karoo Large Igneous Province (LIP) at about 182 Ma during the initial break-up between East and West Gondwana (Aarnes et al. 2011; Burgess et al. 2015; Reeves et al. 2015). The general stratigraphy and basin structure is well known from field investigations and mapping (e.g., Cole 1992; Visser 1997; Johnson et al. 2006; Paton et al. 2006; Tankard et al. 2009; Spikings et al. 2015). However, there is little modern subsurface information available. In the 1960s, a number of seismic lines were acquired crossing the southern part of the basin (see Chap. 2 in this book), and 19 exploration wells of 1–5.5 km depth were drilled by SOEKOR—Southern Oil Exploration Corporation, now PASA (Winter and Venter 1970; Rowsell and de Swardt 1976; Cole 1977). This dataset was augmented by a more recent, near vertical, deep seismic

B. Linol (✉) · N. Chere · T. Muedi · V. Nengovhela · M.J. de Wit
AEON-ESSRI (African Earth Observatory Network-Earth Stewardship Research Institute), Port Elizabeth, South Africa
e-mail: Bastien.aeon@gmail.com

B. Linol · N. Chere · T. Muedi · V. Nengovhela
Geosciences, Nelson Mandela Metropolitan University, Port Elizabeth, South Africa

B. Linol and M.J. de Wit (eds.), *Origin and Evolution of the Cape Mountains and Karoo Basin*,
Regional Geology Reviews, DOI 10.1007/978-3-319-40859-0_1

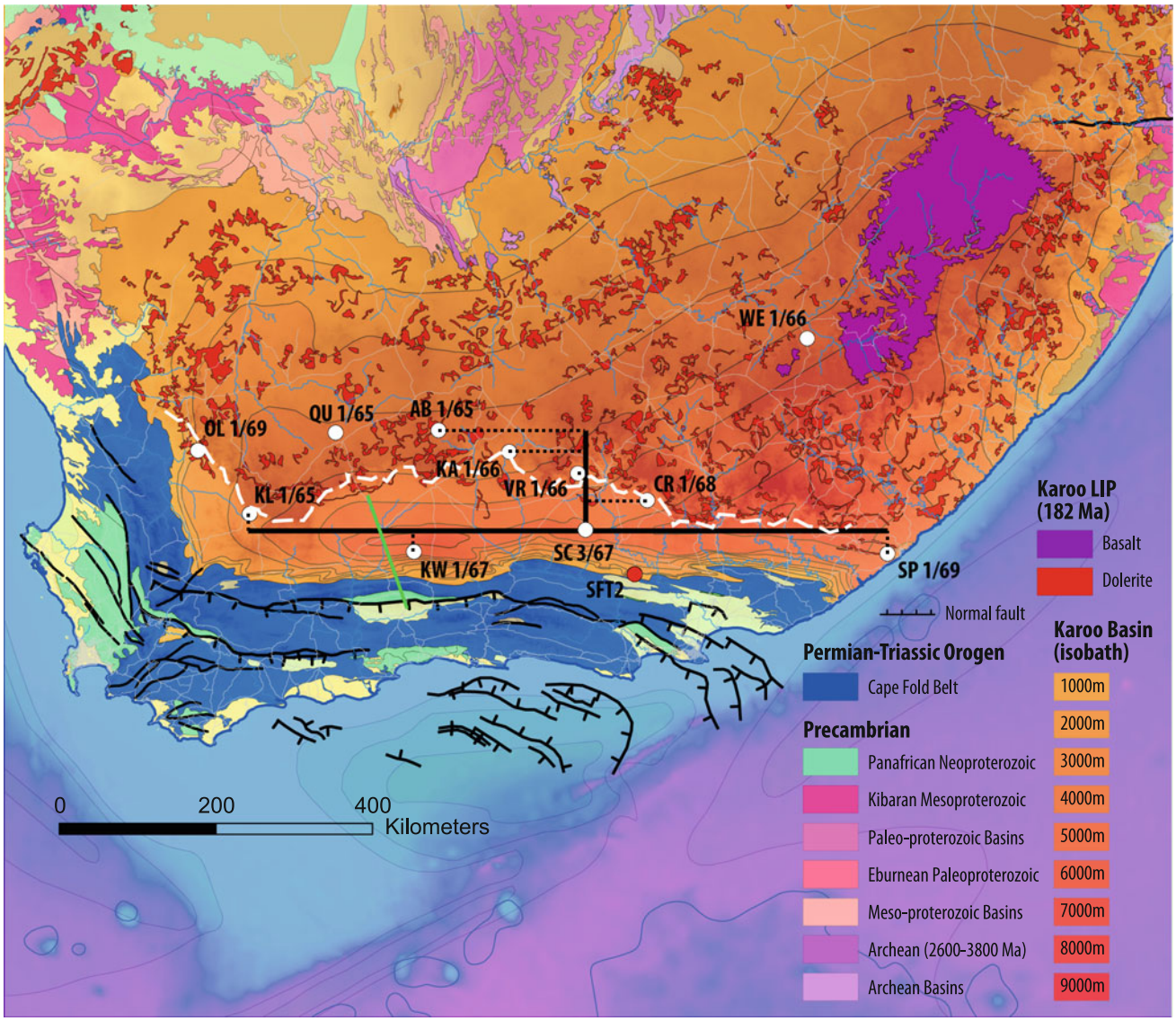

Fig. 1.1 Cape-Karoo geo-tectonic map of southern Africa, showing location of the studied deep boreholes (*white dots*) and correlation profiles (*black lines*), the Inkaba seismic line (*green line*) and AEON's shallow borehole (*red dot*). *White broken line* marks the general edge of the Great Escarpment

reflection profile (Fig. 1.2) of about 100 km across the southwestern Karoo (Lindeque et al. 2011). However, there is still considerable uncertainty about the stratigraphic position of the main sequences at formation and even group level, since calibration between the seismic and well-data (geological and geophysical) is poorly constrained. Traditionally, in the SOEKOR boreholes, the lower stratigraphic boundaries are defined above or below distinctive (black) shales, and upward at the first occurrence of thick (massive) sandstones and/or reddish (red, brown, or purple) shales. Here, we re-describe 11 SOEKOR deep boreholes to address some of these lithostratigraphic uncertainties, and propose preliminary sequence correlations across the southern Karoo Basin based on this new analysis.

1.2 The Cape and Karoo Supergroups

- Surface geology

The Paleozoic-Lower Mesozoic stratigraphic record of southernmost Africa is divided into the Cape and Karoo Supergroups, in turn subdivided into a number of groups and formations (SACS 1980; Shone and Booth 2005; Johnson et al. 2006). The lowermost Cape Supergroup ranges in age from mid-Cambrian (ca. <510 ± 6 Ma; Miller et al. 2016; Chap. 4 this book) to Upper Devonian, and comprises the Table Mountain, Bokkeveld and Witteberg Groups. These sequences consist, respectively, of thick quartz-rich sandstones (~2000–4500 m thick), alternating fine sandstones

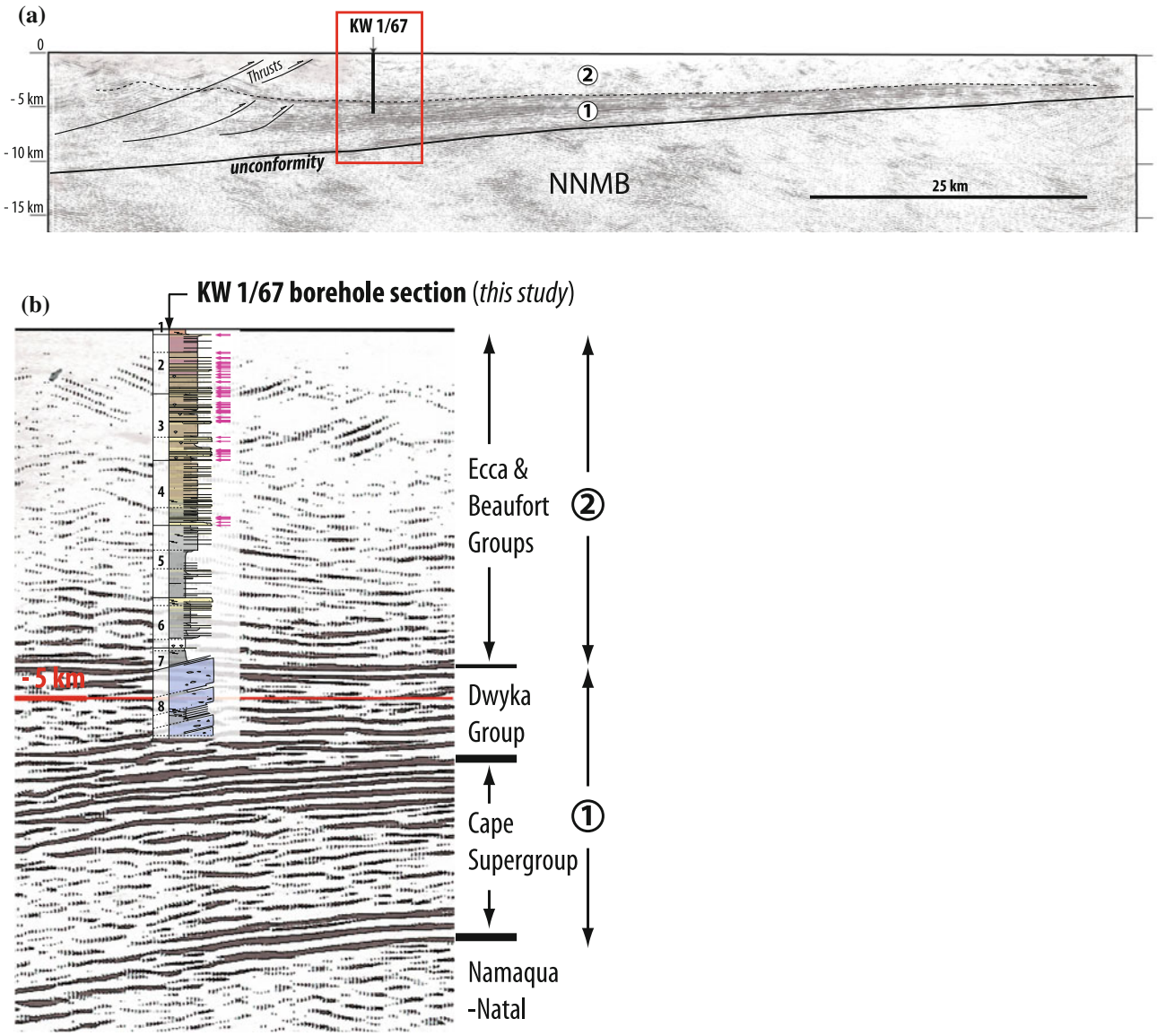

Fig. 1.2 **a** Seismic profile lyA-200501 across the southwestern Karoo Basin (from Lindeque et al. 2011), showing two major seismic-stratigraphic sequences (numbered 1 and 2) unconformably overlying the Namaqua-Natal Metamorphic Belt (NNMB) basement, and **b** calibration against KW 1/67 borehole (Fig. 1.1 for location)

with mudstones (~2200–3500 m thick), and quartzitic sandstones with micaceous mudrocks (~1200–1700 m thick), all deposited regionally from the north along a shallow continental shelf bordering the southwest passive margin of Gondwana (Thamm and Johnson 2006; Chap. 13 this book). Near the top of the Table Mountain quartzites, distinctive glacial deposits, known as the Pakhuis Formation, overlain by deglaciation shales of the Cedarberg Formation form a time horizon that represents the short-lived Late Ordovician glaciation-deglaciation of Gondwana, at about 444 Ma (Vandenbroucke et al. 2009; Rowe and Backeberg 2011). A sequence of younger, Lower Carboniferous glacial deposits separates the uppermost sequences of the Cape Supergroup from the overlying Karoo Supergroup. In the south, the basal contact of the glacial diamictites is a para-unconformity within the uppermost units of the Witteberg Group: the Waaipoort Formation west of longitude 23°E (Streel and Theron 1999), and the Kommadagga Subgroup, which includes diamictites of the Miller Formation, east of longitude 23°E (Thamm and Johnson 2006; Isbell et al. 2008). In the north of the Karoo Basin, an unconformity across Precambrian basement is associated with glacial

pavements, eskers and south-directed paleo-valleys (e.g., Blignault and Theron 2015; Chap. 9 this book), about 150 km to the north of the boreholes described here. The lowermost Karoo glacial sequences form the Dwyka Group, with maximum thicknesses between about 500 and 800 m in the southern part of the basin, and dated from mid-Carboniferous to the Lower Permian (Visser 1997; Bangert et al. 1999), a period when the paleo-South Pole was located some 2000 km east of the Karoo Basin (see Preface of this book). Here, the Dwyka Group comprises four to seven sequences that represent several episodes of advance and retreat of a Gondwana ice cap, terminated sharply by 50–320 m thick black shales of the Prince Albert Formation (formerly Upper Dwyka Shales; Winter and Venter 1970; Anderson 1977). This last deglaciation sequence forms the base of the Ecca Group, dated just before 288–291 Ma based on U-Pb dates of magmatic zircons from thin tuffs found near the base (Bangert et al. 1999; Werner 2006), and with its deposition being genetically linked to the termination of the Dwyka glaciation (Chap. 11 this book). Tillites, diamictites, and deglaciation black shales are in turn overlain by distinctive, white weathered, organic-rich black shales of the Whitehill Formation, maximum 30–80 m thick, followed by rhythmites that contain chert beds (the Collingham Formation, 30–70 m thick; Black et al. 2016) and thick turbidites (e.g., the Ripon, Tierberg, Vischkuil, and Laingsburg Formations; each varying between about 100 and 900 m thick), all of which have abundant volcanic air-fall tuffs dated between 250 and 276 Ma (Fildani et al. 2007; Flint et al. 2011; McKay et al. 2015). However, the younger dates are controversial, because dates of between 255 and 268 Ma have derived also from tuffs in the overlying lower Beaufort Group (Lanci et al. 2013; Rubidge et al. 2013); and because of the presence of Early Triassic fossil reptile *Lystrosaurus* in the basal upper Beaufort Group sediments (Groenewald and Kitching 1995; Chap. 14 this book). Both the Ecca turbidites and the overlying fluvial sediments of the Beaufort Group (in total more than ~4000 m thick) derived predominantly from the south (Cole 1998), relate to the Cape Orogeny active at 253 Ma (Hansma et al. 2015; Chap. 5 this book). Evidence of synsedimentary tectonism, such as sedimentary cannibalism, scours and giant flute casts, can be observed around the Permian-Triassic transition (e.g., the Lootsberg Pass; see Preface of this book). Across the northern and central parts of the basin, the successions are intruded by a suite of dolerite dykes and shallow sill complexes of the Lower Jurassic Karoo LIP (e.g., Duncan et al. 1997; Aarnes et al. 2011; Svensen et al. 2012). These widely outcropping dolerite sills presently define the Great Escarpment that transgresses across the Southern Karoo (Fig. 1.1).

- Subsurface geophysics

Only a single high-resolution seismic section is available, and in which two seismic supersequences are observed (Fig. 1.2a). A lower supersequence of dark reflectors between 1 and 7 km thick corresponds to the combined Cape Supergroup and Dwyka Group, as calibrated from the adjacent KW 1/67 borehole (Fig. 1.2b). In the south-central section, these (lower and mid-Paleozoic) sequences are subhorizontal, thin northward, but are duplicated along shallow listric faults to the south forming the tectonic front of the Cape Fold Belt (Lindeque et al. 2011; Spikings et al. 2015). An upper, seismically more transparent supersequence, between 2.5 and 5 km thick, corresponds to the Permian-Triassic Ecca and Beaufort Groups. Close to its base, inclined seismic reflections (clinoforms) may represent sedimentary progradations (Fig. 1.2a). In the upper part, the seismic section is 'noisy' and here the two groups cannot be separated. Farther inland dolerite intrusions that can be distinguished on other, low-resolution seismic lines prevent detailed stratigraphic correlation of the Karoo sequences between the seismic sections (Chap. 2 this book).

1.3 New Borehole Analysis

Below, 11 deep boreholes are described from our relogging of archived cores (stored at the CGS in Pretoria) at the national core library, combined with reinterpretation of the original SOEKOR mud-logs from the 1960s. The new sections, subdivided into informal litho-units, are presented in Fig. 1.3 together with available biostratigraphic data. The following cores description for the Karoo Supergroup is primarily based on lithofacies, with no lithostratigraphic connotation.

1.3.1 Rocks and Facies Description

- Crystalline basement

Precambrian basement is intersected in the QU, KA, VR, and WE sections, between −2405 and −3692 m depth (Fig. 1.3). It consists of banded leucocratic, mafic gneisses, and granulites. Rocks from the QU and WE sections were dated (SHRIMP U-Pb zircons) at 1.0 and 1.1 Ga, respectively (Eglington and Armstrong 2003), and correlated with the high-grade Mesoproterozoic Namaqua-Natal Metamorphic Belt that underlies most of the southern Karoo Basin (Fig. 1.2; Lindeque et al. 2011).

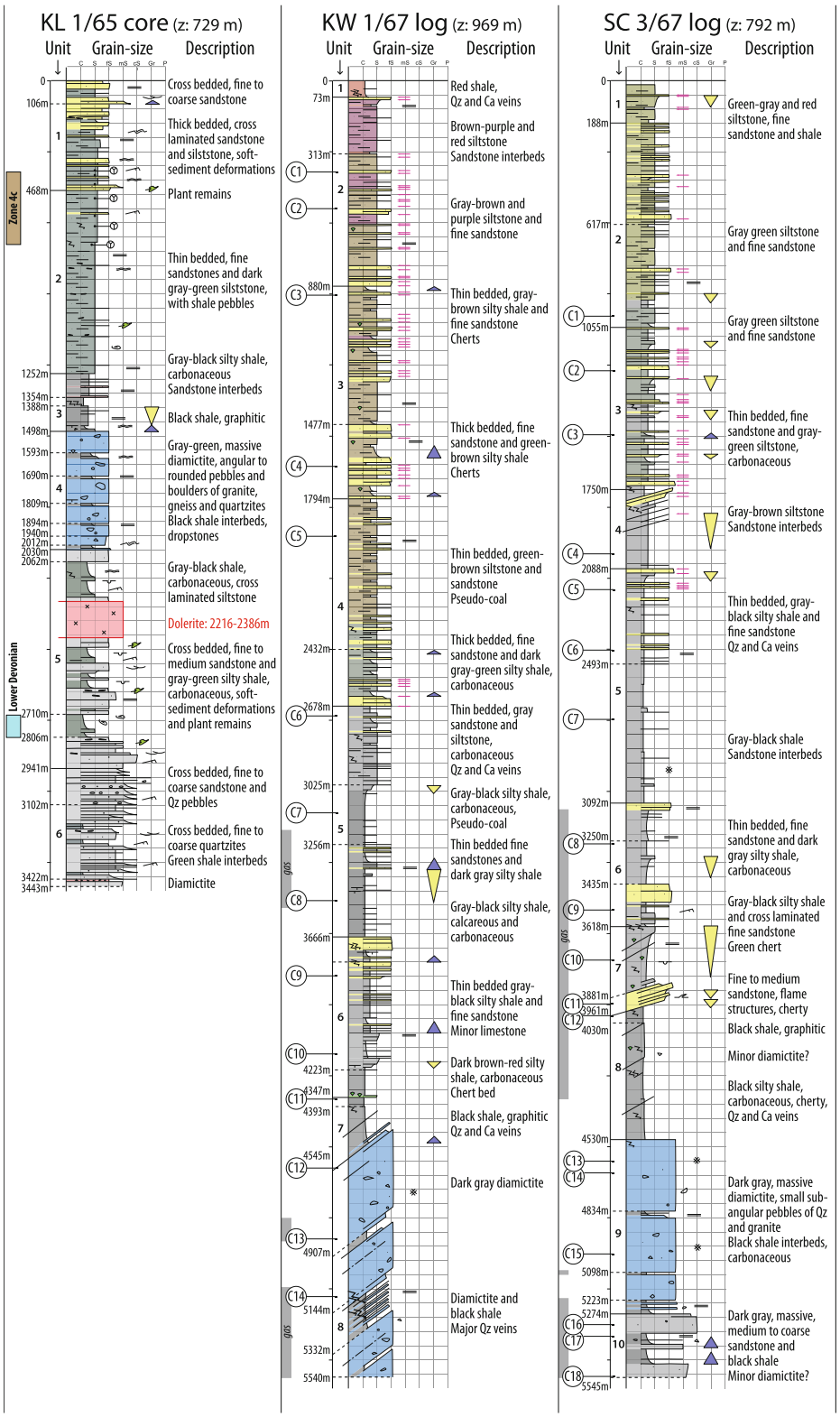

Fig. 1.3 Description of the SOEKOR deep boreholes from the southern Karoo Basin (Fig. 1.1 for location). Depths are converted in meters using the British feet (1' = 0.304 m)

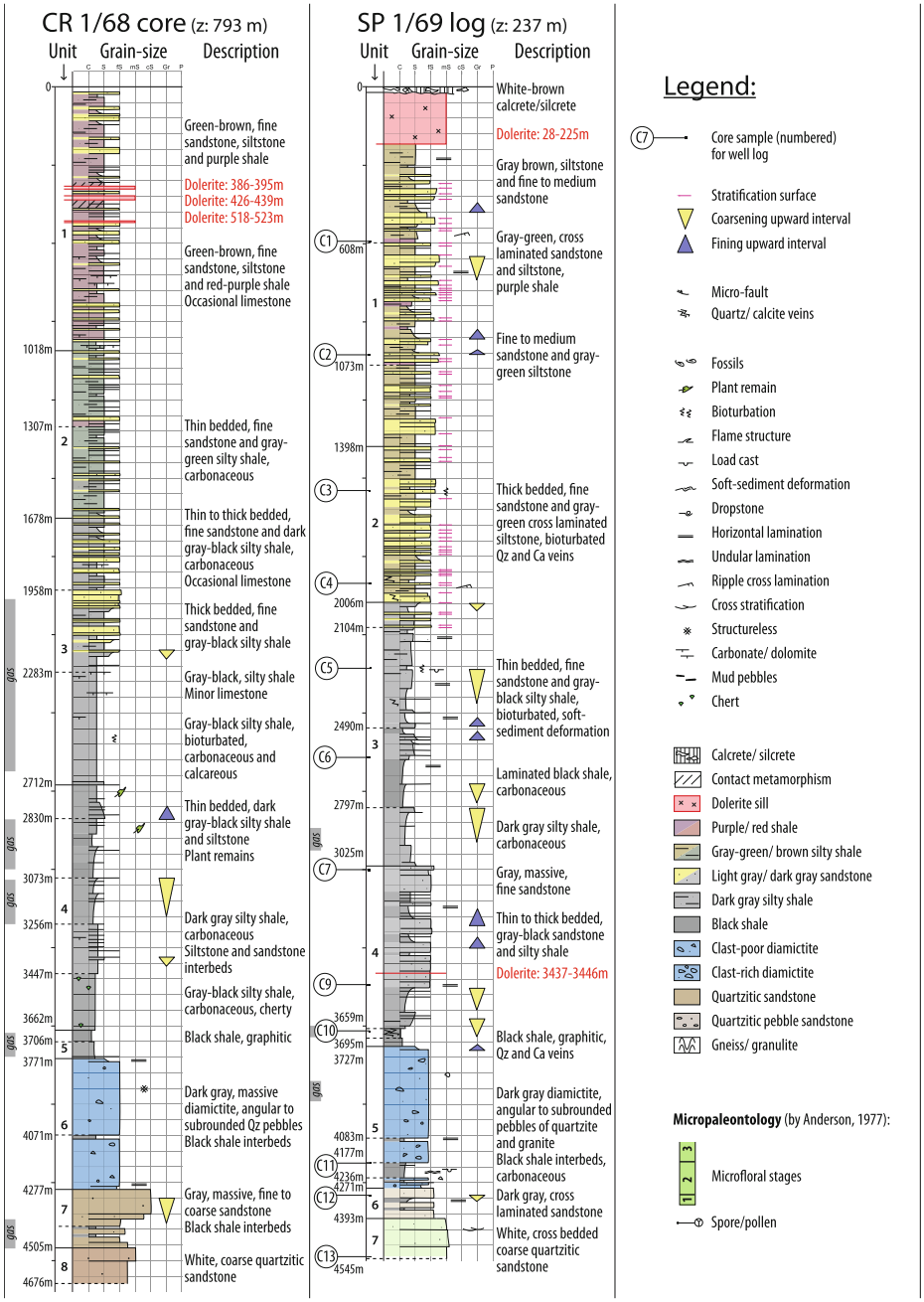

Fig. 1.3 (continued)

- Quartzitic sandstones

Lowermost sequences of white-gray, fine to coarse-grained quartzitic sandstones are described in the OL, KL, CR, VR, SC, and SP sections (Fig. 1.3). These commonly have cross-stratifications (Fig. 1.4a) and ripples, small quartz pebbles, and dark green, or black shales (1–150 m thick), locally with plant remains and marine fossils (trilobites, brachiopods, pelecypods, and gastropods). In the south-western KL section (Fig. 1.3), the succession includes in the lower part a 2 m thick diamictite possibly of glacial origin, and likely correlated with the Pakhuis Formation (upper Table Mountain Group). This is overlain, between −2710 and −2806 m depth, by shale that is dated with marine

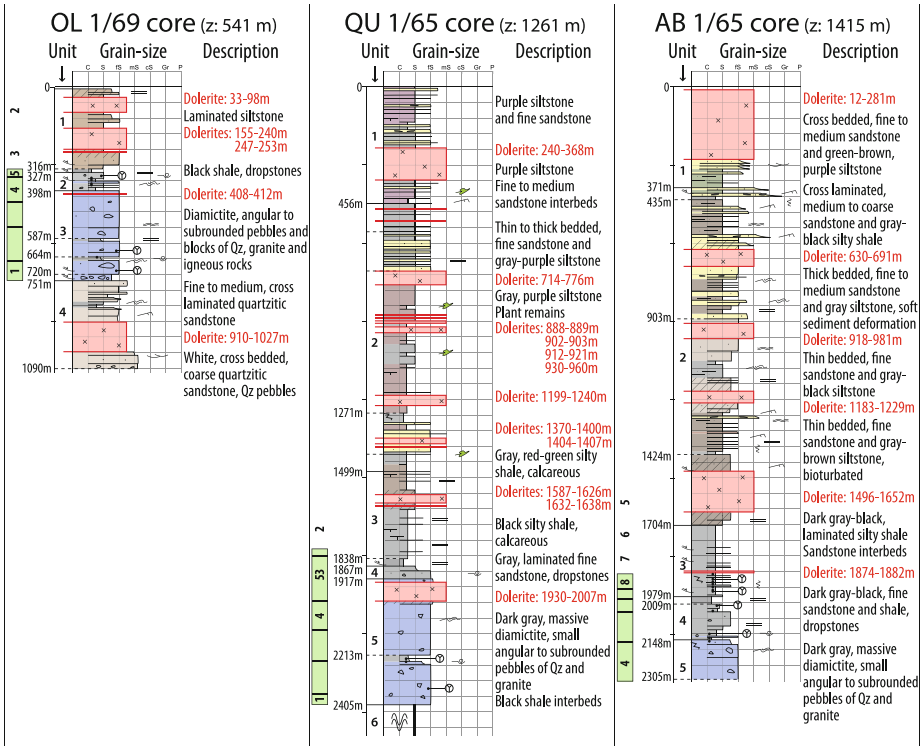

Fig. 1.3 (continued)

invertebrates to the Lower Devonian, and is thus attributed to the Bokkeveld Group.

- Diamictites

Thick diamictites occur in all the studied boreholes (Fig. 1.3), above quartzites of the Cape Supergroup (in the OL, KL, CR, VR, SC, and SP sections) or directly overlying the crystalline basement (in the QU, KA ,and WE sections). These are relatively clast-poor (>40 % sand and finer clastic matrix), massive diamictites composed of a dark gray-black (carbonaceous), argillaceous heterolithic matrix, supporting small (0.5–3 cm) and large (7 cm), angular to subrounded pebbles mainly of quartz and granite. The beds are between 68 and 356 m thick, most commonly with a sharp base and gradational top, separated by black shales (3–60 m thick; Fig. 1.4b) that often display soft sediment deformation structures and contain dropstones. In the westernmost OL and KL sections, the diamictite beds are thinner, ranging between 18 and 119 m thick, and contain large pebbles and boulders (10–50 cm) of more varied lithology, including red quartzites, granite/gneiss and green igneous/mafic rocks. The diamictites are tilted 50–70° in the KW and SC sections (Fig. 1.3), and are locally metamorphosed at contacts with dolerites in the OL and WE sections.

- Black shales

Overlying the diamictites are black shales between 11 and 569 m thick (Fig. 1.3). These dark gray to black mudstones are carbonaceous (organic carbon = 0.2–9.2 %; Rowsell and de Swardt 1976), pyritic, laminated, or massive, and occasionally contain minor limestones or chert (e.g., an 80 cm thick chert horizon in the VR section possibly represents the Matjiesfontein Chert Bed; Viljoen 1992). These facies were deposited from suspension settling of organically enriched muds in anoxic bottom waters (Chap. 11 this book). The bases and tops of the units are either transitional or sharp. The cores are graphite-rich and weathered white due to oxidation of pyrite as it has been exposed to the atmosphere for nearly 50 years. The black shales are often broken-up by intersecting cleavage, fractured by micro-faults and cut by veins of quartz and calcite (Fig. 1.4c), particularly in the southern sections.

- Dark gray-brown silty shales

Above the black shales, thicker units (215–639 m thick) of dark gray-black or gray-brown silty shales are observed in most of the boreholes (Fig. 1.3). These very fine-grained sediments are micaceous, carbonaceous and/or calcareous,

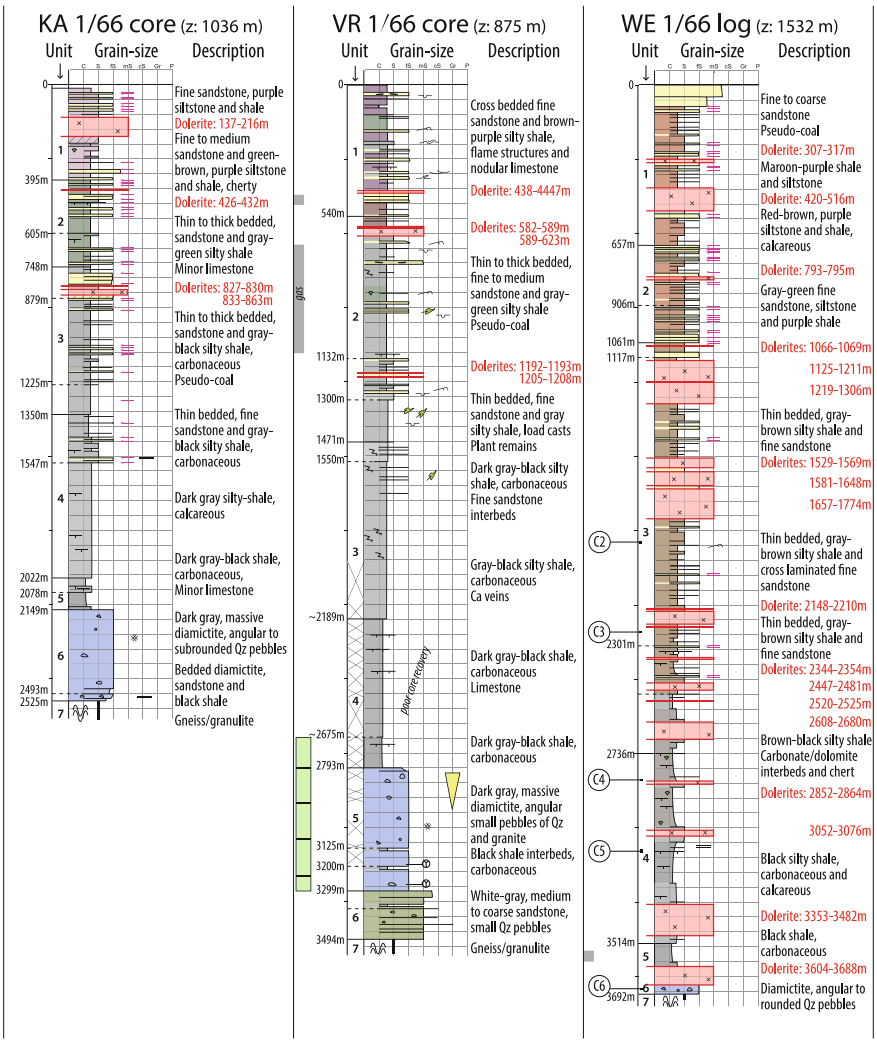

Fig. 1.3 (continued)

thinly laminated (Fig. 1.4e) or massive, and with occasional interbeds (5–20 cm thick) of fine sandstone, siltstone and carbonate/dolomite or chert. The units are deformed (tilted by 20–40°) in the lower and middle parts of the SC section (Fig. 1.3). In the OL, QU, AB, and WE sections the silty shales are intruded by dolerites, and near their contacts are locally recrystallized (see Chaps. 7 and 8 in this book).

- Thin to thick-bedded sandstones and silty shales

Monotonous, 158–1265 m thick successions of interbedded ripple cross-laminated or massive fine sandstones (Fig. 1.4d) with dark gray-green siltstones and silty shales represent alternating low and high-energy flows followed by settling of suspended fines, such as commonly observed in turbidites (e.g., van der Merwe et al. 2009; Jones et al. 2015). The facies have soft sediment deformation structures (convolutions and load casts), and preserve occasional fossil shell marks (in the KL section), plant remains and abundant bioturbations (Fig. 1.4f). The successions generally become thicker bedded upward, with more abundant rip-up clasts and stratification surfaces (Fig. 1.3) that indicate progressively greater rates of deposition and erosion. These strata are subhorizontal, except locally in the uppermost KL section, and are intruded by dolerites at different levels.

- Thick sandstones, siltstones and purple shales

In the uppermost (< 1270 m) part of many sections (Fig. 1.3), alternating green-brown, maroon, purple or red

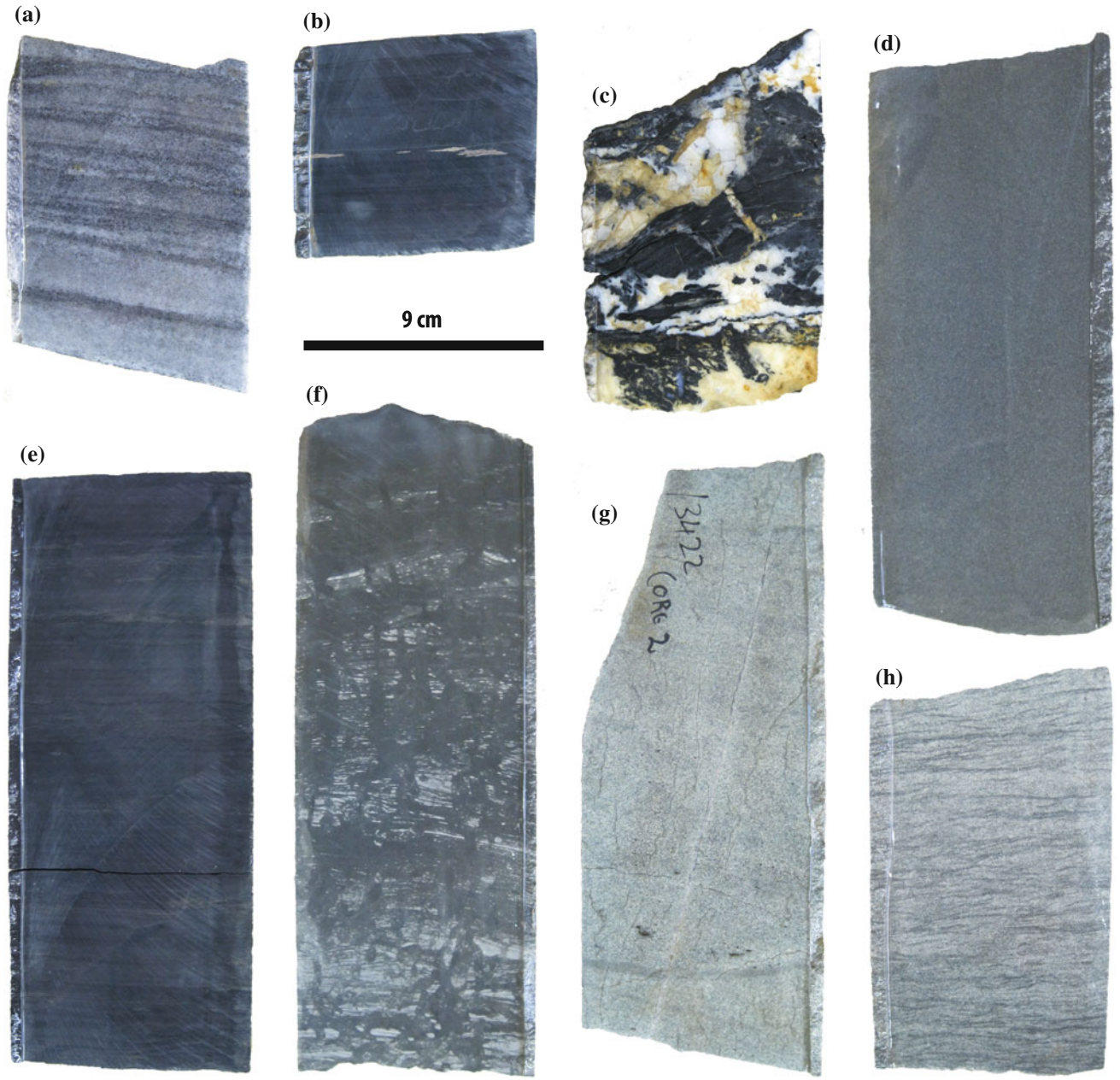

Fig. 1.4 Photos of core samples from the SP 1/69 borehole (Fig. 1.3): **a** Core C12 (−4544 m) of cross-bedded quartzitic medium to coarse-grained sandstone; **b** Core C11 of thinly laminated black shale (e.g., glacial varves) with centimeter-scale pyritic lenses; **c** Core C10 of black shale brecciated by calcite veins; **d** Core C9 (−3041 m) of *dark gray* massive fine to medium-grained sandstone; **e** Core C6 (−2604 m) of *dark gray-black* silty shale with undular lamination; **f** Core C3 (−1568 m) of cross-laminated fine-grained sandstone and *dark gray* siltstone with vertical burrows (e.g., marginal lacustrine); **g** Core C2 (−1040 m) of *green* cross-bedded medium to coarse-grained sandstone; and **h** Core C1 (−600 m) of *gray-green* ripple cross-laminated fine sandstone and siltstone

siltstones and shales comprise thicker (1–40 m thick) and coarser sandstones. These sandstones are fine- to medium-grained, and exceptionally coarse, containing cross-stratifications and ripples (Figs. 1.4g, h) or are massive. Their bases are sharp (erosive), some have flame structures, and their tops generally fine upward to siltstone and shale, characteristic of channel fills. The red-purple siltstones and shales have occasional limestones and carbonate concretions that may represent paleosoils within overbank or abandoned river channel deposits (e.g., Smith and Botha-Brink 2014).

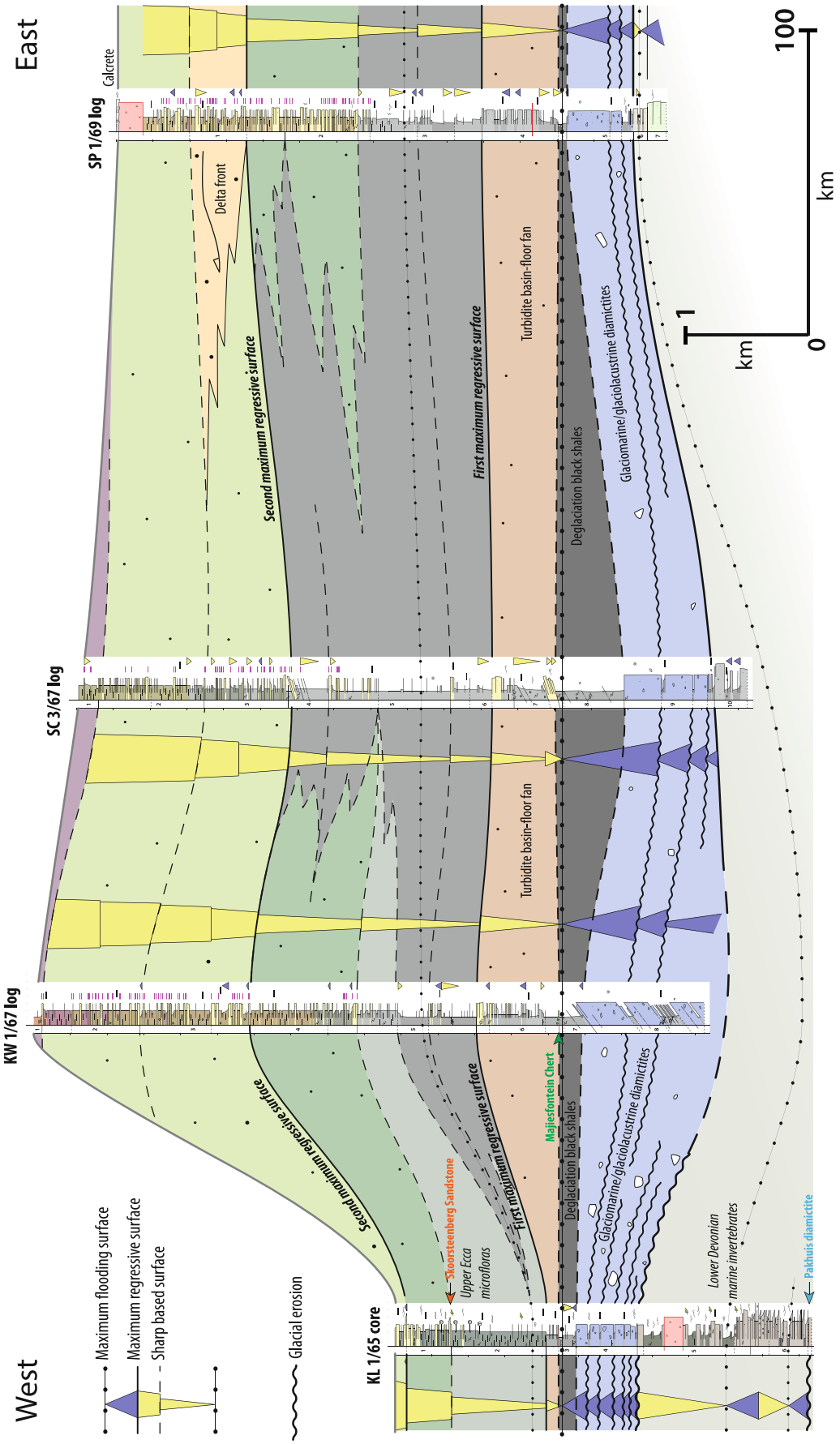

Fig. 1.5 East–West correlation profile, 850 km across the southern Karoo Basin (Fig. 1.1 for location). The datum (*thick dotted line*) is the maximum flooding surface within the Early Permian deglaciation *black* shales (the Prince Albert and Whitehill Formations)

Dolerites

Dolerite intrusions occur in most sections (Fig. 1.3). These are fine- to coarse-grained (0.5–4 mm), and represent thin (0.5–10 m thick) to thick sills (30–269 m thick). They frequently occur close or at major lithological contacts and tend to be thicker higher in the sections (e.g., in the QU, AB, KA, and SP sections). Associated metamorphism effects, mostly confined to the surrounding section (Chaps. 7 and 8 this book), are most visible within the silty and sandy lithologies, including discoloration, recrystallization (silicification) and disseminated gas vesicles (1–10 cm in diameter).

1.3.2 Paleo-Environment Interpretations and Sequences Correlation

Based on facies models and vertical analysis of deepening and shallowing depositional sequences (transgressions and regressions) along the borehole logs, new correlations are proposed along an 850 km long E-W profile across the southern Karoo Basin (Fig. 1.5). This sequence correlation profile largely ignores the formal lithostratigraphy (Winter and Venter 1970).

- Glacial and deglaciation model

The massive diamictites overlain by black shales with dropstones are interpreted to have been deposited from rapid rain-out of suspended sediments and ice-rafted debris from icebergs, ice sheets and glacier surfaces at variable distances away from the terrestrial ice margin. These facies associations that characterize the Dwyka Group (Visser 1997) thicken from 532–544 to 744 m in the center of the correlation profile (Fig. 1.5). The uppermost diamictites are regionally covered by black shales that, based on biostratigraphy, can be equated to the Lower Permian Prince Albert and Whitehill Formations (Anderson 1977). The deglaciation shales record a rapid maximum flooding of the basin, and therefore are a relative short time-line for regional correlations (datum in Fig. 1.5). This major transgression possibly resulted from glacio-eustatic sea level rise and/or local isostatic crustal flexure in response to the final (Sakmarian) Dwyka deglaciation of southern Gondwana, around 290 Ma (Visser 1997; Scheffler et al. 2006; Milani and de Wit 2008; see also Chap. 17 in this book).

- Turbidites and basin-floor fan model

Overlying the black shales, thin-bedded successions of turbidite are characteristic of distal basin-floor environments, such as for example for the Vischkuil and Ripon Formations (van der Merwe et al. 2009; Flint et al. 2011; Jones et al. 2015). Across the central and eastern parts of the profile (Fig. 1.5), the lowermost turbidites form distinct 634–681 m thick coarsening-upward sequences that suggest progradation of depositional lobes in a mid- to outer-fan setting, and terminated at the top by a first marked, basin-wide regressive surface overlain by thick silty shales. Superimposed successions of alternating fine sandstones with mudstones become regionally thicker bedded upward with progressively more abundant sandstones and stratification surfaces (Fig. 1.5), indicative of a major regression, most likely linked to Permian-Triassic deformations and uplift of the Cape Fold Belt along the southwestern margin of Gondwana (Milani and de Wit 2008; Tankard et al. 2009).

- Alluvial model

Uppermost cross-bedded sandstones and red-purple siltstones and shales with pedogenic carbonate are characteristic of river and alluvial plain deposits, and can be correlated to the Beaufort Group (Smith and Botha-Brink 2014; Chap. 14 this book). But the base of these fluvial (lacustrine?) and deltaic sequences is challenging to map in the well-data because core samples and mud-log descriptions are not often diagnostic of a subaerial depositional environment. Instead, a second basin-wide regressive surface (or rapid shallowing) is tentatively correlated between the sections (Fig. 1.5). This surface corresponds to the first cross-bedded coarse sandstone in the upper KL core (at −106 m depth), and to the onset of the most abundant stratification surfaces in the KW and SC wells (at −1794 and −1750 m depths respectively), as well as to the base of distinctive fining upward sequences of channels fills in the SP section (at −1073 m depth). In the latter, superimposed coarser sandstones and coarsening-upward intervals suggest the progradation of delta fronts (Fig. 1.5).

1.3.3 Basin Structure and Geometry of Dolerite Intrusions

The basin structure and distribution of dolerites in subsurface is imaged with borehole correlations projected along a N-S profile, 150 km long across the center of the southern Karoo Basin (Fig. 1.6).

Across this correlation profile, Precambrian basement shallows, over a distance of 23 km, from -3494 m in the VR section to −2525 m depth in the KA section (Fig. 1.6). The overlying Cape Supergroup rapidly pinches out northward between the same borehole sections. Interbedded tillites/diamictites and black shales of the Dwyka Group thin more progressively northward, from 744 m (in the SC section) to 376 m (in the KA section), over a distance of 84 km. Overlying black shales of the lowermost Ecca Group are notably thick (569 m) in the southernmost SC section, likely

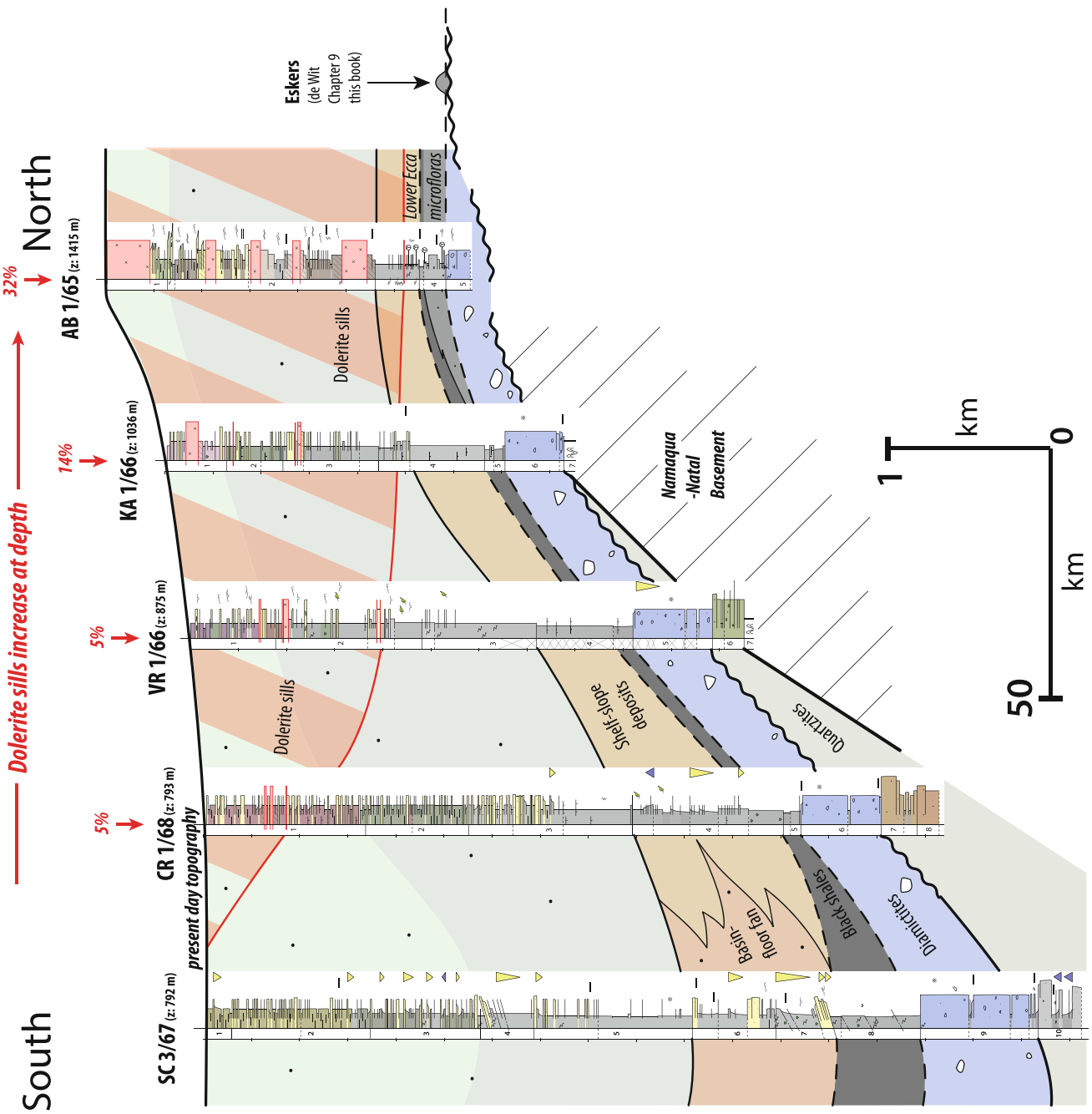

Fig. 1.6 North–South correlation profile, 150 km across the south-central Karoo Basin (Fig. 1.1 for location). Note the progressive increase of dolerite sills to the north (percentage of dolerite thickness in *red*)

duplicated due to folding and/or thrusting, and are between 109 and 127 m thick in the CR, VR, and KA sections (Fig. 1.6). These become sandier in the AB section, corresponding to 139 m bedded fine sandstone covered by 30 m thinly laminated shales, both containing Early Permian palynomorphs (Anderson 1977). The overlying turbidite fan deposits in the SC section grade laterally northward to silty shales and siltstones that become more carbonated, characteristic of shallower shelf-slope deposits (e.g., Jones et al. 2015).

In the southern part of the profile (Fig. 1.6) the Karoo sequences have more abundant quartz and calcite veins, and in the SC section the bedding is rotated (with dips up to 50°) between about −1750 and −2088 m, and again between −3618 and −4530 m depth. These tilts could relate to subsurface structures of the Cape Fold Belt, as observed in the seismic data (Fig. 1.2), and mapped at surface as far as 40 km to the north of the main tectonic front (Booth and Goedhart 2014).

Dolerite intrusions are more abundant and thickest in the northern boreholes (Fig. 1.6). In the AB section, dolerite sills represent 32 % of the total intruded thickness. Comparatively, they become thinner and progressively less abundant southward: KA = 14 %, VR = 5 %, and CR = 5 % of AB; and they intrude systematically at shallower levels (Fig. 1.6).

1.4 Conclusion

Our revised lithostratigraphic sections from the old SOEKOR deep boreholes in the southern Karoo Basin all show at their lower parts distinctive diamictites and black shales, in total between 435 and 1313 m thick, corresponding to the Dwyka Group and the Prince Albert-Whitehill Formations. The basal contact varies from erosion across the Namaqua-Natal basement and Cape Supergroup rocks in the western and northern sections, to alternating diamictites with black shales in the southeastern sections, suggestive of a more conformable transition toward the south. The uppermost Ecca and Beaufort Groups are preserved between 398 and 4545 m thick; however, surface characteristics of the two groups and their different formations, as defined in the field, cannot be distinguished with confidence because of lateral facies changes, variation in diagenesis, local deformation, and metamorphism associated with the numerous dolerite intrusions. Resolving the Karoo Basin subsurface stratigraphy thus will require additional chronostratigraphy and, for example, chemostratigraphy as recently applied to the Lower Permian black shales that are presently under investigation for shale gas potential, and which can be complemented with 3-D basin modeling.

Acknowledgments The authors acknowledge the support by the DST/NRF of South Africa. We thank the Council for Geosciences in Pretoria for providing the original SOEKOR well logs and for their help in accessing and sampling the archived cores. We also thank Doug Cole for a critical review and advice. This is AEON contribution number 155.

References

Aarnes I, Svensen H, Poltea S and Planke S (2011) Contact metamorphic devolatilization of shales in the Karoo Basin, South Africa, and the effects of multiple sill intrusions. Chem Geol 281:181–194.

Anderson JM (1977) The Biostratigraphy of the Permian and Triassic Part 3. A review of Gondwana Permian palynology with particular reference to the northern Karoo Basin, South Africa. Memoirs of the Botanical Survey of South Africa 41, 133p, several charts, 188 plates.

Bangert B, Stollhofen H, Lorenz V, Armstrong R (1999) The geochronology and significance of ash-fall tuffs in the glaciogenic Carboniferous-Permian Dwyka Group of Namibia and South Africa. J Afri Earth Sci 29:33–49.

Black D, Booth P and de Wit M (2016) Petrographic, geochemical and petro-physical analysis of the Collingham Formation near Jansenville, Eastern Cape, South Africa—potential cap rocks to shale gas in the Karoo. S Afri J Geol 119. doi:10.2113/gssajg.119.1.0.

Blignault HJ and Theron JN (2015) The facies association tillite, boulder beds, boulder pavements, liquefaction structures and deformed drainage channels in the Permo-Carboniferous Dwyka Group, Elandsvlei area, South Africa. S Afri J Geol 118:157–172.

Booth PWK and Goedhart ML (2014) Thrust faulting in the northernmost foreland zone of the Cape Fold Belt, Fort Beaufort, Eastern Cape, South Africa. S Afri J Geol 117.2:301–315. doi:10.2113/gssajg.117.2.301.

Burgess SD, Bowring SA, Fleming TH and Elliot DH (2015) High-precision geochronology links the Ferrar large igneous province with early-Jurassic ocean anoxia and biotic crisis. Earth Planet Sci Lett 415:90–99.

Cole DI (1977) Core description of uranium anomalies found in boreholes QU 1/65 and SA 1/66 from the southern Karoo with an interpretation of the depositional environments. Report, Geological Survey, South Africa, No G/277.

Cole DI (1992) Evolution and development of the Karoo Basin. In: de Wit MJ and Ransome IGD (eds) Inversion Tectonics of the Cape Fold Belt, Karoo and Cretaceous Basins of Southern Africa. A.A. Balkema, Rotterdam, pp. 87–99.

Cole DI (1998) Palaeogeography and palaeocurrent distribution of the Beaufort Group in the Karoo basin, South Africa, during the Late Permian. J Afr Earth Sci 27(1A):46–47.

Duncan RA, Hooper PR, Rehacek J, Marsh JS and Duncan AR (1997) The timing and duration of the Karoo igneous event, southern Gondwana. J Geophys Res 102:18127–18138.

Eglington BM, Armstrong RA (2003) Geochronological and isotope constraints on the Mesoproterozoic Namaqua–Natal belt: evidence from deep borehole intersections in South Africa. Precambrian Res 125:179–189.

Fildani A, Drinkwater NJ, Weislogel A, McHargue, T, Hodgson, DM and Flint SS (2007) Age Controls on the Tanqua and Laingsburg Deep-Water Systems: New Insights on the Evolution and Sedimentary Fill of the Karoo Basin, South Africa. J Sediment Res 77(11):901–908.

Flint SS, Hodgson DM, Sprague AR, Brunt RL, Van der Merwe WC, Figueiredo J, Prélat A, Box D, Di Celma C and Kavanagh JP (2011) Depositional architecture and sequence stratigraphy of the Karoo basin floor to shelf edge succession, Laingsburg depocentre, South Africa. Mar Pet Geol 28:658–674.

Groenewald GH and Kitching JW (1995) Biostratigraphy of the Lystrosaurus Assemblage Zone, In: Rubidge BS (ed) Biostratigraphy of the Beaufort Group (Karoo Supergroup). South African Committee for Stratigraphy, Biostratigraphic Series 1, Council for Geoscience, Pretoria, pp. 35–39.

Hansma J, Tohver E, Jourdan F, Schrank C and Adams D (2015) The Timing of the Cape Orogeny: New 40Ar/39Ar age constraints on deformation and cooling of the Cape Fold Belt, South Africa. Gondwana Res. doi:10.1016/j.gr.2015.02.005.

Isbell JL, Cole DI and Catuneanu O (2008) Carboniferous - Permian glaciation in the main Karoo Basin, South Africa: Stratigraphy, depositional controls, and glacial dynamics. In: Fielding CR, Frank TD and Isbell JL (eds) Resolving the Late Paleozoic Ice age in Time and Space. Geol Soc Am Spec Pap 441:71–82.

Johnson MR, Van Vuuren CJ, Visser JNJ, Cole DI, Wickens HV, Christie ADM, Roberts DL and Brandl G (2006). Sedimentary rocks of the Karoo Supergroup. In: Johnson MR, Anhaeusser, CR and Thomas RJ (eds) The Geology of South Africa, Geological Society of South Africa, Johannesburg/Council for Geoscience, Pretoria, pp. 461–499.

Jones GED, Hodgson DM and Flint SS (2015) Lateral variability in clinoform trajectory, process regime, and sediment dispersal patterns beyond the shelf-edge rollover in exhumed basin margin-scale clinothems. Basin Res 27:657–680. doi:10.1111/bre.12092.

Lanci L, Tohver E, Wilson A and Flint S (2013) Upper Permian magnetic stratigraphy of the lower Beaufort Group, Karoo Basin. Earth Planet Sci Lett 375:123–134.

Linol B, de Wit MJ, Milani EJ, Guillocheau F, Scherer C (2015) Chapter 13: New regional correlations between the Congo, Paraná and Cape-Karoo Basins of southwest Gondwana. In: de Wit MJ, Guillocheau F and de Wit MJC (eds) The Geology and Resource Potential of the Congo Basin, Regional Geology Reviews. Springer-Verlag, Berlin Heidelberg, pp. 246–268. http://dx.doi.org/10.1007/978-3-642-29482-2_13.

Lindeque A, de Wit MJ, Ryberg T, Weber M and Chevallier L (2011) Deep Crustal Profile Across the Southern Karoo Basin and Beattie Magnetic Anomaly, South Africa: an Integrated Interpretation with Tectonic Implications. S Afri J Geol 114(3–4):265–292.

McKay MP, Weislogel AL, Fildani A, Brunt RL, Hodgson DM and Flint SS (2015) U-PB zircon tuff geochronology from the Karoo Basin, South Africa: implications of zircon recycling on stratigraphic age controls. Int Geol Rev 57:393–410. http://dx.doi.org/10.1080/00206814.2015.1008592.

Milani EJ, and de Wit MJ (2008) Correlations between the classic Paraná and Cape Karoo sequences of South America and southern Africa and their basin infills flanking the Gondwanides: du Toit revisited. In: Pankhurst RJ, Trouw RAJ, Brito Neves BB and de Wit MJ (eds) West Gondwana: Pre-Cenozoic Correlations Across the South Atlantic Region. Geol Soc London Spec Publ 294:319–342.

Miller W, Armstrong R and de Wit MJ (2016) Geology and U/Pb geochronology of the Gamtoos Complex and lower Paleozoic Table Mountain Group, Cape Fold Belt, Eastern Cape, South Africa. S Afri J Geol 119. doi:10.2113/gssajg.119.1.0.

Paton DA, Macdonald DIM and Underhill JR (2006) Applicability of thin or thick skinned structural models in a region of multiple inversion episodes; southern South Africa. J Struct Geol 28:1933–1947.

Reeves C, Teasdale, J and Mahanjane ES (2015) Insight into the East Coast of Africa from a new tectonic model of the early Indian Ocean. Extended abstract, Geological Society of Houston/Petroleum Exploration Society of Great Britain, London, September 2–3.

Rowe CD and Backeberg NR (2011) Discussion on: Reconstruction of the Ordovician Pakhuis ice sheet, South Africa by H.J. Blignault and J.N. Theron. S Afri J Geol 114:95–102. doi:10.2113/gssajg.114.1.95.

Rowsell DM and De Swardt AMJ (1976) Diagenesis in Cape and Karoo sediments, South Africa, and its bearing on their hydrocarbon potential. Trans Geol Soc S Afr 79:81–145.

Rubidge BS, Erwin DH, Ramezani J, Bowring SA and De Klerk WJ (2013) High-precision temporal calibration of Late Permian vertebrate biostratigraphy: U-Pb zircon constraints from the Karoo Supergroup, South Africa. Geology 41(3):363–366.

SACS-South African Committee for Stratigraphy (1980) Stratigraphy of South Africa. Part 1. (Compiled by L.E. Kent). Lithostratigraphy of the Republic of South Africa, South West Africa/Namibia, and the Republics of Bophuthatswana, Transkei and Venda. Handbook 8, Geological Survey, South Africa, 690p.

Scheffler K, Bühmann D and Schwark L (2006) Analysis of late Palaeozoic glacial to postglacial sedimentary successions in South Africa by geochemical proxies – Response to climate evolution and sedimentary environment. Palaeogeogr Palaeoclimatol Palaeoecol 240:184–203.

Shone RW and Booth PWK (2005) The Cape Basin, South Africa: a review. J Afri Earth Sci 43:196–210.

Smith RMH and Botha-Brink J (2014) Anatomy of a mass extinction: Sedimentological and taphonomic evidence for drought-induced die-offs at the Permo-Triassic boundary in the main Karoo Basin, South Africa. Palaeogeogr Palaeoclimatol Palaeoecol 396:99–118.

Spikings AL, Hodgson DM, Paton DA and Spychala YT (2015) Palinspastic restoration of an exhumed deepwater system: A workflow to improve paleogeographic reconstructions. Interpretation 3(4)71–87. http://dx.doi.org/10.1190/INT-2015-0015.1.

Streel M and Theron JN (1999) The Devonian-Carboniferous boundary in South Africa and age of the earliest episode of the Dwyka glaciation: New palynological result. Episodes 22:41–44.

Svensen H, Corfu F, Polteau S, Hammer Ø and Planke S (2012) Rapid magma emplacement in the Karoo Large Igneous Province. Earth Planet Sci Lett 325–326:1–9.

Thamm AG and Johnson MR (2006) The Cape Supergroup. In: Johnson MR, Anhaeusser CR and Thomas RJ (eds) The Geology of South Africa. Geological Society of South Africa, Johannesburg/Council for Geoscience, Pretoria, pp. 443–460.

Tankard A, Welsink H, Aukes P, Newton R and Stettler E (2009) Tectonic evolution of the Cape and Karoo basins of South Africa: Mar Pet Geol 26(8):1379–1412.

Vandenbroucke TRA, Gabbott SE, Paris F, Aldridge RJ and Theron JN (2009) Chitinozoans and the age of the Soom Shale, an Ordovician black shale Lagerstätte, South Africa. J Micropalaeontol 28:53–66.

Van der Merwe WC, Hodgson DM and Flint SS (2009) Widespread syn-sedimentary deformation on a muddy deep-water basin-floor: the Vischkuil Formation (Permian), Karoo Basin, South Africa. Basin Res 21:389–406. doi:10.1111/j.1365-2117.2009.00396.

Viljoen JHA (1992) Lithostratigraphy of the Collingham Formation (Ecca Group), including the Zoute Kloof, Buffels River and Wilgehout River Members and the Matjiesfontein Chert Bed. Catalogue of South African Lithostratigraphic Units, SA Committee for Stratigraphy, South Africa, 10p.

Visser J (1997) Deglaciation sequences in the Permo-Carboniferous Karoo and Kalahari basins of southern Africa: a tool in the analysis of cyclic glaciomarine basin fills. Sedimentology 44(3):507–521.

Werner M (2006) The stratigraphy, sedimentology and age of the Late Palaeozoic Mesosaurus Inland Sea, SW-Gondwana: new implications from studies on sediments and altered pyroclastic layers of the Dwyka and Ecca Group (lower Karoo Supergroup) in southern Namibia. Unpublished PhD Thesis, University of Würzburg, Germany, 428p.

Winter HDIR and Venter JJ (1970) Lithostratigraphic correlations of recent deep boreholes in the Karoo-Cape sequence. In: Haughton SH (ed) 2nd IUGS Symposium on Gondwana Stratigraphy and Paleontology, Pretoria, South Africa, pp. 395–408.

Seismic Imaging of Dolerite Sills in the Karoo Basin, with Implications for Shale Gas Potential

2

Stephanie Scheiber-Enslin, Susan Webb, and Musa Manzi

Abstract

Seismic data provide a unique opportunity to understand the subsurface structure of dolerite sills that have intruded the Karoo Basin at multiple levels. These sills have intruded close to the Whitehill Formation at several locations within the basin, and may impact shale gas exploration of this horizon. In the southeastern Karoo Basin, around Queenstown, seismic data reveal the presence of 5–30 km wide saucer-shaped sills with vertical thickness of up to ~270 m each, and dips of between 2° and 8° at shallow stratigraphic levels. Farther south, dolerite sheets near Somerset-East are imaged down to a depth of ~5 km and extend for over 150 km, with dips of between 3° and 13°. These dips increase closer to the adjacent Cape Fold Belt in the south. Around Lesotho, at the highest stratigraphic levels, intrusions are dominated by dykes and fluid vents that are evident on seismic data as regions of diffused reflectivity. The lowest concentration of dolerite is found in a region in the south-central part of the basin around the town of Graaff-Reinet. Here intrusions are confined to the Beaufort Group, ~ 1000 m above the shale reservoir. This change in dolerite distribution will influence the location of shale gas exploration.

Keywords

Karoo dolerites • Hydrothermal vents • 2D seismic • Shale gas

2.1 Introduction

Termination of the Karoo Basin sedimentation was characterized by a massive outpouring of lavas around 182 Ma, forming the Karoo Large Igneous Province (LIP, Duncan et al. 1997; Chap. 7 this book). Along with this outpouring, magma intruded as dykes and sills at multiple levels within the basin. These intrusions change from dominant dykes and saucer-shaped sills within the upper and mid-stratigraphic levels (Stormberg and Beaufort Groups), to extensive sub-horizontal sills and sheets within the lower stratigraphic levels (Ecca and Dwyka Groups and basement; Du Toit 1920; Chevallier and Woodford 1999; van Zijl 2006). The upper stratigraphic levels in the east are also disrupted by fluid vents interpreted as hydrothermal (Svensen et al. 2006), while breccia pipes are associated with the deeper shales that outcrop in the northwest (Svensen et al. 2007).

There is a change in the distribution of dolerites throughout the basin. The largest concentration of dolerites is in the northwestern and eastern parts of the basin (with a combined dolerite thickness of >150 m in each well), with intrusions at all stratigraphic levels (Fig. 2.1, Cawthorn 2012; Scheiber-Enslin et al. 2014). There is a significant drop in dolerite volume in the south-central part of the basin (with a combined dolerite thickness of < 150 m in each well), with intrusions limited to the Beaufort Group (Fig. 2.1). This volume drops close to zero, south of the "dolerite line" where no intrusions are intersected in wells or outcrop. This change in distribution has been linked to the location of the magma source supplying the LIP off the west

S. Scheiber-Enslin (✉)
Council for Geoscience, Pretoria, South Africa
e-mail: steph.scheiber@gmail.com

S. Scheiber-Enslin · S. Webb · M. Manzi
School of Geosciences, University of the Witwatersrand, Johannesburg, South Africa

B. Linol and M.J. de Wit (eds.), *Origin and Evolution of the Cape Mountains and Karoo Basin*,
Regional Geology Reviews, DOI 10.1007/978-3-319-40859-0_2

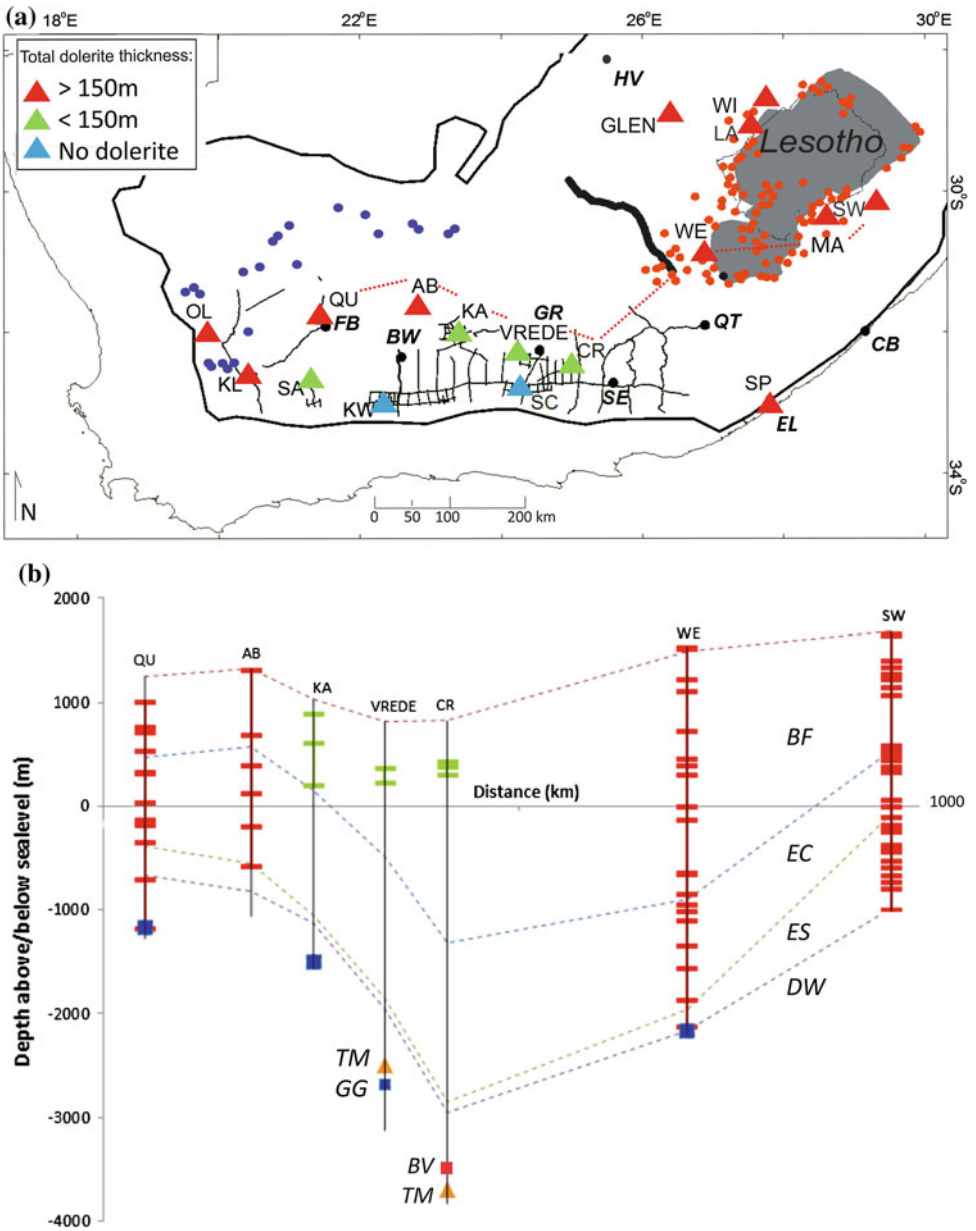

Fig. 2.1 **a** Location map showing the occurrence of dolerites within deep Soekor wells (*triangles*) within the Karoo Basin (*thick black outline*) (modified from Scheiber-Enslin et al. 2014). Wells in the southwest and east intersect >150 m thickness of dolerite (*red triangles*), while those in the south-central Karoo Basin intersect <150 m dolerites (*green triangles*), and those farthest south show no dolerite intersections (*blue triangles*). The *grey* region marks the Drakensberg Group lava cover over the country of Lesotho. The fluid vents in the central Karoo (*red dots*) and breccia pipes in the northwestern Karoo (blue dots) are indicated (Svensen et al. 2004; Svensen et al. 2007). Studied seismic data over the basin include a high-resolution 2D Anglo-American line RT480 (*thick black line*) and historic 2D SOEKOR survey (*thin black lines*). The towns and cities of Fraserburg (FB) in the southwestern part of the basin, Beaufort West (BW) and Graaff-Reinet (GR) in the south-central basin, and Somerset-East (SE), East London (EL) and Queenstown (QT) in the southeastern Karoo Basin are marked. The organic rich shale layer of the Whitehill Formation pinches out between Hertzogville (HV) and Coffee Bay (CB). **b** Profile showing the vertical distribution of dolerites *(green and red horizontal dashes)* within the wells connected by a *dotted red line* in **a**. This is determined from unpublished SOEKOR well logs available from the Council for Geoscience. In the southwest (wells QU1/65 and AB1/65) and east (wells WE1/66 and SW1/67) dolerites have intruded all stratigraphic levels: Dwyka (DW), Ecca Shales (ES), Ecca (EC) and Beaufort Groups (BF); while in the south-central region (wells KA1/66, VREDE1/66, CR1/68) dolerites are limited to the BF

and southeast coast of South Africa (Chevallier et al. 2001; Scheiber-Enslin et al. 2014).

Knowledge of the geometry of these types of intrusions are, in general, limited to information gleaned from well and outcrop data. The Karoo Basin provides a unique opportunity in this respect as intrusions have largely been uncovered by erosion, e.g., the Golden Valley Sill Complex in the southeastern Karoo Basin (Galerne et al. 2011). However, recently digitized historic Soekor seismic data (Scheiber-Enslin et al. 2014) and higher resolution Anglo-American seismic data (Webb et al. 2015) allow the horizontal and vertical extent, and dip of these intrusions in the subsurface to be resolved.

Understanding the geometry of these intrusions is important as several have intruded close to important sedimentary layers such as the Whitehill Formation, which is the current focus of shale gas exploration (Decker and Marot 2012). Previous hydrocarbon exploration was carried out by SOEKOR in the 1960s and early 1970s. No economically recoverable oil was found, but over a 23 h period well CR1/68 yielded gas at a rate of 1.83 million scf/day (Leith 1970; Rowsell and De Swardt 1976). It is thought that further tight gas is locked in the Ecca shales. The Karoo dolerite intrusions may in some cases have heated the shale gas layer/s, which needs to be accounted for when evaluating its gas potential (Aarnes et al. 2011). In addition, these sills and dykes can be highly fractured at surface, but at depth are possibly impermeable, providing seals and traps that could also be targets during exploration. The most important issue in the immediate future, however, will be how the fractures associated with these intrusions can provide additional pathways along which fluids can flow (Chevallier et al. 2004).

The available seismic data in the Karoo Basin is summarised in this chapter, along with additional geophysical data that shed light on the dolerite intrusions, basin depths and basin structures.

2.2 Seismic Data

2.2.1 SOEKOR Data

During the SOEKOR phase of exploration an extensive network of 13,000 line-kilometres of 2D seismic data and deep wells (up to 5 km, Fig. 2.1) were collected. While this original seismic data is not archived, redigitized paper copies from Falcon Oil and Gas are used in this study (data managed by Council for Geoscience (CGS) and Petroleum Agency of South Africa (PASA)). These data were originally collected using a dynamite source with an average charge of 20 kg in 15–18 m deep holes (Fatti and du Toit 1970). The majority of the lines are single fold with an average of 24 traces per shot point. The dominant frequency for the survey is 40 Hz. Assuming a velocity of 5550 m/s for the dolerites, the data have a vertical resolution of ~70 m. Thus, features smaller than this are not identifiable.

Several limitations apply to this dataset. Without well control, multiples or "ringing" are often seen below sills that cannot be differentiated from actual intrusions. This is a result of frequencies being lost as these high impedance dolerites bodies (horizontally and vertically) reflect back energy, leading to a poor signal-to-noise ratio for the deeper reflectors. Sill terminations can also be difficult to resolve due to interference of reflected energy. For this reason we excluded SOEKOR seismic data around Lesotho from this study. A final error of a few hundred metres or less is due to imprecise location of the shot points as these were digitized from maps (Bada, personal communication, 13 December 2011).

2.2.2 Anglo-American Seismic Data

Deep, 2D high-resolution seismic data RT480 in the central Karoo Basin was acquired in 1992 by the Gold Division of Anglo-American Corporation of South Africa (now AngloGold Ashanti Ltd) (de Wit and Tinker 2004). The southern and deeper portion of the seismic profile was previously interpreted by de Wit and Tinker (2004) to constrain crustal structures across the Kaapvaal Craton and Natal-Namaqua crust. The seismic data are characterized by a seismic zero phase wavelet with a dominant frequency of 60 Hz, an average velocity of 6200 m/s, and wavelength of approximately 103 m. The vertical resolution limit of these data according to the Widess criteria is approximately 25 m (Widess 1973). The seismic data has a useful frequency spectrum of 15–60 Hz. The data is dominated by low frequencies because the objective of the survey was to image the deep buried strata (3–4.5 km depths), with the seismic penetrating to the base of the crust (16 s two-way travel times). In this study, we focus on the top 2 s of the data to image dolerite sills and dykes, as well as fluid vents within the upper Karoo stratigraphy. Acquisition parameters are summarised in Webb et al. (2015).

2.3 Methods

2.3.1 SOEKOR Data

Processing steps applied to the SOEKOR seismic data are described by Fatti (1970). It is noted that variable velocities in the weathered and sub-weathered layers made it difficult to compute the static corrections accurately (Fatti 1987). An elevation datum of 700 m was used in the project. These

seismic data are here interpreted to better understand the subsurface distribution and geometry of sills and inclined sheets within the Karoo Basin. At shallower levels several bright reflectors on the seismic data represent these dolerite sills and inclined sheets. In many instances, outcrop and/or magnetic data are used to confirm sills and sheets on the seismic sections where they meet the Earth's surface. Well data are used to confirm the dolerite bodies in the subsurface where possible.

For this study, continuous reflectors representing main stratigraphic horizons on the SOEKOR seismic data were also mapped using previously interpreted Soekor seismic profiles (Fatti 1970; Fatti and du Toit 1970; Fatti 1987), as well as recent seismic data collected in the southwestern Karoo Basin (Lindeque et al. 2011; Loots 2013). Four strong reflectors are visible at greater depths on the majority of the seismic sections that extend down to crystalline basement. The two strongest reflectors that are most laterally continuous represent "Old Faithful" and the top of the basement (GG) (Fatti 1970). "Old Faithful" is thought to represent either the top of the Dwyka Group or the Whitehill Formation within the lower Ecca Group (ES) (Fatti 1970; Lindeque et al. 2011; Chap. 1 this book). Exact stratigraphic correlation is difficult due to limited velocity data, and therefore in this study we assume that "Old Faithful" represents the top of the Whitehill Formation (see Chap. 1 in this book for further discussion). This horizon provides a strong reflection due to the acoustic impedance contrast between the lower velocity of this carbon-rich layer (~4000 m/s) and the surrounding rock (~5000 m/s) (Fatti and du Toit 1970). The remaining weaker reflectors are interpreted to represent the Witteberg-Bokkeveld contact (BV) and the top of the Table Mountain Group (TBM) of the Cape Supergroup. No significant reflectors were imaged from these data in the upper Ecca and Beaufort Groups.

No direct velocity measurements were made during the original survey in the southwestern Karoo Basin. However, an expanding spread velocity profile was collected along line SWK01. Interval velocities were calculated for the lower stratigraphic units from these data, i.e. 5060 m/s for the ES-BV interval; 5350 m/s for the ES-TBM interval; 5560 m/s for the ES-Basement interval (Fatti and Du Toit 1970). These velocities are similar to those determined during more recent seismic tomography studies (4500–5300 m/s; Stankiewicz et al. 2007). These interval velocities are used to calculate velocities for individual horizons using depth and velocity ratios. Additional velocity measurements include sonic logs for wells WE1/66 and SP1/69 in the central and eastern Karoo Basin (Fatti 1987). These data are combined with time and depth data from the seismic section-well pairs in this study (Fig. 2.2). These pairs are determined using the two-way travel times (TWT) of the first continuous strong reflector representing approximately the Whitehill Formation (ES), and the corresponding total vertical depths (TVD) for this horizon from the Soekor wells (MacKay 2013). The best-fit second-order polynomial to these data was used to convert TWT to depth for this survey. A limitation of this method is that velocities are averaged over a large area, thus assuming a constant lateral velocity in the study area. This adds uncertainty to the data as varying dolerite distribution and regional facies changes exist (Chap. 1 this book) within the basin will cause velocities to vary. Tectonic events will also impact velocity measurements within the Cape Fold Belt (CFB) as horizons are affected by folding and faulting, resulting in shallower depth intersections.

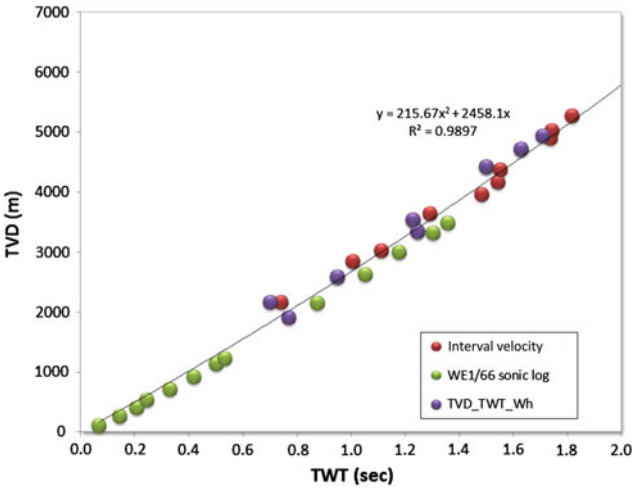

Fig. 2.2 Time-depth plots for Soekor seismic data. The total vertical depth (TVD) of the Whitehill Formation from well logs (Rowsell and De Swardt 1976) and the two-way travel times (TWT) of the first continuous strong reflector (interpreted as the Whitehill Formation) are plotted (TVD_TWT_Wh). Interval velocities determined by Fatti and du Toit (1970) are also plotted (Interval velocity), as well as the sonic velocity log from well WE1/66 (Fatti 1987). A second-order binomial curve is fit to the data with a y-intercept of zero (R^2 = 0.9897), providing a TVD to TWT conversion

2.3.2 Anglo-American Data

These seismic data are interpreted to better understand the subsurface geometry of sills and fluid vents within the central Karoo Basin (Fig. 2.1). Data was re-processed using new velocity fields and migration techniques. This allowed for the detection of sills and dykes that fall below convention vertical seismic resolution limits (<70 m). We used a standard post-stack migration but focused on important processing steps required for high-resolution imaging, such as field static corrections, f-k filtering, velocity analysis and Kirchhoff migration (see Webb et al. 2015 for details).

2.4 Results and Discussion

2.4.1 Dykes and Hydrothermal Vents

The central Karoo Basin is characterized by a greater extent of upper Karoo stratigraphy, with a remnant of the Stormberg Group preserved below the Lesotho lavas. Intrusions occur largely as dykes and saucer-shaped sills in this region possibly due to a reduced overburden during intrusion (Du Toit 1920; van Zijl 2006). In addition, the interaction of these sills with sediments in this region resulted in the explosive release of material in the form of vents interpreted as hydrothermal in origin (Svensen et al. 2006), or possible gas escape structures (Boyd et al. 2011). The explosive release of gas through these hydrothermal vents, as well as degassing from breccia pipes in the northwestern Karoo Basin, has been proposed as a significant contributor to climate change at 182 Ma (Svensen et al. 2004; Svensen et al. 2007).

In general, vertical features are not evident on seismic data; however, several regions of diffuse reflectivity are evident on the Anglo seismic line RT480 southwest of Lesotho (Fig. 2.3) and could be due to dykes or vents (Webb et al. 2015). Vertical displacement of material is evident from the upwarping of sediments surrounding the vents. Ground truth is needed to confirm the causative body. The end of the seismic line correlates with a large vent composed of breccia, agglomerate and tuff, and surrounded by basalt. If ground truthing reveals a hydrothermal vent, then this is the first subsurface evidence where vents have been imaged in the Karoo Basin.

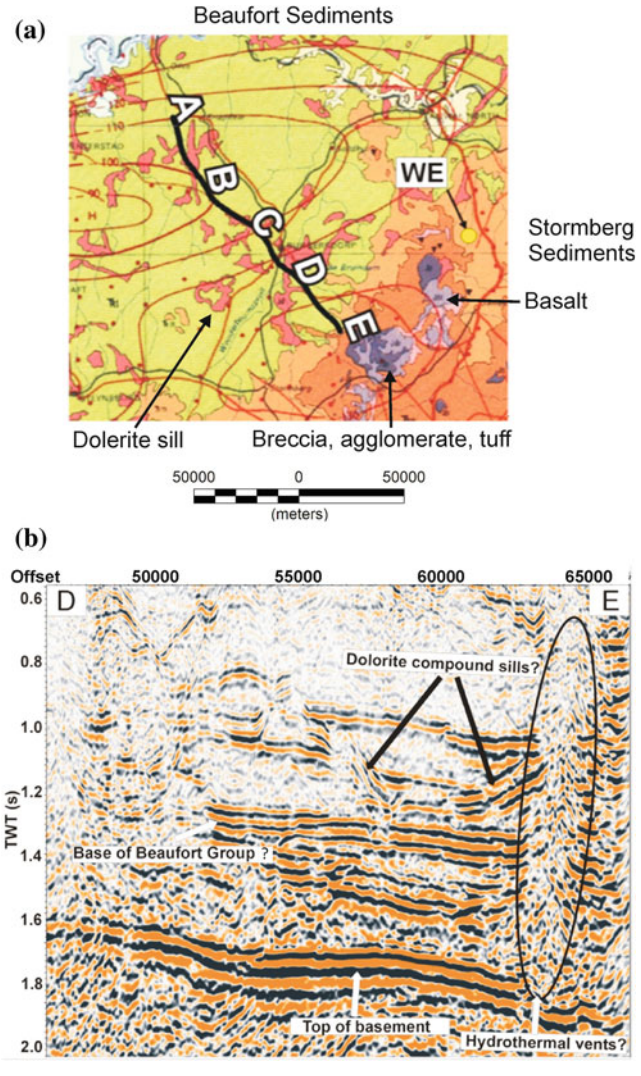

Fig. 2.3 **a** 1:1000,000 geological map showing Anglo seismic line RT480, with segments AB, BC, CD and DE marked. Segment DE is shown in **b** (modified from Webb et al. 2015). The section shows high-resolution imaging of dolerite compound sills and a vertical structure that could be linked to a gas escape feature cross-cutting the Ecca and Beaufort Groups, or a dyke. The top of the basement and the possible base of the Beaufort Group are indicated based on well WE1/66 farther to the east

2.4.2 Saucer-Shaped Sills

From the surface to the base of the Beaufort Group, sill structures are imaged on the seismic data (Fig. 2.4; Webb et al. 2015). These represent the circular or elliptical-shaped sills seen in outcrop throughout the Beaufort Groups (the Burgersdorp Formation) of the Karoo Basin (Du Toit 1920;

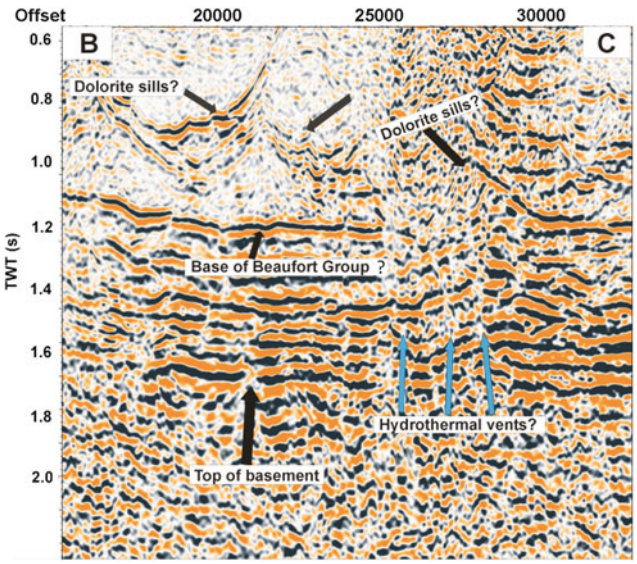

Fig. 2.4 Segment BC of Anglo seismic line RT480 (modified from Webb et al. 2015). See Fig. 2.3 for location. The section is interpreted to show high-resolution imaging of interconnected dolerite sills (compound sill or sill complex) and possible gas escape features cross-cutting the Ecca and Beaufort Groups. The top of the basement is indicated, as well as the possible base of the Beaufort Group based on well WE1/66

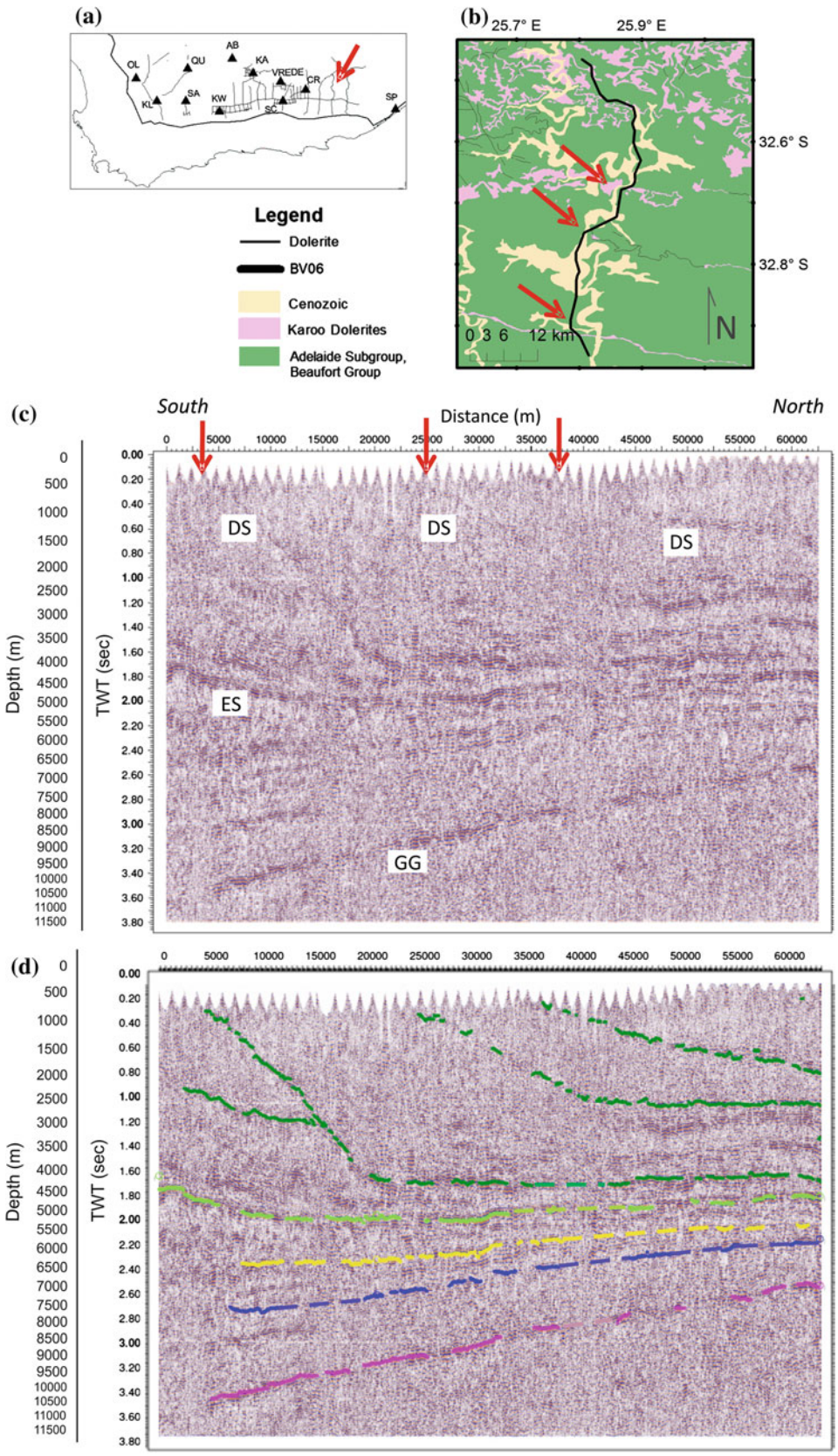

Fig. 2.5 **a** Location map of Soekor seismic profile BV06 in the southeastern Karoo Basin (*red arrow*), east of the town of Somerset-East (modified from Scheiber-Enslin et al. 2014). On the geological map in **b** the seismic profile (*thick black line*) passes over three dolerites sheets (*red arrows*). In **c** the original seismic profile BV06, and in **d** the interpreted seismic profile are shown with the deep reflectors of the Whitehill Formation (ES, *light green line*) and basement (GG, *pink line*) constrained by surrounding seismic lines. Cape Supergroup stratigraphy is interpreted between these horizons (*Bokkeveld Group, yellow line, and Table Mountain Group, blue line*). Shallower reflectors represent dolerite sheets (*DS, dark green*) that are correlated with outcropping dolerites in **b**. These cut through the Beaufort sediments to the surface, and connect to sills at depth. One such sheet appears to have intruded close to the Whitehill Formation (ES). The dip of these sheets steepen from 3°, 5°–6° to 8°–12° respectively to the south. Multiples have been interpreted between these sills

Galerne et al. 2011). Several models of emplacement have been suggested (Chevallier and Woodford 1999; Malthe-Sørenssen et al. 2004; Galland et al. 2006; Polteau et al. 2008; Galerne et al. 2011). Most often these sills occur together as complex interconnected sills extending across multiple levels of the stratigraphy with ends connected by inclined sheets. It has been suggested that such inclined sheets form as the intrusion overcomes the confining stress and a breakout occurs to shallower stratigraphy levels, where it again follows the stratigraphy horizontally (Malthe-Sørenssen et al. 2004). In general, the sills are between 5 and 30 km in diameter, with vertical thicknesses of up to ~270 m each (Scheiber-Enslin et al. 2014). The inclined sheets dip at between 2° and 8°.

These intrusions favour interfaces between weak and strong media (e.g., shale and sandstone; Burchardt 2008). From well core it has been shown that preferential horizons include the Prince Albert-Whitehill Formation contact, as well as along the Dwyka-Ecca Group contact, the upper Ecca-lower Beaufort Group contact, and lithological boundaries within the Beaufort Group (Du Toit 1920; Cole and McLachlan 1994).

2.4.3 Large Sills and Inclined Sheets

Lower in the stratigraphy (Teekloof/Middleton and Abrahamskraal Formations of the Beaufort Group, and Ecca Group) around Somerset East, several large sills and inclined sheets are imaged on the SOEKOR seismic data extending subhorizontally for over 50 km in the subsurface (Fig. 2.5; Scheiber-Enslin et al. 2014). These inclined sheets reach the surface from up to 5 km depth at dips of between 3° and 13°. Several of these sills intrude close to the Ecca shale layers.

The dip of these sheets appear to be affected by the proximity to the CFB, with the closest having steeper dips (Scheiber-Enslin et al. 2014). This relationship could be linked to the existence of the "dolerite line" in the south, i.e. that dipping Karoo Supergroup sediments due to CFB deformation limited the southern extent of the dolerite intrusions. It appears that dolerites do not intrude Karoo Supergroup rocks that dip greater than 15°–20° to the north (Scheiber-Enslin et al. 2014). However, this relationship does not explain why the "dolerite line" is closer to the CFB in the east and further away in the west. An additional influence on the "dolerite line" could be the regional shape of the basin. A depth map created using the Soekor seismic and well data, as well as additional CGS and industry wells show that the basin deepens to the southeast (Fig. 2.6, Scheiber-Enslin et al. 2015). In addition, this map shows that in the southern part of the basin (south of 32°S), the Karoo stratigraphy dips to the south more steeply in the west compared to the east, i.e. there is more rapid deepening in the west compared to the east. This shallower dip of

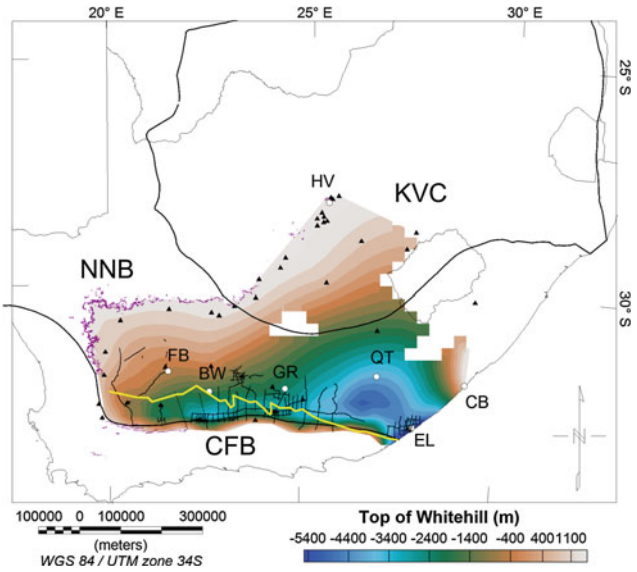

Fig. 2.6 Depth map of the Whitehill Formation relative to WGS84 (modified from Scheiber-Enslin et al. 2015). Data used to constrain the map are marked (seismic = *black lines*; wells = *black triangles*). The dolerite line, south of which no dolerite intrusions are intersected in the wells or outcrop on surface is marked (*yellow line*). The towns of Fraserburg (FB), Beaufort West (BW), Graaff-Reinet (GR), Queenstown (QT) and East London (EL) are marked. The outcropping Whitehill Formation is shown around the edges of the basin (*purple*). The formation pinches out between Hertzogville (HV) and Coffee Bay (CB). The major tectonic provinces are outlined: KVC = Kaapvaal Craton; NNB = Namaqua-Natal Belt; and CFB = Cape Fold Belt

sediments in the southeast could have allowed dolerites sills, which often follow bedding planes, to intrude farther south in this region (Scheiber-Enslin et al. 2015).

2.5 Conclusions

The presence of sills at multiple levels in deep wells and in seismic data suggests that they are pervasive throughout the Karoo Basin, but do not appear to extend south of the "dolerite line". For the future of shale gas exploration to be successful, multiple geophysical methods are needed to understand the geometry and depths of the shale layer, as well as the impact of dolerite intrusions and interpreted vents on this layer (Whitehill Formation).

Examples of studies that have already been conducted include aeromagnetic surveys (Stettler et al. 1999). These data highlight pervasive dolerite sills and dykes at shallow levels in the Karoo Basin. These sills and dykes are easily mapped with the coarse regional magnetic data from the Council for Geoscience (Fig 2.7a, flight height of 100–150 m and line spacing of 1 km). Higher resolution magnetic data in the northwestern Karoo Basin also collected by the Council (flight height of 80 m and line spacing of 200 m) provide better mapping especially of deeper bodies, and highlight bodies that might otherwise be missed using the regional data (Fig. 2.7b and c, Scheiber-Enslin et al. 2014). These high-resolution data indicate the importance of integrated geophysical studies when evaluating the shale gas potential in the Karoo Basin. Additional geophysical methods that have helped map the subsurface fracture system associated with these dykes, as well as the impact of interconnected subsurface structures on aquifers include electromagnetic methods (Chevallier et al. 2004). These structures and fractures could impact gas-groundwater interaction by providing pathways along which fluids can

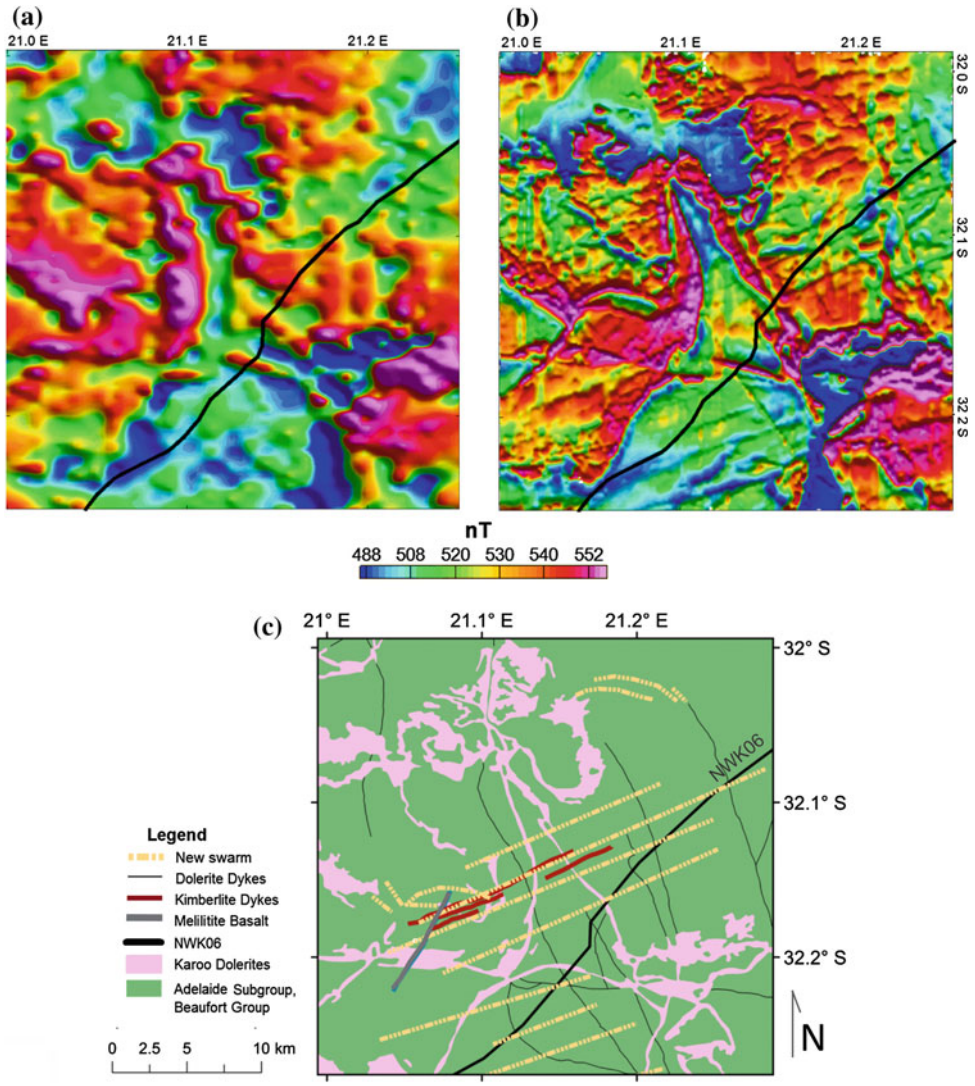

Fig. 2.7 **a** Regional (sun-shading at 45°) and **b** high-resolution (sun-shading at 135°) total magnetic field data for a region in the northwestern Karoo Basin, southwest of the town of Fraserburg (modified from Scheiber-Enslin et al. 2014). These magnetic data maps clearly locate the dolerite sills. Seismic line NWK06 is indicated (*thick black line*). A northwest-trending dolerite dyke swarm is visible on the regional data in **a** and high-resolution data in **b**, and mapped on the geological map in **c** (*thin black lines*, SSAC 1980). An east-northeast trending swarm is only visible on the high-resolution data in **b**. This swarm corresponds with several mapped dykes in **c** (*maroon lines*). The full extent of the swarm is mapped using the magnetic data and overlain on the geological map in **c** (*dashed yellow lines*). An additional northeast trending melitite basalt dyke is mapped from outcrop

mix. Going forward, more geophysical studies will be needed (e.g., Chap. 3 this book).

Acknowledgments We greatly appreciate the software support of Geosoft and Kingdom Suite to this project. We also thank the Department of Science and Technology (DST) for the award of a NRF-PDP grant to Stephanie Scheiber-Enslin and the Norwegian Research Council for research travel grants. We thank the Council for Geoscience and Falcon Oil and Gas for data access. The authors are grateful to Jacek Stankiewicz for improving this chapter greatly through the review process.

References

Aarnes I, Svensen H, Polteau S, Planke S (2011) Contact metamorphic devolitilization of shales in the Main Karoo Basin, South Africa and the effects of multiple sill intrusions. Chemical Geology 281:181–194

Boyd D, Anka Z, Primio RD, Kuhlmann G, De Wit MJ (2011) Passive Margin Evolution And Controls On Natural Gas Leakage In The Orange Basin, South Africa. South African Journal of Geology 114 (3–4):415-432

Burchardt S (2008) New insights into the mechanics of sill emplacement provided by field observations of the Njardvik Sill, Northest Iceland. Journal of Volcanology and Geothermal Research 173:280–288

Cawthorn RG Distribution of Dolerite Sills in the Karoo Supergroup. In: LASI 5 Conference, Port Elizabeth, South Africa, 2012. pp 28–29

Chevallier L, Gibson LA, Nhleko LO, Woodford AC, Nomquphu W, Kippie I (2004) Hydrogeology of fractured-rock aquifers and related ecosystems within the Qoqodala dolerite ring and sill complex, Great Kei Catchment, Eastern Cape. vol Report No. 1238/04. Water Research Commission,

Chevallier L, Goedhart M, Woodford A (2001) The Influence of Dolerite Sill and Ring Complexes on the Occurrence of Groundwater in Karoo Fractured Aquifers: A Morpho-Tectonic Approach. Water Research Commission Report, vol 937/1/01.

Chevallier L, Woodford A (1999) Morpho-Tectonics And Mechanism Of Emplacement Of The Dolerite Rings And Sills Of The Western Karoo, South Africa. South African Journal of Geology 102 (1):43–56

Cole DI, McLachlan IR (1994) Oil shale potential and depositional environment of the Whitehill Formation in the main Karoo basin. Publication (unedited), Geological Survey of South Africa, Library book no 553283COL (Volume I Text; Volume II Tables and Appendixes) Also Report No 1994–0213

De Wit MJ, Tinker J (2004) Crustal structures across the central Kaapvaal craton from deep-seismic reflection data.. South African Journal of Geology 107:185–206

Decker JE, Marot J (2012) Annexure A: Resource Assessment. In: In: Department of Mineral Resources, 2012. Report on Investigation of Hydraulic Fracturing in the Karoo Basin of South Africa. pp 81 p., 15 annexures

Du Toit AI (1920) The Karoo Dolerites. Transactions, Geological Society of South Africa 33:1–42

Duncan AR, Hooper PR, Rehacek J, Marsh JS, Duncan RA (1997) The timing and duration of the Karoo igneous event, Southern Gondwana. Journal of Geophysical Research 102:18127–18138

Fatti L (1970) The use of seismic reflection techniques in the Karoo basin. University of the Witwatersrand, South Africa, Johannesburg

Fatti L (1987) Reflection Seismic Surveys in the Karoo Basin by Soekor. SAGA Yearbook:22–30

Fatti L, Du Toit JJL (1970) A regional reflection-seismic line in the Karoo basin near Beaufort West. Geological Society of South Africa - Transactions and Proceedings 73:17–28

Galerne CY, Galland O, Neumann E-R, Planke S (2011) 3D relationships between sills and their feeders: evidence from the Golden Valley Sill Complex (Karoo Basin) and experimental modelling. Journal of Volcanology and Geothermal Research 202:189–199

Galland O, Cobbold PR, Hallot E, de Bremond d'Ars J, Delavaud G (2006) Use of vegetable oil and silica powder for scale modelling of magmatic intrusion in a deforming brittle crust. Earth and Planetary Science Letters 243:786–804

Leith MJ (1970) Well completion report of SP1/69. Internal Soekor Report vol PSV684a

Lindeque AS, De Wit MJR, T., Weber M, Chevallier L (2011) Deep crustal profile across the Southern Karoo basin and Beattie magnetic anomaly, South Africa: An integrated interpretation with tectonic implications. South African Journal of Geology 114 (3–4):265–292

Loots L (2013) Investigation of the crust in the southern Karoo using the seismic reflection technique. University of the Witwatersrand, South Africa, 128pp

MacKay S (2013) The Interpreter's Guide to Depth Imaging. Society of Exploration Geophysicists Short Course. 604pp

Malthe-Sørenssen A, Planke S, Svensen H, Jamtveit B (2004) Formation of saucer-shaped sills. In: Breitkreuz C, Petford N (eds) Physical geology of High-Level Magmatic Systems, vol 234. Geological Society, London, Special Publication, London, pp 215–227

Polteau S, Mazzini A, Galland O, Planke S, Malthe-Sørenssen A (2008) Saucer-shaped intrusions: Occurrences, emplacement and implications. Earth and Planetary Science Letters 266:195–204

Rowsell DM, De Swardt AMJ (1976) Diagenesis in Cape and Karroo sediments, South Africa, and its bearing on their hydrocarbon potential. Transactions, Geological Society of South Africa 79:81–145

Scheiber-Enslin SE, Ebbing J, Webb SJ (2015) New Depth Maps Of The Main Karoo Basin, Used To Explore The Cape Isostatic Anomaly South African Journal of Geology 118 (3):261–284

Scheiber-Enslin SE, Webb SJ, Ebbing J (2014) Geophysically Plumbing the Main Karoo Basin, South Africa. South African Journal of Geology 117 (2):275–300. doi:10.2113/gssajg.117.2.275

Stankiewicz J, Ryberg T, Schulze A, Lindeque AS, Weber MH, De Wit MJ (2007) Initial results from wide-angle seismic refraction lines in the southern Cape. South African Journal of Geology 110:407–418

Stettler EH, Fourie CJS, Bühmann JR, Hattingh E, Cole P, Kleywegt RJ, Wolmarans LG, Cloete AJ (1999) Magnetics. In: South African Geophysical Atlas. Volume 2 (CD Rom). Council for Geoscience, South Africa,

SSAC (1980) Stratigraphy of South Africa. Part 1 (Compiled by L.E. Kent). Lithostratigraphy of the Republic of South Africa, South West Africa/Namibia, and the Republics of Bophuthatswana, Transkei and Venda. Handbook 8, Geological Survey, South Africa:690

Svensen H, Jamtveit B, Planke S, Chevallier L (2006) Structure and evolution of hydrothermal vent complexes in the Karoo Basin, South Africa. Journal of the Geological Society of London 163:671–682

Svensen H, Planke S, Chevallier L, Malthe-Sörensen A, Corfu F, Jamtveit B (2007) Hydrothermal venting of green-house gases

triggering Early Jurassic global warming. Earth and Planetary Science Letters 256:554–566

Svensen H, Planke S, Malthe-Sørenssen A, Jamtveit B, Myklebust R, Eidem TR, Rey SS (2004) Release of methane from a volcanic basin as a mechanism for initial Eocene global warming. Nature 429:542–545

van Zijl JSV (2006) Physical characteristics of the Karoo sediments and mode of emplacement of the dolerites. South African Journal of Geology 109:329–334

Webb SJ, Manzi M, Scheiber-Enslin SE (2015) Seismic imaging of sills, dykes and hydrothermal vents in the Main Karoo Basin, South Africa: implications for shale gas potential Paper presented at the South African Geophysical Association Biennial Conference, Drakensburg Champagne Sports,

Widess MB (1973) How thin is a thin bed? Geophysics 38:1176–1180

3 Ambient Noise Tomography (Passive Seismic) to Image the Cape-Karoo Transition Near Jansenville, Eastern Cape

Lucien Bezuidenhout, Moctar Doucouré, Viera Wagener, and Maarten J. de Wit

Abstract

During August and September 2015, a seismic network consisting of 17 stations was installed in the south-eastern Cape-Karoo region, near the town of Jansenville. Ambient seismic signals were continuously recorded for a three week period. In this chapter, we reconstruct estimates of the seismic Green's functions between sensor pairs by cross-correlating the ambient seismic signals recorded in the vertical component of each station. The resulting Green's functions contain clear direct Rayleigh wave arrivals. The measured group velocity dispersion curves of the Rayleigh waves were averaged in the period range from 2.5 to 5.5 s (approximately 2–5 km depth). The arrival times of the Rayleigh waves are picked at different periods and then inverted to compute 2-D group velocity maps. This resulted in a velocity model up to depths of 5 km. The results reveal two different velocity regions, broadly corresponding to the Cape Fold Belt and the flanking Karoo Basin. The higher group velocity anomalies (3–5 km in thickness) most likely represent the Carboniferous-Permian sequences of the Karoo Basin (Dwyka-Ecca-Beaufort Groups). A lowermost velocity region in the south-eastern study area could correspond to the Jurassic-Cretaceous sequences of the Algoa Basin that directly overlie the Cape Fold Belt.

Keywords

Ambient noise • Group velocity maps • Tomography • Cape-Karoo contact • Algoa basin

3.1 Introduction

Previous reflection seismic experiments conducted across the Cape Fold Belt and Karoo Basin using active sources have shown that the upper crust, comprising the Paleozoic–Mesozoic Cape and Karoo Supergroups, decreases in thickness from more than 10 km in the south to 2–3 km farther to the north across a distance of about 100 km (Lindeque et al. 2007; 2011; Stankiewicz et al. 2007; Chap. 2 this book). At the front of the Cape Fold Belt, the Karoo Basin sequences are up to 5 km thick as confirmed by deep boreholes (Chap. 1 this book). The most recent reflection data obtained by Lindeque et al. (2007) also contained continuous seismic recordings up to 60 h after each shot. Ryberg (2011) used this 'by product' data to detect refracted and reflected body waves from the cross correlation functions derived from the recordings, indicating that the use of the ambient noise technique in this region is feasible. Since it is more common to investigate the surface wave's component of the ambient noise wave coda, Ryberg (2011) concluded that the high frequency component of the ambient noise wave field consist of refracted and reflected

L. Bezuidenhout (✉) · M. Doucouré · V. Wagener · M.J. de Wit
AEON, Earth Stewardship Science Research Institute, Nelson Mandela Metropolitan University, PO Box 77000Port Elizabeth, 6031, South Africa
e-mail: Lucian.Bezuidenhout@nmmu.ac.za

M. Doucouré
e-mail: Moctar.Doucoure@nmmu.ac.za

V. Wagener
e-mail: Viera.Wagener@nmmu.ac.za

M.J. de Wit
e-mail: Maarten.deWit@nmmu.ac.za

B. Linol and M.J. de Wit (eds.), *Origin and Evolution of the Cape Mountains and Karoo Basin*,
Regional Geology Reviews, DOI 10.1007/978-3-319-40859-0_3

P-waves and could potentially be used as an input for travel time tomography.

Traditional seismic techniques, such as teleseismic observations, do not fully utilize seismic array data. The seismic stations located far from the earthquake lose the high frequency content in the coda due to attenuation and therefore lose spatial resolution in the upper crust (Shapiro et al. 2005). Approximately 50 years ago, Claerbout pointed out that 'by cross-correlating noise traces recorded at two locations (at) on the surface, a wavefield can be constructed that would be recorded at one of the locations if there was a source at the other' (Claerbout 1968). Claerbout's conjecture gained momentum in the seismic community a few decades later after the approach was successfully applied to helioseismic data (Duvall et al. 1993). A few years later Weaver and Lobkis (2001) showed that the Green's function emerges between two ultrasonic sensors when cross-correlating the recorded signal in the presence of a diffuse ultrasonic field. Shapiro et al. (2005) extended this idea and were the first to show that Rayleigh waves emerge from the correlation of ambient seismic noise originating from the oceanic microseisms. This started a revolution in seismology: there was no longer a need for inconvenient controlled seismic sources to image and monitor the earth at different scales; instead each sensor can be used as a virtual seismic source. This passive seismic approach allows for easy deployment of seismic stations, requiring no induced source, thereby permitting access to remote areas. It is also environmentally a low impact technique that is cost effective compared to conventional (active) seismic methods.

In this study, an ambient seismic noise experiment was conducted in an area (approximately 2000 km^2) southeast of Jansenville (Fig. 3.1) to determine and investigate the velocity structures across the transition between the Cape and Karoo Supergroup rock sequences. The Cape Supergroup forms the backbone of the Cape Mountains, extending from the Outeniqua Mountains (near George) in the west, to the Groot Winterhoek Mountains (near Port Elizabeth) in the east. The Cape Supergroup comprises the Table Mountain quartzites, the Bokkeveld shales and sandstones, and the

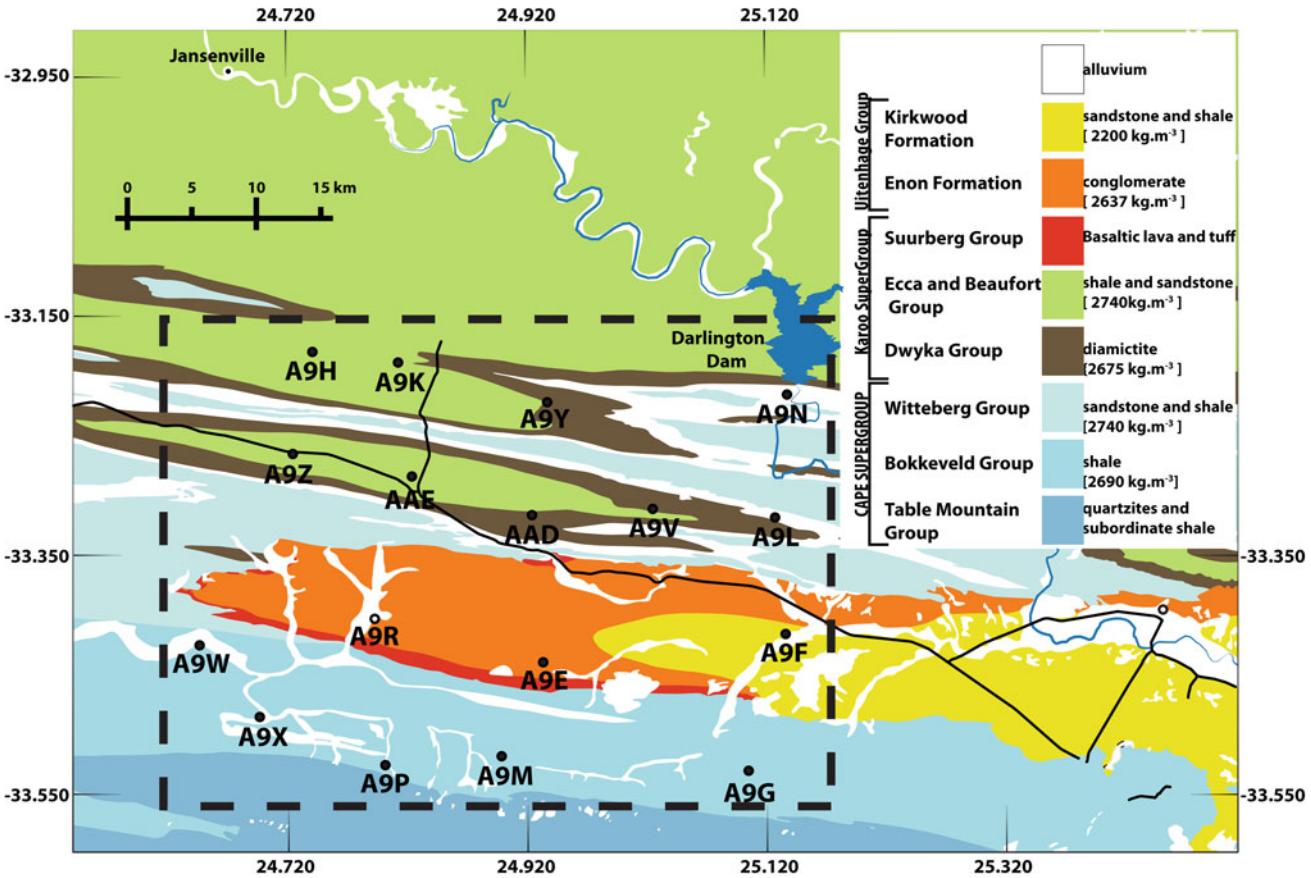

Fig. 3.1 Location of the seismic stations (indicated by *black dots*) and geological setting of the survey area southeast of Jansenville. The *dashed square* outlines the area covered in the tomographic inversion presented in Fig. 3.3. In the legend the average densities for each sequence are shown in *brackets* (from Maré 2012)

Witteberg Group, which consist of quartzite sandstones and micaceous mudrocks (Thamm and Johnson 2006; Tankard et al. 2009). These lower Paleozoic sequences are folded and thrusted northward, reflecting deformation during the Cape Orogeny at about 250 Ma (see Chap. 5 in this book). The overlying Karoo Supergroup comprises Dwyka massive diamictites and black shales of the lowermost Ecca Group (Prince Albert and Whitehill Formations), which are also deformed (Fig. 3.1). The black shales are overlain to the north by thick sequences of mudstone with subordinate sandstone of the Permian–Triassic Ecca and Beaufort Groups (Johnson et al. 2006), which in places are also affected by folding and thrusting related to the Cape Orogeny (Booth and Goodhart 2014). In the southeast of the survey area relatively undeformed and younger Jurassic-Cretaceous rift sediments of the Algoa Basin (between 2 and 10 km thick) consist of tilted conglomerates, sandstones and red mudstones of the Uitenhage Group underlain by a thin sequence of volcanics of the Suurberg Group (Fig. 3.1; Broad et al. 2006; Paton and Underhill 2004; see also Chap. 6 in this book).

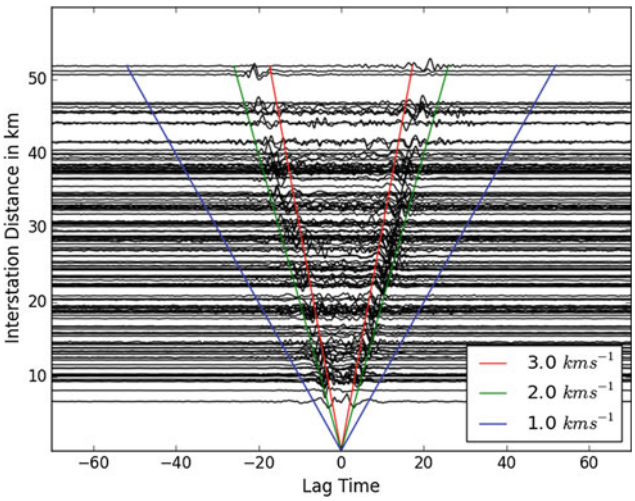

Fig. 3.2 Stacked empirical Green's function for all station pairs plotted as a function of interstation distance. The *positive* and *negative lags* are shown to increase the signal to noise ratio. The *red* and *green solid lines* indicate the arrival of Rayleigh waves between 1.0 and 3.0 kms^{-1}. This velocity is within the expected velocity range of the Rayleigh waves

3.2 Ambient Noise Tomography

3.2.1 Experimental Setup and Data Processing

The experimental setup consisted of 17 three-component short-period seismic sensors (location depicted in Fig. 3.1), each powered by sealed gel battery and connected to a 3-channel seismic recorder (Omnirecs Data-Cube). Time synchronization between stations was achieved by internal GPS modules and signal was recorded at a rate of 100 samples per second. The interstation distances varied between 7 and 52 km (Fig. 3.1).

Minor modifications to the data processing steps, as discussed in detail by Bensen et al. (2007) were performed on our data set. These steps consist of a single station data preparation, cross correlation, stacking, frequency time analysis (FTAN), 2-D inversion and error analysis. Each station records are pre-processed for daily traces. These steps resulted in mean and trend removal, bandpass filtering and spectral whitening of the continuous recordings between 0.01 and 8 Hz. One bit normalization is then applied to these whitened noise records (Bensen et al. 2007; Macquet et al. 2014). Finally, we cross correlate the daily whitened and one bit vertical component traces for all stations pairs. Since there are 17 stations the maximum number of station pairs is 136. The cross correlation functions are then stacked together for positive and negative time lag to improve the signal to noise ratio. Figure 3.2 shows the stacked envelopes of resulting cross correlations between all stations pairs plotted as a function of the interstation distance. The coherency of the signal and the arrival of the Rayleigh waves are clearly evident in Fig. 3.2.

The resulting cross correlation functions are then used to determine the frequency-dependent group and phase velocities of the Rayleigh waves by means of frequency time analysis or FTAN (Dziewonski et al. 1969; Ritzwoller et al. 2002).

To obtain the group velocity map at various periods, 2-D tomographic inversion was performed as described by Barmin et al. (2001) and Mordret et al. (2014). A grid composed of 23 by 29 cells and a grid size of 300 m was used to the 2-D inversion. The Rayleigh wave dispersion group velocity maps were inverted for periods between 1.5 and 5.5 s. Periods below 1.5 s and above 5.5 s resulted in distorted cross correlation functions due to instrumental response. The model used for the inversion had a constant velocity equivalent to that of the mean group velocity for each period. Different periods can be used to sample different depths in the subsurface. Figure 3.3 depicts the lateral variation of the group velocity as a function of period at 1.5, 3, 4.5 and 5 s. Since a Monte Carlo optimization technique was implemented for the inversion, a variance reduction was introduced to enhance the model fitting. Figure 3.3 shows the variance reduction of the travel time residual and the average group velocity at different periods. The variance reduction obtained from the group velocity maps is generally close to 50 % for the different periods, indicating that the modelled group velocity maps fits the data well (Mordret et al. 2015).

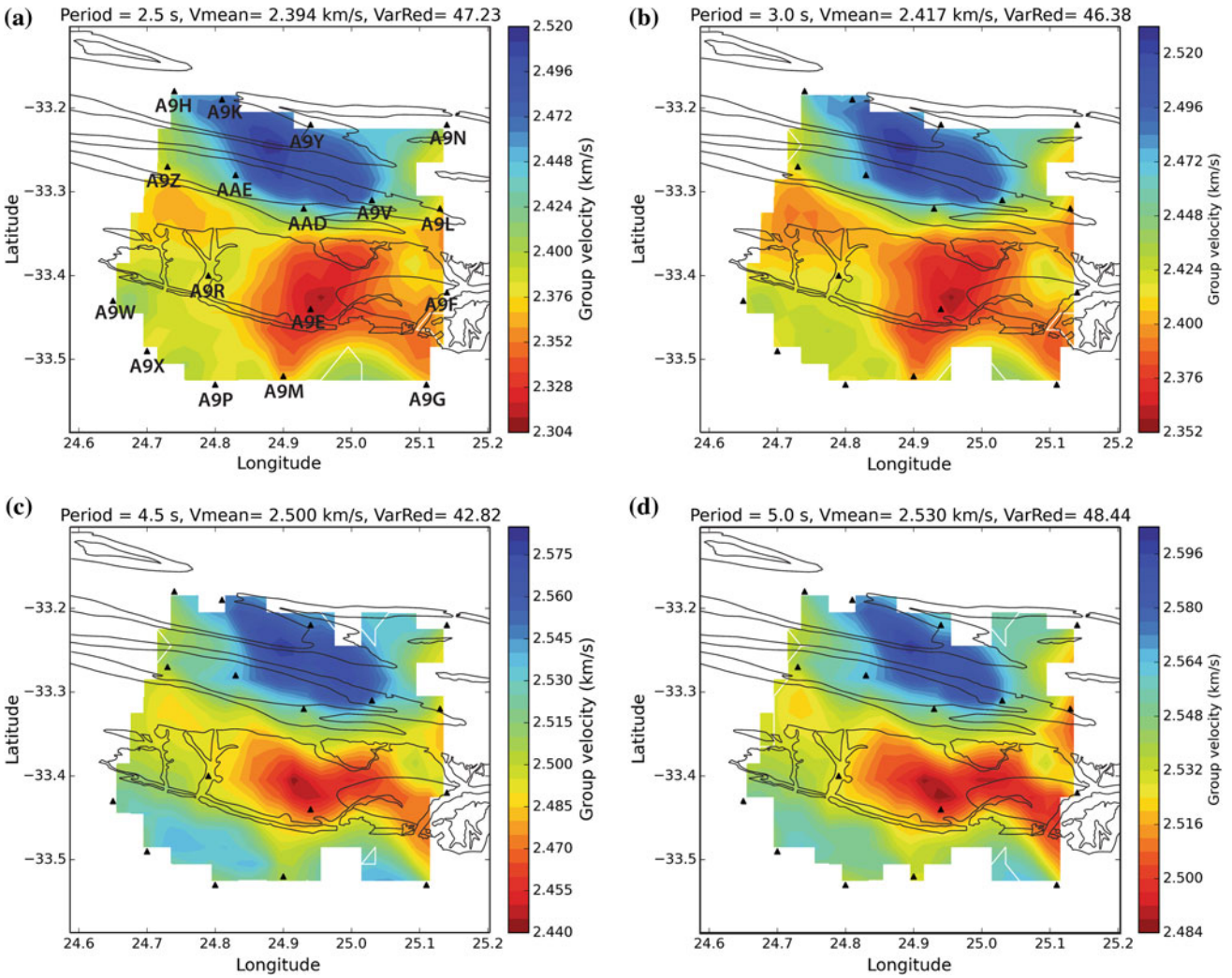

Fig. 3.3 Rayleigh waves group velocity maps at: **a** 2.5; **b** 3.0; **c** 4.5 and **d** 5.0 s. The *black triangles* show the location of the stations. Periods 1.5 and 2.5 s sample approximately the uppermost 2–3 km, and the 4.5 and 5 s sample the uppermost 4–5 km of the subsurface. The mean velocity and the variance reduction are also shown on each map. The *blue colour* indicates the high velocity region and the *red* the low velocity domains. Lithostratigraphic boundaries are from Fig. 3.1

3.2.2 Results and Interpretations

Figure 3.3 shows the group velocity maps for different periods. Higher periods sample deeper into the crust whilst high frequencies (shorter period) image the shallow subsurface (Stankiewicz et al. 2010). The 2.5 s map (Fig. 3.3a) gives an average velocity model of the uppermost 2–3 km, and the 5 s map (Fig. 3.3d) of the uppermost 4–5 km.

Two distinct velocity anomalies are observed in the north and southern sectors of the tomography maps. This could be due to a directional bias in the noise wavefields, which could result in this two-sided effect, although the relative symmetry of stacked cross correlation function (Fig. 3.2) suggest that the noise wavefields are evenly distributed. The two distinct velocity anomalies could thus intuitively coincide with the transition between the Cape Fold Belt and Karoo Basin, respectively. The high velocity region to the north of the study area is consistent with the >5 km thick and dense (lithified fine grained sediments) sequences of the Karoo Basin. A distinct low velocity region in the south of the study area (Fig. 3.3) coincides to the younger Uitenhage Group of the Algoa Basin, consistent with lower compaction and thus lower group velocities. An intermediate velocity region appears at depth >4 km (on the 4.5 and 5.0 s maps) in the south and southwest of the study area, which could possibly mark the southern margin of the Algoa Basin, marked with basaltic volcanics and tuffs (Fig. 3.1). Seismic velocity depends on many parameters such as material (rock)

composition, packing structure, temperature and pressure. Velocity increases with increasing densities. The mean velocity (Fig. 3.3) increases with the sampling period and therefore with depth. This suggests that the Cape and Karoo rock density increases with depth. Karoo rocks, and in particular, the Ecca and Beaufort Groups, are dominated by a fine to coarse grained sandstone and mudstones that are lithified. This is also consistent with a more dense structure. The Ecca and Beaufort Groups have an average density of 2740 and 2720 kg m^{-3}, respectively (Maré 2012). The Algoa Basin sediments that comprise of conglomerates, sandstones and red mudstone have average densities of 2637 and 2200 kg m^{-3}, respectively (Maré 2012). The difference in the two distinct velocity domains in the northern and southern section of the tomography maps can be attributed to the variation in the density of the rocks, with higher density rocks having faster velocities.

3.3 Conclusions

The deployment of 17 passive seismic stations across the Cape-Karoo transition in the Eastern Cape region allowed for a high resolution group velocity maps at depths between 2 and 5 km. By cross-correlating ambient noise between station pairs, arrival times for Rayleigh surface waves were determined. An inversion method was used to extract group velocity maps for different periods. The resulting tomographic maps show two distinct domains, to the north and to the south of the study area, with the transition coinciding broadly to the contact between the Cape Fold Belt and Karoo Basin. The location of this Cape-Karoo transition, with particular emphasis on the Dwyka Group and overlying black shales that constitutes the main target of shale gas exploration cannot be resolved with confidence with the current station layout. In addition, the presence of thick younger sediments of the Algoa Basin in the south-eastern study area significantly dominates the group velocity maps at depths less than 3–4 km. Nevertheless, this study demonstrates the possibility of using ambient seismic noise cross-correlation to image deep geological structures in the Cape-Karoo transition at relatively low cost. Currently, further experiments are ongoing to increase the resolution achieved by this study and to examine the deeper geology of the relatively undeformed Karoo Basin, as well as the influence of groundwater aquifers on seismic velocities.

Acknowledgments The authors would like to thank AEON and the Iphakade programme (DST/NRF) for financial support. We would also like to thank the Members of Sisprobe for assistance with processing. Comments from Bastien Linol and Gerrit Olivier improved the paper. This is AEON contribution number 156.

References

Barmin M, Ritwoller M and Levshin A (2001) A fast and reliable method of surface wave tomography. Pure appl Geophys 158:1351–1375.

Bensen B, Ritzwoller M, Barmin M, Levshin A, Lin F, Moschetti M, Shapiro N and Yang Y (2007). Processing seismic ambient noise data to obtain reliable broad-band surface wave dispersion measurements. Geophys J Int 169:1239–1260. doi:10.111/j.1365-246X.2007.03374.x.

Booth PWK and Goedhart ML (2014). Thrust faulting in the northernmost foreland zone of the Cape Fold Belt, Fort Beaufort, Eastern Cape, South Africa. S Afri J Geol 117(2):301–315. doi:10.2113/gssajg.l.

Broad D, Jungslager A, McLachlan I and Roux J, Offshore Mesozaic Basins (2006). In: Johnson MR, Anhaeusser CR and Thomas RJ (eds) The Geology of South Africa, pp. 553–571.

Claerbout J (1968). Synthesis of a layered medium from its acoustic transmission response. Geophysics 33(2):263–269.

Duvall T, Jeffreis S, Harvey J and Pomarantz M (1993). Time-distance helioseismology. Nature 362:420–432.

Dziewonski A, Bloch S and Landisman M (1969). A technique for analysis for transient seismic signals. Gull Seism Soc Am 59:427–444.

Johnson M, van Vuuren C, Visser J, Cole D, de Wickens A, Christie A, Roberts D and Brandl G (2006). Sedimentary rocks of the Karoo Supergroup. In: Johnson MR, Anhaeusser CR and Thomas RJ (eds) The Geology of South Africa, pp. 461–499.

Lindeque A, Ryberg T, Stankiewicz J, Weber M and de Wit M (2007). Deep crustal seismic reflection experiment across the Southern Karoo Basin, South Africa. S Af J Geol 110:419–438. doi:10.2113/gssajg.110.2/3.419.

Lindeque A, de Wit M, Ryberg T, Weber M and Chevallier L (2011). Deep Crustal Profile Across The Southern Karoo Basin And Beattie Magnetic Anomaly, South Africa: An Integrated Interpretation With Tectonic Implications. S Af J Geol 114:265–292.

Macquet, M, Paul A, Pedersen H, Villasenor A, Chevrot S, Sylvander M, Wolyniec D and Pyrope Working Group (2014). Ambient noise tomography of the Pyrenees and the surrounding regions: inversion for a 3-D Vs model in the presence of a very heterogeneous crust. Geophys J Int 199:402–415.

Maré L. P (2012). Council for Geoscience Petrophysical Properties Atlas.

Mordret A, Rivet A, Landes M and Shapiro M (2015). Three-dimensional shear velocity anisotropic model of Piton de la Fournaise Volcano (La Reunion Island) from ambient noise. J Geophys Res Solid Earth 120:406–427. doi:10.1002/2014JB011654.

Mordret A, Landes M, Shapiro M, Singh S and Roux P (2014). Ambient noise surface wave tomography to determine the shallow shear velocity structure at Valhall: Depth inversion with a Neighborhood Algorithm. Geophys J Int 193(3):1514–1525.

Paton D and Underhill J (2004). Role of crustal anisotropy in modifying the structural and sedimentological evolution of extensional basins: the Gamtoos Basin, South Africa. Basin Res 16:339–369. doi:10.1111/j.1365-2117.2004.00237.x.

Ritzwoller M, Shapiro M, Barmin M and Levshin L (2002). Global surface wave diffraction tomography. J Geophys Res 107 (B12):2335. doi:10.1029/2002JB001777.

Ryberg T (2011). Body wave observation from cross-correlation of ambient seismic noise: A case study from the Karoo, RSA. Geophys Res Let 38:L13311 doi:10.1029/2011GL047665.

Shapiro N, Campillo M, Stehly L and Ritzwoller M (2005). High resolution surface-wave tomography from ambient seismic noise. Science 07(5715):233–236.

Stankiewicz J, Rydberg T, Haberland C, Natawidjaja F and Natawidjaja D (2010). Lake Toba vancano magma chamber imaged by ambient seismic noise tomography. Geophys Res Let 37. doi:10.1029/2010GL044211.

Stankiewicz J, Rydberg T, Schulze A, Lindeque A, Weber M.H and de Wit MJ (2007). Initial results from wide-angle seismic refraction lines in the southern Cape. S Af J Geol 110:407–418. doi:10.2113/gssajg.110.2/3.407.

Tankard A, Welsink H, Aukes P, Newton R and Stettler E (2009). Tectonic evolution of the Cape and Karoo Basins of South Africa. Mar Pet Geol. doi:10.1016/j.marpetgeo.2009.01.022.

Thamm A and Johnson M (2006). The Cape Supergroup. In: Johnson MR, Anhaeusser CR and Thomas RJ (eds) The Geology of South Africa, pp. 443–459.

Weaver R and Lobkis O (2001). On the emergence of the Green's function in the correlation of a diffuse field. J acoust Soc Am 110:3011–3017.

Part II
Structural Geology

4 New Structural Data and U/Pb Dates from the Gamtoos Complex and Lowermost Cape Supergroup of the Eastern Cape Fold Belt, in Support of a Southward Paleo-Subduction Polarity

Warren Miller, Maarten J. de Wit, Bastien Linol, and Richard Armstrong

Abstract

Recent seismic profiling, together with new field mapping and U-Pb zircon geochronology, suggest south-dipping plate subduction polarity linked to the Permo-Triassic Cape Fold Belt of South Africa, during the Gondwanide Orogen. Here, we present further evidence that rocks of the Gamtoos Complex, predating the deposition of the Lower Paleozoic Cape Supergroup, west of Port Elizabeth, form part of an accretionary prism, or lower detachment, of décollement horizons in the "pre-Cape" basement sequences that extend into the overlying quartzites and phyllites of the lower Table Mountain Group (Cape Supergroup) as splay faults penetrating into the upper sequences of the eastern section of the Cape Fold Belt.

Keywords

Cape Fold Belt • Tectonics • Gamtoos complex • U-Pb geochronology

4.1 Introduction

The Cape Fold Belt (CFB) forms part of a large Phanerozoic belt, known as the Gondwanide Orogen that flanked the southeastern paleo-Pacific margin of the supercontinent Gondwana (Fig. 4.1). This belt extends down the western coast of South America, across Argentina (as the Sierra de la Ventana), southern South Africa (as the CFB), the Falkland Islands, Antarctica, and into Eastern Australia and Tasmania (e.g. Dalziel 2000). The CFB is a fossil tectonic front outcropping along the southern tip of South Africa where it deforms siliciclastic rocks of the Cape Supergroup and lower Karoo Supergroup dating from lower Cambrian to the Permian (Fildani et al. 2009; Miller et al. 2016). Age constraints on deformation of the CFB are largely based on K/Ar and Ar/Ar dating of micas in cleaved metasedimentary rocks that range between 248–276 Ma (Hälbich 1993; Hansma et al. 2015; Chap. 5 this book). Recent gravimetric, magnetic and seismic data (Pángaro and Ramos 2012) together with plate reconstruction models reveal that a continuous fold belt, extending 600 km from the Argentinean coast with a ca. 45° change in structural orientation, known as the Colorado Syntaxis, mirrors and connects with the Cape Syntaxis in South Africa (Fig. 4.1). It has been suggested that the configuration of the Cape-Ventana Fold Belt could reflect a buttressing effect due to the northward propagation of the allochthonous Patagonian Block, and its collision with the Rio de la Plata and Kalahari Shields (e.g. Ramos 2008; Fig. 4.1).

W. Miller (✉)
AEON-ESSRI (African Earth Observatory Network—Earth Stewardship Science Research Institute) and Department of Geosciences, Nelson Mandela Metropolitan University, Port Elizabeth, Beacon Bay, P.O. Box 15585East London, 5205, South Africa
e-mail: w.miller.aeon@gmail.com

M.J. de. Wit · B. Linol
AEON-ESSRI (African Earth Observatory Network—Earth Stewardship Science Research Institute), Nelson Mandela Metropolitan University, Port Elizabeth, P.O. Box 77000Port Elizabeth, 6031, South Africa
e-mail: maarten.dewit@nmmu.ac.za

B. Linol
e-mail: bastien.aeon@gmail.com

R. Armstrong
RSES (Research School of Earth Science), Australian National University, RSES, Australian National University Building, 142 Mills Road ACT 0200, Canberra, Australia
e-mail: richard.armstrong@anu.edu.au

B. Linol and M.J. de Wit (eds.), *Origin and Evolution of the Cape Mountains and Karoo Basin*,
Regional Geology Reviews, DOI 10.1007/978-3-319-40859-0_4

Fig. 4.1 Map of south-west Gondwana showing the main tectonic features during the Paleozoic with the Gondwanide Orogen. 1 = Colorado Syntaxis; 2 = Cape Syntaxis; 3 = Cape Antitaxis

In this study we measure tectonic structures and date detrital zircons from fine clastic units of the Gamtoos Complex and lowermost units of the lower Table Mountain Group in the easternmost part of the CFB, near Port Elizabeth. This helps to understand the geodynamics of the belt that in turn have influenced the evolution of large Paleozoic-Mesozoic basins to the north.

4.2 Tectonic Setting

Models for tectono-genesis of the CFB are controversial and often oversimplified. Most popular models have designated a transpressional regime and/or subducting regime to account for its deformation. Little success has been accredited to these models since they do not appeal to the lack or presence of all the associated tectonic features and their presumed links to magmatic arcs and accretionary structures to the south. Subduction polarity has often been regarded as dipping at low angles (Lock 1980) to high angles (Tankard et al. 2012), towards the direction and beneath the CFB, and hence the Permian-Triassic Karoo Basin is generally interpreted as a retro-arc foreland basin propagating northward. The existence of a hinge line observed in the stratigraphy of the Karoo Basin has also been associated with a retro-arc foreland basin model (Catuneanu et al. 2002; Rutherford et al. 2015). However, these models have recently been challenged, preferring southward-directed subduction, and thus challenging the prevailing tectonic setting for the Karoo Basin.

Three major models are summarised

1. Early models describe a northward-dipping subduction zone with a paleo-position to the south of the CFB, forming a fold-and-thrust belt (top to north) and associated "cordillera-type" foreland Karoo Basin to the north (Hälbich 1983a, b, c, 1993; Thomas et al. 1993; Catuneanu et al. 1998, 2002; Johnson et al. 2006; Tankard et al. 2009). These models interpret a large linear (sub-parallel) magnetic anomaly beneath the Karoo Basin, referred to as the Beattie Magnetic Anomaly (BMA), to represent a deeply buried (>6 km) "fossil" suture zone representing the collision of the Kalahari Shield with a landmass to the south (De Beer and Meyer 1984). However, recent seismic and magnetotelluric work has shown that the BMA is not a Paleozoic subduction zone, but rather a complex remnant of magnetised rocks of the Namaqua-Natal basement (Weckmann et al. 2007a, b; Stankiewicz et al. 2008; Lindeque et al. 2011; Scheiber-Enslin et al. 2014). The lack of a distant volcanic arc system and tectonic root related to the CFB in southern Africa during north-facing subduction continues to bring into question the validity of a cordillera-type retro-arc model.
2. More recent models invoke the CFB as a sinistral Permian-Triassic strike-slip orogeny by oblique reactivation of a southern part of the Namaqua-Natal Metamorphic Belt (Johnston 2000; Tankard et al. 2012). This reactivation zone is also inferred to link to a Precambrian subduction zone rooted in the BMA. But, there has been no field evidence that records consistent horizontal lineations in the CFB to support a strike-slip model.
3. Alternatively, Lindeque et al. (2011) modelled the CFB similar to the Jura Mountains in the western Alps, consisting of a major terrane collision, due to southward subduction with a southward polarity. This model, based on high-resolution seismic data, describes far-field

compressional tectonics, exerted towards the current location of the CFB, as blind thrusts, and accounts for the absence of a tectonic root to the CFB (e.g. Stankiewicz and de Wit 2013). Such a "Jura-type" model is also presently used for the Sierra de la Ventana Fold Belt of Argentina (Ramos 1988, 2008). In South Africa, the general south-dipping thrust faults are inferred to coalesce into a common south-dipping décollement or mega-detachment below the Cape Supergroup, at depths below 8 km (Hälbich and Swart 1983; de Wit and Ransome 1992; Paton et al. 2006).

4.3 New Field Observations Along the Western Coast of Port Elizabeth

The Gamtoos Complex forms part of the lowermost basement sequences of the eastern CFB. It is exposed in a tectonic window 70 km long and 5 km wide in the Eastern Cape region, near Port Elizabeth. The study area is located along the coast between Schoenmakerskop, through Sardinia Bay, Claasens Point, Lauries Bay, Kini Bay, Seaview and Maitlands River Mouth (Fig. 4.2).

4.3.1 Lithostratigraphy and Structure

The Gamtoos Complex comprises three main sequences, as defined by Nolte (1990) and Miller et al. (2016): (1) pale grey calcareous rocks of the Kaan Sequence; (2) grey to black grits and phyllites of the Kleinrivier Sequence; and (3) pale arenitic quartzites and shales of the Van Stadens Sequence (Fig. 4.2), all of which are separated by tectonic contacts and internal discontinuities. The complex is tectonically separated from an overlying basal unit of boulder conglomerates, named the lower Sardinia Bay Formation that forms the base of the Table Mountain Group, with the contact located at Sardinia Bay (Fig. 4.2). Overlying these basal conglomerates of the Cape Supergroup are feldspathic quartzites, interbedded with subordinate conglomerates and black phyllites (upper Sardinia Bay Formation). The latter is separated from the underlying Kleinrivier Sequence of the Gamtoos Complex by a thrust fault, near Lauries Bay (Fig. 4.2).

We recorded four events of deformation (D_1–D_4) in the study area (Fig. 4.2). The emphasis here is on the two earliest events (D_1–D_2) and their relationship with primary bedding (S_0) (Fig. 4.3). The first is a slaty cleavage (S_1) parallel to bedding (Figs. 4.3a, d, e). This fabric is deformed by a compressive crenulation cleavage (S_2) that is axial planar to tight to isoclinal folds (F_2), striking south-east to north-west and dipping to the south-west (Figs. 4.3 and 4.4) South-west plunging lineations in the form of slickenlines and intersection lineations ($S_{0/1}/S_2$) are here present in the quartz vein-rich shales and grits. These slickenlines and intersection lineations plunge steeply to the south-west near Kini Bay (Fig. 4.2) within the Kleinrivier Sequence, but become less steep in shale outcrops within the Kaan Sequence, near Claasens Point. In the shales of the upper Sardinia Bay Formation, the intersection lineations and slickensides are horizontal (Fig. 4.2). Both S_1 and S_2 are recorded in the Gamtoos Complex and upper Sardinia Bay Formation (Figs. 4.3b, d).

In the black phyllites at Kini Bay, Claasens Point and Sardinia Bay, these early deformation episodes are accompanied by dense-concentrations of veins comprising predominantly white crystalline quartz (Figs. 4.3a, b, c, d). The earliest vein emplacement episode is parallel to S_0/S_1 (Fig. 4.3b), while a subsequent (second generation) dense vein system is associated with the axial planar south-west-dipping S_2 cleavage (Figs. 4.3a, c.).

All these structural features, together with the general north-verging, south-dipping axial planar cleavage and associated folding recognised throughout the CFB, are consistent with a model configuration whereby subduction polarity was to the south (de Wit 1977; Ramos 2008; Lindeque et al. 2011; Pángaro and Ramos 2012; Miller et al. 2016).

4.4 New U-Pb Zircon Geochronology

4.4.1 Detrital Zircon Dates

U-Pb zircon geochronology was carried out on 448 detrital zircon grains sampled from nine separate lithological units from the Gamtoos Complex and lower Table Mountain Group, and dated by Sensitive High Resolution Ion Microscopy Reverse Geometry (SHRIMP RG) performed at the Research School of Earth Science (RSES), Australia National University, Canberra (Miller et al. 2016). The results show two major zircon populations with age-peaks centred at 1090 and 530 Ma, and subordinate populations between 1800 and 3420 Ma (Fig. 4.5).

Maximum ages from the Gamtoos Complex and lowermost Table Mountain Group in the study area are summarised in Table 4.1. The maximum age of the Sardinia Bay

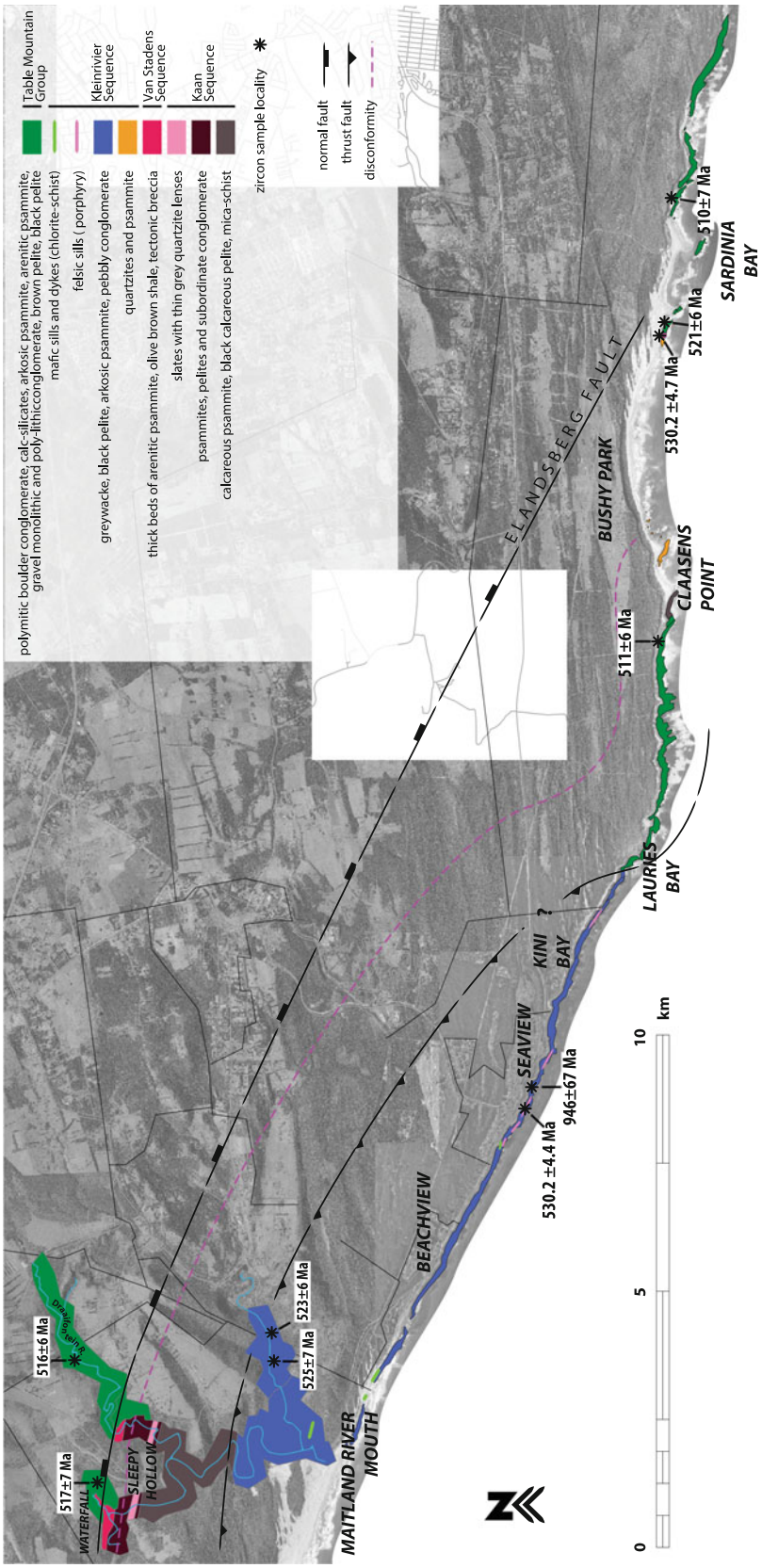

Fig. 4.2 Geological map of the study area between Maitland River and Schoenmakerskop. Black stars show the new maximum detrital dates and igneous concordant dates from U/Pb zircon analysis

Fig. 4.3 Phyllites of the Gamtoos Complex and overlying lower Table Mountain Group: **a** thin section of the phyllites showing S_1 parallel to S_0 overprinted by crenulation cleavage S_2, also hosting dense veining, at Kini Bay of the Kleinrivier Sequence; **b** early vein and slaty cleavage and the crosscutting S_2 crenulation cleavage that forms the predominant cleavage measured in the study area in the Kleinrivier Sequence; **c** clear crosscutting relationship between early and late stage quartz veins; **d** open F_2 folded ca. 10 cm thick bedded phyllites, with bedding-parallel quartz veins. Note the finer lithologies and veins have formed parasitic folds; **e** finely alternating layers of silty and muddy lithologies in the Upper Sardinia Bay Formation of the Table Mountain Group with S1 cleavage parallel to bedding and S_2 crenulation cleavage axial planar to open. These structural features are identical to those found in the Gamtoos phyllites at Kini Bay

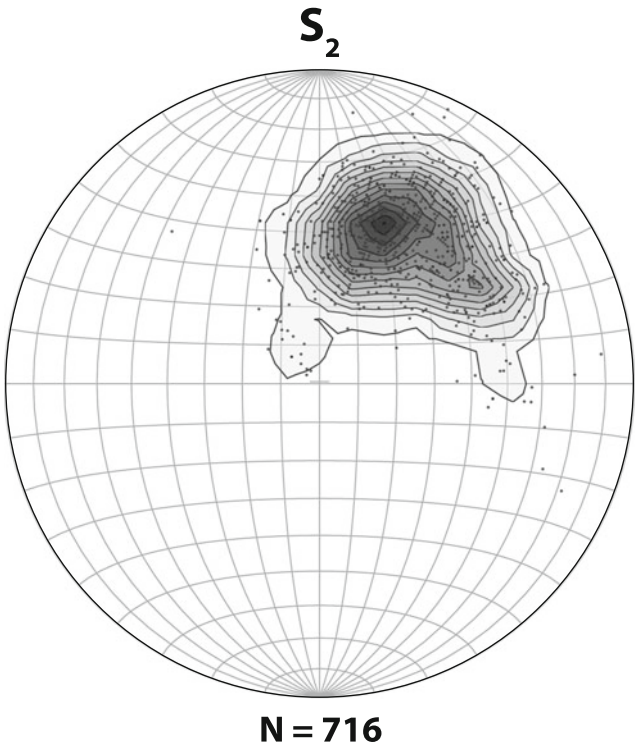

Fig. 4.4 Equal area southern hemisphere stereonet showing the southward-dipping axial planar crenulation cleavage (S_2), measured in the study area

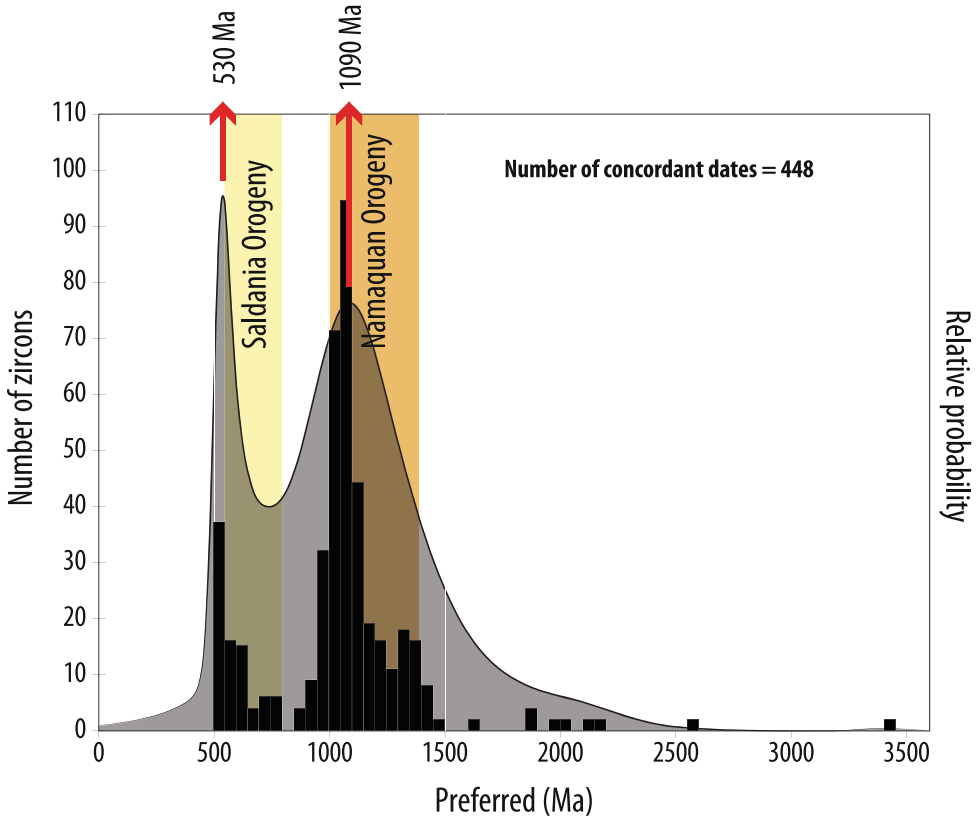

Fig. 4.5 Detrital zircon dates for the Gamtoos Complex and lower Table Mountain Group. Only concordant data are shown. Cambrian to mid-Neoproterozoic = 22 %; early-Neoproterozoic to early-Mesoproterozoic = 75 %; older = late-Paleoproterozoic to Paleo-Archean = 3 %

Table 4.1 Youngest detrital zircon dates from the Gamtoos Complex and lowermost Cape in the study area

Sequence/Formation	Sample	Youngest zircon
Peninsula	Dc179	516 ± 5 Ma
Conformity?		
Upper Sardinia Bay	Di125	510 ± 6 Ma
	Dc177	510 ± 7 Ma
	Dc155	511 ± 6 Ma
Conformity?		
Lower Sardinia Bay	Dc176	521 ± 6 Ma
	Di094	517 ± 7 Ma
Angular unconformity		
Van Stadens		
Sharp discontinuity		
Kaan		
Conformity?		
Kleinrivier	Di084	523 ± 6 Ma
	Di085	525 ± 7 Ma
	Dc088	946 ± 67 Ma
Lauries Bay fault		

Formation is placed within the third and fourth stages of the Cambrian with youngest zircons dated at 517 ± 7 Ma (lower sequence) and 510 ± 6 Ma (upper sequence). The maximum age for the overlying Peninsula Formation is placed in the upper Cambrian and determined from a youngest detrital zircon of 516 ± 5 Ma.

4.4.2 Igneous Zircon Dates

U-Pb geochronology from 35 igneous zircons was measured on a felsic sill and granite boulder. Thirteen concordant dates for the felsic sill at Seaview give a weighted mean age of 530 ± 4 Ma. Seventeen concordant dates from a granite boulder at Sardinia Bay give a weighted mean of 530 ± 5 Ma (Fig. 4.2). The Seaview felsic sill is deformed with its hosting greywackes and black shales of the Kleinrivier Sequence, and in places can be seen to cut these metasedimentary rocks (Miller et al. 2016). The Sardinia Bay granite boulders occur at the base of the lower Sardinia Bay Sequence. Exposed boulders are up to 2 m in diameter and were deposited with the hosting pebble and boulder conglomerates. The age of these igneous rocks coincide with the Cambrian magmatism of the Cape Granite Suite (Armstrong et al. 1998; Scheepers and Poujol 2002; Chemale et al. 2011).

A maximum age from greywackes in the Kleinrivier Sequence is determined from the youngest zircon date of 946 ± 67 Ma (Table 4.1), and with a minimum age of 530 ± 4 Ma from the igneous zircons sampled from the intruding Seaview felsic sill. These ages place the sequence somewhere in the Fortunian Stage of the Cambrian (Cohen et al. 2013). Miller et al. (2016) indicate that these ages are not entirely consistent, and further detrital zircon geochronology is necessary to establish greater stratigraphic accuracy.

4.4.3 Discussion on the Maximum Age of Deformation and Its Role in the Gondwanide Orogen

Age data from the study area alone is restrictive in determining the age of deformation in the Gamtoos Complex and overlying Table Mountain Group. However, the relative age of deformation can be constrained combining structural analyses and U/Pb geochronology presented above.

Structural features in the Kleinrivier and Kaan Sequences are identical to shales in the upper Sardinia Bay Formation, suggesting that deformation occurred subsequent to the youngest zircon in these sequences (< 510 ± 6 Ma). Such an event in the CFB is only recognised as occurring during the mid- to late Paleozoic (Hansma et al. 2015; Chap. 5 this book). This implies that these sequences were not affected by and likely post-dated any inferred Pan African deformation (ca. 545 Ma). Previous interpretations have suggested that a Precambrian deformation existed in rocks underlying the Table Mountain Group throughout the CFB in South Africa (Broquet 1992; Catuneanu et al. 1998; Gresse et al. 2006), but this notion has been contested (Barnett et al. 1997; Lindeque et al. 2011; Miller et al. 2016), suggesting that Pan African deformation only exists along the western limb of the CFB. Deformation of the CFB is interpreted to be related to an allochthonous Patagonia landmass that collided with south-west Gondwana along an accretionary prism (subduction zone) in the Permian-Triassic more than ~1000 km to the south (Pankhurst et al. 2006; Fig. 4.6a). However, little agreement exists between the precise position of major tectonic boundaries, as well as subduction polarity (de Wit and Ransome 1992; Ramos 2008). Evidence presented here from the lower sequences of the eastern CFB, and in particular the finer units of the Gamtoos Complex and overlying Table Mountain Group, suggest a plate boundary connected to an accretionary wedge to the south. This evidence is reflected in the field as early compressive structures (S_1 and S_2) in phyllites of the above-mentioned sequences, corresponding vein systems that are likely related to a major detachment zone.

Plate reconstructions of south-west Gondwana place the position of relevant paleo-sutures and magmatic arcs in Patagonia and Antarctic Peninsula (Figs. 4.6a, b, c) to better reconcile the tectonic position and tectono-genesis of the

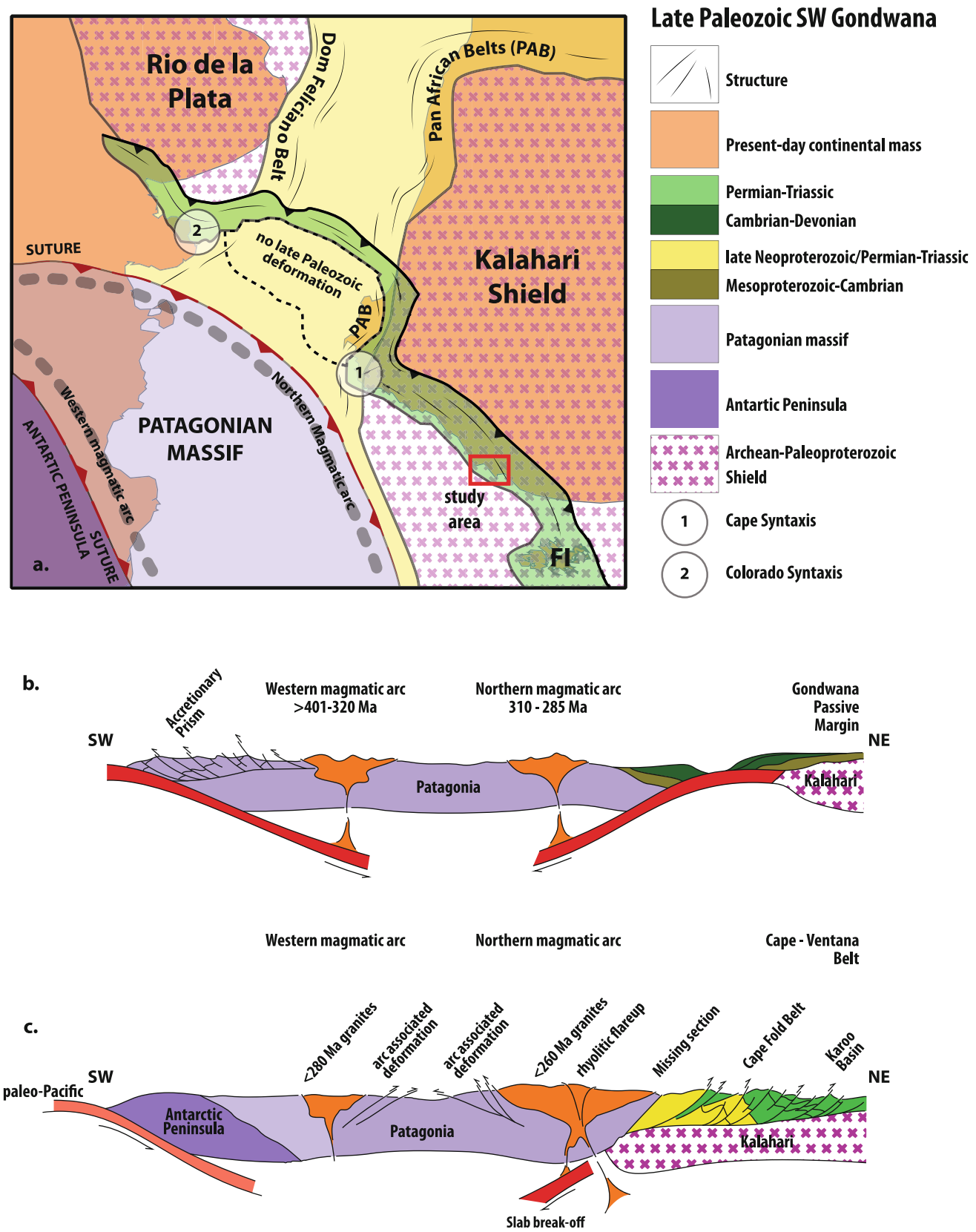

Fig. 4.6 **a** Geological reconstruction map of south-west Gondwana showing the position of Late Paleozoic deformation associated with the CFB and Sierra de la Ventana (*green*), as well as the position of Patagonia and surrounding Kalahari and Rio de la Plata Shields. The red square illustrates the location of field mapping and sample collection (modified after Pángaro and Ramos 2012); **b** Schematic cross-section through south-west Gondwana prior to ca. 300 Ma and; **c** subsequent to Late Paleozoic deformation (c. 200 Ma) (modified after Ramos 2008)

CFB (de Wit 1977; Pankhurst et al. 2006; Ramos 2008). Subduction and collision between the Patagonian landmass and the Rio de la Plata-Kalahari Shields should have resulted in a recognisable pattern of magmatism and metamorphism in the CFB, with magmatic evidence for the postulated northward subduction model. However, evidence for a magmatic arc exists only south of the paleo-position of the CFB (e.g. de Wit 1977; Pankhurst et al. 2006). The debate advocating the existence of a related suture zone situated between the Patagonia landmass and the Rio de la Plata-Kalahari Shields is inferred from the Colorado magnetic discontinuity (Max et al. 1999; Ramos 2008).

4.5 Conclusion

The main characteristics of the Gamtoos Complex and lower Table Mountain Group rocks are summarised below

- The metasedimentary rocks of the study area are deformed by two early structural events (S_1 and S_2), with contemporary emplacement of at least two dense and widespread quartz vein systems.
- The structural grain throughout the study area is concordant with the overlying structural grain measured in the CFB, in the Eastern Cape.
- Both the Gamtoos Complex and the lower Table Mountain Group were deposited during the early Cambrian, although the age of the Kleinrivier Sequence remains uncertain.
- All the sequences in the study area were likely deformed only during the Permo-Triassic (see also Chap. 5 in this book).

To conclude the main lithological and structural features discussed above are consistent with a southward-dipping subduction zone to the south within the Gondwanide, south of the CFB. A major basal thrust or décollement surface is located in the basal "pre-Cape" sequences, with splay faults that penetrate into the lower Table Mountain Group. Recent interpretations that the CFB and Sierra de la Ventana are similar in deformation style to the Jura Mountains (Ramos 2008; Lindeque et al. 2011; Pángaro and Ramos 2012; Miller et al. 2016) are complemented here by southward-dipping and tectonic fabrics.

Acknowledgments We would like to thank Prof Peter Booth for his thorough review. His contributions and detailed comments were invaluable to the completion of the text and figures. This is AEON contribution number 157.

References

Armstrong RA, de Wit MJ, Reid D, York D Zartman R (1998) Cape Town: Table Mountain reveals rapid Pan-African uplift of its basement rocks. J Afr Earth Sci 27:10–11

Barnett W, Armstrong R, de Wit M (1997) Stratigraphy of the upper Neoproterozoic Kango and Lower Palaeozoic Groups of the Cape Fold Belt revisited. S Afr J Geol 100:237–250

Broquet CAM (1992) The sedimentary record of the Cape Supergroup: A review In: de Wit MJ, Ransome IGD (eds) Inversion Tectonics of the Cape Fold Belt, Karoo and Cretaceous Basins of Southern Africa. AA Balkema, Rotterdam, the Netherlands 159–184

Catuneanu O, Hancox P, Rubidge B (1998) Reciprocal flexural behaviour and contrasting stratigraphies: a new basin development model for the Karoo retroarc foreland system South Africa. Basin Res 10(4):417–439

Catuneanu O, Hancox, P, Cairncross B, Rubidge B (2002) Fore-deep submarine fans and fore-bulge deltas: orogenic off-loading in the under-filled Karoo Basin. J Afr Earth Sci 33:489–502

Chemale F, Scheepers R, Gresse PG, Van Schmus WR (2011) Geochronology and sources of late Neoproterozoic to Cambrian granites of the Saldania Belt. Int J Earth Sci, 100:431–444

Cohen KM, Finney SC, Gibbard PL, Fan JX (2013) The ICS International Chronostratigraphic Chart. Episodes 36:199–204

Dalziel I (2000) Laurentia-Kalahari collision and the assembly of Rodinia. J Geol 108:499–513

De Beer J, Meyer R (1984) Geophysical Characteristics of the Namaqua-Natal Belt and its boundaries, South Africa. J Geodyn 13(5):473–494

De Wit M (1977) The evolution of the Scotia Arc as a Key to the reconstruction of southwestern Gondwanaland. Tectonophysics 37:53–81. doi:101016/0040-1951(77)90039-7

De Wit M, Ransome I (1992) Inversion tectonics of the Cape Fold Belt, Karoo and Cretaceous basins of Southern Africa. AA Balkema, Rotterdam, Netherlands, p 280

Fildani A, Weislogel A, Drinkwater NJ, McHargue T, Tankard A, Woodens J (2009) U-Pb zircon ages from the southwestern Karoo Basin, South Africa-Implications for the Permian-Triassic boundary. Geol 37:719–722.

Gresse PG, Von Veh MW, Frimmel HE (2006) Namibian, (Neoproterozoic) to early Cambrian successions In: Johnson MR, Anhaeusser CR, Thomas RJ (eds) the Geology of South Africa. Geol Soc Afr 395–420

Hälbich I, Swart J (1983) Structural zoning and dynamic history of the cover rocks of the Cape Fold Belt. Geol Soc Afr, Special Publication 12:75–100

Hälbich I (1983a) A tectogenesis of the Cape Fold Belt (CFB). Geol Soc S Afr Spec Publ 12:165–175

Hälbich, I (1983b) A geodynamic model for the Cape Fold Belt2 (CFB). 177–184 Geol Soc Afr, Special Publication 12:184

Hälbich I (1983c) Geodynamics of the Cape Fold Belt in the Republic of South Africa, a summary 21–29 In: Rast N, Delany FM (eds) Profiles of Orogenic Belts Geodynamics Series. Geol Soc Am 10:310

Hälbich I (1993) (Compiler) Global Geoscience Transect 9. The Cape Fold Belt - Agulhas Bank transect across Gondwana Suture, Southern Africa. Am Geophys Union Spec Publ 202:18

Hansma J, Tohver E, Jourdan F, Schrank C, Adams D (2015) The Timing of the Cape Orogeny: New 40Ar/39Ar age constraints on deformation and cooling of the Cape Fold Belt, South Africa. Gondwana Res doi:101016/jgr201502005

Johnson M, van Vuuren C, Visser J, Cole D, Wickens H, Christie A, Roberts D, Brandl G (2006) Sedimentary Rocks of the Karoo Supergroup In: Johnson MR, Anhaeusser CR, Thomas RJ (eds) The Geology of South Africa. Geol Soc Afr 461–499

Johnston S (2000) The Cape Fold Belt and Syntaxis and the rotated Falkland Islands: dextral transpressional tectonics along the southwest margin of Gondwana. J Afr Earth Sci 31(1):51–63

Lindeque A, de Wit M, Ryberg T, Weber M, Chevallier L (2011) Deep crustal profile across the southern Karoo Basin and Beattie Magnetic Anomaly, South Africa: An integrated interpretation with tectonic implications. S Afr J Geol 114:265–292

Lock B (1980) Flat-plate subduction and the Cape Fold Belt of South Africa. Geol 8:35–39

Max M, Ghidella M, Kovacs L, Paterlini M, Valladares J (1999) Geology of the Argentine continental shelf and margin from aeromagnetic survey. Mar and Petrol Geol 16(1):41–4

Miller W, Armstrong R, de Wit M (2016) Geology and U/Pb geochronology of the Gamtoos Complex and lower Paleozoic Table Mountain Group, Cape Fold Belt, Eastern Cape, South Africa. S Afr J Geol 119(1)

Nolte C (1990) Structure and Tectonostratigraphy of the Gamtoos Belt. Master's thesis, University of Port Elizabeth 237

Pángaro F, Ramos V (2012) Paleozoic crustal blocks of onshore and offshore central Argentina: New pieces of the southwestern Gondwana collage and their role in the accretion of Patagonia and the evolution of Mesozoic South Atlantic sedimentary basins. Mar and Petrol Geol 37:162–183

Pankhurst R, Rapela C, Fanning C, Márquez M (2006) Gondwanide Continental Collision and the Origin of Patagonia. Earth-Sci Reviews 763(4):235–257

Paton D, Macdonald D, Underhill J (2006) Applicability of thin or thick skinned structural models in a region of multiple inversion episodes; southern South Africa. J Struct Geol 28:1933–1947

Ramos VA (1988) Tectonics of the late Proterozoic-early Paleozoic: a collisional history of Southern South America. Episodes 11: 168–174

Ramos VA (2008) Patagonia: A Paleozoic continent adrift? J S Am Earth Sci 26(3):235–251

Rutherford A, Rubidge B, Hancox P (2015) Sedimentology and palaeontology of the Beaufort Group in the Free State province supports a reciprocal foreland basin model for the Karoo Supergroup South Africa. S Afr J Geol 118(4):355–372

Scheepers R, Poujol M (2002) Up-Ub zircon age of the Cape Granite Suite ignimbrites: characteristics of the last phases of the Saldanian magmatism. S Afr J Geol 105:163–178

Scheiber-Enslin S, Ebbing J, Webb S (2014) An Integrated Geophysical Study of the Beattie Magnetic Anomaly, South Africa. Tectonophysics 636:228–243

Stankiewicz J, Parsiegla N, Ryberg T Gohl, K Trumbull R, Weckmann U, Weber M (2008) Crustal structure of the southern margin of the African continent: results from geophysical experiments. J Geophy Res 113:B10313

Stankiewicz J, de Wit M (2013) 35 billion years of reshaped Moho, southern Africa. Tectonophysics 609:675–689

Tankard A, Welsink H, Aukes P, Newton R, Stettler E (2009) Tectonic evolution of the Cape and Karoo Basins of South Africa. Mar Petrol Geol 26:1379–1412

Tankard A, Welsink H, Aukes P, Newton R, Stettler E (2012) Chapter 23: Geodynamic interpretation of the Cape and Karoo basins, South Africa In: Roberts DG, Bally AW (eds) Phanerozoic Passive Margins, Cratonic Basins and Global Tectonics Maps Amsterdam: Elsevier 869–945

Thomas R, Eglington B, Bowring S, Relief E, Walraven F (1993) New isotopic data from a Neoproterozoic porphyritic granitoid-charnockite suite from Natal, South Africa. Precambrian Res 62:83–101

Weckmann U, Jung A, Branch T, Ritter O (2007a) Comparison of electrical conductivity structures and 2D magnetic modelling along two profiles crossing the Beattie Magnetic Anomaly, South Africa. S Afr J Geol 110:449–464

Weckmann U, Ritter O, Jung A, Branch T, de Wit M (2007b) Magnetotelluric Measurements across the Beattie Magnetic Anomaly and the Southern Cape Conductive Belt, South Africa. J Geophys Res 112

An Overview of Cape Fold Belt Geochronology: Implications for Sediment Provenance and the Timing of Orogenesis

5

Scarlett C.J. Blewett and David Phillips

Abstract

The Cape Fold Belt (CFB) is a 1300 km long fold-and-thrust mountain belt along the western and southern coastlines of South Africa. A limited understanding of the sedimentary provenance history and poor constraints on the timing of deformation has restricted the ability to provide a coherent tectonic model for the evolution of the CFB. Provenance studies on the Cape Supergroup, which dominates CFB outcrop, are largely limited to U-Pb dating of detrital zircons, which indicate the Namaqua-Natal Metamorphic Complex and Pan-African orogenic belts as likely sources for much of the detritus. Early geochronological studies constraining the timing of deformation in the CFB utilized $^{40}Ar/^{39}Ar$ step-heating analysis of bulk mineral separates. In these studies, dominant age domains were interpreted as multiple episodes of deformation. More recent $^{40}Ar/^{39}Ar$ results, from single muscovite grains and aggregate samples, were interpreted in terms of a bimodal tectonic evolution (ca. 270 Ma and ca. 251 Ma) for the CFB. In the present study, preliminary high precision $^{40}Ar/^{39}Ar$ step-heating analyses were carried out on >100 single muscovite grains from the Cape Supergroup of the Eastern Cape area. These results identify a large detrital muscovite population >440 Ma, confirming sedimentary contributions from Pan-African aged rocks of the Saldanian Orogen and associated Cape Granites, and possibly the East African-Antarctic Orogen. Similar muscovite ages at ca. 253 (Ma) are interpreted as constraining the final stage(s) of CFB orogenesis. Intermediate ages between 255 and 440 Ma are attributed to mixed age populations of detrital and metamorphic micas and/or partial resetting/recrystallization of these components by the low-grade CFB metamorphism. The significant detrital population and presence of partially overprinted micas highlights the risks of using bulk mineral separates, as per previous studies. Collectively, the current geochronological data do not support discrete deformation events, but also do not rule out the possibility of earlier or long-lived deformation events. Consequently, available models for the timing of CFB deformation should be treated with caution.

Keywords

Cape Fold Belt • Geochronology • Provenance • Orogenesis • $^{40}Ar/^{39}Ar$ • ARGUSVI • Muscovite

S.C.J. Blewett (✉) · D. Phillips
School of Earth Sciences, The University of Melbourne, Parkville, VIC 3010, Australia
e-mail: blewetts@unimelb.edu.au

B. Linol and M.J. de Wit (eds.), *Origin and Evolution of the Cape Mountains and Karoo Basin*, Regional Geology Reviews, DOI 10.1007/978-3-319-40859-0_5

5.1 Introduction

Geochronology and thermochronology studies of orogenic belts, such as the Cape Fold Belt (CFB) of South Africa, provide important information regarding the source(s) of detrital sediments and the deformational history of these terranes. The CFB is a component of a larger orogenic belt flanking the margin of southwest Gondwana, which extended from the Sierra de la Ventana Fold Belt of Argentina, across southern Africa, and east through the Falkland Islands and the Ellsworth–Whitmore Mountains of Antarctica (Curtis and Hyam 1998; Rapela et al. 2003; Pángaro and Ramos 2012; see also Chap. 4 in this book). Despite comprising a significant portion of the Gondwana margin, the tectonic evolution of the CFB is still poorly understood, due to incomplete lithological, structural, and geochronological constraints.

The Paleozoic Cape Supergroup dominates CFB outcrops and comprises predominantly quartzites, sandstones, and shales, which are divided (from oldest to youngest) into the Table Mountain, Bokkeveld and Witteberg Groups (SACS 1980). Depositional ages are estimated at between 510 and 350 Ma, based on detrital zircons and paleontology (Miller et al. 2016; and see Chaps. 4 and 13 in this book for details). Detrital zircon provenance studies suggest the Cape Supergroup is largely derived from sources such as the Mesoproterozoic Namaqua-Natal Metamorphic Complex (1200–1000 Ma) situated to the immediate north of the CFB, and Pan-African orogenic belts (650–500 Ma) on the African and South American continents (Fourie et al. 2011; Vorster 2013; Miller et al. 2016).

Attempts that have been made to constrain the timing of CFB deformation have utilized the $^{40}Ar/^{39}Ar$ dating method (Gentle et al. 1978; Hälbich et al. 1983; Gresse et al. 1992). The latter two studies suggested that CFB deformation occurred over a series of tectonic pulses. More recently, Hansma et al. (2015) undertook $^{40}Ar/^{39}Ar$ analyses of muscovite samples from three traverses across the CFB. Based on their data, these authors inferred a bimodal distribution of CFB deformation, at ca. 270 Ma and ca. 251 Ma. A further three samples identified detrital components (>400 Ma) indicating a dominantly Pan-African source. Although CFB deformation may well have been episodic, the available geochronological dataset is almost certainly too limited to define sediment source regions, the timing of specific orogenic events, or the causes of CFB orogenesis.

The current contribution provides a review of past geochronological studies in the CFB and presents preliminary, high precision $^{40}Ar/^{39}Ar$ dating results for single muscovite grains from the Eastern Cape region of the CFB. The new age data highlight the complexities inherent in $^{40}Ar/^{39}Ar$ studies and suggest variable sources for detrital grains, but provide definitive evidence for only one deformation event. This chapter also outlines future geochronological and tectonic studies that are required to resolve the evolution of this portion of the southern Gondwanan margin.

5.2 Geological Setting

The CFB comprises Neoproterozoic-Cambrian metasediments of the Pan-African Orogen and other tectonic inliers (650–550 Ma; Barnett et al. 1997; Gresse et al. 2006), the Cambrian Cape Granite Suite (~555–510 Ma; da Silva et al. 2000; Chemale et al. 2011), the Lower to mid-Paleozoic Cape Supergroup (~510–350 Ma; Broquet 1992; Miller et al. 2016), and Upper Paleozoic to Lower Mesozoic parts of the Karoo Supergroup (~300–180 Ma; Bangert et al. 1999; Jourdan et al. 2008).

The CFB is composed of a NNW trending western branch and a southern branch with an E-W axial orientation (Fig. 5.1). These branches are linked by a 'syntaxis' inland of Cape Town. East-west elongated inliers in the southern branch expose mega-antiforms of Precambrian basement rocks that also outcrop in the western branch. At Port Elizabeth at the eastern extremity of the CFB, the structural grain trends offshore at an 'antaxis' that continued into the Falkland Islands when this region was joined to the east coast of South Africa (e.g., Johnston 2000), before activation of the Alghulas Fracture Zone and the opening of the southern ocean (Gohl et al. 2011).

CFB deformation extends 250 km from the southern African coastline into the Karoo Basin to the north. North-directed compression resulted in a general decrease in deformation intensity from the south to the north, with metamorphic grades reaching lower greenschist facies conditions (Hälbich and Cornell 1983; Frimmel et al. 2001). Pressure-temperature estimates decrease only slightly from approximately 2.5 kb/350 °C in the south, to around 1.5 kb/210 °C in the Karoo Basin in the north (Hälbich and Cornell 1983).

The western CFB displays gentle and relatively open folds, whereas the southern branch is more intensely deformed, with steeply dipping to overturned beds, chevron folding, and complex cross-cutting relationships between folding and faulting (Hälbich 1983; Booth 1996, 1998; Chap. 4 this book). CFB deformation produced an axial-planar cleavage that generally dips to the south. Thrust faults are well documented in the southern branch of the CFB and occur throughout the Cape Supergroup and into the Beaufort Group of the overlying Karoo Supergroup (Booth and Goedhart 2014). Thrust sheets hundreds of meters thick are major features in the CFB, and are suggested to account

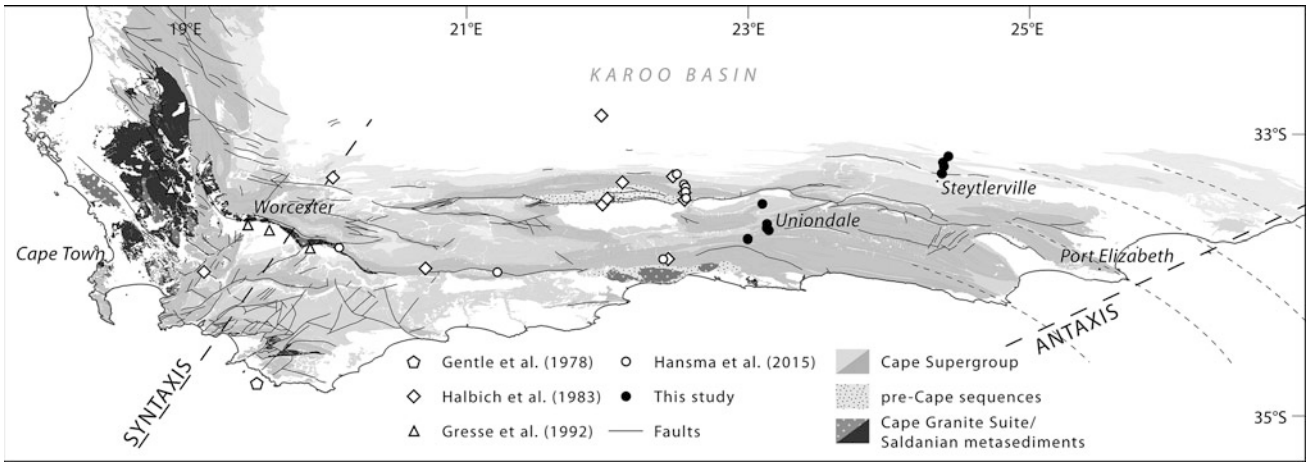

Fig. 5.1 Simplified geological map of the Cape Fold Belt including locations of previous and current geochronological studies relating to CFB orogenesis

for the abnormally large thickness of quartzite, as less competent shale horizons are thinned-out or completely eliminated by numerous thinner thrusts (<1 m thick) (Booth and Shone 2002).

A number of competing tectonic models exist for the evolution of the CFB (discussed in more detail by Miller et al. 2016; and see Chap. 4 of this book). Recent interpretations of seismic reflection profiles by Lindeque et al. (2011) identify thick- and thin-skinned deformation in the CFB, aided by the presence of a south-dipping mega-detachment below the Cape Supergroup (de Wit and Ransome 1992; Paton et al. 2006; Chap. 4 this book). A subduction zone located in the far south is suggested to have driven compression in the CFB, with Mesozoic extension and subsequent separation of South America and Africa during Gondwana break-up removing evidence of a collision zone (Lindeque et al. 2011).

5.3 Detrital Zircon Geochronology in the CFB

To provide context for the detrital muscovite ages discussed in subsequent sections, the following section offers a brief overview of detrital zircon studies conducted on the Cape Supergroup. See Andersen et al. (2016) for a detailed review of previous provenance studies in the CFB.

Geochronological investigations into the source(s) of the Cape Supergroup sediments are limited to LA-ICPMS U-Pb dating of detrital zircons (Fourie et al. 2011; Vorster 2013) and SHRIMP U-Pb dating of detrital zircons (Lower Table Mountain Group only; Miller et al. 2016). Throughout the sedimentary succession, Mesoproterozoic (1200–1000 Ma), Neoproterozoic-Cambrian (650–500 Ma) and Ordovician-Silurian (500–400 Ma) age populations of zircons are identified. The first two detrital zircon age domains are the most prominent, and attributed to the Namaqua-Natal Metamorphic Complex and Pan-African orogenic belts of Africa and South America (i.e., the Dom Feliciano-Gariep-Saldania and Damara-Lufilian orogens), respectively. Miller et al. (2016) propose the Mozambique Belt, of the East African-Antarctic Orogen, as a likely source for detrital zircons with ages between ca. 950 and 500 Ma. No specific terrane(s) has been identified as providing sediment that would account for the 500–400 Ma zircon age group reported by Fourie et al. (2011) and Vorster (2013).

5.4 Previous $^{40}Ar/^{39}Ar$ Constraints on the Timing of CFB Deformation

Gentle et al. (1978) made the first attempt at constraining the timing of metamorphic overprinting by the CFB deformation. These authors recognized recrystallized and neo-crystallized mica in a sample from the Pan-African Haelkraal granite dredged from the sea south-west of Cape Agulhas (Fig. 5.1). $^{40}Ar/^{39}Ar$ step-heating analysis of a single biotite concentrate produced a supposed plateau age of 248.3 ± 1.5 Ma. Although the step-heating spectrum displays a flat segment, the uncertainties for each step are not shown and no methodology or analytical data are reported. Consequently, the ca. 248 Ma biotite age can only be viewed as providing an approximate deformation or cooling age.

Hälbich et al. (1983) and Gresse et al. (1992) provided more detailed geochronological studies of CFB orogenesis. Hälbich et al. (1983) carried out $^{40}Ar/^{39}Ar$ step-heating analyses on axial-planar muscovite aliquots from eleven samples from the lower Cape Supergroup and underlying

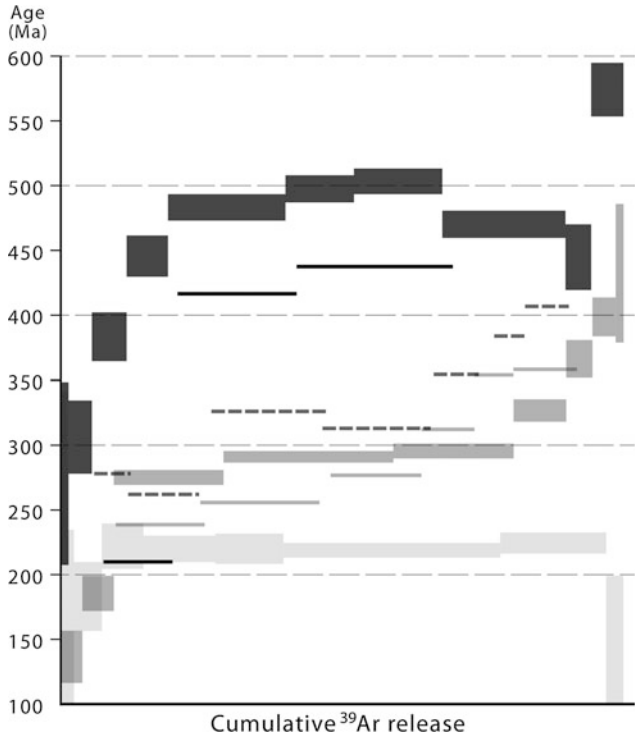

Fig. 5.2 Examples of step-heating age spectra from Hälbich et al. (1983) (*shaded lines**), and Gresse et al. (1992) (*shaded boxes*). *No uncertainties are reported for the apparent age of individual heating steps by Hälbich et al. (1983)

Pan-African metasediments (Fig. 5.1). Three samples yielded staircase step-heating age spectra, with apparent ages ranging from ~200–450 Ma (Fig. 5.2). These spectra are typical of samples that have undergone partial loss of radiogenic argon due to thermal (or chemical) overprinting or contain mixed age populations (McDougall and Harrison 1999). Descriptions of these samples note the presence of occasional detrital grains realigned along cleavage planes, which supports a mixed age population. Three samples produced flatter age spectra (concordance between some heating step ages), but no statistical plateau ages are reported. These three samples were interpreted as defining distinct tectonic events at ca. 278 and ca. 258 Ma (Hälbich et al. 1983). The remaining five age spectra are discordant, with most apparent ages within the interval 230–300 Ma, suggesting that these bulk mineral samples contain mixtures of altered, detrital, partially recrystallized and neo-crystallized components. By combining the spectra of all eleven samples, Hälbich et al. (1983) concluded that CFB deformation was episodic, with significant pulses at 278, 258, 247, and 230 Ma.

Gresse et al. (1992) subsequently conducted ^{40}Ar/^{39}Ar step-heating analyses on six whole rock, cleavage-bearing samples, including five Pan-African samples (greywackes, phyllites, and one sericitized quartz porphyry), and one sample from the Witteberg Group, the uppermost sequence of the Cape Supergroup (Fig. 5.1). Some samples produced staircase step-heating age spectra, with apparent step ages ranging from 200 to 600 Ma (Fig. 5.2). The older age spectrum (Fig. 5.2, dark gray boxes) indicates the presence of detrital components. One plateau age of 221 Ma was attained from the Saldaninan quartz porphyry (truncated by an unconformity at the base of the Table Mountain Group and therefore pre-Cape Supergroup in age), which was described as having a strong penetrative sericite-dominated matrix overprinted by chloritoid crystals (Gresse et al. 1992) (Fig. 5.2, pale-gray boxes). This age either represents an alteration artifact due to the presence of chloritoid overgrowth, or a sericite cooling age. All remaining age spectra are discordant, with apparent ages generally increasing with temperature (cumulative % ^{39}Ar released; e.g. Fig. 5.2, mid-gray boxes). Gresse et al. (1992) combined the age spectra of all six samples and proposed tectonic events at 294, 276, 259, 239, and 223 Ma. An alternative interpretation is that these age spectra reflect mixed age populations from detrital and metamorphic micas and/or partially reset detrital micas.

The main problem with the two above-mentioned studies is that step-heating analyses of bulk mineral separates or whole rock samples risk the possibility of including detrital muscovite grains and/or partially recrystallized micas. Consequently, the individual age spectra almost certainly reflect mixed age populations. Incorporation of detrital muscovite grains and preexisting metamorphic micas is especially problematic in the Cape Orogen, because the low grade of metamorphism (<350 °C; Hälbich and Cornell 1983; Frimmel et al. 2001) would not have reset the argon isotopic systematics of pre-existing muscovite grains (ca. 425 °C isotopic closure temperature; Harrison et al. 2009). The closure temperature for biotite is ca. 300 °C (McDougall and Harrison 1999), which might explain why Gentle et al. (1978) achieved relatively reproducible ages from their step-heating experiment.

More recently, Hansma et al. (2015) reported ^{40}Ar/^{39}Ar results for 16 muscovite samples from five sample locations in the central portion of the CFB (Fig. 5.1). Their results appear to constrain CFB deformation to a 35 Ma period, between 281 and 246 Ma. The data acquisition and data reporting for this publication are more consistent with current protocols for ^{40}Ar/^{39}Ar dating (see Renne et al. 2009). However, some anomalies are apparent and the data interpretation is somewhat enigmatic (see below).

According to Hansma et al. (2015), the step-heating analyses were conducted by laser step-heating of single muscovite grains, except for two samples reported as muscovite 'packages' referring to multi-grain separates. However, the supplementary ^{40}Ar/^{39}Ar analytical dataset indicates that some samples were step-heated using a

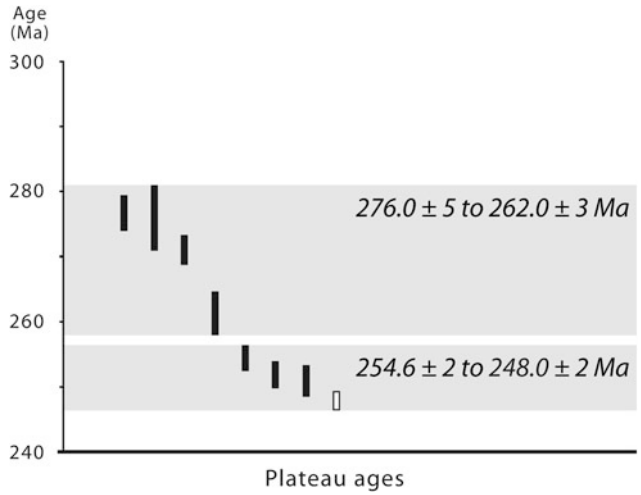

Fig. 5.3 The plateau ages of seven $^{40}Ar/^{39}Ar$ single-grain and bulk muscovite separates (*black symbol*; Hansma et al. 2015), and one $^{40}Ar/^{39}Ar$ biotite age (*white symbol*; Gentle et al. 1978), used by Hansma et al. (2015) to infer bimodal deformation for the CFB (*grey shading*)

furnace, with a further three samples clearly documented as muscovite aggregates rather than single grains. As outlined above, the use of multi-grain mineral aggregates risks inclusion of detrital or inherited components, and thus the possibility of mixed ages that are older than the time of deformation (see Fergusson and Phillips 2001).

Three samples in the Hansma et al. (2015) study yielded older $^{40}Ar/^{39}Ar$ step-heating plateau ages ranging from 477 to 559 Ma, which were attributed to detrital micas and interpreted as provenance ages. Six samples (four muscovite aggregates and two reported 'single' grain) produced discordant age spectra, and were excluded by the authors from further consideration. We suggest that these discordant age spectra might represent either a mixed population of detrital and metamorphic micas and/or partial resetting of predominantly detrital components. The remaining seven samples show concordant age spectra and yield suggested plateau ages (<70 % ^{39}Ar release) of 251 ± 2.4, 252 ± 2.1, 254.6 ± 2.1, 261.4 ± 3.4, 271.1 ± 2.2, 276 ± 5, 276.7 ± 2.8 Ma. Hansma et al. (2015) used this dataset, and the biotite age of Gentle et al. (1978), to infer a bimodal deformation sequence for the Cape Orogeny (Fig. 5.3). It is noteworthy that the 'detrital' ages and most of the older CFB deformation population are from samples collected in the far north of the CFB, whereas the youngest age population is exclusive to the southernmost samples (see Hansma et al. 2015 Fig. 15).

Hansma et al. (2015) suggested that the older age population (276–262 Ma) represents the onset of orogenesis, with the younger population (255–248 Ma) recording either the cooling history of exhumed rocks or a second phase of deformation. An alternative interpretation is that the older age group reflects either a mixture of older detrital/metamorphic micas and neo-crystallized muscovite, and/or partial resetting of detrital components, possibly due to more intense deformation and/or higher metamorphic grades in the south. Therefore, although multiple episodes of deformation in the CFB are certainly possible, a conservative interpretation of the available data is that the final phase of deformation likely occurred at ca. 250 Ma, with no definitive evidence for earlier events.

5.5 New High Precision $^{40}Ar/^{39}Ar$ Dates for CFB

In an attempt to resolve the above ambiguities, the present study is focused on sampling muscovite-bearing shear zones, quartzite and shale outcrops across the eastern segment of the CFB. Preliminary $^{40}Ar/^{39}Ar$ results for *single* muscovite grains are presented below. A major difference between this study and previous work is the use of a new generation ARGUSVI multi-collector mass spectrometer that is capable of a >10-fold improvement in analytical precision, compared to older mass spectrometer systems.

5.5.1 Sampling and Methodology

The 13 samples selected for $^{40}Ar/^{39}Ar$ analysis were collected from areas where detailed structural information is available (Fig. 5.1 and Table 5.1). In order to investigate the possibility of multiple phases of deformation, particular attention was paid to selecting samples from variously angled thrusts, cleavages and folds, as well as from undeformed outcrops that would be dominated by detrital components (Fig. 5.4). A total of 105 single muscovite grains were analyzed, employing a two-step-heating routine to assess contributions from detrital grains in samples selected to determine the timing of deformation.

Samples were crushed using a manual stainless steel crusher and sieved to 90–250 μm size fractions. Muscovite grains were handpicked under a binocular microscope, avoiding grains displaying visible alteration to minimize possible argon loss or recoil effects (see McDougall and Harrison 1999). Samples were cleaned in 5 % nitric acid (HNO_3), distilled water and acetone before being loaded into aluminum foil packets. Packets were weighed and placed in a quartz vial (irradiation can UM#67) along with the flux monitor Fish Canyon Tuff sanidine (FCT 28.02 ± 0.14 Ma (1σ); Renne et al. 1998). Can UM#67 was irradiated for 120 h in the CLICIT facility of the Oregon State University TRIGA reactor.

$^{40}Ar/^{39}Ar$ single muscovite grain step-heating analyses were carried out utilizing a multi-collector Thermo Fischer Scientific ARGUSVI mass spectrometer in the Noble Gas

Table 5.1 Sample locations and descriptions

Sample	Group	Formation	Area	Description	Structural geology reference
ST4	WG	Dirkskraal	Steytlerville	Detrital	1
ST5	WG	Witpoort	Steytlerville	Detrital	1
ST6	WG	Weltevrede	Steytlerville	H shear	1
ST7A	WG	Floriskraal	Steytlerville	V cleavage	1
ST7B	WG	Floriskraal	Steytlerville	H shear	1
ST8A	WG	Witteberg	Steytlerville	V cleavage	1
ST8B	WG	Witteberg	Steytlerville	H shear	1
U5A	TMG	Skurweberg	Uniondale	H shear	2
U5B	TMG	Skurweberg	Uniondale	V shear	2
U6A	TMG	Skurweberg	Uniondale	V shear	2
U6B	TMG	Skurweberg	Uniondale	V shear	2
U10A	TMG	Baaviankloof	Uniondale	V shear	2
P5B	TMG	Baaviankloof		H shear	

WG: Witteberg Group, TMG: Table Mountain Group. V: vertical, H: horizontal. References for structural studies are as follows, 1: Booth (1996; 1998); Booth et al. (2004), 2: Booth and Shone (1999); Booth (2011)

laboratory of the School of Earth Sciences at the University of Melbourne. Details of the instrument and analytical procedures are described by Phillips and Matchan (2013). Age calculations are reported in Table 5.2.

5.5.2 $^{40}Ar/^{39}Ar$ Results

$^{40}Ar/^{39}Ar$ step-heating results obtained for a total of 105 muscovite grains from 13 samples are illustrated in Fig. 5.5. Table 5.2 provides a selection of representative apparent ages. All errors from this study are reported with 2σ uncertainties. For most grains, the apparent age for the low-temperature laser heating step is younger than that of the high-temperature laser fusion step. Overall, high-temperature (fusion) apparent ages range from 249.7 ± 1.2 Ma to 626.8 ± 3.6 Ma. Of these, 75 grains (71 %) across all samples yielded fusion ages above 440 Ma (Fig. 5.5a).

In the case of the youngest grains (<300 Ma), the age difference between the low- and high-temperature step decreases significantly (Fig. 5.5b). There is a concentration of ages at 250 Ma: four grains from samples ST7A, ST7B, U5A produce an average age of 253.3 ± 1.9 Ma (2sd). This age falls within the range of 254.6 ± 2.1 to 248.0 ± 2 Ma for the younger Cape Orogen event proposed by Hansma et al. (2015), but is significantly more precise.

5.5.3 Discussion

Muscovite grains that record fusion ages between ca. 630 and 440 Ma (n = 75) are interpreted to be detrital grains; preserving either the age of crystallization, or cooling, in rocks from igneous or metamorphic terranes. Pan-African tectonic rocks of the proximal Saldanian Orogen to the west (including the Cape Granite Suite at 555–510 Ma) are the most likely source for a proportion of the detrital muscovite population. However, the lower limit of the detrital age range extends beyond the last phase of Saldanian orogenesis, i.e., the emplacement of post-tectonic A-type granites (530–500 Ma; Chemale et al. 2011). Armstrong et al. (1998) reported $^{40}Ar/^{39}Ar$ ages of 536 ± 1 Ma for biotite and muscovite from the Cape Granite (540 ± 4 Ma; U-Pb SHRIMP zircon) and proposed a cooling rate of 4 million years between granite emplacement and the isotopic closure temperature of the micas (300–400 °C). However, this rate is too rapid to account for the youngest detrital muscovite ages. It is possible that the younger muscovite ages (500–440 Ma) reflect provenance from parts of the Saldanian Orogen that cooled at slower rates, or from an entirely different source terrane.

Pan-African aged tectonism is inferred from U-Pb SHRIMP dating of metamorphic and magmatic zircon and $^{40}Ar/^{39}Ar$ and K-Ar dating of mica and hornblende from mylonitic and magmatic rocks from the Dronning Maud Land sector of eastern Antarctica. These techniques yield ages between 565–500 Ma and 530–470 Ma respectively,

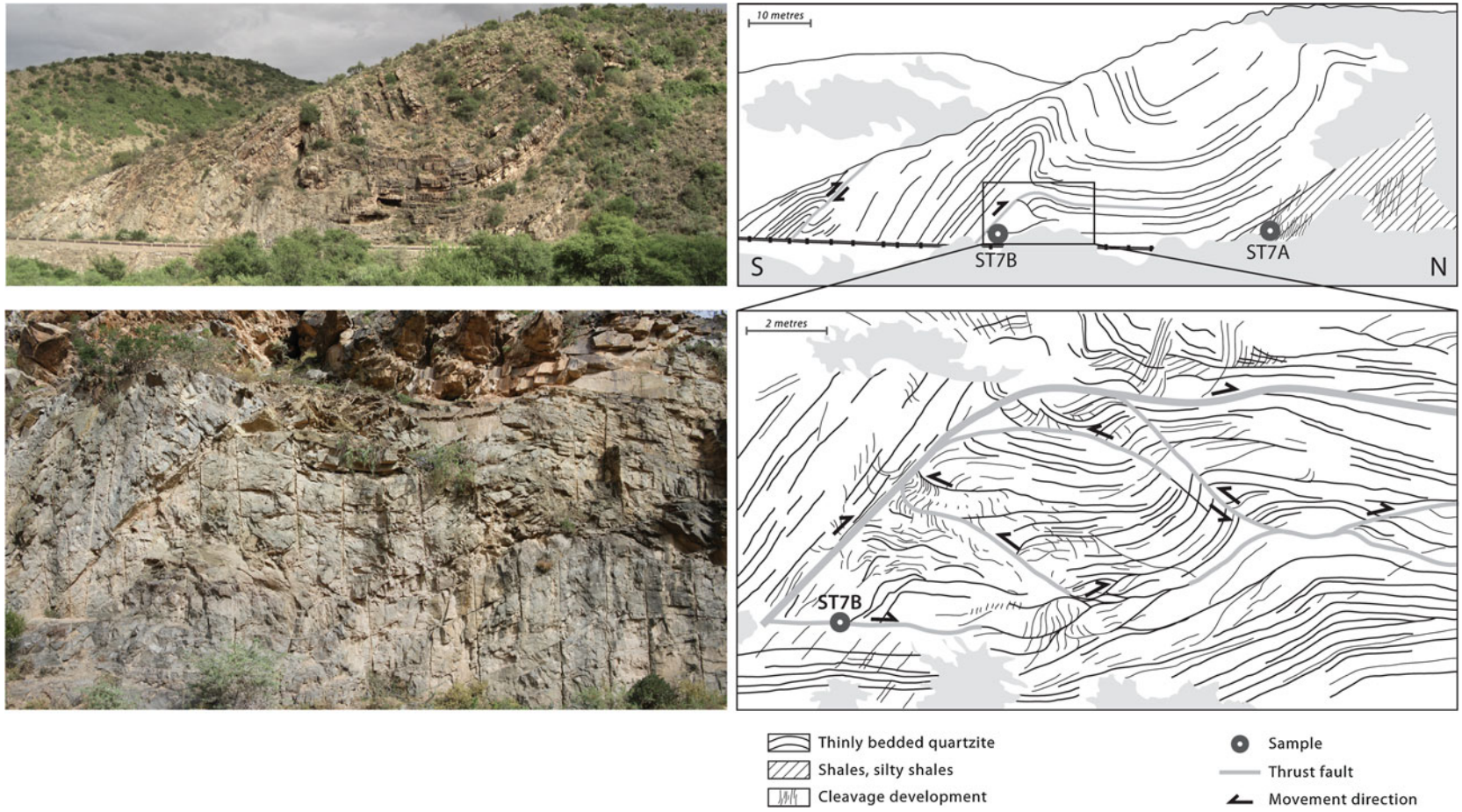

Fig. 5.4 Photographs of an outcrop in the Steytlerville area accompanied by structural interpretation showing multiple, cross-cutting shear zones (sketches on *right*; modified from Booth (1996)). Samples showing well-developed cleavage were selected for $^{40}Ar/^{39}Ar$ geochronology

Table 5.2 Representative ARGUSVI $^{40}Ar/^{39}Ar$ laser step-heating apparent age data for selected CFB muscovite grains

Grain ID	Low-temperature heating step		Fusion step	
	Apparent age (Ma)	±2σ	Apparent age (Ma)	±2σ
U5A-8	257.6	0.7	249.7	1.2
ST7A-5	254.5	0.6	252.1	0.4
ST7A-8	251.3	1.1	253.2	0.4
ST7B-5	249.6	0.5	254.4	0.3
U6B-5	257.2	0.6	267.9	0.6
ST8B-6	300.7	0.3	302.9	5.2
U6A-5	276.2	0.4	330.9	0.3
U6A-7	328.1	0.3	351.0	1.0
P5B-7	457.6	0.8	374.3	2.8
ST4-3	362.0	2.9	380.5	0.7
U5B-5	432.6	0.4	440.6	0.5
ST5-4	394.5	1.4	455.8	3.3
ST8A-2	436.8	0.5	462.4	0.6
ST6-4	434.1	1.3	462.7	1.4
ST4-6	457.5	0.9	467.1	3.7
U5B-1	420.8	0.5	471.3	0.5
U5A-6	467.7	0.8	473.8	21.6
ST5-1	451.7	0.7	475.8	1.8
ST7B-3	464.9	0.7	480.7	0.9
ST7B-9	468.2	0.7	484.1	0.6
ST8A-6	468.2	0.8	489.1	4.0
ST8B-I	511.7	0.6	494.7	0.5
U6B-3	466.3	0.6	508.7	10.4
ST5-3	511.2	1.5	513.7	22.3
P5B-8	484.9	0.5	514.3	12.0
U10A-3	489.7	0.7	530.4	0.8
ST8A-5	509.3	0.9	543.7	4.1
U10A-9	571.1	0.6	626.8	3.6

Data are sorted by increasing fusion step age

[a] Data are corrected for mass spectrometer backgrounds, discrimination, radioactive decay and interference corrections). Errors exclude uncertainties in the J-value (propagating this error only has an effect in the third decimal place)

[b] Interference corrections: $(^{36}Ar/^{37}Ar)_{Ca} = (2.5782 \pm 0.0018) \times 10^{-4}$; $(^{39}Ar/^{37}Ar)_{Ca} = (6.5620 \pm 0.0164) \times 10^{-4}$; $(^{40}Ar/^{39}Ar)_{K} = (1.00 \pm 0.05) \times 10^{-10}$; $(^{38}Ar/^{39}Ar)_{K} = (1.2246 \pm 0.0028) \times 10^{-2}$

[c] J-value is 0.0321127678 ± 0.0000124705 (0.039 %;1σ), based on an age of 28.0200 ± 0.1597 Ma (1σ) for FC sanidine (Renne et al. 1998)

[d] Atmospheric $^{40}Ar/^{36}Ar$ ratio of 298.56 ± 0.31 (Lee et al. 2006)

[e] FCT sanidine age of 28.02 ± 0.14 Ma (lo) (Renne et al. 1998)

[f] Decay constant of Steiger and Jäger (1977) are used

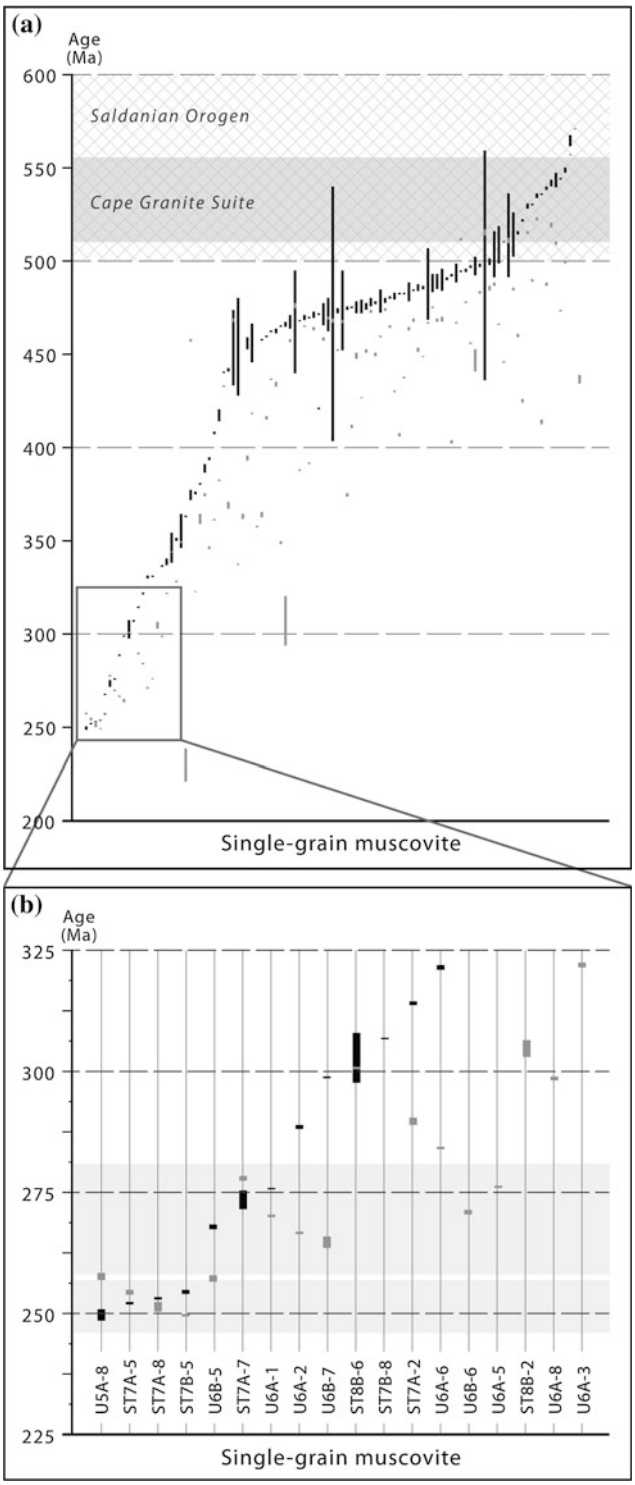

Fig. 5.5 Apparent ages of heating steps for single muscovite grains analyzed in this study. The length of each data symbol represents 2σ analytical errors. **a** Apparent ages for low-temperature steps (*gray*) and fusion steps (*black*) plotted in comparison to the Saldanian Orogen (650–500 Ma; Barnett et al. 1997; Gresse et al., 2006), and the Cape Granite Suite (555 to ~510 M; da Silva et al. 2000; Chemale et al. 2011). **b** magnification of data range between 225–325 Ma with the two age domains of Hansma et al. (2015) superimposed (*gray shading*)

with the hornblende and mica ages corresponding well to the youngest of the observed detrital muscovites in the CFB (Jacobs et al. 1995, 2003; Board et al. 2005). In some

reconstructions of Gondwana (e.g. Jacobs et al. 1998; Jacobs and Thomas 2004), the Dronning Maud Land terrane is considered the southern-most part of the East African-Antarctic Orogen, and was located to the east of the Cape Basin during the Early Phanerozoic. Therefore, it could have feasibly supplied a portion of the younger detrital material. Alternatively, the younger ages could represent partial overprinting related to the CFB deformation.

The average age of the four youngest fusion ages (253.3 ± 1.9 Ma) is considered to reflect the final period of late Permian CFB deformation. Three of the four youngest grains are from fold and fault structures in the Steytlerville area, and confirm that the deformation processes in Fig. 5.4 were active during this period. The scattering of muscovite fusion ages between ~255 and 440 Ma, and the variability in apparent ages between heating steps, suggest these grains are detrital, but affected by partial loss of radiogenic argon due to CFB deformation and related fluid flow (e.g., Egle et al. 1998), and/or alteration. From these data, there is no clear indication of older deformation periods.

The occurrence of so few deformation-related ages in the suite of 105 grains implies that only some shear zones, or very localized areas within shear zones, experienced metamorphic conditions sufficient to grow new muscovite or completely overprint detrital muscovite. The high percentage of detrital mica ages and intermediate ages, suggesting varying degrees of radiogenic argon loss, indicate that the mica-defined foliations visible in cleavage-bearing samples are the result of rotation and realignment of preexisting grains. These findings are consistent with the low P-T estimates for metamorphism in the CFB mentioned above. Ages obtained in this study potentially identify zones where tectonism and associated fluid flow were particularly focused (e.g., structures samples in the Steytlerville area providing ~253 Ma muscovite ages), as well as structures active at shallower crustal levels (e.g., shear zones with no CFB deformation-related ages), where metamorphic conditions were less intense.

5.6 Conclusions

- U-Pb analyses of Cape Supergroup detrital zircon grains show major age populations at 1200–1000 and 650–500 Ma (Fourie et al. 2011; Vorster 2013; Miller et al. 2016), suggesting the Namaqua-Natal Metamorphic Complex and Pan-African orogenic belts as dominant sediment sources. Definitive source(s) for detrital zircons age 500–400 Ma are yet to be identified.
- Previous $^{40}Ar/^{39}Ar$ analyses were mostly conducted on muscovite aggregates and yield discordant age spectra with ages generally increasing with temperature. Ages older than ~400 Ma are interpreted to indicate the presence of detrital muscovite grains. Younger ages have been used previously to infer multiple deformation events at: 278, 258, 247, and 230 Ma (Häbich et al. 1983); 294, 276, 259, 239 and 223 Ma (Gresse et al. 1992); 270 and 251 (Hansma et al. 2015).
- High precision $^{40}Ar/^{39}Ar$ analyses of single muscovite grains in the current study show a range of apparent ages from ~250 Ma to ~630 Ma. Muscovite grains >440 Ma are considered to be a detrital population, predominantly sourced from the Pan-African Orogens and the Cape Granites.
- This overview demonstrates the risk of producing mixed age spectra when $^{40}Ar/^{39}Ar$ step-heating experiments are conducted on multi-grain samples that potentially comprise detrital and partially reset components older than the period of deformation under investigation.
- It is concluded that the main phase of CFB deformation occurred at approximately 253 Ma. At present, there is insufficient data to confirm a polyphase history for CFB deformation.

5.7 Challenges for the Future

To ascertain the complete sedimentary evolution of the CFB, a more systematic study across the entire CFB and throughout the Cape Supergroup sedimentary sequence is needed. Due to the differences in isotopic closure of zircon and muscovite (>900 °C; Lee et al. 1997, and 425 °C; Harrison et al. 2009, respectively), provenance studies should consider the use of both U-Pb dating of zircon and $^{40}Ar/^{39}Ar$ dating of muscovite to identify remote sources, and the most recent and nearby sources. Additional $^{40}Ar/^{39}Ar$ geochronological investigations, geochemical, isotopic, and thermochrological studies in potential source areas would reinforce potential links between sources and sinks. The information from such provenance studies should provide insights into exhumation rates of source terranes and potentially the arrangements of neighboring crustal fragments.

Improved constraints on the timing of orogenesis, including defining the onset, duration, and any potential phases of deformation, in the CFB will require further detailed sample characterization (i.e., microprobe investigations to identify potential geochemical differences between age populations), coupled with further single grain, high precision $^{40}Ar/^{39}Ar$ analysis of samples across the CFB. Due to the low-grade nature of metamorphism within the CFB, future studies should consider the complementary use of zircon and apatite (U-Th)/He analyses, which could provide insights into the cooling history through 200 °C. These geochronological methods would be particularly useful for dating deformation structures in the Karoo Supergroup sediments (i.e., the Beaufort Group), to investigate the waning stages of CFB orogenesis.

Acknowledgments The authors thank Maarten de Wit, Peter Booth, Bastien Linol, and Warren Miller for their guidance and assistance in the field. Dr. Erin Matchan and Stan Szczepanski are thanked for technical assistance in the $^{40}Ar/^{39}Ar$ laboratory. Insightful and constructive comments were greatly appreciated from reviewers Jan Kramers and Maarten de Wit.

References

Andersen, T., Kristoffersen, M. and Elburg, M., 2016. How far can we trust provenance and crustal evolution information from detrital zircons? A South African case study, Gondwana Research (2016), doi:10.1016/j.gr.2016.03.003

Armstrong, R.A., de Wit, M.J., Reid, D., York, D. and Zartman, R., 1998. Cape Town: Table Mountain reveals rapid Pan-African uplift of its basement rocks. Journal of African Earth Science, 27, 10–11.

Bangert, B., Stollhofen, H., Lorenz, V. and Armstrong, R., 1999. The geochronology and significance of ash-fall tuffs in the glaciogenic Carboniferous-Permian Dwyka Group of Namibia and South Africa. Journal of African Earth Sciences, 29, 33–49.

Barnett, W., Armstrong, R. and de Wit, M.J., 1997. Stratigraphy of the Upper Neoproterozoic Kango and lower Palaeozoic Table Mountain Groups of the Cape Fold Belt revisited. South African Journal of Geology, 100, 237–250.

Board, W.S., Frimmel, H.E. and Armstrong, R.A., 2005. Pan-African tectonism in the western Maud Belt: P–T–t path for high-grade gneisses in the H.U. Sverdrupfjella, East Antarctica. Journal of Petrology, 46, 671–699.

Booth, P.W.K., 1996. The relationship between folding and thrusting in the Floriskraal Formation (upper Witteberg Group), Steytlerville, Eastern Cape. South African Journal of Geology 99, 235–243.

Booth, P.W.K., 1998. The effect of thrusting on fold style and orientation, Weltevrede Formation (Cape Supergroup), Steytlerville, Eastern Cape. South African Journal of Geology 101, 27–37.

Booth, P.W.K., 2011. Stratigraphic, structural and tectonic enigmas associated with the Cape Fold Belt: challenges for future research. South African Journal of Geology, 114, 235–248.

Booth, P.W.K. and Goedhart, M.L., 2014. Thrust faulting in the northernmost foreland zone of the Cape Fold Belt, Fort Beaufort, Eastern Cape, South Africa. South African Journal of Geology, 117, 301–315.

Booth, P.W.K. and Shone, R.W., 1999. Complex thrusting at Uniondale, eastern sector of the Cape Fold Belt, Republic of South Africa: structural evidence for the need to revise the lithostratigraphy. Journal of African Earth Sciences, 29, 125–133.

Booth, P.W.K. and Shone, R.W., 2002. A review of thrust faulting in the Eastern Cape Fold Belt, South Africa, and the implication for current lithostratigraphic interpretation of the Cape Supergroup. Journal of African Earth Sciences, 34, 179–190.

Booth, P.W.K., Brunsdon, G. and Shone, R.W., 2004. A Duplex Model for the Eastern Cape Fold Belt? Evidence from the Palaeozoic Witteberg and Bokkeveld Groups (Cape Supergroup), Near Steytlerville, South Africa. Gondwana Research, 7, 211–222.

Broquet, C.A.M., 1992. The sedimentary record of the Cape Supergroup: a review. In: de Wit, M.J., Ransome, I.G.D. (Editors), In: M. J. de Wit and I.G.D. Ransome (Editors). Inversion tectonics of the Cape Fold Belt, Karoo and Cretaceous Basins of Southern Africa. Balkema, Rotterdam, Netherlands, 159–183.

Chemale, F., Scheepers, R., Gresse, P.G. and Van Schmus, W.R., 2011. Geochronology and sources of late Neoproterozoic to Cambrian granites of the Saldania Belt. International Journal of Earth Sciences, 100, 431–444.

Curtis, M.L. and Hyam, D.M., 1998. Late Palaeozoic to Mesozoic structural evolution of the Falkland Islands: a displaced segment of the Cape Fold Belt. Journal of the Geological Society, 155, 115–129.

da Silva, L.C., Gresse, P.G., Scheepers, R., McNaughton, N.J., Hartmann, L.A. and Fletcher, I.R., 2000. U-Pb SHRIMP and Sm-Nd age constraints on the timing and sources of the Pan-African Cape Granite Suite, South Africa. Journal of African Earth Sciences, 30, 795–815.

de Wit, M.J. and Ransome, I.G.D., 1992. Regional inversion tectonics along the southern margin of Gondwana. In: M.J. de Wit and I.G.D. Ransome (Editors). Inversion tectonics of the Cape Fold Belt, Karoo and Cretaceous Basins of Southern Africa. Balkema, Rotterdam, Netherlands, 15–21.

Egle, S., de Wit, M.J. and Hoernes, S., 1998. Gondwana fluids and subsurface palaeohydrology of the Cape Fold belt and the Karoo Basin, South Africa. Journal of African Earth Sciences, 27, 63–64.

Fergusson, C.L. and Phillips, D., 2001. ^{40} and K-Ar age constraints on the timing of regional deformation, south coast New South Wales, Lachlan Fold Belt: problems and implications. Australian Journal of Earth Sciences, 48, 395–408.

Fourie, P. H., Zimmermann, U., Beukes, N. J., Naidoo, T., Kobayashi, K., Kosler, J., Nakamura, E., Tait, J. and Theron, J.N., 2011. Provenance and reconnaissance study of detrital zircons of the Palaeozoic Cape Supergroup in South Africa: Revealing the interaction of the Kalahari and Río de la Plata Cratons. International Journal of Earth Sciences, 100, 527–541.

Frimmel, H.E., Fölling P.G. and Diamond, R., 2001. Metamorphism of the Permo-Triassic Cape Fold Belt and its basement, South Africa. Mineral Petrology, 73, 325–346.

Gentle, R.I., Hooker, P.J., Fitch, F.J. and Miller, J.A., 1978. Evidence for Cape Fold Belt overprinting of the Groot Haelkraal granite during the Upper Permian. Transactions of the Geological Society of South Africa, 81, 105–107.

Gohl, K., Uenzelmann-Neben, G. and Grobys, N., 2011. Growth and dispersal of a southeast African Large Igneous Province. South African Journal of Geology, 114, 379–386.

Gresse, P.G., Theron, J.N., Fitch, F.J. and Miller, J.A., 1992. Tectonic inversion and radiometric resetting of the basement in the Cape Fold Belt. In: M.J. de Wit and I.G.D. Ransome (Editors). Inversion tectonics of the Cape Fold Belt, Karoo and Cretaceous Basins of Southern Africa. Balkema, Rotterdam, Netherlands, 217–228.

Gresse, P.G., Von Veh, M.W. and Frimmel, H.E., 2006. Namibian, (Neoproterozoic) to early Cambrian successions. In: M.R. Johnson, C.R. Anhaeusser and R.J. Thomas, (Editors), The Geology of South Africa, Geological Society of South Africa, Council For Geoscience, 395–420.

Hälbich, I.W. and Cornell, D.H., 1983. Metamorphic history of the Cape Fold Belt. In: A.P.G. Söhnge and I.W. Hälbich (Editors) Geodynamics of the Cape Fold Belt, Special Publications of the Geological Society of South Africa, Johannesburg. 12, 131–148.

Hälbich, I. W., 1983. Disharmonic folding, detachment and thrusting in the Cape Fold Belt. In: A.P.G. Söhnge and I.W. Hälbich (Editors), Geodynamics of the Cape Fold Belt. Special Publications of the Geological Society of South Africa, Johannesburg, 12, 115–124.

Hälbich, I.W., Fitch, F.J. and Miller, J.A., 1983. Dating the Cape Orogeny. In: A.P.G. Söhnge and I.W. Hälbich (Editors), Geodynamics of the Cape Fold Belt. Special Publications of the Geological Society of South Africa, Johannesburg, 12, 75–100.

Hansma, J., Tohver, E., Schrank, C., Jourdaan, F. and Adams, D., 2015. The timing of the Cape Orogeny: New 40Ar/39Ar age constraints on deformation and cooling of the Cape Fold Belt, South Africa. Gondwana Research, doi:10.1016/j.gr.2015.02.005.

Harrison T. M., Célérier J., Aikman A. B., Hermann J. and Heizler M. T., 2009. Diffusion of ^{40}Ar in muscovite. Geochimica et Cosmochimica Acta 73, 1039– 1051.

Jacobs, J., Ahrendt, H., Kreutzer, H., Weber, K., 1995. K–Ar, ^{40}Ar–^{39}Ar and apatite fission track evidence for Neoproterozoic and Mesozoic basement rejuvenation events in the Heimefrontfjella and Mannefallknausane (East Antarctica). Precambrian Research, 75, 251–263.

Jacobs, J., Fanning, C.M., Henjes-Kunst, F., Olesch, M. and Paech, H.-J., 1998. Continuation of the Mozambique belt into East Antarctica: Grenville-age metamorphism and polyphase Pan-African high-grade events in central Dronning Maud Land. Journal of Geology, 106, 385–406.

Jacobs, J., Fanning, C.M. and Bauer, W., 2003. Timing of Grenville-age vs. Pan-African medium- to high grade metamorphism in western Dronning Maud Land (East Antarctica) and significance for correlations in Rodinia and Gondwana. Precambrian Research, 125, 1–20.

Jacobs, J. and Thomas, R.J., 2004. Himalayan-type indenter-escape tectonics model for the southern part of the late Neoproterozoic–early Paleozoic East African-Antarctic orogen. Geology, 32, 721–724.

Johnston, S., 2000. The Cape Fold Belt and Syntaxis and the rotated Falkland Islands: dextral transpressional tectonics along the southwest margin of Gondwana. Journal of African Earth Sciences, 31, 51–63.

Jourdan, F., Féraud, G., Bertrand, H., Watkeys, M.K., Renne, P.R., 2008. The ^{40}Ar/^{39}Ar ages of the sill complex of the Karoo large igneous province: implications for the Pliensbachian–Toarcian climate change. Geochem. Geophys. Geosyst., 9, Q06009. doi:10.1029/2008GC001994.

Lee, J. K. W., Williams, I. S. and Ellis, D. J., 1997. Pb, U and Th diffusion in natural zircon. Nature 390, 159–162.

Lee, J.-Y., Marti, K., Severinghaus, J.P., Kawamura, K., Yoo, H.-S., Lee, J.B. and Kim, J.S., 2006. A redetermination of the isotopic abundances of atmospheric Ar. Geochimica et Cosmochimica Acta, 70, 4507–4512.

Lindeque, A., de Wit, M.J., Ryberg, T., Weber, M. and Chevallier, L., 2011. Deep crustal profile across the southern Karoo Basin and Beattie Magnetic Anomaly, South Africa: An integrated interpretation with tectonic implications. South African Journal of Geology, 114, 265–292.

McDougall I. and Harrison T. M., 1999 Geochronology and Thermochronology by the ^{40}Ar/^{30}Ar Method. Oxford University Press, New York, 1999.

Miller, W., Armstrong, R.,and de Wit, M., 2016. Geology and U/Pb geochronology of the Gamtoos Complex and lower paleozoic Table Mountain Group, Cape Fold Belt, Eastern Cape, South Africa. South African Journal of Geology, 119, 147–170.

Pángaro, F. and Ramos, V.A., 2012. Paleozoic crustal blocks of onshore and offshore central Argentina: New pieces of the southwestern Gondwana collage and their role in the accretion of Patagonia and the evolution of Mesozoic south Atlantic sedimentary basins. Marine and Petroleum Geology, 37, 162–183.

Paton, D.A., Macdonald, D.I.M. and Underhill, J.R., 2006. Applicability of thin or thick skinned structural models in a region of multiple inversion episodes; southern South Africa. Journal of Structural Geology, 28, 1933–1947.

Phillips, D. and Matchan, L., 2013. Ultra-high precision ^{40}Ar/^{39}Ar ages for Fish Canyon Tuff and Alder Creek Rhyolite sanidine: New dating standards required? Geochimica et Cosmochimica Acta, 121, 229–239.

Rapela, C.W., Pankhurst, R.J., Fanning, C.M. and Grecco, L.E., 2003. Basement evolution of the Sierra de la Ventana Fold Belt: new evidence for Cambrian continental rifting along the southern margin of Gondwana. Journal of the Geological Society, London, 160, 613–628.

Renne P.R., Swisher C.C., Deino A.L., Karner D.B., Owens T.L. and De Paolo D.J., 1998. Intercalibration of standards, absolute ages and uncertainties in ^{40}Ar/^{39}Ar dating. Chem. Geol. 145, 117–152.

Renne, P.R., Deino, A.L., Hames, W.E., Heizler, M.T., Hemming, S. R., Hodges, K.V., Kopers, A.A.P., Mark, D.F., Morgan, L.E., Phillips, D., Singer, B.S., Turrin, B.D., Villa, I.M., Villeneuve, M. and Wijbrans, J.R., 2009. Data reporting norms for ^{40}Ar/^{39}Ar geochronology. Quaternary Geochronology, 4, 346–352.

SACS (South African Committee for Stratigraphy), (1980): Stratigraphy of South Africa. Part I. (Compiled by L.E. Kent). Lithostratigraphy of the Republic of South

Steiger, R.H. and Jäger, E., 1977. Subcommission on geochronology: convention on the use of decay constants in geo- and cosmochronology. Earth and Planetary Science Letters, 36, 359–362.

Vorster, C. 2013. Laser ablation ICP-MS age determination of detrital zircon populations in the Phanerozoic Cape and Lower Karoo Supergroups (South Africa) and correlatives in Argentina. Unpublished PhD. Thesis, University of Johannesburg, South Africa, 648p.

Part III
Magmatism and Metamorphism

New Evidence for the Correlation of Basalts of the Suurberg Group with the Upper Part of the Karoo Basalt Sequence of Lesotho

6

J.S. Goonie Marsh

Abstract

Tholeiitic basalts build the Mimosa Formation, the uppermost stratigraphic unit of the Suurberg Group in the northern part of the Algoa Basin. Exposures are very poor and the tectonic significance of the Suurberg rocks and the origin of the Mimosa basalts are contentious. Drilling of stratigraphic boreholes at four localities allowed detailed sampling of the basalts from two cores 90 km apart for geochemical, age and palaeomagnetic investigations. $^{40}Ar/^{39}Ar$ dating of plagioclase from one sample yielded an imprecise plateau age of 194 ± 12 Ma which is within error of the age of the short-lived Karoo volcanism in Lesotho. Whole-rock geochemistry indicates that the Mimosa basalts are equivalent to the Senqu magma type which builds a thick sequence of flows in the upper part of the Lesotho sequence. Mimosa basalts have normal magnetic polarity as do the Senqu basalts. All these data support a correlation between the Mimosa basalts and those in the upper part of the basaltic sequence in Lesotho.

6.1 Introduction

The Jurassic Suurberg Group outcrops along the northern margin of the Algoa Basin, principally between Kirkwood and Paterson and in the Kirkwood Panhandle (Fig. 6.1). Exposures are very poor and comprehensive descriptions of lithology and stratigraphy have relied on both field mapping (Rogers 1905; Haughton and Rogers 1924; Hill 1975) and a number of borehole cores drilled by the Geological Survey of South Africa (Hill 1992). The Suurberg Group unconformably overlies folded and eroded rocks of the Witteberg Group (Cape Supergroup) and Dwyka Group (Karoo Supergroup) and is in turn overlain by sandstones and conglomerates of the Upper Jurassic Enon Formation. The Suurberg Group comprises a lower clastic package of breccia, conglomerate, shale, sandstone and volcaniclastic deposits (the Slagboom and Coerney Formations) overlain by a sequence (up to 140 m thick) of pahoehoe flows of tholeiitic basalt (Mimosa Formation).

J.S. Goonie Marsh (✉)
Department of Geology, Rhodes University, Grahamstown, 6140, South Africa
e-mail: goonie.marsh@ru.ac.za

The exact stratigraphic status of the Suurberg Group, particularly the origin of the basaltic lavas is controversial. This arises from their isolation within the Cape Fold Belt with no visible physical connection to the main mass of Mesozoic mafic lavas and intrusions, namely those of the Karoo Supergroup, far to the north in the interior of southern Africa. Additionally, poor outcrops and their lack of continuity make it difficult to unravel fully the field relationships of the Suurberg Group. There is even uncertainty as to the existence of the Suurberg Fault (Hill 1975) which earlier workers described as defining the northern contact between the Suurberg Group and the older Palaeozoic Cape Fold Belt rocks (e.g. Rogers and Du Toit 1909, 366–369). With regard to the Mimosa basalts, major questions over which opinion is divided relate to the precise age of the volcanic rocks, whether they are correlatives of the Drakensberg Group in Lesotho, and whether they originate from local or remote eruption sites. Resolution of these issues is important for better understanding the original extent of the Karoo Igneous Province and the location of its feeding system.

Following earlier suggestions (e.g. Haughton and Rogers 1924; Du Toit 1954) a general correlation of basalts of the Mimosa Formation with those of the Drakensberg Group of

B. Linol and M.J. de Wit (eds.), *Origin and Evolution of the Cape Mountains and Karoo Basin*,
Regional Geology Reviews, DOI 10.1007/978-3-319-40859-0_6

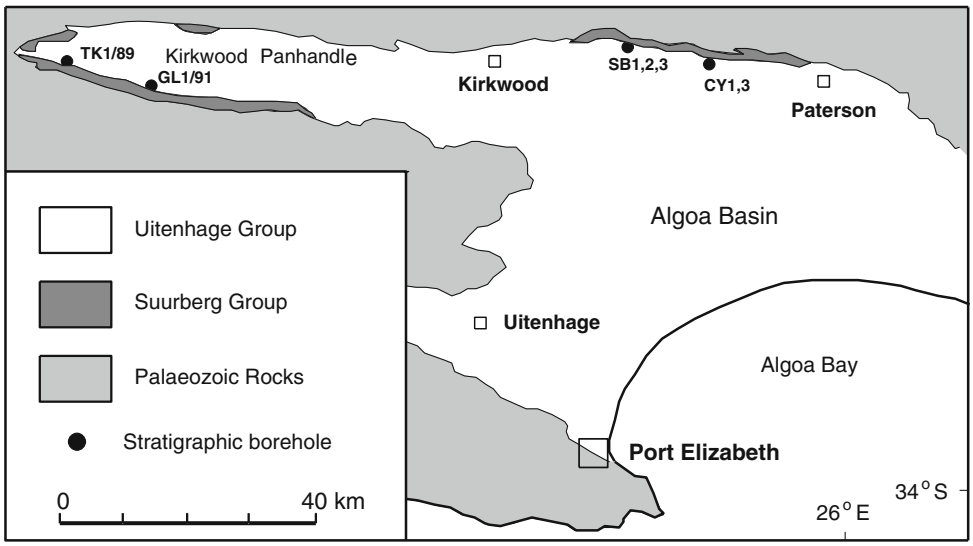

Fig. 6.1 Simplified geological map of the Algoa Basin showing outcrops of the Suurberg Group and the localities of the stratigraphic boreholes

the Karoo Supergroup is now accepted (Hill 1992). This is based on broad palaeontologically defined Jurassic age for the Suurburg sequence and later supported by an old single K/Ar age of 162 ± 7 Ma (McLachlan and McMillan 1976) which lies in the 200–150 Ma range of ages once believed to have characterized Karoo volcanism (Fitch and Miller 1984). New age and palaeomagnetic data (Moulin et al. 2011; Svensen et al. 2012; Burgess et al. 2015) have revised estimates for the duration and timing of volcanic activity building the Drakensberg Group to less than 1 Ma at about 183 Ma and this calls for a review of the proposed correlation. In addition, several stratigraphic boreholes drilled between 1987 and 1991 have allowed unprecedented access to sample material from the Mimosa Formation and a more detailed comparison with basaltic lavas of the Drakensberg Group.

6.2 The Current Study

The Geological Survey of South Africa drilled stratigraphic boreholes through the Suurberg Group at four locations (Fig. 6.1). Detailed sampling of the Mimosa Formation was carried out in two of these boreholes some 90 km apart: SB2/88 (Slagboom, east of Kirkwood) and TK1/89 (Tyger Kop, western end of Kirkwood panhandle). The Slagboom borehole contains a 111 m thick sequence of flows as well as a 3.3 m intrusion some 25 m below the base of the lava sequence and 1.5 m above the basal contact with tillites of the Dwyka Group. At least six separate flow lobes are present in the sequence as indicated by the presence of oxidized flow crusts and thin interbedded sedimentary layers. About half the sequence thickness is made up of the basal flow, which is 55 m thick. In TK1/91, the basaltic sequence is about 75 m thick and built of five flow lobes with the uppermost flow of 52 m dominating the succession. This thick flow has a 2 m thick flow breccia at its base and a centrally located 10 m thick zone characterized by pegmatoidal schlieren. In both cores, the flow lobes exhibit a threefold subdivision based on amygdale distribution typical of pahoehoe flows (Aubele et al. 1988): a thin amygdaloidal basal zone with pipe amygdales, a core zone which is largely amygdale-free, and a thick upper zone of abundant spherical amygdales.

Where possible, a sample from each flow lobe was collected from the amygdale-free core zone of the flow and in many lobes more than one sample was collected, particularly in the thick lobes. Twenty-one samples were collected from TK1/89, including a sample of a pegmatoidal segregation. Twenty-three samples were collected from the lava sequence in SB2/88 and one sample from the intrusion.

6.2.1 Petrography

Petrographic features of lava flows are variable through the flow, and the descriptions given here largely relate to the amygdale-free core zones from which samples were taken. The basalts are hypocrystalline, equigranular with intersertal to hyalophitic textures and are variably altered. Average grain size varies from 0.3 to 0.8 mm but in some samples there are gradations to aggregates of larger crystals up to 1.5 mm. In the pegmatoidal zone of TK1/89, grain sizes range up to 7 mm. Only one flow, the basal flow in TK1/89, has a distinct glomerporphyritic texture with aggregates of plagioclase laths up to 1.5 mm long in a groundmass with

grains size <0.2 mm. Dominant minerals are zoned euhedral plagioclase and subhedral clinopyroxene. Discrete pigeonite and augite occurs throughout the 52 m thick flow in TK1/89, but in other flows pigeonite forms cores and rims to augite. Pseudomorphs after olivine occur in several flows and late crystallizing opaque oxides are ubiquitous accessory minerals. The intrusion in SB2/88 is medium grained, has an ophitic to poikilophitic texture with laths of plagioclase averaging 0.3 mm in length enclosed by large augite grains up to 2 mm in size.

6.2.2 Geochemistry

Samples were pulverized using Mn-steel jaw crusher and swing mill, with care taken to remove any amygdales containing secondary minerals during crushing. All samples were analysed by XRF-spectrometry with a Philips PW1480 spectrometer at Rhodes University. Major elements were determined on glass fusion discs and trace elements on pressed powder pellets as described in Duncan et al. (1984). Analyses are summarized in a number of variation diagrams (Figs. 6.2, 6.3, 6.4 and 6.5).

The basalts are typical continental tholeiites with a modest range in composition (MgO = 5.5 to 7.6 %). There is a substantial overlap in composition in samples from the two cores with those from the base of SB2/33 extending to more primitive compositions. The intrusion in SB2/88, SB-1 is the most primitive sample in terms of MgO, Cr and Ni, but in terms of immobile incompatible elements (i.e. Zr, Nb, P, Ti, Ce) it plots with the bulk of the basalt samples and is clearly of the same magma type. Basalts with <6 % MgO

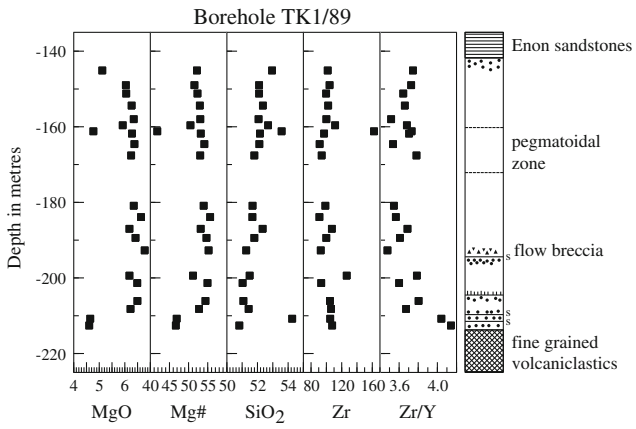

Fig. 6.2 Graphic log of the Mimosa basalts in borehole TK1/89 with accompanying vertical variation of some geochemical parameters. S—thin sedimentary horizon between flows

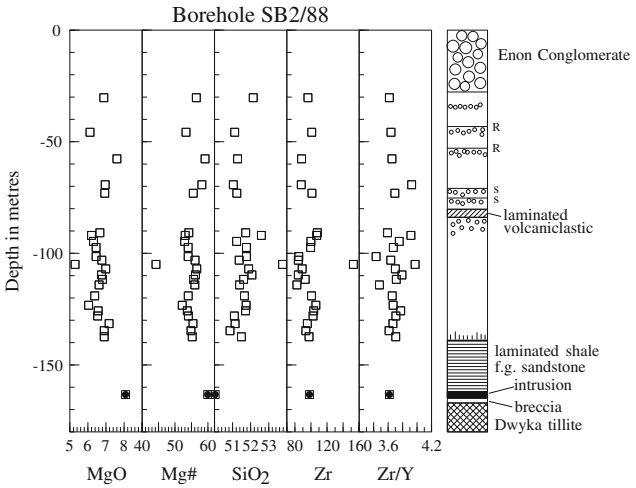

Fig. 6.3 Graphic log of the Mimosa basalts in borehole SB2/88 with accompanying vertical variation of some geochemical parameters. R—oxidized flow top; S—thin sedimentary horizon

show an incoherent scatter in their major element compositions which is not replicated amongst trace elements, especially the immobile elements. Two of these, the pegmatoid TK-48 and sample SB-13 have compositions which are consistent with being fractional crystallization derivatives from the main bulk of basalt samples, but the remaining samples (TK-27, 28, 52) have probably had their compositions modified by alteration to reflect spuriously low MgO relative to immobile elements such as TiO_2, P_2O_5 and Zr (Figs. 6.4 and 6.5). It is noteworthy that these samples are from amygdaloidal zones of flows and also have the highest LOI. No flows of intermediate composition, such as the two surface samples reported by Marsh et al. (1979), were encountered in the cores.

Leaving aside the altered and differentiated samples, Figs. 6.4 and 6.5 demonstrate that the concentrations of both major and, more significantly, a range of trace elements in the Mimosa basalts overlap almost completely with those of the Lesotho Formation of the Drakensberg Group. This compositional similarity was previously remarked on by Marsh et al. (1979) but the current comparison involves much larger databases for both suites of lavas. Marsh et al. (1997) showed that the compositional range of basalts in the Lesotho Formation was relatively small but vertical variations in ratios of immobile incompatible elements as well as other geochemical parameters in eight serial sections through the Lesotho remnant yielded a consistent pattern. This allowed a geochemical stratigraphy for the >1.5 km thick lava sequence to be defined and discrimination diagrams for geochemical stratigraphic units to be established. The geochemical stratigraphy has enabled stratigraphic

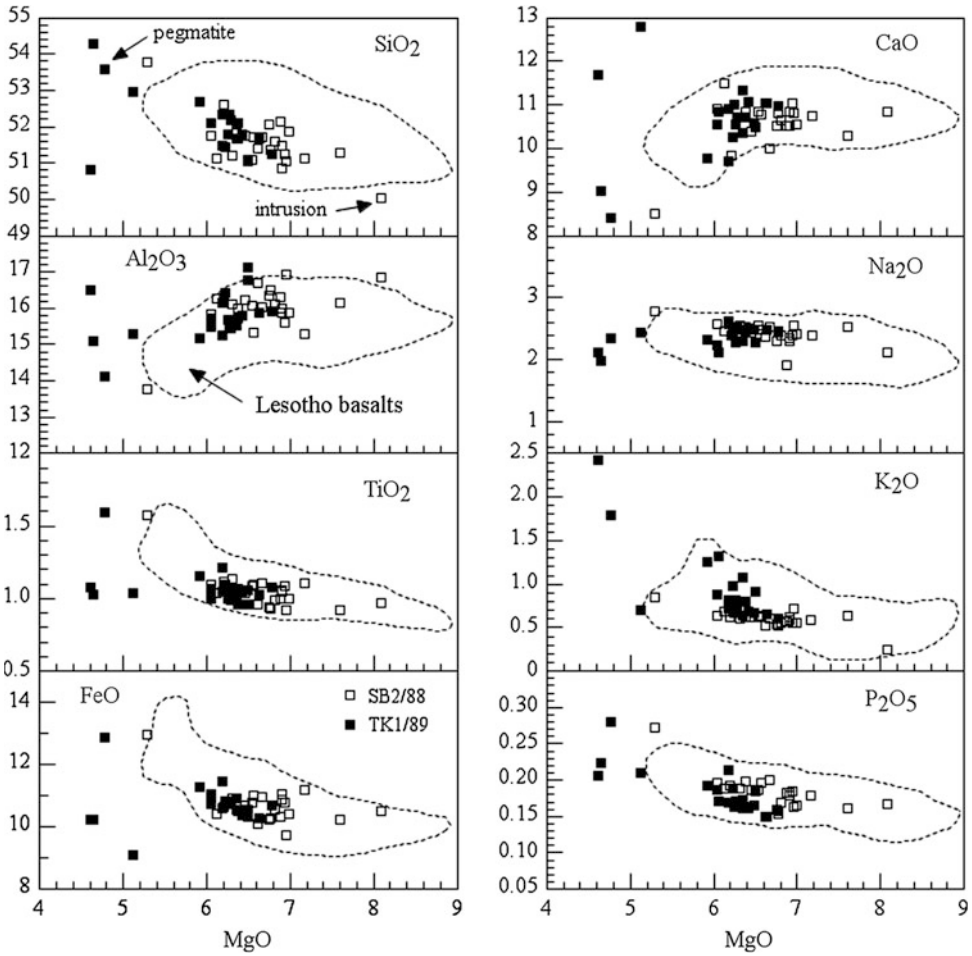

Fig. 6.4 Major element variation diagrams for Mimosa basalts and comparison with the compositional field of basalts from the Lesotho Formation (>600 analyses from Marsh et al. 1997 and unpublished)

correlations between remnants of Karoo volcanic sequences to be established, as demonstrated by Marsh et al. (1997) for correlation between the Springbok Flats remnant and Lesotho, separated by a distance of about 400 km. Figure 6.6 shows the Mimosa basalts plotted on a discrimination diagram for Lesotho Formation stratigraphic units. The geochemical correspondence between the Mimosa basalts and those lavas defining the Senqu unit in the upper part of the Lesotho Formation is clear. Samples which scatter to lower Mg# are the evolved or altered samples discussed above and can be ignored for correlation purposes.

6.2.3 Ar–Ar Dating and Palaeomagnetism

$^{40}Ar/^{39}Ar$ dating of a multigrain plagioclase separate from TK-47 was carried out by Kirstein (1997) and yielded a poor plateau age of 194 ± 12 Ma. This is within error of the 183 ± 1 Ma age for the Karoo recommended by Duncan et al. (1997) based on Ar–Ar dating and the more recently determined average U/Pb age of 182.6 ± 0.2 Ma (Svensen et al. 2012) for dolerites from across the Karoo Basin as well as the age of the larger Karoo-Ferrar province established by Burgess et al. (2015).

Hargraves (deceased) carried out a palaeomagnetic study of 15 cores collected from both TK1/89 and SB2/88. The data have never been published but in a personal communication to the author (1995), he reported that all samples gave stable and consistent results and had normal polarity. The volcanic sequence of Lesotho has a single well-established polarity reversal within a few hundred metres of the base of the lava pile (Van Zijl et al. 1962; Moulin et al. 2011). The Barkly East Formation and the lowermost lavas of the Lesotho Formation have reversed polarity whereas the bulk of the lava pile is characterized by normal directions. On the basis of simple polarity comparisons, the Mimosa basalts would be correlatives of the upper part of the Lesotho Formation.

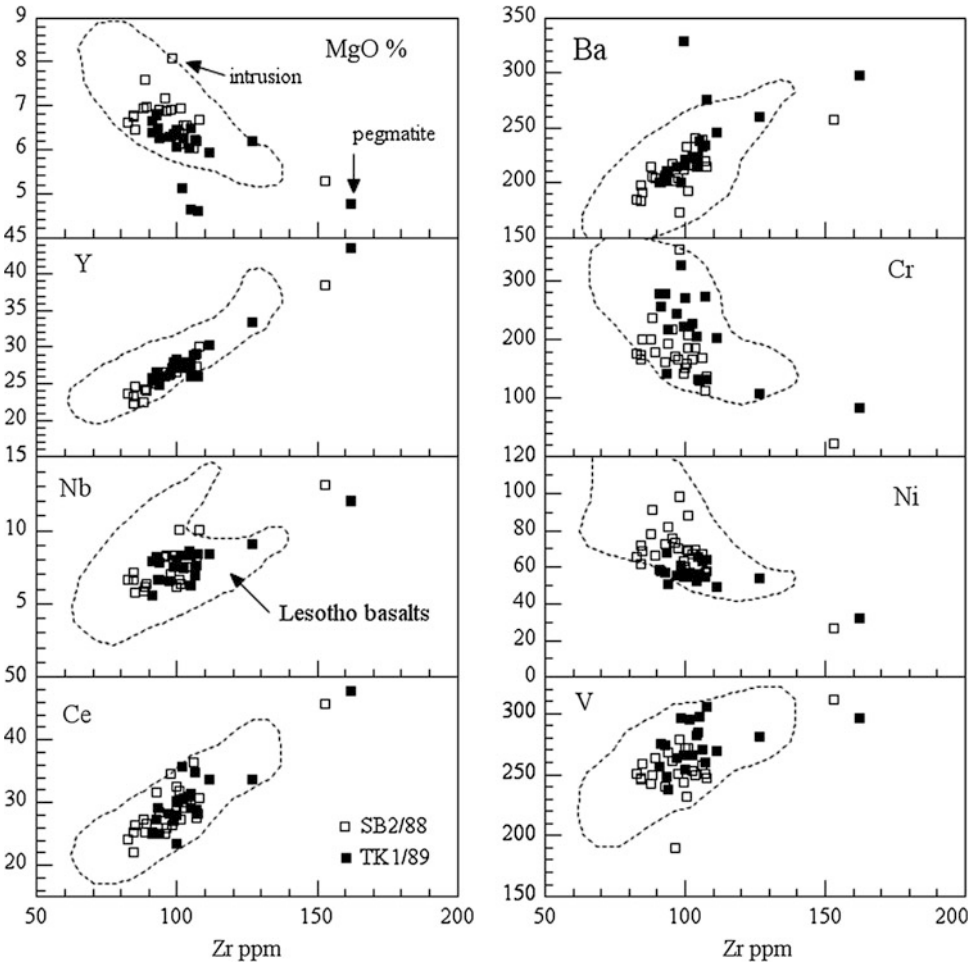

Fig. 6.5 Trace element variation diagrams for Mimosa basalts and compositional field for basalts from the Lesotho Formation

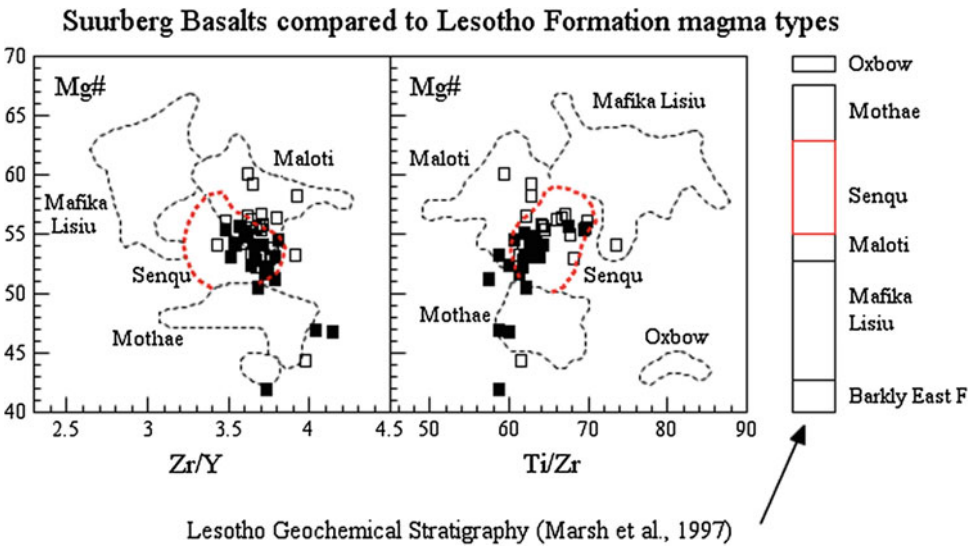

Fig. 6.6 Geochemical discrimination diagram showing composition of Mimosa basalts compared to compositional fields for different magma types in the Lesotho Formation (Marsh et al. 1997)

6.3 Discussion

As pointed out in the introduction, the origin of the Suurberg volcanic rocks has proved controversial. Rogers (1905) and Hill (1975) considered them to be of local derivation. The former author was of the opinion that they were emplaced by magmas rising along a supposed Suurberg Fault, which formed the northern boundary of the Algoa Basin, whereas Hill, finding no evidence for the Suurberg Fault, believed that eruptions were from a number of vents along a "weak zone" in the Cape Fold Belt prior to the formation of the Algoa Basin. He presented no evidence for the existence or location of the "weak zone" or vents, other than to propose that the quartzite breccias and conglomerates of the Slagboom Formation represented "vent-opening" breccias, although he could not dismiss the possibility that the Slagboom Formation was a talus breccia. Conversely, Haughton and Rogers (1924) correlated the lavas with the Karoo basalts based on petrographic similarity, evidence which would be considered rather weak in modern studies, and Du Toit (1954) suggested that the Suurberg basalts were a down-faulted remnant of the vast sheet of flood basalts extending southwards from the Lesotho remnant.

Broad stratigraphic and palaeontological evidence allows for the Mimosa basalts to be included as part of the Karoo volcanic event, and age, palaeomagnetic and geochemical data presented here are entirely consistent with the Mimosa basalts being correlated with the basalts of the Senqu geochemical type in the upper part of the Lesotho basaltic sequence. Mitha (2006) has demonstrated that Senqu basalts were erupted from fissures (now represented by dykes) around the Lesotho remnant. Flood basalt lava lobes emplaced through inflation are known to be voluminous, extending hundreds of kilometres from their vents (Self et al. 1997). They also build constructional volcanic edifices on the land surface and have remarkable geochemical homogeneity (Hooper 1997), the very characteristic which allows for geochemistry to be used for stratigraphic subdivisions and correlation in flood basalt suites of all ages worldwide. It is therefore plausible that flood basalt flows extended southwards overstepping underlying Stormberg Group sedimentary sequence and continuing across folded and eroded lower Karoo and Upper Cape Supergroup sequences of the Cape Fold-Thrust Belt. Development of a southern foreslope in response to orogenic unloading (Catuneanu et al. 1998) may explain why only the uppermost Karoo lavas extended onto the eroded northern margin of the Cape Fold Belt. Subsequent extension, heralding Gondwana break-up, resulted in the formation of a number of half grabens, including the Algoa Basin, to the south of approximately E-W normal faults which were reactivated steep reverse faults. This downfaulting could have preserved the Upper Karoo basalts, which overstepped onto the folded and eroded Cape Fold belt as the Mimosa Formation in the northern Algoa Basin.

The scenario proposed above argues for a distal origin for the Mimosa basalts and accords with the suggestion of Du Toit (1954). The proposal of Hill (1975) for emplacement of the Mimosa basalt from local eruptive vents would require the presence of crustal magma chambers containing magma of the Senqu geochemical type in the Cape Fold Belt beneath the northern part of the Algoa Basin. It is reasonable to expect that such magma chambers should be physically linked to the main mass of Karoo intrusions in the main Karoo basin, but there is no evidence for this as the southern limit of Karoo dolerite outcrops lies over 60 km to the north.

A distal origin faces additional problems. First, it does not account adequately for the silicic volcaniclastic rocks of the Coerney Formation, which underlie the Mimosa basalts. These volcaniclastic rocks featured in Hill's (1975) arguments for the presence of local eruptive centres. It should be noted that volcaniclastic 'tuffs' occur throughout the Karoo sedimentary succession in the main Karoo Basin and are believed to have a distal source, being derived from the magmatic arc far to the south of the Cape Fold Belt (e.g. McKay et al. 2015). A similar source for the Coerney volcaniclastics cannot be ruled out. Second, the dolerite dyke intruding the Coerney Formation (this is the intrusion in SB2/88, see Fig. 6.3) at Slagboom (Hill 1975, p. 131) may also suggest that the basalts were emplaced from local vents. However, it is also possible that the intrusion represents the distal end of a surface lava flow from a remote source which has invaded the underlying Coerney Formation. Such invasive flows are not uncommon. In the Miocene Columbia River Flood Basalt Province, a distal invasive-flow origin has been convincingly demonstrated for numerous dykes and other intrusions in pre-volcanic marine and deltaic sedimentary rocks on the Oregon coast. These intrusions were previously regarded as evidence for eruptive vents but have, in fact, been fed by surface Columbia River basalt flows, some of which have travelled 100s of kilometres from remote vents on the inland plateau before diving into the unconsolidated sedimentary substrata (Pfaff and Beeson 1989; Wells et al. 1989). Unfortunately, the outcrops of the intrusion in the roadcut at Slagboom have recently been completely destroyed during construction of a game fence and the field relationships, which might throw light on the true nature of the intrusion, are not exposed.

In conclusion an unequivocal scenario for the origin of the Suurberg basalts remains elusive. There is a clear need for high-precision age data such as U–Pb age dating of zircon from the Coerney Formation and particularly the tuffs interbedded with the basalts of the Mimosa Formation. Poor exposures seriously limit obtaining the field evidence

necessary to decide whether the basalts were emplaced from local or distal sources. This study presents strong evidence for correlating the Mimosa basalts with the upper part of the Drakensberg Group of Lesotho and argues for their derivation from distal sources in the Karoo Basin.

Acknowledgments This study was funded by the National Research Foundation of South Africa. Thanks are due to Robbie Hill, previously of the Geological Survey of South Africa, for facilitating access to the borehole cores investigated in this study. Comments by Maarten de Wit and Dave Bell (NMMU) improved the manuscript. An EXCEL spreadsheet with the analyses of the basalts is available on request from the author.

References

Aubele JC, Crumpler LS, Elston WE (1988) Vesicle zonation and vertical structure of basalt flows. Journal of Volcanology and Geothermal Research 35: 349–374.

Burgess SD, Bowring SA, Fleming TH, Elliot DH (2015) High precision geochronology links the Ferrar large igneous province with early Jurassic anoxia and biotic crisis. Earth and Planetary Science Letters 415: 90–99.

Catuneanu O, Hancox PJ, Rubidge BS (1998) Reciprocal flexural behaviour and contrasting stratigraphies: a new basin developmental model for the Karoo retroarc foreland system. South Africa Basin Research 10:417–439.

Du Toit AL (1954) Geology of South Africa (3rd Edition). Oliver and Boyd, Edinburgh, 611 pp.

Duncan AR, Erlank AJ, Betton PJ (1984)Appendix 1: Analytical techniques and database descriptions. Special Publication of the Geological Society of South Africa 13: 389–395.

Duncan RA, Hooper PR, Rehacek J, Marsh JS, Duncan, AR (1997) The timing and duration of the Karoo igneous event, southern Gondwana. Journal of Geophysical Research 102: 18127–18138.

Fitch FJ, Miller JA (1984) Dating Karoo igneous rocks by the conventional K-Ar and $^{40}Ar/^{39}Ar$ age spectrum methods. Special Publication of the Geological Society of South Africa 13: 247–266.

Haughton SH, Rogers AW (1924) Volcanic rocks south of the Zuurberg. Transactions of the Royal Society of South Africa 11: 235–249.

Hill RS (1975) The geology of the northern Algoa Basin, Port Elizabeth. Annals of the University of Stellenbosch, Series A1 (Geology) 1: 105–192.

Hill RS (1992) Suurberg Group including the Slagboom, Coerney, and Mimosa Formations. South African Commission for Stratigraphy, Pretoria, Catalogue of South African Lithostratigraphic Units, No 4, 4 pp.

Hooper PR (1997) The Columbia River Flood Basalt Province: Current status. In: Mahoney JJ, Coffin MF (eds) Large igneous provinces: Continental, oceanic, and planetary flood volcanism. Geophysical Monograph 100: 1–28.

Kirstein LA (1997) Magmatism in southern Uruguay and the early rifting of the South Atlantic. Unpublished PhD thesis, The Open University, 376 pp.

Marsh JS, Lock BE, Fuchter WH (1979) New chemical analyses of the Suurberg volcanic rocks and their significance in relation to Mesozoic volcanism in southern Africa. South African Journal of Science 75: 227–229.

Marsh JS, Hooper PR, Rehacek J, Duncan AR, Duncan RA (1997) Stratigraphy and age of Karoo basalts of Lesotho and implications for correlations within the Karoo Igneous Province. In: Mahoney JJ, Coffin ME (eds) Large igneous provinces: continental, oceanic, and planetary flood volcanism. Geophysical Monograph 100: 247–272.

McKay MP, Weislogel AL, Fildani A, Brunt RL, Hodgson DM, Flint SS (2015) U-Pb zircon tuff geochronology from the Karoo Basib, South Africa: implications of zircon recycling on stratigraphic age controls. International Geology Reviews 57: 393–410.

McLachlan IR, McMillan IK (1976) Review and stratigraphic significance of southern Cape Mesozoic palaeontology. Transaction of the Geological Society of South Africa 79: 197–212.

Mitha VR (2006) An insight into magma supply to the Karoo Igneous Province: A geochemical investigation of Karoo dykes adjacent to the northwestern sector of the Lesotho volcanic remanant. Unpublished MSc thesis, Rhodes University, Grahamstown, 194 pp.

Moulin M, Fluteau F, Courtillot V, Marsh J, Delpech G, Quidelleur X, Gérard M, Jay AE (2011) An attempt to constrain the age, duration and eruptive history of the Karoo flood basalt: Naude's Nek section (South Africa). Journal of Geophysical Research 116, B07403. doi:10.1029/2011JB0018210.

Pfaff VJ, Beeson MH (1989) Miocene basalt near Astoria, Oregon: Geophysical evidence for Columbia Plateau origin. In: Reidel SP, Hooper PR (eds) Volcanism and Tectonism in the Columbia River Flood-Basalt Province. Geological Society of America Special Paper 239: 153–156.

Rogers AW (1905) The volcanic fissure under the Zuurberg. Transactions of the Philosophical Society of South Africa 16: 190–197.

Rogers AW, Du Toit AL (1909) An introduction to the geology of Cape Colony (2nd edition). Longmans Green and Company, London, 491 pp.

Self S, Thordarson T, Keszthelyi L (1997) Emplacement of continental flood basalt lava flows. In: Mahoney JJ, Coffin ME (eds) Large igneous provinces: continental, oceanic, and planetary flood volcanism. Geophysical Monograph 100: 381–410.

Svensen S, Corfu F, Polteau S, Hammer Ø, Planke S (2012) Raped emplacement in the Karoo Large Igneous Province. Earth and Planetary Science Letters 325–326: 1-9

Van Zijl JSV, Graham KWT, Hales AL (1962) The palaeomagnetism of the Stormberg lavas of South Africa 1: Evidence for a genuine reversal of the Earth's field in Triassic-Jurassic times. Geophysical Journal of the Royal Astronomical Society 7: 23–29

Wells RE, Simpson RW, Bentley RD, Beeson MH, Mangan MT, Wright TL (1989) Correlation of Miocene flows of the Columbia River Basalt Group from central Columbia River Plateau to the coast of Oregon and Washington. In: Reidel SP, Hooper PR (eds) Volcanism and Tectonism in the Columbia River Flood-Basalt Province. Geological Society of America Special Paper 239: 113–129.

7 High-Resolution Petrographical and Chemical Scanning of Karoo Sedimentary Rocks Near Dolerite Sill Contacts Reveals Metamorphic Effects on Shale Porosity

Vhuhwavhohau Nengovhela, Maarten J. de Wit, Alan R. Butcher, and Erin Honse

Abstract

Host rock alterations related to high heat flow associated with igneous intrusions play an important role in changing the reservoir characteristics of oil and gas bearing shales. Such effects are common in the Permian black shale formations of the Karoo Basin that were intruded by basin-wide dolerites in the Early Jurassic (~182 Ma). Distinct changes in mineralogy and cracking of organic matter associated with high heat and fluid flow affect the porosity and permeability of host rocks. Analysis of drill core samples of the Karoo black shales close to upper and lower contacts of the dolerite sills indicates increased quartz content, decrease in hydrous minerals, and formation of metamorphic chiastolite. Most importantly, a notable decrease in the porosity is also observed in these samples.

Keywords

Karoo sills • Organic-rich shales • Contact metamorphism • Gas leakage

7.1 Introduction

Contact metamorphism in sedimentary basins is often associated with the emplacement of Large Igneous Provinces (LIP) during continental breakup. LIPs are characterized by voluminous basaltic lava flows and intrusive gabbroic-dolerite suites that are emplaced within the country rocks acting as a plumbing system that feeds the overlying lava sequences. Furthermore, the release of large amounts of gases during LIP-related intrusions has been associated with degassing and devolitilization of methane and carbon dioxide from organic-rich sedimentary rocks. Such events are often contemporaneous with mass extinctions (Aarnes et al. 2010; Sobolev et al. 2011; Ruhl et al. 2011; Keller et al. 2012; Renne et al. 2013; Sell et al. 2014; see also Chap. 17 in this book). Similar gas leakage has been inferred from field observations in the Karoo Basin, where the emplacement of the Karoo LIP into the sedimentary sequences at 182–183 Ma created numerous vents across the basin (Duncan et al. 1997; Svensen et al. 2004, 2006; Aarnes et al. 2011; Burgess et al. 2015; see also Chap. 2 in this book). The fine grained, organic-rich shales of the lower Ecca Group (ca. 300–270 Ma) that are divided into the Prince Albert, Whitehill, and Collingham Formations, have been identified as potential reservoirs of large volumes of unconventional shale gas (Geel et al. 2013, 2015; Black et al. 2016). However, the effects of dolerite sills on shale reservoir characteristics and shale gas potential in the Karoo Basin have been sparsely studied thus far despite the predictions that the intrusions may have significantly affected the total gas reservoirs (Aarnes et al. 2011; Mare et al. 2014; Scheiber-Enslin et al. 2014; Chere 2015; Smithard et al. 2015; Chap. 8 this book). The purpose of this study is to better quantify the extent of thermal alteration of host shales at varying distances from sill intrusions using core samples in

V. Nengovhela (✉) · M.J. de Wit
AEON-ESSRI (African Earth Observatory Network), Nelson Mandela University, Port Elizabeth, South Africa
e-mail: vd.nengovhela@yahoo.com

V. Nengovhela
Department of Geosciences, Faculty of Science, Nelson Mandela Metropolitan University, Port Elizabeth, South Africa

A.R. Butcher
FEI, Cambridge, UK

E. Honse
FEI, Houston, USA

B. Linol and M.J. de Wit (eds.), *Origin and Evolution of the Cape Mountains and Karoo Basin*, Regional Geology Reviews, DOI 10.1007/978-3-319-40859-0_7

order to evaluate the total potential gas loss. We present mineralogy and chemical composition data from core samples from the South African Petroleum Exploration Company (SOEKOR) boreholes selected in close proximity to dolerite sills. High-resolution images of organic matter and porosity are also presented to document the petrophysical changes in the shales as a result of heat transfer from the dolerite sills.

7.2 Dolerite Emplacement in the Karoo Basin

The Karoo dolerite suite comprises dykes, interconnected sills and discordant sheets that acted as shallow feeder systems for the main Karoo LIP flood basalt activity. Across parts of the region, sill intrusions compose >30 % of the thickness of the stratigraphy, with an estimated volume of 340,000 km^3 of the dolerite-gabbro suite (Chevallier et al. 2004, 2011). U/Pb dating of zircon and apatite within coarse gabbroic pegmatites of selected sills give dates of 183 ± 0.5 Ma and 182 ± 0.6 Ma, suggesting that the Karoo intrusives were emplaced contemporaneous with the volcanic rocks of the Drakensberg Group at rates of up to 0.78 km^3/yr (Garlene et al. 2008; Svensen et al. 2012; Burgess et al. 2015). The shape and thickness of sills appear to differ depending on where they occur stratigraphically within the Karoo Basin. For example, sills in the Dwyka Group have a maximum thickness of ca. 130 m. Shales of the overlying Ecca Group are characterized by laterally extensive sills attaining thicknesses up to 200 m. In the Beaufort Group, sandstones are intruded by saucer-shaped sill complexes formed by coalescing of individual sills of variable sizes. Here, large sills may have diameters ranging from 20 to 60 km, within which smaller sills attain diameters of up to several kilometres; and thicknesses that can attain several kilometres (du Toit 1903; Poldervaart and Walker 1942; Ferre et al. 2002; Duncan and Marsh 2006; Maes et al. 2008; Polteau et al. 2008; Garlene et al. 2008; Svensen et al. 2012).

Paleo-gas escape in the Karoo Basin probably at the time of the intrusions is revealed by the occurrence of conical structures referred to as hydrothermal vent complexes and breccia pipes (Svensen et al. 2006, 2008; Chere 2015; Scheiber-Enslin et al. 2014; Chap. 2 this book). These structures are believed to represent pathways through which gas and vapourised water, originating from underlying contact aureoles, were vented into the atmosphere. Dolerite intrusions emplaced throughout the Karoo Basin may thus have resulted in extensive devolatilization of the Permian black shales. An estimated release of more than 2000 Gt of carbon dioxide into the atmosphere was calculated by Svensen et al. (2006, 2007), Lee et al. (2009), Grab and Svensen (2011) and Aarnes et al. (2011). Although such volumes have been contested, the impact of cracking of organic matter and expulsion of the resulting methane from the black shales of the Ecca Group on the Early Jurassic biosphere remains largely understudied.

7.3 Methods

7.3.1 Borehole Logging and Sampling

We present preliminary results from two borehole cores AB 1/65 and QU 1/65 that were drilled in the 1960s by SOEKOR. These cores were logged in 2015 at the National Core Library (Council for Geoscience, Pretoria, South Africa). The boreholes intersect three stratigraphic sequences of the Karoo Supergroup: the Beaufort, Ecca and Dwyka Groups, as well as Karoo dolerite sills that intersect the units at different depths (Fig. 7.1a). The data presented here is based on samples close to: two sills, 2 and 7 m in thickness that intrude the Lower Ecca shales at depths of 1881 and 1887 m in borehole AB 1/65; and a 146 m thick dolerite sill that intruded the Dwyka Group at depth of 1930 m in borehole QU 1/65. A total of five core samples were selected (Fig. 7.1b) for detailed analyses. Samples AB1886 and AB1894 are hornfels samples; AB1903 and QU1855 are shales; and sample QU1894 is a sandstone.

7.3.2 Sample Preparation and Analysis

The core samples were first cut with a diamond blade normal to bedding and mounted on a single stub mount with carbon tape. The sectioned cores were then polished in an Argon Ion Mill. The edges of the uncoated core sections were covered with colloidal silver paint to help disperse charge during high-resolution modular automated processing system (MAPS) imaging in the Helios Dual Beam system. Since minerals in sedimentary rocks have a high resistance, or are insulators, it is important to avoid charging effects by coating the sample with a thin conductive layer. To achieve this, a thin layer of carbon was applied after the initial imaging on the Helios. The samples were then analysed on a Quanta 650 Field Emission Gun (FEG) fitted with QEMSCAN® automated mineral technology at FEI's Digital Rock Laboratory in Houston, USA.

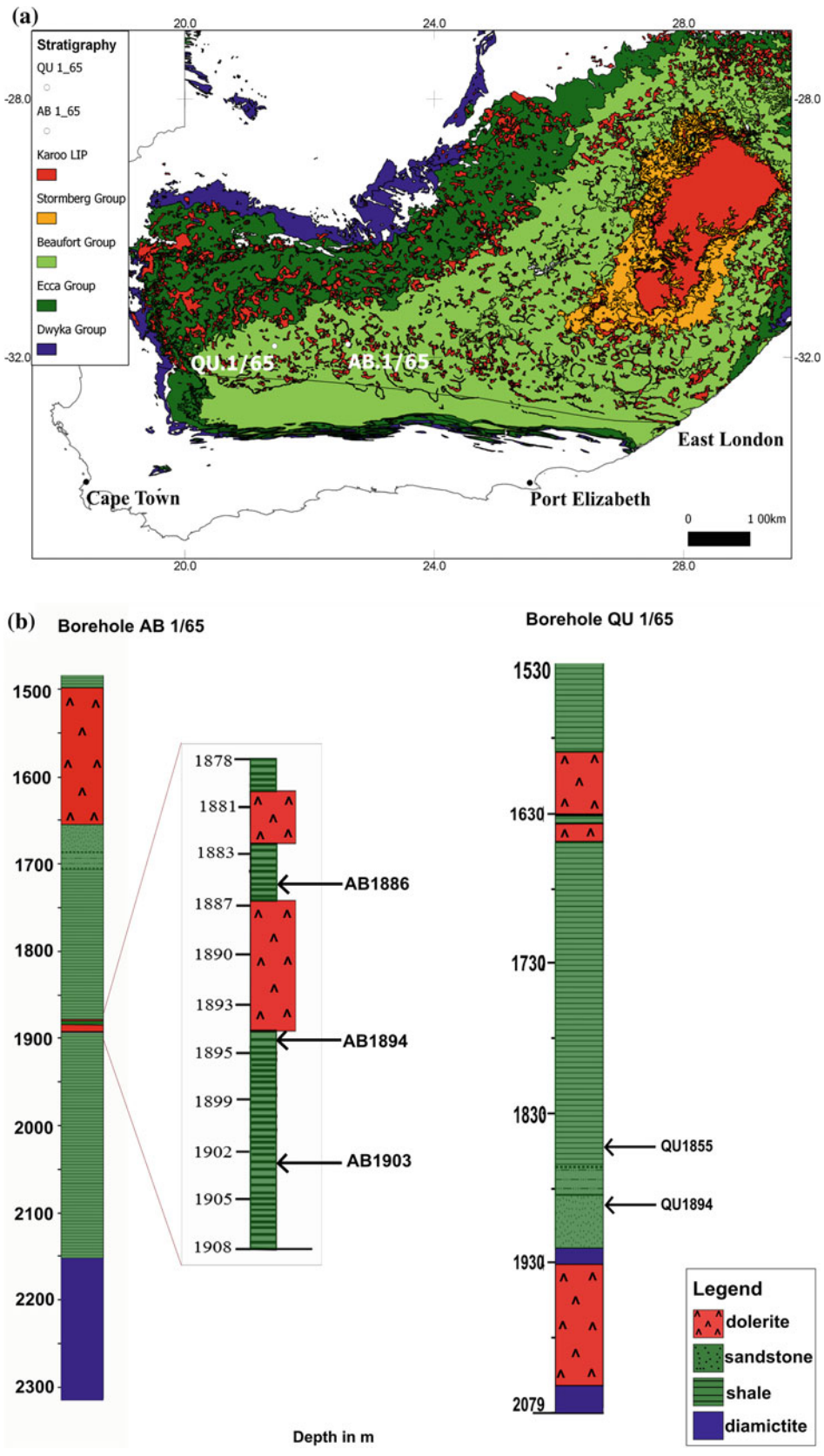

Fig. 7.1 **a** Geological map of the Karoo Basin showing the location of the two studied boreholes: AB 1/65 and QU 1/65. **b** Litho-stratigraphic borehole logs with the position of the samples analysed in this study

7.4 Results

7.4.1 Mineralogy and Elemental Distribution

Samples from borehole AB 1/65 show textural and mineralogical alterations that differ depending on the location of the samples relative to the sill (see Fig. 7.1b for sample location). The texture of AB1886 is typical of hornfels, characterized by very fine grained, white-washed appearance due to high quartz content (Fig. 7.2a). AB1894 has a porphyroblastic texture due to crystallization of metamorphic chiastolite (Fig. 7.2b), now replaced by illite/smectite (7:3). AB1903 is a fine-grained shale with carbonate minerals (Fig. 7.2c). Hornfels samples AB1886 and AB1894 have a higher quartz content of 53.3 and 33.8 wt% compared to the AB1903 shale sample with only 28.2 wt% quartz. High K-feldspar (15.3, 6.5 and 4.0 wt%) and albite (27.5, 19.8 and 12.4 wt%) contents are also observed in these samples. Below the sill, three minerals; anorthite, muscovite, and illite/smectite (7:3) are dominant in samples AB1894 and AB1903. Anorthite (0.60 wt% and 0.5 wt%) and muscovite (4.8 and 2.4 wt%) show decreasing patterns away from the sill, while illite/smectite (7:3) increases from 34.0 to 48.5 wt %. Carbonate minerals siderite (2.9 wt%) and magnesite (0.8 wt%) are limited to AB1903 sample.

Elemental mapping of the above samples reveals the occurrence of elemental sulphur in pyrite in AB1886 (Fig. 7.2d) and AB1903, and the presence of barium, indicative of barite in AB1903; and calcium in magnesite-siderite clusters (Fig. 7.2f).

QU1855 and QU1894 have different mineral compositions (Figs. 7.2g, h); quartz 32.7 wt% and 36.3 wt%, K-feldspar 9.1 wt% and 1.3 wt%, albite 18.4 wt% and 10.8 wt%, muscovite 4.8 wt% and 4.3 wt%, illite/smectite (7:3) 28.2 wt% and 38.3 wt%. Illite/smectite (6:4) occurs in QU1855 with a concentration of 6.8 wt%. These variations in composition are likely due to lithological differences rather than contact metamorphic effect. Elemental distribution map of QU1855 shows minor barium and sulphur likely due to occurrence of barite and pyrite.

7.4.2 Organic Matter and Porosity

High-resolution backscatter electron MAPS images provide visual data on the relationship of organic matter, mineralogy and porosity of the samples. In samples from borehole AB 1/56, porosity varies significantly and seems to be influenced by the mineralogy in the samples (Fig. 7.3). AB1886 has small intermineral pore spaces occurring in between feldspar needles (Fig. 7.3a). Chiastolite crystals occupy the pore spaces in AB1894, where porosity is limited to intergranular grain boundaries (Fig. 7.3b). Carbonate nodules in AB1903 have high intramineral pore spaces (Fig. 7.3c).

In the samples from borehole QU 1/65, porosity varies considerably with QU1855 showing preserved organic matter/bitumen but there is no visible porosity associated with the organic matter or minerals (Fig. 7.3d). QU1894 shows preservation of porosity in areas were quartz, feldspars, and illite form clusters, whilst in areas where quartz is recrystallized, porosity only occurs along grain boundaries (Fig. 7.3e).

7.5 Discussion

7.5.1 Effects of Thin Sills (<10 m Thick) in the Ecca Group

7.5.1.1 Mineralogy

Transformation of smectite to illite through interstratified illite/smectite (I/S) changes the smectite ratio, increases illite crystallinity and the ordering of I/S mixed layer. The I/S mixed layer with illite contents ranging between 60 and 70 % are referred to as better ordered. The reactions are a function of temperature and time and burial depth. Diagenetic processes are estimated to stop at approximately 20 % smectite composition in the I/S system. During contact metamorphism, elevated temperature increases smectite composition in I/S. This reaction is also induced by circulation of K^+, $Al^{3+,}$ and Si^{4+} cations that are necessary for smectite illitization. Ca^{2+}, Mg^{2+}, Fe^{3+}, Na^+ and Si^{4+} are cations released from the reaction, and are then utilized in reactions that precipitate quartz, calcite, mica, feldspar, gypsum and kaolinite. Diagenetic studies show that this transition from randomly ordered to ordered I/S phases occurs at approximately 110 °C and often at depth of 3000 m (the latter being a function of the geothermal gradient in any given basin, e.g. Schleicher et al. 2008). Recently, illite crystallinity studies in contact aureoles of the Whitehill Formation were shown to be in the low grade metamorphism chlorite zone at temperatures of about

Fig. 7.2 Photomicrographs for petrographic analysis of the cores illustrating distribution of minerals (*left images*) and elements (*right images*): ▶ **a** fine-grained hornfels containing quartz (*white*), K-feldspar (*green*), albite (*blue*), muscovite (*brown*); **b** chiastolite porphyroblast (*green*) identified as retrograde illite/smectite **c** fine-grained illite/smectite (7:3) (*green*) with magnesite and siderite (*purple*); **d** sulphur (*yellow*), magnesium (*pink*) occurring in an iron (*blue*) and sodium-rich (*orange*) groundmass **e** chiastolite crystals (*blue*) indicative of high aluminium concentration; **f** magnesite-siderite clusters (*red*) show association with calcium and iron, and barite (*green*); **g** shale with albite (*blue*), quartz (*white*), and illite/smectite(7:3 and 6:4) (green); **h** fine sand with muscovite (*brown*), quartz (*white*) and illite/smectite (7:3) (*green*); **i** sample shows high iron and aluminium concentration (*blue*), barium (*green*), and sulphur (*yellow*); **j** iron and aluminium (*blue*), sulphur (*yellow*), and calcium (*red*)

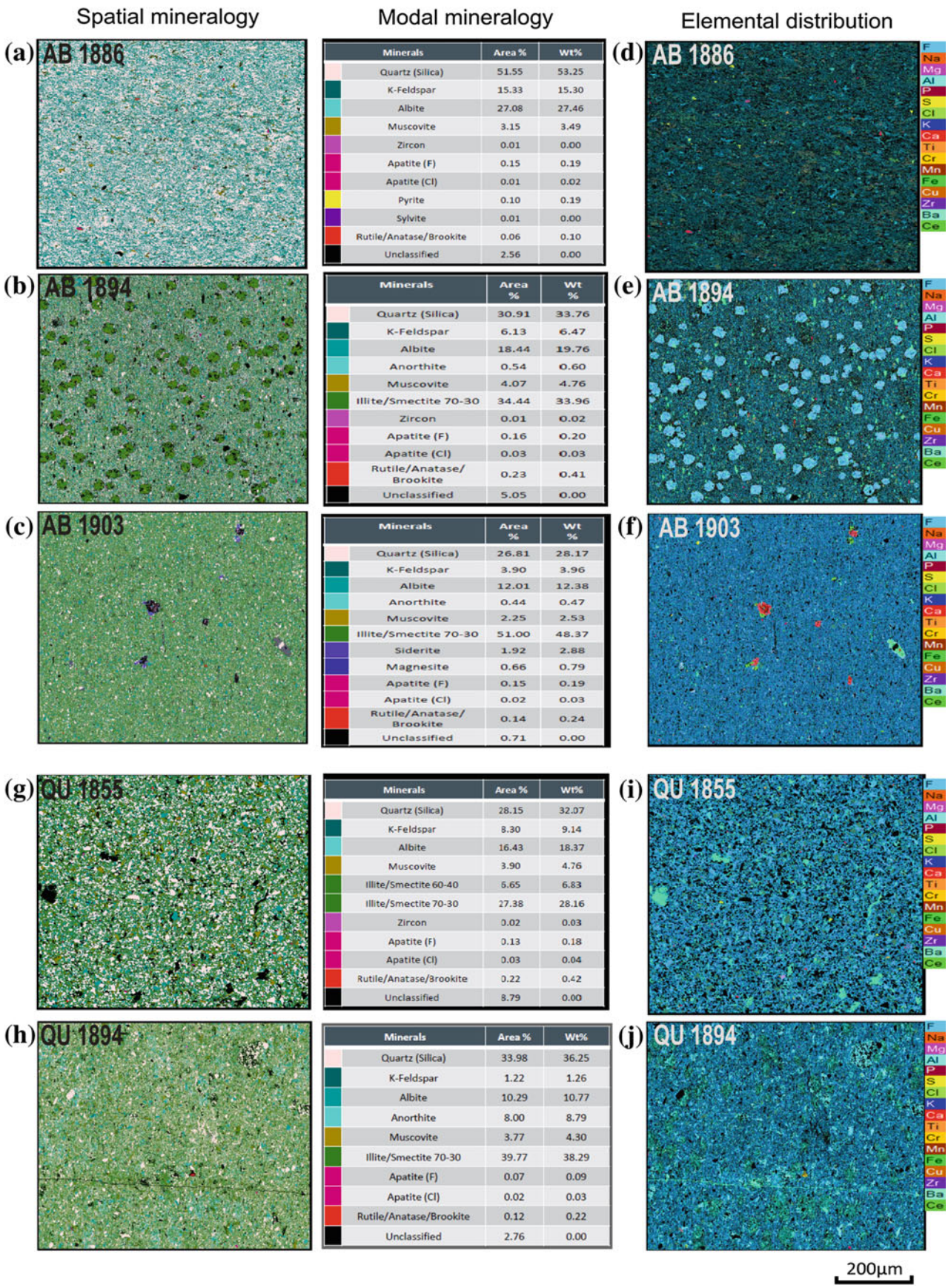

Minerals	Area %	Wt%
Quartz (Silica)	51.55	53.25
K-Feldspar	15.33	15.30
Albite	27.08	27.46
Muscovite	3.15	3.49
Zircon	0.01	0.00
Apatite (F)	0.15	0.19
Apatite (Cl)	0.01	0.02
Pyrite	0.10	0.19
Sylvite	0.01	0.00
Rutile/Anatase/Brookite	0.06	0.10
Unclassified	2.56	0.00

Minerals	Area %	Wt %
Quartz (Silica)	30.91	33.76
K-Feldspar	6.13	6.47
Albite	18.44	19.76
Anorthite	0.54	0.60
Muscovite	4.07	4.76
Illite/Smectite 70-30	34.44	33.96
Zircon	0.01	0.02
Apatite (F)	0.16	0.20
Apatite (Cl)	0.03	0.03
Rutile/Anatase/ Brookite	0.23	0.41
Unclassified	5.05	0.00

Minerals	Area %	Wt %
Quartz (Silica)	26.81	28.17
K-Feldspar	3.90	3.96
Albite	12.01	12.38
Anorthite	0.44	0.47
Muscovite	2.25	2.53
Illite/Smectite 70-30	51.00	48.37
Siderite	1.92	2.88
Magnesite	0.66	0.79
Apatite (F)	0.15	0.19
Apatite (Cl)	0.02	0.03
Rutile/Anatase/ Brookite	0.14	0.24
Unclassified	0.71	0.00

Minerals	Area %	Wt%
Quartz (Silica)	28.15	32.07
K-Feldspar	8.30	9.14
Albite	16.43	18.37
Muscovite	3.90	4.76
Illite/Smectite 60-40	5.65	6.83
Illite/Smectite 70-30	27.38	28.16
Zircon	0.02	0.03
Apatite (F)	0.13	0.18
Apatite (Cl)	0.03	0.04
Rutile/Anatase/Brookite	0.22	0.42
Unclassified	8.79	0.00

Minerals	Area %	Wt%
Quartz (Silica)	33.98	36.25
K-Feldspar	1.22	1.26
Albite	10.29	10.77
Anorthite	8.00	8.79
Muscovite	3.77	4.30
Illite/Smectite 70-30	39.77	38.29
Apatite (F)	0.07	0.09
Apatite (Cl)	0.02	0.03
Rutile/Anatase/Brookite	0.12	0.22
Unclassified	2.76	0.00

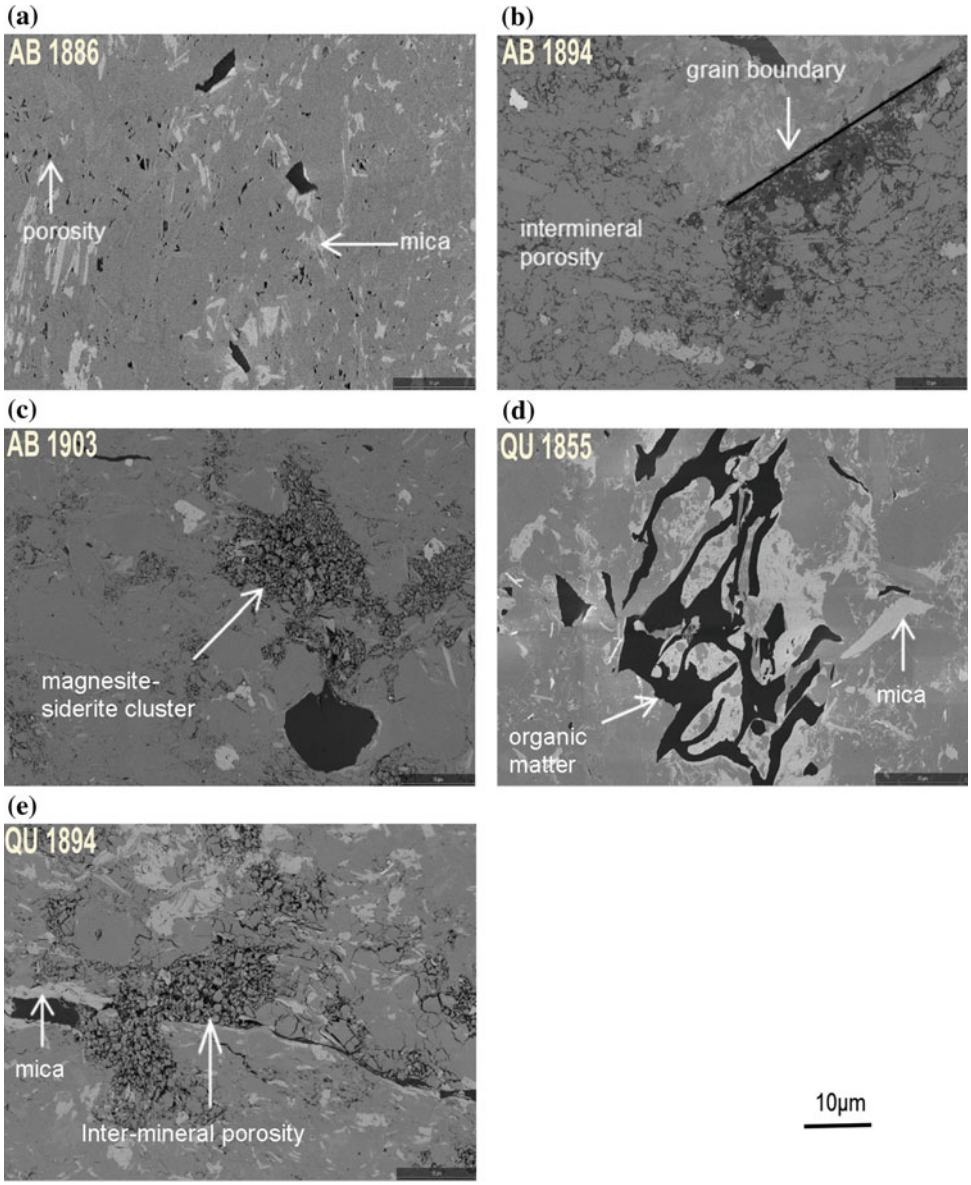

Fig. 7.3 High-resolution backscatter electron MAPS images illustrating the relationship between mineralogy, organic matter, and porosity in the samples: **a** porosity in hornfels sample is preserved in between feldspar needles; **b** porosity at the crystal boundaries of chiastolite crystals; **c** the shale sample shows a high intermineral and intramineral porosity associated with magnesite and siderite clusters; **d** within the shale sample, organic matter (*black*) associated with muscovite (*white*); **e** intermineral porosity (*black*) within quartz and feldspar minerals (*grey*), and on quartz grain boundaries and mica (*white*)

300 °C (Smithard et al. 2015). In our samples however, transformation of smectite to illite in contact aureoles in both shales and sandstones is a consequence of immediate temperature increase during intrusive activity.

Illite porphyroblasts in sample AB1894 are identified as chiastolite crystals using a petrographic optical microscope. These crystals are of an andalusite variety identified with their characteristic cruciform twining towards the centre of the crystals. The high-resolution identification of these crystals as illite can be explained by retrograde metamorphism, which alters the chiastolite to clay and mica minerals (Fig. 7.2b). Thermal modelling (Chap. 8 this book), suggest maximum temperature range of 424–570 °C at the contact zone. It is assumed that at the time, the maximum temperatures were not maintained long enough for the crystals to expel inclusions hence the chiastolite variety was retained. This is congruent with metamorphic studies, which show that under rapid metamorphic crystallization conditions inclusions are retained within crystal structures. Rapid growth of orthorhombic prismatic andalusite crystals results in a preferential adsorption of fluids along the {100} crystal face, forming maltese cross inclusion patterns identified as chiastolite (e.g. Rast 1965; Spry 1969).

7.5.1.2 Porosity

Porosity varies depending on the distance of a sample from a sill intrusion and the new mineral phases produced by the contact metamorphism (Fig. 7.3). Dehydration of existing minerals and recrystallization of quartz and feldspars resulted in a decrease of porosity in the hornfels sample taken

between two thin sills. Growth of chiastolite is observed to decrease the porosity of host rocks, reducing pore spaces at crystal boundaries (Fig. 7.3b). The effects of metamorphism associated with thin sills decreases rapidly with distance from the sill, as observed by the presence of carbonate and sulphate minerals that were not transformed to CO_2 and SO_2 gases, this sample was taken 9 m below a sill (Fig. 7.3c). The carbonate and sulphate minerals have voids in between mineral grains and thus show that the porosity of the host rock was retained. The connectivity of these intermineral voids is yet to be studied, in order to ascertain the permeability of the rocks.

7.5.2 Effects of a 146 m Thick Sill Intrusion in Dwyka

A sill intruding the Dwyka diamictite did not cause detectable thermal alteration of the overlying rocks. The Dwyka Group is intruded by a 146 m thick sill towards the top of the unit. In borehole QU 1/65, the dolerite sill is succeeded by 10 m thick diamictite. Samples QU1855 and QU1894 were selected 37 and 76 m, respectively, above the sill (Fig. 7.1). Mineralogy and textural changes expected in the contact zone are not observed in these samples (Figs. 7.2g, h). It is likely therefore that these samples are too far away from the contact dolerite sill, the heat gradient away from the sill was too great to affect the overlying sandstone and shale beds. These results are compatible with models that show that a maximum temperature of about 590 °C occurs within 10 cm of the contact beyond which temperatures decrease rapidly down to 150 °C (Aarnes et al. 2011).

7.6 Conclusion

A high-resolution petrographical and chemical dataset from shales of the lower Ecca Group at various distances within the contact zones of the intrusive sills in the central Karoo Basin reveals different contact metamorphic patterns. Spatial distribution of minerals and elements indicate new mineral phases (e.g. chiastolite and illite) in the black shales that vary depending on the distance of the sample relative to a sill, with preservation of clay minerals beginning at distances that are equal to the thickness of the sill. The process of transformation of rock forming minerals and growth of new minerals has changed the porosity of the black shales. Growth of new minerals close to sills has decreased the porosity and therefore the capacity of black shales to retain gas. However, the data also shows a possible insulating effect where sills intrude the Dwyka Group rocks since petrographical and elemental changes that accompany contact metamorphism adjacent to this sill were not observed. For more accurate pressure–temperature calculations along contact aureoles, future detailed geothermometry of minerals and thermal modelling will be undertaken.

Acknowledgments The authors would like to thank AEON and the Iphakade programme (DST/NRF) for financial support. We also thank Emese Bordy (University of Cape Town) for carefully reviewing this chapter. This is AEON contribution number 158.

References

Aarnes I, Svensen H, Conolly, JAD and Poldadchikov YY (2010) How contact metamorphism can trigger global climate changes: Modelling gas generation around igneous sills in sedimentary basins. Geochemica et Cosmochimica Acta 74: pp 7179–7195.

Aarnes I, Svensen H, Polteau S and Planke S (2011) Contact metamorphic devolatilization of shales in the Karoo Basin, South Africa, and effects of multiple sill intrusions. Chem Geol 281: pp 181–194.

Black D, Booth P and de Wit M (2016) Petrographic, geochemical, and petro-physical analysis of the Collingham Formation in the context of shale gas from a borehole (STT 2) near Jansenville, Eastern Cape, South Africa-potential cap rock to shale gas in the Karoo. S Afri J Geol 119.1. doi:10.2113/gssajg.119.1.0.

Burgess SD, Bowring SA, Fleming TH and Elliot DH (2015) High-precision geochronology links the Ferrar large igneous province with early Jurassic ocean anoxia and biotic crisis. Earth Planet Sci Lett 415:90–99.

Chevalier L, Gibson LA, Nhleko LO, Woodford AC, Nomquphu W and Kippie I (2004) Hydrogeology of fractured-rock aquifers and related ecosystems in Qoqodala dolerite ring and sill complex, Great Kei catchment, Eastern Cape. Water Research Commision, Report No. 1238/1/04.

Chevallier L, Goedhart AM and Woodford AC (2011) Influence of dolerite sill and ring complexes on the occurrence of groundwater in Karoo fractured aquifers: A morhpo-tectonic approach. Water Research Commission, Report No. 937/1/01.

Chere N (2015) Sedimentological and geochemical investigations on borehole cores of The Lower Ecca Group black shales, for their gas potential-Karoo Basin, South Africa. Unpublished thesis, Nelson Mandela Metropolitan University.

Duncan RA, Hooper PR, Rehacek J, Marsh JS and Duncan AR (1997). The timing and duration of the Karoo igneous event, southern Gondwana. J Geophysical Res 102: pp 18127–18138.

Duncan AR and Marsh JS (2006) The Karoo Igneous Province. In: Johnson MR, Anhaeusser CR, and Thomas RJ (eds) The Geology of South Africa. Geological Society of South Africa, Johannesburg/Council for Gesciences Pretoria, pp 501–520.

Du Toit AL (1903) Union of South Africa, Mines Department Survey. Cape Sheet 27. Maclear-Umtata.

Ferre EC, Bordarier C and Marsh JS (2002) Magma flow inferred from AMS fabrics in a layered mafic sill, Insizwa, South Africa. Tectonophysics 354(1): pp 1–23.

Galerne CY, Neumann ER and Planke S (2008) Emplacement mechanisms of sill complexes: Information from the geochemical architecture of the Golden Valley Sill Complex, South Africa. J Volcanol Geotherm Res 177: pp 425–440.

Geel C, Schulz HM, Booth P, de Wit M and Horsfield B (2013) Shale gas characteristics of Permian black shales in South Africa: results from recent drilling in the Ecca Group, Eastern Cape. Energy Procedia 40: pp 256–265.

Geel C, Schulz HM, Booth P, de Wit M and Horsfield B (2015) Palaeo-environment, diagenesis and characteristics of Permian black shales in the Lower Karoo Supergroup flanking the Cape Fold Belt near Jansenville, Eastern Cape, South Africa: implications for the shale gas potential of the Karoo Basin. S Af J Geology 118 (3): pp 249–274.

Grab S and Svensen H (2011). Rock doughnut and pothole structures of the Clarens Fm. Sandstone in the Karoo Basin, South Africa: Possible links to Lower Jurassic fluid seepage. Geomorphology 131: pp 14–27.

Keller G, Adatte T, Bhowmick PK, Upadhyay H, Dave A, Reddy AN and Jaiprakash BC (2012) Nature and timing of extinctions in Cretaceous-Tertiary planktic foraminifera preserved in Deccan intertrappean sediments of the Krishna–Godavari Basin, India. Earth Planet Sci Lett 341–344: pp 211–221.

Lee CA, Luffi P, Plank T, Dalton H, Leeman WP (2009). Constraints on the depths and temperatures of basaltic magma generation on Earth and other terrestrial planets using new thermobarometers for mafic magmas. Earth and Planetary Sci Lett 279: pp 20–33.

Maes, SM, Ferré EC, Tikoff B, Brown, PE and Marsh JS (2008) Rock magnetic stratigraphy of a mafic layered sill: A key to the Karoo volcanics plumbing system. J Volcanol Geotherm Res 172: pp 75–92.

Mare LP, de Kock MO, Cairncross B and Mouri H (2014) Application of magnetic geothermometers in sedimentary basins: an example from the western Karoo Basin, South Africa. S Afr J Geol 117(1): pp 1–4.

Poldervaart A and Walker F (1942) The petrology of the Elephants head dike and the new Amalfi sheet (Matatiele). T R S S A, pp 95–119.

Polteau S, Mazzini A, Galland O, Planke S and Malthe-Sørenssen A (2008) Saucer-shaped intrusions: Occurrences, emplacement and implications. Earth Planet Sci Lett 266: pp 195–204.

Rast N (1965) Nucleation and Growth of Metamorphic Minerals. In: Pitcher WS, and Flinn GW (eds) Controls of Metamorphism. L G S, pp 73–99.

Ruhl M, Bonis NR, Reichart JS, Damtse JSS and Ku Rschner WM (2011). Atmospheric carbon injection linked to end-Triassic mass extinction. Science 333: pp 430–433.

Renne PR, Deino AL, Hilgen FJ, Kuiper KF, Mark DF, Mitchell WS III, Morgan LE, Mundil R and Smit J (2013) Time scales of critical events around the Creataceous–Paleogene Boundary. Science 339: pp 684–687.

Scheiber-Enslin SE, Webb SJ and Ebbing J (2014) Geophysical plumbling the Main Karoo Basin, South Africa. S A J Geol 117(2): pp 275–300.

Schleicher AM, Warr LN and van der Pluijm BA (2008) On the origin of mixed-layer clay minerals from the San Andreas Fault at 2.5–3 km vertical depth (SAFOD) drillhole at Parkfield, California). Springer-Verlag.

Sell B, Ovtcharova M, Guex J, Bartolini A, Jourdan F, Spangeberg JE, Vicente JC and Schaltegger U (2014) Evaluating the temporal link between Karoo LIP and climatic-biologic events of the Toracian stage with high-precision U-Pb geochronology. Earth Planet Sci Lett 408: pp 48–56.

Smithard T, Bordy EM and Reid D (2015) The effect of dolerite intrusions on the hydrocarbon potential of the lower Permian Whitehill Formation (Karoo Supergroup) in South Africa and southern Namibia. S Af J of Geol 118(4): pp 489–510.

Sobolev SV, Sobolev AV, Kuzmin DV, Krivolutskaya NA, Petrunin AG, Arndt NT, Radko VA and Vasiliev YR (2011) Linking mantle plumes, large igneous provinces and environmental catastrophes. Nature pp 477.

Spry A (1969) Metamorphic textures. The Commonwealth and International Library of Science Technology Engineering and Liberal Studies.

Svensen H, Planke S, Malthe-Sorenssen A, Jamtveit B, Mykle-bust R, Eidem TR and Rey SS (2004) Release of methane from a volcanic basin as a mechanism for Eocence global warming. Nature 429: pp 542–545.

Svensen H, Jamtveit B, Planke S and Chevallier L (2006) Structure and evolution of hydrothermal vent complexes in the Karoo Basin, South Africa. J Geol Soc London 163: pp 671–682.

Svensen H, Planke S, Chevallier L, Malthe-Soressen A, Corfu F and Jamtveit B (2007) Hydrothermal venting of greenhouse gases triggering Early Jurassic global warming. Earth Planet Sci Lett 256: pp 554–566.

Svensen H, Bebout G, Kronz A, Li L, Planke S, Chevallier L, Jamtveit B (2008). Nitrogen geochemistry as a tracer of fluid flow in a hydrothermal vent complex in the Karoo Basin, South Africa. Geochimica et Cosmochimica Acta 72: pp 4929–4947.

Svensen H, Corfu F, Polteau S, Hammer O and Planke S (2012) Rapid magma emplacement in the Karoo Large Igneous Province. Earth Planet Sci Lett 325–326: pp 1–9.

Contact Metamorphism of Black Shales in the Thermal Aureole of a Dolerite Sill Within the Karoo Basin

8

David Moorcroft and Nicolas Tonnelier

Abstract

Recent interest in the shale gas potential of the Karoo Basin has highlighted the metamorphic effects that Jurassic dolerite intrusions may have had on the Lower Ecca Group black shales. We explore the use of metamorphic petrology and Ti in biotite geothermometry to constrain conductive heat flow modelling of a thermal aureole adjacent to two closely spaced, thin dolerite sills intruded into these black shales. Our numerical heat flow modelling shows that a 45 m thick sill may heat a ~100 °C host rock to 650–700 °C at the contacts, and to ~350 °C, 45 m away from the contact. Mineral phase equilibrium modelling constrains minimum temperatures of ~375 °C up to 13 m above the two sills and cooler temperatures farther away and below the sills. Titanium in biotite (TIB) geothermometry results are varied, suggesting disequilibrium conditions within the contact aureole.

Keywords

Contact metamorphism • Sill • Aureole • Convection • Thermobarometry • Biotite

8.1 Introduction

The Karoo Basin covers around 300,000 km^2 of South Africa (Fig. 8.1), and is composed of 2–5 km of clastic sedimentary rocks that are thickest in the south (Lindeque et al. 2011). At about 182–183 Ma, the Karoo Basin was intruded by a complex network of dolerite dykes and sheet-like sills, which form part of the Karoo-Ferrar Large Igneous Province (LIP) (Duncan et al. 1997; Scheiber-Enslin et al. 2014; Burgess et al. 2015). As a consequence of emplacement of the subvolcanic magmatic suite, contact metamorphism has affected the host rock shales adjacent to the intrusions (e.g., Aarnes et al. 2010). The elevated temperatures from cooling intrusions may have had variable influence on the maturation of organic-rich black shales, depending on the extent of the temperature increase (Rowsell and de Swart 1976; Wang et al. 2015). Elevated temperatures within thermal aureoles can favour organic maturation, producing hydrocarbons, but it can also damage existing hydrocarbon reservoirs if temperatures in the contact aureole are too high. The conversion of organic material into hydrocarbons within contact aureoles is considered a rapid process, i.e. 10s–1000s years (Aarnes et al. 2010). Elevated temperatures of just a few hundred degrees may therefore have provided ideal conditions for thermogenic gas production within aureoles.

Rowsell and de Swart (1976) were the first to demonstrate the destructive influence that Karoo dolerite intrusions had on the organic maturation of Karoo shales, using vitrinite reflectance and illite crystallinity measurements (e.g., Wang and Manga 2015). More recently, contact metamorphism of organic-rich shales of the Karoo Basin surrounding dolerite sills has been suggested as a major cause of carbon loss from the black shales, resulting from overpressure and fluid outflows from the contact aureoles (Svensen et al. 2006, Aarnes et al. 2010). Aarnes et al. (2010) developed a convective heat flow model coupled with devolitization models to quantify the amount of fluid released. Their results indicate

D. Moorcroft (✉) · N. Tonnelier
Department of Geosciences, Nelson Mandela Metropolitan University, Port Elizabeth, 6001, South Africa
e-mail: s210088435@nmmu.ac.za

B. Linol and M.J. de Wit (eds.), *Origin and Evolution of the Cape Mountains and Karoo Basin*,
Regional Geology Reviews, DOI 10.1007/978-3-319-40859-0_8

that as much as 2700–16,200 Gt of CH_4 may have been liberated from the Karoo Basin as a result of thermal aureole processes adjacent to dolerite sills. Through systematic variations in model parameters, they show how host rock temperature holds the largest comparative influence in aureole size. The authors also demonstrate how the timing of sill emplacements, and hence the cumulative heating effects can strongly influence the extent of basin-scale devolitization.

Aarnes et al. (2011) further developed a numerical heat flow model to quantify fluid production from shales adjacent to sill intrusions of the Karoo basin. The authors demonstrate how even a thin sill (15.5 m thick), intruding black shales, can generate maximum temperatures of ~600 °C at the sill contacts and several hundred degrees further away within the aureole. Their model, constrained by geochemical and mineralogical data, shows how organic matter is efficiently converted into hydrocarbons within contact aureoles adjacent to intruding sills. Also shown is how multiple sills, simultaneously emplaced, can have an increasing effect on metamorphism and hydrocarbon generation potential.

In this study, we use conventional metamorphic petrology and a biotite geothermometer, coupled with conductive heat flow modelling, to examine the temperatures experienced within a thermal aureole adjacent to a 45 and 4 m thick sills intruded at depth black shales in the west-central Karoo Basin (Fig. 8.1).

8.2 Geological Setting

The Karoo Basin contains the Karoo Supergroup, deposited from Late Carboniferous (~300 Ma) to the Mid-Jurassic (182 Ma), and subdivided into the Dwyka, Ecca, Beaufort and Stormberg Groups (Johnson et al. 2006). Recent interest into the Karoo Basin's shale gas potential has focussed attention on the Lower Permian Ecca Group black shales, most notably the Whitehill Formation and the underlying Prince Albert Formation, which in turn overlies the basal Dwyka Group diamictites. The Prince Albert Formation is a well-laminated olive-grey mudrock that achieves a maximum thickness of ~300 m within the western Karoo Basin (Geel et al. 2013). The overlying Whitehill Formation is a pyrite-bearing black shale comprised mostly of clay minerals with dolomite concretions near its base (Visser 1992; Geel et al. 2013). Ranging in thickness from ~80 m in the south and thinning towards the north, the Whitehill Formation is ~20–30 m thick within the central-western Karoo Basin (Chap. 1 this book). The overlying Tierberg/Collingham Formation is a well-laminated grey mudrock, which reaches

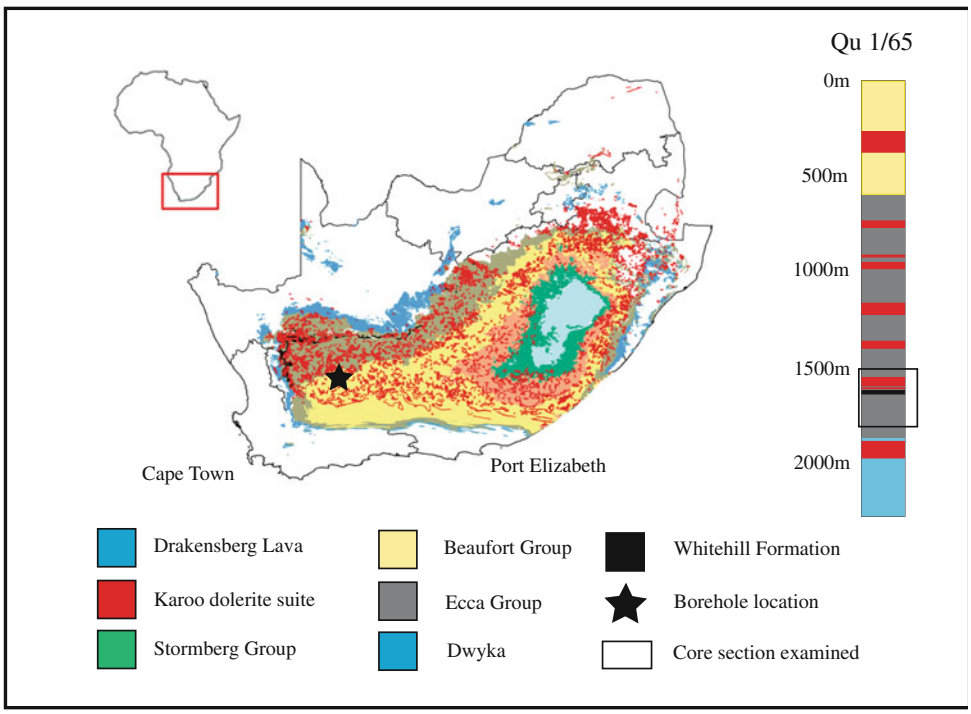

Fig. 8.1 Geological map of the Karoo Basin showing the location of borehole QU 1/65, as well as a simplified stratigraphic well log showing the core-section examined in this study

a maximum thickness of 700 m in the central-western Karoo Basin (Viljoen 1990; Chap. 1 this book).

8.3 Sampling and Methodology

Borehole logging and sampling was conducted on the SOEKOR borehole QU 1/65, drilled in the western Karoo Basin (Fig. 8.1). The complete QU 1/65 drill core (2.5 km in depth) is cut by 12 dolerite sills, ranging from <1 to 130 m in thickness, with a cumulative thickness of 434 m or 17 % of the total section. The core section examined in this study, between 1500 and 1900 m below surface (Fig. 8.2), comprises the Lower Ecca Group black shales, intruded at a depth of 1600 m by two closely spaced dolerite sills (Figs. 8.1 and 8.2). The upper sill is 45 m thick and the lower sill is 4 m thick sill. The two sills are separated by 5 m of host rock.

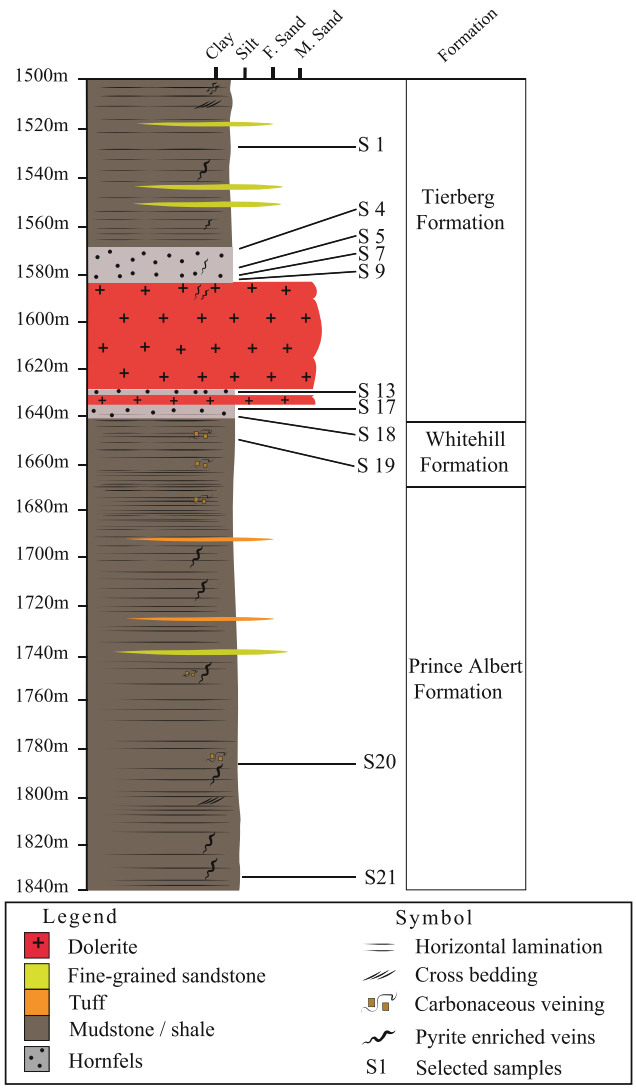

Fig. 8.2 Stratigraphic column of the core section logged and sampled in this study. Stratigraphic boundaries are from the QU 1/65 well completion and log report (du Toit 1967) available from the Council of Geoscience in Pretoria

8.3.1 Mineralogy

15 shale samples were taken from above, below and in-between the two dolerite sills (Fig. 8.2). Petrographic analysis was conducted on polished thin sections. EPMA mineral analysis was conducted using a Jeol JXA 8230 Superprobe at Rhodes University, Grahamstown (South Africa) using acceleration voltage of 15 kV and a probe current of 20 nA. X-Ray Diffraction (XRD) was carried out on selected shale samples using a Bruker D2 PHASER diffractometer at the uYilo testing centre at the Nelson Mandela Metropolitan University in Port Elizabeth (South Africa).

8.3.2 TIB Geothermometry

To infer temperatures in the thermal aureole around the sills, we use the Ti in biotite (TIB) geothermometry calibration of Henry and Guidotti (2002). TIB geothermometry was selected as biotite is a metamorphic mineral found in multiple contact aureole shale samples above the two sills. Biotite was absent within shale host rock more than 13 m away from the sills. We therefore assume that biotite formed in situ during contact metamorphism, and is not a detrital phase.

Temperatures are determined by calculating T from Eq. 8.1:

$$T = \left(\frac{\left[\ln(Ti) - a - c(Xmg)^3 \right]}{b} \right)^{0.333} \quad (8.1)$$

where T is the temperature in °C, Ti is the number of Ti atoms per formula unit (pfu), normalized to 22 oxygens, X_{mg} = Mg/(Mg + Fe) and a, b and c coefficient values are, respectively, a = −2.3594, b = 4.6482 × 10^{-9}, c = −1.7283. The expression is valid for the ranges; X_{mg} = 0.275 − 1.0 and Ti = 0.04 − 0.6 apfu. The uncertainty of the TIB geothermometer is estimated to be 12–24 %.

Chemical disequilibrium of contact metamorphic mineral assemblages is well documented, and it is primarily due to temporal variations within thermal aureoles (e.g., Walther et al. 1984). Even so, pressure-temperature estimates within contact aureoles are commonly made using available mineral assemblages. This is because within metasedimentary contact aureoles, characterized by dehydration mineral reactions, previous studies have constrained reaction temperatures to just 5–30 °C hotter compared to reaction temperatures under equilibrium conditions (Pattison et al. 2011). We therefore

Table 8.1 Approximated model parameters and corresponding notations

Notation	Parameter	Value	Reference
Sill thickness	Sill thickness	45 m	Core log
Depth (m)	Depth of emplacement	3100 m	Core log and Tinker et al. (2008)
T*i*	Initial temperature of melt	1150 °Cs	Falloon et al. (2007)
T*h*	Initial temperature of host rock	97 °C	Brown et al. (1994)
Cps J/kg K	Heat capacity of shale	865	Jones (2003)
Cpm J/kg K	Heat capacity of melt	820	Barker et al. (1998)
Pm kg/m^3	Density of melt	2820	Barker et al. (1998); Jones (2003)
Ps kg/m^3	Density of shale	2540	Jones (2003)
Km W/mK	Thermal conductivity of dolerite	2.05	Jones (2003); Wang et al. (2007)
Ks W/mK	Thermal conductivity of shale	1.88	Jones (2003)

use a phase diagram developed by Aarnes et al. (2010) using Perple_X (Connolly 2005) and a bulk rock composition representative of a typical Ecca Group mudrock (after Caddick and Thompson 2008) to help constrain temperatures in the aureole.

8.3.3 Numerical Modelling of Heat Flow

Two dimensional (2D) conductive heat flow models were generated using the KWare HEAT 3D software (Wohletz 2008). We modelled a cooling sill that has intruded deeply buried shales with inherent low porosity and limited evidence for fluid-flow. For these reasons and for simplicity, we considered heat convection to be negligible and heat transfer to occur exclusively through conduction. KWare HEAT 3D allows for numerical computing of user-defined parameters to solve for the heat conduct equation (Eq. 8.2).

$$\frac{\partial T}{\partial t} = \triangle \cdot (k \triangle T) \tag{8.2}$$

where T = temperature, t = time, $\triangle$ = Laplace operator, k = thermal diffusivity (thermal conductivity/density).

Using Eq. 8.2, a continuous thermal field can be represented as finite temperatures at specified distances away from the heat source at defined intervals. The parameters used in our modelling are presented in Table 8.1.

The sills are located ~1600 m below the current land surface. Tinker et al. (2008) propose that as much as 2–7 km of Karoo Supergroup rocks may have been eroded during the Cretaceous, 60–100 Ma. Since the borehole sampled in this study occur in the western Karoo Basin, we assume a conservative estimation of an additional 1.5 km of eroded overburden. Thus at the time of emplacement, the sill must have been at least 3 km deep. Assuming a geothermal gradient of 25 °C/km (Brown et al. 1994), the host rock temperature would be ~100 °C.

8.4 Results

8.4.1 Petrography and Mineralogy

Shale samples taken more than 30 m above and below the sills (Samples S1–S3, S20, S21) are dominated by mudrock with interspersed fine-grained sandstone horizons (Table 8.2; Fig. 8.2). Mudrock horizons are commonly 5–100 mm thick

Table 2 Selected samples and associated mineral assemblages (Fig. 8.2 for samples location)

Sample	Depth (m)	Distance from upper most and lower most sill contacts	Mineral assemblage
S1	1529	61 m above	Qtz, Alb, Chl, Mont, Kaol
S4	1570	13 m above	Qtz, Alb, Bio, Chl, Mus
S5	1577	6 m above	Qtz, Alb, Bio, K-Fld, Chl, Ill, Mont, Kaol
S7	1580	3 m above	Qtz, Alb, Bio, Chl, Ill
S9	1585	0.1 m above	Qtz, Alb, Bio, Chl, Ill, Kaol
S13	1637	0.3 m below	Qtz, Alb, Chl, Mus, Mont
S18	1640	5 m below	Qtz, Alb, Mus, Kaol, (And)
S19	1650	15 m below	Qtz, Alb, Mus, Dol, (And)
S21	1841	206 m below	Qtz, Alb, Chl, Mus, Mont, Kaol

Mineral abbreviations; And = andalusite, Alb = albite, Bio = biotite, Chl = chlorite, Ill = illite, Kaol = kaolinite, K-Fld = potassium feldspar, Mont = montmorillonite, Qtz = quartz

and are dominated by clay minerals including illite and montmorillonite. The sandstone horizons are commonly 1–20 mm thick and are dominated by sub-angular quartz grains. Sedimentary features such as ripples, graded bedding and flaser bedding are common within samples taken furthest away from the sills.

Samples taken within 13 m above the two sills have a non-foliated, crystalline texture, contrasting with the finely aminated samples taken further from the contact with the upper sill. We defined samples within this 13 m zone above the upper sill as hornfels, i.e. a fine-grained, non-foliated, crystalline rock. Approaching the sills, authigenic muscovite and chlorite intergrowths increase in abundance at the expense of dark clay minerals. This zone corresponds to facies that become progressively paler in colour towards the upper contact of the sill. Metamorphic biotite is present only within the mineral assemblages of samples taken within the hornfels zone. In one of these samples (S5), a single plagioclase-biotite-rich vein contains zoned minerals, and likely formed during the emplacement of the sill (Fig. 8.2). Samples S7 and S8, taken 3 m above the dolerite sills, shows distinct ovoid poikiloblasts, giving the rock samples a 'spotted' hornfels texture (Fig. 8.3c).

Many of the observed features within host rock samples above the upper sill are absent below the sills. Below the two sills, dark clay minerals comprise much of the mineral assemblage within samples directly adjacent to the dolerite contact. Additionally, biotite is absent from all samples taken in-between and below the two sills. Within shale samples S17 and S18, taken below the two sills, distinct, near-rectangular porphyroblasts of chiastolite, were observed within a dark fine-grained matrix (Figs. 8.3e and f). The geochemical compositions of these porphyroblasts most closely resemble micaceous minerals including phlogopite and muscovite, indicating that the porphyroblasts have been retromorphosed. Within shale sample S19, taken

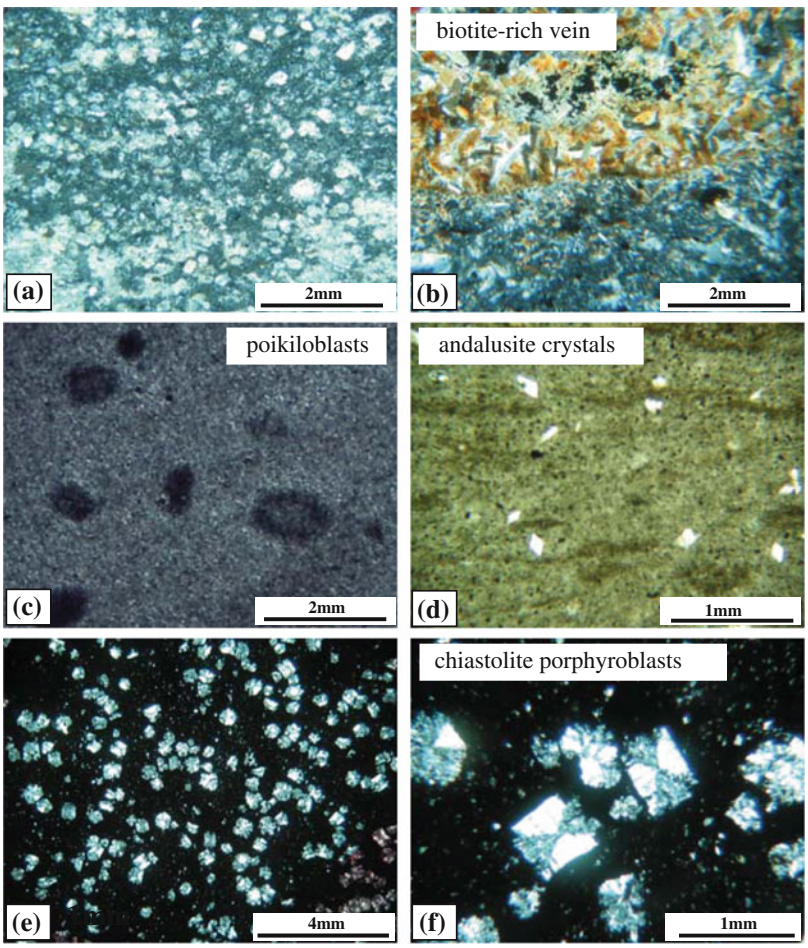

Fig. 8.3 Photomicrographs of selected thin section samples from borehole QU 1/65. **a** A typical hornfels texture showing a fine-grained, non-foliated crystalline groundmass. **b** A biotite-plagioclase-rich vein intruded into a crystalline groundmass of sample S5. **c** A typical 'spotted' hornfels or poikiloblastic texture of sample S8. **d** Andalusite crystals within a dolomitized groundmass of sample S19, taken from the Whitehill Formation. **e** Chiastolite porphyroblasts within a clay mineral groundmass of sample S17. **f** chiastolite porphyroblasts set within a dark, clay mineral groundmass of sample S18, taken 5 m below the dolerite sills (Fig. 8.2 for samples location)

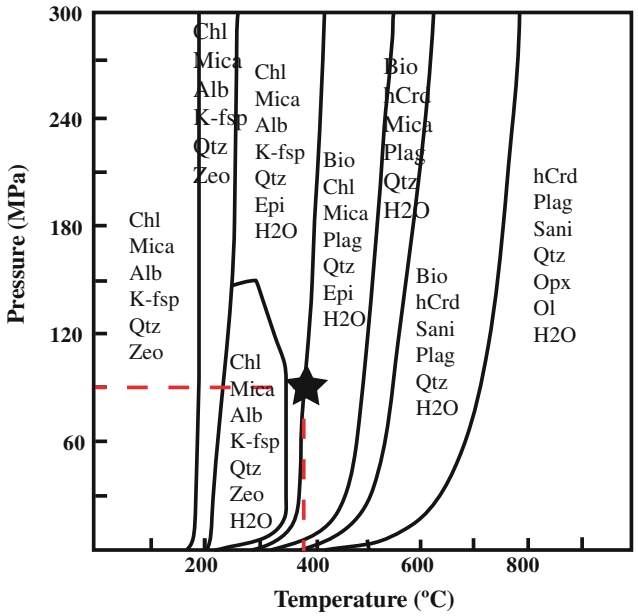

Fig. 8.4 Phase equilibrium diagram showing stable mineral assemblages as a function of temperature and pressure, calculated using Perple_X (Connolly 2005), as adapted from Aarnes et al. (2010). The bulk rock composition used is representative of an average pelite after Caddick and Thompson (2008). The black star indicates the minimum temperatures experienced within 13 m above the dolerite sills, based on the occurrence of metamorphic biotite. Mineral abbreviations: Ab—albite; Bio—biotite; Chl—chlorite; Ep—epidote; hCrd—hydrous cordierite; K-fsp—alkali feldspar; Mica—white mica; Ol—olivine; Opx—orthopyroxene; Plag—plagioclase; Qz—quartz; San—sanidine; Zeo—zeolite

~15 m below the lower sill, grains of andalusite are observed within a fine-grained groundmass of dolomite, quartz, albite and muscovite (Fig. 8.3d).

Variations in the metamorphic mineral assemblages of the samples provide a useful constraint when defining the thermal evolution of rocks within the contact aureole. If we assume chemical equilibrium, the occurrence of metamorphic biotite suggests a minimum temperature of at least 375 °C within 13 m above the upper sill (Fig. 8.4). The occurrence of relict porphyroblasts of chiastolite within samples S18 and S19 are indicative of temperatures between 400 and 550 °C at 1 kbar (e.g., a depth of ca. 3–4 km; Robie and Hemingway 1984; Botha 2010).

8.4.2 Titanium in Biotite (TIB) Thermobarometer

The composition of selected biotite grains and results from the TIB geothermometer after Henry and Guidotti (2002) are shown in Table 8.3. Figure 8.5 shows the temperature results as a function of the distance from the sill. Only three shale samples contained biotite grains suitable for chemical analysis. Temperatures generated from authigenic biotite compositions of sample S4, taken 13 m above the sill are; 422, 428 and 522 °C. Biotite analysed within the matrix of sample S5, produces temperatures of 522 and 543 °C. Biotite analysed from the biotite-plagioclase vein within the same sample infer slightly hotter temperatures of 569, 573 and 607 °C. Temperatures generated from authigenic biotite from sample S7, taken 3 m above the sills, infers temperatures of 570 and 511 °C.

8.4.3 Thermal Modelling

Figure 8.6 represents a 2D conductive heat flow model, designed to examine the cooling history of the thermal aureole surrounding the 45 m thick sill, emplaced instantaneously within the Ecca shales. Results from the TIB geothermometer, as well as mineral phase equilibria modelling are also plotted in Fig. 8.6.

Episodic or not, the timing of emplacement of the Karoo sills is constrained between 182 and 183 Ma (e.g., Svensen et al. 2012; Burgess et al. 2015). Since we cannot constrain the relative timing of emplacement of the two studied sills (or others in the drill core), we only model the heating effects of the 45 m thick sill, excluding the additional heating influence of the underlying 4 m thick sill. We therefore model minimum temperatures experienced within the adjacent host rock.

The thermal model (Fig. 8.6) shows sliding thermal gradients within the contact aureole. Each point within the aureole is subjected to a short thermal pulse, causing increasing and decreasing temperatures lasting a relative short episode of time. Our thermal modelling shows that the peak temperatures are not achieved at the same time in all areas adjacent to the sill. Rocks closest to the sill achieve peak temperatures first when rocks farther away are still heating up; and when rocks closest to the sill begin to cool, rocks farther away from the sill have yet to achieve their peak temperatures. On the basis of our conductive heat flow modelling, maximum temperatures within the aureole are experienced closest to the sill contacts and are in the order of 650–700 °C within 10 years of emplacement. These maximum temperatures at the contact are shown to cool to ~500 °C, 100 years after emplacement. According to our model, host rocks within 5 m of the dolerite sill should experience temperatures of at least 600 °C for a period of 50 years following emplacement of the sill.

Farther away from the sill, the model infers that host rocks within 5–10 m of the sill experience temperatures of 550–600 °C, 50 years after sill emplacement. Comparatively, temperatures generated from biotite compositions analysed from the biotite-plagioclase-rich vein portion of

Table 8.3 Biotite grains used for *geothermobarometry*

Sample	S7_B1	S7_B2	S 5_B1	S 5_B2	S 5_B3	S 5_B4	S 5_B6	S 4_B1	S 4_B2	S 4_B3
Domain	Shale	Shale	Shale	Shale	Plg-bio vein	Plg-bio vein	Plg-bio vein	Shale	Shale	Shale
Mineral	Biotite	Biotite	Biotite	Biotite	Biotite	Biotite	Biotite	Biotite	Biotite	Biotite
SiO_2	37.55	37.23	39.02	39.59	39.12	38.68	39.27	39.81	38.40	40.04
Al_2O_3	16.80	15.30	14.34	14.55	14.93	13.902	14.22	14.53	21.56	22.14
CaO	0.00	0.01	0.10	0.08	0.81	0.168	0.20	1.06	0.07	0.07
F	0.34	0.71	1.48	1.53	1.31	1.095	1.20	1.58	0.13	0.14
MgO	8.53	9.21	14.76	15.42	14.29	13.92	15.38	15.40	8.36	6.38
FeO	16.44	16.73	12.41	12.64	11.87	13.54	12.33	11.25	14.46	13.26
K_2O	8.33	8.61	10.55	10.10	9.62	9.27	10.10	9.94	7.49	9.03
MnO	0.04	0.07	0.07	0.00	0.15	0.06	0.17	0.05	0.09	0.19
Cr_2O_3	0.03	0.02	0.12	0.09	0.09	0.17	0.17	0.20	0	0.00
Na_2O	0.00	0.21	0.43	0.26	0.37	0.40	0.31	0.38	0.04	0.11
TiO_2	4.41	4.62	3.80	2.69	3.24	3.77	2.96	2.36	2.21	2.01
Total	92.51	92.75	97.12	97.03	95.87	95.03	96.40	96.59	92.86	93.38
Mg#	0.307	0.345	0.366	0.549	0.507	0.507	0.555	0.577	0.366	0.325
Ti pfu	0.255	0.157	0.124	0.149	0.181	0.213	0.165	0.131	0.124	0.128
T (°C)	570	511	424	543	573	607	569	522	422	428

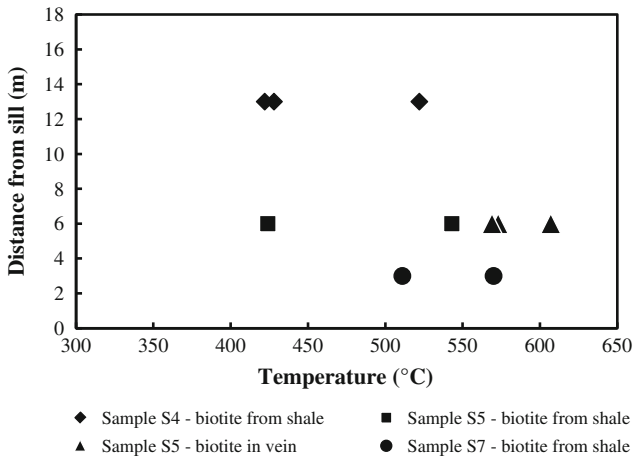

Fig. 8.5 TIB geothermometry results generated using the TIB geothermometer designed for use on metapelitic biotite by Henry and Guidotti (2002)

sample S5, range from 573–607 °C, whilst biotite analysed from the hornfels groundmass portion of sample S5 generates temperatures of 424–543 °C (Figs. 8.5 and 8.6). Available mineral assemblages from samples taken within 13 m above the sill indicate minimum temperatures of 375 °C. Based on our model, host rocks 15–20 m away from the sill experienced temperatures of at least 400–450 °C, 50 years after emplacement. Geothermometry results from sample S4 (13 m away from the sill) indicate temperatures of 422–522 °C.

8.5 Discussion

Our study reveals an asymmetry across the contact aureole with a wider hornfels zone above than below the sills (Fig. 8.2). The presence of biotite within mineral assemblages is only observed above the sills, with the occurrence of a single biotite-plagioclase-rich vein 5 m above the upper contact. These observations suggest that heat transport via vertical fluid flow must have acted as a heat transfer mechanism.

Heat convection is commonly considered a second-order effect, too small to significantly influence the thermal development of a metamorphic system (e.g., Thompson and Connolly 1992). This is particularly relevant when considering deeply buried, well-compacted shales, in which transient permeabilities and the timing of fluid pathway formation are both poorly constrained. For these reasons, heat convection and fluid flow was not constrained in our model. Hydrothermal convection commonly causes isotherms to be more pronounced above intrusions than below, resulting in asymmetrical contact aureoles (Bowers et al. 1990). Asymmetrical contact aureoles are commonly associated with, but not limited to large, >100 m thick intrusions (Rowsell and de Swart 1976; Aarnes et al. 2010). Our thermal modelling furthermore ignores heat generated from crystallization of the magma and heat generation from endothermic metamorphic reactions and radioactive decay. We propose that the inner zone of the thermal aureole recrystallized relatively quickly, forming an 'impermeable' barrier to the upward migration of

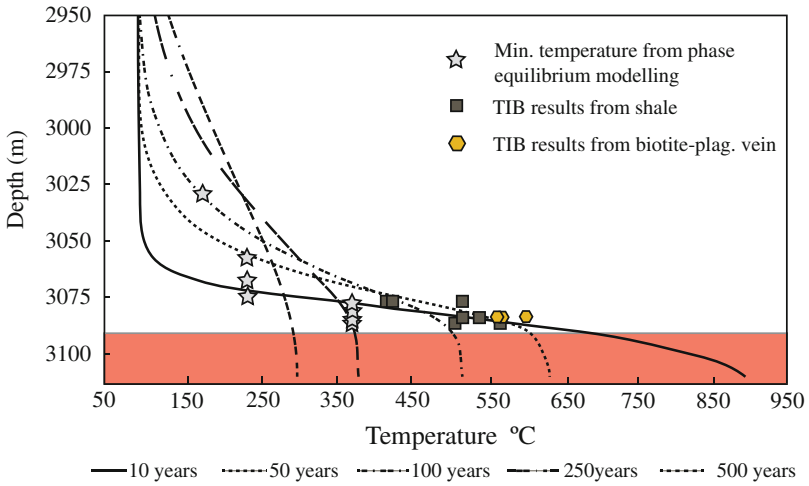

Fig. 8.6 2-D cross-section of the thermal evolution of a contact aureole above the 45 m thick dolerite sill. Geothermometry and mineralogical data are synthesized and overlaid for comparative purposes

hydrous flow within and below the dolerite sills. This can also explain the abundance of hydrous clay minerals within our samples from below the sills and their relative absence within samples taken in-between and above the sills.

Aarnes et al. (2011) model maximum temperatures adjacent to a 15.5 m thick sill as ~600 °C. This is 50–100 °C cooler than temperatures generated in our model, modelling the heating effects of a 45 m thick sill. This difference can largely be accounted for by the difference in the initial host rock temperatures: Aarnes et al. (2011) model a sill intruding a 75 °C host rock, whilst we model a sill intruding a 100 °C host rock (corresponding to a depth of 3 km). We calculated maximum temperatures reached at a distance equal to 100 % of the sill thickness away from the contacts in a 100 °C host rock as ~300 °C, 100 years after emplacement of the sill. By contrast, Aarnes et al. (2010) calculated that in a 75 °C host rock, temperature would reach ~400 °C, 100 m away from the contact of a 100 m thick sill, 100 years after the sill emplacement. This 100 °C temperature difference can be explained partially by the exclusion of the effects of latent heat from crystallization of magma, as well as heat generated from metamorphic mineral reactions in our thermal modelling.

Scheiber-Enslin et al. (2014) have also briefly modelled the heating effects of the sills in borehole QU 1/65 at the depth of our studied interval. They model maximum temperatures experienced 15–40 m below the same sills examined in this study as being in the range of 700–800 °C, 10 years after emplacement. In comparison, our conductive heat flow modelling predicts substantially cooler temperatures of between 350 and 500 °C for rocks at the same depth. Part of this difference can be accounted for by the hotter intrusion temperature (1200 °C) used in their conductive heat flow model, compared to 1150 °C used in our model.

8.5.1 Constraints and Limitation of the Ti-in-Biotite Geothermometry

In order to constrain the validity of our Ti-in-biotite thermobarometry results, we estimated the metamorphic temperature that each of the studied samples underwent based on the observed mineral assemblages (Table 8.2) and a pseudosection/phase diagram calculated for pelitic rock with a composition similar to the Tierberg Formation by Aarnes et al. (2010). We are only able to constrain a minimum temperature of ~375 °C within 13 m above the sills, based on the presence of authigenic biotite. This is consistent with results by Aarnes et al. (2011), who predict a minimum temperature of 350 °C within a similar contact aureole, also based on the growth of metamorphic biotite in a bulk chemical environment similar to ours. Comparatively, Smithard et al. (2015) constrain maximum temperatures of <300 °C, based on the absence of authigenic biotite from mineral assemblages samples of host rocks sampled 1–3 m away from dolerite sills.

Varying chemical compositions and the low total oxide sums of some biotite grains may suggest disequilibrium within the contact aureole (Table 8.2). This is best illustrated by the large spread of temperatures generated by the TIB geothermometer (Fig. 8.5). Our small sample size (10 data points), limited by the fine-grained nature of the mineralogy, and the inherent error of 12–24 % associated with the TIB technique, mean that a more comprehensive examination of the technique is required. However, the results of the TIB geothermometer are in relatively good agreement with temperatures estimated using other methods. For the same rocks, we can constrain absolute minimum temperatures of 300–350 °C based on phase equilibrium modelling, and maximum temperatures of 400–650 °C, based on thermal modelling. The results from the

TIB geothermometer appear to be in good agreement with both methods and give a range of temperature of 422–607 °C.

8.6 Conclusion

Conductive heat flow modelling, comparable to that from other studies, has shown that a 45 m thick sill, intruding at an initial depth of 3 km, can heat a 100 °C black shale host rock to 650–700 °C at the sill contact, and up to 350 °C, 45 m away. Mineral phase equilibrium modelling constrains absolute minimum temperature of 375 °C, for rocks within 13 m above the sill, and 180 °C for rocks farther away. TIB geothermometry results, although limited, provide a meaningful constraint to our thermal modelling results, inferring temperatures comparable to those generated through thermal modelling and those constrained by mineral phase equilibria. The application of the TIB geothermometer warrants a more comprehensive investigation around multiple sills of varying thickness, where it could indicate whether it is a reliable method to model thermal aureole temperature surrounding Karoo dolerite sills. Our thermal modelling focuses on the temperature field of just a single relatively thin sill, not taking into account the effects of multiple intrusions. Future studies should focus on the heating effects of multiple sills, as well as the influence of thicker, 100–300 m dolerite sills.

Acknowledgments Thanks to Maarten de Wit and AEON-ESRI for providing funding which enabled the collection of samples at the Council for Geoscience core shed in Pretoria. The use of the Jeol JXA 8230 Superprobe at Rhodes University, sponsored by the NRF/NEP grant 40113 (UID 74464) is also kindly acknowledged. Thank must also go to Steffan Buettner of Rhodes University and Dr. Bastien Linol (NMMU) for their constructive review of this work. This is AEON publication number 159.

References

Aarnes I, Svensen H, Connolly JAD, Podladchikov YY (2010) How contact metamorphism can trigger global climate changes: Modeling gas generation around igneous sills in sedimentary basins. Geochim Cosmochim 74:7179–7195. doi:10.1016/jgca2010.09011

Aarnes I, Svensen H, Poltea S, Planke S (2011) Contact metamorphic devolatilization of shales in the Karoo Basin, South Africa, and the effects of multiple sill intrusions. Chem Geol 281:181–194. doi:10.1016/jchemgeo201012007

Barker CE, Bone Y, Lewan MD (1998) Fluid inclusion and vitrinite-reflectance geothermometry compared to heat-flow models of maximum paleotemperature next to dikes, western onshore Gippsland Basin Australia. Int J Coal Geol 37:73–111

Bowers JR, Kerrick DM, Furlong KP (1990) Conduction model for the thermal evolution of the Cupsuptic aureole, Maine. Am J Sci 290:644–665

Botha BW (2010) An Overview of Andalusite from Southern Africa: Geology and Mineralogy. The Southern African Institute of Mining and Metallurgy, Refractories 2010 Conference, 8p

Brown R, Gallagher K, Duane M (1994) A quantitative assessment of the effects of magmatism on the thermal history of the Karoo sedimentary sequence. J Afr Earth Sci 18:227–243

Burgess SD, Bowring SA, Fleming TH, Elliot DH (2015) High-precision geochronology links the Ferrar large igneous province with early-Jurassic ocean anoxia and biotic crisis. Earth Planet Sci Lett 415:90–99

Caddick MJ, Thompson AB (2008) Quantifying the tectono-metamorphic evolution of pelitic rocks from a wide range of tectonic settings: mineral compositions in equilibrium 156:177–195. doi:10.1007/s0041000802806

Connolly JAD (2005) Computation of phase equilibria by linear programming : A tool for geodynamic modeling and its application to subduction zone decarbonation. Eart Planet Sci Lett 236:524–541

Duncan RA, Hooper PR, Rehacek J, Marsh JS, Duncan AR (1997) The timing and duration of the Karoo igneous event, southern Gondwana. J Geophys Res 102:127–138. doi:10.1029/97JB00972

Du Toit JJL (1967) QU 1/65 geophysical well logging. Report, Geological Survey, South Africa, No 24/5/67

Falloon TJ, Green DH and Danyushevsky LV (2007) Crystallization temperatures of tholeiite parental liquids: Implications for the existence of thermally driven mantle plumes. Geol Soc of Am, Special Papers 430: 235–260.

Geel C, Schulz HM et al (2013) Shale gas characteristics of Permian black shales in South Africa: Results from recent drilling in the Ecca Group (Eastern Cape). Energy Procedia 40:256–265. doi:10.1016/jegypro20130803

Henry DJ, Guidotti CV (2002) Titanium in biotite from metapelitic rocks: Temperature effects, crystal-chemical controls, and petrologic applications. Am Min 87:375–382

Johnson MR, van Vuuren CJ, Visser JNJ, Cole DI, Wickens HV, Christie ADM, Roberts DL Brandl G (2006) Sedimentary rocks of the Karoo Supergroup. In: Johnson MR, Anhaeusser CR and Thomas RJ (eds). The Geology of South Africa, Geological Society of South Africa, Johannesburg/Council for Geoscience, Pretoria, pp. 461–499

Jones MQW (2003) Thermal properties of stratified rocks from Witwatersrand gold mining areas. J SA Inst Min Metall 173–186

Lindeque A, de Wit MJ, Ryberg T, Weber M Chevallier L (2011) Deep crustal profile across the Southern Karoo basin and beattie magnetic anomaly, South Africa: An integrated interpretation with tectonic implications. S Af J Geol 114:265–292. doi:10.2113/gssajg11434265

Pattison DR, Capitani C et al (2011) Petrological consequences of variations in metamrophic reaction affinity. J Met Geol. doi:10.1111/j15251314201100950

Robie RA, Hemingway BS (1984) Entropies of kyanite, andalusite, and sillimanite: additional constraints on the pressure and temperature of the Al2SiO5 triple point. Am Min 69:298–306

Rowsell DM, de Swart AMJ (1976) Diagenesis in Cape and Karoo sediments, South Africa and its bearing on hydrocarbon potential. Trans Geol Soc S Af 79:81–145

Scheiber-Enslin SE, Webb SJ, Ebbing J (2014) Geophysically Plumbing the Main Karoo Basin, South Africa. S Af J Geol 117:275–300. doi:10.2113/gssajg1172275

Smithard T, Bordy EM, Reid D (2015) The effect of dolerite intrusions on the hydrocarbon potential of the Lower Permian Whitehill Formation (Karoo Supergroup) in South africa and Southern Namibia: A preliminary study. S Af J Geol 118(4)489–510. doi:10.2113/gssajg.118.4.489

Svensen H, Jamtveit B, Planke S, Chevallier L (2006) Structure and evolution of hydrothermal vent complexes in the Karoo Basin, South Africa. J Geol Soc Lon 163:671–682

Svensen H, Corfy F, Ploteau S, Hammer O, Planke S (2012) Rapid magma emplacement in the Karoo Large Igneous Province. Earth Planet Sci Lett 325–326:1–9

Tinker J, de Wit MJ, Brown R (2008) Linking source to sink: Evaluating the balance between onshore erosion and offshore sediment accumulation since Gondwana break-up, South Africa. Tectonophysics 455:94–103

Thompson AB, Connolly AD (1992) Migration of metamorphic fluid: some aspects of mass and heat transfer. Earth Sci Rev 32:107–121

Viljoen JHA (1990) K-bentonites in the Ecca Group of the south and central Karoo. S Af J Geol 94:576–579

Visser JNJ (1992) Deposition of the Early to Late Permian Whitehill Formation during a sealevel highstand in a juvenile foreland basin. S Af J Geol 95:181–193

Walther JV, Wood BJ (1984) Rate and mechanism in prograde metamorphism. Contrib Mineral Petrol 88:246–259

Wang D, Lu X, Zhang X, Xu S, Hu W, Wang L (2007) Heat-model analysis of wall rocks below a diabase sill in Huimin Sag, China compared with thermal alteration of mudstone to carbargilite and hornfels and with increase of vitrinite reflectance. Geophys Res Let 34:L16312. doi:10.1029/2007GL030314

Wang D, Manga M (2015) Organic matter maturation in the contact aureole of an igneous sill as a tracer of hydrothermal convection. J Geophys Res Sol Earth 120:4102–4112 doi:10.1002/2015JB011877

Wohletz K (2008) KWare Heat3D. http://www.lanl.gov/orgs/ees/geodynamics/Wohletz/KWare/Index.htm

Part IV
Stratigraphy and Sedimentary Systems

Dwyka Eskers Along the Northern Margin of the Main Karoo Basin

9

Mike C.J. de Wit

Abstract

Diamond-bearing gravels of the Lichtenburg—Ventersdorp area of the North West Province are associated with sinuous North–South orientated 'runs' that occur exclusively on a flat erosional surface comprised almost entirely of Malmani Subgroup dolomites (Transvaal Supergroup). This unconformity, which developed over a period of 80 Myr prior to deposition of the Pretoria Group sediments, was exhumed in pre-Karoo times, and again in post-Gondwana times. Glacial pavements and isolated remnants of thin Karoo sediments are also found across this polyphase erosional surface. The coarse-grained gravels, (texturally diamictites) that make up the runs and within sinkholes directly or indirectly linked to the runs, have been mined since 1926 and have produced some 12 million carats of diamonds. The runs are narrow, elongated, positive ridges that meander across the dolomite surface. They are up to 30 km long, between 80 and 300 m wide and up to 20 m high. They consist either of sediments interpreted as glacial diamictites, locally derived breccias, or both. The runs have been interpreted by previous workers as post-Gondwana drainage deposits linked to southward flowing Tertiary or Pleistocene river systems. However, no Cenozoic fossils or artefacts have been reported in almost 90 years of mining. Here, new data are presented, including field evidence, geomorphological studies, age-dating from inclusions in diamond and zircon analyses that indicate that the runs are paleo-eskers that were formed during final deglaciation of the Permo-Carboniferous Dwyka continental ice sheet. The eskers represent the infillings of ice-walled stream channels and record deposition of poorly sorted sediment in subglacial drainage networks. Diamictites and their associated internal structures are interpreted as outwash fans or deltas deposited at the front of the glaciers, and fed by the eskers during ice retreat. The age of the deposits is constrained by two populations of agates within the diamictites, which are linked to two separate volcanic units of the Pretoria Group. The youngest ages of detrital zircons from the diamictites are of Kibaran age (ca. 1 Ga), whilst diamonds from the eskers support a Neoproterozoic to Cambrian (600–500 Ma) source for the diamonds. The absence of diamonds from Mesozoic kimberlites, and of Cenozoic fossils, supports the conclusion that the runs are of Karoo age.

M.C.J. de Wit (✉)
University of Pretoria, Pretoria, South Africa
e-mail: mdewit@tsodiloresources.com

M.C.J. de Wit
Tsodilo Resources Ltd., Barberton, South Africa

B. Linol and M.J. de Wit (eds.), *Origin and Evolution of the Cape Mountains and Karoo Basin*,
Regional Geology Reviews, DOI 10.1007/978-3-319-40859-0_9

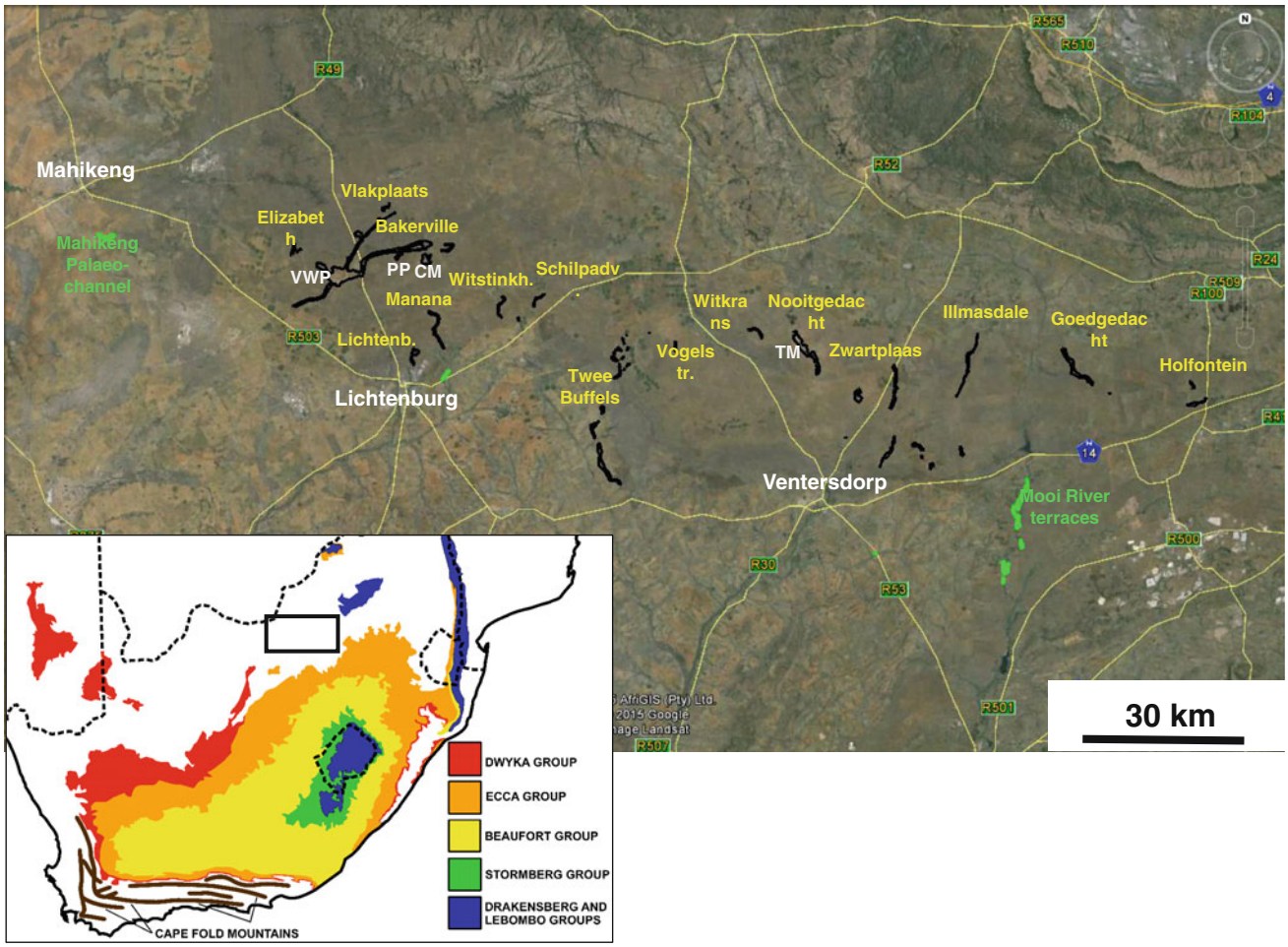

Fig. 9.1 Main gravel 'runs' (*black*) in the Lichtenburg—Ventersdorp area. Younger reworked deposits in *green*. Carlisonia Mine (CM), Pienaars pothole (PP), Van Wyks Pothole (VWP), Tirisano Mine (TM). Background from Google Earth; Insert after Oggmus

9.1 Introduction

Diamond-bearing gravels of the Lichtenburg—Ventersdorp area are associated with sinuous ridges or 'runs', a term first used by Du Toit (1935) to describe these narrow, elongated and sometime sinuous, positive ridges that occur at an elevation of some 1500 m on a flat to very gently southward sloping surface comprised almost entirely of dolomites of the Malmani Subgroup of the Transvaal Supergroup. The runs, referred to as the 'older gravels' (Du Toit 1951), are mainly composed of gravels and breccias, course sands and minor clay units. The runs, close to Randfontein in the East to midway between Lichtenburg and Mahikeng in the West (Fig. 9.1), cover an area of approximately 150 km (E–W) by 40 km (N–S). In the West, around Lichtenburg, they are orientated northeast-southwest; in the central parts near Ventersdorp, north–south; and close to Randfontein, northwest-southeast (Fig. 9.1). Reworked or younger gravels occur as terraces to the south along the Mooi River, and to the southwest near Mahikeng as a palaeo-river channel (Fig. 9.2).

Diamond mining in the Lichtenburg area (known as the Northern Field), and around Ventersdorp (the Eastern Field) started around 1926. Diamonds in the Southern Field (Schweizer-Reneke, Wolmeranstad, Bloemhof) were discovered earlier, but these deposits are not discussed here in detail. The total recoveries from all three fields up to 1984 was 14.4 Mct (Marshall 1987), most of which came from the Northern Fields (9.7 Mct), with the Eastern and Southern Fields each contributing some 2.7 and 2.0 Mct, respectively.

Most researchers have advocated a depositional origin for the gravel runs by surface streams in post-Karoo, and likely Late Mesozoic and Cenozoic times (Harger 1928; Wellington 1929; Williams 1932; Sinclair 1940; Du Toit 1935 and 1951; Cooks 1968; Mayer 1973; Partridge and Maud 1987; Stratten 1979 and Marshall 1990). Stettler (1979), de Wit (1981), and Marshall and Norton (2009) suggested that the

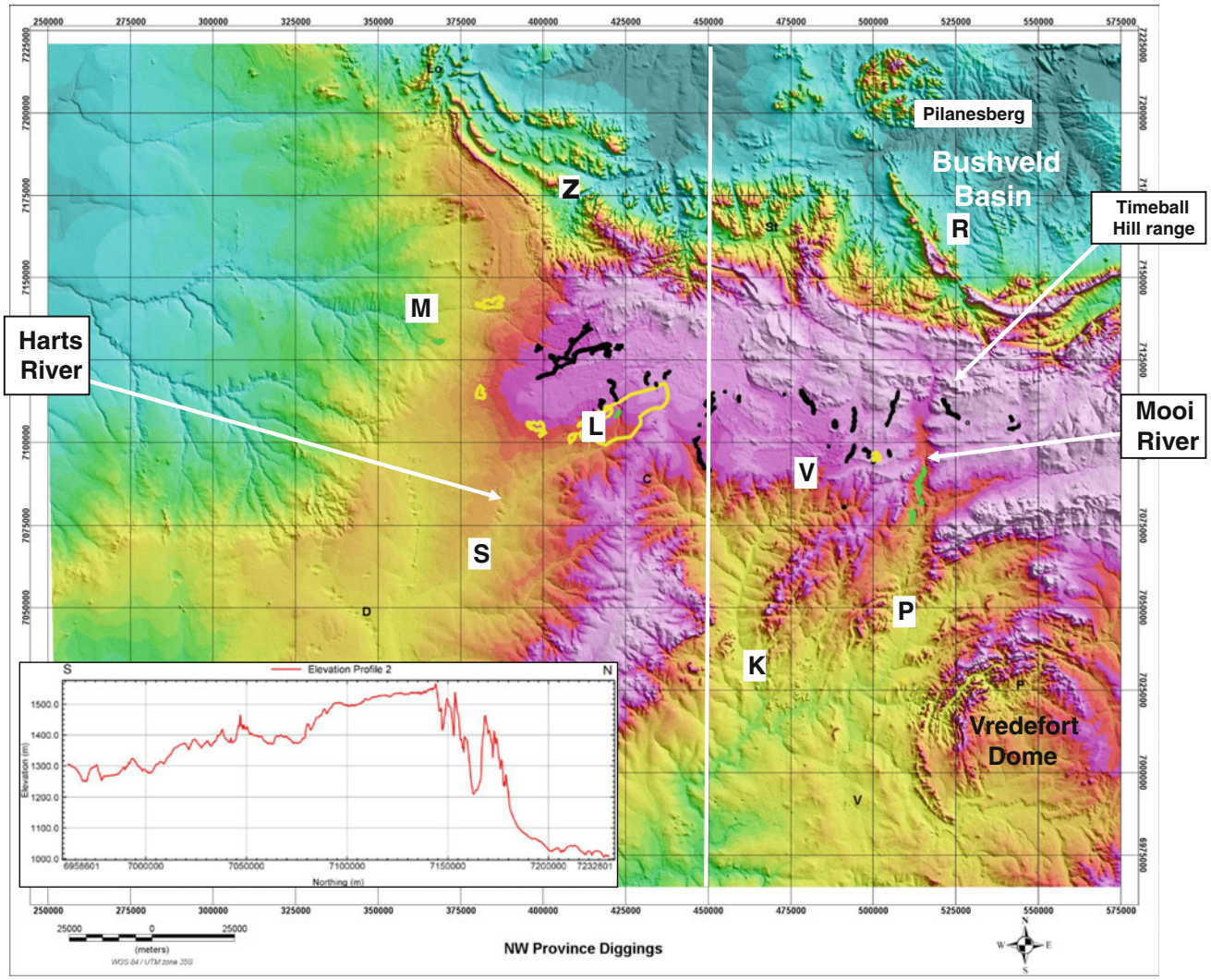

Fig. 9.2 Elevation map based on STRM 1 Arc—Second global: older gravel 'run' (*black*), reworked younger gravel (*green*), remnant Karoo (*yellow*). Insert: North–South profile (at 450 k easting; white line on map) across the dolomite plain (between 7090 and 7140 K m northing). *Note* The Mooi River valley cuts through this dolomite surface. Kleksdorp (K), Lichtenburg (L), Mahikeng (M), Magaliesburg (MB), Potchefstroom (P), Rustenburg (R), Schweizer-Reneke (S), Ventersdorp (V), Zeerust (Z)

runs were controlled by leached and/or fractures zones in the dolomites and that the gravels were deposited in a karst system. De Wit et al. (1998) reported preliminary data from mantle zircons and indicator minerals in the runs that suggest input from local, but as yet undiscovered kimberlites.

9.2 Geomorphological Setting

Flanking the diamond-bearing gravel runs directly to the North is the Griqualand-Transvaal axis, referred to by Wellington (Wellington 1929) as the *Vaal-Limpopo watershed*. The axis has a maximum elevation of just over 1600 m. It is asymmetrical, with a short, steep gradient (9.3 m/km see profile of Fig. 9.2) into the Bushveld Basin to the North, and a remarkably even and very gently sloping dolomite surface (0.8 m/km) to the South that hosts the gravel runs. Du Toit (1933) recognized that the Griqualand-Transvaal axis is not a tectonic axis of uplift but rather a hinge possibly related to subsidence of the adjacent Bushveld Basin to the North. The pre-Karoo dolomite surface that forms the gentle slope on the southern side has remained almost untilted (Du Toit 1933). On this surface, numerous sinkholes and caves have developed within the dolomites, some of which are demonstrably of pre-Karoo age. For example on Ryedale 75IQ a karstic depression is filled with Lower Karoo sediments (Pack et al. 2000). The Mooi River, the only major valley that cuts across the gently sloping dolomite surface, is 'U' shaped, almost 100 m deep, and is the northerly extension of the Virginia Valley, a major

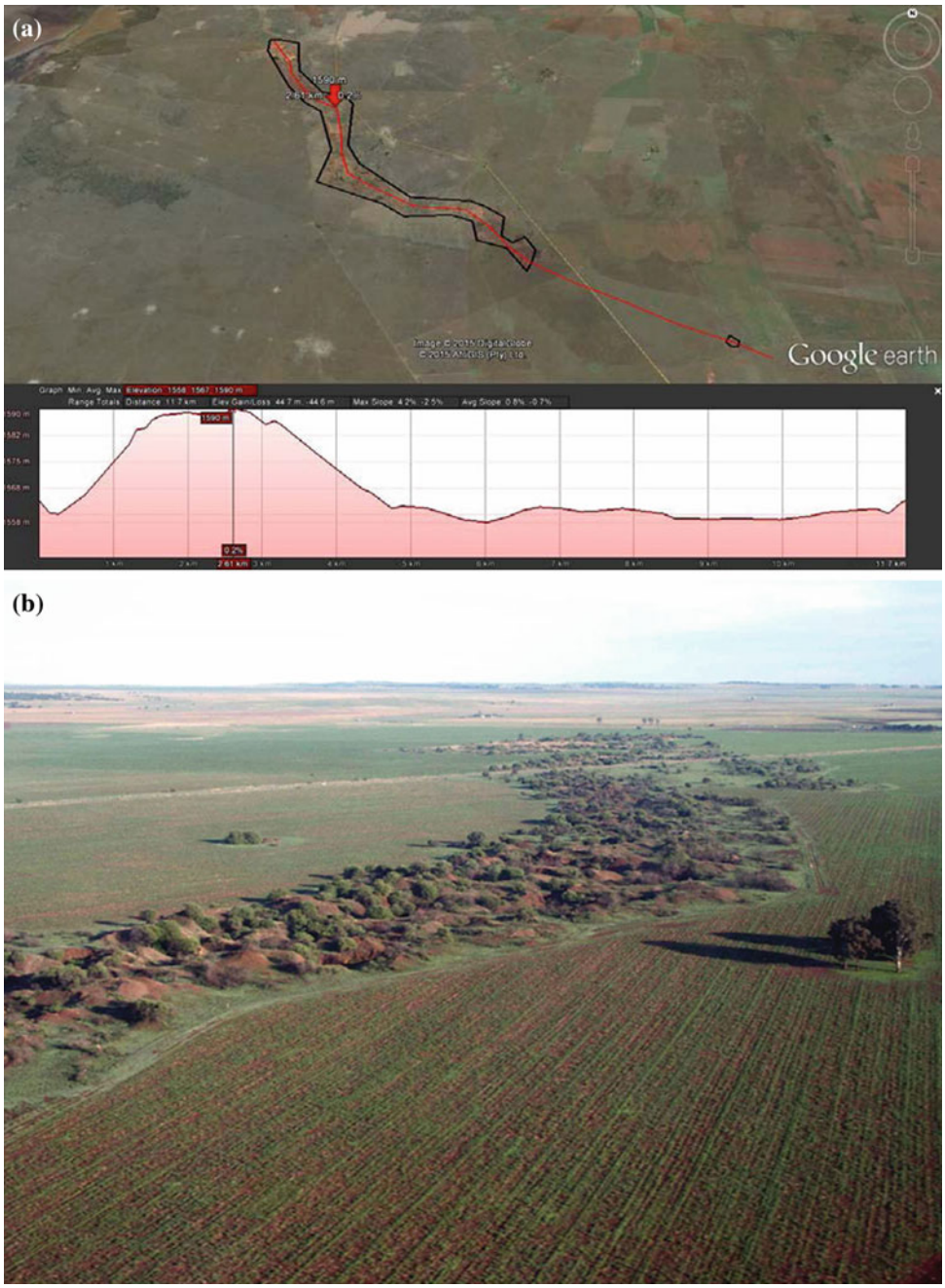

Fig. 9.3 **a** *Outline* of the Goedgedacht 'run' (*black*) with the *profile line* (*red*). Profile showing elevation in meters highlighting the major uphill section in the upper part of the run as well as its overall zero-gradient. **b** View looking north at the northern end of the Zwartplaas gravel 'run' meandering across the dolomite erosion surface

Carboniferous glacial valley that fed into the main Karoo Basin to the south (Visser and Kingsley 1982).

9.3 Ancient and Re-Exhumed Erosion Surface

As a result of a significant fall in sea level at the end of the Transvaal carbonate phase, chert breccias and conglomerates formed across the karst topography of the dolomites. The breccias and conglomerates (now silicified) comprise the Rooihoogte Formation, which cuts across older underlying lithologies of the Malmani Subgroup as an erosional sequence (Eriksson et al. 2001). This unconformity is overlain by younger Pretoria Group sediments and volcanics, and thus represents a time gap of at least 80 Myr (Eriksson et al. 2001). The Rooihoogte karstic sediments preserved on the dolomite plain indicate that this surface represents a major pre-Pretoria Group (i.e. ca. 2.2 Ga) erosion surface, reworked in the Palaeozoic, and upon which Dwyka glacial deposits (including the runs described below) are well preserved (Figs. 9.1, 9.2 and 9.3).

Visser (1987a) named an East–West orientated Carboniferous mountainous region, which included the

Transvaal dolomites, across much of northern South Africa, the Cargonian Highlands. To the south, a palaeo-escarpment separates the Cargonian Highlands from the main Karoo Basin. Pre-Karoo valleys, such as the Kaap and Virginia valleys, cut into this escarpment, and the northerly extension of the latter can be traced through Potchefstroom along the Mooi River valley across the dolomites as far as the Timeball Hill range.

In the Northern Field, close to Lichtenburg, and within the Harts River valley, there are some well-exposed glacial pavements on Ventersdorp sequences (Von Backström et al. 1953). Glacial scratches and grooves on small (ca. 3–5 m length) roches moutonnées suggest ice flow from northeast to southwest. These exhumed glacial pavements suggest that the pre-Karoo Harts River valley is linked to the Kaap Valley. Three gravel runs, Manana, Witstinkhoutboom and Schildpadverdriet, all terminate short of this pre-Karoo valley and were most likely feeding into it (Fig. 9.2).

Ten kilometres west-southwest of Ventersdorp there are polished surfaces with crescentic chatter markings on quartzites of the West Rand Group. The polished surfaces are reminiscent of those described as glacial polish over many parts of southern Africa (Ward et al. 2014). Similar crescentic markings occur on a quartz vein beneath Schilpadverdriet gravel run. Percussion scars are common on boulders in several of the runs. Such scars require collisions of clasts under high energy conditions that were unlikely to have occurred in meandering rivers on the flat, subhorizontal dolomite plain, unless within focussed subglacial channels.

Remnants of Dwyka and Lower Ecca Group sediments are preserved around Lichtenburg in the limestone quarries west of the town, and as Dwyka black shales, varvites, diamictites, sandstones and conglomerates overlying the Ventersdorp Supergroup east of Lichtenburg (Lynn 2014).

To the north of Lichtenburg within the Bakerville diamond diggings, Du Toit (1951) described Karoo sediments within the Pienaars pothole (Ruigtelaagte 353JP). Within the southern part of the Carlisonia mine, on the farm Welverdiend 361JP and less than 5 km east of Pienaars pothole, there are some isolated blocks of pale red and cream coloured cross-bedded medium-grained pebbly sandstones. Based on lithological similarities, these sandstones have tentatively been correlated to the Upper Karoo-aged Mosolotsane Formation in Botswana and the Lisbon Formation in the Ellisras Basin (Bordy et al. 2010).

Du Toit (1951) mentioned silicified Karoo wood from Welverdiend 361JP and Ruigtelaagte 353JP. Recently a boulder-size piece of silicified wood was recovered from Pienaars pothole and identified as Karoo age *Agathoxylon* (Marion Bamford, pers comm 2010). In addition, Harger (1928) describes a fossil tree trunk of 1.8 m from Grasfontein 356JP which resembles gymnosperm and is known from the Upper Karoo Molteno beds (Du Toit 1951).

Approximately 45 km east-northeast of Lichtenburg, Harger (1928) described an old shaft into Dwyka shales resting directly on dolomite; and 20 km east-northeast of Ventersdorp on the farm Ryedale 75IQ there is a ferromanganese mine hosted in Ecca Group shales containing well-preserved imprints of *Glossopteris* leaves (Pack et al. 2000) in a shallow depression resting on Malmani dolomite.

Across the Southern Field, Von Gottberg (1970) described remnants of Karoo sequences on the exhumed pre-Karoo topography, with glacial features including striated pavements, polished surfaces and roches moutonnées that show the region was eroded by Dwyka glaciers moving from North to South. The semi-consolidated clayey and sandy boulder diamictites in this area was intruded by Karoo dolerites (Von Gottberg 1970) and covered by thin upper Karoo sediments. Only in the pre-Karoo valleys such as upper Harts valley, are thick Ecca and Dwyka Group sediments lithified. There is no direct evidence to suggest that this area was covered by Karoo volcanics.

A black ferromanganese wad, part of the so-called Waterval saprolite, is well preserved within the upper part of the Ecca Group near Ventersdorp (e.g. Ryedale 75 IQ; Beukes et al. 1999). This saprolite is thought to have developed along the post-Gondwana African land surface during periods of deep humid weathering in the Late Mesozoic and early Cenozoic (Partridge and Maun 1987; Beukes et al. 1999).

9.4 Apatite Fission Track Analysis (AFTA)

AFTA analysis has been used extensively in southern Africa to extract low temperature thermal history from rocks as they cool through the upper 3–5 km of the crust (Brown et al. 2002). The technique has been applied to constrain the magnitude and timing of crustal denudation when combining the AFTA ages with the measured track length distribution (Jaspen et al. 2006; Wildman et al. 2015).

Over much of the margins of southern Africa, ages are well below 150 or even 100 Ma suggesting substantial (post-Gondwana rifting) denudation to explain the observed cooling (Brown et al. 2002; Wildman et al. 2015), although there is also evidence to suggest that the Cretaceous heat flow was higher.

From AFTA of surface and borehole samples of the elevated area of the North West Province of South Africa, which includes the Lichtenburg/Ventersdorp area, the modelled thermal history indicates that an accelerated cooling event, interpreted to reflect uplift and erosion, took place

Table 9.1 Length and gradient of main gravel runs

Primary gravels			
	Length (km)	Farms: start - finish	Average gradient (m/km or ‰)
Bakerville Run	30.8	Pypklip–La Reystryd	1.01
Vlakplaats Run	14.8	Geluksdal–Bakerville	−0.14
Manana Run (only)	7.6	Lichb. Reserve–Manana	0.53
Witstinkhoutboom Run	4.5	Witstinkhoutboom–Roodepan	0.22
Schilpadverdriet Run	2.9	Schilpadverdriet	1.38
Twee Buffels Run	28.9	Goedvooruitzicht–Wildfontein	1.63
Nooitgedacht Run	8.8	Nooitgedacht–Zwartrand	1.48
Zwartplaas Run	17.7	Zwartpaas–Uitkyk	1.13
Illmasdale Run	11.2	Avondson–Oatlands	−0.45
Goedgedacht Run	11.7	Klipgat–Buchansvale	0
Reworked deposits			
Mafikeng deposit	3.1		6.25
Mooi River terraces	31.2	Klerkskraal dam–Du Toitspruit	1.96

somewhere between 700–450 Ma (Green et al. 2009; Mackintosh 2013). It shows that there was limited cover on the pre-Karoo dolomite surface in this area since around 300–350 Ma and that the Cretaceous cooling event seen along the coastal areas, is not recorded in this part of South Africa (Wildman et al. 2011). This is contrary to the large amount of unroofing interpreted to have taken place in the interior of South Africa during the Cretaceous by Stanley et al. (2013).

9.5 Gravel Runs

All the runs have gradients less than 1.6 m/km and several significantly so (Table 1). Furthermore the Goedgedacht run has an average gradient of zero and the Vlakplaats and Illmasdale runs have negative average gradients (−0.14 and −0.45 m/km, respectively) indicating that these southward directed runs were 'flowing uphill' (Fig. 9.3a). However, under ice and as long as the surface slope of the glacier decreases in a downflow direction, glaciers can flow 'uphill' or against a reversed bedslope (Van der Veen 2013).

The older deposits or 'primary gravels' occur as 'runs', and in 'potholes' and fissure fills, on the previously described ancient surface. These are generally made up of coarse-grained, very poorly sorted gravel, both matrix and clast supported and contain clasts that range from angular to well rounded (Du Toit 1951). 'Potholes' is an incorrect but engrained term for sinkholes, where gravels accumulated and where karstification processes have been ongoing (e.g. the Pienaars, Van Wyks and Tirisano potholes). Many occur close to, but not necessarily within, the gravel runs. The fissure fills are deep, narrow linear structures infilled with gravel and generally bounded by almost vertical dolomite walls. Examples are found on Grasfontein 356JP (King, Malan and Van Wyk fissures) and Goedvooruitzicht 120IP.

The runs vary from 3 to over 30 km in length, are some 70 m wide on average but can be as wide as 300 m in isolated areas (Table 9.1). The runs are positive features of up to 20 m high (Fig. 9.3b). The gradient and morphology of the 29 km long Twee Buffels run, the only one that is partially deposited on Ventersdorp bedrock, remains unchanged across the contact between the Malmani dolomites and the Ventersdorp lava. This shows that the gravels did not protect the underlying dolomite rock from a general lowering of the dolomite surface by solution processes, and hence did not transform incised channels within the dolomite to elevated ridges or runs (previously referred to as 'inverted topography', e.g. Du Toit 1951).

The main lithofacies encountered in the 'older gravels' in the runs and potholes are summarized in Table 9.2. Sediments are very poorly sorted and have been described as coarse-grained with a clayey matrix (Marshall and Norton 2009), and as coarse-muddy gravel (Stettler 1979). The presence of muscovite as a large component in the clay fraction, and the absence of feldspar in Dwyka Group sediments in the northern part of the Karoo Basin (Bühmann and Bühmann 1990), indicate that the clay fraction is mostly primary in these older gravels.

The term diamictite is appropriate for the gravel making up the runs (most sediments are at loosely- or semi-lithified), since diamictite refers to any poorly sorted clast-sand-mud admixture regardless of depositional environment (Eyles et al. 1983). The Malmani bedrock has been modified by

Table 9.2 Bedrock- and lithofacies types

Code	Facies	Description
Bedrock' facies		
BBcsh	Shattered bedrock	In situ matrix-poor, clast-supported diamictite, bedrock fragments are angular and blockey, have well-defined bedrock fabric, very locally derived
BBm	Bedrock breccia	Massive to locally normally graded clast- to matrix-supported, lacks obvious clast macrofabric, clasts mainly angular to sub-angular, bedrock clasts only, randomly orientated clasts
BB(t)	Tectonised bedrock breccia	Stratified bedrock residue in which the variably developed layering (defined by grain size, clast macrofabric and matrix content) is deformed by locally developed open folds, large bedrock raft highly fractured
Lithofacies		
Dmm	Diamictite—matrix supported, massive	Structureless mud/sand/pebble admixture, clasts may be angular to rounded, matrix is highly variable from clay to coarse sand but generally a fine silty-clay, no immediate and preferred clast orientation, bedrock (angular to sub-rounded) and foreign (sub-rounded to rounded)
Dcm	Diamictite—clast supported, massive	Clast-supported structureless mud/sand/pebble admixture, rare clast imbrication, clasts compositions—locally derived sub-angular to sub-rounded (mainly chert) and foreign rounded clasts (often polished), rare imbrication
Dcs	Diamictite—clast supported, stratified	Textural differentiation within diamict, stratification more than 10 % of unit thickness, gravel and diamictite units interbedded, units not laterally extensive, presence of pods of gravel
Dcg	Diamictite—clast supported, graded	Diamict exhibits vertical grading in clast content
Gm	Gravel—massive or cludely bedded, clast supported	Horizontally bedded or gently dipping (Gp), metre scale beds, laterally extensive, very coarse-grained, interbedded sand units
Sm	Silty sands - massive	Massive or crudely bedded silty sand,may be pebbly
Fm	Clay - massive	Generally red coloured

glacial activity as discussed above, and in the process produced several altered bedrock facies. Firstly, in situ shattered and fractured bedrock with associated closely packed bedrock breccia (BBsh), such as in the old Welverdiend workings (Fig. 9.4a), has been attributed to frost shattering. Frost action is supported by several ice wedges found on some of the Dmm facies in the Manana run. Second, bedrock breccias (BBm) have locally derived and randomly orientated angular clasts (Fig. 9.4b), and are generally devoid of any bedrock macrofabric but grade upwards into the Dmm/Dcm facies (Fig. 9.4c) with a decrease in size and frequency of bedrock clasts, and an increasing proportion of foreign clasts. The BBm matrix is fine grained and quartz-rich with some kaolinite. This has been interpreted as the transition from brittle shearing at the ice-bed interface to ductile deformation as diamictite thickness increases. Third, folded bedrock breccias (BB(t)) of mainly chert, grading into Dcm diamictite composed of highly concentrated angular bedrock clasts with shattered chert rafts, are seen in the more elevated sections, such as the Lichtenburg Townlands (Fig. 9.4d). These features are interpreted as a product of glaciotectonic brecciation. Similar facies have been described by Visser (1987a, b) from a borehole near Winburg on a pre-Karoo 'high', covered with brecciated and glaciotectonised bedrock, grading upwards into a poorly sorted conglomerate.

The most common lithofacies are matrix- and clast-supported diamictites (Dmm and Dcm) which are interpreted as eskers formed by proximal accretion along the axis of sub-glacial tunnels. They have been referred to as R-channels (Boulton et al. 2009), which are flow-parallel streams in sub-glacial tunnels that arch up onto the ice, leaving behind positive ridges once the ice has melted such as those found in Quaternary sequences of northern Europe (e.g. Karukäpp 2005). Eskers have the capacity to efficiently discharge large meltwater fluxes (Boulton et al. 2009). My interpretation is that the diamictite runs were deposited sub-glacially in ice tunnels during the Dwyka deglaciation. Diamictite facies with some internal structure are either graded or stratified (Dmg or Dcs). Gravel facies Dcs/Gm are exposed at the Tirisano mine on the Nooigedacht run overlying the basal Dmm/Dcm units, and in the lower end of the Bakerville run. These are generally subhorizontal or dip at very low angles to the south, and are interpreted as outwash fans deposited during ice retreat by eskers formed in deltaic or fan environments with large volumes of water bringing sediments that were released during the ice melt. The Nooitgedacht fan is a relatively flat feature and extends beyond the main mining pit that lies at the intersection of two fractures orientated roughly NS and EW (Marshall and Norton 2012).

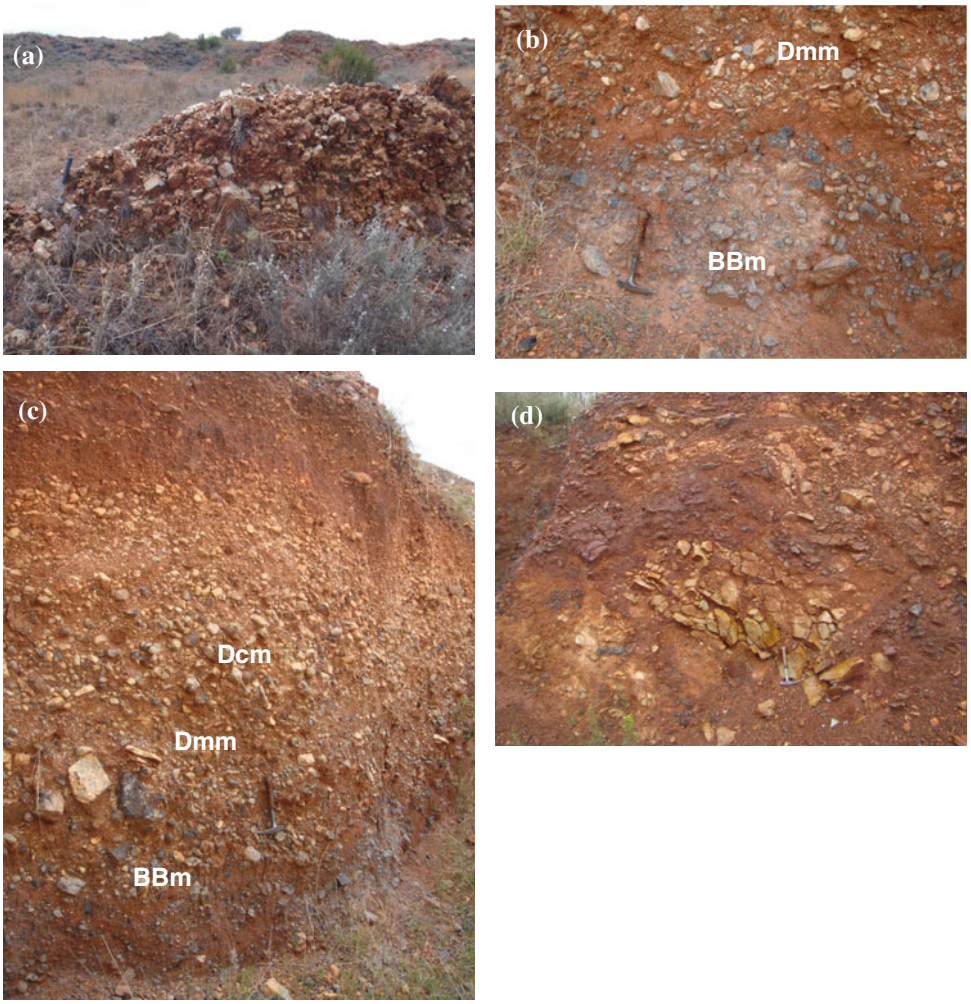

Fig. 9.4 **a** In situ shattered bedrock breccia, with high density of chert fracturing and little or no displacement, directly below the gravel deposit on Welverdiend (facies BBsch). This shattering is interpreted as the result of frost action. **b** Bedrock breccia (BBm) overlain by matrix-supported diamictite (Dmm) in the Manana 'run'. **c** Bedrock breccia (BBm) at the base overlain by Dmm and Dcm, respectively, in the Manana 'run'. **d** Layered bedrock residue deformed by locally developed folds and shattered bedrock rafts interpreted as glaciotectonic structures (BB(t) facies). Hammer for scale

On relatively flat surfaces, water velocities in ice tunnels are high, falling in a narrow range between 2 and 6 m/s (Boulton et al. 2009). The presence of transported oversize material with percussion damaged surfaces in the Dmm/Dcm units of some of the runs, support such high flow regimes. Boulton et al. (2009) further showed that the spacing between eskers on flat surfaces is typically between 8 and 25 km depending on the transmissivity. The average spacing of the runs on the pre-Pretoria Group surface is 13.6 km, very similar to the spacing of eskers in northern Estonia (11.3 km; Rattas 2007), where eskers have very similar morphologies and distribution patterns to the gravel runs of the North West Province.

9.6 Clay Mineralogy

Marshall and Norton (2009) reported XRD analysis of samples taken from various gravel units on the Nooitgedacht run north of Ventersdorp (Table 9.3). These samples are all broadly similar, with quartz (50–60 %), kaolinite (20–30 %), goethite (10–15 %) and mica (10–11 %) making up the dominant phases. Samples from around Lichtenburg (Robb 1994) have the same constituents with quartz, goethite, muscovite and kaolinite as the main components (Table 9.3). The survival of muscovite in many of the gravel samples suggests that these sediments were not exposed to intense weathering prior and during deposition. Interestingly muscovite is also a major component in Lower Karoo sediments in the Bothaville area (Bühmann and Bühmann 1990), whilst kaolinite has been reported from the Vryheid Formation of the Ecca Group (Bredell 1978; Bühmann and Bühmann 1990). Although the intense Cretaceous weathering on the African erosion surface would have added to the kaolinite in the sediments, there is strong evidence to suggest that kaolinite in Permian sediments was early diagenetic or post-depositional (Bühmann and Bühnmann 1990), and formed under the influence of acidic (freshwater) and not marine pore waters (Bühmann and Bühmann 1990). The presence of goethite and haematite can be ascribed to groundwater remobilisation of iron and manganese from the Malmani dolomites (Pack et al. 2000).

Table 9.3 Clay mineralogy of selected samples

Site	Run	Material	Main components as determined by XRD (calculated percentages)									Total	XRF	Possible source
	Deposit		Quartz	Kaolinite	Goethite	Muscovite	Vermiculite	Smectite	Hematite	Chlorite	Others			
Ryedale*	Illmasdale	Reddish gravel	28	53	19							100		
Ryedale*	Illmasdale	White clay		100							Jarosite tr	100		
Zwartplaas*	Zwartplaas	Reddish gravel	45	27	18	10					Alunite tr	100		
Roodepan*	Zwartplaas	White clay	2	87	6	5					Feldspar tr	100		
Zwartrand 1*	Nooitgedacht	Red/brown gravel	14	29	19	10			10	8	Amphibole 10 %	90		
Zwartrand 2*	Nooitgedacht	Greenish/grey clay	29	37	9			25			Feldspar tr	100		Mafic component
Welverdiend 1*	Welverdiend Dep	Black	33	14	15	13					Talc? 9 %	75		
Welverdiend 2*	Welverdiend Dep	Dark red clay	50	24	12	14						100		
Carlesonia (Wel)*	Welverdiend Dep	Red clay	28	51	13	8						100		Lava?
Pienaars Pothole*	Bakerville	Brown gravel		24	20			56				100		Mafic
Pienaars Pothole*	Bakerville	Purple sed		89		3			4	4	Jarosite tr	100		
Pienaars Pothole*	Bakerville	White clay		94				6			Dolomite tr	100		
Gravitatie 1*	Bakerville	Grey/brown	6	7	5	4	78				Jarosite tr	100		Ultramafic
Gravitatie 1*	Bakerville	Red clay	25	32	20	14		11				102		Mafic
Gravitatie 1*	Bakerville	Red gravel	35	28				37				100		Mafic
S1*	Bakerville	Red gravel	23	46	16	15					Mircocline? Rutile?	100		
S1*	Bakerville	White		95								100		
Uitgevonden 1*	Bakerville	White/grey			15		85					100	Ni–1270 Cr–2003	Ultramafic
Uitgevonden 1*	Bakerville	Greenish clay	48				52					100		Ultramafic?
Uitgevonden 1*	Bakerville	Pinkish	63	24	6	7						100		
Kings Pothole *	Grasfontein Dep	Dark grey	42		16	17		14			Serpentine 11 %, Feldspar tr	89		Mafic component

(continued)

Table 9.3 (continued)

Site	Run	Material	Main components as determined by XRD (calculated percentages)									Total	XRF	Possible source
	Deposit		Quartz	Kaolinite	Goethite	Muscovite	Vermiculite	Smectite	Hematite	Chlorite	Others			
LGP—T[o]	Nooitgedacht	Gravel sample	53.1	25.2	12.5	9.2						100		
LGP—H[o]	Nooitgedacht	Gravel sample	48.2	29.7	11.2	10.9						100		
TZP—T[o]	Nooitgedacht	Gravel sample	63.4	20.4	10.4	5.8						100		
TZP—H[o]	Nooitgedacht	Gravel sample	60.5	22.8	11.2	5.4						100		
UGP—T[o]	Nooitgedacht	Gravel sample	48.8	31.6	14.6	5.0						100		
UGP—2[o]	Nooitgedacht	Gravel sample	55.0	26.3	15.6	3.1						100		
*Robb (1994)														
[o]Coetzee (2001)														

Several samples from Lichtenburg indicate that some of the clays have been derived from weathered mafic and ultramafic rocks (Table 9.3), and these are probably the local sources for the unabraded agates in the gravels.

9.7 Agate Populations

There are two populations of agates in the gravels. First there are the wine-coloured carnelians and yellow chalcedonies, which are restricted to certain major 'potholes' and runs North of Lichtenburg. These are absent in the Ventersdorp area. The carnelians and chalcedonies generally have fresh surface textures showing little or no sign of abrasion (Fig. 9.5a). Pipe carnelians are common, especially associated with the deeper 'potholes'. Du Toit (1951) suggested that the carnelian and chalcedony pebbles were derived from the Karoo volcanics in the Bushveld Basin; however, a more likely source is the Bushy Bend amygdaloidal lavas (ca. 2.3–2.4 Ga) that occur between the basal Rooihoogte and overlying Timeball Hill Formations of the Pretoria Group (Eriksson et al. 1994; Coetzee 2001). These only occur as isolated occurrences in the southwest of the Transvaal Basin, and have been described from Potchefstroom (Lenhardt et al. 2012), from Gopane and eastern Botswana (Eriksson et al. 1994), and from near Pretoria (van der Neut 1990). According to Coetzee (2001) these lavas, which are intimately associated with the Rooihoogte Formation, occurred mainly as restricted fissure eruptions between Potchefstroom and Ventersdorp, which includes the Lichtenburg area, and as far East as Botswana.

Second, the pale colourful agates are generally banded with white, grey and black colours. These are mostly well-rounded, and highly abraded with smooth surfaces. These are found in most of the gravels in the region, both in Lichtenburg and Ventersdorp, but in lower and more variable concentrations. The likely source for these agates is the Hekpoort volcanics (ca. 2.2 Ga) that attain a thickness of 1100 m in the southcentral part of the Transvaal Basin (Lenhardt et al. 2012). Single lava flows can be up 60 m thick varying from massive to vesicular. In the North West Province these occur northeast of the Lichtenburg/Ventersdorp area between Zeerust and Magaliesburg.

9.8 Diamonds and Zircons

The main observations from a parcel of 166 diamonds from Van Wyk's pothole is that more than 50 % of the diamonds are classified as boart, many of the stones are fragile and cracked, and there is no evidence of significant transportation (Robinson 2004). This population clearly suggests that

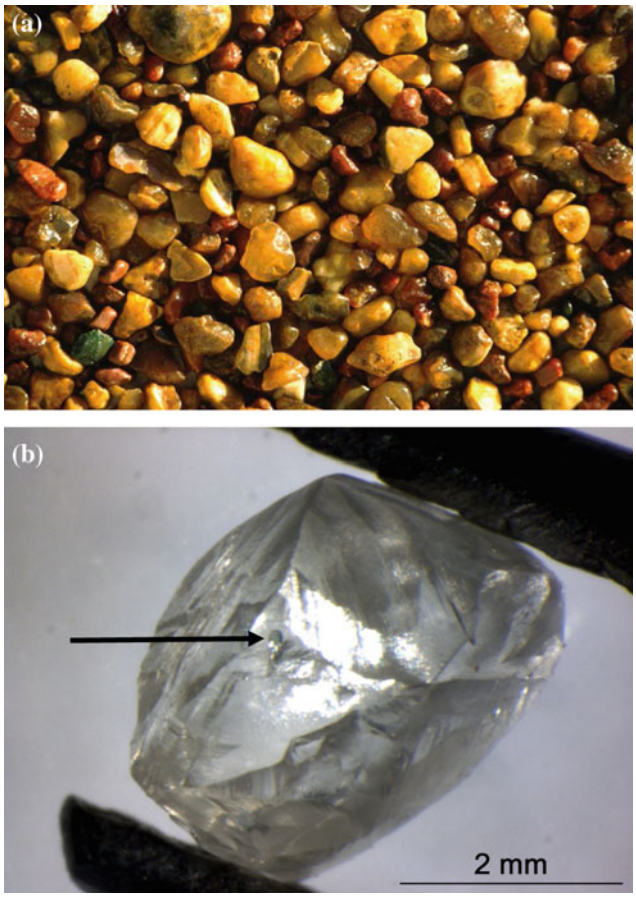

Fig. 9.5 **a** Locally derived carnelians and chalcedonies from Pienaars pothole. Note irregular shapes and pitted surfaces of many of the unabraded agates. Bar is 2 cm. **b** Diamond from MSG (Van Wyks pothole) with clinopyroxene inclusion used for Ar/Ar dating pointed out by *arrow*

the diamonds have a local proximal source. Two of the diamonds with clinopyroxene inclusions were sent to Phillips (University of Melbourne) for Ar^{40}/Ar^{39} step-heating analysis (Fig. 9.5b). The results for both inclusions were indistinguishable and indicate an emplacement age of between 500 and 600 Ma (Dave Phillips, pers comm 2013). This precludes the older Premier kimberlite (ca. 1.2 Ga) and younger southern African Cretaceous/Jurassic kimberlites as possible sources for the diamonds (Dave Phillips, pers comm 2013). Low-U and probably mantle-derived zircons from concentrates of the diamond workings at Pienaar's pothole give an age range between 489 and 664 Ma (de Wit et al. 1998), supporting the inference of a late Neoproterozoic to Cambrian kimberlite source.

Detrital crustal zircons were also recovered from Karoo sediments from Welverdiend and Pienaar's pothole and the following ages were obtained: Welverdiend (3148 ± 140, 2824 ± 51, 2067 ± 53 and 1046 ± 30 Ma) and Pienaar's pothole (3144 ± 58, 2044 ± 21 with a single grain at

2809 ± 98 Ma) (Van der Linde 2015). The youngest ages are Kibaran, and others are Bushveld and Archaean in age, so no 'young' crustal zircons have been recovered in Lichtenburg.

9.9 Discussion and Conclusions

In summary, it is suggested that a gently dipping dolomite surface was scoured during Dwyka times by an ice cap and at least two major valley glaciers (valleys now occupied by the Mooi and Harts Rivers), and numerous smaller valley glaciers that fed into the main Karoo Basin to the South and West. This surface, on which the Dwyka gravel runs were subsequently deposited, was initially shaped over a period of at least 80 Myr in pre-Pretoria Group times, and thereafter episodically re-exhumed possibly from post-Waterberg to Pre-Karoo times; during Dwyka times; and again during the Mesozoic-Cenozoic. It contains remnants of pre-Pretoria karst sediments, Dwyka glacial markings and eskers, remnants of isolated Karoo sequences, and evidence of the Cretaceous African landsurface and younger Cainozoic erosion cycles. It is therefore a relatively thin surface 'layer', or a significant 'palimpsest' that represents a long history of deposition, erosion and non-deposition, locally preserved as condensed sequences, of which the eskers are small remnants.

The gravel 'runs' around Lichtenburg and Ventersdorp are remnants of sub-glacial deposits preserved on an old erosion surface that has been shaped since pre-Pretoria Group times. They are mainly present as diamictites deposited as southward flowing eskers during the final stages of the Gondwana-wide Dwyka glaciation. Analyses of inclusions in diamond and zircons support this time frame; and the fact that the agate populations most likely relate to the Pretoria Group and not to the Karoo volcanics adds further weight to the diamictites being of Dwyka age.

Acknowledgment The author wishes to acknowledge De Beers Exploration for the zircon analysis, Jeff Harris and Dave Phillips for the diamond data, Edgar Stettler for Lichtenburg drilling data, Rockwell Diamonds for providing the clay analysis, Tania Marshall for generously providing photos and unpublished reports, McDonald Kahari for helping with the topographical image, and Tania, John Ward and Maarten de Wit for discussions and suggestions on the 'western Transvaal'. Mike Lynn, Jeff Harris and Dave Phillips are thanked for their valuable comments and edits.

References

Beukes, N.J., van Niekerk, H.S., and Gutzmer J., 1999. Post Gondwana land surface and pedogenetic ferromanganese deposits on the Witwatersrand at the West Wits Gold Mine, South Africa. South African Journal of Geology, 102 (1), 65–82.

Bordy, E.M., Segwabe, T., and Makuke B., 2010. Sedimentology of the Upper Triassic – Lower Jurassic (?) Mosolotsane Formation (Karoo Supergroup), Kalahari Karoo Basin, Botswana. Journal of African Earth Sciences, 58, 127–140.

Boulton, G.S., Magdorn, M., Maillot, P.B. and Zatsepin, S., 2009. Drainage beneath ice sheets: groundwater-channel coupling and the origin of esker systems from former ice sheets. Quaternary Science Reviews, 28, 621–638.

Bredell, J.H., 1978. Prospecting for refractory clays on the East Rand. Geological Survey of South Africa, Bulletin, 62, 20 pp.

Brown, R.W., Summerfield, M.A. and Gleadow, A.J.W., 2002. Denudational history along a transect across the Drakensberg Escarpment of southern Africa derived from apatite fission track thermochronology. Journal of Geophysical Research, 107 (B120, 2350).

Bühmann, C. and Bühmann, D., 1990. Clay minerals as palaeoenvironment indicators exemplified on a Karoo sequence from the Bothaville area, South Africa. South African Journal of Geology, 93 (3), 505–513.

Coetzee, L.L., 2001. Genetic stratigraphy of the Paleoproterozoic Pretoria Group in the Western Transvaal. Unpublished MSc thesis, University of Johannesburg, 212 pp.

Cooks, J. 1968. Paleodreineringslyne in die Wes-Transvaalse karstgebied. South African Geographical Journal, 50, 101 – 109.

De Wit, M.C.J., 1981. Geophysical investigation and geological interpretation of part of the diamondiferous gravels on the Grasfontein farm (356 JP), west of Bakerville. Unpublished MSc thesis, University of Pretoria, South Africa, 93 pp.

De Wit, M.C.J., Morelli, C. and Skinner, C.P.S., 1998. A reinterpretation of the Lichtenburg diamond deposits. Extended abstracts of the 7th International Kimberlite conference, Cape Town, South Africa, 195.

Du Toit, A.L., 1933. Crustal movement as a factor in the geographical evolution of South Africa. The South African Geographical Journal, XVI, 2 – 20.

Du Toit, A.L., 1935. The Diamondiferous alluvials. Explanation for sheet 53, Geological Survey of South Africa, Pretoria, Chapter X, 49 – 64.

Du Toit, A.L., 1951. Diamondiferous gravels of Lichtenburg. Geological Survey of South Africa, Memoire, 44, 58 pp.

Eriksson, P.G., Engelbrecht, J.P., Res, M., Harmer, R.E., 1994. The Bushy Bend Lavas, a new volcanic member of the Pretoria Group, Transvaal Sequence. South African Journal of Geology, 97 (1), 1 –7.

Eriksson, P.G., Altermann, W., Catuneanu, O., van der Merwe, R., Bumby, A.J., 2001. Major influences on the evolution of the 2.67 – 2.1 Ga Transvaal basin, Kaapvaal craton. Sedimentary Geology, 1410142, 205–231.

Eyles, N., Eyles, C.H. and Miall, A.D., 1983. Lithofacies types and vertical profile models; an alternative approach to the description and environmental interpretation of glacial diamict and diamictite sequences. Sedimentology, 30, 393–410.

Green P., Swart, R., Jacob, J., Ward, J. and Bluck, B., 2009. Thermochronology and landscape development in southern Africa. PESGB HGS, Africa meeting, Extended abstracts, 7 pp.

Harger, H., S., 1928. Discussion of Draper's paper 'On the Association of Diamonds with the Chert Bed of the Districts of Ventersdorp and Lichtenburg'. Proceedings of the Geological Society of South Africa, XXX, xxxix- xliv.

Jaspen, P., Bonow, J.M., Green, P.F., Chalmers, J.A., Lidmar-Bergström, K., 2006. Elevated passive continental margins: long-term highs or Neogene uplifts? New evidence from West Greenland. Earth Planetary Science letters, 248(1), 330–339.

Karukäpp, R., 2005. Eskers in the periphery of their distribution in North Estonia. Proceedings of the Estonian Academy of Sciences, Geology, 54 (1), 26–39.

Lenhardt, N., Eriksson, P.G., Catuneanu, O., Bumby, A.J., 2012. Nature of and controls on volcanism in the c. 2.32 – 2.06 Ga

Pretoria Group, Transvaal Supergroup, Kaapvaal Craton, South Africa. Precambian Research, 212–215, 106- 123.

Lynn, M.D., 2014. Lichtenburg Project, Site Visit Report. The MSA Group (Pty) Ltd report on behalf of: The Gold Company (Pty) Ltd, J2903, 12 pp.

Mackintosh, V., 2013. The application of apatite (U-Th)/He thermochronology to constraining the cooling, erosion and uplift history of southern Africa. Internal report, School of Geographical and Earth Sciences University of Glasgow, 5 pp.

Marshall, T.R., 1987. Alluvial diamond occurrences of the western and south western Transvaal – a compilation of production data. Economic Research Unit, University of the Witwatersrand, Johannesburg, Information Circular, no. 194.

Marshall, T.R., 1990. The nature, origin and evolution of the diamondiferous gravels of the southwestern Transvaal. Unpublished PhD thesis, University of the Witwatersrand, Johannesburg, South Africa, 211 pp.

Marshall, T.R. and Norton, G.A., 2009. The nature of the alluvial diamond deposits of the Ventersdorp district, north West Province, South Africa. South African journal of Geology, 112, 109–124.

Marshall, T.R., and Norton, G.A., 2012. Report on the Tirisano Alluvial Diamond project, Ventersdorp District, South Africa, for Rockwell Diamonds INC, 113 pp.

Mayer, J.J., 1973. Morphotectonic development of the Harts River Valley in relation to the Griqualand-Transvaal axis and the Vaal and Molopo rivers. Transactions of the Geological Society of South Africa, 73, 183 – 194.

Pack, A., Gutzmer J., Beukes, N.J., and van Niekerk, H.S., 2000. Supergene Ferromanganese Wad deposits derived from Permian Karoo Strata along the Late Cretaceous-Mid-Tertiary African Land Surface, Ryedale, South Africa. Economic Geology, 95, 203–220.

Partridge, T.C. and Maud, R.R., 1987. Geomorphic evolution of southern Africa since the Mesozoic. South African Journal of Geology, 90, 179– 208.

Robb, V.M., 1994. Clay analysis of twenty one samples for the Western Transvaal clay project. Anglo American Research Laboratory (Pty) Ltd, Report M94/0489, 7 pp.

Robinson, D.N., 2004. The characteristics of diamonds, also studies by infrared absorption from 'Mike-se Gat', adjacent to Van Wyks Pothole, Lichtenburg, Internal report for Synodinos, 8 pp.

Sinclair, W.E., 1940. Alluvial diamonds in South Africa: a retrospective account of the Lichtenburg Diggings, one of the world's big alluvial diamond fields. Mining Magazine, 62 (4), 213 – 219.

Stanley, R.S., Flowers, R.M. and Bell, D.R. 2013. Kimberlite (U-th)/He dating links surface erosion with lithospheric heating, thinning, and metasomatism in the southern African plateau. Geology, 41 (12), 1243–1246.

Stettler, E.H., 1979. A geological and geophysical investigation of the diamond runs on Ruigtelaagte and vicinity, in the Bakerville area, Lichtenburg District. Unpublished MSc thesis, University of Pretoria, South Africa, 112 pp.

Stratten, T., 1979. The origin of the diamondiferous alluvial gravels in the southwestern Transvaal. In: A.M. Anderson and W.J. von Biljon (editors), Some sedimentary basins and associated ore deposits of South Africa. Special Publication of the Geological Society of South Africa, 6, 219–228.

Rattas, M., 2007. Spatial distribution and morphological aspects of eskers and bedrock valleys in north Estonia: implications for the reconstruction of a subglacial drainage system under the late Weichselian Baltic ice stream. In Johansson, P. and Sarala, P. (editors), Applied Quaternary research in the central part of glaciated terrain, Geological Survey of Finland, Special Paper, 46, 63 –68.

Van der Linde, G., 2015. U-Pb ages of detrital zircons from EIA662 and EIA664 (RSA140026). De Beers Group Services, report 157790, 12 pp.

Van der Neut, M., 1990. Afsettingstoestande van die Pretoria Groep gesteentes in die Pretoria-Bronkhorstspruit-Delmas gebied. Unpublished MSc thesis, University of Pretoria.

Van der Veen, C.J., 2013. Fundamentals of Glacier dynamics. 2nd Edition, CRC Press, 363 pp.

Visser, J.N.J. and Kingsley, C.S., 1982. Upper Carboniferous glacial valley sedimentation in the Karoo Basin, Orange Free State. Transactions of the Geological Society of South Africa, 85, 71 –79.

Visser, J.N.J., 1987a. The palaeogeography of part of southwestern Gondwana during the Permo-Carboniferous glaciation. Palaeogeography, Paleoclimatology, Palaeoecology, 61, 205–219.

Visser, J.N.J., 1987b. The influence of topography on the Permo-Carboniferous glaciation in the Karoo Basin and adjoining areas, southern Africa. In: D.H. Elliot, J.W. Collison, G.D. McKenzie and S.M. Haban (editors), Gondwana Six: Stratigraphy, Sedimentology and Paleontology, 41, 123 – 129.

Von Backström, J.W., Schumann, F.W., Le Roex, H.D., Kent, L.E., du Toit, A.L., 1953. The geology of the area around Lichtenburg. Geological Survey of the Union of South Africa.

Von Gottberg, B., 1970. The occurrence of Dwyka rocks and glacial topography in the South-western Transvaal, 73, 99 – 106.

Ward, J.D., Bluck, B.J., Swart, R., Jacob, R.J., de Wit, M.C.J. and Spaggiari, R.I., 2014. Concave polished rock patches: pointers to widespread pre-Karoo landscape remnants in southern Africa. Abstract Roy Miller Symposium – Celebrating 50 years of Geological Service to Namibia.

Wellington, J.H., 1929. The Vaal Limpopo watershed. The South African Geographical Journal, XII, 36 –45.

Wildman, M., Beucher, R., Brown, R. W., Persano, C., and Stuart, F. (2011, December). Exhumation and erosion rates in southern Africa from apatite fission track and (U-Th)/He analysis: state of research, ongoing work and future perspectives. In *AGU Fall Meeting Abstracts* (Vol. 1, p. 2564).

Wildman, M., Brown, R., Watkins, R., Carter, A., Gleadow, A., Summerfield, M., 2015. Post break-up tectonic inversion across the southwestern Cape of South Africa: new insights from apatite and zircon fission track thermochronometry. Tectonophysics, 654, 30–55.

Williams, A.F., 1932. The Genesis of the Diamond. Ernest Benn Ltd, London, Vol 2, 354 – 636.

Spatiotemporal Sedimentary Facies Variations in the Lower Permian Whitehill Formation, Ecca Group, Karoo Basin

10

Kenneth Chukwuma and Emese M. Bordy

Abstract

The Lower Permian Whitehill Formation in the Karoo Basin is a potential shale gas unit in South Africa. Recharacterizing this heterogeneous formation and explaining the spatiotemporal variations in its geometry, texture, bedding features, composition, and distribution of organic carbon content is necessary, because gas recovery can be strongly influenced by these characteristics of the host rock. Here, we report on these rock property variations and their sedimentological controls in light of recent advances in shale sedimentology by combining field descriptions, petrographic observations and geochemical proxies. We distinguish five sedimentary facies (F1–F5) that suggest changes in the Early Permian depositional conditions from overall low energy in F1 and F2, allowing pelagic snow aggregates to cover the basin floor, to higher energy in F3, F4, and F5, bringing terrestrial detritus via hyperpycnal and diluted mud flows, which possibly originated from summer melting of mountain glaciers in the Cargonian Highlands flanking the northern margin of the Karoo Basin.

Keywords

Karoo basin • Shale gas • Permian • Mud depositional setting • Sedimentary facies

10.1 Introduction

The Lower Permian Whitehill Formation (WHF) has attracted attention from geologists for over a century (e.g., Rogers and Du Toit 1909; Schwarz 1912; Cunningham-Craig 1914) due to the oil shale potential, abundant but low diversity fossil biota and conspicuous white-weathering characteristics of this black, carbonaceous shale unit. Currently, renewed interest in the WHF is due to its perceived shale gas potential (e.g., Decker and Marot 2012; Geel et al. 2013, 2015; Smithard et al. 2015). However, despite a large number of publications on its lithology (e.g., Cole and McLachlan 1991; Visser 1992), sedimentology (e.g., Visser 1992), paleontology (e.g., Oelofsen 1981, 1987) and hydrocarbon potential (e.g., Rowsell and de Swardt 1976; Cole and McLachlan 1991; Geel et al. 2013; Smithard et al. 2015), the WHF remains poorly understood. For instance, while reference is often made to this black, thinly laminated, carbonaceous formation as a typical anoxic facies, no consensus exists on the palaeo-water depths (e.g., Oelofsen 1981, p. 21, 143; Cole and McLachlan 1991, p. 381) or salinity levels (e.g., Faure and Cole 1999 vs. Scheffler et al. 2006). Furthermore, the widely accepted anoxic facies model requires refinement to explain why the WHF contains more siltstone and very fine-grained sandstone than 'black shale' in the northeastern part of the Karoo Basin (e.g., Cole and McLachlan 1991; Werner 2006). Its regional geometry (e.g., thinning from SW to NE) and style of mud sedimentation (e.g., Visser 1992; Werner 2006) also need additional research. The distribution of organic carbon in the formation is uneven both laterally across the basin and vertically within stratigraphic sections (Cole and McLachlan 1991; Geel et al.

K. Chukwuma · E.M. Bordy (✉)
Department of Geological Sciences, University of Cape Town, Cape Town, 7701, South Africa
e-mail: emese.bordy@uct.ac.za

K. Chukwuma
e-mail: chkken003@myuct.ac.za

B. Linol and M.J. de Wit (eds.), *Origin and Evolution of the Cape Mountains and Karoo Basin*,
Regional Geology Reviews, DOI 10.1007/978-3-319-40859-0_10

2013; Smithard et al. 2015). While some areas are enriched in total organic carbon (up to 17 % TOC; Cole and McLachlan 1991), others are organic carbon-lean with less than 1 % TOC. Quantifying the interplay of syn- vs. post-depositional controls (e.g., structural deformation and metamorphism) on the TOC distribution in the WHF on a basinal scale is lacking, with the exception of a few localities that were studied in recent publications (e.g., Geel et al. 2013; Smithard et al. 2015, see also Chaps. 7 and 8 in this book).

Recently, significant hydrocarbon reserves have been associated with 'black shales' globally. This, together with developments in horizontal drilling and multistage fracture stimulation technology have triggered an unprecedented interest in the sedimentology and stratigraphy of these 'black shales' worldwide (e.g., Bohacs et al. 2005; Macquaker et al. 2010; Lazar et al. 2015; Wilson and Schieber 2015), and nationally in the WHF, the singular rock unit with ambient qualities for shale gas exploitation in South Africa. This study aims to: document the variations in the internal composition and primary sedimentary features of the WHF, and to analyze the link between the facies changes and the dynamics of sedimentation in time and space.

10.2 Geological Background

The WHF is part of the Permian Ecca Group, which in turns is part of the Upper Carboniferous to Lower Jurassic Karoo Supergroup. With an estimated thickness ranging between 30 to no more than 100 m, the WHF forms an outcrop belt along the western and southern portion of the Karoo Basin. It has been identified in the subsurface, where it ranges in depth from 1600 to 3000 m below surface, and thus the formation occupies an area of $\sim$235,000 km^2 in the western half of the basin (inset Fig. 10.1; Visser 1992; Tankard et al. 2012). Stratigraphically, the WHF occurs between the Prince Albert and Collingham Formations in the south and between the Prince Albert and Tierberg Formations in the west. It is correlated with the upper part of coal-bearing Vryheid Formation in the northeastern part of the basin (Cole and McLachlan 1991; Visser 1992). Based on palynology, litho- and bio stratigraphy, the WHF is also correlated with the Irati Formation in the Paraná Basin of southeastern Brazil (Oelofsen 1987; Chap. 18 in this book). In spite its tuffaceous beds, radiometric dates are not available for the WHF in South Africa. Absolute dates from the WHF correlative units are 280.5 $\pm$ 2.1 Ma in Namibia (Werner 2006) and 278.4 $\pm$ 2.2 Ma in Brazil (Santos et al. 2006), and therefore the WHF in South Africa is inferred to be Kungurian in age.

At outcrop-scale, the white-weathering formation is distinguished from the dark to olive gray lithologies of the under- and overlying Prince Albert and Collingham/Tierberg Formations. When freshly exposed, the WHF is predominantly black (Fig. 10.2), thinly laminated shale with vertical and lateral variations in silt content (Oelofsen 1981, 1987; Cole and McLachlan 1991; Visser 1992). Nodules of carbonate, pyrite and chert, evaporites (e.g., gypsum, halite), as well as pale gray to yellowish thin tuffaceous beds are also present (e.g., McLachlan and Anderson 1977, 1979; Oelofsen 1981, 1987; Cole and McLachlan 1991; Visser 1992; Faure and Cole 1999; Werner 2006). Visser (1992) subdivided the WHF into SW deep- and NE shallow-water facies mainly based on the distribution of post-depositional, diagenetic sedimentary features (e.g., chert) and not on the primary characteristics of the sedimentary facies such as lithology, texture, suite of sedimentary structures, geometry, fossils (e.g., Tucker 2011).

The lower part of the WHF is largely unfossiliferous, whereas the upper half hosts a highly diverse fossil assemblage comprising aquatic mesosaurid reptiles, palaeoniscid fish, crustaceans, insects, as well as terrestrial plant debris (e.g., palynomorphs, gymnosperms wood, *Glossopteris* sp. leaves, club mosses—McLachlan and Anderson 1973, 1977; Oelofsen 1981; Cole and McLachlan 1991). Ichnofossils, in addition to unidentified bioturbation, include arthropod tracks, fish swimming traces and coprolites (Oelofsen 1981, 1987). The stratigraphic distribution of the fossils as well as carbon and pyrite prompted McLachlan and Anderson (1977) and Oelofsen (1981, 1987) to argue for a stratified Early Permian water body in the Karoo Basin (see also Chap. 11 in this book), where the anoxic reducing bottom conditions contrasted the oxygenated surface conditions that supported free swimming, benthic and platonic organisms. Paleontological evidence for a marine affinity of the WHF fossils is lacking (e.g., McLachlan and Anderson 1973, 1979; Faure and Cole 1999).

10.3 Methods

WHF outcrops were studied to capture the facies heterogeneity, which can be detected in the texture, fabric and bedding features as well as composition. The exposed WHF strata were logged sedimentologically, photographed, and sampled along the entire outcrop belt, except in the easternmost part of the Eastern Cape where the WHF is very poorly exposed (Fig. 10.1). The microtexture, mineralogy of the matrix fraction and cement were established using standard petrographic investigations and Carl Zeiss MERLIN and EVO high resolution field emission scanning electron microscope (FE-SEM) with nanoscale and micro- and cryo-EDS operated mainly in back scatter and cathode luminescence modes between 20 and 30 kV at 9–11 mm working distance. Total organic carbon content was measured with LECO CS244 carbon analyzer at the Indian Institute of Technology in Bombay.

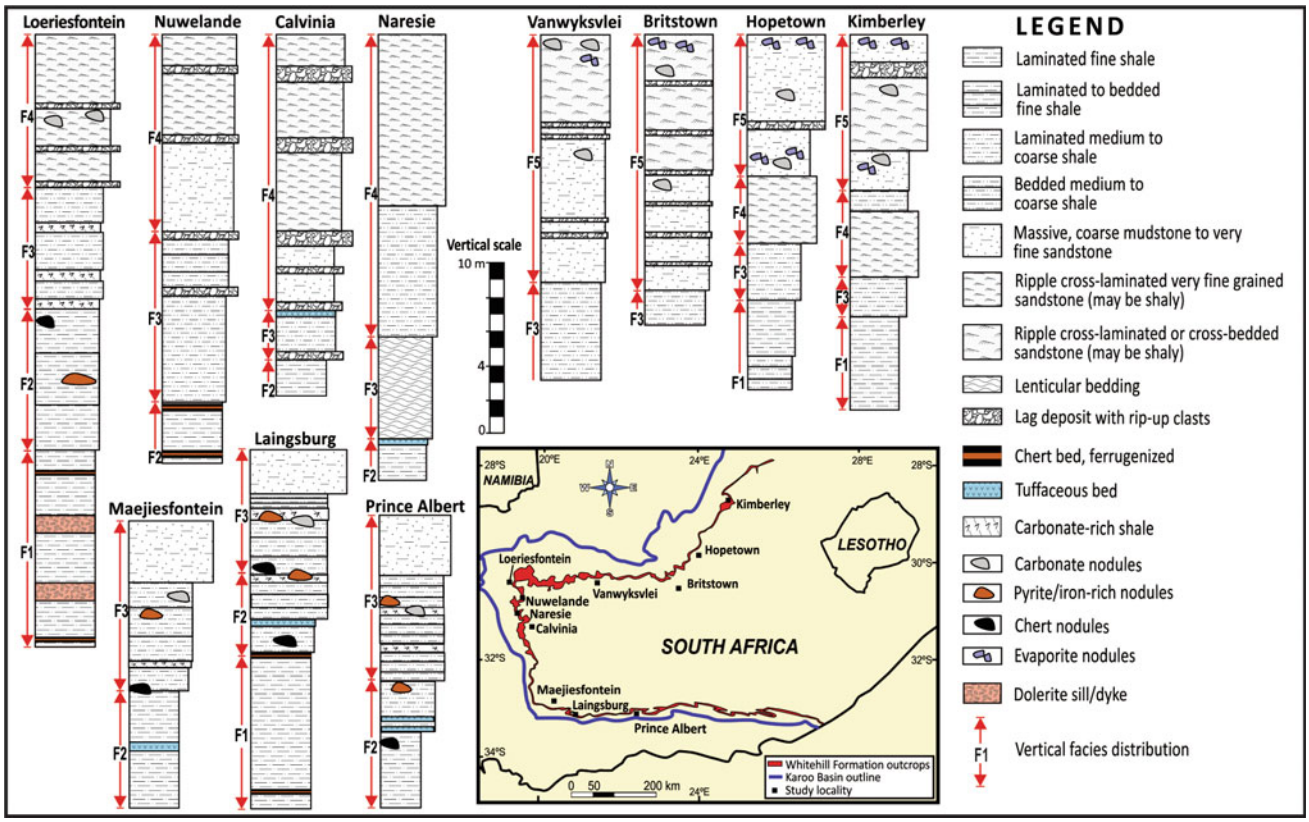

Fig. 10.1 Simplified sedimentological logs of the WHF measured in selected outcrops in the western Karoo Basin. Thicknesses reported are not the maximum thickness of the formation at those localities, but the maximum exposed thickness of the facies at each locality. The base of F1 and top of F5 when exposed are either sharp or gradational. For log locations refer to the inset map which also shows the areal distribution of the WHF outcrops in the basin. Note that F4 and F5 are only found along the northern margin of the WHF outcrop area

10.4 Observations

Five distinctive facies (F1–F5) of the WHF can be recognized (Table 10.1) that include fine- to coarse-grained shales (*sensu* Lazar et al. 2015) with a variety of primary sedimentary features, which are mainly fine laminations, very thin and thin (1–5 cm) beds in F1 and F2 that give way to an upward increasing abundance horizontal- to low-angle cross-laminations, internal scours, sharp bedding planes, diffuse bedding, as well as, normal graded beds (from coarse silt to clay) in F3, F4 and F5 (Fig. 10.4, Table 10.1). Ripple cross-laminations with forest dip directions ranging between 44° and 78° (E–NE) were measured in F4 and F5 between Calvinia and Loeriesfontein (Figs. 10.1 and 10.4). Body fossils of mesosaurid reptiles, palaeoniscoid fish, plant fragments, fish trails were observed in F3, F4 and F5 between Calvinia and Vanwyksvlei (Figs. 10.1 and 10.2). The southern KB outcrops only yielded some poorly preserved plant fragments in F3 (e.g., east of Prince Albert; Fig. 10.2). In contrast the facies contain variable quantities of organic carbon that ranges from 0.1 to 16.5 wt% in F5 and F2, respectively. Dark colored chert and carbonate concretions (up to 3 m in diameter) and beds (up to 1.4 m) are common in the lower part of the formation, particularly in F2, and light gray to yellowish carbonate and evaporite concretions are mainly present in F4 and F5. Yellowish-weathering thin tuffaceous beds occur throughout the formation (e.g., an 8 cm layer was recorded in F3 near Calvinia; Fig. 10.1). Primary fabrics are occasionally overprinted by secondary alteration features (e.g., mineral filled cracks). In the Tankwa area, the shales are gently deformed and dip southward between 2° and 6°, whereas between Calvinia and Loeriesfontein the dip is 2°–3° northward. Between Vanwyksvlei and Hopetown, the shales dip southward at 2° and 7°. In contrast to the northern study sites, bed thickness and orientation are harder to define in the south due to structural deformation associated with the Cape orogeny (Fig. 10.1).

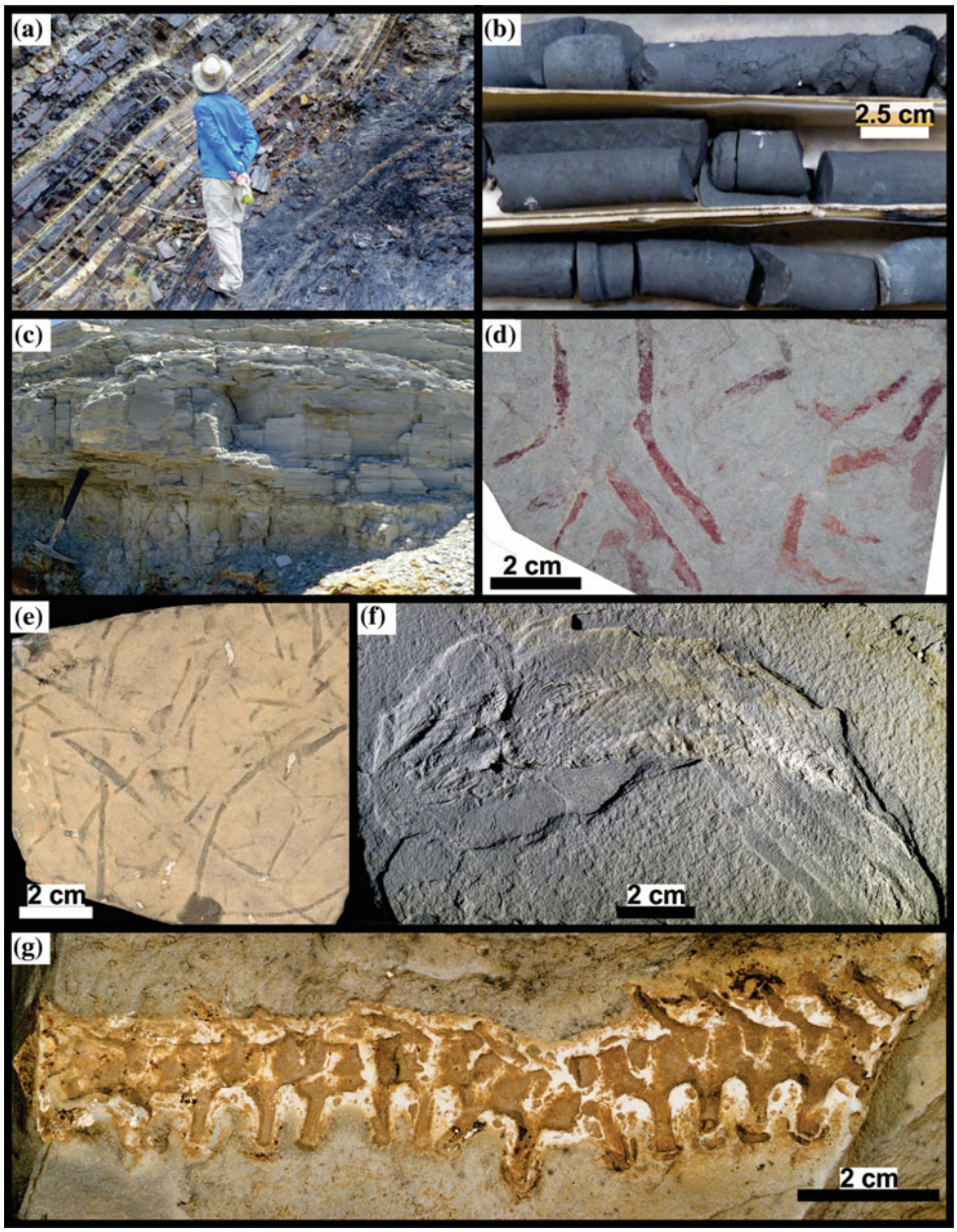

Fig. 10.2 **a** Outcrop image of the crisp contact between Whitehill and Collingham Formations (on the *right* and *left*, respectively) near Laingsburg. **b** Freshly drilled outcrop samples obtained with a portable hand drill fitted with a 400 × 25 mm drill barrel. Core diameter is 2.5 cm. **c** Sharp-based and normally graded light gray to white shales and very fine-grained sandstones are common in the northern outcrop area (F5). Hammer is 31.3 cm long. **d** Plant fragments in middle WHF (near Prince Albert; F3). **e** Trace fossil are common in the in middle WHF (near Nuwelande; F3). **f** Body fossil of palaeoniscid fish found in F4 near Nuwelande. **g** Body fossil of mesosaurid reptile (dorsal spine) found in F4 near of Calvinia. Mesosaurids were endemic to SW Gondwana in the Early Permian

10.5 Discussion

10.5.1 Depositional Processes

Dominance of biogenic detritus, thin laminations and close association between clay fraction and organic matter (OM—e.g., flattened algal macerals; Fig. 10.2) packaged as organo-minerallic aggregates ('org-min-a') in F1 and F2 indicate that these sediments were: (1) produced in an overall low energy water body away from the reach of coarse clastic sedimentary detritus and (2) settled out of buoyant suspensions in form of pelagic snow aggregates (e.g., Fowler and Knauer 1986; Bohacs et al. 2005; Macquaker et al. 2010). Mud-size particles do not only settle out of suspension individually, but often clump together due to physical coagulation and/or zooplankton-mediated aggregation (e.g., Nittrouer et al. 1986; Alldredge and Gotschalk 1990). In the latter, the organo-minerallic aggregates are glued together by extra-cellular muco-polysaccharides and exopolymeric secretions of plankton (e.g., Fowler and Knauer 1986; Faure and Cole 1999).

The disseminated fine-grained (<5 μm) pyrite framboids in F1 (Fig. 10.2) suggests that this facies may have been deposited on the basin floor where sulfidic and anoxic conditions existed (Demaison and Moore 1980; Wignall and Newton 1998; Lazar et al. 2015). In contrast, pyrite grains aligning

Table 10.1 Summary of the sedimentary facies in the Whitehill Formation (also see Figs. 10.1, 10.2, 10.3 and 10.4). Fossils content is based on observations in this study and reports in Oelofsen (1981)

Facies code	Facies description	Sedimentary process interpretation
F1	Thinly and horizontally laminated (~5 mm-thick), black, carbonaceous, fine shale with an average TOC of 4.4–7.8 wt%; contains flattened organo-minerallic aggregates (oma), amorphous organic carbon, fecal pellet-like materials, disseminated fine-grained (<5 μm) pyrite framboids/concretions, and minor silt-size quartz with some pyrite-filled hair cracks; few grains of barite; the matrix is clay (illite-smectite), amorphous organic carbon (aoc), chert/quartz. No fossils found or reported to date	High bioproductivity; suspension settling of pelagic snow on the basin floor at the anoxic and sulfidic water–sediment interface
F2	Laminated to bedded, black, splintery argillaceous fine shale with a maximum TOC of ~16.5 wt%; Contains silt-size quartz, clay, aoc, fecal pellets, algal maceral and pyrite majorly aligned along bedding planes; Few mm to 10 m diameter diagenetic nodules common in upper section; the matrix is clay, carbonate, aoc, quartz. No fossils found or reported to date	Suspension settling of pelagic snow under intermittent anoxic and sulfidic iron-poor sediment-water conditions. Initial high bioproductivity was interrupted, resulted in early cementation and remineralization
F3	Sharp-based, horizontally laminated to bedded occasionally burrowed, diminutive normally graded, dark gray siliceous-calcareous-argillaceous medium shale; Contains silt-size quartz, clay, aoc, fecal pellets and lags of rip-up shale particles, with an average TOC of 1.6 wt%; the matrix is clay, quartz, carbonate. Trace fossils are common (include: fish swimming traces, arthropod tracks, horizontal and interconnecting burrows); fragmentary plant fossil east of Prince Albert	Erosion and redeposition of muddy substrate by currents in sustained bed-load transport; incipient oxic bottom waters
F4	Horizontal and ripple cross-lamination, diffused bedding, internal scouring, gray siliceous medium shale with continuous nonparallel down-lapping (concave-up) geometries and triplet features; average TOC: 1.01 wt%; the matrix is quartz, carbonate ≫ clay. Mesosaurid reptiles and palaeoniscoid fish are abundant in the lower part of F4	Progressive dominance of waning wave-enhanced sediment gravity flows and bed-load dominated currents; often transient oxic bottom waters, especially in the upper part of F4
F5	Horizontal and ripple cross-lamination to massive, diffused bedding, light gray siliceous coarse-grained shale with continuous nonparallel down-lapping (concave-up) geometries and triplet features; thicker beds than in F4; average TOC: 0.58 wt%; the matrix is quartz and carbonate. Palaeoniscoid fish, and in the upper part, pygocephalomorphic crustaceans (e.g., *Notocaris tapscotti*) are abundant	Rapid, *en masse* deposition of sand and silt in hyperpycnal flows and bed-load dominated currents; often fully oxygenated water body

bedding planes of F2 indicate presence of free oxygen at the sediment–water interface (e.g., Lazar et al. 2015). The intergranular pores-filling clays and quartz in F1 and F2 (Fig. 10.2) indicate their diagenetic origin (e.g., Macquaker et al. 2014; Lazar et al. 2015). The diagenetic nodules with well-developed carbonate cement, and pre-compaction microcrystalline pyrite cement in F2 (Fig. 10.2) further attests that the pore water contained microbial reduced sulfate whose solutes filled the pores prior to compaction and initiated the growth of nodules, following a pause in sedimentation(e.g., Dean and McArthur 1989; Macquaker and Gawthorpe 1993). Furthermore, the change from thin lamination of F1 to alternation of laminated and non-laminated beds in F2 (Figs. 10.1 and 10.3) suggest disruption to the anoxia during F1.

The marked increase in the quantity of coarse-grained silt and very fine-grained sand particles from F3 to F5, together with an upward increasing abundance of horizontal- to cross-laminations, internal scours, sharp bedding planes, diffuse bedding, as well as, normal graded beds (Figs. 10.1, 10.2, 10.3 and 10.4; Table 10.1) are interpreted as products of sustained lateral sediment transport by turbulent flows with waxing and waning current energies (Macquaker et al. 2010; Wilson and Schieber 2015). The increasingly higher energy levels during deposition of F3–F5 are also attested by several shale layers with subrounded to subangular rip-up particles with diameters up to 1.1 mm (Fig. 10.1). These intraformational shale particles (Fig. 10.3g, h) may also be used as an indirect evidence for the above postulated pause

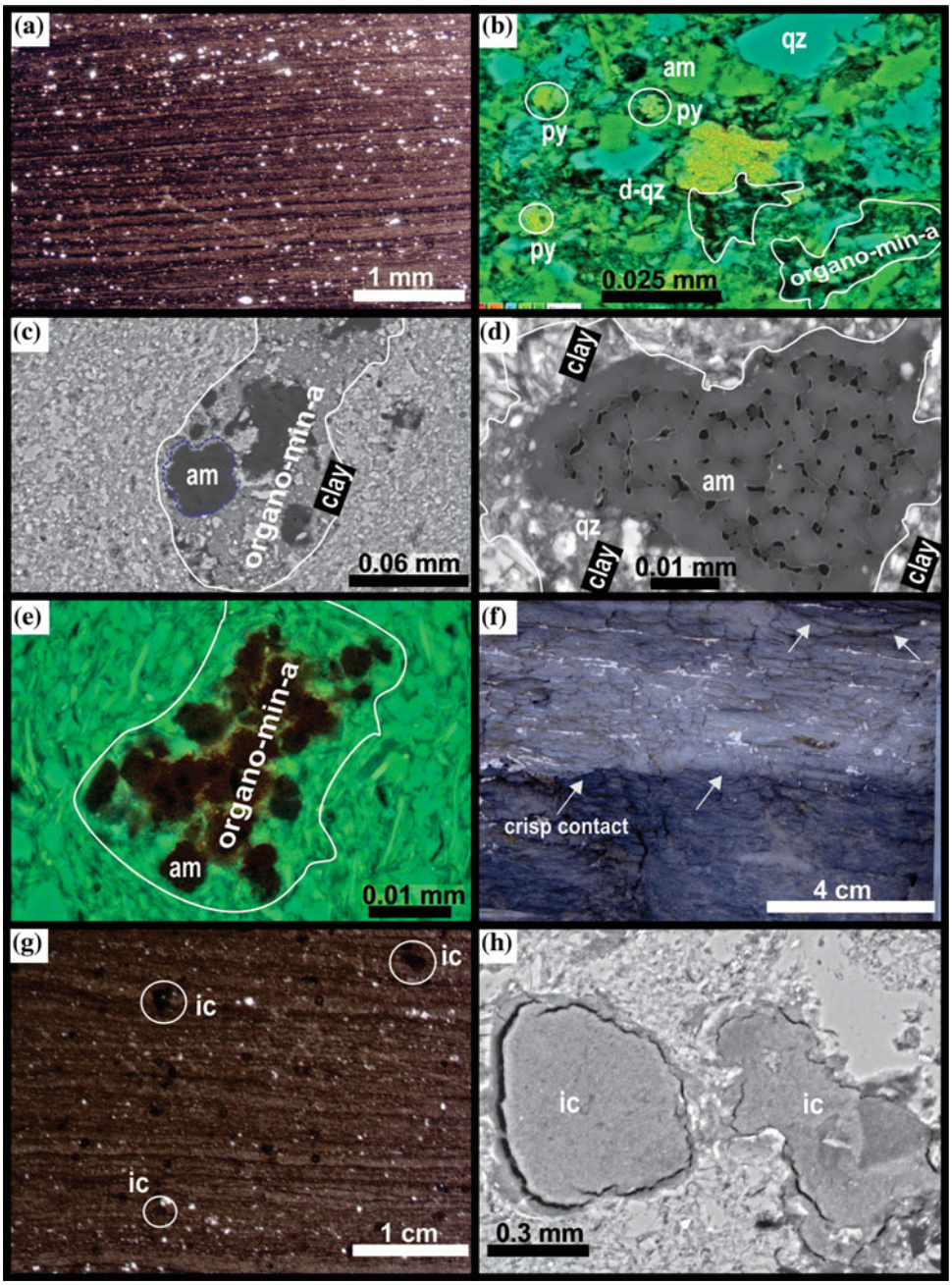

Fig. 10.3 Micro-sedimentary features (structure, fabric, texture) of F1, F2 and F3 in the WHF. **F1 a** Optical photomicrograph of uniform, continuous horizontal laminations. **b** Back-scattered electron photomicrograph of disseminated pyrite (py) and the association of algal macerals (am), pellets, and clay that form organo-minerallic aggregates (org-min-a—*white outlines*). Diagenetic quartz (d-qz) infills intergranular pores. Organic carbon, pre-compaction microcrystalline carbonate and pyrite cement indicate that pore waters controlled microbial reduction. The sulfate, likely derived from the water column, infilled the sediment pores pre-compaction and/or during a pause in sedimentation (e.g., Dean and McArthur 1989; Macquaker and Gawthorpe 1993). **F2 c** Back-scattered electron photomicrograph of close knitting between algal macerals and clays ('org-min-a'—*white outline*). **d** Close-up of features in the am shown in **c**. The 'org-min-a' are larger in F2 compared to F1. Pores are filled by quartz and clay. **e** Close-up of the algal macerals (am) and organo-minerallic aggregate (org-min-a—*white outlines*). **F3 f** Horizontally laminated to bedded, medium shales with crisp contacts (arrows). **g** Optical photomicrograph of intraclasts (ic) and vertical variability in lamina thickness. **h** Back-scattered electron photomicrograph of G showing the close-up of the subrounded to subangular intraclasts (ic), which are rip-up shale particles with diameters up to 1.1 mm

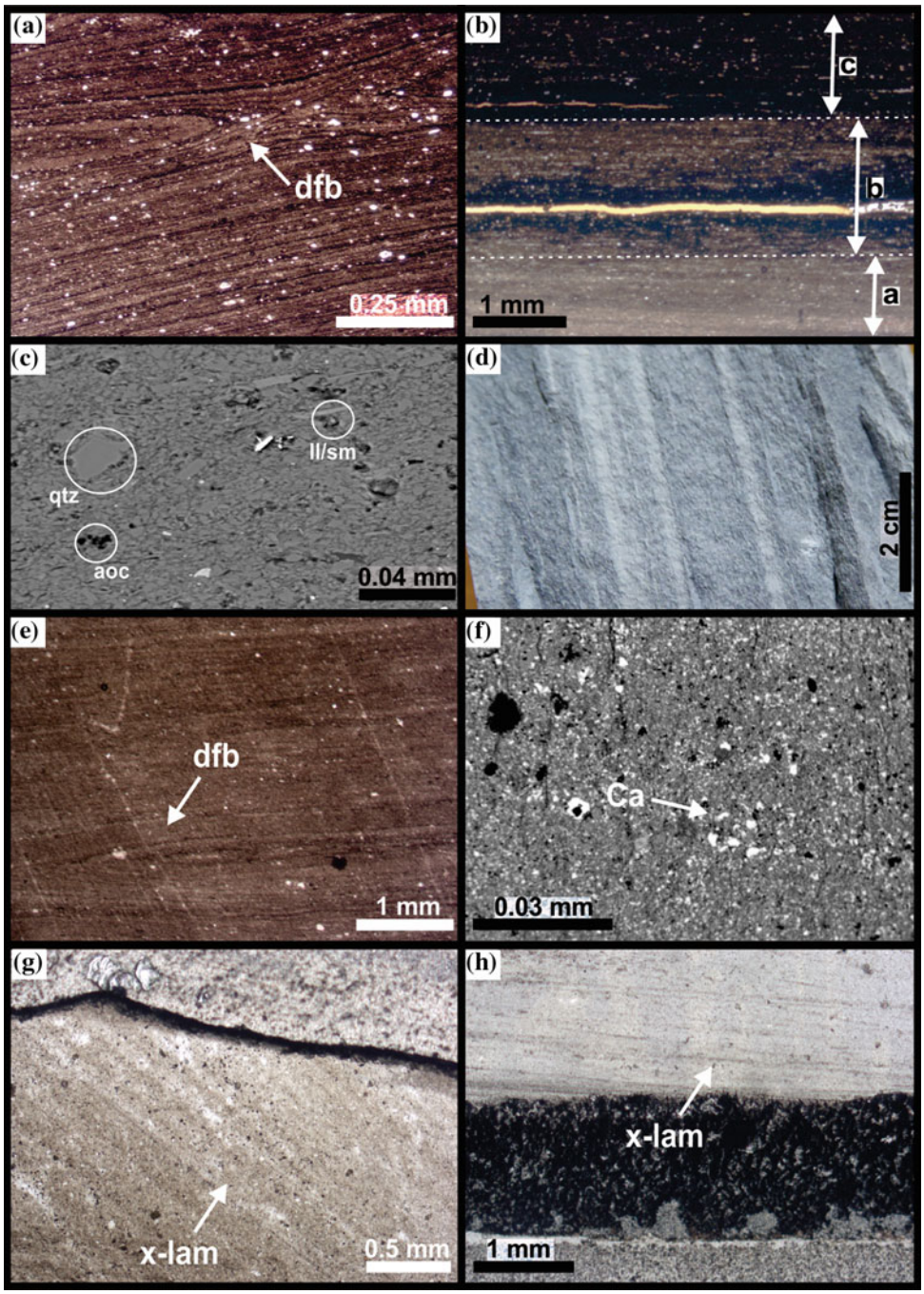

Fig. 10.4 Micro-sedimentary features (structure, fabric, texture) of F4 and F5 in the WHF. **F4 a** Optical photomicrographs of diffused bedding (dfb) and concave upward geometries. **b** Optical photomicrograph of triplet feature. Note the gradual increase in clay content (darker laminae). **c** Back-scattered electron photomicrograph illustrating the dominance of clay and quartz particles. **F5 d** Horizontal interlamination of clay- and silt-rich layers in a shale hand specimen. **e** Optical photomicrographs of diffused bedding (dfb) and concave upward geometries. **f** Back-scattered electron photomicrograph illustrating the grain size and mineral composition (mainly clay and quartz) in **c**. **g** Optical photomicrograph of ripple cross-lamination (x-lam). Note the steep dip angle of the foresets, truncated by an erosion surface. **h** Optical photomicrograph of low-angle ripple cross-lamination (x-lam) in tangential contact with the lower bedding plane

in sedimentation that might have contributed to the consolidation of the previously deposited mud (F1–F2). The medium to coarse shale beds with sharp bases, horizontal and ripple cross-laminations, diminutive normal grading, and diffused bedding in F3–F5 (Figs. 10.1, 10.2, 10.3 and 10.4; Table 10.1), coupled with the higher abundance of trace and body fossils, suggest increasing oxygenation levels and higher clastic/nutrient influx to the basin floor, which were significant changes in sedimentary conditions relative to those lower energy and more anoxic ones that dominated during F1–F2. These interpretations are also supported by the northeast–southwest aligned fossils in F4–F5 and very low amplitude oscillation ripple marks found by Oelofsen (1981, p. 24) near Hopetown, Loeriesfontein and Calvinia. These symmetrical ripple marks recovered by Oelofsen occur within a facies that could correspond to the transition

of F3 and F4. The overall facies descriptions and interpretations presented here are also in line with sedimentological results of Cole and McLachlan (1991).

10.5.2 Orientation of the Basinal Paleo-slope

Palaeoslope of the basin at the time of deposition of the WHF is difficult to establish, because of the monotony of finely laminated shales with palaeocurrent indicators limited to rare cross-laminations, ripple marks and orientation of fossils (i.e,. 47 mesosaurid and 138 pygocephalomorphic crustacean specimens reported in Oelofsen 1981; his Figs. 9 and 10). Sedimentological and taphonomic evidence suggest that the ripples and the northeast–southwest aligned fossils were generated by weak, localized oscillatory flows rather than strong, unidirectional, basinal bottom currents. These localized flow indictors are unsuitable to infer the Early Permian basinal palaeoslope orientation (cf. Tucker 2011). Notwithstanding the lack of reliable primary palaeocurrent indicators in the WHF, the basinal distribution of the F3–F5 (Fig. 10.1) may be linked to a south-southwestward dipping WHF palaeoslope.

10.5.3 Depositional Setting Interpretations

Our results are in line with previous interpretations that suggest stratified and brackish water body across southwest Gondwana during the Kungurian (e.g., McLachlan and Anderson 1973; Faure and Cole 1999; Werner 2006; Flint et al. 2011). During the deposition of facies that are unfossiliferous and have high organic carbon content (F1 and F2), we interpret that the surface waters contained nutrients (e.g., N, Si, P, Fe) that enabled high primary productivity of OM, which was preserved together with fine-grained sediments on the basin floor under reducing (oxygen-depleted) conditions. Sediment-laden underflows subsequently entered the basin along its northern margin, possibly from summer melting of mountain glaciers north of the Karoo Basin (Cargonian Highland; see also Chap. 9 in this book). Consequently, the biogenic constituents produced were diluted by progressively higher input of terrestrial detritus. The contrast between the brackish and freshwater fluids possibly triggered thermohaline currents as the hyperpycnal riverine discharge plunged into the basin floor, eroding and resuspending the muddy substrate. Considering the basinal extent of F3 (Fig. 10.1), bottom hugging currents (diluted mud flows) probably moved the sediment over large distances on relatively low gradient slopes (<0.7°—e.g., Mulder et al. 2003; Bhattacharya and MacEachern 2009). Similar processes and features were observed on modern muddy shelves near river mouths (Friedrichs and Wright 2004), for example, at the mouths of the Yellow (Wright et al. 2001) and Amazon Rivers (Kineke et al. 1996), along the northern California coast (Eel River; Nittrouer et al. 1986; Wright et al. 2001), and in laboratory experiments (e.g., Schieber and Yawar 2009). Our depositional model (Fig. 10.5), which proposes an overall shallowing upwards trend and basinward migration of the shoreline along the southward dipping WHF palaeoslope, is supported by: (1) up-section increase in grain size, thickness, sharp bedding planes, graded intervals, layers with rip-up shale particles; (2) the spatiotemporal distribution of the facies—i.e., the basinal extent of F1–F3 versus the restricted nature of F4 and F5 along the northern margin of the basin (Fig. 10.1); and (3) reduced TOC in F4 and F5.

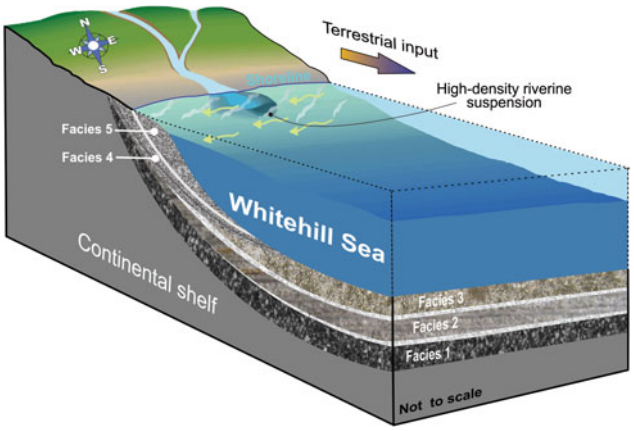

Fig. 10.5 Summary of the depositional model for the WHF showing spatial distribution of the five facies (F1–F5) deposited by diverse sedimentary processes. The near-uniform and basinal extent as well as predominant fine-grained size of F1 and F2 point to a low energy shelfal setting, away from coarse clastic inputs, in the distal parts of a large water body. Increase in grain size and detrital fractions in F3–F5 indicate progradation in a regressing water body. Compositional and textural differences of the facies (Figs. 10.1, 10.2, 10.3 and 10.4; Table 10.1) attest to variable provenance and complex sediment dispersal histories

10.6 Conclusion

Five distinctive facies in WHF reveal that in addition to the quiet settling of suspended particles, more energetic depositional processes were also present in the Karoo Basin during the Early Permian. The WHF facies and their basinal distribution are linked to: (1) primary sediment production within the basin, (2) terrestrial clastic input from the Cargonian Highlands in the north to the basin, and (3) post-depositional alterations. F1 and F2 are interpreted as biologically produced pelagic snow aggregates that were deposited on the basin floor, remote from coarse sediment sources and under anoxic to dysoxic conditions, favorable to preservation of organic carbon, especially in the lower part

of F2. Terrestrial detritus is increasingly more dominant from F3 to F5, and this upward increase in clastic grains is interpreted to be linked to underflows from summer melting of mountain glaciers north of the Karoo Basin that fed the sediment-laden hyperpycnal currents along the northern margin of the basin and mud flows further to south. In summary, the temporal and spatial variations in the internal composition, primary sedimentary structures and distribution of organic matter in the WHF reflect the diversity of sedimentary conditions (e.g., sediment supply, energy levels, mode of transport) in time and space within the Early Permian Karoo Basin.

Acknowledgments We would like to give special thanks to our friends and colleagues Francisco Paiva and Sanda Spelman for field assistance. We thank Nicholas Laidler for his invaluable lab assistance. We also gratefully acknowledge the very constructive reviews by Hans-Martin Schultz, Maarten de Wit and Bastien Linol. The financial support of the Faculty of Science at the University of Cape Town toward this research is hereby acknowledged. Opinions expressed and conclusions arrived at are those of the authors and are not necessarily to be attributed to the UCT.

References

Alldredge AL, Gotschalk CC (1990) The relative contribution of marine snow of different origins to biological processes in coastal waters. Cont Shelf Res 10:41–58

Bhattacharya JP, MacEachern JA (2009) Hyperpycnal rivers and prodeltaic shelves in the Cretaceous seaway of North America. J Sed Res 79:184–209

Bohacs KM, Grabowski GJ, Carroll AR, Mankiewicz PJ, Miskellgerhardt KJ, Schwalbach JR, Wegner MB, Simo JA (2005) Production, destruction, and dilution: the many paths to source-rock development. In Harris NB (ed) The deposition of organic carbon-rich sediments: SEPM Spec Pub 82, 61–101

Cole DI, McLachlan IR (1991) Oil potential of the Permian WHF Shale Formation in the main Karoo Basin, South Africa. In: Ulbrich H, Rocha-Campos AC (eds), Gondwana Seven Proceedings, pp 379–390

Cunningham-Craig EH 1914 Report on the petroleum prospects in the Union of South Africa. The Government Printing and Stationery Office, Pretoria, UG3, pp 28

Dean WE, McArthur MA (1989) Iron-sulfur-carbon relationships in organic-carbon-rich sequences: Cretaceous western seaway. Am J Sci 289:708–743

Decker J, Marot J (2012) Investigation of hydraulic fracturing in the Karoo of South Africa. Annexure A, Resource Assessment, Petroleum Agency SA. Available at: http://www.dmr.gov.za/publications/viewdownload/182/854.html

Demaison GJ, Moore GT (1980) Anoxic environments and oil source bed genesis. AAPG Bulletin 64:1179–1209

Faure K, Cole D (1999) Geochemical evidence for lacustrine microbial blooms in the vast Permian main Karoo, Parana, Falkland Islands and Huab basins of southwestern Gondwana. Palaeogeography, Palaeoclimatology, Palaeoecology 152:189–213

Flint SS, Hodgson D, Sprague AR, Brunt RL, Van der Marwe WC, Figueiredo J, Prélat A, Box D, Di Celma C, Kavanagh JP (2011) Depositional architecture and sequence stratigraphy of the Karoo basin floor to shelf succession, Laingsburg depocentre, South Africa. Mar Pet Geo 28:658–674

Fowler SW, Knauer GA (1986) Role of large particles in the transport of elements and organic compounds through the oceanic water column. Prog Oceanogr 16:147–194

Friedrichs CT, Wright LD (2004) Gravity-driven sediment transport on the continental shelf: implications for equilibrium profiles near river mouths. Coast Eng 51:795–811

Geel C, Schulz H-M, Booth P, de Wit M, Horsfield B (2013) Shale gas characteristics of Permian black shales in South Africa: results from recent drilling in the Ecca Group Eastern Cape. Energy Procedia 40:256–265

Geel C, de Wit M, Booth P, Schulz H-M, Horsfield B (2015) Palaeo-environment, diagenesis and characteristics of Permian black shales in the lower Karoo Supergroup flanking the Cape Fold Belt near Jansenville, Eastern Cape, South Africa: Implications for the shale gas potential of the Karoo Basin. SAJG 118:248–274

Kineke GC, Sternberg RW, Trowbridge JH, Geyser WR (1996) Fluidmud processes on the Amazon continental shelf. Cont Shelf Res 16:667–696

Lazar OR, Bohacs KM, Macquaker JHS, Schieber J, Demko TM (2015) Capturing key attributes of fine-grained sedimentary rocks in outcrops, cores, and thin sections: nomenclature and description guidelines. J Sed Res 85:230–246

Macquaker JHS, Gawthorpe RL (1993) Mudstone lithofacies in the Kimmeridge Clay Formation, Wessex Basin, Southern England: implications for the origin and controls of the distribution of mudstones. J Sediment Petrol 63:1129–1143

Macquaker, JHS, Keller MA, Davies SJ (2010) Algal blooms and "marine snow": mechanisms that enhance preservation of organic carbon in ancient fine-grained sediments. J Sed Res 80:934–942.

Macquaker, JHS,Taylor KG, Keller MA, Polya D (2014) Compositional controls on early diagenetic pathways in fine-grained sedimentary rocks: Implications for predicting unconventional reservoir attributes of mudstones. AAPG Bull 98:587–603

McLachlan IR, Anderson AM (1973) A review of the evidence for marine conditions in Southern Africa during Dwyka times. Palaeontol Afr 15:37–64.

McLachlan IR, Anderson AM (1977) Carbonates, "stromatolites" and tuffs in the lower Permian White Band Formation. SAJG 73:92–94

McLachlan IR, Anderson AM (1979) The oil-shale potential of the Early Permian White Band Formation in Southern Africa. Geol Soc S Afr Spec Publ 6:83–86

Mulder T, Syvitski JPM, Migeon S, Faugères, JC, Savoye B (2003) Marine hyperpycnal flows: initiation, behavior and related deposits: a review. Mar Pet Geo 20:861–882. doi:10.1016/j.marpetgeo.2003.01.003

Nittrouer CA, Curtin TB, DeMaster DJ (1986) Concentration and flux of suspended sediment on the Amazon continental shelf. Cont Shelf Res 6:151–174

Oelofsen BW (1981) An anatomical and systematic study of the Family Mesosauridae (Reptilia: *Proganosauria*) with special reference to its associated fauna and palaeoecological environment in the WHF Sea. Unpublished PhD thesis, University of Stellenbosch, South Africa, pp 259

Oelofsen BW (1987) The biostratigraphy and fossils of the Whitehill and Irati Shale Formations of the Karoo and Parana Basins. In: McKenzie GD (ed), Gondwana Six Proceedings, pp 131–138

Rogers, A. W, Du Toit, A. L (1909) An introduction to the Geology of Cape Colony. Longmans, Green and Co. New York, Bombay, pp 491

Rowsell DM, de Swardt AMJ (1976) Diagenesis in Cape and Karroo sediments, South Africa, and its bearing on their hydrocarbon potential. Trans Geol Soc S Africa 79:81–145

Santos RV, Souza PA, Souza de Alvarenga CJ, Dantas EL, Pimentel MM, Gouveia de Oliveira C, Medeiros de Araújo L (2006) Shrimp U–Pb zircon dating and palynology of bentonitic layers from the Permian Irati Formation, Paraná Basin, Brazil. Gondwana Res 9:456–463

Schieber J, Yawar Z (2009) A new twist on mud deposition: mud ripples in experiment and rock record. The Sed Record 7:4–8

Smithard T, Bordy EM, Reid D (2015) The effect of dolerite intrusions on the hydrocarbon potential of the lower Permian WHF Formation (Karoo Supergroup) in South Africa and southern Namibia: A preliminary study. SAJG 118:489–510

Scheffler K, Buehmann D, Schwark L (2006) Analysis of late Palaeozoic glacial to postglacial sedimentary successions in South Africa by geochemical proxies - Response to climate evolution and sedimentary environment. Palaeogeog palaeoclim palaeoecol 240: 184–203

Swartz EHL (1912) South African Geology. Blackie and Son Ltd, London, Glasgow, Bombay, pp 200

Tankard A, Welsink H, Aukes P, Neweighton R, Stettler E (2012) Geodynamic interpretation of the Cape and Karoo basins, South Africa. In: Roberts, D.G, Bally, A.W (Editors), Regional Geology and Tectonics: Phanerozoic Passive Margins, Cratonic Basins and Global Tectonic Maps. Elsevier, U.K, pp 869–945

Tucker ME (2011) Sedimentary rocks in the field; A practical guide. Blackwell, Oxford, pp 275

Visser JNJ (1992) Deposition of the Early to Late Permian Whitehill Formation during a sea-level highstand in a juvenile foreland basin. SAJG 95:181–193

Werner M (2006) The stratigraphy, sedimentology and age of the Late Palaeozoic Mesosaurus Inland Sea, SW-Gondwana: new implications from studies on sediments and altered pyroclastic layers of the Dwyka and Ecca Group (lower Karoo Supergroup) in southern Namibia. Unpublished PhD Thesis, University of Würzburg, Germany, pp 428

Wignall PB, Newton R (1998) Pyrite framboid diameter as a measure of oxygen deficiency in ancient mudrocks. Am J Sci 298:537–552

Wilson RD, Schieber J (2015) Sedimentary facies and depositional environment of the Middle Devonian Geneseo Formation of New York, USA. J Sed Res 85:1393–1415

Wright LD, Friedrichs CT, Kim SC, Scully ME (2001) Effects of ambient currents and waves on gravity-driven sediment transport on continental shelves. Mar Geol 175:25–45

11 Is the Postglacial History of the Baltic Sea an Appropriate Analogue for the Formation of Black Shales in the Lower Ecca Group (Early Permian) of the Karoo Basin, South Africa?

Hans-Martin Schulz, Naledi Chere, Claire Geel, Peter Booth, and Maarten J. de Wit

Abstract

The Early Permian black shales of the Prince Albert and Whitehill Formations (lower Ecca Group) of the Karoo Basin were deposited in the immediate aftermath of the Carboniferous glaciation across Gondwana. Their preserved geochemical and mineralogical signals indicate that organic carbon production and preservation changed in time and space due to variations in marine incursions into a fresh water lake. We propose that the Post-Pleistocene glaciation history of the Baltic Sea of northern Europe provides a modern analogue for the deposition of TOC-enriched fine-grained sediments of the lower Ecca Group. The low sulphur contents of the Prince Albert Formation reflects deposition in a water body influenced by melting water, at least in the lower part. In contrast, the depositional environment of the TOC-rich Whitehill Formation reflects processes that can be compared with those of deep basins in the subrecent Baltic Sea, where the preservation of organic carbon in the sediments is controlled by a stable water stratification comprising anoxic bottom water, with high total dissolved solids, overlain by lighter freshwater with high bio-productivity at surface.

Keywords

Black shale • Organic carbon • Early permian • Karoo basin • Deglaciation

11.1 Introduction

Melt water has a direct influence on the deposition of muds rich in organic matter. Strong continental run-off of cold and nutrient-poor water masses controls oceanic circulation patterns (e.g. Fichot et al. 2013) and was often a key factor for black shale deposition during Earth history (Lüning et al. 2000). Today some of these black shales host significant shale gas resources, e.g. the Lower Palaeozoic 'Hot shales' in northern Africa (Algeria) and possibly Upper Palaeozoic (Karoo) black shales in sub-Saharan Africa.

Around 4.5–5 million km^2 of sedimentary basins of southwest Gondwana host black shales of the Lower Permian Prince Albert and Whitehill Formations (in South Africa), and their equivalent formations, e.g. in Brazil, and possibly the DR Congo (Linol et al. 2015), indicating similar depositional conditions on a continental scale (Johnson et al. 1997). Here we explore how melting during the Early Permian deglaciation and later processes may have controlled organic matter-rich mud deposition in the Karoo Basin, based on comparison with the Quaternary analogue of the Baltic Sea (Fig. 11.1).

H.-M. Schulz (✉)
Helmholtz Centre Potsdam—GFZ German Research Centre for Geosciences, Telegrafenberg, 14473 Potsdam, Germany
e-mail: schulzhm@gfz-potsdam.de

N. Chere · P. Booth · M.J. de Wit
AEON-ESSRI and Geosciences, Nelson Mandela Metropolitan University, Port Elizabeth, 6031, South Africa

C. Geel
Geosciences, University of Cape Town, Cape Town, 7700, South Africa

B. Linol and M.J. de Wit (eds.), *Origin and Evolution of the Cape Mountains and Karoo Basin*, Regional Geology Reviews, DOI 10.1007/978-3-319-40859-0_11

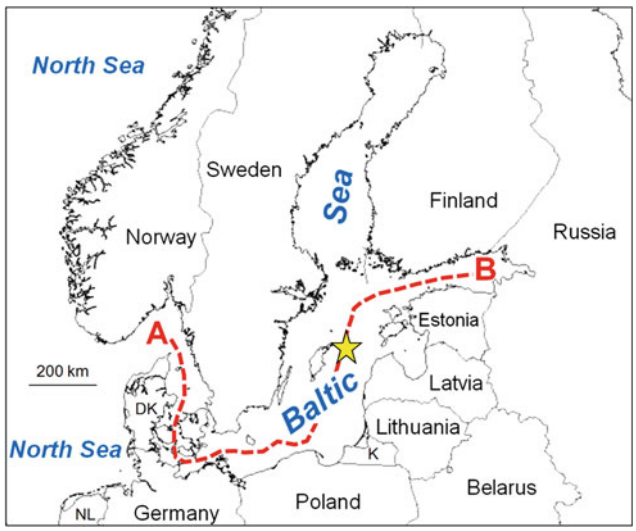

Fig. 11.1 Geographical overview of the Baltic Sea region. *Yellow star symbol* indicates the location of the Eastern Gotland basin

11.2 Melt Water Control on Black Shale Deposition

11.2.1 A Brief Review

The lateral and vertical variability of thickness, lithology, mineralogy, geochemistry, and total organic carbon (TOC) content, etc., in black shale reflects changes in the depositional environment, and stores a wealth of information about palaeoclimate and palaeoceanography. Whilst such signals are often overprinted by diagenetic processes during burial, they can still be resolved using modern analytical methods. The analysis of the link between past climates and unconventional hydrocarbons in shale leads to the conclusion that glacial periods during Earth's history and especially subsequent deglaciation periods have had strong influences on today's large shale gas and shale oil occurrences and resources worldwide, e.g. Formolo et al. (2008) (North America), or Schulz et al. (2015) (northern Europe). Previous work has linked global marine transgressive events with the deposition of many well-known conventional petroleum source rocks (e.g. Craig et al. 2009). Some of these transgressive events have been shown to be related to Palaeozoic deglaciation episodes following the Hirnantian (Late Ordovician) and the Carboniferous–Permian glaciations (Le Heron et al. 2009). Across western North Africa, for example, coupled interactions of retreating ice sheets, glacier melting and marine ingressions during the Late Ordovician-Early Silurian transition (~445–440 Ma) led to widespread black shale deposits that are today thermally mature and enriched in gas that is still retained in nanometre-sized pores (Lüning et al. 2000; Le Heron et al. 2009). These shales are thus a current hot spot for exploration of unconventional gas, especially in Algeria (U.S. Energy Information Administration EIA 2013).

After the Late Carboniferous-Permian glaciation large scale melting occurred progressively southward across central and southern Gondwana as recorded in the then linked Congo-Karoo-Paraná Basins of Africa and South America, ending in the Early Permian. During this time, extensive black organic shales were also deposited in the southern Gondwana basins, such as those preserved as in the lower Ecca Group of the Karoo Basin.

Below, we first summarize the extensively studied geo-bio evolution of the Baltic Sea in northern Europe during the late Quaternary. In a next step, we present data from this short-lived basin that potentially serves as an analogue-baseline from which we compare the depositional, diagenetic, and geochemical signals from the black shales of the lower Ecca Group.

11.2.2 The Late Pleistocene to Holocene History of the Baltic Sea

Following the last glacial maximum at ca. 22 ka BP, deglaciation of the Baltic Basin began 15–17 ka BP and ended at 11–10 ka BP, by which time the entire basin was deglaciated (Andrén et al. 2011). Subsequently, the water body of the Baltic Sea Basin experienced multiple phases with variations in salinity due to changing water exchange with the North Sea marine basin. Thus oceanographic variations were essentially controlled by the gradual melting of the Scandinavian Ice Sheet and related global climate change. This caused highly and locally different glacio-isostatic compensatory movements within the Baltic Basin and led to variations in the exchange with open marine waters of the North Sea (Björck 2008; Andrén et al. 2011). Accordingly, the depositional environments varied in time and space, as did the bio-productivity within the water bodies. Today, the Baltic Sea is characterized by a marked halocline that prevents vertical water exchange and results in anoxic bottom conditions in the deeper subbasins (Fig. 11.2). Below, we summarize the main phases of the evolution of the Baltic Sea during this period (after Andrén et al. 2011 if not otherwise cited) to enable comparison with the black shale formations of Gondwana.

Phase 1: Baltic Ice Lake (16.0–11.7 ka BP)

Melt water filled the Baltic Ice Lake that grew in size due to the northward retreat of the ice sheet. As a result a glacio-lacustrine depositional environment prevailed in which glacially varved clays with dropstones were deposited in

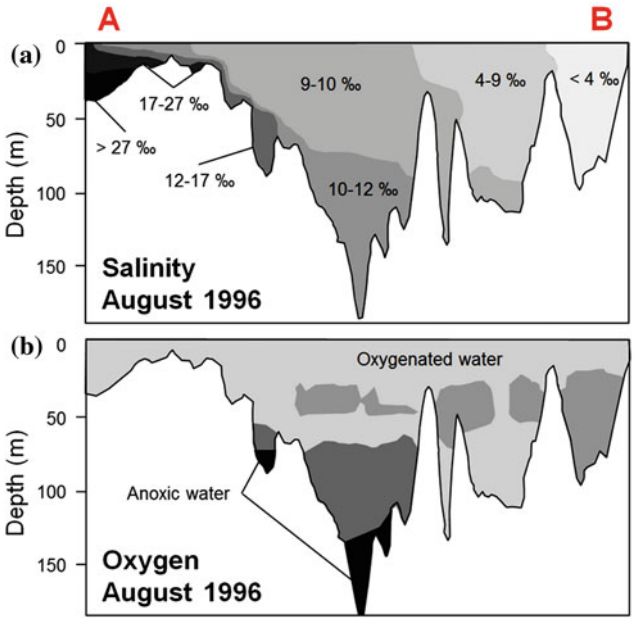

Fig. 11.2 Transect *A* to *B* across the Baltic Sea basin (see Fig. 11.1 for transect location) schematically showing lateral and vertical changes in salinity (**a**) and relative oxygen content (**b**). Data modified after Emeis (2011)

proximal areas of the ice sheet, while homogeneous clay was deposited in more distal areas. Organic productivity was very low, and the Baltic Ice Lake sediments are poor in total organic carbon (Fig. 11.3a). The lake covered areas of the today's southern and central Baltic Sea, which are underlain by subglacial "*Geschiebemergel*" (for comparison note that Dwyka diamictites in the Karoo Basin are glaciomarine or glaciolacustrine; Catuneanu et al. 2005).

Phase 2: Yoldia Sea (11.7–10.7 ka BP)

After the Pleistocene, and during rapid global warming, saline waters from the North Sea entered the Baltic Basin through narrow straits, creating conditions conducive to sedimentation of varves with occasional sulphide layers (distal facies, Fig. 11.3b). As the hinterland was increasingly uplifted isostatically, straits between the Baltic and the North Sea shallowed, preventing saline water from dispersing into the Baltic, and reversing the Yoldia Sea into a freshwater basin. At the end of this stage most of the Baltic Basin was deglaciated, and its outflow became restricted. Sedimentation changed into deposition of varved glacial clay in the Bothnian Bay and into postglacial sedimentation in the central and southern part of the basin.

Phase 3: Ancylus Lake Sea (10.7–9.8 ka BP)

Melt water input with low nutrient contents created an aquatic environment with low bio-productivity (proximal facies, Fig. 11.3b), with well-mixed oxygenated water due to the absence of halocline. The sediments of this large freshwater lake are thus poor in organic carbon, but contain sulphide layers due to potential H_2S diffusion from younger sediments (Sohlenius et al. 2001).

Phase 4: Initial Littorina Sea (9.8–8.5 ka BP)

After the final melting of the Scandinavian ice sheet, occasional saline incursions flooded the Baltic Basin, which by now was at an equivalent level to the North Sea. The organic carbon content of the sediments often rises gradually throughout this stage, because nitrogen-fixing cyanobacteria were abundant.

Phase 5: Littorina Sea (8.5 ka BP–Present)

A rising sea level caused flooding of straits and an estuarine circulation system that promoted stratification and bottom water anoxia in the deep basins (Fig. 11.3c). Organic-rich sediments were deposited as a result of an increase in biological activity, with rising sea surface temperatures of more than 16 °C (Kabel et al. 2012). Incursions of saline, oxygen-rich waters from the North Sea frequently replaced the oxygen depleted deep water (Neumann et al. 1997; Figs. 11.2a, and 11.3c).

In summary, the sediments of the different postglacial stages in the Baltic Sea vary in thickness and lithology. In today's depocentre (e.g. Gotland Basin), the total postglacial sediment column reaches a thickness of between 8.5 m (Harff et al. 2011) to more than 11 m (Emeis 2011).

11.2.3 Comparison with the Lower Permian Ecca Black Shales of the Karoo Basin

By comparison to the Baltic Basin, the Karoo Basin is different in origin, both time-wise and likely in architectural detail. However, the following provides a first order comparison related to fresh (glacial) and marine water interaction, and resulting circulation and deposition.

A sequence of processes similar to the Baltic Sea evolution may have affected the Karoo Basin during and after the melting of the large Gondwana ice caps. New seaways likely opened, during which marine waters possibly flooded areas that were covered by glacigene sediments of the Dwyka Group. During glacial deposition, apparent first marine transgressions occurred during the latest Carboniferous, which are interpreted to represent interglacial periods (Visser 1993, 1996; Bangert et al. 2000; Chap. 9 this book), and during which deposition of organic matter-rich mud occurred (Scheffler et al. 2006). The Dwyka Group is conformably overlain by mudrocks of the Prince Albert Formation and followed by the Whitehill Formation of the lower Ecca Group. However, lateral facies transitions and hiatuses or erosional boundaries exist, and in places the

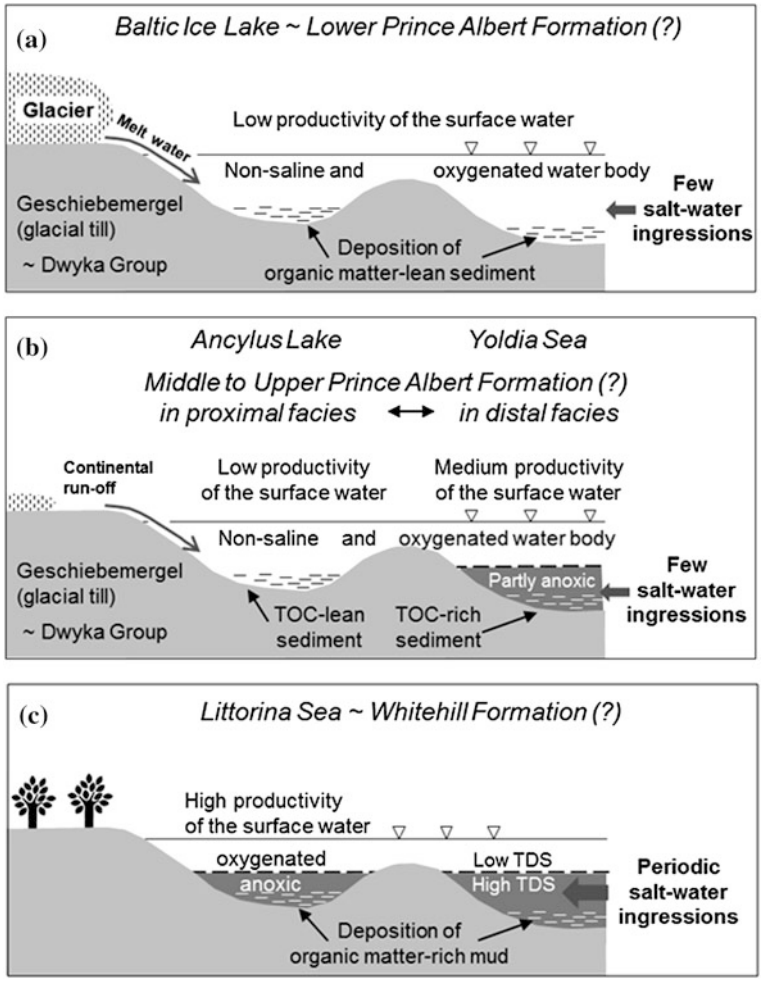

Fig. 11.3 Schematic diagrams showing different stages of the Baltic Sea evolution. **a** Baltic Ice Lake (16–11.7 ka BP). During the melting of glaciers at the end of the Pleistocene, the southern and central Baltic Basin was partly filled by glacial till ("Geschiebemergel" in German is equivalent of diamictite). Processes creating such sediments in the Baltic resemble those in the Karoo Basin during deposition of the diamictites of the Dwyka Group (cf. "valley" and "shelf" facies; Visser 1996). In the Baltic Sea low nutrient contents in the melt water led to deposition of organically lean sediments, resembling those of the lower Prince Albert Formation. **b** Lateral variations of the middle and upper part of the Prince Albert Formation in terms of thickness, lithology, TOC content and pyrite content can be explained by the lateral extension of saline water influxes that controlled regionally different water stratification. This is observed in Baltic Sea stages of the Yoldia Sea (11.7–10.7 ka BP) and the Ancylus Lake Sea 10.7–9.8 ka BP. **c** Present-day Baltic Sea since ~9.8 ka BP. Periodic saltwater incursions from the North Sea fill the deep basins of the Baltic Basin causing stable water stratification. North Sea water masses with higher content of total dissolved solids (TDS) fill the deep basins periodically, and are overlain by lighter Baltic Sea water with lower TDS contents. The Karoo Basin during sedimentation of the TOC-rich Whitehill Formation resembles this oceanographic environment in the Baltic Sea. However, the Baltic Sea history is complex, and these three very schematic diagrams are used only to illustrate the most basic stages to explain times of TOC-lean or TOC-rich deposition in the Karoo Basin

Prince Albert Formation has an unconformable contact where the Dwyka deposits are missing (Isbell et al. 2008). The sediments of the Prince Albert Formation regionally coarsen northward, and are overlain by the TOC-rich Whitehill Formation in the western and central parts of the basin (Visser 1993; Cole et al. 1994).

Geochemical data of the Whitehill Formation are presented in Fig. 11.4. The data are derived from cores of the borehole SFT2 drilled near Jansenville (Eastern Cape) in the southeastern Karoo Basin flanking the tectonic front of the Cape Fold Belt (thermal maturity ~4 % R_r; Geel et al. 2013, 2015), and from cores of the borehole KL 1/65 drilled near Sutherland (Western Cape) in the west-central part of the basin with uncertain thermal maturity (Chere 2015). We compare these data sets with that from the Baltic Sea deposits, in the context of geochemical 'events'.

Phase 1: Prince Albert Formation (~290–280 Ma)

The sediments of the Prince Albert Formation are poor in TOC, and contain dropstones and distinctive phosphate

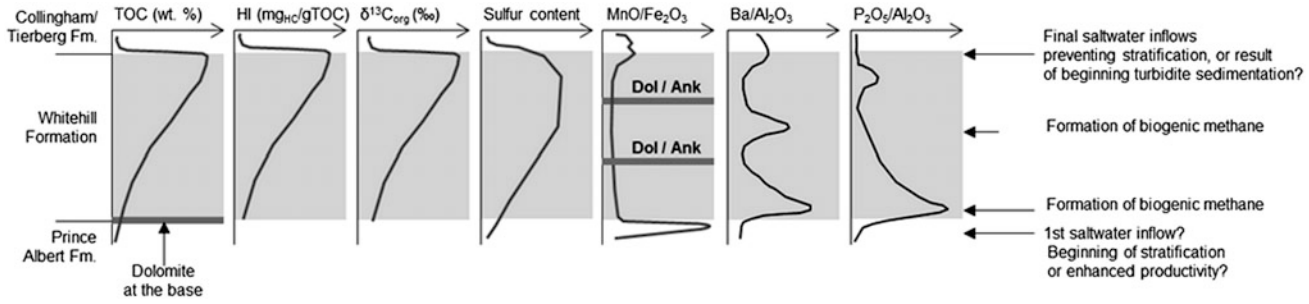

Fig. 11.4 Generalized patterns of selected geochemical proxies in the Whitehill Formation to illustrate palaeoceanographic processes. Data gained by analyses of core samples from a borehole drilled near Jansenville in the Eastern Cape, close to the tectonic front of the Cape Fold Belt (details in Geel et al. 2013, 2015). Sulphur occurs throughout the Whitehill Formation and is fixed to pyrite

nodules near the base (Chere 2015; Geel et al. 2015). This suggests that during deposition, a sufficient content of convertible TOC was available to release dissolved phosphate for mineralization, and that productivity was probably enhanced by volcanic ashes (known from Namibia; Stollhofen et al. 2000; Werner 2006). However, as the today's TOC content is less than 1 %, low surface water bio-productivity can be assumed, which simulates depositional conditions during the Baltic Ice Lake and Ancylus Lake phases (Fig. 11.3a, b). Sr isotope values of the phosphate nodules in the lower part of the Prince Albert Formation are similar to those of calcite concretions in the underlying Dwyka Group deposits (Herbert and Compton 2007). This suggests that fresh water conditions persisted at this stage in the Karoo Lake. The rare occurrence of pyrite in the Prince Albert sediments points to limited sulphate availability in the pore waters, probably from weak marine incursions, similar to that found in the Yoldia Sea deposits of the Baltic Basin (Fig. 11.3b).

Phase 2: Whitehill Formation (~280–276 Ma)

The depositional environment of the Whitehill Formation marks a significant change as the sediments are progressively enriched in TOC and in sulphur content (Fig. 11.4). This implies that marine waters may have continuously infiltrated the southern Karoo Basin at that time that led to a stratified water body with anoxic, denser bottom water and that, at least during onset of deposition of the Whitehill black shales, significant saline-water influxes occurred. A high MnO/FeO ratio (Fig. 11.4) also points to a saline water influx, similar to the episodic saline inflow events into the Baltic Sea (Neumann et al. 1997). High P_2O_5/Al_2O_3 ratios near the base of the Whitehill Formation (Fig. 11.4) indicate phosphogenesis, which is a well-documented feature during the onset of black shale deposition in many petroleum-bearing basins (cf. Schulz et al. 2002; Schulz and Bechtel 2011; Fig. 11.4). Biomarker investigations of a single sample from the Whitehill Formation (Tmax: 431 °C, corresponds to 0.5 % R_r) also suggest deposition under anoxic conditions in a saline lacustrine palaeo-environment (Summons et al. 2008). This interpretation implies that whereas the Karoo Basin underwent marine flooding, it was later at least temporally isolated again from the open ocean (Fig. 11.3). Importantly, a high abundance of 3-methylhopane indicates intense methane cycling due to a low sulphate water body (Summons et al. 2008). High values of the Ba/Al ratio in the Whitehill Formation (Fig. 11.4) indicate barite precipitation, and may reflect the presence of a sulphate/methane transition zones (cf. Arning et al. 2015). By analogy with the TOC content of the Whitehill Formation, the increase in hydrogen indices relates either to enhanced bio-productivity or to a stabilized water stratification with anoxic bottom water (Fig. 11.4). In contrast to the underlying and overlying sediments, the increased δ^{13}Corg values point to intensified methanogenesis during early diagenesis in the sediments of the Whitehill Formation and that the remaining organic matter therefore became isotopically heavier. Alternative hypotheses suggest that the ^{13}C enrichment and the similarity of organic matter from other southwestern Gondwana basins (Paraná Basin, Huab Basin) may be attributed to drawdown of dissolved inorganic carbon (DIC) by algal blooms (Faure and Cole 1999; Summons et al. 2008). Isotopic investigations of intercalated carbonates (partly as nodules) support this hypothesis. The δ^{13}C values of carbonates increase from −15 ‰ in the Prince Albert Formation to values as high as −1 ‰ in the Whitehill Formation, whereas the δ^{18}O values of carbonates increase from +7 ‰ in the Prince Albert Formation to values as high as +25 ‰ in the Whitehill Formation (Faure and Cole 1999).

Phase 3: Collingham Formation

The mudstones of the Collingham Formation which may be as thick as 30–70 m in the southern and western Karoo Basin are considered to be the result of suspension and turbidite flow deposition (Johnson et al. 1997; Chap. 1 this book), and are not related to deglaciation. However, the

beginning of this sedimentation style was probably coupled to reoxygenation, as reflected by a high MnO/FeO ratio (Fig. 11.4). Both deposition style and reoxygenation gave rise to the low TOC content of the Collingham Formation.

11.3 Conclusions

The comparison between the depositional evolution of the Baltic Sea and the post-glaciation history stored in the fine-grained lower Ecca Group sediments in the Karoo Basin shows both similarities and differences. These can be linked to (i) lateral facies changes in time and space, and (ii) a different basin architecture (regional versus supercontinental-scale). It remains unclear, for example, how long deglaciation affected the depositional environment of the Prince Albert Formation (~290–280 Ma) as Haldorsen et al. (2001) found that the Early Permian deglaciation of the northeast Karoo Basin occurred during thousands rather than millions of years. However, a general similarity of retraceable events can explain the occurrence of TOC-rich intervals recorded in both basins. The black shales were deposited under anoxic bottom water conditions caused by stable water stratification in which denser saline bottom water was overlain by a lighter surface water with lower total dissolved solid contents. Today, organic matter-rich mud deposition in the deep Baltic Sea basins is caused by water masses of different salinities and densities, and melting water is not a controlling factor. It needs further investigations to find out whether the black shale deposition of the Whitehill Formation was caused by transgression and/or (by analogy to the today's Baltic Sea) by circulation restrictions rather than by water stratification due to lighter melt water. The deposition of the Prince Albert Shale occurred over a period of about 10 or more million years (Stollhofen et al. 2008), and melting of Gondwana ice sheets was not a factor in development of the Whitehill Formation black shales (see also the markable sulphur contents in the Whitehill Formation in Fig. 11.4).

The termination of black shale sedimentation was probably caused by the onset of turbidite deposition from the south during Collingham Formation times. However, analysis of the detailed processes in the Karoo Basin, as presented here, will require samples from different boreholes across the basin for systematic and high resolution geochemical analyses, if meaningful proxies for palaeoceanographic conditions are to be unravelled.

Acknowledgments We thank Prof. John Isbell (University of Wisconsin-Milwaukee, U.S.A.) and Dr. Bastien Linol (Nelson Mandela Metropolitan University, Port Elizabeth, South Africa) for their constructive comments and recommended revisions that have helped improve this manuscript. This AEON contribution number 160.

References

Andrén, T., Björck, S., Andrén, E., Conley, D., Zillén, L., and Anjar, J. (2011): The Development of the Baltic Sea Basin During the Last 130 ka. In: Jan Harff, Svante Björck, Peer Hoth (Eds.): The Baltic Sea Basin. Chapter 4, pp. 75–97. Springer.

Arning, E. T., Gaucher, E. C., van Berk, W., Schulz, H.-M. (2015): Hydrogeochemical models locating sulfate-methane transition zone in marine sediments overlying black shales: A new tool to locate biogenic methane? - Marine and Petroleum Geology, 59, p. 563–574.

Bangert, B., Stollhofen, H., Geiger, M., and Lorenz, V. (2000): Fossil record and high-resolution tephrostratigraphy of Carboniferous glaciomarine mudstones, Dwyka Group, southern Namibia. Communs geol. Surv. Namibia, 12, p. 265–276.

Björck, S. (2008): The late Quaternary development of the Baltic Sea basin. In The BACC Author Team (Eds.): Assessment of climate change for the Baltic Sea Basin, Springer-Verlag Berlin Heidelberg, 398–407.

Catuneanu, O., Wopfner, H., Eriksson, P. G., Cairncross, B., Rubidge, B. S., Smith, R. M. H., and Hancox, P. J. (2005): The Karoo basins of south-central Africa. Journal of African Earth Sciences 43(1–3), 211–253.

Chere, N. (2015): Sedimentological and geochemical investigations on borehole cores of the Lower Ecca Group black shales, for their gas potential - Karoo Basin, South Africa. MSc thesis, Nelson Mandela Metropolitan University, Port Elizabeth, South Africa. 175 pages.

Cole, D. I., Christie, and A. D. M. (1994): A palaeoenvironmental study of black mudrock in the glacigenic Dwyka Group from the Boshof–Hertzogville region, northern part of the Karoo Basin, South Africa. In: Deynoux, M., Miller, J. M. G., Domack, E. W., Eyles, N., Fairchild, I. J., and Young, G. M. (Eds.): Earth's Glacial Record. Cambridge Univ. Press, pp. 204–214.

Craig, J., Thurow, J., Thusu, B., Whitham, A. & Abutarruma, Y. (2009): Global Neoproterozoic Petroleum Systems: The Emerging Potential in North Africa. Geological Society, London, Special Publications, 326, 1–25.

Emeis, K.-C. (2011): Die lange und wechselvolle Geschichte der Ostsee. Talk, Stralsund, Germany. 33 slides.

Fichot, C. G., Kaiser, K., Hooker, S. B., Amon, R. M. W., Babin, M., Bélanger, S., Walker, S. A., and Benner, R. (2013): Pan-Arctic distributions of continental runoff in the Arctic Ocean. Sci. Rep. 3, 1053; 6 pp.

Formolo, M.J., Salacup, J.M., Petsch, S.T., Martini, A.M., Nüsslein, K. (2008): A new model linking atmospheric methane sources to Pleistocene glaciation via methanogenesis in sedimentary basins. Geology 36(2), 139–142.

Geel, C., Schulz, H.-M., Booth, P., de Wit, M., Horsfield, B. (2013): Shale gas characteristics of Permian black shales in South Africa: results from recent drilling in the Ecca Group (Eastern Cape). - Energy Procedia 40, 256–265.

Geel, C., de Wit, M., Booth, P., Schulz, H.-M., Horsfield, B. (2015): Palaeo-environment, diagenesis and characteristics of Permian black shales in the Lower Karoo Supergroup flanking the Cape Fold Belt near Jansenville, eastern Cape, South Africa: Implications for the shale gas potential of the Karoo Basin. South African Journal of Geology 118(3), 249–274.

Faure, K. and Cole, D. (1999): Geochemical evidence for lacustrine microbial blooms in the vast Permian Main Karoo, Parana´, Falkland Islands and Huab basins of southwestern Gondwana. Palaeogeography, Palaeoclimatology, Palaeoecology 152, 189–213.

Haldorsen, S., Von Brunn, V., Maud, R., and Truter, E. D. (2001): A Weichselian deglaciation model applied to the Early Permian

glaciation in the northeast Karoo Basin, South Africa. Journal of Quaternary Science 16(6), 583–593.

Harff, J., Endler, R., Emelyanov, E., Kotov, S., Leipe, T., Moros, M., Olea, R., Tomczak, M., and Witkowski, A. (2011): Late Quaternary Climate Variations Reflected in Baltic Sea Sediments. In: Jan Harff, Svante Björck, Peer Hoth (Eds.): The Baltic Sea Basin. Chapter 4, pp. 99–132. Springer.

Herbert, C. T., and Compton, J. S. (2007): Depositional environments of the lower Permian Dwyka diamictite and Prince Albert shale inferred from the geochemistry of early diagenetic concretions, southwest Karoo Basin, South Africa. Sedimentary Geology 194, 263–277.

Isbell, J. L., Cole, D. I., and Catuneanu, O. (2008): Carboniferous-Permian glaciation in the main Karoo Basin, South Africa: Stratigraphy, depositional controls, and glacial dynamics. Geological Society of America Special Papers 441, 71–82.

Johnson, M. R., van Vuuren, C. J., Visser, J. N. J., Cole, D. J., Wickens, H. de V., Christie, A. D. M., Roberts, D. L. (1997): The foreland Karoo Basin, South Africa. In: Selley, R.C. (Ed.), African Basins-Sedimentary Basins of the World. Elsevier, Amsterdam, 269–317.

Kabel, K., Moros, M., Porsche, C., Neumann, T., Adolphi, F., Andersen, T. J., Siegel, H., Gerth, M., Leipe, T., Jansen, E., and Sinninghe Damsté, J. S. (2012): Impact of climate change on the Baltic Sea ecosystem over the past 1,000 years. Nature Climate Change 2, 871–874.

Le Heron, D. P., Craig, J., and Etienne, J. L. (2009): Ancient glaciations and hydrocarbon accumulations in North Africa and the Middle East. Earth-Science Reviews 93, 47–76.

Linol, B., De Wit, M., Barton, E., Guillocheau, F., De Wit, M., and Colin, J.-P. (2015): Paleogeography and tectono-stratigraphy of Carboniferous-Permian and Triassic "Karoo-like" sequences of the congo basin. In: Maarten J. de Wit, François Guillocheau, Michiel C.J. de Wit (Eds.): Geology and Resource Potential of the Congo Basin, Springer, pp. 111–134, Regional Geology Reviews.

Lüning, S., Craig, J., Loydell, D. K., Štorch, P., Fitches, B. (2000): Lower Silurian `hot shales' in North Africa and Arabia: regional distribution and depositional model. Earth-Science Reviews, 49 (1–4), 121–200.

Neumann, T., Christiansen, C., Clasen, S., Emeis, K.-C., and Kunzendorf, H. (1997): Geochemical records of salt-water inflows into the deep basins of the Baltic Sea. Continental Shelf Research 17(1), 95–115.

Scheffler, K., Buehmann, D., and Schwark, L. (2006): Analysis of late Palaeozoic glacial to postglacial sedimentary successions in South Africa by geochemical proxies – Response to climate evolution and sedimentary environment. Palaeogeography, Palaeoclimatology, Palaeoecology 240, 184–203.

Schulz, H.-M., and Bechtel, A. (2011): Organic-inorganic interactions during phosphogenesis in the Western Central Paratethys (Late Eocene, Austrian Molasse basin). Journal for the Geological Sciences 39(1), 58–81.

Schulz, H.-M., Sachsenhofer, R. F., Brechtel, A., Polesny, H., and Wagner, L. (2002): The origin of hydrocarbon source rocks in the Austrian Molasse Basin (Eocene-Oligocene transition). - Marine and Petroleum Geology 19(6), 683–709.

Schulz, H.-M., Biermann, S., van Berk, W., Krüger, M., Straaten, N., Bechtel, A., Wirth, R., Lüders, V., Schovsbo, N. H., and Crabtree, S. (2015): From shale oil to biogenic shale gas: retracing organic-inorganic interactions in the Alum Shale (Furongian-Lower Ordovician) in southern Sweden. AAPG Bulletin 99(5), 927–956.

Sohlenius, G, Emeis, K. C., Andrén, E., Andrén, T., and Kohly, A. (2001) Development of anoxia during the fresh–brackish water transition in the Baltic Sea. Marine Geology 177: 221–242.

Stollhofen, H., Stanistreet, I.G., Bangert, B., and Grill, H. (2000): Tuffs, tectonism and glacially related sea-level changes, Carboniferous-Permian, Southern Namibia. Palaeogeogr., Palaeoclimat., Palaeoecol. 161: 127–150.

Stollhofen, H., Werner, M., Stanistreet, I.G., and Armstrong, R.A. (2008): Single zircon U/Pb dating of Carboniferous-Permian tuffs, Namibia, and the intercontinental deglaciation cycle framework.- In: Fielding, Chr.R., Frank, T.D. & Isbell, J.L. (Eds.) Resolving the Late Paleozoic Ice Age in time and space, Geol. Soc. Amer. Spec. Paper 441:83–96.

Summons, R. E., Hope, J. M., Swart, R., and Walter, M. R. (2008): Origin of Nama Basin bitumen seeps: Petroleum derived from a Permian lacustrine source rock traversing southwestern Gondwana. Organic Geochemistry 39, 589–607.

U.S. Energy Information Administration EIA (2013): Technically Recoverable Shale Oil and Shale Gas Resources: Algeria. U.S. Department of Energy, Washington, DC 20585, 28 pp.

Visser, J. N.J. (1993): Sea-level changes in a back-arc-foreland transition: the late Carboniferous-Permian Karoo Basin of South Africa. Sedimentary Geology 83, 115–131.

Visser, J. N.J. (1996): Controls on Early Permian shelf deglaciation in the Karoo Basin of South Africa. Palaeogeography, Palaeoclimatology, Palaeoecology 125, 129–139.

Werner, M. (2006): The stratigraphy, sedimentology and age of the Late Palaeozoic Mesosaurus Inland Sea, SW-Gondwana: new implications from studies on sediments and altered pyroclastic layers of the Dwyka and Ecca Group (lower Karoo Supergroup) in southern Namibia. Unpublished PhD Thesis, University of Würzburg, Germany. 428 pp.

Geochemistry of the Pronksberg Bentonite of the Upper Elliot Formation (Early Jurassic), Eastern Cape, South Africa

12

Emese M. Bordy and Miengah Abrahams

Abstract

Located within the continental red beds of the upper Elliot Formation (Eastern Cape, South Africa), the Lower Jurassic Pronksberg bentonite is in close proximity to the boundary between the Triassic and Jurassic, which coincides with one of Earth's largest mass extinction events. Sedimentological, mineralogical, and major and trace element geochemical data indicates that: (1) the bentonite formed by devitrification of felsic volcanic ash; (2) the deposit was reworked by gentle currents in an ephemeral lake where intense chemical weathering of the volcanic ash occurred; and (3) the source of the original felsic volcanic material was probably in southwest Gondwana (now South America) where explosive silicic igneous activity has been documented not only in the Permian, but also in the Late Triassic and Early Jurassic.

Keywords

Bentonite geochemistry • Felsic volcanic ash • Karoo basin • Elliot formation

12.1 Introduction

Globally, the Triassic–Jurassic boundary coincides with one of Earth's five large mass extinction events, a record of which is expected to be contained within the Upper Triassic–Lower Jurassic Elliot Formation in southern Africa (Fig. 12.1a). However, the exact stratigraphic position of the Triassic–Jurassic boundary in this region remains largely unknown, due to the lack of radiometric dates from the upper Karoo Supergroup. Here, we present the geochemistry of a detrital zircon-bearing, ~1 m thick bentonite layer located in the upper Elliot Formation (UEF) at Pronksberg Mountain (Fig. 12.1b) with the aim of determining its origin. The U–Pb radiometric dating of the zircons extracted from the bentonite is currently underway. The bentonite is a pale yellow, massive claystone and is interbedded with pale purple, silty, very fine grained sandstones (Figs. 12.1c–f). The bentonite is confined to a stratigraphic horizon ~60 m below the lithostratigraphic contact of the Clarens and Elliot formations, and ~75 m below the base of the Drakensberg Group (Figs. 12.1a–b), which on Pronksberg is represented by both basaltic rocks and dacites. The latter is part of a felsic igneous rock suite within the Karoo Large Igneous Province (Marsh and Eales 1984).

12.2 Geological Background

Bentonites consist of smectite group minerals (chiefly montmorillonite), which mostly form via in situ alteration (i.e. devitrification and hydration) of glassy volcanic ash or tephra with a parent rock composition ranging from dacitic to rhyolitic (Johnson 1971; Eisenhour and Reisch 2006). Evidence for the igneous ejecta origin of bentonites in general is petrographic (e.g. euhedral minerals, glass shards or fragmented crystals within a clayey groundmass), and geochemical (e.g. major and rare earth element content consistent with a volcanic origin). Bentonites are useful stratigraphic correlation tools, and often contain zircon

E.M. Bordy (✉) · M. Abrahams
Department of Geological Sciences, University of Cape Town, Cape Town, 7701, South Africa
e-mail: emese.bordy@uct.ac.za

B. Linol and M.J. de Wit (eds.), *Origin and Evolution of the Cape Mountains and Karoo Basin*,
Regional Geology Reviews, DOI 10.1007/978-3-319-40859-0_12

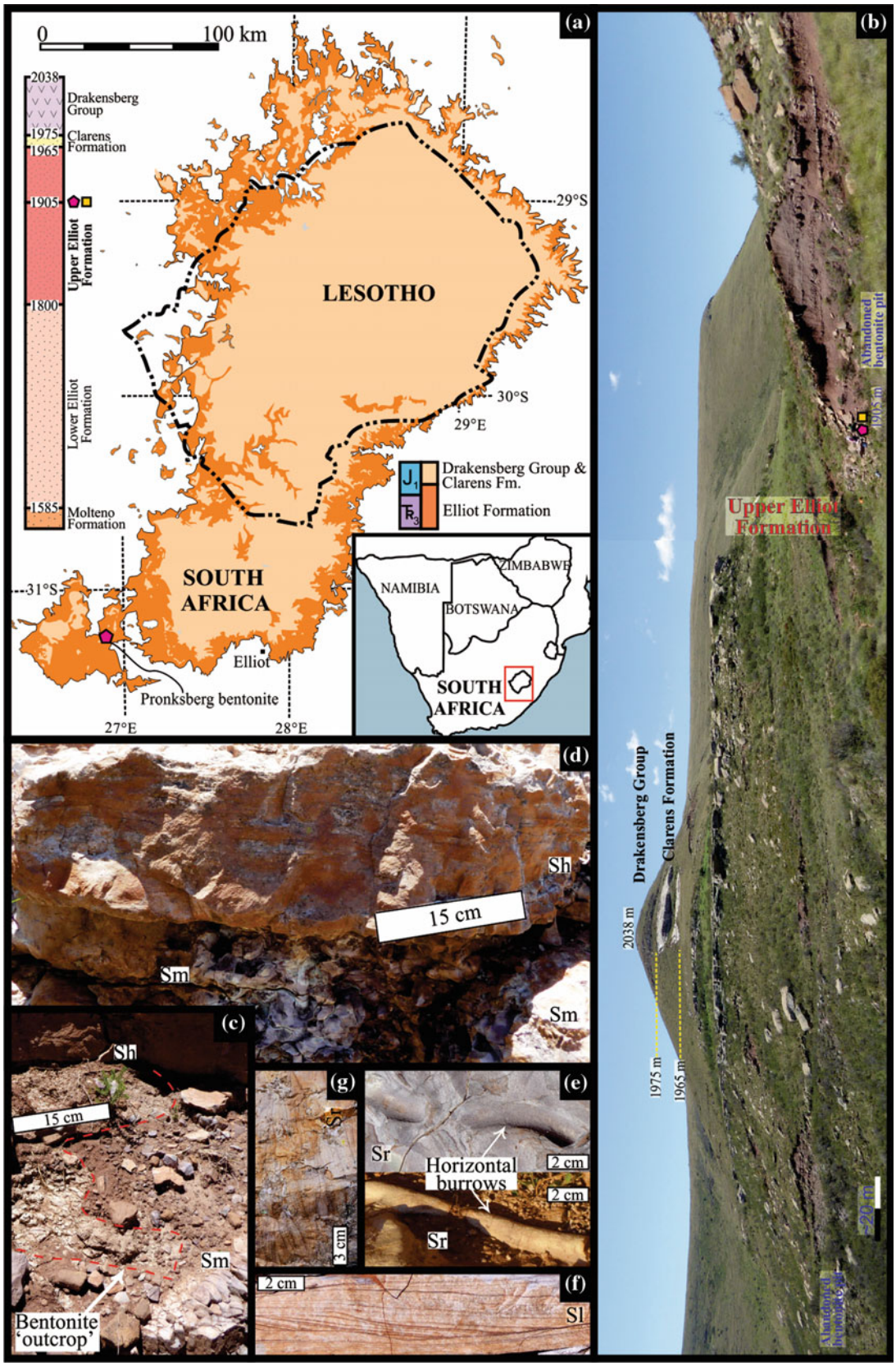
(a)
0
100 km
2038
1975
1965
1905
1800
1585
Drakensberg Group
Clarens Formation
Upper Elliot Formation
Lower Elliot Formation
Molteno Formation
LESOTHO
SOUTH AFRICA
29°S
30°S
29°E
31°S
27°E
28°E
Elliot
Pronksberg bentonite
Drakensberg Group & Clarens Fm.
Elliot Formation
ZIMBABWE
NAMIBIA
BOTSWANA
SOUTH AFRICA
(b)
Abandoned bentonite pit
Upper Elliot Formation
Drakensberg Group
Clarens Formation
2038 m
1975 m
1965 m
20 m
(c)
Sh
15 cm
Sm
Bentonite 'outcrop'
(d)
Sh
15 cm
Sm
Sm
(e)
Sr
Horizontal burrows
2 cm
2 cm
Sr
(f)
2 cm
Sl
(g)
3 cm

◀ **Fig. 12.1** Location, stratigraphy and field relations of the Pronksberg bentonite (Lower Jurassic, Eastern Cape, South Africa). **a** Simplified regional geological map of the Elliot Formation within southern Africa and stratigraphic column at Pronksberg. Numbers within the column are the heights (metres asl) of the key stratigraphic surfaces and the relative position of the analyzed samples. **b** Landscape view of Pronksberg mountain showing aspects of the local geology and two abandoned bentonite pits, some 200 m apart. All *pits* are in the same stratigraphic horizon and position along the southern slope of the mountain and traceable for ~1.5 km; the bulk of the bentonite was mined out in the mid-1970s. The bentonite and interbedded sandstones sample localities are marked with a *pentagon* and *rectangle*, respectively. **c** Poorly exposed bentonite under- and overlain by sandstones (Sh, Sm). **d** Horizontally laminated (Sh) sandstone underlain by strongly bioturbated, massive sandstone (Sm). Note the nodular fabric from the intense bioturbation; the style of bioturbation is attributable to aquatic invertebrates. **e** Two well-preserved horizontal burrows in ripple cross-laminated sandstone (Sr). **f** Low-angle cross-bedded (Sl). **g** Ripple cross-laminated sandstone (Sr). All sandstones are very fine grained

crystals suitable for fission-track and U–Pb radiometric dating (Bohor and Triplehorn 1993).

Generally, the bentonite-hosting UEF has an unconformable contact with the Molteno Formation and a conformable, chiefly gradational contact with the Clarens Formation in the Karoo Basin (Bordy and Eriksson 2015 and references therein). Overall, the sedimentary rocks of the UEF consists of silty, massive or laminated, often pedogenically altered mudstones with intermittent fine to very fine grained, deep red to maroon sandstones (Bordy and Eriksson 2015). The UEF mudstones contain a large diversity of vertebrate fossils, including sauropodomorph dinosaurs, turtles, fish, amphibians, crocodilians, advanced therapsids and early mammals (Bordy and Eriksson 2015). Furthermore, petrified wood, freshwater crustaceans and diverse assemblages of vertebrate and invertebrate trace fossils along with carbonized and calcretized root traces, calcareous concretions, irregular mottles, desiccation cracks and mud drapes are also present. All in all, the sedimentological and palaeontological evidence indicates a semi-arid fluvio-lacustrine system with a highly seasonal discharge, prone to flash floods (Bordy et al. 2004).

12.3 Methodology

Outcrop information (e.g. photographs, sketches, GPS positions and comprehensive field notes) and samples were collected on Pronksberg. Further laboratory studies in the Department of Geological Sciences at University of Cape Town included: (a) standard petrographic analysis for grain size and sedimentary fabric assessment; (b) X-ray diffractometry (XRD) on powered samples using a Phillips PW 1390 XRD machine with a Cu K-α X-Ray tube, accelerating voltage of 40 kV and a 25 mA current and a Bruker Topas 4.1 software for mineral phase identification; (c) wavelength dispersive X-ray fluorescence spectrometry (XRF) on powdered rock samples using a PANalytical Axiois XRF spectrometer with a rhodium end window X-ray tube and wavelength dispersion spectrometer for the major and trace elements analysis in the bentonite and interbedded sandstone; and (d) inductively coupled plasma mass spectrometry (ICP-MS) for the rare earth element (REE) analysis of the bentonite. For the latter, Thermo-Fisher X-Series II quadrupole ICP-MS fitted with a New Wave UP213 solid-state laser ablation system was used on 5000-times diluted powdered samples (after digestion and baking). All analytical results are available on request from the first author.

12.4 Results

Petrographic thin section of the very fine grained sandstones interbedded with the bentonite shows a poorly sorted, submature texture. The sandstones contain a high proportion of clay-size particles and low sphericity, angular to sub-angular (rarely sub-rounded) monocrystalline quartz that do not show undulose extinction. Glass shards or fragmented mineral grains were not observed. XRD analysis positively identified montmorillonite, illite, albite and quartz in the bentonite. In addition, the interbedded sandstone also contains analcime.

The major element composition of the bentonite and the interbedded sandstone are similar when compared to the average geochemical composition of the UEF mudstones (Fig. 12.2a). Furthermore, all samples are depleted in major oxides with respect to the host UEF mudstones with the exception of SiO_2, Al_2O_3, as well as MgO in the bentonite and Na_2O in the interbedded sandstone (Fig. 12.2a). With the exception of Na, the bentonite is very slightly enriched in major elements relative to the interbedded sandstone, which in turn is enriched in Na relative to the UEF mudstones. The latter can be also illustrated with the K_2O/Na_2O ratio, which is 2.13 in the bentonite and 0.08 in the interbedded sandstone, respectively.

The trace element concentration in the bentonite and the interbedded sandstone are similar to that of the UEF mudstones (Fig. 12.2b). With the exception of Ba, Rb, Cu and Cr, the bentonite and interbedded sandstone are enriched in trace elements relative to the host UEF. The ICP-MS results of REE element analysis of the bentonite (Fig. 12.2c) show a light REE enrichment relative to heavy REE and no Ce, but a detectable Eu anomaly.

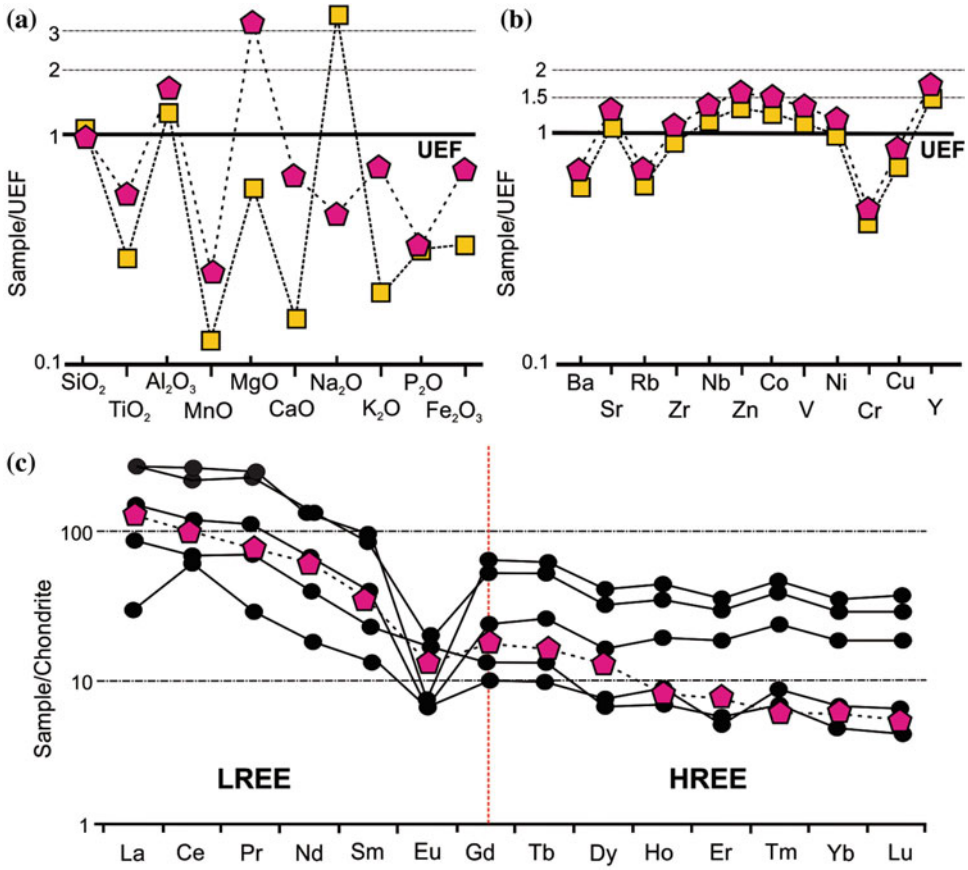

Fig. 12.2 Geochemical plots of the Pronksberg bentonite and interbedded sandstone. Spider plot of average **a** major and **b** trace element concentrations for bentonite (*pentagons*) and interbedded sandstone (*rectangles*) normalized against the average geochemical composition of the UEF mudstones (UEF data from Sciscio and Bordy 2016), **c** Chondrite-normalized REE profile of the Pronksberg bentonite sample (*pentagon*) and South American volcanogenic rocks (*black circles*). The latter were sourced from the Permo–Triassic Choiyoi Silicic Magmatic Province (data from Sun 1982; Rocha-Campos et al. 2011)

12.5 The Relation of the Pronksberg Bentonite to Permian Karoo Tuffaceous Beds

Tuffaceous beds within the Karoo Supergroup were initially reported by Southern Oil Exploration Corporation (SOEKOR) in 1966 and subsequently described by numerous authors (e.g. Johnson 1971; Keyser and Zwanda 1988; McLachlan and Jonker 1990; Viljoen 1994, 1998; Foulkes 2009). To understand the relationship between the Pronksberg bentonite and older Karoo tuffaceous deposits, we compared the geochemistry of the bentonite to: Permian K-bentonite beds (Ecca Group—Viljoen 1994), Permian tuffaceous beds (Ecca Group—McLachlan and Jonker 1990), Permian pyroclastics (Beaufort Group—Keyser and Zawanda 1988 and Permian ash beds (Beaufort Group—Foulkes 2009) (Fig. 12.3).

12.6 Interpretations

Illite and montmorillonite are considered probable weathering products in relatively dry climates, the dominant climatic condition during the deposition of the Elliot Formation (Bordy and Eriksson 2015; Sciscio and Bordy 2016). This climate is confirmed by the chemical index of alteration (CIA) of the Pronksberg bentonite and interbedded sandstone (Fig. 12.4a). The CIA values (Fig. 12.4b) also indicate that the bentonite is more chemically altered by weathering than the interbedded sandstone and UEF mudstones.

The major element composition of ideal bentonites approximates montmorillonites. However, Al_2O_3 and Na_2O contents of the Pronksberg bentonite are depleted and its CaO content is slightly elevated for its silica content relative to montmorillonite. The departures from an ideal montmorillonite composition may be explained by sedimentary mixing of the freshly deposited volcanic ash with detrital quartz or via chemical weathering of volcanic ash to smectite, which is a hydration reaction that requires Mg, and produces excess silica and alkali ions (Keyser and Zawanda 1988). The latter may take place, to different degrees of completeness, according to the following reaction series: silicic volcanic glass + water ➔ montmorillonite + silica + ions in solution ➔ montmorillonite/illite mixed layer clay + analcime and quartz ➔ albite + illite + quartz (Viljoen 1994). The Na depletion may result from Na leaching during the devitrification of volcanic glass, which in turn could have enriched the interbedded sandstone in Na_2O. The

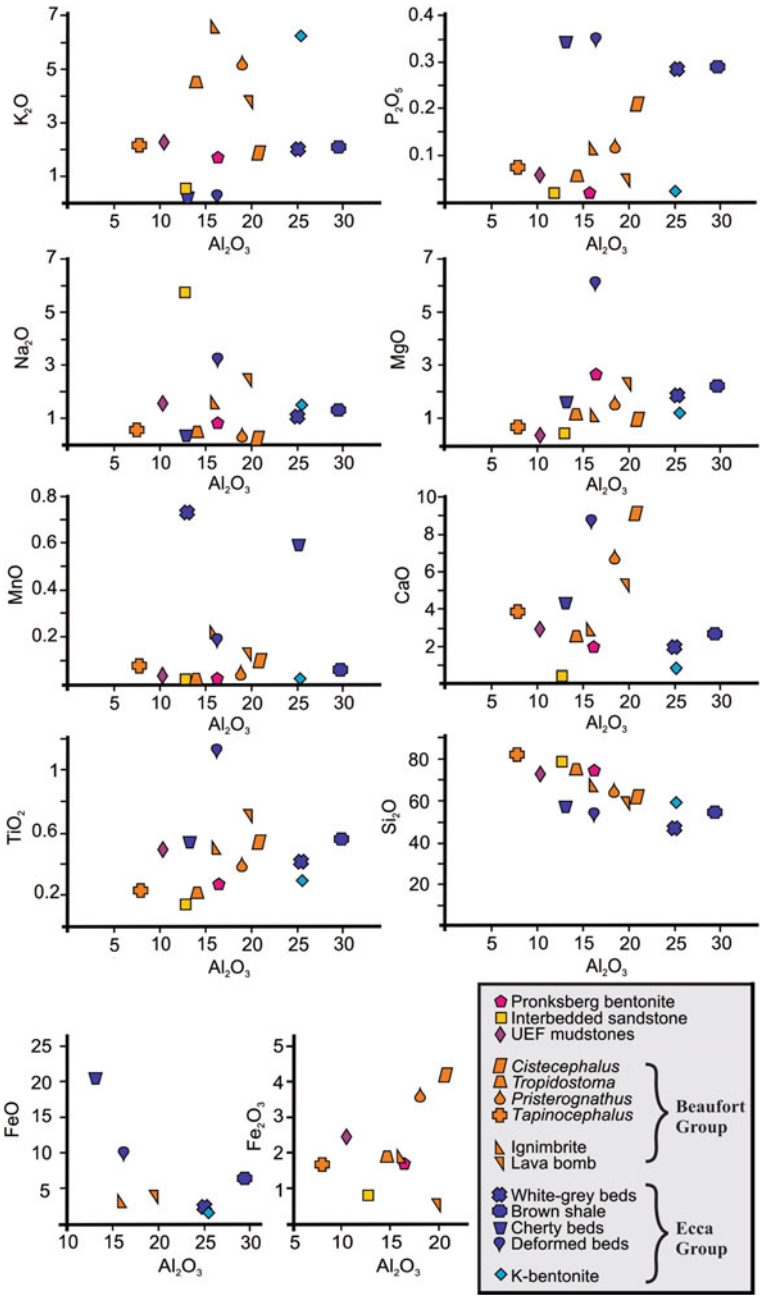

Fig. 12.3 Harker diagrams for major element composition of the Pronksberg bentonite, interbedded sandstone, average UEF mudstone and older Karoo tuffaceous deposits. All plotted data are on an anhydrous basis

latter is present in the zeolite analcime, which can form from volcanic glass in tuffs in alkaline environments such us ephemeral lakes (e.g. Larsen et al. 1991). With respect to SiO_2, the low Al_2O_3 and Na_2O and elevated CaO contents may also reflect the fairly intense weathering of the bentonite.

In the studied Karoo volcaniclastic samples, the temporal increase in Si coupled with a decrease in Al (Fig. 12.3a) may represent increasing quartz content, which might reflect a progressively more felsic source and/or the recycled nature of the deposits (i.e. silica dilution due to magmatic versus sedimentary processes). These major element variations shown in Fig. 12.3 do not form strong enough trends to suggest that the Karoo volcaniclastics are genetically linked or have a common source. Furthermore, due to interlaboratory analytical errors (e.g. bias from the potentially different analytical techniques, differences in accuracy) and the low number of comparative studies, the emerging trends are not considered here convincing to deduce any temporal changes in the geochemistry of these deposits. Conversely, these major element plots are useful to demonstrate that the analyses scatter quite widely with no trend. This scatter may indicate different original ash compositions, different alteration processes leading to different alteration assemblages,

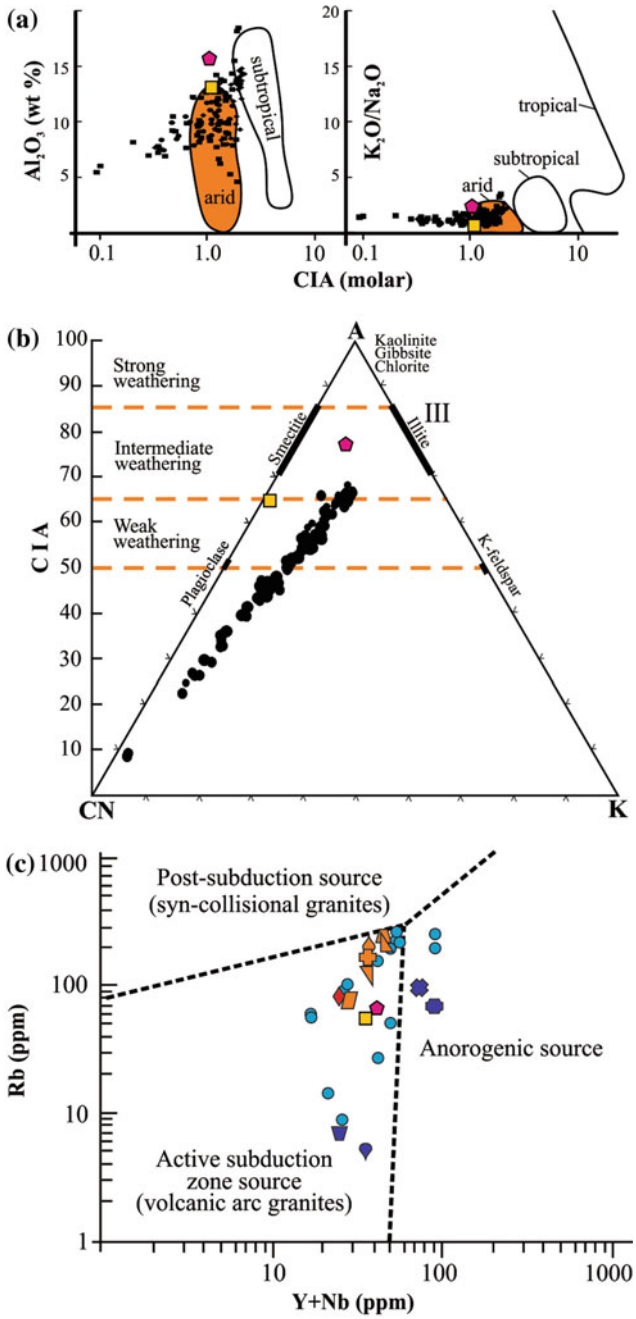

Fig. 12.4 **a** CIA (molar) versus the ratio K_2O/Na_2O and Al_2O_3 plots suggest that the Pronksberg bentonite (*pentagon*) and interbedded sandstone (*rectangle*) were deposited during dry climatic conditions as the rest of the UEF samples (*black symbols*). **b** The A-CN-K [Al_2O_3−(CaO + Na_2O)−K_2O] ternary diagram shows that the Pronksberg bentonite and interbedded sandstone are more chemically weathered than the UEF mudstones (*black dots*), **c** Tectonic discrimination plot using Rb versus Y + Nb trace elements for the Pronksberg bentonite, interbedded sandstones, average mudstone UEF (*black dots*), older Karoo tuffaceous deposits (see Fig. 12.3 for legend) and South American bentonites (*blue dots*). Tectonic fields are from Pearce et al. (1984)

different amounts of non-volcanic clastic input in these Permo–Triassic Karoo tuffaceous deposits.

Trace element (Rb/Y + Nb)-based tectonic setting discrimination diagram (Fig. 12.4c) indicates a source rock in a subduction zone for the Pronksberg bentonite, interbedded sandstone, Permian Karoo tuffaceous deposits as well as Permo–Triassic volcanogenic deposits in South America (Keyser and Zawanda 1988; McLachlan and Jonker 1990; Foulkes 2009; Rocha-Campos et al. 2011). While no distinct temporal trends can be detected in Rb/Y + Nb content, the strong clustering of nearly all Karoo and most South American samples in the active subduction zone field is evident. Strong clustering is also apparent in the Nb/Y–Zr/TiO_2 discrimination diagram of the López-Gamundí (2006—his Fig. 12.3), and shows the common rhyolitic–rhyodacitic composition of the Permian Karoo and South American volcaniclastics (Parana Basin and Central Andes, Chile). As for the Pronksberg bentonite, it plots in the rhyolite field of the silica versus Nb/Y-based rock classification diagram of Winchester and Floyd (1977). The trace element data in this study are also consistent with modern tephra sourced from volcanos above active subduction zones (Tomlinson et al. 2015). Finally, an active continental margin setting or at the very least a felsic magmatic source is also supported by the Scandium (9 ppm) versus Vanadium (49 ppm) content of the Pronksberg bentonite (Bhatia and Crook 1986).

The REE profiles of the Pronksberg bentonite are also consistent with a felsic volcanic source (Fig. 12.2c; Rocha-Campos et al. 2011). While the slight depletion of HREE relative to LREE together with the moderate negative Eu anomaly and lack of Ce anomaly are characteristics of bentonites that originate from volcaniclastic materials with a dacitic to rhyolitic source (Bohor and Triplehorn 1993; Eisenhour and Reisch 2006; Rocha-Campos et al. 2011). However, these geochemical results should be used cautiously, because the bentonites and the sedimentary rocks inevitably record not only the original geochemical composition of their source rocks but also a series of complex syn- and post-depositional processes as the sediment evolves from source to sink (Weltje and von Eynatten 2004). It is this alteration that deterred the confident use of major element based discrimination diagrams in this study (Ryan and Williams 2007). This is mainly because compositional modifications most profoundly impact on major element geochemistry of sediments, especially in continental settings, where highly mobile elements (e.g. Ca, K, Na) are readily released during mineral breakdown and can be leached away from the deposits.

12.7 Discussion

12.7.1 Bentonite Depositional Model

Mineralogical studies of the Pronksberg bentonite, during the 1970s and this study, show that it primarily contains montmorillonite and ~5 % quartz (Schmidt 1976). In addition, Schmidt (1976) mentioned minor amounts of cristobalite, which together with the small quantities of quartz were used by Heckroodt (1991) to suggest that the bentonite resulted from the in situ alteration of volcanic tephra. Johnson (1971) asserted that the tephra was wind-transported to the location of deposition, followed by sub-aerial and subsequent sub-aqueous reworking and alteration, but provided no evidence for these statements. On the other hand, Schmidt's (1976) evidence for deposition within a water body is the occurrence of bedding laminations and thin lenses of sandstone within the bentonite. The primary sedimentary structures in the sandstone interbeds, namely ripple cross-lamination, horizontal lamination and low-angle cross-bedding, as well as the laterally extensive beds (Fig. 12.1b), suggest an alternation of low/medium and upper flow regime currents in an overall low energy setting. Therefore, the depositional environment of the original volcanic ash is interpreted as a shallow ephemeral lake that was occasionally stormy enough to allow the transport of sand size particles in currents. Mud drapes associated with the various sedimentary structures indicate intermittent, short periods of quiet conditions in which mud size particles settled from suspension in these temporary lakes, where during distant volcanic explosions, airborne ash would also collect, and subsequently alter, before being sub-aqueously reworked. The ephemeral nature of the lacustrine depositional environment is consistent with the trace fossil evidence observed in the field (e.g. Fig. 12.1d) as well as with the overall semi-arid palaeoenvironment reconstructed for the Elliot Formation (Bordy and Eriksson 2015; Sciscio and Bordy 2016).

12.7.2 Bentonite Origin

Syntheses of previous reports on tuffaceous beds within the Late Paleozoic basins of Gondwana found a common South American, more specifically Choiyoi Silicic Magmatic Province source for the Permian volcaniclastics in southwestern Gondwana (Lopez-Gamundi 2006; Rocha-Campos et al. 2011; Sato et al. 2015; Linol et al. 2015). This hypothesis is founded on the following key arguments: the Choiyoi magmatism is felsic in nature and therefore highly explosive; the proximity of the studied areas to the Choiyoi Province; pene-contemporaneous formation and geochemical compatibility of the volcaniclastics (ibid). The southwestern Gondwana source of Permian tuffaceous beds in the Karoo Supergroup has been debated by Keyser and Zawanda (1988) and McLachlan and Jonker (1990), who suggested a more proximal source for the Karoo tuffaceous beds, possibly in the north. Keyser and Zawanda (1988) argue for a northern source for the pyroclastics based on southerly palaeocurrents observed in the host sedimentary rocks; however, this conclusion requires more evidence as the sources of clastic sediment and volcanic material do not have to be in the same region. McLachlan and Jonker (1990) suggest a source as close as 100 km based on observed thick beds and glass shards up 70 µm in size. While the thickness and size of ejecta have an inverse relationship with distance from the source (Pyle 1989), this basic relationship only holds for an eruption of a given magnitude. Considering that, to-date, geological supporting evidence for this proximal volcanic eruption source within southern Africa is lacking, the possible explanation for the thickest Karoo tuffaceous beds would be a distal supervolcano event, in combination with upper atmospheric currents supplying volcanic dust to southwestern Gondwana (e.g. Linol et al. 2015). A likely volcanic eruption source to the southwest was first shown by Viljoen (1998) who demonstrated, at least for the tuffaceous beds in the Lower Permian Ecca Group, a decrease in abundance and thickness in tuffaceous beds northwards and eastwards within the Karoo Basin.

A geochemical comparison of the Pronksberg bentonite to younger felsic rocks in the lowermost Drakensberg Group (e.g. Pronksberg dacite—Marsh and Eales 1984) was inconclusive for establishing their potential common magma source. Although the Pronksberg bentonite and dacite are geochemically similar, this similarity is considered apparent here. This is not only because the documented 'continental crustal' geochemical signature of the earliest Drakensberg volcanics is virtually indistinguishable from that of products of silicic magmatism at subduction zones (Marsh 2010), but mostly because: (1) these lowermost Drakensberg volcanics have an anhydrous mineralogy (e.g. plagioclase, pyroxene, Ti-magnetite) suggestive of a rather non-explosive eruption history (Marsh 2010); (2) the coeval lowermost Drakensberg volcaniclastics are rare and highly localized (laterally restricted); and (3) the Pronksberg bentonite and dacite are, currently, considered to be up to 10 Ma apart in age. This age gap would make a local volcanic source of Pronksberg bentonite an unlikely early herald of the copious amounts of basaltic magma associated with the Karoo Large Igneous Province.

Field observations in the current study provide no direct indication for the source location of the Pronksberg bentonite, however, the geochemical signatures of the bentonite suggest a source in a magmatic province with felsic explosive volcanism, possibly in southwest Gondwana (now South America). Here, products of felsic igneous activities,

some of them highly explosive, have been documented in the Late Triassic (Rhaetian) and Earliest Jurassic among others from northern Peru, Chilean Precordillera, central western Argentina and Central Patagonia (e.g. Álvarez et al. 1995; Álvarez and Ramos 1999; Pankhurst et al. 2006; Ottone et al. 2014; Wotzlaw et al. 2014; Sato et al. 2015). Although the explosive felsic magmatism in South America around the Triassic-Jurassic boundary is not normally linked to active subduction, but extension, it has been related to post-subduction processes (e.g. break-off of the subducted slab—Pankhurst et al. 2006), possibly to explain the explosive nature. This explanation is important because rift related felsic eruptions are not as highly explosive as those related to subduction zones.

12.8 Conclusion

The Pronksberg bentonite in the UEF, only 60 m below the lower contact of the Clarens Formation, was sampled in order to determine its origin and the relationship to older Karoo tuffaceous beds. Geochemical investigations of the major and trace elements in weathered, whole rock samples as well as field observations showed that the bentonite had been reworked. The CIA of the bentonite indicates that it is more weathered than its UEF host rocks. This may be due to the primary ashfall deposit of felsic origin having undergone sub-aqueous weathering in an ephemeral lake. The most likely source for the bentonite is southwest Gondwana (now South America), where explosive felsic igneous activities have been documented not only in the Permian, but also across the Triassic-Jurassic boundary.

Acknowledgements Most of all, we would like to thank Goonie Marsh for the countless stimulating discussions. Our special thanks go to our friends and colleagues Rugshana Daniels, Blair McPhee and Lara Sciscio for field and lab assistance. Albert and Susanna Roodt are acknowledged for graciously allowing us access to the abandoned bentonite pits on Pronksberg. We thank Chris Harris and Agnes Odri for improving an earlier version of the manuscript, and reviewers Jurie Viljoen and Maarten de Wit for their constructive comments. The financial support of the National Research Foundation of South Africa via its African Origins Platform and Completive Program for Rated Researches grants (#82606, #93544) to EMB is hereby acknowledged. Opinions expressed and conclusions arrived at are those of the authors only.

References

Álvarez PP, Benoit SV, Ottone EG (1995) Las formaciones Rancho de Lata, Los Patillos y otras unidades mesozoicas de la Cordillera Principal de San Juan. Rev Asoc Geol Argent 49:123–142.

Álvarez PP, Ramos VA (1999) The Mercedario rift system in the principal Cordillera of Argentina and Chile. J South Am Earth Sci 12:17–31.

Bohor BF, Triplehorn DM (1993) Tonsteins: Altered Volcanic-Ash Layers in Coal-Bearing Sequences: Boulder, Colorado. Geol Soc Am, pp 47.

Bordy EM, Hancox PJ, Rubidge BS (2004) Fluvial style variations in the Late Triassic–Early Jurassic Elliot Formation, main Karoo Basin, South Africa. JAES 38:383–400.

Bordy EM, Erikson P (2015) SACS Elliot Formation (Late Triassic - Early Jurassic), Karoo Supergroup, South Africa. SAJG 107:397–412.

Bhatia MR, Crook, KAW (1986) Trace element characteristics of greywackes and tectonic discrimination of sedimentary basins. Contrib Mineral Petrol 92:181–192.

Eisenhour D, Reisch F (2006) Bentonite. In: Kogel JE, Trivedi N, Barker JM, Krukowski ST (eds), Industrial Minerals and Rocks. 7th Ed. Colorado: SME Inc., 357–368.

Foulkes S (2009) A geochemical analysis of volcanic ashes in the Pristerognathus, Tropidostoma and Cistecephalus Assemblage Zones of the Beaufort Group, Karoo Supergroup, in the Eastern Cape, South Africa. Unpublished Honours thesis, Rhodes University, Grahamstown, South Africa, pp 56.

Heckroodt R (1991) Clay and clay materials in South Africa. J South Afr Inst Min Metall 91:343–363.

Johnson MR (1971) Provisional geological report: an occurrence of bentonite in the Pronksberg (Mountain), Wodehouse District CP. Geol Surv S Afr Pretoria, 0012 6/196, pp 7.

Keyser N, Zawanda PK (1988) Two occurrences of ash-flow tuff from the lower Beaufort Group in the Heilbronn-Frankfort area, northern Orange Free State. SAJG 91:509–521.

Larsen G, Plum KH, Forster H (1991) Zeolites and other hydrothermal alteration products of synthetic glasses. Eur J Mineral 3:933–941.

Linol B, de Wit M, Barton E, de Wit MJC, Guillocheau F (2015) U–Pb detrital zircon dates and source provenance analysis of Phanerozoic sequences of the Congo Basin, central Gondwana. Gondwana Res 29:208–219.

Lopez-Gamundi O (2006) Permian plate margin volcanism and tuffs in adjacent basins of west Gondwana: Age constraints and common characteristics. J South Am Earth Sci 22:227–238.

Marsh JS (2010) Karoo andesites and dacites. Abstract book of the 2nd Annual Igneous and Metamorphic Studies Group Meeting (January, 2010) Grahamstown, South Africa. Unpaginated.

Marsh JS, Eales H.V (1984) Chemistry and petrogenesis of igneous rocks of the Karoo Central area, southern Africa, Special Publication of the Geological Society of South Africa 13:27–68.

McLachlan IR, Jonker JP (1990) Tuff beds in the northwestern part of the Karoo Basin. SAJG 93:329–338.

Ottone E, Monti M, Marsicano C, de la Fuente M, Naipauer M, Armstrong R, Mancuso A (2014) A new Late Triassic age for the Puesto Viejo Group (San Rafael depocenter, Argentina): SHRIMP U-Pb zircon dating and biostratigraphic correlations across southern Gondwana. J South Am Earth Sci 56:186–199.

Pankhurst RJ, Rapela CW, Fanning CM, Márquez M (2006) Gondwanide continental collision and the origin of Patagonia. Earth-Sci Rev 76:235–257.

Pearce JA, Harris NBW, Tindle AG (1984) Trace element discrimination diagrams for the tectonic interpretation of granitic rocks. J Petrol 25:956–983.

Pyle D (1989) The thickness, volume and grainsize of tephra fall deposits. B Volcanol 51:1–15.

Rocha-Campos AC, Basei MA, Nutman AP, Kleiman LE, Varela R, Llambias E, Canile FM, da Rosa OCR (2011) 30 million years of Permian volcanism recorded in the Choiyoi igneous province (W Argentina) and their source for younger ash fall deposits in the Paraná Basin: SHRIMP U–Pb zircon geochronology evidence. Gondwana Res 19:509–523.

Ryan KM, Williams DM (2007) Testing the reliability of discrimination diagrams for determining the tectonic depositional environment of ancient sedimentary basins. Chem Geol 242:103–125.

Sato A M, Llambias EJ, Basei MAS, Castro CE (2015) Three stages in the Late Paleozoic to Triassic magmatism of southwestern Gondwana, the relationships with the volcanogenic events in coeval basins. J South Am Earth Sci 63:48–69.

Schmidt ER (1976) Clay. In: Coetzee C (ed) Mineral resources of the Republic of South Africa. Fifth edition. Geol Surv S Afr Pretoria Handb 7:275–286.

Sciscio L, Bordy EM (2016) A preliminary geochemical study of the Upper Triassic-Lower Jurassic Elliot Formation in southern Africa. JAES http://dx.doi.org/10.1016/j.jafrearsci.2016.03.014.

Sun SS (1982) Geochemical composition and origin of Earth's primitive mantle. Geochim Cosmochim Acta 46:179–192.

Tomlinson E, Smith C, Albert P, Aydar E, Civetta L, Cian IR, Cubukcu E, Gertisser R, Isaia R, Menzies M, Orsi G, Rosi M, Zanchetti G (2015) The major and trace element glass compositions of the productive Mediterranean volcanic sources: tools for correlating distal tephra layers in and around Europe. Quat Sci Rev 118:48–66.

Viljoen JHA (1994) Sedimentology of the Collingham Formation, Karoo Supergroup. SAJG 97:167–183.

Viljoen JHA (1998) Distribution of altered volcanic ash beds in the Dwyka and Ecca Groups of the main Karoo Basin, South Africa. JAES Special Abstracts Issue, Gondwana 10: Event Stratigraphy of Gondwana 27:204–205.

Weltje GJ, von Eynatten H (2004) Quantitative provenance analysis of sediments: review and outlook. Sediment Geol 171:1–11.

Winchester JA, Floyd PA (1977) Geochemical discrimination of different magma series and their differentiation products using immobile elements. Chem Geol 20:325–343.

Wotzlaw JF, Guex J, Bartolini A, Gallet Y, Krystyn L, McRoberts CA, Taylor D, Schoene B, Schaltegger U (2014) Towards accurate numerical calibration of the Late Triassic: high-precision U-Pb geochronology constraints on the duration of the Rhaetian. Geology 42:571–574.

Part V
Paleontology and Paleo-Environments

Vertebrate Biostratigraphy of the Witteberg Group and the Devonian-Carboniferous Boundary in South Africa

13

Robert W. Gess

Abstract

Witteberg Group rocks are Late Devonian to Early Carboniferous in age. Comparison with Laurasian sea-level curves has correlated the earliest Carboniferous Tournasian transgression, with the argillaceous Kweekvlei Formation, overlying the arenaceous Witpoort Formation. The Devonian/Carboniferous boundary is globally characterised by a Mass Extinction which extinguished the entire grade of placoderm fish and radically reduced sarcopterygian and acanthodian diversity, preluding an Early Carboniferous radiation of actinopterygians. Analysis of Cape Supergroup biostratigraphy reveals that a fauna preservationally dominated by placoderms, sharks, and gyracanthid acanthodians may be traced from the Upper Bokkeveld Group through the Wagondrift Formation (Witteberg Group) to the Witpoort Formation, wherein it displays an increased diversity of placoderms, as well as sarcopterygians. Overlying strata contain no placoderms or sarcopterygians, but present are some relict sharks and acanthodians, and an increasing abundance of actinopterygians. This congruence confirms sea-level curve based age estimates of the Witteberg Group and the position of the Devonian/Carboniferous boundary.

Keywords

Witteberg group • Biostratigraphy • Hangenberg • Famennian • Placoderms

13.1 Introduction

Witteberg Group rocks are considered Late Devonian to Early Carboniferous in age (Streel and Theron 1999). This is based principally on comparison of putative sea-level changes with Laurasian sea-level curves, and includes correlation of the earliest Carboniferous Tournasian transgression, with onset of the argillaceous Kweekvlei Formation, overlying the arenaceous Witpoort Formation (Cooper 1986). More recent research on early vertebrate faunas is reviewed below and used to test previous theories on the age of the Witteberg Group. Globally recognised higher taxonomic level vertebrate extinctions at the end of the Devonian period (Sallan and Coates 2010), are used to provide a basis for comparison. Strong evidence for the stratigraphic placement of the Devonian/Carboniferous boundary is provided.

R.W. Gess (✉)
NRF DST Centre of Excellence in Palaeosciences Member, Albany Museum, Grahamstown, South Africa
e-mail: robg@imaginet.co.za

13.2 Stratigraphy of the Witteberg Group

The Witteberg Group (Cape Supergroup) occurs from near Fish River, south east of Grahamstown (Eastern Cape, South Africa) westward along the Cape Fold Belt to the Cedarberg in the Western Cape. It is the youngest of three main divisions of the tripartite Ordovician to Carboniferous Cape Supergroup.

Lower Witteberg Group rocks comprise marginal marine-derived quartzites and shales, forming the culmination of a coarsening up sequence that began in the underlying mudstone dominated Bokkeveld Group. In the Eastern Cape, the lower Witteberg is subdivided into a basal unit of interbedded shale and quartzite, the Weltevrede Formation,

B. Linol and M.J. de Wit (eds.), *Origin and Evolution of the Cape Mountains and Karoo Basin*,
Regional Geology Reviews, DOI 10.1007/978-3-319-40859-0_13

overlain by an increasingly quartzitic unit, the Witpoort Formation, which comprises predominately quartz arenites, wackes and subarkoses with minor interbeds of shale. These are overlain by the mudstone and siltstone dominated Lake Mentz Subgroup, which comprises three Formations. Initially deposited argillaceous strata are assigned to the Kweekvlei Formation. These coarsen upward towards the overlying Floriskraal Formation, which presents a relatively brief return to episodes of arenitic deposition, interbedded within finer sedimentary rocks. The Waaipoort Formation is again dominated by finer grained facies including mudstone, siltstone and fine to medium-grained sandstone, and forms the last laterally extensive unit of the Witteberg Group. Within the Eastern Cape, discontinuous arenites and diamictites that patchily overlie the Waaipoort Formation are assigned to the Kommadagga Subgroup (Thamm and Johnson 2006).

13.3 Age Estimates of the Witteberg Group

Cooper (1986) correlated putative South African sea-level changes with Laurasian sea-level curves to determine the ages of units within the Cape Supergroup, postulating a Late Devonian (Famennian) age for the Witpoort Formation and a late Givetian to Frasnian age for the underlying Weltevrede subgroup. He considered the 358.9 Ma Devonian-Carboniferous boundary to be at, or near, the contact between the clean white quartzites of the Witpoort Formation (which he correlated with the Famennian—latest Devonian—regression) and the fine black sediments of the overlying Kweekvlei Formation (which he interpreted as a reflection of the Tournasian—earliest Carboniferous transgression).

This was consistent with Gardiner (1969; 1973) and Marias' (1963) interpretation of the diverse Actinopterygian (ray-finned) fish fauna known from the Waaipoort Formation as being Visean in age, and the occurrence of the Givetian to Frasnian articulate brachiopod, *Tropidolepis*, near the top of the Weltevrede subgroup (Boucot et al. 1983). On the basis of the scant palaeobotanical record, however, Plumstead (1967) and Anderson and Anderson (1985) had previously suggested that the entire Witteberg Group was Middle to Late Devonian in age. An early palynological study by Stapleton (1977), likewise suggested a Middle to late Devonian age for the Waaipoort Formation. By contrast palynological analysis by Streel and Theron (1999), of a single sample from the Waaipoort Formation, was interpreted as indicating a late Tournasian to Visean age for the Waaipoort Formation and was presented as evidence in support of Cooper (1986) and his placement of the Devonian-Carboniferous boundary between the Witpoort and Kweekvlei Formations (Streel and Theron 1999). Floral records from the Witpoort Formation, Waterloo Farm lagerstätte, furthermore include the presence of the cosmopolitan progymnosperm tree, *Archaeopteris* (Anderson et al. 1995) (Fig. 13.1), usually indicative of a latest Devonian Frasnian to Famennian age (Algeo et al. 2001).

Ongoing research into the vertebrate faunas of the Witteberg Group, however, provides a far more precise manner of defining the position of the Devonian-Carboniferous boundary in South Africa.

Fig. 13.1 Witpoort Formation (Witteberg Group): two leaf bearing penultimate axes of *Archaeopteris notosaria*, together with two small herbaceous lycopod axes (*top right*), from the Waterloo Farm lagerstätten. Scale bar = 5 cm

13.4 The End-Devonian Extinction Event

A severe global extinction event affecting plants, invertebrates and vertebrates, marks the end of the Devonian, and apparently spanned the Famennian as a series of sub-events, which were taxonomically selective. Each of these appears to be associated with a brief global transgressive event, which can be correlated across and between continents (Algeo et al. 2001). Eustatic changes have been attributed to Gondwanan glaciation (Streel et al. 2000), but this fails to adequately explain extreme levels of anoxia indicated (Algeo et al. 2001). Climatic instability during the Late Devonian may have been triggered by rapid global spread of the first (*Archaeopteris,* Progymnosperm) forests during the Frasnian, compounded by colonisation of dryer areas by the first seed-plants towards the end of the Famennian (Algeo et al. 2001).

The most important and widespread two of these sub-events, which practically bracket the Famennian (Streel et al. 2000), are the Kellwasser extinction event, which approximately coincides with the Frasnian/Famennian boundary (and mainly affected invertebrate and plant communities), and the Hangenberg extinction event, near the end of the Famennian and therefore the Devonian/Carboniferous boundary (Algeo et al. 2001).

The Hangenberg extinction event coincides with widespread extinction of fish taxa. Sallan and Coates (2010) demonstrated that reports linking significant loss of vertebrate taxa to the Kellwasser event are the result of incomplete sampling of the Famennian fossil record. Over 50 % of gnathostome (jawed vertebrate) diversity, including more than 40 % of gnathostome higher groups, was lost during the Hangenberg Event. Significantly the End-Devonian Mass Extinction Event -(EDME) resulted in the abrupt extinction of all placoderm (armour-plated) fish, and the majority of acanthodian (spiny-finned) and sarcopterygian (lobe-finned) fish. This laid the way for a great radiation of actinopterygian (ray-finned) fish and chondrichthyans (sharks and their kin) during the Carboniferous (Sallan and Coates 2010). Having been a minor component of faunas during the Devonian, Actinopterygians have dominated aquatic ecosystems ever since.

A noted lack of abundance of vertebrate fossils collected from the earliest Carboniferous Visean stage (known as Romer's Gap) has been postulated as a possible post extinction lull in abundance and diversity (Sallan and Coates 2010). Rapid recovery of diversity following the EDME event is however indicated by demonstration of early radiations of lungfish and tetrapods during the Visean (Smithson et al. 2012, 2015).

13.5 Review of Vertebrate Occurrences in the Upper Bokkeveld and Witteberg Groups

Faunal remains from the lowermost Witteberg Group Wagondrift Member of the Weltevrede Subgroup are very sparse and fragmentary, however, they strongly indicate a continuation of better preserved faunas recorded from the upper Bokkeveld Group.

13.5.1 Adolphspoort Formation (Traka Subgroup, Bokkeveld Group) and Klipbokkop Formation (Bidouw Subgroup, Bokkeveld Group)

The Adolphspoort (Traka Subgroup) of the southern arm of the Cape Supergroup outcrop is approximately laterally equivalent to the Klipbokkop (Bidouw Subgroup) of the Bokkeveld Group occurring in the Western arm (Theron and Johnson 1991), and contains a comparable vertebrate fauna. Both are associated with lycopod remains and bivalves.

The fossiliferous horizons of the Adolphspoort Formation are interpreted as marginal marine delta top deposits (Almond and Evans 1996; Almond *pers comm*. 2009). Collecting was first conducted by Abraham de Vries, a farmer at the Warmwaterberg in the Klein Karoo. His early material provided the type material of *Barrydalaspis theron*i (Chaloner et al. 1980) (Fig. 13.2a), an arthrodire placoderm possibly congeneric with *Groenlandaspis*. Chaloner et al. (1980) noted the presence of a spine bearing oblique tuberculated ribs, which they attributed to the climatiform acanthodian, *Gyracanthides.* They considered it almost identical to that of *Gyracanthides warreni* from the Aztec Siltstone of Victorialand (Chaloner et al. 1980) (*c.f.* Fig. 13.2b).

Almond and Evans (1996) recognised that additional specimens collected by de Vries included spines and teeth comparable to the pan-Gondwanan chondrichthyan, *Antarctilamna* (Fig. 13.2d), as well as other unidentified spines attributed to small to moderate sized acanthodians. In September 2007, the author (RG) collected a spine comparable to that of *Plesioselachus* at Hondewaterstasie (Fig. 13.2c).

The contemporaneous Klipbokkop Formation, in the Cederberg, contains remains of a similar fauna, also interpreted as having been deposited on a restricted marine or freshwater delta top (Almond and Evans 1996). It includes disarticulated acanthodian and *Antarctilamna*-like fin spines

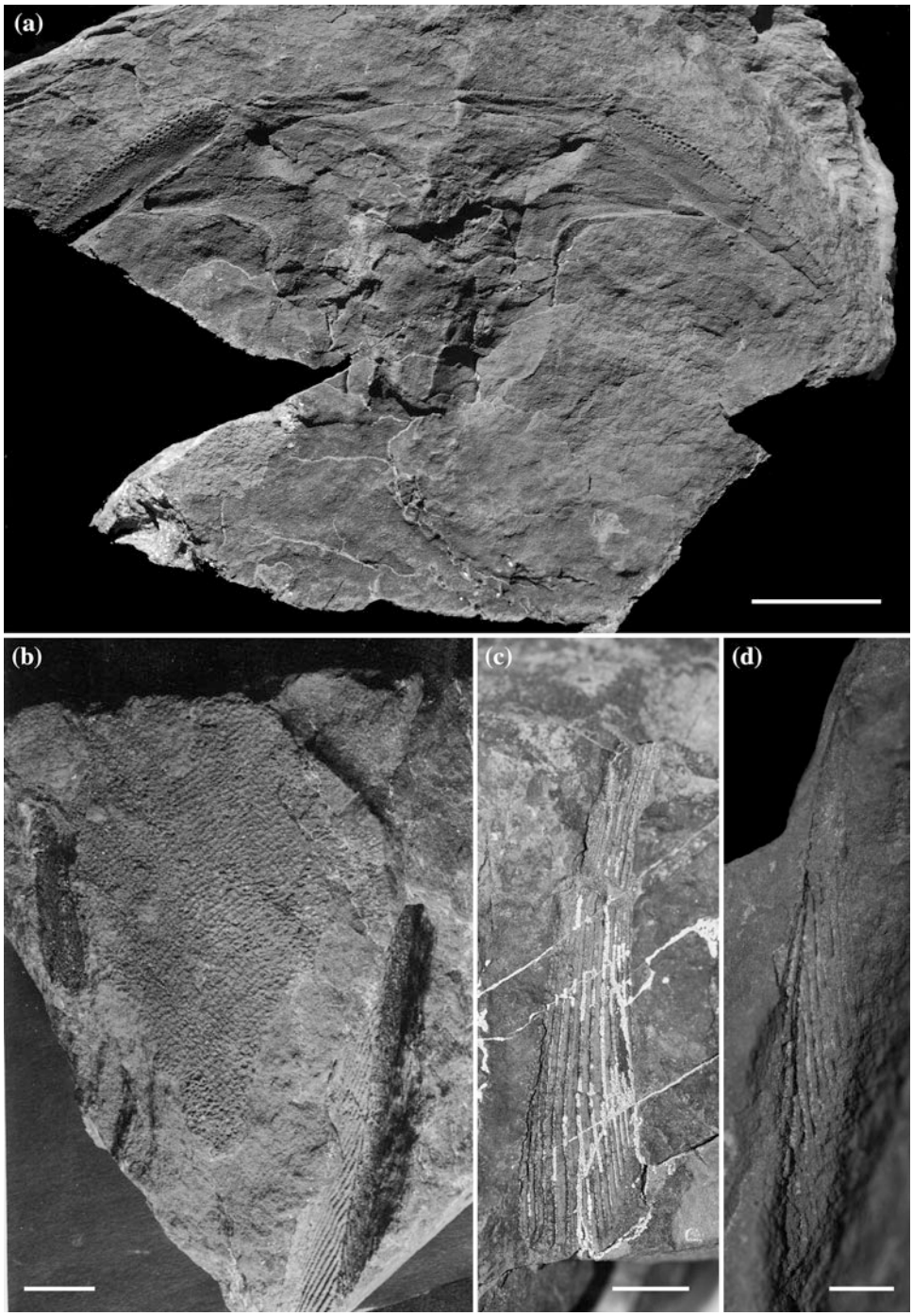

Fig. 13.2 Adolphspoort Formation (Traka Subgroup, Bokkeveld Group): selection of vertebrate fossils; **a** *Barrydaleaspis theroni* holotype, arthrodire placoderm ventral trunk armour, scale bar = 2 cm; **b** partial ventral impression of gyracanthid acanthodian, **c** *Plesioselachus*-like shark dorsal fin spine; **d** *Antarctilamna*-like shark dorsal fin spine. Scale bars in **b**–**d** = 1 cm

and placoderm plates (Almond and Evans 1996) comparable to *Barrydaleaspis* (RG). In addition, isolated shark teeth have been compared to *Antarctilamna*, *Portalodus* and *Aztecodus* (previously described from the Givetian Aztec Siltstone of Antarctica) and fragments of a primitive holonematid arthrodire placoderm have been reported (Anderson et al. 1999b).

13.5.2 Wagendrift Formation (Basal Weltevrede Subgroup, Witteberg Group)

The Wagendrift Formation of the Witteberg Group has provided scant fragmentary fossil fish material from a single mud chip-dominated lag deposit at Rooiberg (south of Laingsburg) interpreted as having originated along a prograding,

storm-dominted, siliclastic shoreline (*pers. comm*. Almond and Evans 1997). Ichnofossils in the Wagen Drift Formation reflect restricted, marginal marine to brackish estuarine palaeoenvironments (*pers. comm*. Almond and Evans 1997). From fossil material in the collection of the Council of Geosciences and field observation the assemblage from the Wagendrift Formation includes small elongate shark-like fin spines with noded ribs of the *Plesioselachus* type, in addition to placoderm remains reminiscent of *Barrydaleaspis* (*Groenlandaspis*). This evidence suggests a continuity with the fauna described from the Adolphspoort and Klipbokkop Formations of the Bokkeveld.

13.5.3 Witpoort Formation (Witteberg Group)

The Witpoort Formation is a quartz arenite dominated unit interpreted as having been deposited in a number of sub environments along a sandy linear coastline. Vertebrate fossils are almost exclusively known from the black shale of the Waterloo Farm lagerstätten, near Grahamstown. This black shale lens is interpreted as a product of anaerobic sediments deposited in a quiet embayment near the mouth of an estuarine lagoon, and fossils also include a diverse Late Devonian flora (Gess and Hiller 1995). The fauna is far more diverse than those discussed above, though it also retains taxa similar to most of those reported. To some extent its greater recorded diversity no doubt derives from remarkable fossil preservation potential in a low energy environment that preserved many delicate organisms (e.g. Gess et al. 2006), coupled with rigorous prospecting over several decades. Nonetheless the unique presence of a number of organisms comprising robust elements suggests a real increase in diversity, perhaps related to a partial break down of Agulhas Sea endemism.

The lamprey *Priscomyzon riniensis* (Gess et al. 2006) (Fig. 13.3a) is the only agnathan. Antiarch placoderms are represented by *Bothriolepis africana* (Long et al. 1997) (Fig. 13.3b). Collections are numerically dominated by the arthrodire placoderm, *Groenlandaspis riniensis* (Long et al. 1997) (Fig. 13.3d). Other arthrodires include *Africanaspis doryssa* (Long et al. 1997) (Fig. 13.3c) and a second *Africanaspis* species, both characterised by extremely high median dorsal plates.

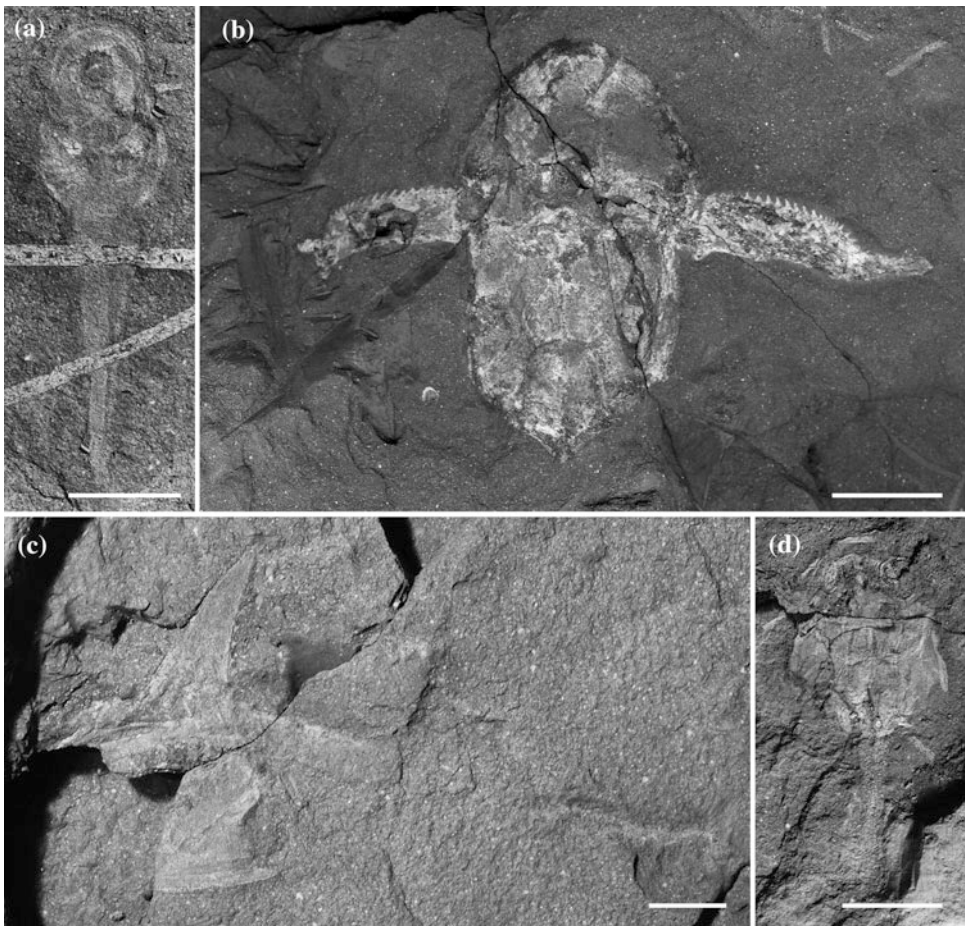

Fig. 13.3 Witpoort Formation (Witteberg Group): selection of vertebrate fossils from the Waterloo Farm lagerstätten; **a** *Priscomyzon riniensis* holotype, agnatha, whole-bodied lamprey in ventral view; **b** *Bothriolepis africana*, subadult antiarch placoderm head and trunk armour in dorsal view; **c** *Africanaspis doryssa*, arthrodire placoderm trunk armour and tail impression in lateral view; **d** *Groenlandaspis riniensis*, juvenile arthrodire placoderm head and trunk armour with tail impression in dorsal view. Scale bars = 1 cm

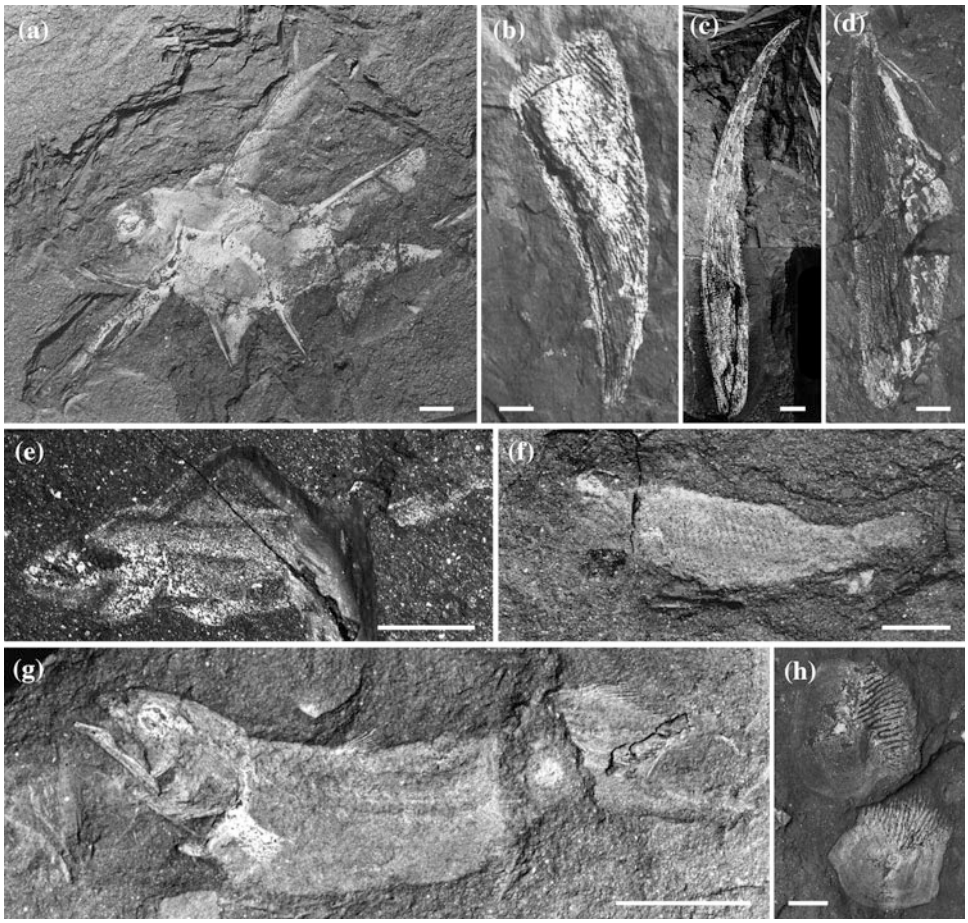

Fig. 13.4 Witpoort Formation (Witteberg Group): selection of vertebrate fossils from the Waterloo Farm lagerstätten; **a** *Diplacanthus acus* holotype, whole-bodied diplacanthid acanthodian in lateral view; **b** gyracanthid acanthodian fin spine, **c** *Plesioselachus macracanthus*, shark anterior dorsal fin spine; **d** *Antarctilamna ultima*, shark, anterior dorsal fin spine of holotype; **e** juvenile whole-bodied shark in lateral view, probably *Antarctilamna ultima*; **f** juvenile whole-bodied actinopterygian in lateral view; **g** *Serenichthys kowiensis* holotype, sarcopterygian, whole-bodied juvenile actinistian (coelacanth) in lateral view; **h** isolated osteolepiform sarcopterygian body scales, c.f. *Hyneria*. Scale bars **a**–**d** = 1 cm, **e**, **f** = 5 mm, **g**, **h** = 1 cm

Acanthodians are fairly diverse, though not commonly preserved, and include a large gyracanthid (Gess and Hiller 1995) (Fig. 13.4b), a diplacanthid, *Diplanthus acus* (Gess 2001) (Fig. 13.4a) and an acanthodid (RG obs.). Chondrichthyans included *Antarctilamna ultima*, (Gess and Coates 2015a) (Figs. 13.4d, e) and *Plesioselachus macracanthus* (Anderson et al. 1999a; Gess and Coates 2015a) (Fig. 13.4c).

Small actinopterygians are uncommonly preserved (Gess and Coates 2008) (Fig. 13.4f). Sarcopterygians include numerous juvenile (post yolk-sac) coelacanths, *Serenichthys kowiensis* (Gess and Coates 2015b) (Fig. 13.4g), a dipnoan comparable to *Andreyevichthys* and a sizable tristichopterid, similar to *Hyneria* (Gess and Coates 2008).

13.5.4 Kweekvlei and Foriskraal Formations (Lake Mentz Subgroup, Witteberg Group)

Vertebrate fossils are virtually unknown from these lowermost two units of the Lake Mentz Subgroup that were deposited following relative deepening of sea levels. A thin lag conglomerate low in the Kweekvlei Formation has yielded a partial shark spine at Hilton Farm, north of Grahamstown, that may be an antarctilamnid (author's observations), whereas Evans (2005) recorded actinopterygian and acanthodian fragments at the base of the Floriskraal Formation at Koega.

13.5.5 Waaipoort Formation (Lake Mentz Subgroup, Upper Witteberg Group)

The Waaipoort Formation consists of mudstones, siltstones and fine sandstones and has most commonly been interpreted as a marginal marine environment, possibly lagoonal (e.g. Theron 1993) or deltaic (e.g. Matshobo 1994). Localities with fish fossils are fairly widespread and, at most of these, the fish are present in calcitic or phosphatic nodules. At a single locality, Schiethoogte in the Eastern Cape, a 15 cm thick black layer consisting of siltstone and fine-grained sandstone contains two thin horizons closely packed with the remains of exclusively actinopterygian fish (Fig. 13.5a). These clearly represent mass mortality events

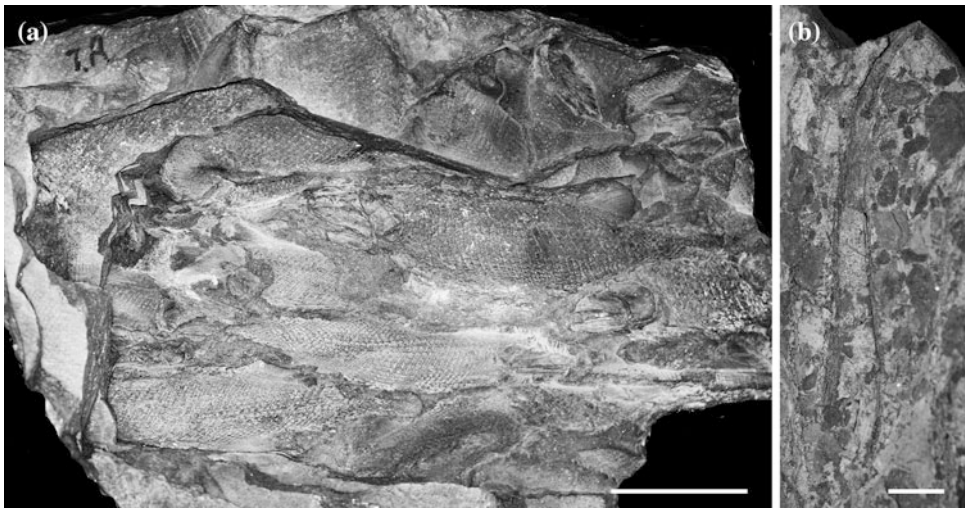

Fig. 13.5 Waaipoort Formation (Witteberg Group): selection of vertebrate fossils; **a** mass death assemblage of actinopterygian fish in lateral view, from Schiethoogte, scale bar = 5 cm; **b** *Plesioselachus*-like shark anterior dorsal fin spine from Soetendalsvlei, scale bar = 1 cm

(Marais 1963; Evans 2005), possibly resultant from anoxic episodes (Evans 1997). Jubb (1965) described *Mentzichthys walshi* and Gardiner (1969) described a further 10 species of actinopterygian, which included six additional genera, from various outcrops in the Waaipoort Formation. These were *Mentzichthys theroni*, *Mentzichthys maraisi*, *Mentzichthys jubbi*, *Australichthys longidorsalis*, *Aesturichthys fulcratus*, *Willowmoreichthys striatulus*, *Sundayichthys elegantulus*, *Dwykia analensis*, *Adroichthys tuberculatus* and *Soetendalichthys comtoni.*

Gardiner considered that many of these genera were closely related to those of the Tournasion to Visean Cementstone Group of Scotland (Gardiner 1969). Evans (1997; 2005) demonstrated the need for a thorough taxonomic revision of Waaipoort Formation fish and concluded that 15 "palaeoniscoid" actinopterygian species are represented.

A number of partial acanthodian spines (Gardiner 1973; Evans 1997) and also scales have been reported from some of the nodule bearing localities (Evans 1997). Spines with noded oblique ridges, sometimes associated with acanthodian-like scale impressions were identified as *Gyracanthides* (Evans 1997).

Gardiner (1973) placed one isolated spine in the genus *Acanthodes,* however, he went on to correctly comment that the multiple (smooth) ridges on this specimen preclude this identification, as *Acanthodes* has a single ridge. Membership of the Acanthodidae has not been unequivocally established.

Shark material, differing from that found in the Devonian was almost certainly wrongly identified as being ctenacanthiform (Evans 1997 and 1999). A small spine fragment was examined by Long and Evans who compared its ornament to that of *Antarctilamna* specimens from the Adolphspoort Formation (Evans 1997). An additional shark spine (Fig. 13.5b), identified by Evans (1997) as '? Acanthodii problematicum' was re-examined (RG) and identified as the dorsal fin spine of a *Plesioselachus*-like taxon. As *Plesioselachus* spines have a similar ornament to those of *Antarctilamna*, the fragment previously reported could be from a *Plesioselachus* spine.

13.6 Discussion

When the fossil vertebrate occurrences from the Cape Supergroup are tabulated together with the proposed stratigraphic dating of Cooper (1986) it is possible to explore biostratigraphic patterns (Fig. 13.6).

It is clear that by upper Bokkeveld times a marginal marine community had developed, the remains of which are dominated by groenlandaspid phlyctaeniid arthrodire placoderms, together with sharks including antarctilamnids and plesioselachids, as well as various acanthodians, including gyracanthids.

These groups are all seen to persist until the late Witpoort Formation (Witteberg Group), where they are preserved together with a range of additional placoderms, more delicate acanthodians (that are largely recognised due to soft tissue preservation), small numbers of actinopterygians and a range of sarcopterygians. The robust nature of the placoderm and larger sarcopterygian remains suggest that these would most likely have been preserved in earlier strata. An augmentation of the ecosystem with taxa presumably derived by migration from lower latitudes is therefore suggested. This may have been facilitated by a slight warming of polar coastal waters due to changes in oceanic circulation towards the end of the Devonian (Streel et al. 2000). It is furthermore consistent with a globally observed breakdown of Early to Middle Devonian provincialism and a move towards greater cosmopolitanism in the Late Devonian (Young 1993), possibly caused by the increasing proximity of Laurussia and Gondwana (Young 1993; Streel et al. 2000).

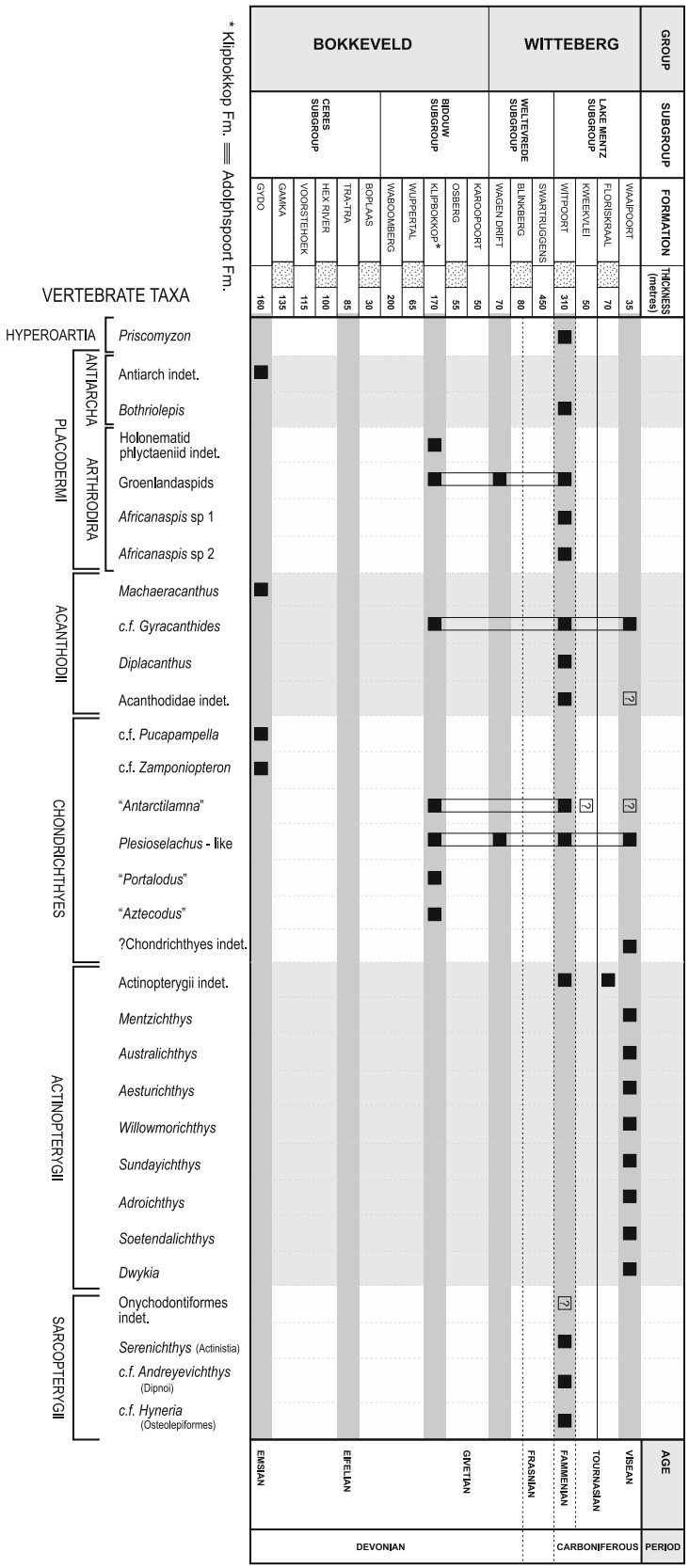

Fig. 13.6 Stratigraphic distribution and ranges of vertebrate taxa in the Bokkeveld and Witteberg Groups. Figure combining the stratigraphic column of Theron and Thamm (1990) (incorporating the sea-level-based dating of Cooper 1986), with published and unpublished records of vertebrate fossils

What is most marked, however, about the emerging biostratigraphic pattern, is the total absence of placoderm remains in strata that are stratigraphically younger than the Witpoort Formation. This is particularly pertinent due to the high preservational potential of placoderm dermal plates and their high diversity in the Witpoort Formation. In addition upper Witteberg strata have, as yet, yielded no sarcopterygian remains.

Although sparse vertebrate fossils are known from the overlying Kweekvlei and Foriskraal Formations (Lake Mentz Subgroup, Witteberg Group) they are restricted to the remains of *Antarctilamna*-like sharks, unidentified acanthodians and actinopterygians.

When abundant vertebrate fossils are, once more, encountered in the fossil record, within Waaipoort Formation (Lake Mentz Subgroup, Witteberg Group) strata, these are overwhelmingly dominated by diverse actinopterygian taxa. Only gyracanthid and possibly acanthodid acanthodians together with certain sharks appear to form a continuity with earlier communities. Additional sharks also appear to be present.

These changes are entirely consistent with global changes if the Devonian-Carboniferous boundary is situated at the end of the Famennian aged Witpoort Formation as suggested by Cooper (1986). Globally the End-Devonian Extinction Event, in the latest Famennian, resulted in the total extirpation of all placoderm groups, irrespective of environmental setting. Of the acanthodians only gyracanthids and acanthodids survived the end of the Devonian (gyracanthids subsequently survived until the Late Carboniferous, and acanthodids until the Early Permian). In addition, many Sarcopterygian groups were decimated, including most osteolepids. Vertebrate fossils are less commonly known from the Tournasion (a time of hypothetical lack referred to as Romers Gap) whilst an unprecedented radiation of actinopterygians is seen to colonise vacant niches thereafter.

13.7 Conclusion

Congruence between the vertebrate biostratigraphy of the upper Cape Supergroup and that observed globally during the Late Devonian and Early Carboniferous, provides the strongest yet confirmation for the proposed dating of this portion of the sratigraphic succession on the basis of sea-level fluctuations (Cooper 1986). This is also consistent with other, more incidental palaeontological evidence. Correlation of the Witpoort Formation with the Famennian (latest subdivision of the Devonian) is therefore considered well-established and placement of the Devonian-Carboniferous boundary immediately above the Witpoort Formation is confirmed.

Acknowledgements This research was supported by the Palaeontological Scientific Trust (PAST), National Research Foundation (NRF) and the Department of Science and Technology (DST) of South Africa. The support of the South African DST/NRF Centre of Excellence in Palaeosciences (CoE in Palaeosciences) towards this research is hereby acknowledged. The input of John Almond, regarding the Bokkeveld Group, over many years, is appreciated. The reviewers, particularly Dr Michael Coates of the University of Chicago, are thanked for their constructive comments.

References

Algeo TJ, Scheckler E, Maynard JB (2001) Effects of the Middle to Late Devonian Spread of Vascular Land Plants on Weathering Regimes, Marine Biotas and Global Climate. In: Gensel PG, Edwards D (eds) Plants Invade the Land: Evolutionary and Environmental Perspectives. Columbia University Press, New York, p 213–236.

Almond JE, Evans FJ (1996) Early—Middle Devonian fish faunas from the Bokkeveld Group, South Africa. In: Abstracts from the 9th Biennial Conference of the Palaeontological Society of South Africa, Stellenbosch, 23–25 September 1996.

Almond J, Evans F (1997) Personal Communication with Gess RW in Belville, Western Cape, South Africa.

Anderson JM, Anderson HM (1985) The Palaeoflora of Africa: Prodromus of Southern African megafloras, Devonian to Lower Cretaceous. Balkema, Rotterdam.

Anderson HM, Hiller N, Gess RW (1995) *Archaeopteris* (Progymnospermopsida) from the Devonian of southern Africa. Bot J Linn Soc. 117: 305–320.

Anderson ME, Long JA, Gess RW, Hiller N (1999) (a) An unusual new fossil shark (Pisces: Chondrichthyes) from the Late Devonian of South Africa. Records of the Western Australian Museum **57**: 151–156.

Anderson ME, Long JA, Evans FJ, Almond JE, Theron JN, Bender PA (1999) (b) Biogeography of South African Devonian fish. Records of the Western Australian Museum **57**: 157–168.

Boucot AJ, Brunton CHC, Theron JN (1983) Implications for the age of South African Devonian rocks in which *Tropidolepis* (Brachiopoda) has been found. Geol Mag 120: 51–58.

Chaloner WG, Forey PL, Gardiner BG, Hill AJ, Young VT, (1980). Devonian fish and plants from the Bokkeveld Series of South Africa. Annals of the South African Museum 81: 127–157.

Cooper MR (1986) Facies shifts, sea-level changes and event stratigraphy in the Devonian of South Africa. S Afr J Sci 82: 255–258.

Evans FJ (1997) Palaeobiology of Early Carboniferous fishes and contemporary lacustrine biota of the Waaipoort Formation (Witteberg Group), South Africa. MSc dissertation, University of Stellenbosch.

Evans FJ (1999) Palaeobiology of Early Carboniferous lacustrine biota of the Waaipoort Formation (Witteberg Group), South Africa. Palaeontologia Africana 35:1–6.

Evans FJ (2005) Taxonomy, Palaeoecology and Palaeobiogeography of some Palaeozoic Fish of Southern Gondwana. PhD thesis, University of Stellenbosch.

Gardiner BG (1969) New palaeoniscoid fish from the Witteberg series of South Africa. Zoo J Linn Soc 48: 423–452.

Gardiner BG (1973) New Palaeoniscoid fish remains from Southern Africa. Palaeontologia Africana 15: 33–35.

Gess RW (2001) A new species of *Diplacanthus* from the Late Devonian (Famennian) of South Africa. Annales de Paléontologie 87: 49–60.

Gess RW, Coates, MI, Rubidge BS (2006) A lamprey from the Devonian period of South Africa. Nature 443, 981–984.

Gess R, Coates M (2008) Vertebrate Diversity of the Late Devonian (Famennian) Deposit near Grahamstown, South Africa. J Vertebr Paleontol 28 (3).

Gess RW, Coates MI (2015) High Latitude Chondrichthyans from the Late Devonian (Famennian) Witpoort Formation of South Africa. Palaeontologische Zeitschrift 89: 147–169.

Gess RW, Coates MI (2015) (b) Fossil juvenile coelacanths from the Devonian of South Africa shed light on the order of character acquisition in actinistians. *Zool Journal Linn Soc* 175: 360–383.

Gess RW, Hiller N (1995) A preliminary catalogue of fossil algal, plant, arthropod, and fish remains from a Late Devonian black shale near Grahamstown, South Africa. Annals of the Cape Provincial Museums (natural History) 19: 225–304.

Jubb RA (1965) A new palaeoniscid fish from the Witteberg Series (Lower Carboniferous) of south Africa. Annals of the South African Museum 48: 267–272.

Long JA, Anderson ME, Gess RW, Hiller N (1997) New placoderm fishes from the Late Devonian of South Africa. J Vertebr Paleontol 17: 253–268.

Marais JAH (1963) Fossil fishes from the Upper Witteberg beds near Lake Mentz, Jansenville District, Cape Province. Annals of the Geological Survey of South Africa 2: 193–198.

Matshobo LC (1994) The geology of the area between Alicedale and Kommadagga. Honours Disertation, Rhodes University, Grahamstown.

Plumstead EP (1967) A general review of the Devonian fossil plants found in the Cape System of South Africa. Palaeontologia africana 10: 1–83.

Stapleton RP (1977) Carboniferous unconformity in southern Africa. Nature 268: 222–223.

Sallan LC, Coates MI (2010) End Devonian extinction and a bottleneck in the early evolution of modern jawed vertebrates. P Natl Acad Sci USA 107: 10131–10135.

Smithson TR, Wood SP, Marshall JEA, Clack JA (2012) Earliest Carboniferous tetrapod and arthropod faunas from Scotland populate Romer's Gap. P Natl Acad Sci USA 109: 4532–4537.

Smithson TR, Richards KR, Clack JA (2015) Lungfish diversity in Romer's Gap: reaction to the end-Devonian extinction. Palaeontology 59(1): 29–44.

Streel M, Caputo MV, Loboziak S, Melo G (2000) Late Frasnian-Famennian climates based on palynomorph analyses and the question of the Late Devonian glaciations. Earth-Sci Rev **52**: 121–173.

Streel M, Theron J (1999) The Devonian-Carboniferous boundary in South Africa and the age of the earliest episode of the Dwyka glaciation: new palynological evidence. Episodes 22: 41–44.

Thamm AG, Johnson MR (2006) The Cape Supergroup. In: Johnson MR, Anhaeusser CR, Thomas RJ (eds). The Geology of South Africa. Geological Society of South Africa, Johannesburg/Council for Geoscience, Pretoria p 443–460.

Theron JN (1993) The Devonian-Carboniferous boundary in South Africa. Annales de la Societe geologique de Belgique 116(2): 291–300.

Theron JN and Thamm AG (1990) Stratigraphy and sedimentology of the Cape Supergrouop in the Western Cape. Guidebook PR2, Geocongress '90. Geological Society of South Africa. p 64.

Theron JN, Johnson MR (1991) Bokkeveld Group (including the Ceres, Bidouw & Traka subgroups), In: Johnson MR (ed), SACS catalogue of South African Lithostratigraphic units, 3, p 3–5.

Young GC (1993) Vertebrate faunal provinces in the middle Palaeozoic. In Long JA (ed) Palaeozoic vertebrate biostratigraphy and biogeography: p 293–323, Belhaven Press, London.

Advances in Nonmarine Karoo Biostratigraphy: Significance for Understanding Basin Development

14

Bruce S. Rubidge, Michael O. Day, Natasha Barbolini, P. John Hancox, Jonah N. Choiniere, Marion K. Bamford, Pia A. Viglietti, Blair W. McPhee, and Sifelani Jirah

Abstract

The nonmarine Permo-Jurassic deposits of the Karoo Supergroup of South Africa have long been a world standard for tetrapod biostratigraphy. Recent and ongoing research is revising the palaeoflora and palaeofauna of these sedimentary strata with an unprecedented level of stratigraphic precision. This work has shown that: Permian palynomorphs are useful for correlating time-equivalent lithostratigraphic units in different sectors of the basin; that there is a marked end-Guadalupian diversity drop in tetrapods; that the *Dicynodon* Assemblage Zone can be subdivided, and should be renamed as the *Daptocephalus* Assemblage Zone; that the *Cynognathus* Assemblage Zone has a robust threefold subdivision; and that the name *Euskelosaurus* for the *Euskelosaurus* Range Zone is invalid and should be replaced. This work, together with new radiometric dates from the Karoo Supergroup, has dramatically enhanced our understanding of the timing of major evolutionary events in terrestrial ecosystems and provides strong evidence for tectonic controls on accommodation and sedimentation in the Karoo Basin during the Permo-Jurassic, within an overall flexural basinal setting.

Keywords

Palaeozoic • Mesozoic • Karoo Supergroup • Stratigraphy • Non-mammalian synapsid • Sauropodomorph

14.1 Introduction

The Karoo Supergroup of South Africa hosts a temporally extensive palaeontological record of terrestrial life, extending from the Middle Permian until the Early Jurassic (Rubidge 2005). It is particularly noted for its wealth of fossil tetrapods, including non-mammalian synapsids, temnospondyl amphibians and archosauriformes. The rocks of the Karoo Basin are also an excellent source of palaeobotanical fossils (Anderson and Anderson 1985; Bamford 2000; Prevec et al. 2010) and palynomorphs (Barbolini 2014; see references therein), but these have received less research attention than the tetrapods.

Early researchers working on the Karoo Basin realised the utility of fossil tetrapods for biostratigraphy, especially in light of the paucity of lithological marker beds. Their research paved the way for more refined biostratigraphic subdivision of the Beaufort Group (e.g. Rubidge 1995) and the Stormberg Group (Kitching and Raath 1984). In addition, three palynostratigraphic schemes spanning the Carboniferous-Jurassic have been drawn up for the northern and southern Karoo Basin (Barbolini 2014; see references therein). Fossil wood has also been used to create a biostratigraphic subdivision that can be correlated with the vertebrate biozones (Bamford 1999). Recent advances in Karoo biostratigraphy have improved our ability to correlate fossil-bearing continental successions across Pangea, our

B.S. Rubidge (✉) · M.O. Day · N. Barbolini · P.J. Hancox · J. N. Choiniere · M.K. Bamford · P.A. Viglietti · B.W. McPhee · S. Jirah
Evolutionary Studies Institute and School of Geosciences, University of the Witwatersrand, Johannesburg, PO Wits 2050, South Africa
e-mail: bruce.rubidge@wits.ac.za

B. Linol and M.J. de Wit (eds.), *Origin and Evolution of the Cape Mountains and Karoo Basin*, Regional Geology Reviews, DOI 10.1007/978-3-319-40859-0_14

understanding of past extinction events, and allowed for refined temporal control for development models.

14.2 Biostratigraphy

The lithological nature of the Ecca-Beaufort contact is now well documented (Rubidge et al. 2000) and is marked by a change in fluvial style, from subaqueous delta-dominated, to subaerial shoreline-dominated systems (Rubidge et al. 2000). Palaeontological evidence demonstrates that this contact is diachronous (e.g. Rubidge 2005). The lowest Beaufort Group strata along the southwestern margin of the basin yield tetrapod fossils assignable to the *Eodicynodon* Assemblage Zone (AZ), while in the northeast the lowest Beaufort strata contain fossils of the younger *Dicynodon* AZ (Fig. 14.1). This observation is supported by palynological data (Barbolini 2014) in that the northern Volksrust (Ecca Group) microflora shows greatest similarity to the southern Abrahamskraal Formation (*Tapinocephalus* AZ—Beaufort Group), suggesting that the Volksrust and Abrahamskraal formations were deposited synchronously.

The Guadalupian-aged Abrahamskraal Formation and eastern equivalent, the Koonap Formation (Fig. 14.2) is present only in the south of the basin and is the oldest lithostratigraphic unit of the Beaufort Group (Johnson et al. 2006). The *Eodicynodon* and *Tapinocephalus* AZ faunas that it hosts primarily comprise basal members of most major therapsid groups except the cynodonts. For the *Tapinocephalus* AZ, taxonomic studies have provided major insight into the diversity and stratigraphic ranges of dicynodonts (e.g. Angielczyk and Rubidge 2013), therocephalians (Abdala et al. 2014), dinocephalians (Güven et al. 2013) and gorgonopsians (Kammerer et al. 2015), which has been crucial to biostratigraphic work.

Many species (up to 80 %) have their Last Appearance Datum (LAD) near the top of the Abrahamskraal Formation, which represents the transition from the *Tapinocephalus* AZ to the succeeding *Pristerognathus* AZ (Day et al. 2015). An ID-TIMS date of ~260.26 Ma for the base of the overlying Teekloof Formation suggests this may correspond with the marine late-Capitanian mass extinction (Day et al. 2015). The base of the Teekloof, and in the east the Middleton Formation, comprises a laterally extensive, sandstone-dominated package that in the west is known as the Poortjie Member. The Poortjie Member primarily hosts a *Pristerognathus* AZ fauna, which represents the early recovery from the late-Capitanian extinction, and the beginnings of the Lopingian fauna (Day et al. 2015; Fig. 14.3).

The extent and definition of the early Lopingian *Tropidostoma* and *Cistecephalus* AZs has not changed since the last review of Rubidge (1995), and corresponds to the upper Middleton and lower Balfour formations (Fig. 14.2). Concern over the similarity and stratigraphic overlap between

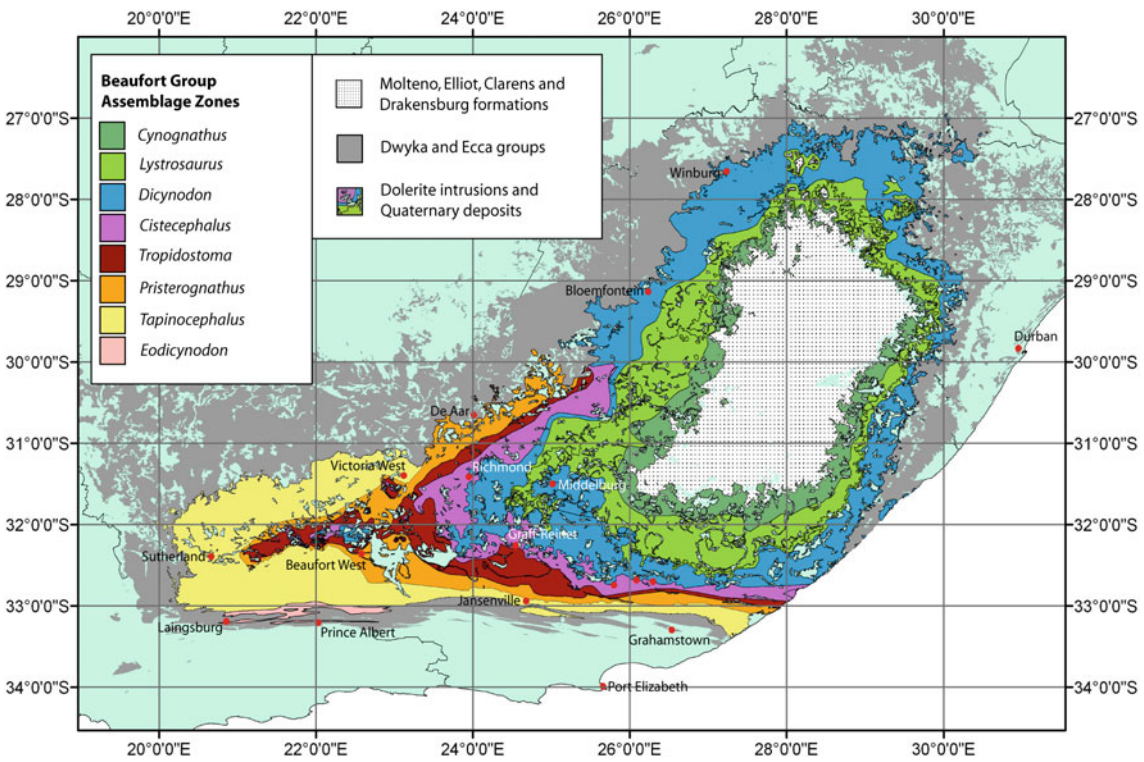

Fig. 14.1 Biozonation of the Beaufort Group based on vertebrate collections records (after van der Walt et al. 2010)

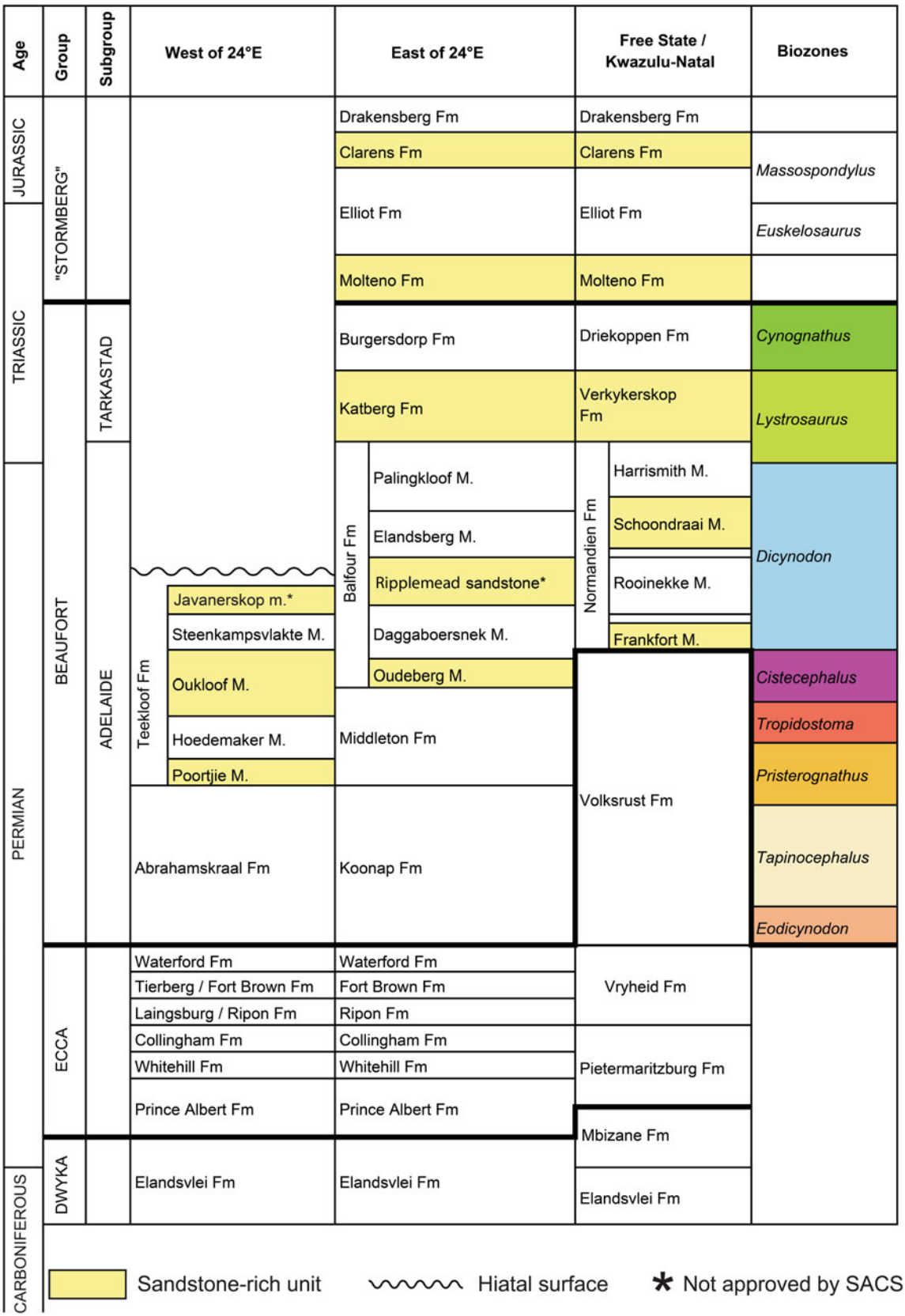

Fig. 14.2 Litho- and biostratigraphic subdivisions of the Karoo Supergroup

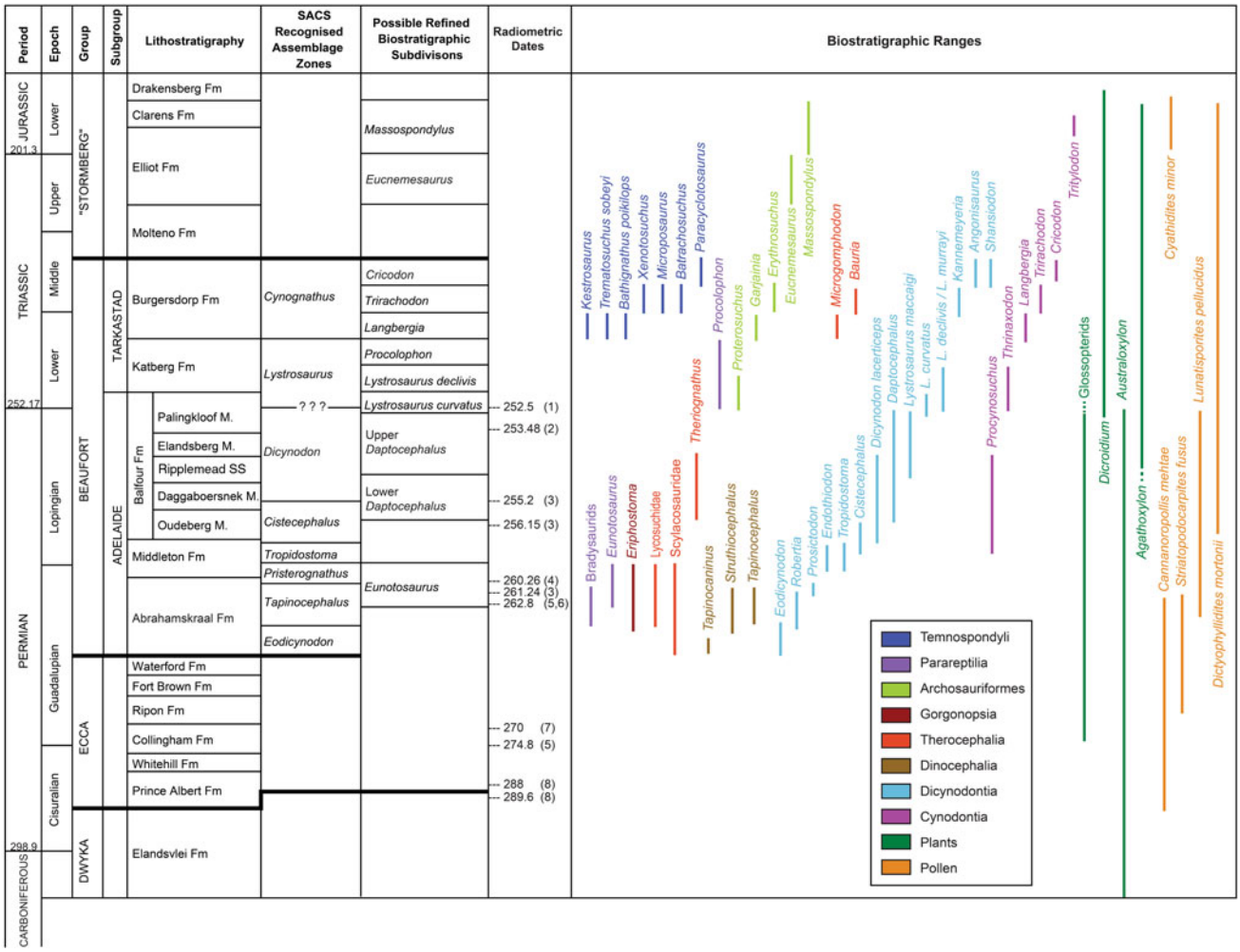

Fig. 14.3 Stratigraphic ranges of key tetrapod, palynomorph, and fossil wood taxa in the main Karoo Basin. References for dates presented are: 1. Coney et al. (2007), 2. Gastaldo et al. (2015), 3. Rubidge et al. (2013), 4. Day et al. (2015), 5. Fildani et al. (2007), 6. Fildani et al. (2009), 7. Turner (1999), 8. Bangert et al. (1999)

the dicynodont index species *Tropidostoma microtrema* and the long ranging genus *Oudenodon bainii* precipitated a study that found the two genera to be distinct using morphometric analyses of snout shape and skull dimensions (Botha and Angielczyk 2007). *O. bainii* first occurs in the *Tropidostoma* AZ and so its FAD is not a good indicator for the base of the *Cistecephalus* AZ, as previously considered.

The *Daptocephalus* (previously the *Dicynodon*) AZ, which spans the uppermost Permian strata (Balfour, upper Teekloof and Normandien Formations), has recently been re-established for the youngest Permian biozone of the Beaufort Group, and two subdivisions have been proposed therein (Viglietti et al. 2016), new lithostratigraphic subdivision has also been proposed (Viglietti 2016), although not yet officially accepted by SACS (Fig. 14.2). The Javanerskop member is an arenaceous unit that appears in the upper Teekloof Formation. The Barberskrans Member is renamed the Ripplemead Member because Tordiffe's (1978) Barberskrans Member is shown to be part of the Oudeberg Member (Viglietti 2016). The new *Daptocephalus* AZ resulted from the recognition that the three index fossils used to define the former *Dicynodon* AZ (*Dicynodon lacerticeps*, *Theriognathus microps*, and *Procynosuchus delaharpeae*) have their FAD below its traditionally recognized lower boundary, and have ranges mostly restricted to the lower portion of the biozone, well below the Permo-Triassic boundary (PTB) in the southern portion of the basin (Viglietti et al. 2016). This resulted in an informal subdivision of the biozone where the appearance of *Daptocephalus leoniceps* and *Theriognathus microps* defines the base of the lower *Daptocephalus* AZ subzone, and the appearance of *Lystrosaurus maccaigi* defines the base of the upper subzone. The upper *Daptocephalus* AZ terminates with the disappearance of *Daptocephalus leoniceps* at the PTB (Smith and Botha-Brink 2014). Although *Lystrosaurus* is present in the upper subdivision of the upper *Daptocephalus*

AZ, this is not recognized as part of the *Lystrosaurus* AZ because the species found there, *L. maccaigi*, is limited to the Permian. The Upper *Daptocephalus* AZ also retains a Permian fauna, prior to the major faunal turnover observed at the inferred PTB (Smith and Botha-Brink 2014; Viglietti et al. 2016).

The Karoo Basin preserves one of the few relatively complete terrestrial PTB successions in the world and as a result, is a rare window into terrestrial ecosystems during the greatest mass extinction event in Earth's history. Events prior to this extinction, and its aftermath in the terrestrial realm, have received attention in the Karoo Basin from varied scientific disciplines including palaeontology, sedimentology, taphonomy, palaeomagnetics and stratigraphy (Viglietti et al. 2016; Smith and Botha-Brink 2014; Gastaldo et al. 2015). Karoo Basin rocks indicate changes in fluvial style during the transition from the Permian to Triassic, and are believed to relate to vegetation die-off and the onset of drier, warmer, and highly seasonal conditions by the Early Triassic (Smith and Botha-Brink 2014). These changes have for some time been demonstrated to coincide with a three-phased extinction of numerous non-mammalian synapsid genera, disappearance of most of the glossopterid flora, as well as a temporary spike in abnormal tri- and tetra-saccate pollen over the PTB (Prevec et al. 2010; Smith and Botha-Brink 2014).

A high precision age of 253.48 ± 0.15 Ma (early Changhsingian) was recently obtained from zircons in a silicified ash close to the inferred PTB in South Africa (Gastaldo et al. 2015) (Fig. 14.3). These authors also report on an apparently Permian dicynodontoid skull and *Glossopteris* flora preserved in strata defined as earliest Triassic due to the presence of intraformational conglomerate lags within this same interval. In combination with their estimated average depositional rates, they suggest this is evidence for the PTB and the *Daptocephalus-Lystrosaurus* AZ boundary being stratigraphically higher than is currently reported by the disappearance of taxa in the phased extinctions of Smith and Botha-Brink (2014). However, ash layers in the Beaufort Group commonly show evidence for reworking (Rubidge et al. 2013; McKay et al. 2015), intraformational conglomerates are common in the upper *Daptocephalus* AZ strata, and average depositional rates cannot be inferred for fluvial rocks, which are defined by frequent periods of erosion and non-deposition (Miall 2014). Furthermore, the dicynodontoid skull in question is poorly preserved within a conglomeritic lag and could result from reworking of floodplain sediments (Smith and Botha-Brink 2014).

New findings show that the PTB is not a conformable boundary across the Karoo Basin, as demonstrated by a significant thinning of strata in a northerly direction, and the disappearance of *Daptocephalus* AZ taxa below the PTB in the southern part of the basin (Viglietti 2016; Viglietti et al. 2016). Thus, in the south of the basin (i.e. the proximal sector) there is a more complete record of this extinction event than in the north (i.e. the distal sector). This supports work by Gastaldo et al. (2009) who regard the laminated PTB red beds described by Smith and Botha (2005) in the Bethulie area (in the distal part of the Karoo Basin) as laterally discontinuous and non-synchronous. Furthermore, in the most distal portions of the basin, the PTB is marked by an unconformity and is not preserved (Rutherford et al. 2015).

The Triassic Tarkastad Subgroup has been the focus of significant research both in terms of biostratigraphy and lithostratigraphy (Hancox 1998; Neveling 2002). The arenaceous Katberg Formation has previously been considered to have resulted from either tectonic uplift in the Cape Fold Belt (CFB), tectonic quiescence in the CFB (Catuneanu et al. 1998) or, more recently, to changing fluvial styles attributable to the die-off of vegetation at the PTB (Smith and Botha-Brink 2014). The overlying Burgersdorp Formation is a predominantly argillaceous sequence that conformably overlies the Katberg Formation in the south and west of the basin. Neveling (2002) questioned the long-held belief that no overlap exists between the faunas of the *Lystrosaurus* and *Cynognathus* AZs, showing that this does not hold in the southern and western regions of the basin. These studies revealed an increase in procolophonid abundance towards the top of the biozone above the LAD of *Lystrosaurus*. There may therefore be merit in re-instating the *Procolophon* Zone, between the LAD of *Lystrosaurus* and the FAD of elements of the *Cynognathus* AZ.

Recent work has shown that *Cynognathus* extends throughout the temporal range of the *Cynognathus* AZ, and is the most appropriate index taxon for the biozone. Additional collecting in this biozone has also allowed for the establishment of threefold subdivision initially based on the FADs of various temnospondyls and archosaurs (Shishkin et al. 1995), and more recently on the trirachodontid cynodonts *Langbergia*, *Trirachodon* and *Cricodon* (Hancox et al. submitted). This in turn has allowed for refined correlation of the Early-Middle Triassic Pangean continental deposits (Hancox et al. submitted). Ottone et al. (2014) obtained a SHRIMP $^{238}U/^{206}Pb$ age of 235.8 ± 2.0 Ma, for an ignimbrite from between the Quebrada de los Fósiles and Río Seco de la Quebrada formations in Argentina, which have been correlated with the *Trirachodon* and *Cricodon* subzones of the *Cynognathus* AZ. This age assignation, if correct, implies that the upper *Cynognathus* AZ would have been deposited some 10 Ma later than currently accepted, and implies long periods of non-deposition in the Triassic Beaufort and a 15 Ma temporal range for *Cynognathus.*

Leaf impressions of the *Glossopteris* flora occur throughout the Permian (Anderson and Anderson 1985) but ecological variations confound the use of the leaves for biostratigraphic purposes. Reproductive structures are more

useful, but are much rarer (Prevec et al. 2010). Silicified wood occurs throughout the Karoo Supergroup and can be used for low resolution biostratigraphy as well as to provide information on vegetation and climate.

The occurrence of wood-species that have long time ranges is useful for standardising growth ring analyses and climate reconstruction (Chap. 16 this book). Dwyka Group woods from Namibia have preserved central pith of various types, and to date, woods with pith have not been found in the Ecca Group or younger strata (Bamford 2000). In the Karoo Basin of South Africa *Australoxylon* is present from the Ecca Group into the upper Beaufort (Upper Permian) and a new wood, *Agathoxylon,* is present from the base of the Normandien Formation, the northern equivalent of the upper Balfour Formation. The range of *Agathoxylon karooensis* is restricted to the Normandien Formation, whereas that of *Agathoxylon africanum* extends throughout the Triassic (Bamford 1999).

Apart from dinosaur footprints, the overlying Upper Triassic Molteno Formation does not host fossil tetrapods, but does have a rich fish, insect and *Dicroidium* megaflora (Anderson and Anderson 1985). Although the Molteno Formation has a high diversity of plants, only three wood genera are represented, *Agathoxylon*, *Podocarpoxylon* and *Rhexoxylon*. Palynological diversity of the Molteno Formation is not higher than that of other Karoo formations, suggesting that the huge diversity of macroplants represents a sampling and preservation bias, rather than higher plant diversity during the Late Triassic (Barbolini 2014).

Sauropodomorph dinosaurs form the basis of Stormberg Group biostratigraphy (Kitching and Raath 1984) and the current biostratigraphic scheme consists of a lower '*Euskelosaurus*' and an upper *Massospondylus* Range Zone (RZ) (Kitching and Raath 1984). This RZ subdivision is generally coincident with a lithostratigraphic boundary between the lower and upper Elliot Formation (Bordy et al. 2004a), which is thought to also mark the Triassic-Jurassic boundary (Olsen and Galton 1984). This biostratigraphic zonation of Kitching and Raath (1984) has not gained widespread acceptance because of the shortage of detailed stratigraphic data for key fossil discoveries, and taxonomic issues with '*Euskelosaurus' sp.* This "catch all" genus has now been shown to contain several valid genera, including *Antetonitrus*, *Plateosauravus* and *Eucnemesaurus* (McPhee et al. 2014). Of the lower Elliot Formation genera, *Eucnemesaurus* appears to be the best biostratigraphic marker taxon for the Triassic strata (McPhee et al. 2015a) (Fig. 14.3). Other relatively large-bodied sauropodomorph taxa, such as *Antetonitrus,* occur only in the upper part of the Elliot Formation, and are thus presumably Early Jurassic.

Preliminary results suggest that the sauropodomorph fauna of the Early Jurassic *Massospondylus* RZ is much more diverse than previously thought. Importantly it contains taxa with a broader range of body sizes than the former '*Euskelosaurus*' RZ (McPhee et al. 2015b). Ongoing fieldwork to improve the stratigraphic and taxonomic precision of dinosaur taxa will help refine biostratigraphic subdivision of the Elliot and Clarens formations.

14.3 Basin Development

The retroarc foreland basin model for the main Karoo Basin is pervasive because it best explains the out-of-phase deposition of lithostratigraphic units. Catuneanu et al. (1998) showed that flexural tectonics partitioned the Karoo Basin into proximal foredeep, central forebulge, and distal backbulge flexural provinces. Orogenic loading and unloading caused changes in position of the forebulge and foredeep. This resulted in deposition in the proximal (with reference to the Gondwanan Mobile Belt) or distal regions of the Karoo Basin. Flexural tectonics is interpreted as being the result of subduction of the Palaeo-Pacific plate under southern Gondwana at a low angle (i.e., flat slab subduction) (Catuneanu et al. 1998). The drag force generated by viscous mantle corner flow, coupled to the low angle of the subducting plate, caused orogenic loading and subsidence (and the accommodation space for the deposition of lithostratigraphic units) to happen out of phase throughout the Karoo Basin (Mitrovica et al. 1989). The southern margin of the basin is bounded by the CFB and links have been made between dated periods of coaxial compressional deformation in this zone (Hansma et al. 2015) and sedimentary responses in the Karoo Basin (Catuneanu et al. 1998). The problem of reliable time resolution has recently been improved by radiometric dates (Fildani et al. 2009; Rubidge et al. 2013; Day et al. 2015; Gastaldo et al. 2015) in combination with better biostratigraphic resolution (Fig. 14.3).

At the base of the Beaufort Group, improvements in the dating of tetrapod biozones directly overlying the Ecca Group show that beginning in the Wordian, the Ecca Sea underwent a regression that began from the southwest margin of the basin (*Eodicynodon* AZ deposition) and prograded northeastwards to the southern Free State Province by the late Wuchiapingian. This regression might not have occurred at an even rate and evidence for this comes from exposures north of the Orange River, where the *Pristerognathus* AZ, which directly overlies the Ecca Group, is in turn overlain directly by the *Daptocephalus* AZ (Welman et al. 2001). This suggests that regression was punctuated, with little change in the position of the shoreline in the early Wuchiapingian (Day 2013). Biostratigraphic correlation with the marine/lacustrine rocks of the northern Ecca Group suggests that while Guadalupian–Lopingian Permian fluvial

deposition of the Beaufort Group took place in the south of the basin, contemporaneous deposition of subaqueous Ecca Group sedimentary rocks (Volksrust Formation) occurred in the northern distal sector (Catuneanu et al. 1998; Rubidge 2005; Barbolini 2014) (Fig. 14.2).

An age of 260.4 Ma for the top of the Koonap Formation (Day et al. 2015) and biostratigraphic correlation suggest that the base of the Teekloof (Poortjie Member) and Middleton formations are the same age. The association of the terminal *Tapinocephalus* AZ tetrapod extinctions with the base of the arenaceous Poortjie Member implicates climatic influences as the cause of both, but this is unsure. Although the formation of the Poortjie Member has been attributed to increased aridification and a consequent reduction in vegetation cover and increase in weathering of the source region (Cole and Wipplinger 2001), recent sedimentological studies of channel sandstones invoke tectonics rather than climate as the most likely cause for the lithological changes (Paiva 2015). This could coincide with the end of a deformation phase in the CFB, recently recalibrated to have lasted from ~275–260 million years ago (Hansma et al. 2015; but see Chap. 5 of this book for alternative interpretations).

Rutherford et al. (2015) have shown that during the Upper Permian and Lower Triassic, certain parts of the Beaufort Group stratigraphic succession that are present in the southern part of the Karoo Basin are absent in the central Free State. This suggests either a depositional hiatus, or a period of erosion at the beginning and the end of *Lystrosaurus* AZ, as well as the end of *Cynognathus* AZ times, and that during these depositional hiatuses or periods of erosion, deposition or preservation of the rock record was restricted to the proximal sector. Similarly, Neveling (2002) recognized that the Katberg Formation comprises different units, with the lowermost unit being restricted to the proximal sector, the middle (Swartberg Member) being present throughout the basin, and the uppermost unit present only in the proximal sector. Such an arrangement indicates a proximal migration of the depocentre, and thus an increase in accommodation space in the proximal sector, in response to a short period of tectonic loading.

The uppermost Katberg Formation fines upwards into the Burgersdorp Formation, which contains a *Langbergia* subzone assemblage (Fig. 14.3). This latest Lower Triassic unit does not show contrasting stratigraphies in the proximal and distal sectors of the basin, indicating that continental fluvial deposition was taking place in both sectors (Neveling 2002). The progressively smaller surface areas of the Middle Triassic *Trirachodon* and *Cricodon* subzones, however, indicates a receding basin through time (Hancox 1998), with no deposition or erosion in the distal sector. Biostratigraphic refinement of the Burgersdorp Formation and its contained *Cynognathus* AZ fauna (Shishkin et al. 1995; Hancox et al. submitted) has shown that the Beaufort–Stormberg contact in the south represents only the latest Middle Triassic (Ladinian), whereas in the north it represents the entire Middle Triassic, a period of up to 10 million years. Recognition of such regional unconformities is important, as they are indicative of significant base level changes.

The nature of the contact between the Molteno and overlying Elliot formations is not yet properly understood, but it appears that this most likely followed the same path that had been set in Burgersdorp and Molteno times, when the basin initially receded and later expanded (Bordy et al. 2005). Ultimately, the fluvially deposited Elliot Formation occupied both northerly and southerly positions in the basin, although still only within the distal portion of the basin. Continental fluvial deposition continued in the Early Jurassic in an increasingly arid environment and ultimately led to the expansive erg in South Africa represented by the Clarens Formation, which appears to have stretched at least across Zimbabwe (Forest Sandstone Formation) and Namibia (Etjo Formation), and even across to the American continent (Rubidge 2005).

The retroarc foreland basin hypothesis has been questioned in recent years by authors who propose fault controlled subsidence and extension (Tankard et al. 2012), continent–continent collision (Lindeque et al. 2011), and asymmetrical subsidence (Fildani et al. 2009) models for the Karoo Basin. It is however only the timing of the onset of flexural tectonics that has been seriously disputed. It is now clear that by the deposition of the Dwyka Group, flexural tectonics were already in place as evidenced by a foredeep transgressed by an interior seaway, a forebulge uplifted above base level with continental ice sheets, and a shallow backbulge depocenter to the north (Catuneanu 2004). This means the Karoo Basin was most likely a foreland basin from its formation and these conditions continued into the Stormberg Group (Bordy et al. 2004b).

The only problematic issue with the foreland model has been the difficulty in correlating tectonic paroxysms with sedimentation events in the Karoo Basin. New $^{40}Ar/^{39}Ar$ age constraints on the deformation in the CFB has contributed to this debate, most recently by Hansma et al. (2015), as cause-and-effect relationships between source area orogenesis and sedimentation in the Karoo are dependent on reliable chronological constraints. This work constrains a broad period of orogenesis from ~275–260 Ma and also constrains a later phase of what may be cooling (or possibly a second period of deformation) from 255–245 Ma (Hansma et al. 2015). Reciprocal cyclical deposition of the Katberg and Burgersdorp formations (Catuneanu et al. 1998) implies the continuation of orogenic activity in the Lower Triassic, but the age constraints for CFB deformation are too broad to conclusively link putative orogenic pulses with cyclical deposition within the basin. Nevertheless, strong evidence

exists for flexural tectonics controlling deposition of the Karoo Supergroup.

Acknowledgment This work was supported by the University of the Witwatersrand, the DST-NRF Centre of Excellence in Palaeosciences, The NRF African Origins Platform, and the Palaeontological Scientific Trust and its Scatterlings of Africa Programmes. We are indebted to Maarten de Wit and Bastien Linol and an anonymous reviewer for very helpful comments which have greatly improved the paper.

References

Abdala NF, Kammerer CF, Day MO, Jirah S and Rubidge BS (2014) Adult morphology of the therocephalian *Simorhinella baini* from the Middle Permian of South Africa and the taxonomy, geographic and temporal distribution of the Lycosuchidae. J Paleontol 88 (6): 1139–1153.

Anderson JM and Anderson HM (1985) Palaeoflora of southern Africa: Prodromus of South African megafloras, Devonian to Lower Cretaceous. Balkema, Rotterdam, 423 pp.

Angielczyk KD and Rubidge BS (2013) Skeletal morphology, phylogenetic relationships and stratigraphic range of *Eosimops newtoni* Broom, 1921, a pylaecephalid dicynodont (Therapsida, Anomodontia) from the Middle Permian of South Africa. Journal of Systematic Palaeontology 11 (2): 191–231.

Bamford MK (1999) Permo-Triassic fossil woods from the South African Karoo Basin. Palaeontologia africana 35: 25–40.

Bamford MK (2000) Fossil woods of Karoo aged deposits in South Africa and Namibia as an aid to biostratigraphic correlation. J Afr Earth Sci 31: 119–132.

Bangert B, Stollhofen H, Lorenz V and Armstrong R (1999) The geochronology and significance of ash-fall tuffs in the glaciogenic Carboniferous-Permian Dwyka Group of Namibia and South Africa. J Afr Earth Sci 29: 33–49.

Barbolini N (2014) Palynostratigraphy of the South African Karoo Supergroup and correlations with coeval Gondwana successions. Unpublished PhD Thesis, University of the Witwatersrand, Johannesburg, 386 pp.

Bordy EM, Hancox PJ and Rubidge BS (2004a) A description of the sedimentology and palaeontology of the Late Triassic–Early Jurassic Elliot Formation in Lesotho. Palaeontologia africana 40: 43–58.

Bordy EM, Hancox PJ and Rubidge BS (2004b) Basin development during the deposition of the Elliot Formation (Late Triassic-Early Jurassic), Karoo Supergroup, South Africa. South African J Geol 107: 397–412.

Bordy EM, Hancox PJ and Rubidge BS (2005) The contact of the Molteno and Elliot Formations through the main Karoo Basin, South Africa: a second order sequence boundary. South African J Geol 108: 351–364.

Botha J and Angielczyk KD (2007) An integrative approach to distinguishing the Late Permian dicynodont species *Oudenodon bainii* and *Tropidostoma microtrema* (Therapsida: Anomodontia). Palaeontol 50 (5): 1175–1209.

Catuneanu O, Hancox PJ and Rubidge BS (1998) Reciprocal flexural behaviour and contrasting stratigraphies, a new Basin development model for the Karoo retroarc foreland system, South Africa. Basin Res 10: 417–439.

Catuneanu O (2004) Basement control on flexural profiles and the distribution of foreland facies: The Dwyka Group of the Karoo Basin, South Africa. Geology 32: 517–520.

Cole DI and Wipplinger PE (2001) Sedimentology and molybdenum potential of the Beaufort Group in the main Karoo basin, South Africa. Memoir Council for Geoscience, Pretoria, 80, 225 pp.

Coney L, Reimold W, Hancox P, Mader D, Koeberl C, McDonald I, Struck U, Vajda V and Kamo S (2007) Geochemical and mineralogical investigation of the Permian–Triassic boundary in the continental realm of the southern Karoo Basin, South Africa. Palaeoworld 16, 67–104.

Day MO (2013) Middle Permian continental biodiveristy changes as reflected in the Beaufort Group of South Africa: a bio- and lithostratigraphic review of the *Eodicynodon, Tapinocephalus* and *Pristerognathus* Assemblage Zones. Unpublished Ph.D. Thesis, University of theWitwatersrand, Johannesburg, 387 pp.

Day MO, Ramezani J, Bowring SA, Sadler PM, Erwin DH, Abdala F and Rubidge BS (2015) When and how did the terrestrial mid-Permian mass extinction occur? Evidence from the tetrapod record of the Karoo Basin, South Africa. Proceedings of the Royal Society B 20150834. http://dx.doi.org/10.1098/rspb.2015.0834.

Fildani A, Drinkwater N, Weislogel A, McHargue T, Hodgson D and Flint S (2007) Age controls on the Tanqua and Laingsburg deep-water systems: New insights on the evolution and sedimentary fill of the Karoo Basin, South Africa. Journal of Sedimentary Research 77: 901–908.

Fildani A, Weislogel A, Drinkwater N, McHargue T, Tankard A, Wooden J, Hodgson D and Flint S (2009) U-Pb zircon ages from the southwestern Karoo Basin, South Africa: Implications for the Permian-Triassic boundary. Geology 37: 719–722.

Gastaldo RA, Neveling J, Clark CK and Newbury SS (2009) The terrestrial Permian-Triassic boundary event bed is a nonevent. Geology 37: 199–202.

Gastaldo RA, Kamo SL, Neveling J, Geissman JW, Bamford M and Looy CV (2015) Is the vertebrate-defined Permian-Triassic boundary in the Karoo Basin, South Africa, the terrestrial expression of the end-Permian marine event? Geology 43: 1–5.

Güven S, Rubidge BS and Abdala F (2013) Cranial morphology and taxonomy of South African Tapinocephalidae (Therapsida: Dinocephalia): the case of *Avenantia* and R*iebeeckosaurus*. Palaeontologia africana 48: 24–33.

Hancox PJ (1998) A stratigraphic, sedimentological and palaeoenvironmental synthesis of the Beaufort-Molteno contact in the Karoo Basin. Unpublished PhD Thesis, University of the Witwatersrand, Johannesburg, 404 pp.

Hancox PJ, Neveling J and Rubidge BS (Submitted) Biostratigraphic subdivision of the *Cynognathus* Assemblage Zone: implications for global correlation of Lower to Middle Triassic non-marine sequences. Palaeontology.

Hansma J, Tohver E, Jourdan F, Schrank C and Adams D (2015) The Timing of the Cape Orogeny: New 40Ar/39Ar age constraints on deformation and cooling of the Cape Fold Belt, South Africa. Gondwana Res. doi:10.1016/j.gr.2015.02.005.

Johnson MR, van Vuuren CJ, Visser JNJ, Cole DI, Wickens H de V, Christie ADM, Roberts DL and Brandl G (2006) Sedimentary rocks of the Karoo Supergroup. In: Johnson MR, Anhaeusser CR and Thomas RJ (Eds) The Geology of South Africa. Council for Geoscience, Pretoria, 461–501.

Kammerer CF, Smith RM, Day MO and Rubidge BS (2015) New information on the morphology and stratigraphic range of the mid-Permian gorgonopsian *Eriphostoma microdon* Broom, 1911. Papers in Palaeontology 1 (2): 201–221.

Kitching JW and Raath MA (1984) Fossils from the Elliot and Clarens Formations (Karoo sequence) of the northeastern Cape, Orange Free State, and Lesotho, and a suggested biozonation based on tetrapods. Palaeontologia africana 25: 111–125.

Lindeque A, de Wit MJ, Ryberg T, Weber M and Chevallier L (2011) Deep crustal profile across the southern Karoo Basin and Beattie

Magnetic Anomaly, South Africa: an integrated interpretation with tectonic implications. South African Journal of Geology, 114: 265–292.

Miall AD (2014) Fluvial depositional systems. Springer, Switzerland 316 pp.

McKay MP, Weislogel AL, Fildani A, Brunt RL, Hodgson DM and Flint SS (2015) U-PB zircon tuff geochronology from the Karoo Basin, South Africa: implications of zircon recycling on stratigraphic age controls. International Geology Review 57 (4): 393–410.

McPhee BW, Yates AM, Choiniere JN and Abdala F (2014) The complete anatomy and phylogenetic relationships of *Antetonitrus ingenipes* (Sauropodiformes, Dinosauria): implications for the origins of Sauropoda. Zoological Journal of the Linnean Society 171: 151–205.

McPhee BW, Choiniere JN, Yates AM and Viglietti PA (2015a) A second species of *Eucnemesaurus* Van Hoepen, 1920 (Dinosauria, Sauropodomorpha): new information on the diversity and evolution of the sauropodomorph fauna of South Africa's lower Elliot Formation (latest Triassic). Journal of Vertebrate Paleontology 36 (5): e980504.

McPhee BW, Bonnan MF, Yates AM, Neveling J and Choiniere JN (2015b) A new basal sauropod from the pre-Toarcian Jurassic of South Africa: evidence of niche partitioning at the sauropodomorph–sauropod boundary? Scientific Reports 5 (13224): 1–12. doi:doi:10.1038/srep13224.

Mitrovica JX, Beaumont C and Jarvis GT (1989) Tilting of continental interiors by the dynamical effects of subduction. Tectonics 8: 1079–1094.

Neveling J (2002) The biostratigraphy and sedimentology of the contact area between the *Lystrosaurus* and *Cynognathus* Assemblage Zones (Beaufort Group, Karoo Supergroup). Unpublished PhD.thesis, University of the Witwatersrand, Johannesburg, South Africa, 232 pp.

Olsen PE and Galton PM (1984) A review of the reptile and amphibian assemblages from the Stormberg of southern Africa, with special emphasis on the footprints and the age of the Stormberg. Palaeontologia africana 25: 87–110.

Ottone EG, Monti M, Marsicano CA, de la Fuente MS, Naipauer M, Armstrong R and Mancuso AC (2014) A new Late Triassic age for the Puesto Viejo Group (San Rafael depocenter, Argentina): SHRIMP UePb zircon dating and biostratigraphic correlations across southern Gondwana. Journal of South American Earth Sciences 56: 186–199.

Paiva F (2015) Fluvial facies architecture and provenance history of the Abrahamskraal-Teekloof Formation transition (Lower Beaufort Group) in the main Karoo Basin. Unpublished MSc dissertation, University of Cape Town, 98 pp.

Prevec R, Gastaldo RA, Neveling J, Reid SB and Looy CV (2010) An autochthonous glossopterid flora with latest Permian palynomorphs and its depositional setting in the *Dicynodon* Assemblage Zone of the southern Karoo Basin, South Africa. Palaeogeogr Palaeoclimatol Palaeoecol 292: 391–408.

Rubidge BS (Ed) (1995) Biostratigraphy of the Beaufort Group (Karoo Supergroup). SACS Biostratigraphic Series 1, 46 pp.

Rubidge BS, Hancox PJ and Catuneanu O (2000) Sequence analysis of the Ecca-Beaufort contact in the southern Karoo of South Africa. South African Journal of Geology 103(1): 81–96.

Rubidge BS, Erwin DH, Ramezani J, Bowring SA and De Klerk WJ (2013) High-precision temporal calibration of late Permian vertebrate biostratigraphy: U-Pb constraints from the Karoo Supergroup, South Africa. Geology. DOI 10.1130 G33622.1.

Rubidge BS (2005) Re-uniting lost continents–Fossil reptiles from the ancient Karoo and their wanderlust. South African Journal of Geology 108(1): 135–172.

Rutherford AB, Rubidge BS and Hancox PJ (2015) Sedimentology and palaeontology of the Beaufort Group in the Free State Province supports a reciprocal foreland basin model for the Karoo Supergroup, South Africa. South African Journal of Geology 118 (4): 355–372.

Shishkin MA, Rubidge BS and Hancox PJ (1995) Vertebrate biozonation of the Upper Beaufort Series of South Africa – a new look on correlation of the Triassic biotic events in Euramerica and southern Gondwana. In: Sun A and Wang Y (eds): Sixth Symposium on Mesozoic Terrestrial Ecosystems, Short Papers. China Ocean Press, Beijing, 39–41.

Smith RMH and Botha J (2005) The recovery of terrestrial vertebrate diversity in the South African Karoo Basin after the end-Permian extinction. Comptes Rendus Palevol 4: 623–636.

Smith RM and Botha-Brink J (2014) Anatomy of a mass extinction: Sedimentological and taphonomic evidence for drought-induced die-offs at the Permo-Triassic boundary in the main Karoo Basin, South Africa. Palaeogeography, Palaeoclimatology, Palaeoecology 396: 99–118.

Tankard A, Welsink H, Aukes P, Newton R and Stettler E (2012) Geodynamic interpretation of the Cape and Karoo basins, South Africa. In: Phanerozoic Passive Margins, Cratonic Basins and Global Tectonic Maps. Elsevier, 869–945. DOI:10.1016/B978-0-444-56357-6.00022-6.

Turner BR (1999) Tectonostratigraphical development of the Upper Karoo foreland basin: Orogenic unloading versus thermally-induced Gondwana rifting. Journal of African Earth Sciences 28: 215–238.

Viglietti PA, Smith RMH, Angielczyk KD, Kammerer CF, Fröbisch J and Rubidge BS (2016) The *Daptocephalus* Assemblage Zone (Lopingian), South Africa: A proposed biostratigraphy based on a new compilation of stratigraphic ranges. J Afr Earth Sci 113: 153–164.

Viglietti PA (2016) Stratigraphy and sedimentary environments of the late Permian *Dicynodon* Assemblage Zone (Karoo Supergroup, South Africa) and implications for basin development. Unpublished PhD Thesis, University of the Witwatersrand, Johannesburg, 273 pp.

Van der Walt M, Day M, Rubidge BS, Cooper AK and Netterberg I (2010) A new GIS based biozone map of the Beaufort Group (Karoo Supergroup), South Africa. Palaeontologia africana 45: 1–5.

Welman J, Loock JC and Rubidge BS (2001) New evidence for diachroneity of the Ecca-Beaufort contact (Karoo Supergroup, South Africa). South African Journal of Science, 97: 320–322.

A Review of Stratigraphic, Geochemical, and Paleontologic Data of the Terrestrial End-Permian Record in the Karoo Basin, South Africa

15

Johann Neveling, Robert A. Gastaldo, Sandra L. Kamo, John W. Geissman, Cindy V. Looy, and Marion K. Bamford

Abstract

The Karoo Basin has long been considered to contain the type stratigraphic succession for the terrestrial expression of the end-Permian mass extinction. A detailed extinction model, based on biostratigraphic and geologic data, has proposed rapid environmental change that coincides with a vertebrate biozone boundary, which was postulated to have been caused by increased aridity. Our sedimentologic, geochronologic, palaeomagnetic, and geochemical data collected from reported boundary sections, show that the link between the floral and faunal turnover and marine end-Permian event is tenuous. A review of existing, as well as our own palaeontological data, interpreted within a robust stratigraphic and sedimentologic framework, further indicate that ecological change was more subtle and protracted than currently modeled, and reflects the complex way in which the ancient Karoo landscape responded to changes in several extrinsic factors.

15.1 Introduction

The continental stratigraphic record in the Karoo Basin, South Africa, plays a central role in our understanding of the terrestrial ecosystem response to the end-Permian mass extinction. The basin formed in southern Gondwana during the Late Paleozoic and contains a sedimentary succession that records deposition from the Late Carboniferous to Middle Jurassic. Research on the events reported to be associated with the end-Permian crisis focused on an interval encompassing the two uppermost lithologic members recognized in the Balfour Formation, a part of the fully continental Beaufort Group. The Elandsberg Member consists predominantly of greenish gray mudstone and is overlain by the Palingkloof Member, characterized by greenish gray and grayish red mudstone which is, in turn succeeded by the largely arenaceous Katberg Formation (SACS 1980).

15.2 Background

The rich fossil record of tetrapods preserved in the Beaufort Group allowed for the establishment of an eightfold (Fig. 15.1) biozone subdivision (Rubidge 1995; see also Chap. 14 in this book). The origin of this scheme can be traced to that of Broom (1906), who proposed a sixfold subdivision and presumed the *Lystrosaurus* beds (i.e., the *Lystrosaurus* AZ in the modern scheme) to be Early Triassic in age; all preceding units were considered Permian. The

J. Neveling (✉)
Council for Geosciences, Pretoria, South Africa
e-mail: jneveling@geoscience.org.za

R.A. Gastaldo
Colby College, Waterville, ME, USA

S.L. Kamo
Jack Satterly Geochronology Laboratory, University of Toronto, Toronto, Canada

J.W. Geissman
University of Texas at Dallas, Richardson, TX, USA

C.V. Looy
University of California at Berkeley, Berkeley, CA, USA

M.K. Bamford
Evolutionary Studies Institute, University of the Witwatersrand, Johannesburg, South Africa

B. Linol and M.J. de Wit (eds.), *Origin and Evolution of the Cape Mountains and Karoo Basin*,
Regional Geology Reviews, DOI 10.1007/978-3-319-40859-0_15

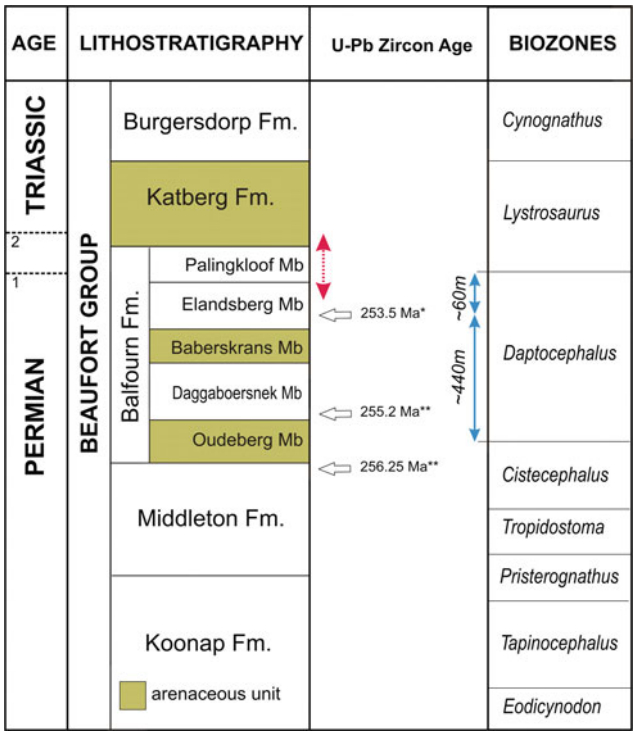

Fig. 15.1 Lithostratigraphy, biostratigraphy, and chronometric ages of the Beaufort group. Stippled line 1 represents the previously reported position of the PTB (Smith and Botha-Brink 2014). Stippled line 2 represents the hypothesized position of the PTB proposed by Gastaldo et al. (2015). The empty arrows depict the stratigraphic positions of volcanic ash beds that yielded the U-Pb ID-TIMS ages reported by Gastaldo et al. 2015 (*) and Rubidge et al. 2013 (**). The stippled double arrow depicts the position of the boundary interval described in the literature (Smith and Ward 2001; Smith and Botha-Brink 2014). The solid double arrows depict the approximate stratigraphic distance from the porcellanite reported by Gastaldo et al. (2015) to the base (~440 m) and top (~60 m) of the *Daptocephalus* AZ. The position of the base of the *Daptocephalus* AZ is based on Viglietti et al. (2016)

assignment of these lower biozones, of which the *Dicynodon* Assemblage Zone (AZ) is the youngest (Keyser and Smith 1978), received wide acceptance (Rubidge 1995; Rubidge et al. 2013). In contrast, the Triassic age of the *Lystrosaurus* AZ had been questioned, but most workers by the 1980s, agreed with its assignment to the earliest Triassic (see summary in Neveling 2004). The *Dicynodon* AZ, which recently has been redefined as the *Daptocephalus* AZ (Viglietti et al. 2016), traditionally has not been considered to share any taxa with the *Lystrosaurus* AZ (Kitching 1977), although Hotton (1967) first reported overlap in the stratigraphic ranges of the index taxa. Anderson and Cruickshank (1978) first correlated the sharp faunal turnover between these two biozones with the end-Permian crisis. This was supported by Smith (1995), who argued that the faunal turnover at the top of the *Daptocephalus* AZ was broadly time-equivalent with the extinction in the marine record.

In the first detailed study of this biozone contact, Smith (1995) demonstrated overlap of more than 20 m in the stratigraphic ranges of the, then, index taxa *Dicynodon* and *Lystrosaurus*, based on investigations at the Bethulie locality (southern Free State). The faunal boundary was placed at the base of the Palingkloof Member, which was interpreted to record a change in fluvial architecture from high sinuosity to low sinuosity river systems. This change in sedimentary regime was attributed to both increasing aridity and uplift in the Cape Fold Belt.

After incorporating data from additional sections, the position of the faunal boundary subsequently was reassigned to the lower part of the Palingkloof Member (Smith and Botha 2005, 2006), while a distinct lithofacies sequence was described (with subtle variation) as characteristic of the boundary interval (Fig. 15.1). In summary, the base of the interval comprises massive, greenish gray siltstone with subordinate, thick sandstone bodies in which fossils of the *Daptocephalus* AZ are preserved. This interval is interpreted to represent meandering fluvial deposits (Ward et al. 2000). The highest record of the *Daptocephalus* AZ is reported from an overlying interval of massive, mottled maroon and greenish gray mudrock, with thin tabular sandstone bodies (Smith and Ward 2001; Botha and Smith 2006; Smith and Botha-Brink 2014). A third facies, first introduced by Ward et al. (2000) and subsequently associated by many with the Permo-Triassic Boundary (PTB) itself, is described as consisting of very thinly bedded (Tucker, 1989) siltstone–mudstone couplets, each 1–3 cm thick (Smith and Ward 2001; Smith and Botha-Brink 2014). This 3–5 m thick interval has been referred to as "*…a stratigraphically unique unit…*" (Smith and Ward 2001, p.1148) that can "*…be used as a mappable unit…and a datum…*" (Smith and Botha-Brink 2014, p. 103) to correlate between widely distributed sections (Smith and Botha-Brink 2014, p. 110). This assumption was contradicted by Ward et al. (2012), who reported the facies from horizons above and below the PTB. Massive maroon and olive-gray siltstone, in which the *Lystrosaurus* AZ fauna is preserved, overlies this facies, followed stratigraphically by the multistoried channel sandstones of the Katberg Formation.

Ward et al. (2000) proposed that a shift in climatic conditions initiated the transition from high to low sinuosity fluvial architectures. According to their model, long-term deterioration of the terrestrial ecosystem, with a final pulse of increased ecological stress, culminated in wide-spread die-off of vegetation (Ward and Smith 2001; Ward et al. 2005; Smith and Botha 2005). The proposed vegetational collapse and loss of the *Glossopteris* flora caused the demise of the *Daptocephalus* AZ fauna, and the loss of vegetation cover resulted in the deposition of their laminated interval, which they identified as a datum throughout the basin.

This model, however, was developed in the absence of palaeobotanical data. The plant record for the central and southern parts of the basin of this interval, at the time, was considered almost barren. Subsequent studies have demonstrated the presence of macrofossil plants and palynomorphs where they were considered to be absent (Prevec et al. 2010; Gastaldo et al. 2015). Smith and Ward (2001), supporting Smith (1995) and subsequently followed by Smith and Botha (2005, 2006; Smith and Botha-Brink 2014), proposed aridification as the most likely causal mechanism of environmental stress. This interpretation was based on changes in fluvial style, reddening of floodplain paleosols, vertebrate taphonomy, and reinterpretation of the red siltstones as loess deposits (Smith 1995; Smith and Ward 2001; Smith and Botha-Brink 2014). Yet, tetrapod fossil data suggest that these conditions were not sufficiently severe to prevent rapid, post-extinction recovery of the vertebrate fauna (Botha and Smith 2006).

Until recently, no geochronologic data were available to validate the hypothesized correlation of the *Daptocephalus-Lystrosaurus* AZ contact with the end-Permian marine extinction. Hence, chemostratigraphic and magnetostratigraphic methods were attempted. Macleod et al. (2000) correlated a negative $\delta^{13}C$ excursion, obtained from pedogenic carbonate nodules (and supported by a smaller excursion from vertebrate tusks) within the interval of biostratigraphic overlap, with the PTB. Yet, Gastaldo et al. (2014) demonstrated that this correlation is doubtful because most pedogenic carbonate cements from this interval were formed in poorly drained soils and, therefore, do not reflect the isotopic composition of atmospheric CO_2. Ward et al. (2005) presented magnetostratigraphic records from sections spanning this interval and used a composite polarity record for the Karoo Basin to correlate with the extant global geomagnetic polarity time scale for the PTB. Although their data show the end-Permian interval to lie within a normal polarity magnetozone, which Lucas (2009) interpreted as evidence that this biozone contact predates the marine extinction, their overall polarity pattern for Old Lootsberg Pass could not be repeated by Gastaldo et al. (2015).

15.3 Materials and Methods

Detailed sedimentological investigations were undertaken at all reported PTB localities including Old Lootsberg Pass (Blaauwater 67), Blaauwater 65, Lootsberg Pass (Lucerne 70), Old Wapadsberg Pass (Farm 527), and the Bethulie locality (Bethel 763, Heldenmoed 677; Fig. 2). Stratigraphic sections were measured using standard field methods and a Jacob staff with leveling eyepiece. Architectural elements and lateral facies relationships were identified using photomosaics, some obtained using drone technology, and correlating sections by tracing bounding surfaces along strike physically in the field.

15.4 Observations and Discussion

Recently acquired data do not corroborate the widely accepted model of an abrupt, three-phased faunal turnover, and facies sequence advanced in the literature. A reassessment of published biostratigraphic data from the Bethulie locality reveals discrepancies in the stratigraphic position reported for some specimens (e.g. RS67 in Smith and Botha-Brink 2014, Figs. 4 and 12, Supplementary Table 1) and variances between the reported and actual stratigraphic position of specific collection sites relative to the inferred PTB (Battifarano et al. 2015). A similar field-based review of reported fossil localities at the Old Wapadsberg locality suggests that at least two *Daptocephalus* AZ specimens (RS174, reported as *Dicynodon lacerticeps*; RS175, *Lystrosaurus maccaigi*) overlap the stratigraphic ranges of the *Lystrosaurus* AZ faunal elements, such as *Lystrosaurus murrayi* (e.g. RS102, RS103), by more than 30 m, contradicting published stratigraphic ranges (Smith and Botha-Brink 2014, Fig. 12). This suggests that vertebrate taxon ranges need to be reassessed and implies that the taxa of the *Daptocephalus* AZ may not have experienced a phased, near coeval extinction, but coexisted with the fauna of the overlying *Lystrosaurus* AZ for a much longer time than currently assumed.

Accurate stratigraphic placement of biostratigraphic data points is hampered by a dearth of dependable, local and regional geological datums in the studied succession. The reported laminated siltstone–mudstone "event bed" interval (Smith and Ward 2001) is absent from the sections we measured on the farm Blaauwater 65, as well as from two gulley sections on the farm Lucerne 70 known to yield fossils from the boundary interval. This facies also is absent from the proposed biozone boundary at Old Lootsberg Pass (Blaauwater 67). In contrast, we documented very thinly bedded siltstones at two stratigraphic intervals, separated by about 50 m of section (Fig. 15.3), above the placement of the vertebrate-defined PTB. Similarly, several laminated siltstone intervals are exposed above the proposed boundary at Old Wapadsberg Pass.

Lateral correlation of the exposures at Old Lootsberg Pass demonstrates that the laminated siltstone intervals are laterally equivalent to multistoried channel sandstones (Fig. 15.3). This corroborates our earlier observations at Bethulie (Gastaldo et al. 2009), which were subsequently

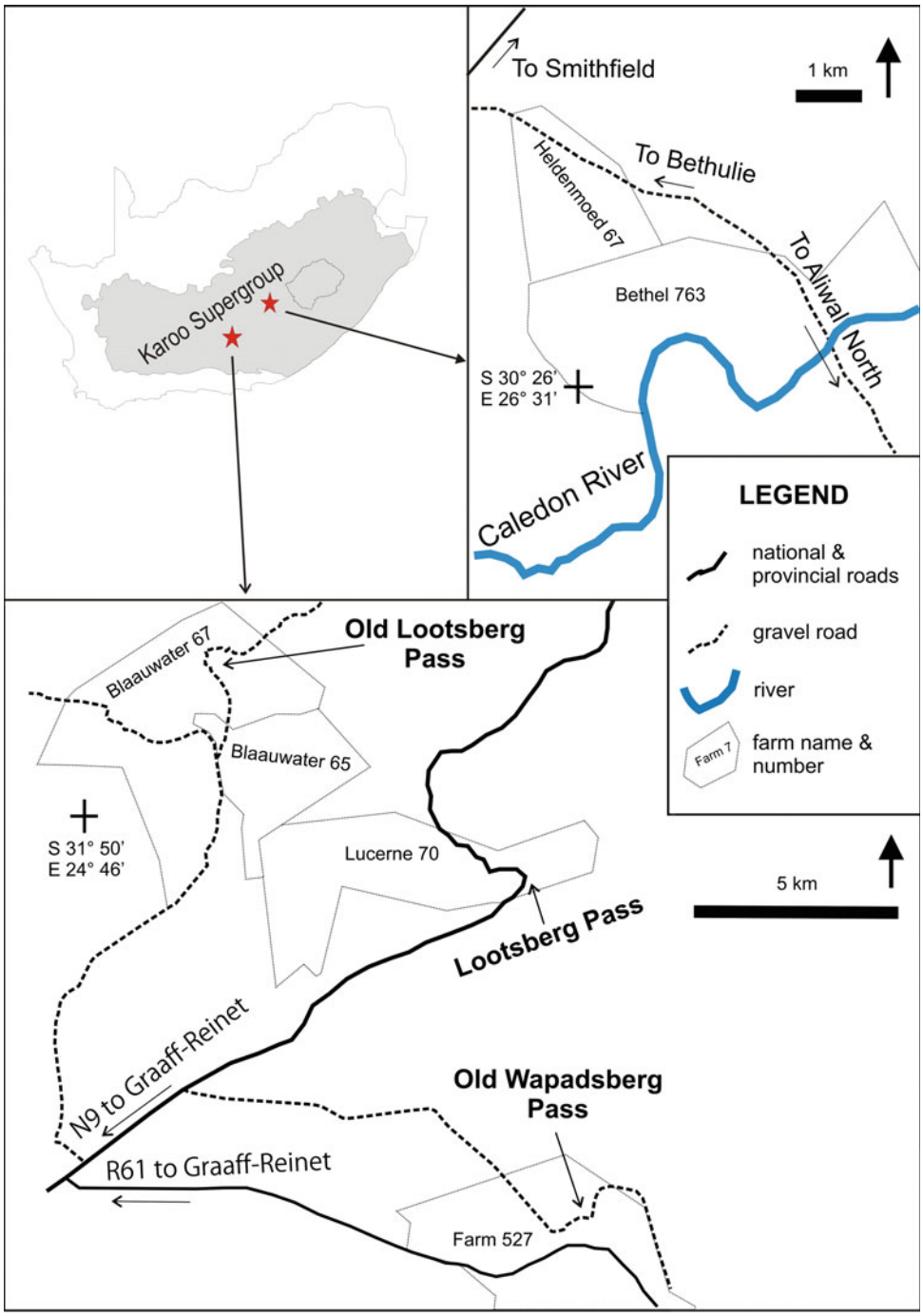

Fig. 15.2 Locality map showing the Lootsberg-Wapadsberg and Bethulie localities. The shadowed area in the small-scale map of South Africa represents the Karoo Supergroup

acknowledged by Ward et al. (2012), that this facies is neither unique nor isochronous. Its occurrence at multiple horizons and well-established, lateral association with channel deposits support the interpretation that it represents the distal facies associated with channel avulsion events on the early *Lystrosaurus* AZ landscape, as presently recognized.

Evidence for rapid environmental change or extreme aridity as a biological kill mechanism remains tenuous. The proposed loessic origin of the massive gray-red siltstones of the lowermost *Lystrosaurus* AZ is not supported by the lateral variation displayed by this lithology above the reported biozone boundary at several localities (Gastaldo and Neveling, 2016). Thick units of greenish gray siltstone at Old Lootsberg Pass grade into grayish red siltstone over a lateral distance of less than 1 km (Fig. 15.3); a similar condition exists at Bethulie, where a lateral change in siltstone color can be traced over a distance less than 0.2 km. Both occurrences are incompatible with the unit's proposed aeolian origin. Rather, this alteration is interpreted as

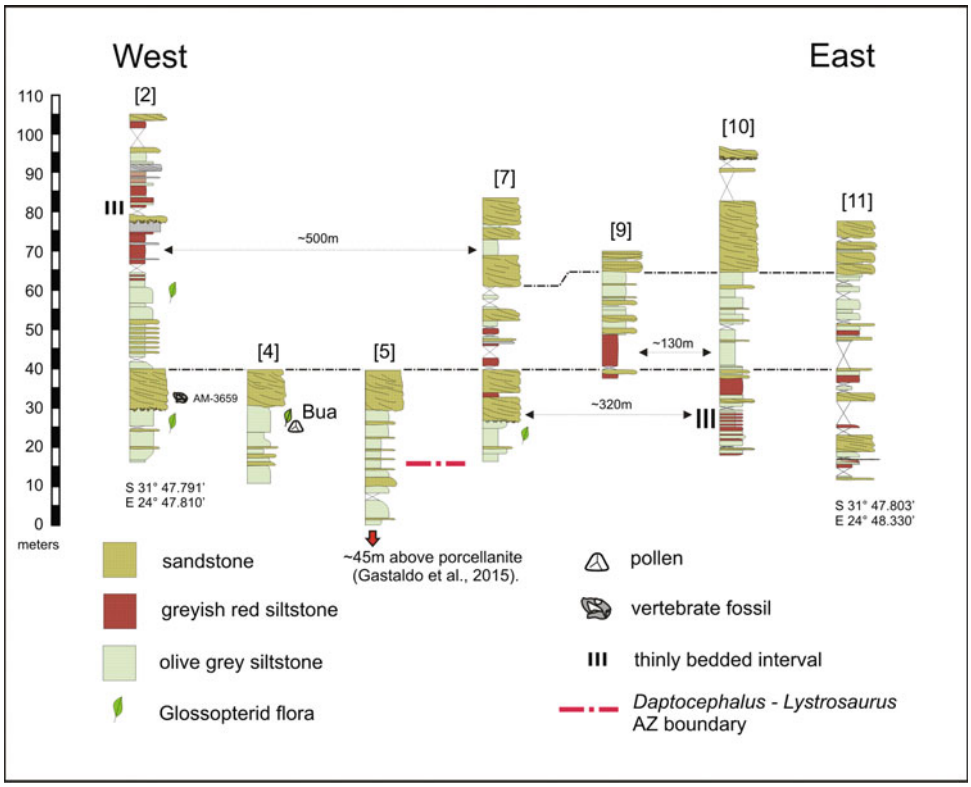

Fig. 15.3 Seven stratigraphic sections, with palaeontological data, measured at the Old Lootsberg Pass locality and correlated by tracing bounding surfaces in the field. Only seven of the original 11 sections (identified by number) are shown here. The position of the *Daptocephalus—Lystrosaurus* AZ boundary (previously correlated with the PTB) is based on the supplementary data of Smith and Botha-Brink (2014), used in conjunction with global positioning system coordinates provided by Smith. The lateral distances between selected sections are depicted by the double arrows

indicative of varying local pedogenic conditions on the ancient floodplain.

With the exception of paleo-calcic Vertisol remnants contained in lenses of reworked nodule conglomerate (Pace et al. 2009; Gastaldo et al. 2013), geochemical data (Tabor et al. 2007; Gastaldo et al. 2014) indicate that the pedogenic horizons above and below the reported vertebrate biozone boundary developed in seasonally to perennially wet soils. Moist soil conditions are supported by the paleobotanical record of a glossopterid flora (Prevec et al. 2010), 10–55 m above the reported biozone boundary at Old Lootsberg Pass; the upper localities occur within the *Lystrosaurus* AZ (Gastaldo et al. 2015). The presence of pollen produced by gymnosperms (e.g., conifers and peltasperms) not represented in the macrofloral assemblages, and representing taxa that are considered to represent vegetation that grew on well-drained soil conditions, are indicative of pedogenically drier conditions somewhere in the basin. Macrofossils with similar botanical affinities only made their appearance in post-extinction Karoo Basin floras (Anderson and Anderson 1985). The sudden appearance of reworked nodule conglomerates containing Vertisol remnants is also indicative of a shift to a more seasonally dry climate, but the extrinsic factors that influence fluvial style include both climate and tectonism (Allen et al. 2013). The fact that a change in fluvial depositional style persisted in the overlying Katberg Formation, combined with its thickness (SACS 1980) and changes in fluvial style observed upsection, suggest that tectonic influence has been underestimated in recent fluvial models for this interval.

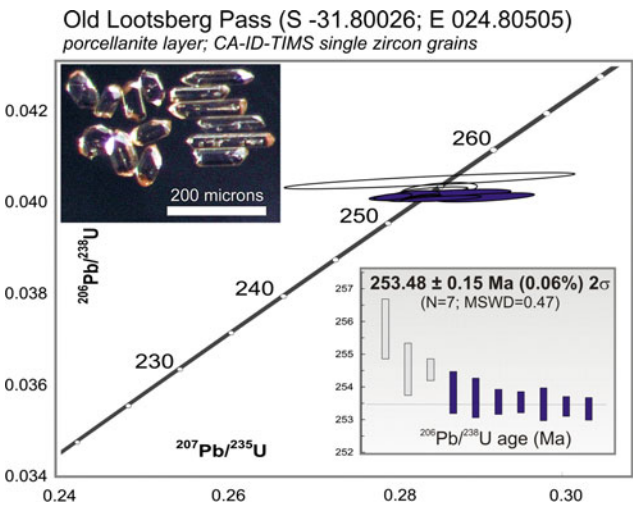

Fig. 15.4 Concordia diagram showing U-Pb ID-TIMS data for chemically abraded, single zircon grains from a volcaniclastic layer ~60 m below the purported *Daptocephalus-Lystrosaurus* AZ contact, Old Lootsberg Pass section, Karoo Basin, South Africa. The procellanite bed is dated at 253.48 ± 0.15 Ma based on the seven youngest zircon grains (of eleven grains dated). Insets are: a photomicrograph of representative zircon grains similar to those that were analyzed; a plot of $^{206}Pb/^{238}U$ ages (data for oldest not plotted)

A U-Pb ID-TIMS age of 253.48 ± 0.15 Ma (Fig. 15.4) recently was reported from a silicified ash bed situated ~60 m below the inferred biozone boundary (as based on data presented by Smith and Botha-Brink 2014) at Old Lootsberg Pass. This maximum depositional age determination is early Changhsingian (Gastaldo et al. 2015). When compared with existing U-Pb ages for older Adelaide Subgroup strata (Beaufort Group; Rubidge et al. 2013), reported biozone thickness for the *Daptocephalus* AZ (Viglietti et al. 2016), and high stratigraphic position of the ash bed within this biozone (Fig. 15.1), the most parsimonious conclusion is that there is a very low probability that the faunal turnover between the *Daptocephalus* and *Lystrosaurus* AZs represents the terrestrial expression of the marine mass extinction event. This interpretation is supported by new magnetostratigraphic data that show the upper part of the *Daptocephalus* AZ, with the exception of one thin reverse polarity magnetozone immediately above the silicified bed, and the lower part of the *Lystrosaurus* AZ is located predominately in normal polarity magnetozones. This differs significantly from the global pattern close to the PTB, and indicates that it is unlikely that the biozone transition crosses the PTB. It also implies that the fauna of the latter biozone was already well established by the latest Permian.

15.5 Conclusions

Recent results indicate that the previous efforts to utilize magnetic polarity and chemostratigraphic data from the Karoo Basin to correlate stratigraphy in the Beaufort Group with the global PTB record are untenable. This is underscored by recent geochronologic data reported from this interval at Old Lootsberg Pass. An assessment of lateral facies relationships demonstrates that it is impossible to accurately correlate successions between different localities, or even between outcrops at a single locality, without tracing boundary surfaces in the field. Hence, without the development of a lithostratigraphic framework in which lateral relationships are understood, only generalizations about paleobiological data can be attempted.

A reassessment of biostratigraphic data suggests that the faunal turnover between the *Daptocephalus* and *Lystrosaurus* AZs was not of a cataclysmic nature (Roopnarine and Angielczyk 2015). Rather, we hypothesize that the turnover was more protracted than current models suggest. This is mirrored by the paleobotanical and palynological record, with the presence of the wetland glossopterid flora in the lowermost *Lystrosaurus* AZ, and the simultaneous presence of drought-tolerant forms, representing vegetation outside of the macrofloral taphonomic window. Although this suggests, together with pedogenic data, that there was a gradual trend in increasing seasonality, conditions were not as dry as portrayed, implying that increasing seasonal drying, alone, cannot explain the faunal change. Rather, we argue that a more nuanced interpretation should be adopted for this transition. The sedimentologic and biostratigraphic records of the uppermost Balfour Formation provide evidence for the varying ways in which the fluvial landscape responded, at different tempos, to a number of extrinsic factors including climate change, tectonic influences and, perhaps, also faunal migration, on local to regional scales.

Acknowledgments We thank J. Kingwill and L. Kingwill (Blaauwater, South Africa), S.D. Theron (Bethel, South Africa), and P. Loock (Quaggas Fontein, South Africa) for accommodating our multiple requests to work on their property. We also thank R.M.H. Smith for providing their original vertebrate database, including global positioning system coordinates of all specimens. R. Prevec is thanked for research contributions made during earlier work and especially for finding and identifying the palaeobotanical remains. Comments made by C. Fielding and S. Lucas greatly improved the original manuscript. This research was supported by the Council for Geoscience, South Africa; U.S. National Science Foundation grants EAR-0749895, EAR-0934077, and EAR-1123570; a Fulbright Award to Gastaldo (Geology Department, Rhodes University); and funding to Geissman from the University of Texas at Dallas.

References

Allen, J.P., Fielding, C.R., Rygel, M.C., Gibling, M.R (2013) Deconvolving signals of tectonic and climate controls from continental basins: An example from the Late Palaeozoic Cumberland Basin, Atlantic Canada. Journal of Sedimentary Research 83: 847–872.

Anderson, J.M., Anderson, H.M. (1985) Palaeoflora of southern Africa. Prodomus of South African megafloras Devonian to Lower Cretaceous. Balkema, Rotterdam, Netherlands.

Anderson, J.M., Cruickshank, A.R.I. (1978) The biostratigraphy of the Permian and the Triassic, Part 5. A review of the classification and distribution of Permo-Triassic tetrapods. Palaeontologia africana 21: 15–44.

Battifarano, O.K., Churchill, A. N., Gastaldo, R.A., Neveling, J., Geissman, J.W. (2015) Lithostratigraphy and lateral variation in vertebrate biostratigraphy near the Permian-Triassic boundary at Bethulie, South Africa. In: Abstracts of the GSA Annual Meeting, 47(7), Baltimore, Maryland, USA, 1–4 November 2015.

Botha, J., Smith, R.M.H. (2006) Rapid vertebrate recuperation in the Karoo Basin of South Africa following the End-Permian extinction. Journal of African Earth Sciences 45: 502–514. doi:10.1016/j.jafrearsci.2006.04.006.

Broom, R. (1906). On the Permian and Triassic faunas of South Africa. Geological Magazine, Decade 5(3): 29–30.

Gastaldo, R.A. Kamo, S.L., Neveling, J., Geissman,, J.W., Bamford, M., Looy, C.V. (2015) Is the vertebrate defined Permian–Triassic Boundary in the Karoo Basin, South Africa, the terrestrial expression of the End Permian marine event? Geology 43: 939–942. doi:10.1130/G37040.1.

Gastaldo, R.A., Knight, C.L., Neveling, J., Tabor, N.J. (2014) Latest Permian paleosols from Wapadsberg Pass, South Africa: Implications for Changhsingian climate. Geological Society of America Bulletin126: 665–679. doi:10.1130/B30887.1.

Gastaldo, R.A., Neveling, J. (2016) Anatomy of a mass extinction: Sedimentological and taphonomic evidence for drought-induced die-offs at the Permo- Triassic boundary in the main Karoo Basin, South Africa: Comment. Palaeogeography, Palaeoclimatology, Palaeoecology 447: 88–91.

Gastaldo, R.A., Neveling, J., Clark, C.K., Newbury, S.S. (2009) The terrestrial Permian-Triassic boundary event bed is a non-event: Geology 37: 199–202. doi:10.1130/G25255A.1.

Gastaldo, R.A., Pludow, P.A., Neveling J. (2013). Mud aggregates from the Katberg Formation, South Africa: Additional evidence for Early Triassic degradational landscapes. Journal of Sedimentary Research, 83: 531–540.

Hotton, N. (1967) Stratigraphy and sedimentation in the Beaufort Series (Permian-Triassic), South Africa. In: Teichert, Yochelson (Eds.), Essays in Paleontology and Stratigraphy, University of Kansas Special Publication 2: 390–428.

Keyser, A.W., Smith, R.M.H. (1978) Vertebrate biozonation of the Beaufort Group with special reference to the western Karoo Basin. Annals of the Geological Survey 12: 1–35.

Kitching, J.W. (1977) The distribution of the Karoo vertebrate fauna. Memoir of the Bernard Price Institute for Palaeontological Research, University of the Witwatersrand 1.

Lucas, S.G. (2009) Timing and magnitude of tetrapod extinctions across the Permo-Trioassic boundary. Journal of Asian Earth Science, 36, 491–502. doi:10.1016/j.jseaes.2008.11.016.

MacLeod, K.G., Smith, R.M.H., Koch, P.L., Ward, P.D. (2000) Timing of mammal-like reptile extinctions across the Permian-Triassic boundary in South Africa. Geology 28: 227–230.

Neveling, J. (2004) Stratigraphic and sedimentological investigation of the contact between the *Lystrosaurus* and the *Cynognathus* Assemblage Zones (Beaufort Group: Karoo Supergroup). Council for Geoscience Bulletin 137.

Pace, D.W., Gastaldo, R.A., Neveling, J. (2009) Aggradational and Degradational Landscapes in the Early Triassic of the Karoo Basin and Evidence for Dramatic Climate Shifts Following the P/Tr Event. Journal of Sedimentary Research 79: 276–291.

Prevec, R., Gastaldo, R.A., Neveling, J., Reid, S.B., Looy, C.V. (2010) An autochthonous glossoperid flora with Latest Permian palynomorphs from the *Dicynodon* Assemblage Zone of the southern Karoo Basin, South Africa: Palaeogeography, Palaeoclimatology, Palaeoecology 292: 391–408. doi:10.1016/j.palaeo.2010.03.052.

Roopnarine, P.D., Angielczyk, K.D. (2015) Community stability and selective extinction during the Permian-Triassic mass extinction. Science 350: 90–93. doi:10.1126/science.aab1371.

Rubidge, B.S. (ed). (1995) Biostratigraphy of the Beaufort Group (Karoo Supergroup). South African Commission on Stratigraphy, Biostratigraphic Series 1.

Rubidge, B.S., Erwin, D.H., Ramezani, J., Bowring, S.A., De Klerk, W.J. (2013) High-precision temporal calibration of Late Permian vertebrate biostratigraphy: U-Pb zircon constraints from the Karoo Supergroup, South Africa. Geology 41: 363–366. doi:10.1130/G33622.1.

Smith, R.H.M. (1995) Changing fluvial environments across the Permian-Triassic boundary in the Karoo Basin, S. Africa and possible causes of tetrapod extinctions: Palaeogeography, Palaeoclimatology Palaeoecology 117: 81–104.

Smith, R.H.M., Botha, J. (2005) The recovery of terrestrial vertebrate diversity in the South African Karoo Basin after the end-Permian extinction. Compte Rendu Palevol. 4: 555–568.

Smith, R.H.M., Botha-Brink, J. (2014) Anatomy of a mass extinction: Sedimentological and taphonomic evidence for drought-induced die-offs at the Permo-Triassic boundary in the main Karoo Basin, South Africa. Palaeogeography, Palaeoclimatology, Palaeoecology 396: 99–118. doi:10.1016/j.palaeo.2014.01.002.

Smith, R.M.H., Ward, P.D. (2001) Pattern of vertebrate extinctions across an event bed at the Permian-Triassic boundary in the Karoo Basin of South Africa. Geology 28: 227–230.

South African Committee for Stratigraphy. 1980. Stratigraphy of South Africa. Part 1: Lithostratigraphy of the Republic of South Africa, South West Africa/ Namibia, and the republics of Bophuthatswana, Transkei and Venda. Geological Survey, South Africa, Handbook 8: 535–548.

Tabor, N.J., Montañez, I.P., Steiner, M.B., Schwindt, D. (2007) $\delta^{13}C$ values of carbonate nodules across the Permian-Triassic boundary in the Karoo Supergroup (South Africa) reflect a stinking sulfurous swamp, not atmospheric CO2. Palaeogeography, Palaeoclimatology, Palaeoecology 252: 370–381.

Tucker, M.E. (1989) The field description of sedimentary rocks. Geological Society of London Handbook. Open University Press, United Kingdom.

Viglietti, P.A., Smith, R.M.H., Angielczyk, K.D., Kammerer, C.F., Fröbish, J., Rubidge, B.S. (2016) The *Daptocephalus* Assimblage Zone (Lopingian), South Africa: A proposed biostratigraphy based on a new compilation of stratigraphic ranges. Journal of African Earth Science 113: 153–164.

Ward, P.D., Montgomery, D.R., Smith, R.H.M. (2000) Altered river morphology in South Africa related to the Permian-Triassic extinction. Science 289: 1740–1743.

Ward, P.D., Botha, J., Buick, R., Dekock, M.O., Erwin, D.H., Garrison, G., Kirschvink, J., Smith, R.H.M. (2005) Abrupt and gradual extinction among Late Permian land vertebrates in the Karoo Basin, South Africa. Science 307: 709–714. doi:10.1126/science.1107068.

Ward, P.D., Retallack, G.J., Smith, R.M.H. (2012) The terrestrial Permo-Triassic event bed is a non-event Comment. Geology. 40: e256.

Fossil Woods from the Upper Carboniferous to Lower Jurassic Karoo Basin and Their Environmental Interpretation

16

Marion K. Bamford

Abstract

Silicified fossil woods are scattered through the Karoo sequence and can be used to give an indication of the past vegetation and climate. It is not yet possible to relate the wood species directly to the leaf species, but having wood types that extend through a long period of time is most useful for standardising the growth ring analyses. A relatively diverse flora has been recorded from the Carboniferous-Permian Dwyka and Ecca Groups of the western Kalahari Basin in north central Namibia. Lower Permian Ecca woods are widespread in southern Africa but of low diversity with only two genera, *Australoxylon* and *Prototaxoxylon. Australoxylon* continues into the Lower Beaufort (Upper Permian) and a new wood, *Agathoxylon* is present. The latter continues throughout the sequence and one species survives well after the end Permian extinction. *Podocarpoxylon* is present from the Upper Beaufort onwards. Although the Molteno (mid to Upper Triassic) has a very high diversity of plants and depositional environments there are only three wood genera, *Agathoxylon, Podocarpoxylon* and *Rhexoxylon*. Preliminary research on the growth rings of these gymnospermous woods is presented here and shows that there is some variation in climate over time, as expected, but also along the northeast–southwest axis. This axis is parallel to the lines of palaeolatitude so the variation in the climate signal may also be a result of local environmental conditions, or influenced by the distance from the seaway or hinterland.

Keywords

Gymnosperms • Growth rings • Permian • *Agathoxylon*

16.1 Introduction

Although the Karoo Basin is better known for a rich fossil record of vertebrates from the Upper Carboniferous Dwyka Group to the Lower Jurassic Clarens Formation, there are also numerous well preserved pollen, leaf and wood floras (Anderson 1977; MacRae 1988; Aitken 1994; Barbolini 2014; Anderson and Anderson 1985; Prevec et al. 2009; Bamford 1999, 2004). To date, the emphasis has been on taxonomy and floral diversity, although application of biostratigraphy to complement the vertebrate biozones has also been investigated (Bamford 1999; Barbolini 2014).

The environment and climate of the Karoo Basin during the Upper Carboniferous to Lower Jurassic Periods in which the plants and animals lived are of great interest to palaeosciences because of the extensive and almost uninterrupted fossil record, including the progressive warming from the Carboniferous to the Triassic, and the end Permian mass extinction events. Various physical methods, therefore, have been used to attempt to reconstruct the palaeoenvironments, such as the sedimentology (Smith 1990), but as all of the animals and most of the plants are extinct, it is difficult to use many of the palaeoecological tools that are available. The Nearest Living Relative or Correspondence Analysis approach, for example, can be used where the climatic

M.K. Bamford (✉)
Evolutionary Studies Institute and School of Geosciences, University of the Witwatersrand, P Bag 3, Johannesburg, WITS 2050, South Africa
e-mail: Marion.bamford@wits.ac.za

B. Linol and M.J. de Wit (eds.), *Origin and Evolution of the Cape Mountains and Karoo Basin*, Regional Geology Reviews, DOI 10.1007/978-3-319-40859-0_16

tolerance and ranges of the modern analogue are assumed to apply to the fossil. Another example is the use of light stable isotopes to reconstruct past temperatures and humidity (e.g. Berner 2006), but with older fossil assemblages the risk of contamination and alteration of materials increases significantly due to diagenesis and weathering (e.g. Prevec et al. 2009).

Physiognomy is another useful non-taxonomic approach where the functional adaptation of an organ can be used to infer climate, such as leaf area increasing with moisture, stomatal density varying with CO_2 concentrations, or bovid limb flexibility increasing with denser vegetation, to mention but a few. One approach that is commonly used for much younger floras is dendroclimatology where the growth ring widths and cellular details of historic or palaeontological woods are measured and compared with the same species or closely related species of modern woods. The latter method has not previously been applied to Karoo woods. Since woods tend to be rather conservative evolutionarily, and some of the Karoo wood types resemble modern gymnosperm woods, this study attempts for the first time to test the feasibility of the method in the Karoo.

A linked approach is to measure the intra-ring variability of the tracheid cells within one growth ring (Falcon-Lang 2000) to provide an indication of leaf longevity and deciduous versus evergreen habit. Once growth rings in the Karoo woods have been recognised and consistently defined this method can be applied to various wood genera and species.

16.2 Materials and Methods

16.2.1 Fossil Woods

Over 500 samples of silicified woods from the Karoo Basin are housed in the Palaeobotany Collection of the Evolutionary Studies Institute, University of the Witwatersrand. Study of thin sections of the best preserved and well provenanced samples, 83 of the 305 samples sectioned to date, under optical microscope has enabled identification to species level in most cases (Bamford 1999, 2000). Anatomical features, distribution and stratigraphic range of the woods have been recorded (Fig. 16.1, Table 16.1) and then these samples are related to the estimated palaeolatitude (Fig. 16.2). This is a preliminary study to determine qualitatively if there is a climate signal from the fossil woods of the Karoo basin that would warrant a more detailed and quantitative study.

Wood samples were selected for this preliminary study based on stratigraphic range, locations with at least five samples of one particular taxon, and a wide geographical distribution (palaeo east–west and palaeo north–south) in order to determine if there are noticeable differences in growth rings. The localities selected for this study (Fig. 16.2) are palaeo west: Sutherland, palaeo east Harrismith; palaeo south: Queenstown (samples still to be sectioned) and palaeo northeast: Senekal. In the discussion the numbers of samples studied for this project are given. A complete list of woods is in the ESI Catalogue.

16.2.2 Growth Ring Types and Widths

In gymnosperm woods the annual growth rings are recognised as palimpsests of latewood and earlywood. Earlywood is produced during the active growing season (spring and summer with longer day length and higher temperatures) and the tracheid walls tend to be thinner and the lumen larger than the slower growing latewood tracheids (autumn and/or winter with shorter day length and lower temperatures; Fig. 16.3, Table 16.1). The proportions of earlywood to latewood vary depending on the climate and on the genetic control of the taxon. In addition, the transition from earlywood to latewood varies from very gradual to abrupt. Transition from latewood to earlywood can be imperceptible to very distinct (Creber and Chaloner 1984). In highly seasonal climates the growth rings can be very clear, but in less seasonal to non-seasonal climates the rings may be indistinct to absent, again controlled by climate and/or genome. Furthermore, where there is little variation in climate from year to year there will be little variation between successive ring widths, and the wood is termed "complacent". In contrast, where there is much variability in climate year to year and ring widths vary greatly, the wood is termed "sensitive" (Chaloner and Creber 1990).

Each growth ring generally represents an annual cycle, and counting them can also be used to age the tree. The ring width is a direct reflection of the productivity of the tree with high growth rates being shown by rings over 5 mm in width, medium rate 3–5 mm wide and a low rate for rings of 1 mm and less (Chaloner and Creber 1990, based on modern woods). Growth rings can include false rings caused by traumatic events, for example short periods of extreme dryness or cold, causing the cessation of growth, or lack of sunlight from ash or dust clouds. Traumatic rings can be caused by fire, defoliation or disease and is expressed in the wood as erratic or patchy growth, deformed cells or canals (Barefoot and Hankins 1982).

The first step is to recognise the types of growth rings (Fig. 16.3) and then measure their widths. Wide rings with many cells imply rapid growth and therefore adequate growing conditions (higher temperatures and water availability). In order to minimise the genetic influence, measurements from the same species or genus of wood should be taken from a wide geographical region and over a long time range.

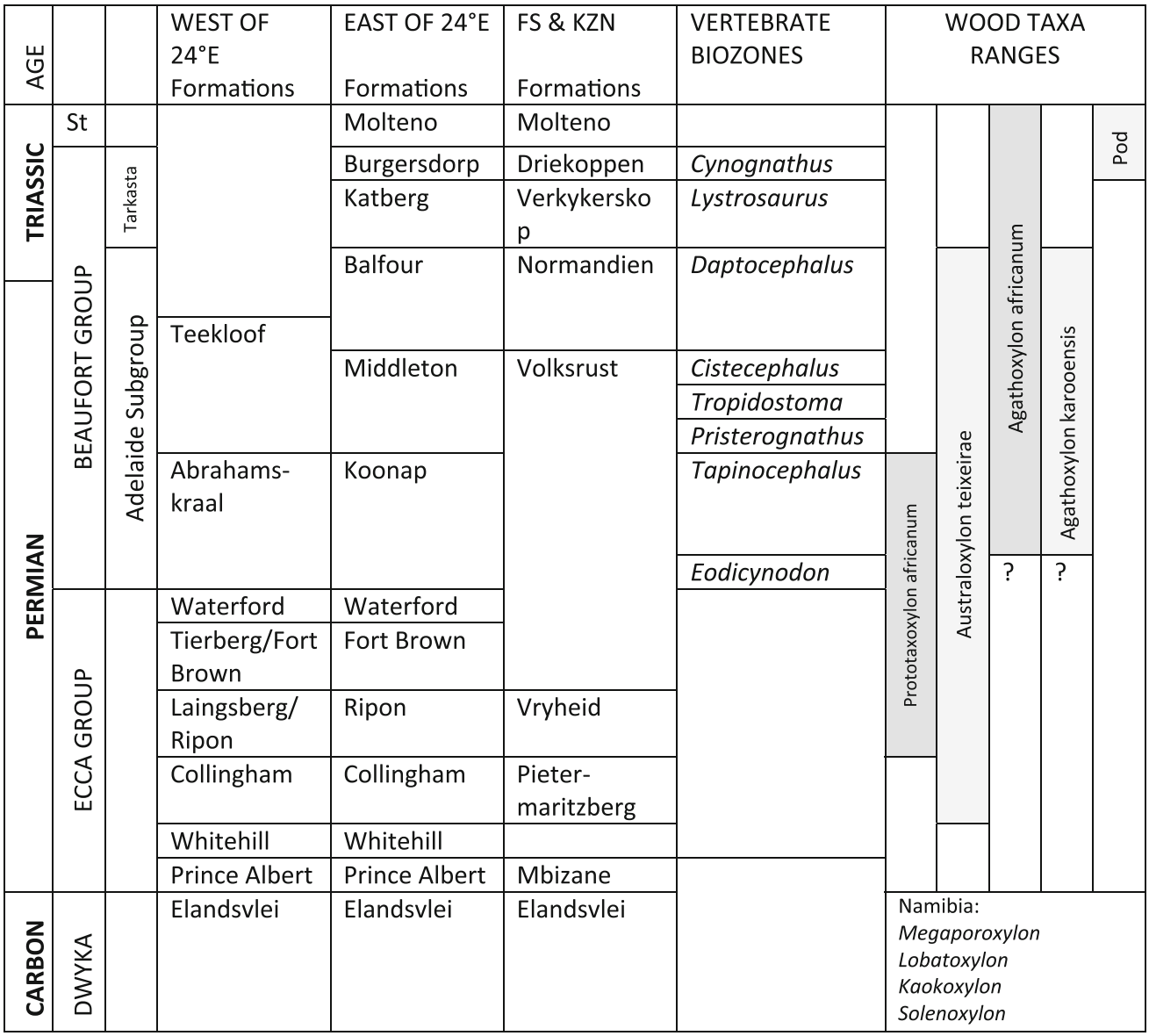

Fig. 16.1 Stratigraphy of the Karoo Basin and ranges of the fossil wood genera. Compiled from Bamford (1999), Rubidge (1995), Rubidge (2005), Viglietti et al. (2016) and a few selected radiometric carbon dates: Dwyka-Ecca boundary >289.6 Ma (Bangert et al. 1999); middle of Abrahamskraal/Koonap Formations 262.8 Ma (Fildani et al. 2007, 2009), top of Teekloof Formation ca 255.2 Ma (Rubidge et al. 2013), mid Balfour Formation 253.48 (Gastaldo et al. 2015), P-Tr boundary 252.17 Ma (Cohen et al. 2013, updated). See Chap. 14 in this book for more details on stratigraphy and radiometric dates, and Barbolini et al. submitted. *Abbreviations* *St* = Stormberg Group; *Tarka* = Tarkstad subgroup; *Podo* = *Podocarpoxylon*. *Note* *Rhexoxylon* occurs only in the Molteno whereas *Podocarpoxylon* extends into the Upper Cretaceous

16.3 Results

16.3.1 Analysis of Karoo Wood Growth Rings

There are only five genera of fossil woods known from the main Karoo Basin (Walton 1925, Marguerier 1973, Bamford 1999, 2000, 2004) and they are distinguished by two main features: the distribution of bordered pits on the tracheid walls, and types and numbers of pits in the crossfields (Table 16.2, Fig. 16.4). For all these Karoo woods the rays are uniseriate with smooth walled cells and the rays range in height from a few cells to over 30 cells. There are no ray tracheids, no canals, none to very little axial parenchyma and only occasionally resiniferous contents in the cells.

Table 16.1 Six types of growth rings that have been recognised by Creber and Chaloner (1984) to which a new category for the Karoo woods (S) is added

Ring type	Description	Climate interpretation
A	Sharp earlywood–latewood transition, usually with narrow latewood	Good water supply
B	Gradual earlywood–latewood transition, usually with wide latewood	Long growing season with adequate water supply
C	Very gradual earlywood–latewood transition	Little change throughout the growing season
D	Uniform growth but terminal event to retard or stop growth, ring boundary is visible	Uniform growing season
E	Same as D but the ring boundary is very difficult to see	Uniform growing season
O	No growth rings	Uniform climate, no seasonality
S (new)	Shear zones present and usually associated with narrow latewood	Unknown

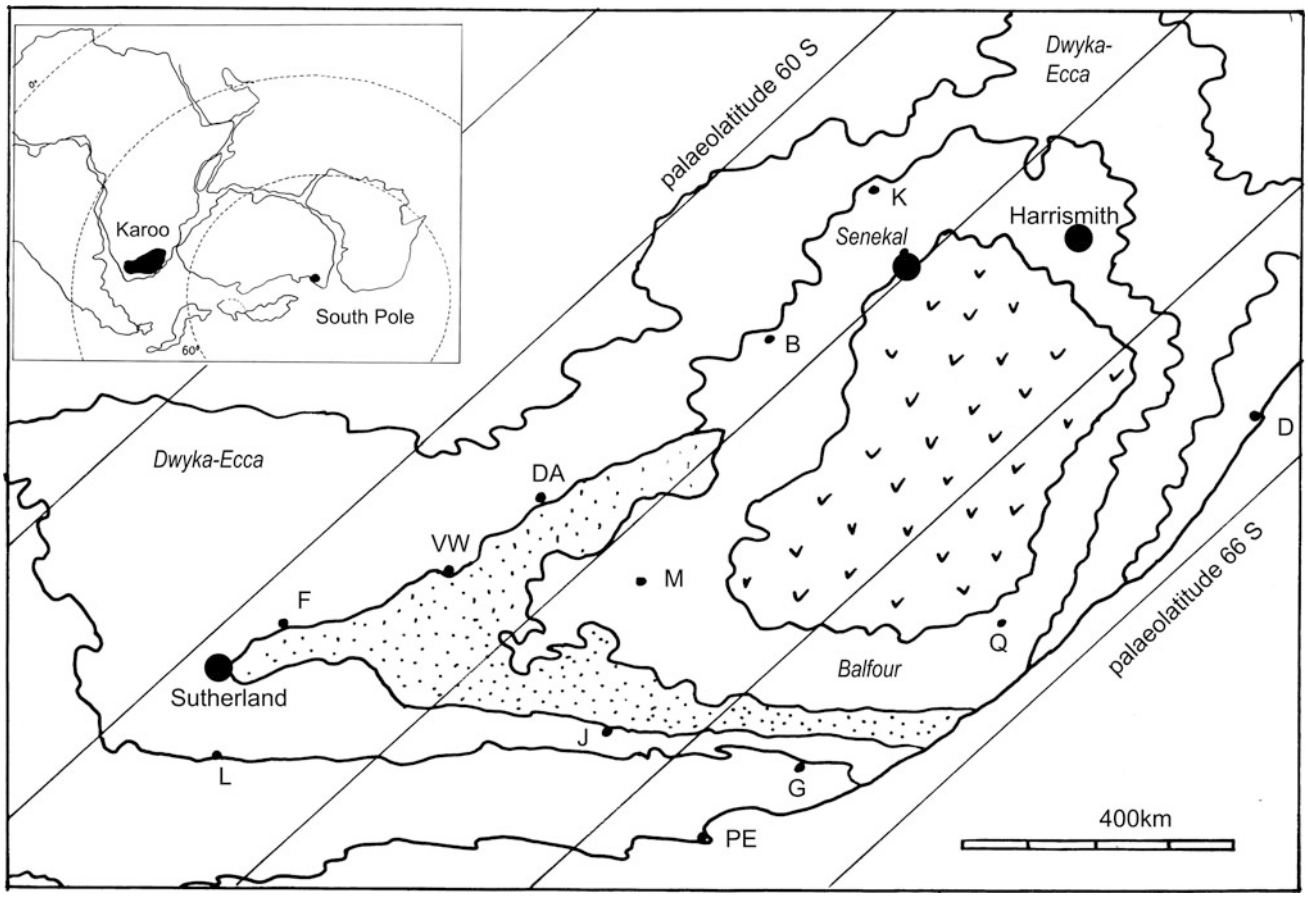

Fig. 16.2 Map of the Karoo Basin showing the estimated palaeolatitude during Late Permian times (based on McLoughlin 2001). Large dots represent the fossil wood localities. Dwyka-Ecca strata—white background; Balfour strata—inner white background; Beaufort Teekloof/Middleton strata—*dotted*; Triassic-Jurassic strata—small 'v' background. *Abbreviations B*—Bloemfontein, *D*—Durban, *DA*—De Aar, *F*—Fraserburg, *G*—Grahamstown, *J*—Jansenville, *K*—Kroonstad, *L*—Laingsburg, *M*—Middleburg, *PE*—Port Elisabeth, *Q*—Queenstown, *S*—Sutherland, *VW*—Victoria West

Late Carboniferous Dwyka woods have been described from the Karoo in Namibia. Like woods from South America, they have various types of central pith surrounded by secondary xylem that is similar to the Permian conifer woods. These woods were described from the Kaokoveld, northwestern Namibia, and they include *Solenoxylon* (with three species), *Lobatoxylon* (1), *Megaporoxylon* (3), *Kaokoxylon* (2) and *Phyllocladopitys* (1) (Kräusel and Range 1928).

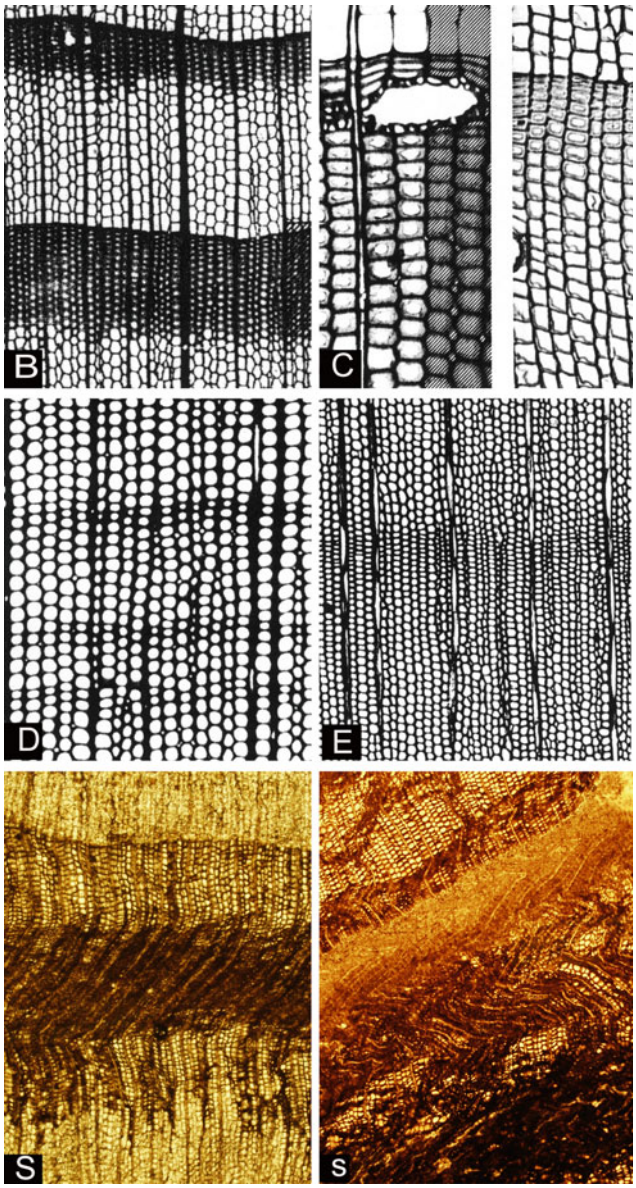

Fig. 16.3 Illustration of types of growth rings based on Creber and Chaloner (1984; first four figures) and Karoo woods. **b** Distinct growth rings with abrupt transition from earlywood (*light cell walls*) to latewood (*dark cell walls*). **c** Gradual transition from earlywood to latewood; canal visible in *left* of picture, **d** indistinct growth rings seen as three bands where the cell walls are marginally thicker. **e** Indistinct growth rings with one band of slightly foreshortened cells. **S** Shear zones typical of Karoo woods. **s** Extreme distortion of wood and shear zones

It is not known to which plants the woods are associated and the growth rings have not been studied to date. Equivalent floras are absent from the main Karoo Basin except for a few samples in the southwestern part of the basin (Anderson and McLachlan 1976). This region was in the northern part of the basin in Palaeozoic times, and farther from the Dwyka ice cap (McLoughlin 2001).

Early Permian woods comprise two species of *Prototaxoxylon* and two of *Australoxylon*. In most samples rings are absent (Type D of Creber and Chaloner 1984) but some have very faint rings, Type E (Figs. 16.3 and 16.4). *Prototaxoylon* does not range beyond the end of the Abrahamskraal/Koonap Formations and *Australoxylon* does not range beyond the end of the Permian (or below the top of the Balfour/Normandien Formations). Glossopterids for the most part do not survive into the Triassic thus making A*ustraloxylon* a good contender for being the wood of at least some of the glossopterid leaves. A deciduous habit has been proposed for the glossopterids based on leaf layers in many of the floras but the *Australoxylon* woods do not show clear growth rings (Fig. 16.4).

The Beaufort/Middle Permian woods are not diverse with only the longer ranging *Agathoxylon africanum* and short ranging *Agathoxylon karooensis* (Fig. 16.1). They have distinct growth rings but with an indistinct transition and very narrow latewood, ranging from 3–10 cells wide (Fig. 16.4). In most cases the earlywood is very wide, over 250 cells or 2–6 mm. A notable feature of these woods is the shear zones which appear dark to the naked eye and under the microscope are seen as bands of distorted or skewed thick-walled cells. The shear zones vary in width but are mostly wider than the latewood bands. They are sometimes closely associated with latewood bands. It is difficult to interpret the shear zones: the thick-walled cells resemble latewood cells but as they are distorted this implies a structural weakness relative to the thin-walled earlywood or thick-walled latewood cells.

From the Upper Beaufort/Burgersdorp Formation onwards *Podocarpoxylon* woods are present. The species diversity is unknown for the earlier members as they are usually poorly preserved. Growth rings are indistinct to absent with very narrow bands of latewood when it is present (Fig. 16.5).

Exclusive to the Middle to Late Triassic Molteno Formation are several species of *Rhexoxylon*, an unusual wood with lobed xylem growing from two cambial rings (Fig. 16.5). It is associated with the *Dicroidium* flora but not to any taxon (Walton 1925; Archangelsky and Brett 1961). Growth rings are distinct but with such a complicated anatomy it is not possible to determine the growth pattern or climate.

16.3.2 Palaeolatitude

The Dwyka woods all come from the same area in Namibia so it is not possible to compare the range in growth rings. Woods of *Prototaxoxylon* and *Australoxylon* have a much

Table 16.2 Fossil woods from the Karoo Basin with distinguishing features, stratigraphic range and type of growth rings (distinct, indistinct and shear zones). Based on Bamford (1999) with the taxonomy updated in Bamford and Philippe (2001) and Rößler et al. (2014). Alternate, compressed pitting is also called "araucarian pitting". Uniseriate to biseriate, opposite pitting that is not compressed is also known as "abietinian pitting". Oculipores = bordered pits of various types, cuppressoid, taxodioid, araucarioid, podocarpoid (cf. oopores = no border)

Taxon	Tracheid pitting	Cross-field pitting	Stratigraphical range	Growth rings
Megaporoxylon kaokense	Pith plus secondary xylem; 1–2 seriate, alternate, contiguous to compressed	1 large oopore	Dwyka	Distinct; very narrow latewood
Megporoxylon scherzi	Pith plus secondary xylem; uniseriate and contiguous (biseriate and alternate)	1–2 large oopores	Dwyka	Distinct, abundant latewood; gradual transition of earlywood to latewood
Prototaxoxylon africanum	Uniseriate and contiguous; rarely alternate, biseriate and contiguous. Strong spiral thickening	2–5 oculipores	Ecca and Lower Beaufort Abrahamskraal	Indistinct to absent; some with shear zones
Prototaxoxylon uniseriale	Uni- and biseriate, alternate, contiguous. Fine spiral thickening	2–8 oculipores	Abrahamskraal	Indistinct; 4–7 mm wide
Australoxyon teixeirae	Clusters; uni- and bi- seriate, opposite and alternate	3–7 oculipores	All Permian	Distinct, very narrow latewood (2–5 cells); some with shear zones
Australoxylon natalensis	Clusters; 1–4 seriate, opposite and alternate	3–4 (−7) oculipores	Normandien	Distinct and indistinct rings, narrow latewood
Agathoxylon africanum	Alternate, biseriate, compressed, rarely contiguous	2–7 oculipores	Normandien, Katberg, Burgersdorp	Distinct; 2 mm wide; many shear zones
Agathoxylon karooensis	Alternate, 1–3 seriate, compressed, rarely contiguous	2–4 oculipores	Normandien/Balfour (not Triassic)	Distinct; 6 mm wide; many shear zones
Podocarpoxylon spp.	Uniseriate, separate to contiguous but never compressed	1–2 oculipores	Upper Beaufort, Triassic to Recent	Indistinct
Rhexoxylon africanum	Lobed wood; 1–3 seriate, alternate and compressed	1–3 oopores	Molteno, Triassic only	Distinct but discontinuous
Rhexoxylon tetrapteridoides	Lobed wood, 1–3 seriate, alternate and compressed	1 oopore	Molteno Triassic only	Distinct but discontinuous

wider distribution but the growth rings are indistinct to absent so it is not possible to compare them. *Agathoxylon* woods, however, have growth rings and are widely distributed in the main Karoo Basin. Samples from the vertebrate biozones have been plotted on the map showing the palaeolatitude and Groups (because of the low time resolution within the biozones and radiometric dates that are still under scrutiny; Chap. 14 this book) and their growth rings compared qualitatively (Table 16.2).

Two collections (more than five samples in each) of *Agathoxylon africanum* from the Lower Beaufort/Abrahamskraal Formation, one collection from north of Sutherland with palaeo-position to in the westernmost part of the basin and approximately 61 degrees south, and the other from the eastern side of the basin and about 63° south are compared (Fig. 16.2, based on McLoughlin (2001) and the palaeolatitudes are estimates only). The palaeo-altitude is unknown but high ground could also affect the local climate. To the west of the southern African landmass was a sea incursion between Africa and South America. To the east of the Karoo Basin were vast expanses of land of Antarctica and Australia (the hinterland). Fossil woods from near Sutherland (24 samples) have a few indistinct growth rings and many shear zones, whereas the woods from near Harrismith (5 samples) have narrow but distinct latewood and a few shear zones. The width of growth rings from all the woods varies considerably. This implies that the Harrismith woods show more seasonality, possibly because they are farther south and farther inland than the Sutherland woods. Ignoring altitudinal effects, one would expect that the flora closer to the pole would show more seasonality or colder climate. The latitudinal variation is only about 4–5 degrees, but it is possible that the generally more extreme climate of the interior enhances the effect of latitude on floras closer to the South Pole.

There are no Upper Beaufort sediments to the far west but central and eastern floras can be compared. Woods of *Agathoxylon africanum* from the Balfour Formation at the Lootsberg Pass (9 samples) and Aliwal North (16 samples) have mostly distinct growth rings and very narrow latewood

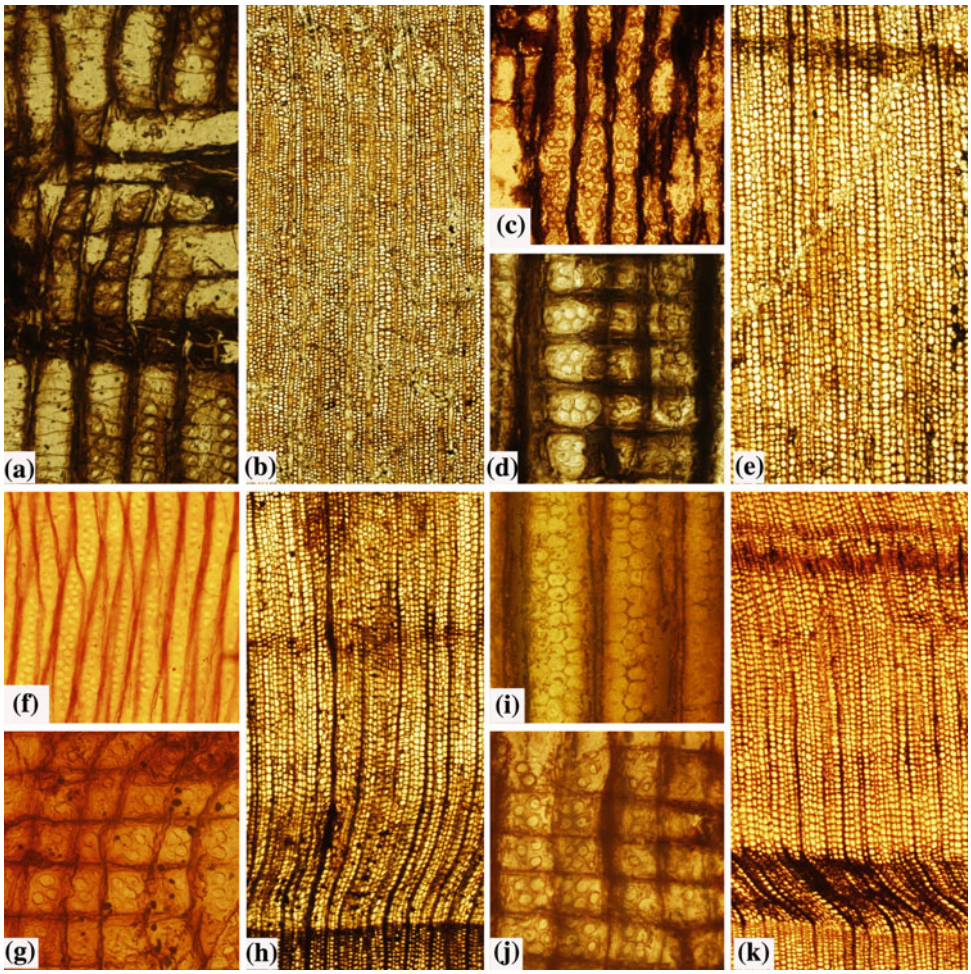

Fig. 16.4 Photomicrographs of fossil woods from the Karoo Basin. **a**, **b** *Prototaxoxylon africanum.* **a** Radial longitudinal section (RLS) of pitting on the radial walls of tracheids and spiral thickening (*lower part*) and round to oval cross-field pits with narrow walls, **b** transverse section of wood (TS) with regular, more or less square cross-section of tracheids. A faint ring boundary is seen at the *top*. **c**, **d**, **e** *Australoxylon teixeirae*. **c** RLS tracheid pitting, **d** RLS, cross-field pitting, **e**, TS growth ring visible at the *top*. **f**, **g**, **h** *Agathoxylon africanun*. **f** RLS tracheid pitting, **g**, RLS, cross-field pitting, **h**, TS indistinct ring growth ring visible at the *top* and a distinct one at the *bottom*. **i**, **j**, **k** *Agathoxylon karooensis*. **i** RLS tracheid pitting, **j** RLS, cross-field pitting, **k** TS growth ring visible at the *top* but a shear zone associated with a growth ring boundary at the *bottom*

bands plus some shear zones. They represent the central Karoo Basin during the Upper Permian. From the eastern basin Normandien Formation in the Harrismith and Senekal area (7 and 5 samples) the growth rings are much the same as those from the central part. These sites are within the same line of latitude, approximately 63° south, so one would expect a similar climate signal. Using the palaeo-map (Fig. 16.2) the projected distance of the slightly older Sutherland floras from the marine incursion compared to the distance of the Lootsberg Pass flora is much the same. Therefore the location relative to the marine incursion or hinterland does not appear to be important, and latitude has more influence on climate. Analysis of the woods from near Queenstown (a few degrees farther south), still to be sectioned, would add useful data to these comparisons.

Triassic fossil wood collections are not numerous enough from which to make any comparisons. Woods from Zimbabwe and new collections from Zambia, which appear to have very wide growth rings, were in the subtropical regions and may present contrasting or complementary information about the palaeoclimate of the Karoo Basin. More sub-Saharan Africa studies are needed.

16.3.3 Comparison with Other Climate Indicators

Sediments of the Abrahamskraal/Koonap Formations are interpreted by many authors (e.g. Smith 1990), to reflect high energy braided river systems that grade into a lower energy meandering stream system so there was plenty of water available for vegetation but no indication of temperature or seasonality. The fauna of the *Tapinocephalus* Assemblage Zone does not shed any light on the climate, nor does the flora because many plants are extinct, and the lower plants (ferns, lycopods and sphenophytes) require locally moist conditions. Coals of this time period are preserved in the northeastern part of the basin and indicate relatively warm and humid conditions.

The Karoo depocentre began to shrink as conditions dried out, as indicated by the Middle to Upper Beaufort Balfour/Normandien sediments (Upper Permian). In the Balfour Formation there are braided river sequences grading upwards into meandering stream systems and in the Normandien Formation there are meandering stream sediments with channels in wide semi-arid floodplains. The

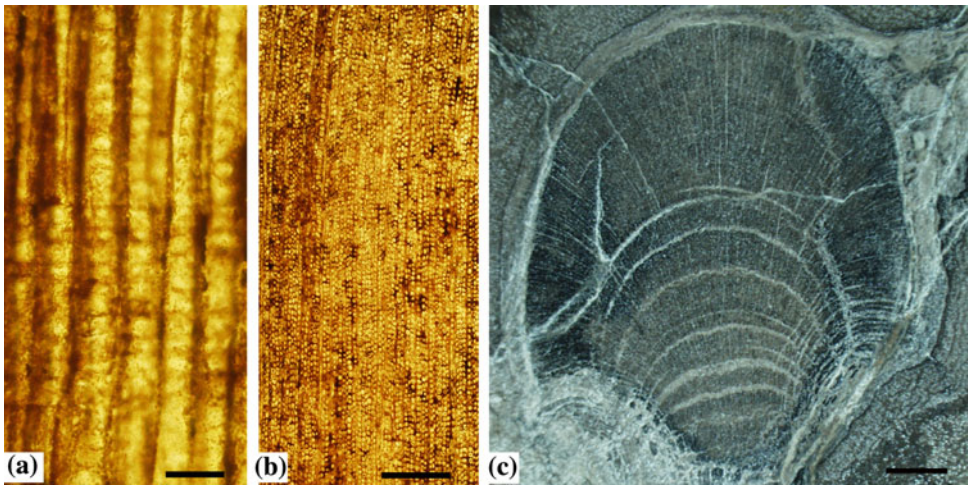

Fig. 16.5 Photomicrographs of fossil woods from the Karoo Basin. **a**, **b** *Podocarpoxylon* sp. **a** RLS tracheid pitting is uniseriate and not compressed. **b** TS no growth rings visible. **c** *Rhexoxylon* sp. TS. One lobe shown of many in a cross-section. White bands are the growth ring boundaries

Normandien floras (Anderson and Anderson 1985; Prevec et al. 2009) do not differ significantly from the slightly older Abrahamskraal or Volksrust Formation floras with *Glossopteris* leaves dominant in both.

16.4 Conclusion

A preliminary assay of the thin sections of fossil woods in the collections of the Evolutionary Studies Institute has shown that there are climate signals in the Beaufort woods. *Prototaxoxylon*, an Ecca-Lower Beaufort wood, does not show any differences in the indistinct growth rings between the older Waterford/Fort Brown Formations and the younger Abrahamskraal Formation, but this is based on only five samples from the two formations and qualitative data. A larger sample and more detailed study are required. Similarly *Australoxylon* from the Waterford/Fort Brown, Abrahamskraal and Balfour/Normandien Formations shows no difference over time. Future studies would include all possible localities with at least five samples, preferably more so that variation due to non-climatic factors can be minimised.

Of the two species of *Agathoxylon*, both originating in the Abrahamskraal Formation, *A. karooensis* does not survive the Permo–Triassic boundary. Therefore, intensive sampling and analyses of these woods throughout the Balfour/Normandien Formations could potentially show climatic fluctuations. In contrast the other species, *A. africanum*, extends well into the Triassic. These woods have broad shear zones throughout their time range but some of the younger ones also have distinct growth rings, but what this indicates is still to be determined.

Dwyka woods, with their central pith, were present during the periods of deglaciation and, when compared with similar woods from other Gondwana regions, may show an interesting adaptation to the climate. The Ecca woods are more difficult to interpret, but the Beaufort and Triassic woods appear to have subtle climate signals. Measurements and detailed analyses of existing fossil wood samples, and new collections to fill in the time and spatial gaps, will provide a useful and independent indicator of climate conditions in the Karoo Basin.

Acknowledgments The University of the Witwatersrand and NRF are acknowledged for financial support and equipment. The many geologists and palaeontologists who have collected wood samples for me to analyse are thanked as without their efforts this project would not have been possible. The invitation to participate in the Cape-Karoo Imbizo at the Nelson Mandela Metropolitan University from Maarten de Wit and Bastien Linol is gratefully acknowledged.

References

Aitken G (1994) Permian palynomorphs from the Number 5 Seam, Ecca Group, Witbank Highveld Coalfields, South Africa. Palaeontologia africana 31:97–109.

Anderson AM and McLachlan IK (1976) The plant record in the Dwyka and Ecca series (Permian) of the southwestern half of the Great Karoo Basin. Palaeontologia africana 19:31–42.

Anderson JM (1977) The biostratigraphy of the Permian and Triassic Part 3. A review of gondwanan Permian palynology with particular reference to the northern Karoo Basin, South Africa. Memoirs of the Botanical Survey of South Africa No 41, 1–133.

Anderson JM and Anderson HM (1985) Palaeoflora of Southern Africa: Prodromus of South African megafloras, Devonian to Lower Cretaceous. A.A. Balkema, Rotterdam. 423 pp.

Archangelsky S and Brett DW (1961) Studies on Triassic fossil plants from Argentina. I. *Rhexoxylon* from the Ischigualasto Formation. London Philosophical Transactions of the Royal Society 244 (706):1–19.

Bamford MK (1999) Permo-Triassic fossil woods from the South African Karoo Basin. Palaeontologia africana 35:25–40.

Bamford MK (2000) Fossil woods of Karoo aged deposits in South Africa and Namibia as an aid to biostratigraphic correlation. Journal of African Earth Sciences 31:119–132.

Bamford MK (2004) Diversity of the woody vegetation of Gondwanan southern Africa. Gondwana Research 7:153–164.

Bamford MK and Philippe M (2001) Jurassic-Early Cretaceous Gondwanan homoxylous woods: a nomenclatural revision of the genera with taxonomic notes. Review of Palaeobotany and Palynology 113:287–297.

Bangert B, Stollhofen H, Lorenz V, Armstrong R (1999) The geochronology and significance of ashfallout tuffs in the glaciogenic Carboniferous-Permian Dwyka Group of Namibia and South Africa. Journal of African Earth Sciences 29:33–49.

Barbolini N (2014) Palynostratigraphy of the South African Karoo Supergroup and correlations with coeval Gondwana successions. Unpublished PhD Thesis, University of the Witwatersrand, Johannesburg.

Barbolini N, Bamford MK and Rubidge BS (in press) Radiometric dating demonstrates that Permian spore-pollen zones of Australia and South Africa are diachronous. Gondwana Research.

Barefoot AC and Hankins FW (1982) Identification of Modern and Tertiary Woods. Clarendon Press, Oxford. 189 pp.

Berner RA (2006) GEOCARBSULF: a combined model for Phanerozoic O_2 and CO_2. Geochimica et Cosmochimica Acta 70:5653–5664.

Chaloner WG and Creber GT (1990) Do fossil plants give a climatic signal? Journal of the Geological Society, London 147:343–350.

Cohen K, Finney S and Gibbard P (2013, updated) The ICS International Chronostratigraphic Chart. Episodes 36:199–204.

Creber GT and Chaloner WG (1984) Influence of environmental factors on the wood structure of living and fossil trees. Botanical Review 50:357–448.

Falcon-Lang H (2000) The relationship between leaf longevity and growth ring markedness in modern conifer woods and its implications for palaeoclimatic studies. Palaeogeography, Palaeoclimatology, Palaeoecology 160:317–328.

Fildani A, Drinkwater N, Weislogel A, McHargue T, Hodgson D and Flint S (2007) Age controls on the Tanqua and Laingsburg deep-water systems: New insights on the evolution and sedimentary fill of the Karoo Basin, South Africa. Journal of Sedimentary Research 77:901–908.

Fildani A, Weislogel A, Drinkwater N, McHargue T, Tankard A, Wooden J, Hodgson D and Flint S (2009) U-Pb zircon ages from the southwestern Karoo Basin, South Africa: Implications for the Permian-Triassic boundary. Geology 37:719–722.

Gastaldo RA, Kamo SL, Neveling J, Geissman JW, Bamford M and Looy CV (2015) Is the vertebrate defined Permian-Triassic boundary in the Karoo Basin, South Africa, the terrestrial expression of the end-Permian marine event? Geology 10: 1–5.

Kräusel R and Range P (1928) Beitäge sur Kenntnis der Karruformation Deutsch-Südwest-Afriakas. Beitage zur geologischen Erforschung der Deutschen Schutzgebeite 20:1–54.

MacRae CS (1988) Palynostratigraphic correlation between the Lower Karoo sequence of the Waterberg and Pafuri coal-bearing basins and the Hammanskraal plant macrofossil locality, Republic of South Africa. Memoirs Geological Survey of South Africa 75:1–217.

Marguerier J (1973) Paléoxylologie du Gondwana Africain. Etudes et affinités du genre *Australoxylon*. Palaeontologia africana 16:37–58.

McLoughlin S (2001) The breakup history of Gondwana and its impact on pre-Cenozoic floristic provincialism. Australian Journal of Botany 49: 271–300.

Prevec R, Labandeira CC, Neveling J, Gastaldo RA, Looy C and Bamford MK (2009) Portrait of a Gondwanan ecosystem: A new Late Permian locality from KwaZulu-Natal, South Africa. Review of Palaeobotany and Palynology 156:454–493.

Rößler R, Philippe M, van Konijnenburg-van Cittert JHA, McLoughlin S, Sakala J, Zijlstra G et al. (35 coordinating authors) (2014). Which name(s) should be used for Araucaria-like fossil wood? – Results of a poll. Taxon 63(1):177–184.

Rubidge BS, (ed) (1995) Biostratigraphy of the Beaufort Group (Karoo Supergroup): Geological Survey of South Africa Biostratigraphic Series, no. 1, p. 1–46.

Rubidge BS (2005) Reuniting lost continents—fossil reptiles from the ancient Karoo and their wanderlust. South African Journal of Geology 108, 135–172.

Rubidge BS, Day MO, Barbolini N, Hancox PJ, Choiniere J, Bamford MK, Viglietti PA, McPhee B and Jirah S (2016) Advances in non-marine Karoo biostratigraphy: significance for understanding basin development. In: Origin and Evolution of the Cape Mountains and Karoo Basin: Geo-biohistory in a terrain with Shale Gas Resources and need for Conservation. (Eds) Bastien Linol & Maarten de Wit. Springer, Regional Geology Reviews 8643.

Rubidge B, Erwin DH, Ramezani J, Bowring SA and de Klerk WJ (2013) High-precision temporal calibration of Late Permian vertebrate biostratigraphy: U-Pb zircon constraints from the Karoo Supergroup, South Africa. Geology 41: 363–366.

Smith RMH (1990) A review of stratigraphy and sedimentary environments of the Karoo Basin of South Africa. Journal of African Earth Sciences 10:117–137.

Viglietti PA, Smith RMH, Angielczyk KD, Kammera CF, Fröbisch J, Rubidge BS (2016) The Daptocephalus Assemblage Zone (Lopingian), South Africa: A proposed biostratigraphy based on a new compilation of stratigraphic ranges. Journal of African Earth Sciences 113, 153–164.

Walton J (1925) On some South African fossil woods. Annals of the South African Museum 22:1–26.

Organic Carbon Isotope Stratigraphy of the Karoo Supergroup

17

Maarten J. de Wit

Abstract

Carbon isotopes are being used increasingly for high resolution chemostratigraphy. $\delta^{13}C$ variations provide relative temperature scales that can be complemented with litho- and bio-stratigraphy to reconstruct local ecosystem and global climate shifts. We present the first Karoo terrestrial organic carbon isotope curve, calibrated against U/Pb zircon dates from interbedded ash-fall tuffs, which can be used for correlation between separate terrestrial Gondwana basins and with marine sequences elsewhere. We identify a number of distinct shifts in the carbon isotope stratigraphy of the Karoo and explore these to discuss punctuated and gradational changes linked to local paleoenvironments and global climates, from polar to desert conditions, over a span of about 200 million years that includes two major extinction events.

Keywords

Terrestrial chemical stratigraphy • Carbon isotopes • Climate • Ecosystem fluctuations

17.1 Introduction

Terrestrial sequences are difficult to correlate with their marine counterparts (Ager 1973). Traditional stratigraphic tools based on palaeontology from these different paleo-ecosystems need independent data to verify stratigraphic equivalence, and common calibrated standards are scarce. Chrono-stratigraphy using radiometric age dating often depends on the presence in both environments of contemporaneous volcanic material with igneous minerals that can be dated with confidence, but volcanic events are rarely frequent or regional enough to provide detailed resolution. Magneto-stratigraphy can best resolve some of these issues, but primary paleo-magnetic signatures may be re-magnetised during diagenesis, basin fluid-flow and low-grade metamorphism, particularly in Paleozoic sequences (McCabe and Elmore 1989; Smith 1999). Such secondary effects have, for example, reset the magnetic fingerprints of large sections of the Karoo Basin sediments (Bachtadse et al. 1987; Opdyke et al. 2001; Ward et al. 2005).

More recently, chemical stratigraphy has been explored as a tool for geological correlations, particularly using strontium, carbon and oxygen isotopes (e.g., Veizer et al. 1999; Grossman 1994). In the case of strontium isotopes, however, marine and terrestrial sequences are buffered through their very different oceanic and terrestrial fluid-rock reservoirs, respectively, and are therefore not useful as stratigraphic tools to correlate between marine and terrestrial environments. On the other hand, light stable isotopes of carbon and oxygen isotopes acquire equilibrium between hydrosphere reservoirs and the atmosphere within a relative short space of time (e.g., Ruddiman 2000). For all practical stratigraphy purposes, isotopic ratios of carbon and oxygen in marine and terrestrial environments change in tandem and are recorded, by proxy, in their respective biomass. Variations in isotope ratios of carbon in organic matter and

With contributions from AEON research associates James Alexander, John Decker, Joy Ghosh, Nicolas Rakotosolofo, and Stephanie de Villiers.

M.J. de Wit (✉)
AEON, Africa Earth Observatory Network, Nelson Mandela Metropolitan University, Port Elizabeth, South Africa
e-mail: maarten.dewit@nmmu.ac.za

B. Linol and M.J. de Wit (eds.), *Origin and Evolution of the Cape Mountains and Karoo Basin*,
Regional Geology Reviews, DOI 10.1007/978-3-319-40859-0_17

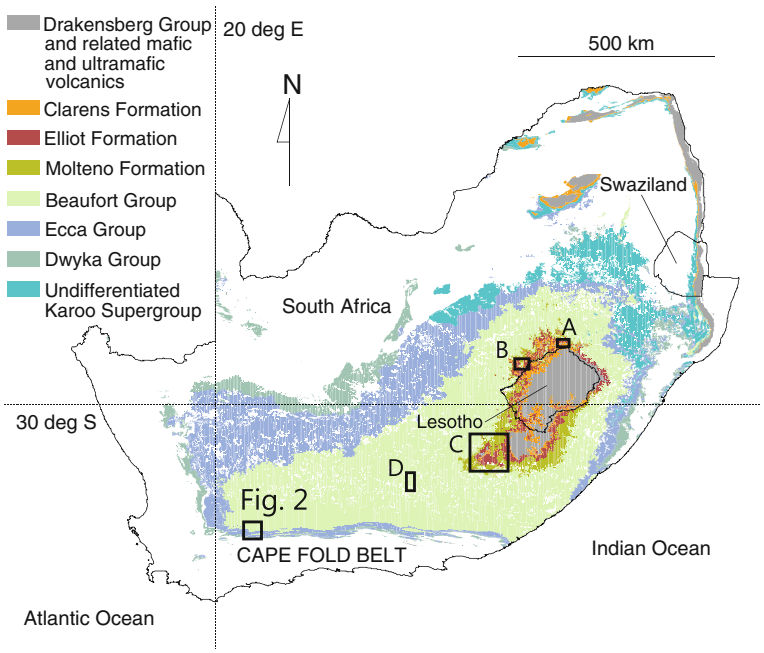

Fig. 17.1 Simplified geology of the Karoo Basin (outcrop map) with sampled locations *(squares)*. A = Emeus, near Golden Gate; B = Bramleyshoek; C = Region of Molteno fossil sites sampled from the Anderson Collection (see text); D = P-T boundary along the Lootberg Pass. Details of Waaipoort-Dwyka-lower Beaufort sections near Laingsburg are shown in Fig. 17.2

carbonates can potentially therefore provide reliable signatures for stratigraphic correlations between terrestrial and marine sequences. This has been used successfully, for example, to correlate repeated marine incursions in Jurassic terrestrial sediments (Jenkyns et al. 2002) and to track the history of Cenozoic glaciations on a global scale using marine sediments and terrestrial ice cores (e.g., Raymo 1994), respectively.

Plants in different terrestrial environments use the same atmospheric chemistry to photosynthesise, and isotopic fractionation of carbon isotopes during photosynthesis is well understood. Therefore, variations in the ratio of organic carbon isotopes of fossil organic remains (or penecontemporaneous carbonates) in sediments (e.g., $^{12}C/^{13}C$, expressed as $\delta^{13}C_{org}$) are useful proxy for changes in coupled atmospheric/oceanic/biosphere conditions related, for example, to global climate change (e.g., Berner 1990; Faure et al. 1995; de Wit et al. 2002). Although fractionation differs between plants that use different photosynthetic pathways, it is generally agreed that before 200 Ma only one type of photosynthetic pathway (C3) had evolved. The organic carbon isotope signatures of Karoo fossil plant materials are therefore usually relatively simple to interpret (Ghosh 1999; de Wit et al. 2002; Decker 2004; Decker and de Wit 2005), and can thus provide a powerful tool to facilitate regional correlation of terrestrial sequences, and to track details of climate changes during evolution of this Gondwana continental interior that was first covered by Antarctic-like ice caps in the Carboniferous and then by Sahara-like dune fields in the Jurassic-Cretaceous, a period of more than 200 million years (see Preface of this book).

This chapter summarises the organic carbon isotope stratigraphy of the Karoo Supergroup across three sequences across the Karoo Basin (Fig. 17.1). The first comprises the Lower Karoo (Carboniferous-Permian) around Laingsburg in the southwest Karoo Basin; the second covers the Upper Karoo (Triassic-Jurassic) from a number of localities in the central sector of the Karoo Basin. These two sequences are linked through a short third sequence across the Permian-Triassic (P-T) boundary (presently dated at 252.17 ± 0.06 Ma; Burgess et al. 2014) in the south-central Karoo exposed around Graaff-Reinet (along the Lootsberg Pass), and which has been sampled also for Carbon isotopes by several other research groups (see for example Chap. 15 of this book).

17.2 Selected Sequences

The first sequence is well-exposed between the contacts of the Lower Paleozoic Cape Supergroup and the overlying Upper Paleozoic part of the Beaufort Group (Fig. 17.2). It represents a near complete sequence from the Upper Carboniferous Waaipoort Formation (upper most Witteberg Group of the Cape Supergroup) to the Middle Permian Waterford-Beaufort boundary of the Karoo Supergroup, and includes the classic Permo-Carboniferous glacial deposits of the Dwyka Group (du Toit 1926; Visser 1987). Of particular interest is to test for climate variation during the time of deposition of the Dwyka Group.

The second sequence traces the organic isotope stratigraphy of the Mesozoic upper Karoo Supergroup. This

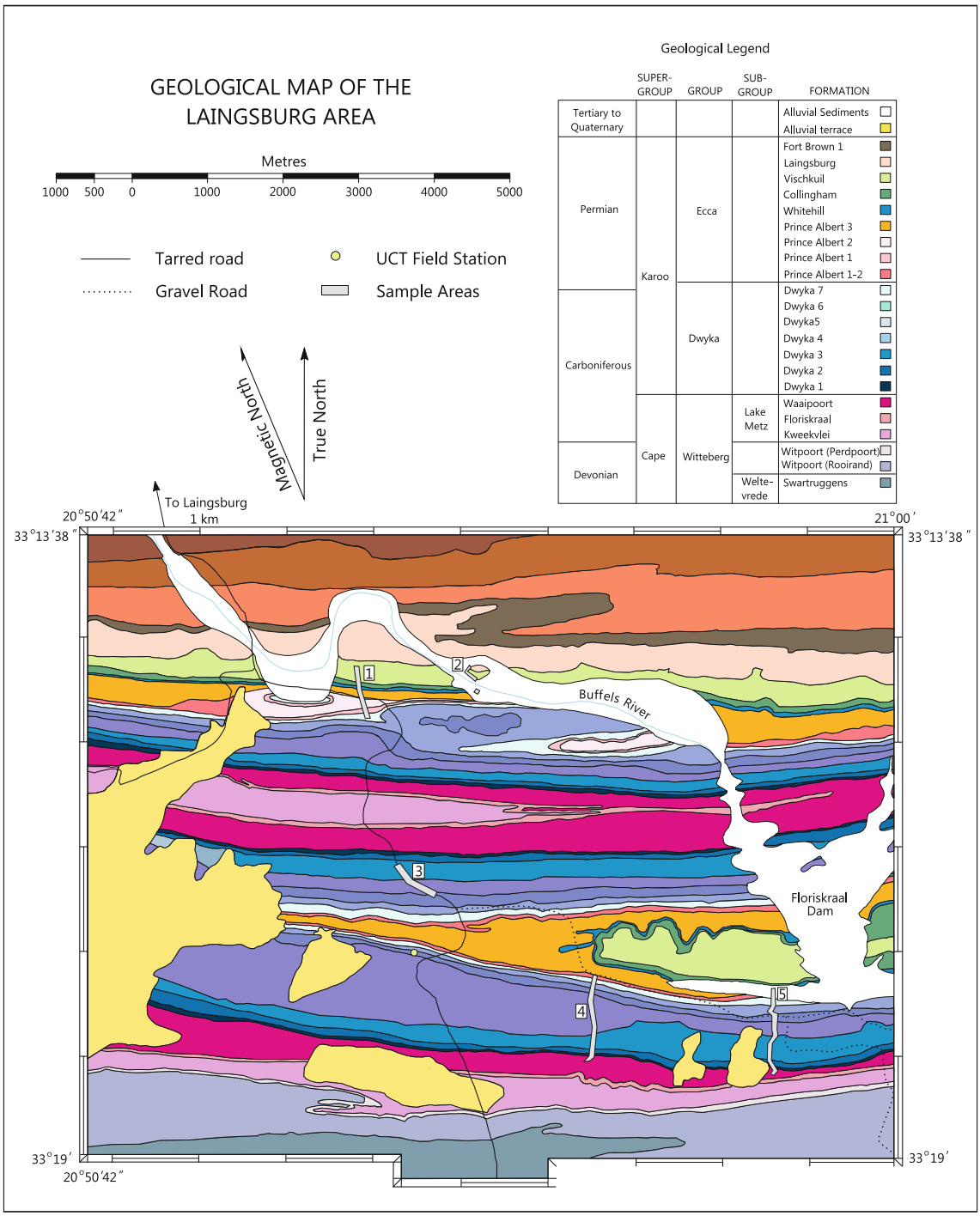

Fig. 17.2 Geological map of the field area south of Laingsburg (modified from Knütter et al. 1995 and Alexander 1999)

sequence is directly overlain by the continental flood basalts of the Jurassic Drakensberg lavas that have been dated at 182–183 Ma (Duncan et al. 1997), and thus limits the upper-bound of our terrestrial organic carbon isotope history to the Lower Jurassic. This carbon isotope curve is derived from plant and insect fossils from the Molteno, Elliot and Clarens Formations, deposited under conditions of increasing aridity from the Late Triassic into the Early Jurassic (Anderson et al. 1999).

Our third $\delta^{13}C_{org}$ section links the lower and upper Karoo sections through the P-T transition in the Beaufort Group, which is based predominantly on vertebrates (Day et al. 2015). Attempts to record the $\delta^{13}C_{org}$ across the P-T boundary of the Karoo Basin have yielded contrasting

results. A gradual negative trend over nearly 20 myrs leading up to the P-T boundary was first identified from different parts of basin using apatite from tusks of the mammal-like reptile *Dicynodon* (as a proxy for the contemporaneous vegetation of these herbivores) and from boreholes through coal-bearing sequences (Thackeray et al. 1990; Faure et al. 1995). Both these studies conclude that the start of a gradual decline in $\delta^{13}C_{org}$ was well on the way before the P-T boundary. A subsequent study of $\delta^{13}C_{carb}$ from carbonate nodules conducted at three nearby sites (Doornplaats, Lootsberg and Bethulie) gave conflicting results (MacLeod et al. 2000), some attributed to secondary alterations (de Wit et al. 2002). We re-examined the Lootsberg section for organic materials preserved in the carbonate nodules. More recent work along detailed lithologic and palaeontological sections (e.g., Gastaldo et al. 2015) is reported in Chap. 15, and is not described further here.

17.3 Geological Background

17.3.1 The Lower Karoo Supergroup: Dwyka to Beaufort Groups

Lithostratigraphic and palynology evidence suggest that the onset of glaciation was in progress during deposition of the uppermost Witteberg Group (the Tournasian Waaipoort Formation; see also Chap. 13 in this book) and that there is minimal hiatus before glaciers advanced across a Witteberg glaciogene surface (Streel and Theron 1999). Thereafter glaciogenic sedimentation and erosion dominated until well into the Early Permian (~288 Ma; Artinskian) accumulating up to 800 m of Dwyka Group diamictites and rhythmites in the southern part of the Karoo Basin, and classical striated pavements along the northern fringes of the basin, respectively (Du Toit 1926; Visser 1987). Local ice-flow directions indicate provenances to the north (Chap. 9 in this book). Between the Early to Late Carboniferous, the South Pole moved from southern Africa to Antarctica; and the northern margins of the ice sheets reached as far as Tanzania, Madagascar, the Central African Republic and Angola (Linol et al. 2016; see Preface of this book). Visser (1987) estimated an ice sheet cover of more than 4 km above the basin floor, similar to that of large parts of present-day East Antarctica.

Whereas many investigators infer a marine setting for the deposition of these diamictites and related varves (e.g., McLachland and Anderson 1973; Johnson et al. 1997 and references therein), there is no unequivocal evidence for this. Marine fossils occur only at the top of the Dwyka along the western margins of the basin, particularly in southern Namibia (Warmbath Basin) and along the deep glacial valley through the Vryburg-Prieska region along the northern extents of the Karoo Basin. These are witness of a short marine transgression at the end of the glaciation (Visser 1987). By contrast, terrestrial plant fragments are common throughout the Karoo Basin, albeit rare in the Dwyka (Plumstead 1964; see also Chap. 16 in this book). It is therefore possible that the entire Dwyka sequence of the Karoo Basin was deposited in a terrestrial setting (du Toit 1926), including those of the overlying organic-rich mudstones of the Prince Albert, Whitehill and Collingham Formations (see Higgs 2010 and references therein; also Chaps. 10 and 11 this book), during which the Karoo Basin may have become a gigantic inland lake up to three times the size of the present Black Sea (e.g., Faure and Cole 1999). These observations imply that during early Dwyka times, the water-lain diamictites may represent glaciogenic lake-sediments deposited peripheral and beneath the major continental ice cap of Gondwana (de Wit et al. in prep).

Two occurrences of rhyolitic-andesitic volcanic tuff are present in the Dwyka Group of southern Africa (Bangert et al. 1999). These were most likely derived from a magmatic arc to the south (Bangert et al. 1999; Linol et al. 2016). U/Pb dating on zircons from tuffs near Laingsburg about 400 m above the base of the Dwyka has yielded a date of 297 ± 1.8 Ma (Bangert et al. 1999). The age of the top of the Dwyka has been similarly derived using zircons dates from tuffs in the lowermost beds of the overlying Prince Albert Formation (288 ± 3 and 289 ± 3.8 Ma). Thus, the Dwyka Group in the southern Karoo Basin spans about 50 million years, with the upper 200 m representing less than 10 million years, or at most 20 ‰ of the glacial period.

Following rapid disintegration of the ice cap at about 290 Ma (Asselian-Sakmarian), glaciogenic sedimentation gave way to slow deposition of black suspended muds of the Prince Albert and Whitehill Formations (for further details see Chaps. 10 and 11 in this book). Geochemistry (Zawada 1988; Faure and Cole 1999) suggests that most of these deposits are fresh to brackish water lake deposits, and a 'Baltic Sea' model has recently been suggested to account for this (see Chap. 10 in this book), and which by then extended across into the Paraná Basin of South America as a gigantic lacustrine basin (Chap. 18 in this book).

The Whitehill Formation, with its characteristic fauna of the fresh water *Mesausaurus* and dragonflies (du Toit 1926; see also Chap. 10 this book) is abruptly overlain by the upward coarsening sequence of turbidites of the Collingham to Laingsburg Formation and the more deltaic sequences of the Ford Brown Formation. These deposits are in turn succeeded by a succession of shore-line and in turn braided-river deposits of the Beaufort Group (see Chap. 14 in this book) that contain the terrestrial mammal-like reptiles, and the Permo-Triassic boundary (e.g., MacLeod et al. 2000; Day et al. 2015; Gastaldo et al. 2015; Chap. 15 in this book).

We use selected U/Pb zircons from tuffs at various locations across the southern Karoo (e.g., Bangert et al. 1999; Fildani et al. 2007; Rubidge et al. 2013; McKay et al. 2015; Day et al. 2015; Gastaldo et al. 2015) to further "calibrate" our $\delta^{13}C_{org}$ stratigraphy sections.

17.3.2 The Upper Karoo Supergroup: Molteno, Elliot and Clarens Formations

Karoo terrestrial sedimentary sequences terminate at the boundary with the overlying Drakensberg flood basalts, dated at 182 ± 1 Ma (Duncan et al. 1997). Formerly known as the Stormberg Group (Bordy et al. 2004), these siliciclastic formations have been interpreted to represent contemporaneous environments in a systems tract shifting towards a southerly source (Turner 1983, 1999; Smith et al. 1993; Bordy et al. 2004). No geochronological data exists for this section of the Upper Karoo Supergroup (but see Chap. 12 in this book for a date to be published soon from a tuff in the upper Elliot Formation).

The lower Molteno Formation is dominated by coarse sandstones, interbedded with grey shales and occasional seams of coal (du Toit 1926, 1954), and is thought to have been deposited by perennial, high energy, low-sinuosity braided streams (Turner 1983). It is the most productive macroflora-bearing formation in terms of both diversity and localities, offering the clearest available window globally onto the floral and insect diversity during the Late Triassic (Anderson and Anderson 2003; Anderson et al. 1999; Scott et al. 2004; see the Preface and Chap. 16 in this book). Thus, the Molteno plant and insect fossils provide the most robust $\delta^{13}C_{org}$ proxy for Late Triassic (Carnian) terrestrial environments in southern Gondwana and global atmosphere conditions.

The overlying Elliot Formation is characterised by purple and red mudstones and shales with calcareous nodules, red sandstones and thickly bedded yellow and white feldspathic sandstones (Decker 2004; Bordy et al. 2004; Chap. 12 this book). The Elliot has been interpreted as alluvial floodplain deposits with interacting fluvial and aeolian processes during increasingly arid conditions (see Bordy et al. 2004 and Decker and de Wit 2005 for references). Overlying the Elliot Formation is the Clarens Formation, dominated by massive aeolian sandstones (du Toit 1926), in addition to facies representing distal alluvial fan and playa lake environments (Smith et al. 1993; Bordy et al. 2004). The lowermost flows of the overlying Drakensberg basalts often fill the morphology of the dune fields of the Clarens Formation, and intercalation of fossiliferous Clarens strata with the overlying lavas and volcanic ashes indicates contemporaneous deposition at circa 183 Ma.

17.4 Sampling

Our samples include organic materials and host rocks cleaned of carbonates. All sampling methods, locations and data, including details of the instrumentation and analytical work, with standards and reproducibility, are described in detail elsewhere (Ghosh 1999; Alexander 1999; de Wit et al. 2002; Decker 2004; Decker and de Wit 2005).

17.5 The Lower Karoo, Laingsburg

150 samples were collected along five transects in the Laingsburg area (Dwyka and Ecca Groups; Figs. 17.1 and 17.2). Sampling was conducted at intervals of between 50 cm to 50 m depending on the litho-stratigraphy and heterogeneity of the sections. Sampling was carried out using a modified lithological map compiled by Knütter et al. (1995; Fig. 17.2). The $\delta^{13}C_{org}$ section in our study area (Fig. 17.2) is represented by about 800 m of lodgement, rain-out and subaqueous and subglacial meltwater sands, suspended mud, and turbidity current sands and silts, deposited in at least seven upward fining cycles (Units 1–7), each starting with thick coarse tillites/diamictites and terminating in thin shale horizons and rhythmites/varves.

17.6 The Permian-Triassic Transition at Lootsberg Pass

For our second section, we separated organic matter preserved in 30 soil carbonate nodules collected along the Lootsberg Pass across the P-T boundary (Fig. 17.1). Details of our sample locations and data are given in Ghosh (1999) and de Wit et al. (2002). This section, as well as other nearby sections, has been studied by numerous people, and Chap. 15 of this book provides a significant summary of the present status.

17.7 The Molteno, Elliot and Clarens Formations

For our third section, 41 Molteno Formation samples for carbon isotope analysis were obtained from the Anderson collections (Anderson and Anderson 2003), housed in National Botanical Institute (NBI), Pretoria (now relocated to the Centre for Paleosciences at University of the Witwatersrand, Johannesburg). Plant, wood, insect fossils and rock samples were obtained from eight different sites (Fig. 17.1), the detailed locations of which are shown in Decker (2004) and Decker and de Wit (2005). 15 rock samples were

collected at a short section (~17 m) across the Molteno/Elliot Formation contact near Bramleyshoek (Fig. 17.1). Outcrop is poor and the contact not well defined (see also Chap. 12 in this book). 44 samples of the Lower and Upper Elliot Formation, basal and lowermost Clarens Formation were collected near Golden Gate (Fig. 17.1).

17.8 A Preliminary Composite Chemo-Stratigraphic Profile for the Karoo Basin

Figure 17.3 is a composite plot showing the measured $\delta^{13}C_{org}$ against time-stratigraphy for the entire Karoo Basin constructed using the above-mentioned data. Selected stratigraphic heights above the lowest sample site are indicated, and from which approximate maximum sedimentation rates can be estimated (Fig. 17.4). $\delta^{13}C_{org}$ has a varied range of values, from −11 to −32 ‰, with majority of samples falling between −21 and −28 ‰. At a broad scale, the variations in $\delta^{13}C$ can be divided into at least eight regimes (I–VIII, Fig. 17.3).

Regime I covers most of the glacial deposits from upper Tournasian (~346 Ma) up until Unit 5 of the Dwyka Group (~297 Ma, lower Asselian). During this ca. 50 myrs time-interval, $\delta^{13}C$ ranges between −22 to −28 ‰ (~25 ± 3 ‰), whilst sedimentation accumulation rates were very low (Fig. 17.4). From there upward, there is a steady increase in $\delta^{13}C$ between −26 and −20 ‰ during the deglaciation period, with a simultaneous increase to higher sediment accumulation rates. The transition to Regime III starts during the last glacial deposits (Regime II), consistent with faster accumulation rates associated with extensive melting and retreat of the ice cover. These conditions terminate abruptly when sediment accumulation rate of fine detritus under anoxic conditions suddenly decreases during the Prince Albert and Whitehill times (~290–276 Ma; Regimes III and IV).

Thereafter there is a steady decrease of $\delta^{13}C$ from −21 to −23 ‰ (Regime V) during a period of high sedimentation rates following the onset of turbidite deposition of the Collingham Formation and which continues up until early Beaufort Group times, after which subaerial sedimentation establishes itself permanently for the rest of the Permian (see Preface and Chap. 14 in this book). An early phase of uplift of the proto-Cape Mountains may have occurred just after the Dwyka Group was deposited, to coincide with the regional (global) increase in burial of carbon, mostly in the form of the extensive Karoo coal deposits at shallow depths throughout Gondwana (Veevers et al. 1994; Ghosh 1999; Faure et al. 1995; de Wit et al. 2002). The $\delta^{13}C_{org}$ of Permian (lower Ecca) coal ranges between −24 and −22 ‰ (Faure et al. 1995); the average $\delta^{13}C_{org}$ in the lower Ecca gas shales of the deeper water deposits range between −24 to −18 ‰ (Fig. 17.5), within the range of −25 to −19 ‰ determined by Geel et al. (2015; see also Chap. 11 in this book).

There is a distinct negative $\delta^{13}C$ shift of about 10 ‰, at first relatively gently, increasing from about −21 to −23 ‰ during deposition of the Karoo turbidites, and thereafter more sharply (following the transition to terrestrial environments) towards the P-T boundary, just below and across which there are rapid fluctuations between −27 and −32 ‰ (Regimes V and VI; see also Thackeray et al. 1990; Faure et al. 1995, MacLeod et al. 2000; de Wit et al. 2002). Soon after the P-T boundary, $\delta^{13}C$ returns to values of around −25 to −21 ‰ by Molteno times in the Triassic (Regime VII), after which arid conditions become established (Regime VIII). Because of a significant hiatus (Regime VII), the rate of increase in $\delta^{13}C$ during the Early Triassic is not known.

17.8.1 Significant Shifts in the Lower Karoo

$\delta^{13}C_{org}$ from the Waaipoort and most of the Dwyka (Regime I) is characterised by small, distinct fluctuations, but one most striking feature of our results is the similar stratigraphic positions and extremely high $\delta^{13}C$ values of two positive spikes in Unit 2 of the Dwyka Group of about –5 and –11 ‰, respectively (Alexander 1999). Because these peaks were detected in two separate transects they likely represent genuine dramatic excursions to extreme cold conditions over a very short stratigraphic section (~25 m), followed by a dramatic return to relative cool temperatures. The actual $\delta^{13}C_{org}$ values reached, −12 to −13 ‰, are similar to that reported for organic material deposited in modern subglacial Antarctic lakes (Bell and Karl 1999; Siegert et al. 2001). It is therefore tempting to contribute this to organic material of similar nature. However, similar large single positive spikes recorded at approximately similar biostratigraphic levels of the Carboniferous sequences of the USA, Europe and Russia could also imply a global atmospheric link related to sudden burial of extensive plant materials (Saltzman et al. 2000; Mii et al. 2001). The ultimate cause of this large event will require more detailed work across the Dwyka and its Gondwana equivalents in central Africa, Madagascar, South America, India, Antarctica.

The shifts in $\delta^{13}C_{org}$ of ~4–6 ‰ over a very short stratigraphic section across the boundaries between Dwyka Units 5–7 (Regime II) could be interpreted as a possible climatic shifts from interglacial to glacial (e.g., Visser 1987). The data in regime II is not of a high enough resolution to resolve this at present. However, the rapid decrease in the $\delta^{13}C_{org}$ at the end of Unit 7 supports an interpretation of rapid climatic warming from the Dwyka to the Prince Albert Formation (see also Chap. 10 in this book). This is consistent

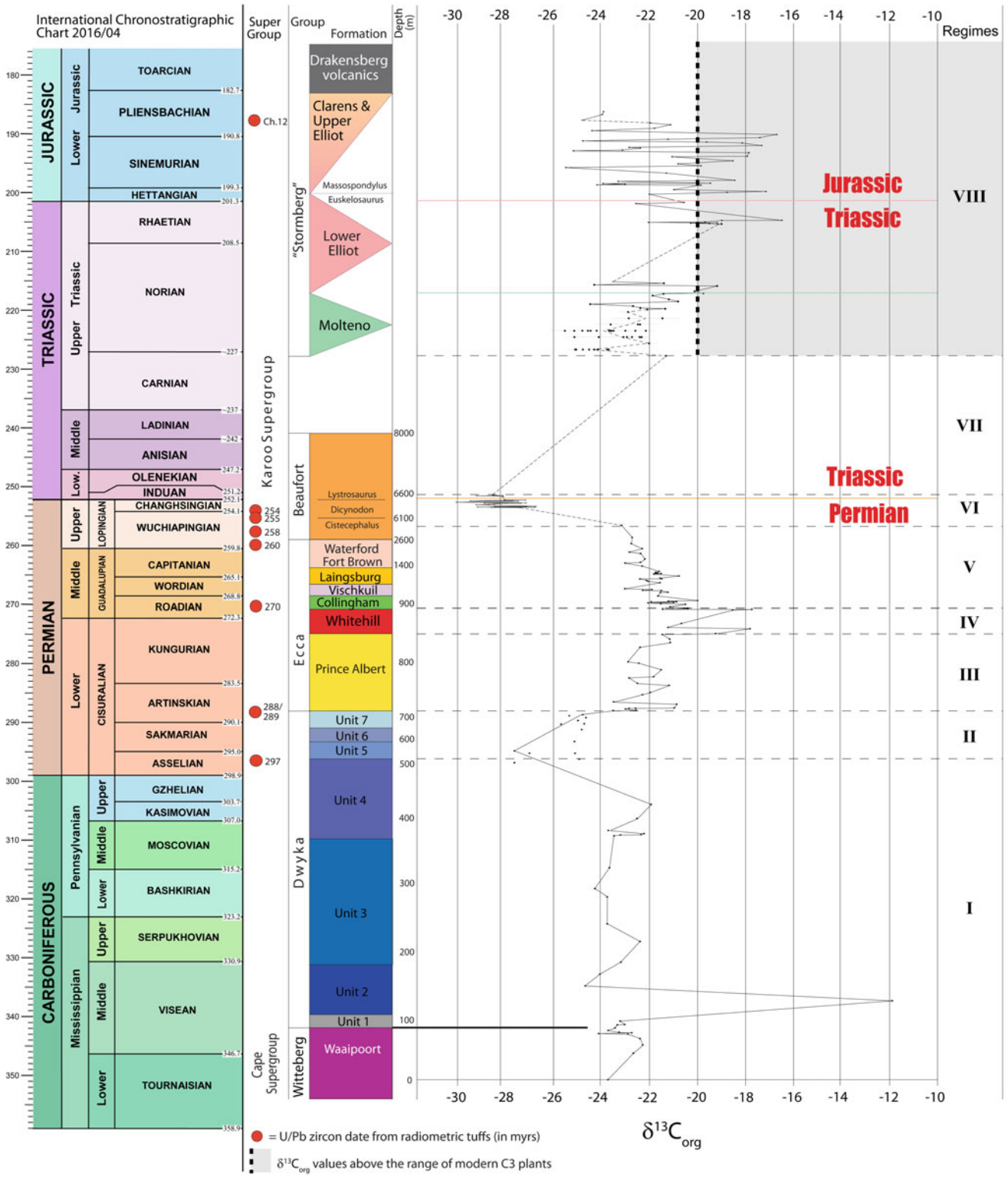

Fig. 17.3 Composite $\delta^{13}C_{org}$ stratigraphy across the south-central Karoo Basin. $\delta^{13}C_{org}$ data across the Dwyka and Ecca Groups (Regimes I–V) are from Alexander (1999) and Ghosh (1999). Data across the Permian-Triassic boundary (Regime VI) are combined from Thackeray et al. (1990); Faure et al. (1995); Gosh (1999), de Wit et al. (2002), and Ward et al. (2005), and are similar to those reported in MacLeod et al. (2000). $\delta^{13}C_{org}$ data from the Triassic sections (Regime VIII) are from Decker (2004) and Decker and de Wit (2004). See text for detailed analyses of the $\delta^{13}C_{org}$ fluctuations

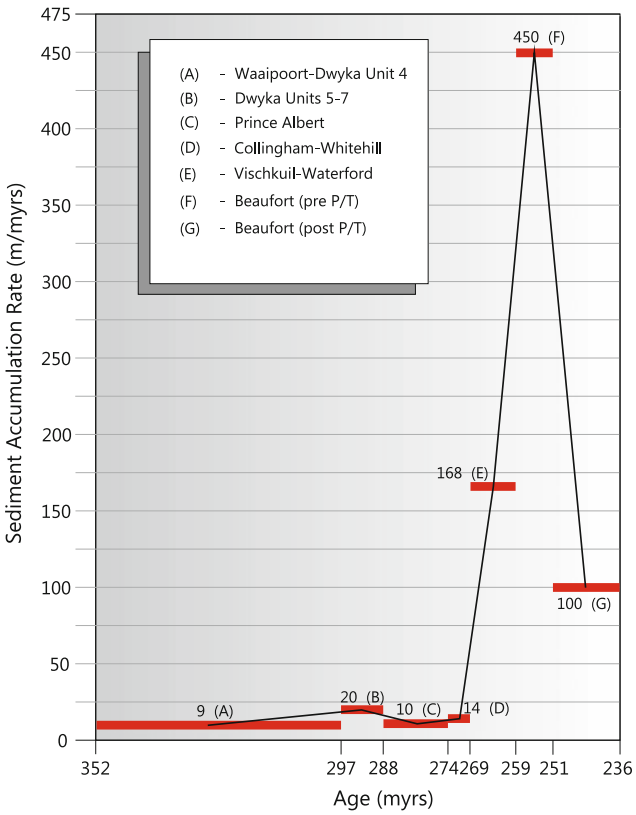

Fig. 17.4 Approximated maximum sediment accumulation rates for the Karoo Basin based on sediment thicknesses of sampled sections and U/Pb zircon dates (de Wit et al. in prep). P/T = Permian-Triassic Boundary

with the Chemical Index of Alteration (CIA) of the Karoo rocks. Dwyka diamictites have a low range of CIA values, consistent with mechanical weathering and cold conditions. By contrast, CIA values for mudrocks in the Dwyka units show wide fluctuating ranges that are interpreted to represent deposition during interglacial episodes, and shales from the overlying Prince Albert Formation have high CIA values suggesting a rapid transition to a much more intensive weathering regime and warmer climatic conditions (Visser and Young 1990).

Of significant interest, is the positive shift of 9 ‰, from −27 to −18 ‰, commencing in Dwyka Unit 5 and terminating at the end of the Whitehill Formation (Regime III/IV). This trend is consistent with increased burial of plant material and the formation/preservation of peat, coal and oil causing a shift to more positive $\delta^{13}C$ values. This period coincides with the formation of the major known coal deposits within the Karoo and other terrestrial Gondwana basins (Veevers et al. 1994; Faure et al. 1995; Ghosh 1999; de Wit et al. 2002), as well as the high TOC of the deep water black shales such as the Whitehill Formation (4.5 weight percent; Geel et al. 2015).

Although $\delta^{13}C_{org}$ variability within the Whitehill Formation (Regime IV) are clearly complex, with large (>3 ‰) internal reversals (Fig. 17.5b), the large and abrupt positive excursion $\delta^{13}C_{org}$ (~5 ‰) confined to the Whitehill Formation (Fig. 17.5 a–c) makes this a distinct chemo-stratigraphic marker that can be traced as far as the Irati Formation in Brazil, with similar bio-, litho- and chemo-stratigraphy (du Toit 1926; Faure et al. 1995; Linol et al. 2016; Chap. 18 of this book). The $\delta^{13}C_{carbonate}$ values in the Whitehill Formation (Fig. 17.5d) are really low and are thus unlikely to be related to marine deposits. Assuming a freshwater origin, therefore, the $\delta^{13}C_{water}$ of the Karoo must have been extremely variable. Variability in $\delta^{13}C_{water}$ can probably explain the $\delta^{13}C_{org}$ variability without invoking a switch between different plant types or algal blooms

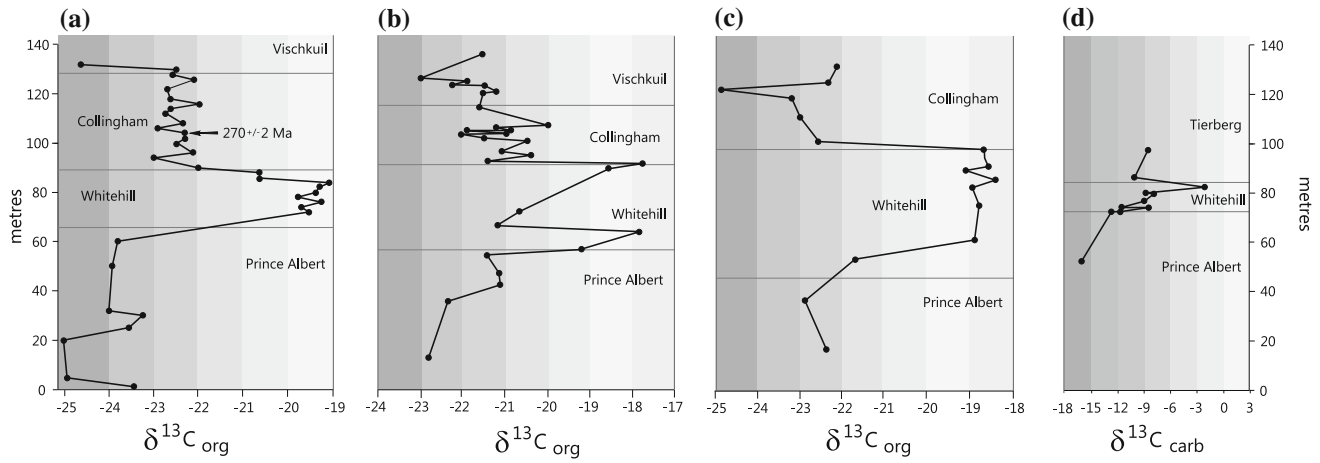

Fig. 17.5 Carbon isotope 'fingerprints' across the *black* gas-shales of the Whitehill Formation. $\delta^{13}C_{org}$ sections **a**–**c** are from sample areas 1, 4 and 5 shown on Fig. 17.2. The $\delta^{13}C_{carbonate}$ section **d** is from Faure et al. (1995). The origin for the distinct C-isotope perturbations across the Whitehill Formation remains to be resolved (see also Chap. 11 in this book)

(e.g., Faure et al. 1995). However, large $\delta^{13}C_{water}$ variations would also imply an isolated environment, closed from the atmosphere in, for example, a subglacial lake environment such as those found beneath present-day Antarctic ice sheets, such as Lake Vostok. This lake, which has been stable for 20 myrs, has a depth of up to 670 m beneath the ~4 km ice sheet of Antarctica and has accumulated up to several hundred metres of glacial sediments (Bell and Karl 1999; Siegert et al. 2001). Because the East Antarctic ice sheet flows across Lake Vostok (and at least 70 other large lakes that have now been identified beneath the ice; Jamieson et al. 2016), it acts as a conveyer belt delivering sediments to the lake bottom, as the base of the ice sheet melts during pressure release. This partial melting of the ice sheet is believed to supply sediments, new water, microbes and possibly gas hydrates to the lake (Bell and Karl 1999). Such an environment could explain the low spore/pollen counts in the lower Dwyka sequences of the southern Karoo.

17.8.2 Significant Shifts Across the P-T Boundary

The $\delta^{13}C_{org}$ shows significant fluctuations in the Upper Permian between −27 and −29 ‰, and a small negative spike (–30 ‰) is discernible (Fig. 17.3) around the P-T boundary. Lack of nodules throughout the section prevented identification of more pronounced spikes. However, there is a significant negative trend in the $\delta^{13}C_{org}$ from a mean around −23 ‰ between ~260 and 270 Ma. The general decline in $\delta^{13}C$ towards the P-T boundary and the general rapid fluctuation across the boundary have been linked to increasing exposure and oxidation of coals across the heartland of Gondwana, and release of methane gas from its continental margins (de Wit et al. 2002), as well as extensive gas emissions during the formation of the Siberian LIP (Svenson et al. 2009; Saunders 2016). But there is no overall agreement about cause and effects of the general decline and subsequent fluctuations across the Karoo P-T boundary (Faure et al. 1995; MacLeod et al. 2000; de Wit et al. 2002; Ward et al. 2005; Day et al. 2015; Gastaldo et al. 2015; Chap. 15 in this book).

17.8.3 Significant Shifts in the Upper Karoo

$\delta^{13}C_{org}$ values for all Molteno Formation samples typically range between −26 and −21 ‰ (Regime VIII; de Wit et al. in prep). Due to the wide range of values at well-sampled locations, no clear stratigraphic trend is observed. The greatest degree of variation occurs at the best-sampled location with well-preserved fossils representing riparian forest habitats. The spectrum of $\delta^{13}C_{org}$ values (for 13 samples) has a range of 4.3 ‰ (Fig. 17.2). Such a range of variation in $\delta^{13}C_{org}$ is greater than the 3.5 ‰ excursion in the $\delta^{3}C_{org}$ of wood observed across the Triassic-Jurassic (T-J) boundary elsewhere (Hesselbo et al. 2002).

Bulk rock (shale) and coal samples generally display isotopic ratios of a similar range, and within error of plant fossils. Isotopic variations do not follow taxonomic trends, supporting that bulk rock analysis is a reasonable alternative to fossil plant analysis when conducting $\delta^{13}C_{org}$ stratigraphy in the Upper Karoo Supergroup. All Molteno samples analysed show $\delta^{13}C_{org}$ values typical of modern C3 plants (Fig. 17.3), although all values lie within the higher end of the range of modern C3 plants, with a value of −24 ‰ (modern C3 plant average −27 ‰). The possible reasons for this are discussed elsewhere (Decker and de Wit 2005), but suffice it to state that the concentration of atmospheric CO_2 at this time was higher than it is today (Berner 1990), and the $\delta^{13}C$ value of atmospheric CO_2 in the Carnian (Molteno times) may have been higher than modern pre-industrial values. Alternatively, the data indicate high water use efficiency in Molteno plants, due to a saline or arid environment, and seasonal aridity may well have been a determining factor.

Details of the chemostratigraphy of the Elliot and Clarens Formations are discussed elsewhere (Decker 2004; Decker and de Wit 2005). $\delta^{13}C_{org}$ values oscillate relatively rapidly between −27 and −15 ‰, with at least seven episodic reversals (Fig. 17.3). The Elliot Formation is distinguished from the Molteno Formation chemostratigraphically by the existence of $\delta^{13}C_{org}$ values higher than −20 ‰. 30 % of the Elliot Formation samples have $\delta^{13}C_{org}$ values above −20 ‰ (Fig. 17.3). These values range as high as −16 ‰ (Decker and de Wit 2005) that occur as distinct, sharp, positive excursions. Most importantly, these positive excursions lie beyond the $\delta^{13}C$ range of modern C3 plants (Fig. 17.3), and have been interpreted as evidence of the episodic dominance of CAM plants (Crassulacean Acid Metabolism, also known as CAM photosynthesis) in response to severe episodes of drought during aridification towards a Jurrasic-Cretacous greenhouse world (Decker and de Wit 2005).

17.9 Discussion and Conclusions

Most, if not all of the Karoo sequences have terrestrial organic materials preserved suitable for Carbon isotope analysis. Organic Carbon isotope signatures ($\delta^{13}C_{org}$) across the Karoo sequences reveal distinct climate and ecosystem changes that can be tested against other stratigraphic observations especially fossils, to help reconstruct robust evolving paleoenvironments. But the work is in early stages and requires, and deserves, more detailed analyses to trace the terrestrial trends across Gondwana as has also been

attempted for India and Madagascar (e.g., Ghosh 1999; Rakatosolofo 1999; de Wit et al. 2002).

Following the formation of lacustrine conditions at the early Visean, Dwyka deposition may have occurred in a large subglacial lake similar to those reported beneath the modern Antarctic ice cap. There is only one recorded layer in the lowermost Prince Albert Formation that may represent a marine incursion, but even in this case, there is significant doubt about the environmental interpretation from this scanty fossil evidence (Ian McLachlan, pers comm 2001); and the stable isotope (carbon and sulphur) evidence to-date on this formation, favours a terrestrial saline lake environment during the immediate post-Dwyka period (Faure et al. 1995; Faure and Cole 1999; see also Chap. 11 in this book). Antarctic-like conditions clearly existed in source areas during deposition of the Dwyka sedimentation, as the South Pole traversed the Karoo (Opdyke et al. 2001; Preface this book). The Dwyka tillites and varves may therefore have formed in a lake, possibly episodically connected to marine waters, and perhaps similar to the present Antarctic subglacial Lake Vostok (Bell and Karl 1999; Siegert et al. 2001; Jamieson et al. 2016). Our field and stable-isotope data also confirm that there were significant interglacial episodes within the last 10 myrs of Dwyka deposition, as was postulated by Visser and Young (1990).

Wopfner (1999) has argued that deglaciation was extremely abrupt (<5 myrs) in the Late Asselian to Early Sakmarian, relatively consistent with the recent dating of the top of the Dwyka at about 290 Ma (Sakmarian-Artinskian transition; Bangert et al. 1999). The partial or total collapse of the ice sheet would in turn have contributed to global sea level rise during general global warming. The short marine incursion along the western part of the basin may represent a related sea level high-stand, but isostatic rebound after deglaciation may have kept the Karoo lake from becoming a large marine basin.

Deposition occurred predominantly in lacustrine environments; the size of the Karoo lake became gigantic following deglaciation, perhaps similar to the moraine blocked lake of the Baltic Sea following the last deglaciation and isostatic equilibration (Chap. 11 this book), which in turn re-established terrestrial conditions for the remained of the history of the interior of southern Africa.

The upper parts of the Karoo sequences contain two of the major extinction events (P-T and T-J) that now require further high resolution carbon isotope testing to reveal their global terrestrial connectivity to rapid, pulsating CO_2 (and related CH_4) emissions from large igneous provinces that are now precisely dated at around 252 Ma and 201 Ma, respectively (e.g., Hesselbo et al. 2002; Svensen et al. 2009; Schoene et al. 2010) as has been done successfully at resolutions well below 100,000 years elsewhere in marine systems (e.g., Ruhl et al. 2011; Burgess et al. 2014; Clarkson et al. 2015). Resolving the causes of the great decline of $\delta^{13}C_{org}$, some 3–4 million years ahead of the P-T boundary (Regime IV); and the large fluctuations well before the T-J boundary (Regime VIII) remain major challenges.

The transition into the Jurassic and Cretaceous hothouse environments is also well archived in the Karoo. Large fluctuations in the isotope ratios document the onset of severe droughts ahead of the onset of regional desertification that continued for at least 50 million years, as witnessed in Namibia, where dune fields, similar to those found intercalated with the lowermost lavas of the Drakensberg basalts in South Africa, are interbedded with the Lower Cretaceous Etendeka flood basalts (~132 Ma; Marsh et al. 2001). In addition, $\delta^{13}C_{org}$ of plant fossils across the T-J boundary have revealed nature's first engineering of CA photosynthesis. Thus, carbon isotope stratigraphy across the Karoo has shown the importance of chemical stratigraphy in unravelling its paleo-history. Combining this tool with other stable isotopes is now needed for a higher resolution.

Acknowledgments Funding for the studies was by NRF to MdW (Open Program). This chapter is a summary of a much more detailed manuscript that has been 'in progress' since 2004, and will be completed in due course. Thanks to B Linol for thorough reviews. This is AEON contribution number 161.

References

Ager DV (1973) The Nature of the Stratigraphic Record. Halsted (Wiley), New York, 114p. (3rd edition 1992, 151p).

Alexander J (1999) Carbon Isotope stratigraphy of Permo-Carboniferous sediments in the Karoo Basin, SE of Laingsburg, South Africa. Unpublished Hons. Thesis, University of Cape Town, 37p.

Anderson JM and Anderson HM (2003). The Heyday of the Gymnosperms: systematics and biodiversity of the Late Triassic Molteno fructifications. Strelitzia, 15, National Botanical Institute, Pretoria, 398p.

Anderson JM, Anderson HM, Archangelsky S, Bamford S, Chandra S, Dettman M, Hill R, Mcloughlin S and Rösler O (1999) Patterns of Gondwana plant colonisation and diversification. J Afr Earth Sci 28:145–168.

Bachtadse V, Van der Voo R and Halbich IW (1987) Paleomagnetism of the western Cape Fold Belt, South Africa, and its bearing on the Paleozoic apparent polar wander path for Gondwana. Earth Planet Sci Lett 84:487–499.

Bangert B, Stollhofen H, Lorenz V and Armstrong R (1999) The geochronology and significance of ashfall tuffs in the glaciogenic Carboniferous-Permian Dwyka Group of Namibia and South Africa. J Afr Earth Sci 29:33–50.

Bell RE and Karl DM (1999) Evolutionary processes a focus of Decade-long ecosysytem study of Antarctic's Lake Vostok. EOS, Trans Am Geophy Union 80:573–579.

Berner RA (1990) Atmospheric carbon dioxide levels over Phanerozoic time. Science 249:1382–1386.

Bordy EM, Hancox PJ, Rubidge BS (2004) Fluvial style variations in the Late Triassic–Early Jurassic Elliot Formation, main Karoo Basin, South Africa. J Afr Earth Sci 38:383–400.

Burgess, S.D., Bowring, S., and Shen, S.Z., 2014, High-precision timeline for Earth's most severe extinction. National Academy of Sciences Proceedings 111:3316–3321.

Clarkson et al. (2015) Ocean acidification and the Permo-Triassic mass extinction. Science 348:229–232.

Day MO, Ramezani J, Bowring SA, Sadler PM, Erwin DH, Abdala F and Rubidge BS (2015) When and how did the terrestrial mid-Permian mass extinction occur? Evidence from the tetrapod record of the Karoo Basin, South Africa. Proc R Soc B 20150834.

Decker JE (2004) Organic Carbon Isotope Stratigraphy of the Mesozoic Upper Karoo Supergroup, Main Karoo Basin, South Africa, in a Seismic Stratigraphic Framework. Unpublished M.Sc. thesis, University of Cape Town, 144p.

Decker JE and de Wit MJ (2005) Carbon isotope evidence for CAM photosynthesis in the Mesozoic. Terra Nova 18:9–17.

De Wit MJ, Ghosh JG, de Villiers S, Rakotosolofo N, Aexander J, Tripathi A and Looy C (2002) Multiple organic carbon isotope reversals across the Permo-Triassic boundary of terrestrial Gondwana sequences: Clues to extinction patterns and delayed ecosystem. J Geol 110:227–24.

Duncan RA, Hooper PR, Rehacek J, Marsh JS, Duncan AR (1997) The timing and duration of the Karoo igneous event, southern Gondwana. J Geophys Res 102:18127–18138.

Du Toit AL (1926) The Geology of South Africa (*3rd edition, 1954*). Oliver and Boyd, Edinburgh.

Faure K, de Wit MJ and Willis JP (1995) Late Permian global coal hiatus linked to ^{13}C depleted CO_2 flux into the atmosphere during the final consolidation of Pangea. Geology 23:507–510.

Faure K and Cole D (1999) Geochemical evidence for lacustrine microbial blooms in the vast Permian Main Karoo, Paraná, Falkland Islands and Haub basins of southwestern Gondwana. Palaeogeogr Palaeoclimatol Palaeoecol 152:189–213.

Fildani A, Drinkwater NJ, Weislogel A, McHargue T, Hodgson DM and Flint SS (2007) Age controls on the Tanqua and Laingsburg deep-water systems: new insights on the evolution and sedimentary fi ll of the Karoo basin, South Africa. J Sediment Res 77:901–908.

Gastaldo RA, Kamo SL, Neveling J, Geissman JW, Bamford M and Looy CV (2015) Is the vertebrate-defined Permian-Triassic boundary in the Karoo Basin, South Africa, the terrestrial expression of the end-Permian marine event? Geology 43:939–942.

Geel C, de Wit M, Booth P, Schulz H-M and Horsfield B (2015) Palaeo-environment, diagenesis and characteristics of Permian black shales in the Lower Karoo Supergroup flanking the Cape Fold Belt near Jansenville, eastern Cape, South Africa: Implications for the shale gas potential of the Karoo Basin. S Afr J Geol 118:249–274.

Ghosh JG (1999) U/Pb geochronology and structural geology across major shear zones of the southern granulite terrain of India and the $\delta^{13}C_{org}$ stratigraphy of the Gondwana coal basins of India: their implication for Gondwana studies. Unpublished PhD thesis, University of Cape Town.

Grossman, E.L. 1994. The carbon and oxygen isotope record during the evolution of Pangea: Carboniferous to Triassic. Geol Soc Am Spec Pap 288:207–228.

Hessselbo SP, Robinson SA, Surlyk F and Piasecki S (2002) Terrestrial and marine extinction at the Triassic-Jurassic boundary synchronized with major carbon-cycle perturbation: A link to initiation of massive volcanism? *Geology* **30**: 251–254.

Higgs R (2010) Comments on 'Sequence stratigraphy of an argillaceous, deepwater basin plain succession: Vischkuil Formation (Permian), Karoo Basin, South Africa' from van der Merwe, Flint and Hodgson (Mar Pet Geol 27: 321–333). Mar Pet Geol 27:2073-2075.

Jamieson SSR, Ross N, Greenbaum JS, Young DA, Aitken ARA, Roberts JL, Blankenship DD, Bo S and Siegert MJ (2016) An extensive subglacial lake and canyon system in Princess Elizabeth Land, East Antarctica. Geology 44:87–90.

Jenkyns HC, Jones CE, Gröke DR, Hesselbo SP and Parkinson DN (2002) Chemostratigraphy of the Jurassic System: applications, limitations and implications for palaeoceanography. J Geol Soc London 159:351–378.

Johnson MR et al. (1997) The Foreland Karoo Basin, South Africa. In: Selley RC (ed) African basins. Sedimentary basins of the World. Elsevier, Amsterdam, pp. 269–317.

Knütter RKC, Fiedler K, Adelman D, Albes D, Zechner J (1995) Geological map of Laingsburg area, 1:25000, Bonn University Unpublished.

Linol B, de Wit MJ, Barton E, de Wit MCJ and Guillocheau F (2016) U–Pb detrital zircon dates and source provenance analysis of Phanerozoic sequences of the Congo Basin, central Gondwana. Gondwana Res 29:208–219.

Marsh JS, Ewart A, Milner SC, Duncan AR and Miller RMcG (2001) The Etendeka Igneous Province: magma types and their stratigraphic distribution with implications for the evolution of the Parana- Etendeka flood basalt province. Bull Volcanol 62:464–486.

McCabe C and Elmore RD (1989) The occurrence and origin of Late Paleozoic remagnitisation in the sedimentary rocks of North America. Rev Geophys 27:471–494.

MacLeod KG, Smith RMH, Koch PL and Ward PD (2000) Timing of mammal-like reptile extinctions across the Permian-Triassic boundary in South Africa. Geology 28:227–230.

McLachlan IR and Anderson AM (1973) A review of the evidence for marine conditions in southern Africa during Dwyka times. Palaeontologica Africana 15:37–64.

McKay MP, Weislogel AL, Fildani A, Brunt RL, Hodgson DM and Flint SS (2015) U-PB zircon tuff geochronology from the Karoo Basin, South Africa: implications of zircon recycling on stratigraphic age controls. Int Geol Rev 57:393–410.

Mii H-S, Grossman EL, Yancey TE, Chuvashow B and Egorov A (2001) Isotopic records of brachiopod shells from the Russian Platform – evidence for the onset of mid-Carboniferous glaciation. Chem Geol 175:133–147.

Opdyke ND, Mushayandebun M and de Wit MJ (2001) A new palaeomagnetic pole for the Dwyka System and correlative sediments in sub-Saharan Africa. J Afr Earth Sci 33:143–154.

Plumstead EP (1964) Gondwana floras, geochronology and glaciation in South Africa. International Geological Congress, 22nd Session, India, pp. 303–319.

Rakotosolofo NA (1999) Geology, Carbon isotope stratigraphy, and palaeomagnetism of the Karoo sequences of the southern Morondava basin, SW Madagascar. Unpublished MSc. thesis, University of Johannesburg (formerly Rand Afrikaans University).

Raymo ME (1994) The initiation of northern hemisphere glaciation. Ann Rev Earth Planet Sci 22:353–383.

Ruddiman WF (2000) Earth's Climate. W H Freeman & Co. NY, 465p.

Rubidge BS, Erwin DH, Ramezani J, Bowring SA and de Klerk WJ (2013) High-precision temporal calibration of Late Permian vertebrate biostratigraphy: U-Pb zircon constraints from the Karoo Supergroup, South Africa. Geology 41:363–366.

Ruhl M, Bonis NR, Reichart G-J, Damsté JSS, Kürschner WM (2011) Atmospheric Carbon Injection Linked to End-Triassic Mass Extinction. Science 333:430–434.

Saltzman MR, González LA and Lohmann KC (2000) Earliest carboniferous cooling step triggered by the Antler orogeny? Geology 28:347–350.

Saunders AD 2016. Two LIPs and two Earth-system crises: the impact of the North Atlantic Igneous Province and the Siberian Traps on the Earth-surface carbon cycle. Geol Mag 153.

Schoene B, Guex J, Bartolini A, Schaltegger U and Blackburn TJ (2010) Correlating the end-Triassic mass extinction and flood basalt volcanism at the 100 ka level. Geology 38:387–390.

Scott AC, Anderson JM and Anderson HM (2004) Evidence of plant–insect interactions in the Upper Triassic Molteno Formation of South Africa. J Geol Soc London 161:401–410.

Siegert MJ, Ellis-Evans JC, Tranter M, Mayer C, Petit J-R, Salamatin A and Priscu JC (2001) Physical, chemical and biological process in Lake Vostok and other subglacial lakes. Nature 414:603–609.

Smith AG (1999) Gondwana: its shape, size and position from Cambrian to Triassic times. J Afr Earth Sci 28:71–97.

Smith RMH, Erickson PA and Botha WJ (1993) A review of the stratigraphy and sedimentary environments of the Karoo-aged basins of southern Africa. J Afr Earth Sci 16:143–169.

Streel M and Theron JN (1999) The Devonian-Carboniferous boundary in South Africa and the age of the earliest episode of the Dwyka glaciation: New palynological result. Episodes, 22:41–44.

Svensen SH, et al. (2009) Siberian gas venting and the end-Permian environmental crisis. Earth Planet Sci Lett 277:490–500.

Thackeray J F, van der Merwe NJ, Lee-Thorpe JA, Sillen A, Lanham J L, Smith R, Keyser A and Monteiro PMF (1990). Carbon isotope evidence for Late Permian therapsids teeth, for a progressive change in atmospheric CO2 composition. Nature 347:751–753.

Turner BR (1983) Braidplain deposition of the Upper Triassic Molteno Formation in the main Karoo (Gondwana) Basin, South Africa. Sedimentology 30:77–89.

Turner BR (1999) Tectonostratigraphical development of the upper Karoo foreland basin: orogenic unloading versus thermally-induced Gondwana rifting. J Afr Earth Sci 28:215–238.

Veevers JJ, Cole DI, Cowan EJ (1994) Southern Africa: Karoo Basin and Cape Fold Belt. In: Veevers, J.J., Powell, McA. (Eds) Permian-Triassic Pangean Basins and foldbelts along the Panthalassan margin of Gondwanaland. Geol Soc Am Mem 184:223–280.

Veizer J *et al*. (1999) $^{87}Sr/^{86}Sr$, $\delta^{13}C$ and $\delta^{18}O$ evolution of Phanerozoic sea water. Chem Geol 161:59–88.

Visser JNJ (1987) The Palaeogeography of part of southwestern Gondwana during the Perm-Carboniferous glaciation. Paleogeogr Palaeoclimat Palaeoecol 61:205–219.

Visser JNJ and Young GM (1990) Major element geochemistry and paleoclimatology of the Permo-Carboniferous glacigene Dwyka Formation and post-glacial mudrocks in southern Africa. Palaeogeogr Palaeoclimat Palaeoecol 81:49–57.

Ward PD, Botha J, Buick R, DeKock MO, Erwin DH, Garrison GH, Kirschvink JL and Smith R (2005) Abrupt and Gradual extinction among Late Permian land vertebrates in the Karoo Basin, South Africa. Science 307:709–714.

Wopfner H (1999) The Early Permian deglaciation event between East Africa and northwestern Australia. J Afr Earth Sci 29:77–90.

Zawada PK (1988) Trace elements as possible paleosalinity indicators for the Ecca and Beaufort Group mudrocks in the southwestern Orange Free State. S Afr J Geol 91:18–26.

Part VI
Geodynamics

18 Correlation and Paleogeographic Reconstruction of the Cape-Karoo Basin Sequences and Their Equivalents Across Central West Gondwana

Bastien Linol, Maarten J. de Wit, Charles H. Kasanzu, Renata da Silva Schmitt, Francisco Jose Corrêa-Martins, and Andre Assis

Abstract

The most iconic stratigraphic sequences of West Gondwana are those of the Cape-Karoo Basin of southern Africa. But time-equivalent, extensive, and thick basin sequences are also preserved in the less well-known Congo Basin of central Africa, and the Paraná and Parnaíba Basins of south-east and north-central South America. Here, we review sedimentological and stratigraphic data of these four very large basins of Central West Gondwana to discuss possible correlations and paleogeographic reconstructions during and following the period of amalgamation of Gondwana and Pangea (ca. 600–300 Ma), and during the subsequent period of break-up of these two supercontinents (ca. 200–120 Ma). The aim is to provide a regional framework to the study of the Cape-Karoo type sections and highlight some of the major uncertainties that remain to be clarified before robust continental-scale geodynamic models and global climatic variability can be verified.

Keywords

West Gondwana • Intracratonic basins • Chronostratigraphy • Paleogeography

18.1 Introduction

Pioneering stratigraphic correlations by Alex du Toit, in the 1930s, first highlighted significant similarities between the sedimentary rock sequences in south-central Africa and eastern South America (Fig. 18.1a), supporting the concept of a united Central West Gondwana Basin. Based on subsequent seismic- and well-data (Milani and de Wit 2008; Lindeque et al. 2011; Daly et al. 2014; Linol et al. 2015a), and recent field investigations in Brazil, the Democratic Republic of Congo (DRC) and South Africa (Fig. 18.1b), we describe the main stratigraphic sequences and sedimentation patterns of the Parnaíba, Paraná and Congo Basins to propose Gondwana-scale correlations and paleogeographic reconstructions with those from the Cape-Karoo Basin that is the focus of this book.

18.2 Regional Stratigraphic Basin Analysis

- Parnaíba Basin

The Parnaíba Basin covers ca. 600,000 km^2 of northeastern Brazil (Fig. 18.1). It preserves depocenters between 1 and 3.5 km in thickness, which record two main episodes of

B. Linol (✉) · M.J. de Wit
AEON-ESSRI (African Earth Observatory Network – Earth Stewardship Research Institute), Nelson Mandela Metropolitan University, Port Elizabeth, South Africa
e-mail: bastien.aeon@gmail.com

C.H. Kasanzu
Geology Department, University of Dar es Salaam, P.O. Box 35052Dar es Salaam, Tanzania

R. da Silva Schmitt · A. Assis
Laboratório do Gondwana – Departamento de Geologia, sala J2-020 – Campus Universitário, Universidade Federal de Rio de Janeiro, Rio de Janeiro, Brazil

F.J. Corrêa-Martins
Departamento de Geociências, Universidade Federal Rural do Rio de Janeiro, Seropédica, Rio de Janeiro, Brazil

B. Linol and M.J. de Wit (eds.), *Origin and Evolution of the Cape Mountains and Karoo Basin*, Regional Geology Reviews, DOI 10.1007/978-3-319-40859-0_18

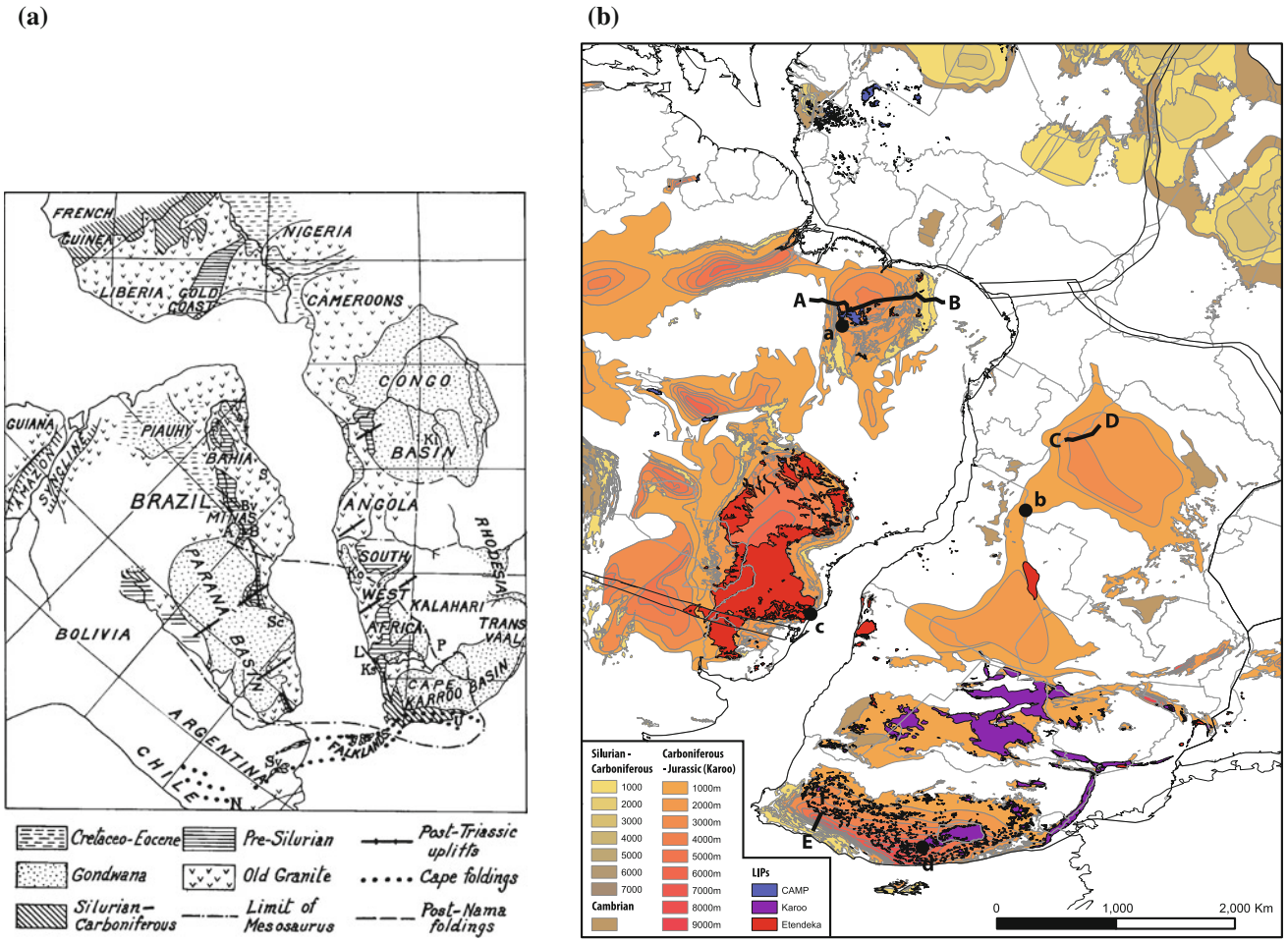

Fig. 18.1 Maps of Central West Gondwana showing stratigraphic correlations between south-central Africa (the Congo and Cape-Karoo Basins) and eastern South America (the Paraná and Parnaíba [Piauhy] Basins): **a** by Alex Logie du Toit (1937); and **b** using rotated Geographic Information System (GIS) data in Gplates (Gurnis et al. 2011), with location of the seismic lines (*black lines*) and field photos (*black dots*) presented in Figs. 18.2 and 18.4, respectively

basin inversion, during the Triassic and during the Late Jurassic-Early Cretaceous (Daly et al. 2014). The basin overlies a subhorizontal peneplain across Precambrian basement (the Amazonian and São Francisco Cratons, and the Parnaíba block; Fig. 18.2a), with locally remnants of Cambro-Ordovician sequences preserved (e.g., Riachão and Jaibaras; Fig. 18.3). The oldest overlying siliciclastic platform sequence of the basin, the Serra Grande Group, comprises thick cross-bedded quartz-rich sandstones with subordinate siltstones and shales (about 900 m thick; Vaz et al. 2007), deposited regionally from the south and southeast, and biostratigraphically dated from the Llandovery to Lower Devonian (Grahn et al. 2005). Near the base, diamictites beds (part of the Ipu Formation; BL personal observations) possibly relate to the Late Ordovician glaciation of Gondwana, as also documented in the Cape and Paraná Basins (but not in the Congo Basin; Milani and de Wit 2008; Linol et al. 2015a; Chap. 1 this book), and which is also widely preserved across north Africa (e.g., Cherns and Wheeley 2009; Torsvik and Cocks 2011; Ghienne et al. 2014). The overlying Devonian-Lower Carboniferous Canindé Group (1200 m thick) starts with tide and storm-related deposits, and black shales rich in organic matter (TOC = 2.0–2.5 %; Milani and Zalán 1999), known as the Pimenteiras Formation (Fig. 18.3) that represent a rapid maximum marine inundation. These shales coarsen upward to sandstones with younger glacial deposits (part of the Cabeças Formation; Caputo et al. 2008). The top of this regressive sequence is marked by an erosional surface, in turn overlain by low-stand delta fronts of the Poti Formation (Fig. 18.3), which possibly relates to eustatic falls in sea level linked to expanding Gondwanan ice caps during the Carboniferous (ca. 300–350 Ma; Vaz et al. 2007; see also Chap. 17 in this book), and/or uplift related to initiation of the Appalachian-Variscan orogens that amalgamated Pangea between about 340 and 270 Ma (Van Staal et al. 2009; Kröner and Romer 2013). An overlying clastic-evaporitic and aeolian sequence, part of the Balsas Group (1300 m

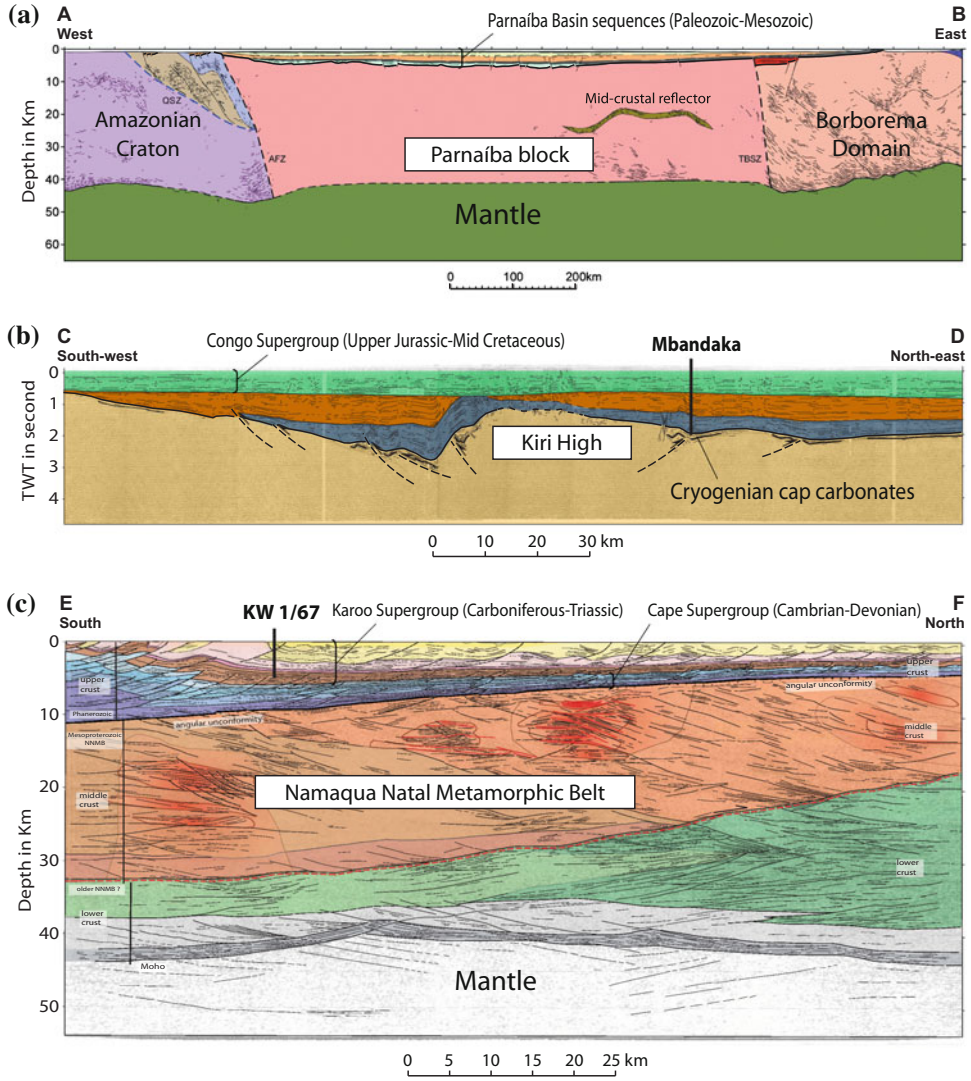

Fig. 18.2 Deep seismic reflection profiles across: **a** the Parnaíba Basin (Daly et al. 2014); **b** central-west Congo (re-interpreted from Daly et al. 1992 by Linol et al. 2015a; Mbandaka = 4.3 km deep borehole drilled by Esso-Zaire in 1981); and **c** the southwest Cape-Karoo Basin (KW 1/67 = 5.5 km deep borehole drilled by SOEKOR in 1967; Lindeque et al. 2011; Chap. 1 this book); Fig. 18.1b for location

thick; Vaz et al. 2007), is dated from the Pennsylvanian to Lower Triassic (Souza et al. 2010), and yields some earliest Permian (Cisuralian) amphibians and reptiles (Cisneros et al. 2015). At the top of this sequence, stromatolitic limestones are unconformably overlain by Triassic and Jurassic aeolian dune sands (the Sambaíba Formation and Mearim Group; Fig. 18.3), deposited during easterly and northeasterly paleo-winds (Fig. 18.4a). The aeolianites are intercalated with at least two mafic sequences, named the Mosquito and Sardinha Formations. The first magmatic sequence (Mosquito) dates at 202–197 Ma (Merle et al. 2011) and is linked to the Central Atlantic Magmatic Province (CAMP) that erupted at 201 Ma (Schoene et al. 2010; Blackburn et al. 2013) during initial opening of the southern North Atlantic Ocean. The second magmatic sequence (Sardinha) is dated at 129–124 Ma, and attributed to rifting phases of the northern South Atlantic opening. In the northern part of the basin, an uppermost 1000 m thick mid-Cretaceous fluvial-marine sequence (the Corda, Grajaú, Codó and Itapecuru Formations; Fig. 18.3) unconformably overly the Jurassic CAMP basalts and red beds, biostratigraphically dated in the lower part to the upper Aptian-Albian.

- The Congo Basin

The Phanerozoic sedimentary cover of the Congo Basin extends ca. 1,800,000 km^2 across central Africa (DRC, Rep. of Congo, Gabon, Angola and the CAR; Fig. 18.1b), and ranges between 1 and 6 km in thickness (Daly et al. 1992; Linol et al. 2015a). The basin is surrounded by amalgamated Archean

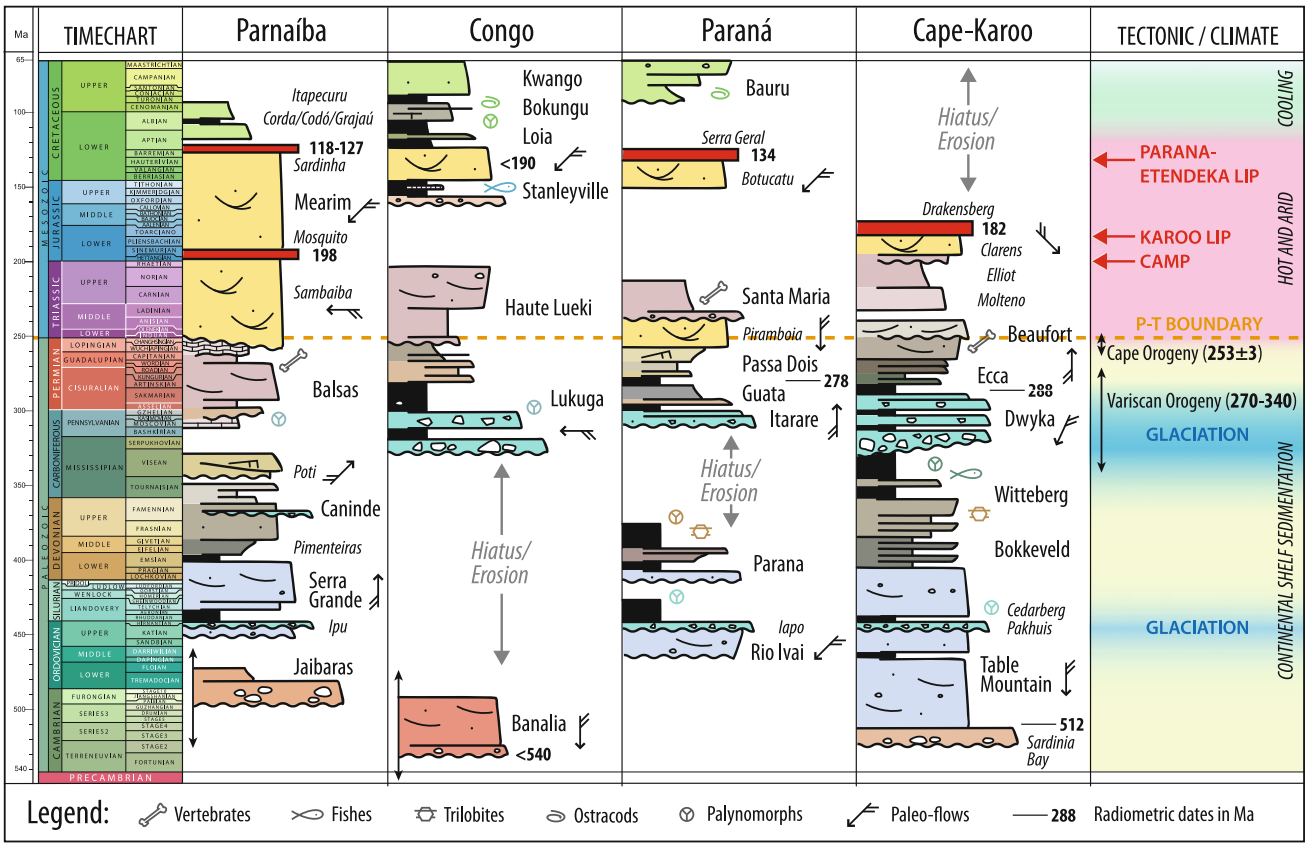

Fig. 18.3 Main stratigraphic sequences of the Parnaíba, Congo, Paraná and Cape-Karoo Basins, and time-correlation with West Gondwana tectonic events, magmatism and climate (from various sources and our own field observations, as described in the text)

Cratons (the Kasai, Cuango, Ntem, Mboumou and Tanzanian Cratons) with peripheral Neoproterozoic fold-and-thrust belts that also form a basement high beneath the basin (the Kiri High; Fig. 18.2b), similar to that observed under the Parnaíba Basin (the Parnaíba block; Fig. 18.2a). Deep borehole cores confirm a lowermost basement sequence of deformed Cryogenian (mid-Neoproterozoic) carbonates and evaporates (Delpomdor et al. 2015; Linol et al. 2015a). Seismic reflection data (Fig. 18.2b) reveal two regional unconformities within the basin fill, originally interpreted as early and late Paleozoic unconformities (Daly et al. 1992), but more recently re-assigned to the Permian-Triassic and the Jurassic, based on seismic stratigraphy recalibrations (see Linol et al. 2015a for details). These two main episodes of basin inversion are interpreted to be related to large-scale intracontinental deformations during the amalgamation of Pangea (ca. 340–270 Ma), and again during the initial period of break-up between East and West Gondwana at around 180–160 Ma (e.g., Reeves 2014).

The lowermost sequence of the Congo Basin is upper Neoproterozoic to lower Paleozoic in age (the Banalia, Inkisi and Biano Groups). It comprises 1000–1500 m thick red beds (conglomerates, quartzitic sandstones and red mudstones; Fig. 18.3) sourced from the exhumed Neoproterozoic belts that surround the basin. This sequence is dated by U-Pb detrital zircons geochronology to have a maximum early Cambrian age (ca. <540 Ma; Linol et al. 2015a). There are no Ordovician-Devonian sequences recognized in the Congo Basin, suggesting a prolonged hiatus of 150 million years of non-deposition and/or erosion. The overlying Carboniferous-Permian Lukuga Group comprises two 'lower glacial beds' with black shales (Milleson et al. 2016), in total between 400 and 800 m thick, sourced from the Tanzanian Highlands flanking the eastern margin of the basin, and sandstones with coal beds and varicolored mudstones (about 200 m thick; Fig. 18.3). The top of this sequence is an angular unconformity covered by conglomerates and red sandstones, up to 1800 m thick in the center of the basin (Fig. 18.2b), attributed to the Triassic Haute Lueki Group (Linol et al. 2015a). This is in turn truncated by another regional erosion surface and covered by red sandstones and fossiliferous mudstones of the Upper Jurassic-Cretaceous Stanleyville, Loia, Bokungu and Kwango Groups (in total between 600 and 1200 m thick; Fig. 18.2b). These ephemeral marine, aeolian, fluvial and lacustrine deposits are Kimmeridgian, Albian-Cenomanian and Upper Cretaceous in age, as dated by palynology and rich fish and crustacean (ostracods) faunas, similar to the Brazilian sequences (Colin 1994; Linol et al. 2015b). In the Congo Basin, the aeolian

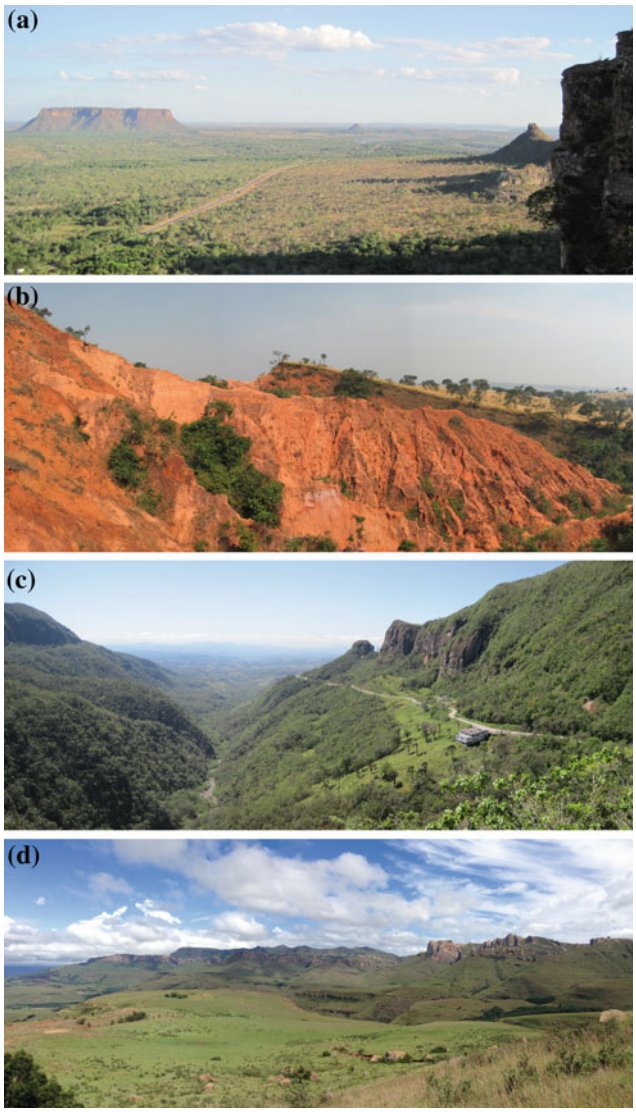

Fig. 18.4 Mesozoic aeolian sequences of West Gondwana: **a** remnants of the Triassic Sambaíba Formation in the southwest Parnaíba Basin (derived from the south); **b** the Kwango Group (Jurassic-Cretaceous) of the southwest Congo Basin deposited from northeasterly paleo-winds; **c** the Botucatu Formation (Lower Cretaceous) near the top of Serra do Rio do Rastro in the southeast Paraná Basin; and **d** the Drakensberg escarpment comprising the aeolian Clarens Formation (foreground; Lower Jurassic) in the eastern Karoo Basin; Fig. 18.1b for location

dunes, named the Dekese Formation (part of the Kwango Group), were deposited also during northeasterly paleo-winds (Fig. 18.4b), and are younger than Lower Jurassic as based on U-Pb dates using detrital zircons (ca. <190 Ma). These correlate to time-equivalent aeolian sequences in Namibia (the Etjo Formation) and eastern Brazil (the Botucatu and Sergi Formations), implying an immense 'Sahara-like' paleo-desert across Central West Gondwana before the opening of the South Atlantic Ocean (Scherer and Goldberg 2007; Linol et al. 2015c). Both the Namibian and Brazilian aeolianites are covered by Lower Cretaceous continental flood basalts of the Paraná-Etendeka Large Igneous Province (LIP) dated between 127 and 137 Ma (Janasi et al. 2011; Pinto et al. 2011); but flood basalts are absent in the Congo.

- The Paraná Basin

The Paraná Basin occupies ca. 1,400,000 km^2 of southern Brazil, Paraguay, northern Argentina and Uruguay (Fig. 18.1b). Its sedimentary fill, up to 5 km in thickness, can possibly be linked to the geodynamic history of the Gondwanides (Milani et al. 2007), an extensive and long-lived Phanerozoic belt along the southern margin of Gondwana marked by successive orogens (the Ocloyic, Precordillera, Chanic and Sanrafaelic Orogenies), and that now form the Andes flanking the southern margin of the basin. No modern seismic sections are available across the Paraná Basin (Milani, pers comm 2016).

The oldest siliciclastic platform sequences, viz. the Ordovician-Lower Silurian Rio Ivaí Group (300–1000 m thick) and the Devonian Paraná Group (1000 m thick) were regionally derived from the north and northeast, and correlate litho- and bio-stratigraphically with the Cape Supergroup of South Africa (Fig. 18.3), including the Upper Ordovician Iapó and Pakhuis glacial deposits, respectively (Milani et al. 2007; Milani and de Wit 2008). In the Paraná Basin, a distinct glacial erosion surface represents a hiatus of ca. 50 million years at the top of the Devonian. Striated glacial pavements indicate regional paleo-flows to the north-northwest, related to glaciers and icebergs originating in southwestern Africa (Gesicki et al. 2002). The overlying glaciomarine turbidites with subordinate varves and tillites of the Itarare Group are up to 1500 m thick and correlate best with the lower Lukuga and Dwyka Groups of the Congo and Karoo Basins, respectively (Linol et al. 2015c). The glacial sequences are overlain by sandstones with coal beds and thick bioturbated siltstones of the Guatá Group (maximum 600 m thick) that record a major maximum marine inundation of the basin around the Sakmarian-Artinskian transition (Milani et al. 2007). This transgressive sequence is in turn overlain by 40–70 m thick black shales, named the Irati Formation (Fig. 18.3), with an organic carbon content as high as 23 % (Milani and Zalán 1999), and which contains the characteristic aquatic reptilian *Mesosaurus* that first permitted Gondwana-scale correlation between South America and southern Africa (Fig. 18.1a; du Toit 1937; see also Chap. 17 in this book). This geochemical and biostratigraphic marker horizon is dated at 278 ± 3 Ma using magmatic zircons from interbedded bentonitic layers (Santos et al. 2006) and thus the same age as the Whitehill Formation of the Karoo Basin in South Africa (see also Chap. 1 in this book). The Irati

Formation is transitionally overlain by a regressive sequence (the Passa Dois Group; maximum 1600 m thick; Fig. 18.3) with younger interlayered ash fall deposits (ca. 270–258 Ma) sourced from abundant Permian arc-volcanism of the proto-Andes (Rocha-Campos et al. 2011; Castillo et al. 2015), and thereafter red beds (the Santa Maria Group; about 300 m thick) containing Middle to Upper Triassic tetrapod fossils. The succeeding widespread aeolian Botucatu Formation (Fig. 18.4b), is conformably overlain by the Serra Geral Basalts of the Paraná-Etendeka LIP (137–127 Ma) that is linked to the onset of break-up and early spreading of the southern South Atlantic (Fromm et al. 2015 and references therein). In the north-central part of the basin, an uppermost 300 m thick Upper Cretaceous fluvial sequence (the Bauru Group; Fig. 18.3) covers the basalts, implying a hiatus of at least 25 million years during the Early Cretaceous.

- The Cape-Karoo Basin

The Cape-Karoo Basin covers ca. 800,000 km^2 of southern Africa, and before Gondwana break-up and the opening of the southern oceans extended eastward to the Falkland Islands and Antarctica (e.g., Marshall 1994; Elliot et al. 2015), and westward to northern Argentina and Brazil (Fig. 18.1a). The stratigraphic record ranges between 3 and 8 km in thickness (Fig. 18.2c) and traditionally divided into the Cape and Karoo Supergroups, which record a transition from passive margin to foreland basin. This inversion resulted from the Sanrafaelic Orogeny (290–245 Ma; Milani and de Wit 2008) within the Gondwanides, and in particular the formation of the Cape-Sierra de la Ventana (SdlV) Fold Belt that extends from southern South Africa to northern Argentina (Pángaro et al. 2015; Chap. 4 this book), dated at 253 Ma using Ar/Ar thermochronology on muscovites (see Chap. 5 in this book). Whilst there is evidence for a southward subduction zone associated with this deformation (Chap. 4 this book), the geodynamic history of the Cape-SdlV Fold Belt is still poorly resolved.

The basal unconformity of the Cape-Karoo Basin is an extensive peneplain across Precambrian basement including the Mesoproterozoic Namaqua Natal Metamorphic Belt and Cambrian Cape Granites (552–510 Ma; Chemale et al. 2011), covered by conglomerates of the Klipheuvel Group in the Western Cape, and the Sardinia Bay Formation (Fig. 18.3) in the Eastern Cape region (Chap. 4 this book). The succeeding lowermost Table Mountain Group is U-Pb dated with detrital zircons to be younger than mid-Cambrian (ca. $< 510 \pm 6$ Ma; Vorster 2013; Chap. 4 this book). This sequence comprises extensive thick quartz-rich sandstones (2000–4500 m thick) intercalating with the Pakhuis tillite and Hirnantian deglaciation shales of the Cedarberg Formation (ca. 444 Ma) that contains spectacular conodonts (Thamm and Johnson 2006). The overlying Bokkeveld and Witteberg Groups (Fig. 18.3), in total between about 3000 and 5200 m thick, comprise alternating tidal and lacustrine deposits, dated with invertebrates and fossil fishes from Devonian to the Mississipian (Chap. 13 this book). All these lower Paleozoic sequences that form the Cape Supergroup and the lowermost platform sequences of the Paraná Basin were derived regionally from the north, indicating a wide shallow marine shelf along the southwest passive margin of Gondwana (Milani and de Wit 2008; Linol et al. 2015c; see also Preface of this book). The overlying Karoo Supergroup starts with Carboniferous-Lower Permian glacial-deglaciation sequences of the Dwyka Group (maximum 500–800 m thick; Chap. 17 this book), which also sourced from the north (Chap. 9 this book). The Dwyka Group is capped by black shales, known as the Prince Albert and Whitehill Formations (Fig. 18.3), that represent a final deglaciation sequence (Chaps. 10 and 11 this book), dated with two thin tuffs near the base at 288–291 Ma (Bangert et al. 1999; Stollhofen et al. 2008). The black shales of the Whitehill Formation (correlated with the Irati Formation in Brazil; Fig. 18.3) are transitionally overlain by rhythmites and coarsening upward turbidites of the Ecca Group, and then fluvial deposits of the Beaufort Group, in total between 700 and 4500 m thick, and both of which are derived from the south in the southern part of the basin (Chap. 1 this book). This thick, regressive, Ecca-Beaufort sequence contains a number of interlayered air-fall volcanic tuffs sourced from the proto-Andes, similar to those described from the Paraná Basin (Linol et al. 2015c), and in its upper part preserves a large diversity of Permian-Triassic mammal-like reptiles (Chap. 14 this book). The overlying Upper Triassic-Lower Jurassic Moltino, Elliot, and Clarens Formations (in total up to 1400 m thick; Fig. 18.3) are increasingly arid and terminate with aeolian dune sands and the Drakensberg Lavas of the Karoo LIP, erupted at 182–183 Ma (Duncan et al. 1997; Burgess et al. 2015; Chaps. 12 and 17 this book).

18.3 Chronostratigraphic Correlation and Paleogeography

Comparison of the stratigraphic sequences of the Parnaíba, Congo, Paraná, and Cape-Karoo Basins (Fig. 18.3) shows that all these very large basins of Central West Gondwana were significantly influenced by the successive climatic and tectonic processes associated with Gondwana's Neoproterozoic-Cambrian amalgamation (the Pan African-Brasiliano orogens; de Wit et al. 2008), its late Paleozoic active margin (the Gondwanides orogens), pan-Gondwanan orogenic events (the Cape and Appalachian-Mauritanian-Variscan Orogenies), and its subsequent break-up during the Jurassic-Cretaceous.

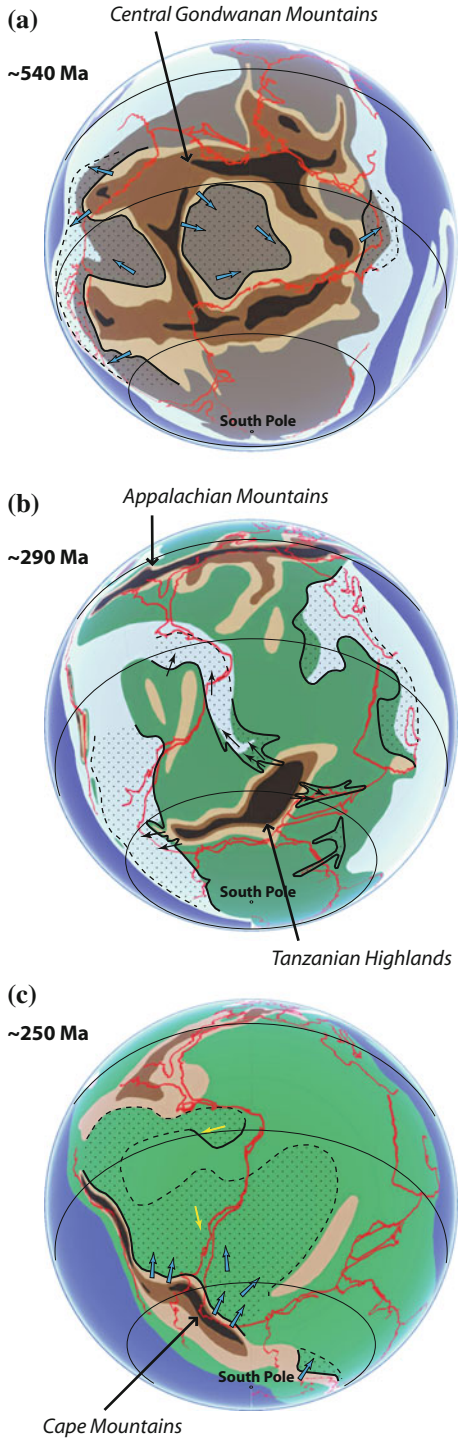

Fig. 18.5 Paleogeographic reconstructions (modified from Scotese 2014) showing major Gondwana mountain systems (*pale* to *dark brown*), basin sequences (*dot pattern*) and sediment dispersal pattern (*arrows: blue* = fluvial, *black* = glacial, *yellow* = aeolian) during: **a** Cambrian; **b** Early Permian; and **c** Early Triassic. Note the rotation of Gondwana relative to the equator during the Early Paleozoic

Following the Pan African-Brasiliano orogens (800–550 Ma; de Wit et al. 2008), continental red bed sediments sourced from extensive Central Gondwana Mountain systems were deposited regionally across the Gondwana interior (in and east-west direction at that time; Fig. 18.5a). These earliest Paleozoic sequences subsequently could provide a large part of sediment detritus to Ordovician-Carboniferous shallow marine platforms bordering the passive margins of Gondwana, and which episodically recorded sea level rises during the Llandovery and Early Devonian, and glaciations, the most marked being the mid-Carboniferous (Dwyka) ice-age. During and following this late Paleozoic period, significant erosion affected south-central Gondwana (Fig. 18.5b), as indicated by abundant glacial pavements and incised paleo-valleys preserved across the Congo, Paraná and northern Karoo Basins, as well as recent thermochronometry data from the Tanzanian and Cargonian Highlands (Kasanzu et al. 2016; Preface this book) that indicate removal of up to 5 km of overburden between 350 and 220 Ma. At higher latitude, across the Parnaíba Basin, only a thin regressive sequence (the Poti Formation) possibly relates to this glaciation (Vaz et al. 2007). Terminal deglaciation during the Early Permian and subsequent isostatic rebound led to widespread deposition of organic-rich black shales and coal beds across southern Gondwana (the Whitehill, Irati, and Lukuga Formations; Fig. 18.3). This was followed by progressively continental sedimentation across the entire interior of Central West Gondwana (Fig. 18.5c), where early mammal-like reptiles evolved.

Basin inversion and/or erosion around the Permian-Triassic transition is recorded in all four basins, which is interpreted to be related to large-scale flexures of the Gondwana continental lithosphere associated with the Appalachian-Mauritanian-Variscan (340–270 Ma) and Cape Orogenies (253 Ma) along the northwest and southwest margins of Gondwana, respectively (Figs. 18.5b, c; Trouw and de Wit 1999; Linol et al. 2015c), similar to that seen in north America (e.g., Pinet 2016). The subsequent Triassic-Jurassic arid sedimentation culminated in widespread deposition of aeolian dunes (the Clarens, Etjo, Botucatu, Sergi, Dekese, Sambaíba and Pastos Bons Formations) during strong surface paleo-winds blowing predominantly from the north to the southwest (Fig. 18.3) towards the proto-Andes (Linol et al. 2015c). This was episodically interrupted by successive eruptions of LIPs, at 201 Ma (CAMP), 182 Ma (Karoo) and 134 Ma (Paraná-Etendeka), during initial phases of opening of the southern North Atlantic, Indian and South Atlantic Oceans, respectively. This extended period of break-up of Gondwana is

recorded in the centers of the Parnaíba, Paraná and Congo Basins by an unconformity and/or a hiatus covered by Upper Jurassic-Cretaceous marine and fluvial deposits (Fig. 18.3). Around the basin margins, and widely across southern Africa, prolonged weathering and exhumation removed a further 2–7 km of overburden during the Kalahari Epeirogeny (de Wit 2007; Brown et al. 2014; Preface this book). The resulting sediment detritus was rapidly shed offshore, potentially contributing significantly to the chemistry of the Cenozoic ocean and atmosphere (Linol et al. 2015d and in prep).

18.4 Conclusion

The Cape-Karoo, Paraná, Congo, and Parnaíba Basins evolved during the amalgamation of Gondwana and Pangea supercontinents (ca. 600–300 Ma), and subsequently through their prolonged break-up history (ca. 200–120 Ma). However, major uncertainties remain to connect these basins physically and genetically:

- Is the initial peneplanation and subsequent onset of sedimentation in the basins varied in time?
- The Paleozoic sequences record episodes of maximum basin deepening that are not well constrained in age. Can they possibly be linked to singular phases of the Gondwanides and Appalachian-Mauritanian-Variscan orogens?
- The most marked ice-age ranges from mid-Carboniferous (Visean) to Early Permian, as the paleo-South Pole moved across Africa (Preface this book). Is this 50 million years period of glaciation diachronous across the Karoo, Kalahari, Congo, Paraná, and Parnaíba Basins?
- How do the magmatic events of the three successive LIPs relate to each other and Pangea-Gondwana break-up?
- What impact do the pre-Jurassic-Cretaceous basin structures have on the post-break-up evolution?

To conclude, more modern chronostratigraphy, seismic and subsidence analysis of these large Gondwana Basins are needed to construct a robust supercontinental-scale geodynamic model, and which could also be complimented by climate simulations based on rigorous sedimentological data from the different continents.

Acknowledgments We appreciate the support from AEON-ESSRI and the DST/NRF of South Africa, and the Gondwana Map Project in Brazil. We thank Mike Daly for a constructive review. This is a contribution to IGCP-628 and AEON publication number 162.

References

Bangert B, Stollhofen H, Lorenz V, Armstrong R (1999) The geochronology and significance of ash-fall tuffs in the glaciogenic Carboniferous-Permian Dwyka Group of Namibia and South Africa. J Afri Earth Sci 29:33–49.

Blackburn TJ, Olsen PE, Bowring SA, McLean NM, Kent DV, Puffer J, McHone G, Rasbury ET and Et-Touhami M (2013) Zircon U-Pb Geochronology links the end-Triassic extinction with the Central Atlantic Magmatic Province. Sci. doi:10.1126/science.1234204.

Brown R, Summerfield M, Gleadow A, Gallagher K, Carter A, Beucher R and Wildman M (2014) Intracontinental deformation in southern Africa during the Late Cretaceous. J Afr Earth Sci 100:20–41. http://dx.doi.org/10.1016/j.jafrearsci.2014.05.014.

Burgess SD, Bowring SA, Fleming TH and Elliot DH (2015) High-precision geochronology links the Ferrar large igneous province with early-Jurassic ocean anoxia and biotic crisis. Earth Planet Sci Lett 415:90–99.

Caputo MV, Melo JHG, Streel M and Isbell JL (2008) Late Devonian and Early Carboniferous glacial records of South America. In: Fielding CR, Frank TD and Isbell JL (eds) Resolving the Late Paleozoic Ice Age in Time and Space. Geol Soc Am Spec Pap 441:161–173. doi:10.1130/2008.2441(11).

Castillo P, Fanning CM, Hervé F and Lacassie JP (2015) Characterisation and tracing of Permian magmatism in the south-western segment of the Gondwanan margin; U–Pb age, Lu–Hf and O isotopic compositions of detrital zircons from metasedimentary complexes of northern Antarctic Peninsula and western Patagonia. Gondwana Res. http://dx.doi.org/10.1016/j.gr.2015.07.014.

Chemale F, Scheepers R, Gresse PG and Van Schmus WR (2011) Geochronology and sources of late Neoproterozoic to Cambrian granites of the Saldania Belt. Int J Earth Sci 100(2):431–444. doi:10.1007/s00531-010-0579-1.

Chernes L and Wheeley JR (2009) Early Palaeozoic cooling events: peri-Gondwana and beyond. In Bassett MG (ed) Early Palaeozoic Peri-Gondwana Terranes: New Insights from Tectonics and Biogeography. Geol Soc London Spec Publ 325:257–278.

Cisneros JC, Marsicano C, Angielczyk KD, Smith RGH, Richter M, Fröbisch J, Kammerer CF and Sadleir RW (2015) New Permian fauna from tropical Gondwana. Nat Commun 6:8676. doi:10.1038/ncomms9676.

Colin J-P (1994) Mesozoic-Cenozoic lacustrine sediments in the Zaïre Interior Basin. In: Gierlowski-Kordesch E and Kelts K (eds) Global Geological Record of Lake Basins. Cambridge University Press 4, pp. 31–36.

Daly MC, Andrade V, Barousse CA, Costa R, McDowell K, Piggott N and Poole AJ (2014) Brasiliano crustal structure and the tectonic setting of the Parnaíba basin of NE Brazil: Results of a deep seismic reflection profile. Tectonics 33:2102–2120. doi:10.1002/2014TC003632.

Daly MC, Lawrence SR, Diemu-Tshiband K, and Matouana B (1992) Tectonic evolution of the Cuvette Centrale, Zaire. J Geol Soc 149 (4):539–546.

Delpomdor F, Blanpied C, Virgone A and Préat A (2015) Chapter 4: Sedimentology and sequence stratigraphy of the Late Precambrian carbonates of the Mbuji-Mayi Supergroup in the Sankuru-Mbuji-Mayi-Lomami-Lovoy Basin (Democratic Republic of the Congo). In: de Wit MJ, Guillocheau F and de Wit MJC (eds) The Geology and Resource Potential of the Congo Basin, Regional Geology Reviews. Springer-Verlag, Berlin Heidelberg, pp. 59–76.

De Wit MJ, Stankiewicz J and Reeves C (2008) Restoring Pan-African-Brasiliano connections: more Gondwana control, less Trans-Atlantic corruption. In: Pankurst RJ, Trouw RAJ, Brito Neves BB and de Wit MJ (eds) West Gondwana: Pre-Cenozoic correlations across the South Atlantic Region. Geol Soc London Spec Publ 294:399–412.

De Wit MJ (2007) The Kalahari Epeirogeny and climate change: differentiating cause and effect from core to space. S Afr J Geol 110 (2–3):367-392.

Duncan RA, Hooper PR, Rehacek J, Marsh JS, Duncan AR (1997) The timing and duration of the Karoo igneous event, southern Gondwana. J Geophys Res 102: 18127–18138.

Du Toit A (1937) Our wandering continents: An Hypothesis of Continental Drifting. Edinburgh: Oliver and Boyd, 366p.

Elliot DH, Fanning CM and Hulett SRW (2015). Age provinces in the Antarctic craton: Evidence from detrital zircons in Permian strata from the Beardmore Glacier region, Antarctica. Gondwana Res 28:152–164.

Fromm T, Planert L, Jokat W, Ryberg T, Behrmann JH, Weber MH and Haberland C (2015) South Atlantic opening: A plume induced break-up? Geology 43(10):931–934.

Gesicki ALD, C. Riccomini C and Boggiani PC (2002) Ice flow direction during late Paleozoic glaciation in western Paraná Basin, Brazil. J South Amer Earth Sci 14:933–939.

Ghienne J-F, Desrochers A, Vandenbroucke TRA, Achab A, Asselin E, Dabard M-P, Farley C, Loi A, Paris F, Wickson S and Veizer J (2014) A Cenozoic-style scenario for the end-Ordovician glaciation. Nat Commun 5:4485. doi:10.1038/ncomms5485.

Grahn Y, de Melo JHG and Steemans P (2005) Integrated chitinozoan and miospore zonation of the Serra Grande Group (Silurian-Lower Devonian), Parnaíba Basin, northeast Brazil. Rev Esp Micropaleontol 37(2):183–204.

Gurnis M, Turner M, Zahirovic S, DiCaprio L, Spasojevic S, Müller RD, Boyden J, Seton M, Vlad Manea C and Bower DJ (2011) Plate tectonic reconstructions with continuously closing plates. Comput Geosci. doi:10.1016/j.cageo.2011.04.014.

Janasi VA, Freitas VA and Heaman LH (2011) The onset of flood basalt volcanism, Northern Paraná Basin, Brazil: A precise U-Pb baddeleyite/zircon age for a Chapecó-type dacite. Earth Planet Sci Lett 302:147–153. doi:10.1016/j.epsl.2010.12.005.

Kasanzu C, Linol B, de Wit MJ, Brown R, Persano C and Stuart FM (2016) From source to sink in Central Gondwana: coeval exhumation of the Precambrian basement rocks of Tanzania and sediment accumulation in the adjacent Congo Basin. Tectonics (under review).

Kroner U and Romer RL (2013) Two plates – Many subduction zones: The Variscan orogeny reconsidered. Gondwana Res 24:298–329. http://dx.doi.org/10.1016/j.gr.2013.03.001.

Lindeque A, de Wit MJ, Ryberg T, Weber M and Chevallier L (2011) Deep Crustal Profile across the Southern Karoo Basin and Beattie Magnetic Anomaly, South Africa: an Integrated Interpretation with Tectonic Implications. S Afr J Geol 114(3–4):265-292.

Linol B, de Wit MJ, Barton E, Guillocheau F, de Wit MJC, Colin, J-P (2015a) Chapter 7: Paleogeography and tectono-stratigraphy of Carboniferous–Permian and Triassic 'Karoo-like' sequences of the Congo Basin. In: de Wit MJ, Guillocheau F, de Wit MJC (eds) The Geology and Resource Potential of the Congo Basin, Regional Geology Reviews. Springer-Verlag, Berlin Heidelberg, pp. 111–134. http://dx.doi.org/10.1007/978-3-642-29482-2_7.

Linol B, de Wit MJ, Barton E, Guillocheau F, de Wit MJC, Colin J-P (2015b) Chapter 8: Facies analysis, chronostratigraphy, and paleo-environmental reconstructions of the Jurassic to Cretaceous sequences of the Congo Basin. In: de Wit MJ, Guillocheau F, de Wit MJC (eds) The Geology and Resource Potential of the Congo Basin, Regional Geology Reviews. Springer-Verlag, Berlin Heidelberg, pp. 135–161. http://dx.doi.org/10.1007/978-3-642-29482-2_8.

Linol B, de Wit MJ, Milani EJ, Guillocheau F, Scherer C (2015c) Chapter 13: New regional correlations between the Congo, Paraná and Cape-Karoo Basins of southwest Gondwana. In: de Wit MJ, Guillocheau, F, de Wit MJC (eds) The Geology and Resource Potential of the Congo Basin, Regional Geology Reviews. Springer-Verlag, Berlin Heidelberg, pp. 246–268. http://dx.doi.org/10.1007/978-3-642-29482-2_13.

Linol B, de Wit MJ, Guillocheau F, de Wit MJC, Anka Z and Colin J-P (2015d) Chapter 10: Formation and collapse of the Kalahari duricrust ['African Surface'] across the Congo Basin, with implications for changes in rates of Cenozoic off-shore sedimentation. In: de Wit MJ, Guillocheau, F, de Wit MJC (eds) Geology and Resource Potential of the Congo Basin, Regional Geology Reviews. Springer-Verlag, Berlin Heidelberg, pp. 193–210. doi: 10.1007/978-3-642-29482-2_10.

Marshall JEA (1994) The Falkland Islands: a key element in Gondwana paleogeography. Tectonics 13:499–514.

Merle R, Marzoli A, Bertrand H, Reisberg L, Verati C, Zimmermann C, Chiaradia M, Bellieni G and Ernesto M (2011) $^{40}Ar/^{39}Ar$ ages and Sr–Nd–Pb–Os geochemistry of CAMP tholeiites from Western Maranhão basin (NE Brazil). Lithos 122:137–151. doi:10.1016/j.lithos.2010.12.010.

Milani EJ and de Wit MJ (2008) Correlations between the classic Paraná and Cape Karoo sequences of South America and southern Africa and their basin infills flanking the Gondwanides: du Toit revisited. In: Pankhurst RJ, Trouw RAJ, Brito Neves BB and de Wit MJ (eds) West Gondwana: Pre-Cenozoic Correlations Across the South Atlantic Region. Geol Soc London Spec Publ 294:319–342.

Milani EJ, Gonçalves de Melo JH, de Souza PA, Fernandes LA and França AB (2007) Bacia do Paraná. Boletim de Geociências da Petrobrás 15(2):265–287.

Milani EJ and Zalán PV (1999) An outline of the geology and petroleum systems of the Paleozoic interior basins of South America. Episodes 22(3):199–205.

Milleson M, Myers TS and Tabor NJ (2016) Permo-carboniferous paleoclimate of the Congo Basin: Evidence from lithostratigraphy, clay mineralogy, and stable isotope geochemistry. Palaeogeogr Palaeoclimatol Palaeoecol 441:26–240. http://dx.doi.org/10.1016/j.palaeo.2015.09.039.

Pángaro F, Ramos VA and Pazos PJ (2015) The Hesperides basin: a continental-scale upper Palaeozoic to Triassic basin in southern Gondwana. Basin Res. doi:10.1111/bre.12126.

Pinet N (2016) Far-field effects of Appalachian orogenesis: A view from the craton. Geology 44(2):83–86.

Pinto VM, Hartmann LA, Santos JOS, McNaughton NJ and Wildner W (2011) Zircon U–Pb geochronology from the Paraná bimodal volcanic province support a brief eruptive cycle at ~ 135 Ma. Chem Geol 281:83–102. doi:10.1016/j.chemgeo.2010.11.031.

Reeves C (2014) The position of Madagascar within Gondwana and its movements during Gondwana dispersal. J Afri Earth Sci 94:45–57.

Rocha-Campos AC, Basei MA, Nutman AP, Kleiman LE, Varela R, Llambias E, Canile FM, da Rosa ODCR (2011). 30 million years of Permian volcanism recorded in the Choiyoi igneous province (W Argentina) and the source for younger ash fall deposits in the Paraná Basin: SHRIMP U–Pb zircon geochronology evidence. Gondwana Res 19(2):509–523.

Santos RV, Souza P, de Alvarenga CJS, Dantas EL, Pimentel MM, de Oliveira CG and de Araújo LM (2006) Shrimp U-Pb zircon dating and palynology of bentonitic layers from the Permian Irati Formation, Paraná Basin, Brazil. Gondwana Res 9(4):456–463.

Scotese CR (2014) PaleoAtlas for ArcGIS, PALEOMAP Project, Evanston, IL.

Scherer CMS and Goldberg K (2007) Palaeowind patterns during the latest Jurassic - earliest Cretaceous in Gondwana: Evidence from aeolian cross-strata of the Botucatu Formation, Brazil. Palaeogeogr Palaeoclimatol Palaeoecol 250(1–4):89-100.

Schoene B, Guex J, Bartolini A, Schaltegger U and Blackburn TJ (2010) Correlating the end-Triassic mass extinction and flood basalt volcanism at the 100 ka level. Geology 38(5):387–390.

Souza PA, Matzembacher LT, Abelha M and Borghi L (2010) Palinologia da Formação Piauí, Pensilvaniano da bacia do Parnaíba: biocronoestratigrafia de intervalo selecionado do poço 1UN09Pi (Caxias, MA, Brasil). Rev Bras Paleontolog 13(1):57–66. doi:10.4072/rbp.2010.1.07.

Stollhofen H, Werner M, Stanistreet IG and Armstrong RA (2008) Single-zircon U-Pb dating of Carboniferous-Permian tuffs, Namibia, and the intercontinental deglaciation cycle framework. Geol Soc Am Spec Pap 441:83–96.

Thamm AG and Johnson MR (2006) The Cape Supergroup. In: Johnson MR, Anhaeusser CR and Thomas RJ (eds) The Geology of South Africa. Geological Society of South Africa, Johannesburg/Council for Geoscience, Pretoria, pp. 443–460.

Torsvik TH and Cocks LTM (2011) The Palaeozoic palaeogeography of central Gondwana. In: Van Hinsbergen DJJ, Buiter SJH, Torsvik TH, Gaina C and Webb S J (eds) The Formation and Evolution of Africa: A Synopsis of 3.8 Ga of Earth History. Geol Soc London Spec Publ 357:137–166.

Trouw RA and de Wit MJ (1999) Relation between the Gondwanide Orogen and contemporaneous intracratonic deformation: J Afr Earth Sci 28(1):203–213.

Van Staal CR, Whalen JB, Valverde-Vaquero P, Zagorevski A and Rogers N (2009) Pre-Carboniferous, episodic accretion-related, orogenesis along the Laurentian margin of the northern Appalachians. Geol Soc London Spec Publ 327:271–316.

Vaz PT, Rezende NGAM, Wanderley Filho JR and Travassos WAS (2007) Bacia do Parnaíba: Boletim de Geociências da Petrobrás 15:253–263.

Vorster C (2013) Laser ablation ICP-MS age determination of detrital zircon populations in the Phanerozoic Cape and Lower Karoo Supergroups (South Africa) and correlatives in Argentina. Unpublished PhD thesis, University of Johannesburg, 626p.

Epilogue: Simplified Cape-Karoo Stratigraphy

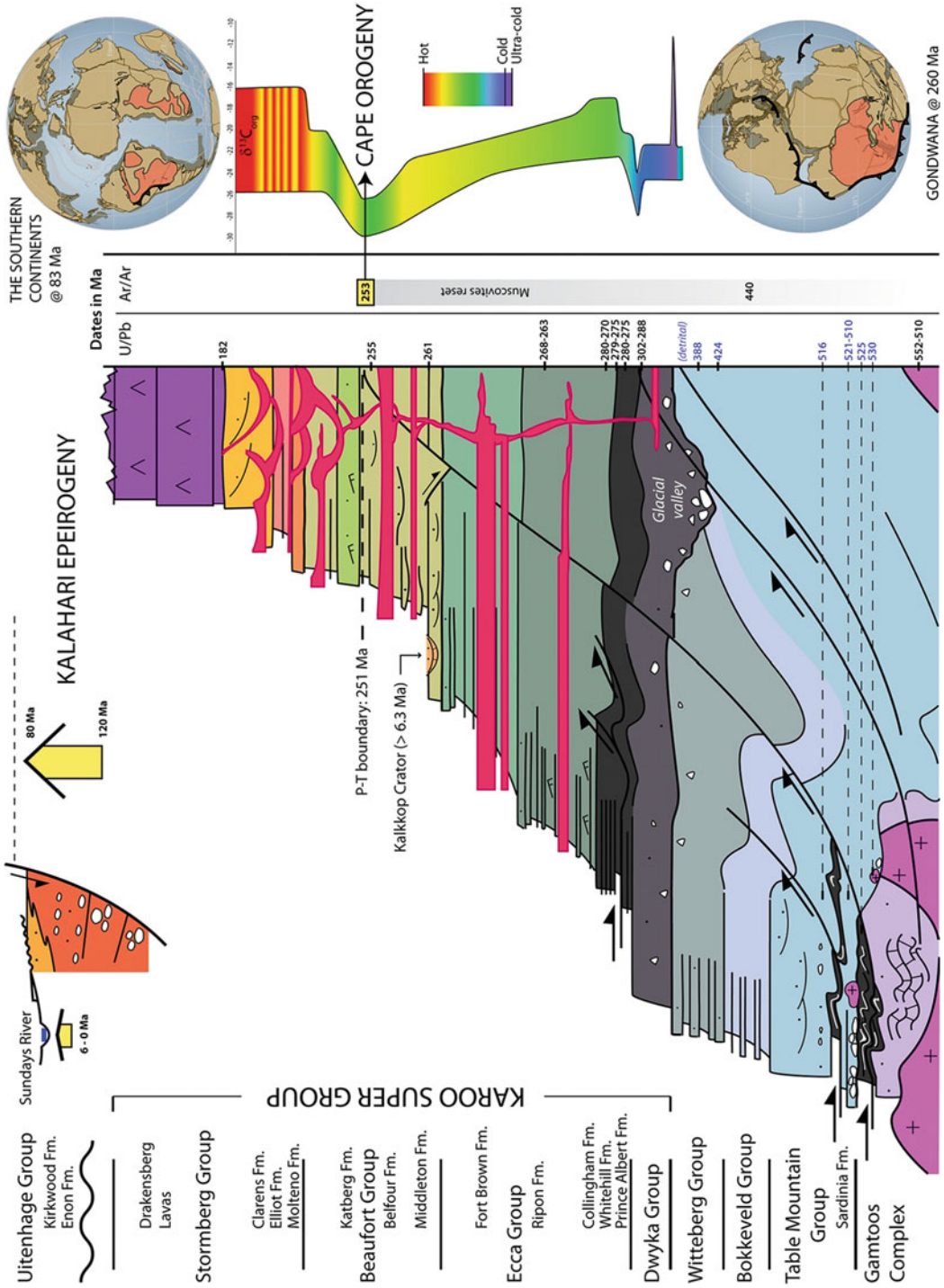

B. Linol and M.J. de Wit (eds.), *Origin and Evolution of the Cape Mountains and Karoo Basin*,
Regional Geology Reviews, DOI 10.1007/978-3-319-40859-0